Title
Trehalose Polymers and Ruthenium-Catalyzed Polymerizations: Synthesis and Applications

Author
Ko, Jeong Hoon

Publication Date
2018

Peer reviewed|Thesis/dissertation

UNIVERSITY OF CALIFORNIA

Los Angeles

Trehalose Polymers and Ruthenium-Catalyzed Polymerizations: Synthesis and Applications

A dissertation submitted in partial satisfaction of the

requirements for the degree Doctor of Philosophy in Chemistry

by

Jeong Hoon Ko

2018

ABSTRACT OF THE DISSERTATION

Trehalose Polymers and Ruthenium-Catalyzed Polymerizations: Synthesis and Applications

by

Jeong Hoon Ko

Doctor of Philosophy in Chemistry

University of California, Los Angeles, 2018

Professor Heather D. Maynard, Chair

Since the definition of polymers as covalently linked macromolecules by Hermann Staudinger in 1920, polymers have become indispensable components of our society as industrial materials, consumer products, and medical devices only to name a few applications. This explosive growth of polymer use in the past century, referred to as "The Plastics Revolution", was driven by research into polymerization techniques for various monomer types appropriate for the desired application. The past two decades have been marked by the development of controlled polymerization methods in addition to advances in new chemical reactions that are highly efficient. The combination of controlled polymerization techniques with methodologies in other fields of organic chemistry is expected to lead to a second plastics revolution, enabling polymers to further enhance our society by materials with new applications.

The first five chapters of this dissertation are related to the use of controlled radical polymerization in combination with methods for protein-polymer conjugation, carbohydrate

synthesis, and click chemistry to enhance the properties of protein drugs. Proteins have many desirable traits for therapeutic use, but their potential has yet to be fully realized due to their low physical stability and rapid clearance from the body by multiple elimination pathways. Synthetic polymers produced from the natural sugar trehalose, which stabilizes proteins in nature, would be effective in protecting various proteins from physical stressors and also *in vivo* clearance when covalently conjugated to proteins.

Even though polymers based on sugars are used for various applications, their syntheses are hindered by the difficulty in monomer synthesis. This is because the multiple hydroxyl groups in sugars have minimal reactivity difference under most reaction conditions, and the reported syntheses are multi-step and low yielding. In Chapter 1, an efficient one-step synthesis of a trehalose monomer was developed using the specific interaction of borinic acids with 1,3-diol of trehalose, thereby overcoming the challenge in carbohydrate monomer synthesis. In Chapter 2, trehalose polymers with varying attachment site of the polymer backbone to the trehalose side chain were synthesized, and the effect of the regioisomers on protein stabilization was evaluated.

In Chapter 3, polymeric hydrogels based on trehalose were used to stabilize proteins important for medical and industrial applications. In the first section, a glucose-responsive trehalose hydrogel was developed to stabilize insulin against heat stress and release insulin in response to high glucose level as in diabetic patients after a meal. The second section presents the industrially scalable synthesis of trehalose hydrogel that did not require any chromatographic purification. The hydrogel fully stabilized phytase, an important animal feed enzyme, under industrially relevant conditions when the hydrogel was used at 10 or higher weight equivalents.

In Chapter 4, trehalose polymers were conjugated to therapeutic proteins to enhance both their stability and *in vivo* pharmacokinetics. The first section demonstrates that this strategy was

effective for insulin as a model protein drug, and the insulin-trehalose polymer conjugate exhibited significantly higher thermal stability and *in vivo* half-life compared to insulin itself. In the second section, the approach was extended to granulocyte colony-stimulating factor (G-CSF). Click chemistry was used for efficient synthesis of the G-CSF-trehalose polymer conjugate. *In vivo* evaluations including bioactivity, biodistribution, toxicity, and immunogenicity were conducted.

Although conjugation of a polymer to a therapeutic protein has benefits that outweigh the costs, the conjugates often have reduced activity due to steric hindrance by the attached polymer. In Chapter 5, a new traceless conjugation method was developed to address this drawback of polymer conjugation to proteins. Traceless conjugation such as the method described herein would help the protein regain full activity while retaining all the benefits of polymer conjugation.

In the last three chapters, ruthenium-catalyzed controlled polymerization techniques were combined with new organic chemistry methodologies to access new types of polymers. In Chapter 6, ruthenium-catalyzed living radical polymerization (Ru-catalyzed LRP) was used to prepare amphiphilic fluorinated random copolymers that encapsulated a fluorinated agrochemical and exhibited interesting self-assembly behavior. In Chapter 7, cyclic ketene acetal was used with Ru-catalyzed LRP to synthesize degradable fluorinated polymers, and their degradation rates were shown to be modulated by the shielding of degradable units by the fluorous side chains. In Chapter 8, aryne chemistry was used to prepare monomers for ring-opening metathesis polymerization (ROMP). Previous syntheses of benzonorbornadiene polymers showed that these polymers are highly unstable and spontaneously oxidize and degrade upon exposure to air. Aryne chemistry enabled the efficient syntheses of monomers with substitution at the benzylic/allylic position, which prevented the resulting polymer from oxidative deformation in air.

The dissertation of Jeong Hoon Ko is approved.

Yi Tang

Joseph Ambrose Loo

Kendall N. Houk

Heather D. Maynard, Committee Chair

University of California, Los Angeles

2018

"[…] the creative function of organic chemistry will continue to augment Nature, with great rewards, for mankind and the chemist in equal measure."

R. B. Woodward, "Synthesis" in *Perspectives in Organic Chemistry*, 1956.

TABLE OF CONTENTS

LIST OF FIGURES

LIST OF SCHEMES

LIST OF TABLES

LIST OF ABBREVIATIONS

13FOMA	1*H*,1*H*,2*H*,2*H*-Perfluorooctyl methacrylate
5FPMA	1*H*,1*H*,2*H*,2*H*,3*H*,3*H*-Perfluoropentyl methacrylate
ACN	Acetonitrile
ACS	American Chemical Society
AcTreMA	Acetylated trehalose methacrylate
AIBN	Azobisisobutyronitrile
ALT	Alanine aminotransferase
APS	Ammonium persulfate
ARC	Animal Research Committee
AST	Aspartate aminotransferase
ATR	Attenuated total reflection
ATRP	Atom transfer radical polymerization
AUC	Area under the curve
BMDO	5,6-Benzo-2-methylene-1,3-dioxepane
BSA	Bovine serum albumin
BTTAA	2-[4-[(Bis[(1-*tert*-butyl-1*H*-1,2,3-triazol-4-yl)methyl]amino)methyl]-1*H*-1,2,3-triazol-1-yl]acetic acid
BUN	Blood urea nitrogen
CBC	Complete blood count
COSY	Correlation spectroscopy
Creat	Creatinine
CTA	Chain transfer agent

CuAAC	Copper-catalyzed azide-alkyne cycloaddition
DART	Direct analysis in real time
DCE	1,2-Dichloroethane
DCM	Dichloromethane
DFO	Deferoxamine
DFT	Density functional theory
DIPEA	*N*,*N*-diisopropylethylamine
DLS	Dynamic light scattering
DMAP	4-(Dimethylamino)pyridine
DMF	*N*,*N*-dimethylformamide
DMI	1,3-dimethyl-2-imidazolidinone
DMSO	Dimethyl sulfoxide
DOSY	Diffusion-ordered spectroscopy
DP	Degree of polymerization
D-PBS	Dulbecco's phosphate buffered saline
DSC	Dynamic scanning calorimetry
EBPA	Ethyl 2-bromo-2-phenylacetate
ECPA	Ethyl-2-chloro-2-phenylacetate
EDC	1-Ethyl-3-(3-dimethylaminopropyl)carbodiimide
EDTA	Ethylenediaminetetraacetic acid
EK	Enterokinase
ELISA	Enzyme-linked immunosorbent assay
ESI	Electrospray ionization

FDA	Food and Drug Administration
FITC	Fluorescein isothiocyanate
FPLC	Fast protein liquid chromatography
FT-IR	Fourier-transform infrared spectroscopy
GAMESS	General Atomic and Molecular Electronic Structure System
GPC	Gel permeation chromatography
GRAS	Generally regarded as safe
HES	Hydroxyethyl starch
HMBC	Heteronuclear multiple bond correlation
HOMO	Highest occupied molecular orbital
HPLC	High performance liquid chromatography
HPMA	*N*-(2-hydroxypropyl) methacrylamide
HRMS	High resolution mass spectrometry
HRP	Horseradish peroxidase
HSQC	Heteronuclear single quantum coherence
Hz	Hertz
ICP-MS	Inductively coupled plasma mass spectrometry
IR	Infrared
ITT	Insulin tolerance tests
LAL	Limulus amebocyte lysate
LC-MS	Liquid chromatography-mass spectrometry
LS	Light scattering
MALDI	Matrix-assisted laser desorption/ionization

MALS	Multi-angle light scattering
MBP	Maltose-binding protein
MW	Molecular weight
MWCO	Molecular weight cut-off
NMP	Nitroxide-mediated polymerization
NMR	Nuclear magnetic resonance
NTA	Nitrilotriacetic acid
OPLS	Optimized potentials for liquid simulations
PAGE	Polyacrylamide gel electrophoresis
PDB	Protein Data Bank
pDNA	Plasmid DNA
PEG	Poly(ethylene glycol)
PEGMA	Poly(ethylene glycol) methyl ether methacrylate
PEP	Proline-specific endopeptidase
PET	Positron emission tomography
PMMA	Poly(methyl methacrylate)
RAFT	Reversible addition-fragmentation chain transfer
RBC	Red blood cell count
RC	Regenerated cellulose
RI	Refractive index
RID	Refractive index detector
ROMP	Ring-opening metathesis polymerization
SDS	Sodium dodecyl sulfate

SEC	Size exclusion chromatography
SEM	Scanning electron microscope
SET	Styrenyl ether trehalose
siRNA	Small interfering RNA
SMD	Solvation model based on density
SOMO	Singly occupied molecular orbital
TBAF	Tetrabutylammonium fluoride
TEMED	Tetramethylethylenediamine
TEV	Tobacco etch virus
TFA	Trifluoroacetic acid
T_g	Glass transition temperatures
TGA	Thermogravimetric analysis
THF	Tetrahydrofuran
TIPS	Triisopropylsilyl
TLC	Thin-layer chromatography
TMB	3,3’,5,5’-Tetramethylbenzidine
TOF	Time-of-flight
TreMA	Trehalose methacrylate
UPLC	Ultra performance liquid chromatography
UV	Ultraviolet
WBC	White blood cell count

ACKNOWLEDGEMENTS

I am forever indebted to my advisor Heather Maynard for both her scientific and career mentorship for the past five years. She has always led by example and has been such a great mentor and teacher. She also encouraged me to pursue my ideas that even I thought were outlandish, and her support has been crucial to making those projects work in the end.

I would like to express my gratitude to my dissertation and oral examination committee for their valuable time. I am especially thankful to Professor Ken Houk for first introducing me to the world of physical organic chemistry, and for our collaborative project. I would like to thank Professor Joe Loo for his advice on mass spectrometry, especially during the quarter when I was taking more mass spectra than TLCs. I am thankful to Professor Yi Tang for his sage advice regarding academic career and other matters. I am also thankful to Professor Jennifer Murphy for her help with the oral examination.

I appreciate all Maynard group members for making our lab a friendly environment and a great place to do chemistry. Juneyoung Lee (June) was an excellent mentor who helped me quickly adjust to Ph.D. research, and exposed me to many of the trehalose projects in the lab. I am grateful for all his help. I would like to thank Yang Liu for teaching me animal experiments, which were crucial for the latter half of my Ph.D. studies. En-Wei Lin is one of the sweetest people I have ever met, and I am glad that I had the chance to work with her on the phytase hydrogel project. I am thankful to Uland Lau for setting the G-CSF project on a solid path and his help even after graduation. I have to say big thanks to Emma Pelegri-O'Day for all her cheerfulness and friendship for all these years we spent together in Ph.D. Marco Messina had to endure my presence in the same office and my bugging him every day with a new paper I would get excited about. I appreciate his patience over the years as well as our project together on trehalose regioisomers. I am thankful

to Kathryn Mansfield for her persistence with all the insulin projects and helping finishing them, and also being a great office mate. I would like to thank Priera Panescu for all her laughter without which the Maynard lab would not be the same anymore, and for her endurance with the trehalose hydrogel project and also for the wonderful introduction at my organic graduate symposium talk. I really appreciate Neil Forsythe and Doug Rose for helping me with projects in my last few months, and for always being there with me in the lab day and night, rain or shine. Arvind Bhattacharya has been a super-first year and helped out in multiple projects, and I am grateful for all his help. I am also thankful to Erhan Bat, Muhammet Kahveci, Jacquelin Kammeyer, Nic Matsumoto, Kathy Nguyen, Cait Decker, Sam Paluck, Natalie Boehnke, Kyle Tamshen, Madeline Gelb, Kathleen Chen, Peter Nauka, Maltish Lorenzo, Warrick Ma, and Omar Ebrahim for their friendship and collaboration on projects.

I have been blessed with many excellent collaborators, who taught me about different fields of research and helped enrich my Ph.D. education. I am very grateful to them and being able to make many exciting discoveries together. I would like to thank Professor Ken Houk again and his talented student Dr. Zhongyue Yang for the collaboration on trehalose regioisomer studies. It has been a true joy working with them, and it always amazes me how effortlessly they can dissect the chemical events with their astute intuition. I am thankful to Professor Neil Garg and his student Dr. Jose Medina for the aryne ROMP project. Apart from having many friends in the Garg lab, this project was a lot of fun and arguably one of my favorites. I believe that benzonorbornadiene polymers that we uncovered will have far-reaching applications in polymer chemistry, and people are already using our approach to access these types of molecules (*Green Chemistry* **2018**, *20*, 1448)! I have been touched by the generous hospitality of Professors Mitsuo Sawamoto, Takaya Terashima, and Makoto Ouchi, as well as Dr. Yuta Koda and Mr. Yoshihiko Kimura during my

10-week stay in Kyoto University and I am thankful for their unlimited support during this time. I would like to thank my undergraduate research advisor Steve Craig at Duke University for allowing me to work with the old gang again – Cameron Brown and Meredith Barbee – on the educational outreach project using the mechanochemically activated spiropyran elastomer. I appreciate Dr. Jin-Wook Lee from Professor Yang Yang's group for the collaboration on perovskite solar cells. I am also very thankful to Professor Paola Picotti and Ms. Monika Pepelnjak at ETH Zurich for being open to our research proposal and being such great collaborators. I also appreciate help from Dr. Jane Strouse for the laborious NMR assignment verification for the regioisomer project, Dr. Frank Ruch and Peter Wallace from Phytex, LLC. for the phytase hydrogel project, and Professor Chrys Wesdemiotis and Ms. Sahar Sallam at University of Akron for their invaluable help in analyzing trehalose polymer-insulin, which were impossible to characterize by mass spectrometry until their assistance.

There are so many mentors and friends in our department that I am thankful for making me feel like a member of the family. I will only mention a few here. I am thankful to Professor Alex Spokoyny for his friendship and his exceptional ability to break down complicated problems, both scientific and career-related, into simple terms and offer a solution whenever I have asked for help. Professor Ellen Sletten is acknowledged here for her expert advice on click chemistry as well as academia in general, and also for constantly calming my nervousness about everything by telling me "you will be fine" during our multiple encounters on the 4th floor of the Molecular Sciences Building. I appreciate Dr. Jon Axtell for his willingness to engage in any random chemistry discussions and for his useful advice, and also for being a great friend and soccer buddy. The "Korean mafia" as Professor Mike Jung would say has grown over the years, and I am thankful for their friendship and scientific help. Dr. Sung-Wook Yi has been always very helpful, and also

taught me tennis for the first couple years. Junyong Kim is my constant go-to for any synthesis questions (or any question in general), and also when I've had too many Subway® sandwiches and want to get something nicer to eat. It has been a pleasure to have Tim Chung and Jin Park as friends and neighbors, and I would like to thank them for helping me with many practice talks. I am thankful to Ha Seong Kim for his advice on statistical mechanics and physical chemistry. I would like to thank Dahee Jung for her friendship over the years. Ga Young Lee has become my new computational chemistry reference after the departure of Zhongyue, and I appreciate her help.

Finally, I would like to thank my parents for their unconditional support in many different forms that made my Ph.D. possible, and my girlfriend Gami Shin for her loving support throughout my Ph.D.

VITA

EDUCATION

B.S.E. in Biomedical Engineering and A.B. in Chemistry with Distinction 2013/5
Duke University, Durham, NC

RESEARCH EXPERIENCE

Graduate student researcher, University of California, Los Angeles 2013/9 – 2018/6
Advisor: Professor Heather D. Maynard

- Synthesized trehalose polymer conjugates to therapeutic proteins and tested their stability and bioactivity *in vivo*.
- Developed regioselective syntheses of trehalose monomers.
- Discovered new traceless conjugation method for protein modification.

Visiting researcher, Kyoto University 2016/6 – 2016/8
Advisors: Professors Mitsuo Sawamoto and Takaya Terashima

- Established a method for tuning the degradation of vinyl fluoropolymers.

Undergraduate researcher, Duke University 2008 – 2009, 2012 – 2013
Advisors: Professors Stephen L. Craig and David Needham

- Studied mechanochemically activated retro Diels-Alder reaction (Craig group).
- Optimized temperature-responsive liposomal formulation of anti-cancer agents (Needham group).

Student research intern, Yonsei University College of Medicine 2011/7 – 2012/6
Advisor: Professor Hae-Jeong Park

- Proposed a new brain atlas based on functional connectivity using graph theory for functional magnetic resonance imaging (fMRI) analysis.

AWARDS

Graduate Research Award for Interdisciplinary Research (UCLA Chem. & Biochem.) 2018
UCLA Dissertation Year Fellowship 2017
UCLA Research Showcase Travel Award for the 251st ACS National Meeting 2015
Associate Trainee, NIH Chemistry-Biology Interface Training Program 2014 – 2017
Outstanding Senior Undergraduate Award, ACS Division of Organic Chemistry 2013
Graduation with Distinction in Chemistry, Duke University 2013
Independent Study Grant, Duke University Undergraduate Research Support 2012

PUBLICATIONS

12. **Jeong Hoon Ko**, Arvind Bhattacharya, Takaya Terashima, Mitsuo Sawamoto, and Heather D. Maynard. Amphiphilic Fluorous Random Copolymer Self-Assembly for Encapsulation of a Fluorinated Agrochemical, *Journal of Polymer Science, Part A: Polymer Chemistry***,** provisionally accepted.

11. Jin-Wook Lee, Zhenghong Dai, Changsoo Lee, Hyuck Mo Lee, Tae-Hee Han, Nicholas De Marco, Oliver Lin, Christopher S. Choi, Bruce Dunn, Jaekyung Koh, Dino Di Carlo, **Jeong Hoon Ko**, Heather D. Maynard, and Yang Yang. Tuning Molecular Interactions for Highly Reproducible

and Efficient Formamidinium Perovskite Solar Cells via Adduct Approach, *J. Am. Chem. Soc.* **2018**, *140*, 6317-6324.

10. Juneyoung Lee, **Jeong Hoon Ko**, Kathryn M. Mansfield, Peter C. Nauka, Erhan Bat, and Heather D. Maynard. Glucose-Responsive Trehalose Hydrogel for Insulin Stabilization and Delivery, *Macromolecular Bioscience* **2018**, *18*, 1700372.

9. **Jeong Hoon Ko**, Takaya Terashima, Mitsuo Sawamoto, and Heather D. Maynard. Fluorous Comonomer Modulates the Reactivity of Cyclic Ketene Acetal and Degradation of Vinyl Polymers, *Macromolecules* **2017**, *50*, 9222.

8. Marco S. Messina,† **Jeong Hoon Ko**,† Zhongyue Yang, M. Jane Strouse, Kendall N. Houk, and Heather D. Maynard. Effect of Trehalose Polymer Regioisomers on Protein Stabilization, *Polymer Chemistry* **2017**, *8*, 4781. († Equal contribution).

7. Cameron L. Brown, Meredith H. Barbee, **Jeong Hoon Ko**, Heather D. Maynard, and Stephen L. Craig. Writing Without Ink: A Mechanically and Photochemically Responsive PDMS Polymer for Science Outreach, *Journal of Chemical Education* **2017**, *94*, 1752.

6. Jose M. Medina,† **Jeong Hoon Ko**,† Heather D. Maynard, and Neil K. Garg. Expanding the ROMP Toolbox: Synthesis of Air-Stable Benzonorbornadiene Polymers by Aryne Chemistry, *Macromolecules* **2017**, *50*, 580. († Equal contribution).

5. Yang Liu,† Juneyoung Lee,† Kathryn M. Mansfield, **Jeong Hoon Ko**, Sahar Sallam, Chrys Wesdemiotis, and Heather D. Maynard. Trehalose Glycopolymer Enhances Both Solution Stability and Pharmacokinetics of a Therapeutic Protein, *Bioconjugate Chemistry* **2017**, *28*, 836.

4. Juneyoung Lee,† **Jeong Hoon Ko**,† En-Wei Lin, Peter Wallace, Frank Ruch, and Heather D. Maynard. Trehalose Hydrogels for Stabilization of Enzymes to Heat, *Polymer Chemistry* **2015**, *6*, 3443. († Equal contribution).

3. Bumhee Park, **Jeong Hoon Ko**, Jong Doo Lee, and Hae-Jeong Park. Evaluation of Node-Inhomogeneity Effects on the Functional Brain Network Properties using an Anatomy-Constrained Hierarchical Brain Parcellation, *PLOS One* **2013**, *8*, e74935.

2. Gijeong Jang, Shin-ae Yoon, Sung-Eun Lee, Haeil Park, Joohan Kim, **Jeong Hoon Ko**, and Hae-Jeong Park. Everyday Conversation Requires Comprehension of Implicated Meanings: Neural Bases of Comprehending Relevance Implicatures in Conversations, *NeuroImage* **2013**, *81*, 61.

1. Eui-Joon Cha, Eue Soon Jang, In-Cheol Sun, In Joon Lee, **Jeong Hoon Ko**, Young Il Kim, Ick Chan Kwon, Kwangmeyung Kim, and Cheol-Hee Ahn. Development of MRI/NIRF 'Activatable' Multimodal Imaging Probe Based on Iron Oxide Nanoparticles, Journal of Controlled Release **2011**, *155*, 152.

Chapter 1.

Regioselective Synthesis of Trehalose Monomers

1.1 Introduction

Trehalose is a naturally occurring sugar composed of two glucose units linked by α,α-1,1 glycosidic linkage. It increases the tolerance of various organisms to extreme environments such as dehydration and heat.[1] Many studies have explored the stabilization mechanism. Although multiple stabilization mechanisms seem to be in effect,[2] preferential exclusion theory[3] is frequently invoked. According to this theory, trehalose has more favorable interaction with water molecules than with biomacromolecules such as proteins and is excluded from the surface. As a result, the protein is preferentially hydrated (and hence the alternative name "preferential hydration hypothesis").[4] Since the unfolded state of a protein has a higher surface area, the folded state is entropically favored in the presence of trehalose (see also depletion interaction in the colloid literature[5, 6]). Trehalose occupies about 2.5 to 2.9 times larger hydration volume than other disaccharides (e.g., sucrose, lactose and maltose),[1, 7] and this larger size has been attributed to the greater effect on preferential exclusion and consequently the superior stabilization effect of trehalose over other sugars for several proteins.[7, 8]

Due to its unique properties, trehalose has been incorporated into synthetic polymers for diverse applications ranging from inhibiting amyloid fibril formation,[9, 10] stabilizing nucleic acid complexes,[11, 12] and protecting proteins from degradation.[13-21] However, many of the trehalose monomers for these studies are synthesized via laborious multi-step syntheses involving protecting group strategies, which are both time-consuming and low-yielding. Miura and co-workers synthesized their trehalose-pendant acrylamide monomer in 8 steps with 16% overall yield.[9] Reineke and co-workers later optimized the synthesis of the same monomer utilizing silyl protecting group instead of an acetyl group in the final stages, but increase in the yield was only 20%.[12] An alternative approach involves chemoenzymatic esterification using enzymes;[21-23]

however, the use of enzymes increases the cost. Moreover, enzyme instability and batch variability are potential concerns, and the scope is limited to ester-based monomers.

To address these limitations, our group has researched protecting group-free chemical syntheses of trehalose monomers (Figure 1-1). In our first report, transacetalization between O4 and O6 of trehalose with a vinyl benzaldehyde acetal yielded a trehalose monomer with acetal linkage between the sugar and the styrenyl group in one step with 41% yield.[13] In addition to direct synthesis without the use of protecting groups, this approach involved only a single step and had a moderate yield that was higher than other multi-step syntheses of trehalose monomers. Subsequently, a trehalose monomer with ether linkage was synthesized by Williamson etherification, which is non-selective and yields various regioisomers.[14, 18] Surprisingly, the secondary alcohol at O4 was found to be more reactive than the primary alcohol at O6 due to the ionic complexation of the sodium ion with the O6 hydroxyl. Density functional theory (DFT) calculations revealed that O6-substituted monomer best retains the native conformation of trehalose (see Chapter 2),[18] but an efficient route to access this monomer remains to be discovered.

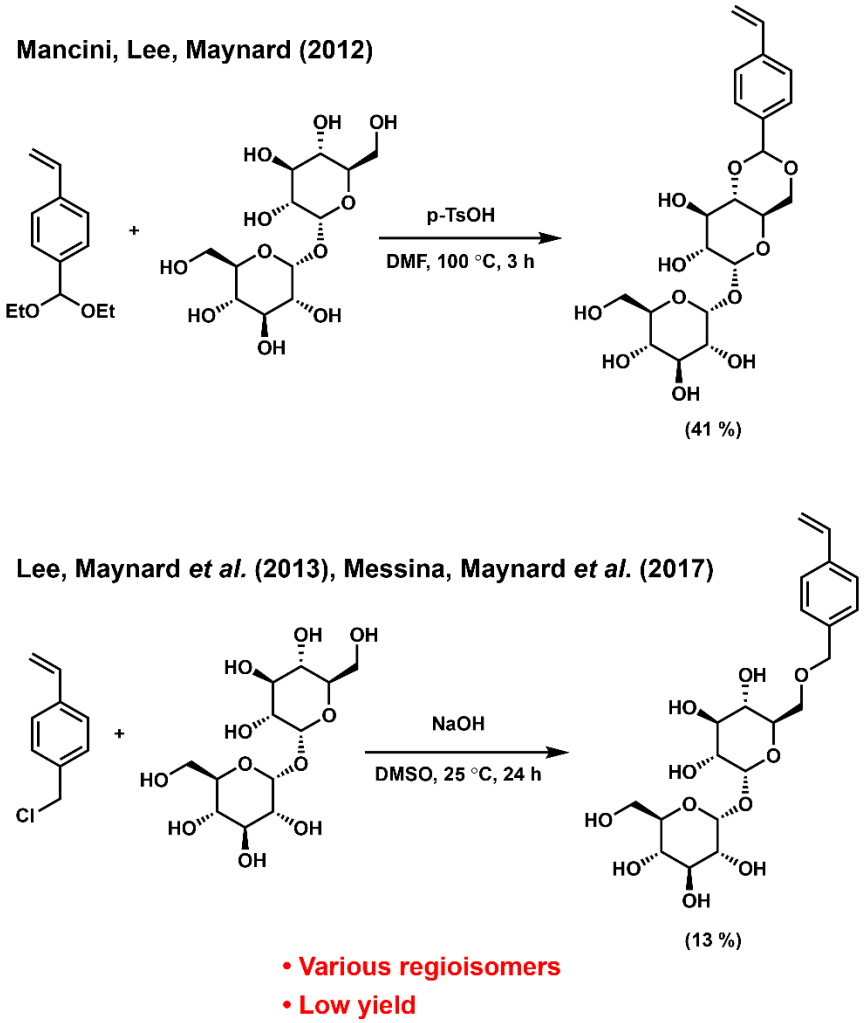

Figure 1-1. Synthesis of trehalose monomers without protecting groups from the Maynard group.

Recently, an effective method to regioselectively modify carbohydrates and other polyols using borinic acids has been developed by Taylor and co-workers.[24-26] Selectivity arises from the ability of borinic acid to form borinate ester with *cis*-1,2- and 1,3-diols, which activates the alcohol towards reaction with an electrophile (Figure 1-2). We envisioned that this chemistry could be used for regioselective trehalose modification since the sugar lacks *cis*-1,2-diols and only has 1,3-diols at the O4 and O6 positions, which should result in selective modification at the O6 position. Although various methods to selectively modify a primary alcohol exist,[27-29] they do not work for

trehalose due to its ionic complexation[18] or they involve organometallic reagents that are incompatible with strongly polar and coordinating solvents such as dimethyl sulfoxide (DMSO) and *N*,*N*-dimethylformamide (DMF) that are required to dissolve trehalose. In this chapter, we will present our results on using the borinic acid reagents to efficiently synthesize an O6-styrenyl trehalose monomer in one step without the use of protecting groups, in addition to attempts at the synthesis of other trehalose derivatives.

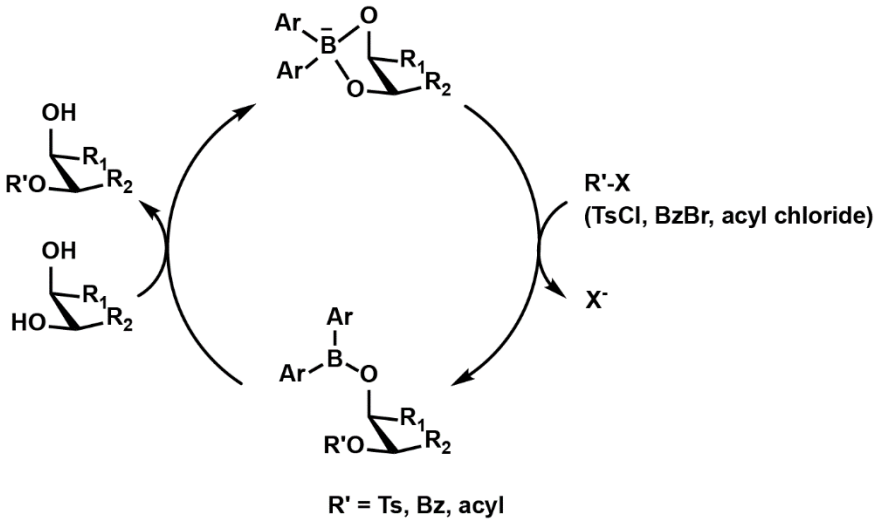

Figure 1-2. Mechanism of regioselective modification of carbohydrates and polyols using borinic acid.[24]

1.2 Results and Discussion

The first borinic acid reagent investigated for regioselective modification of trehalose was 2-aminoethyl diphenyl borate (**1**, Figure 1-3b) reported by Taylor and co-workers.[24] While the previous Williamson etherification using sodium hydroxide in DMSO resulted in all four possible regioisomers and higher substituted products (Figure 1-3a), 10 mol % of **1** with *N*,*N*-diisopropylethylamine (DIPEA) as the base, potassium iodide (KI) to activate the benzyl halide,

and 4 Å molecular sieves exclusively yielded the O6 product in 22% yield (Figure 1-3b). In the absence of the borinic acid, the amount of product obtained was negligible as quantified by high performance liquid chromatography (HPLC) area under the curve (AUC); the reaction also produced other isomers (Experimental Section Figure 1-6). Although the yield from this initial reaction was only 22% as calculated from the calibration curve, it was a significant improvement from the 13% from our previous non-selective route[18] and encouraged further optimization.

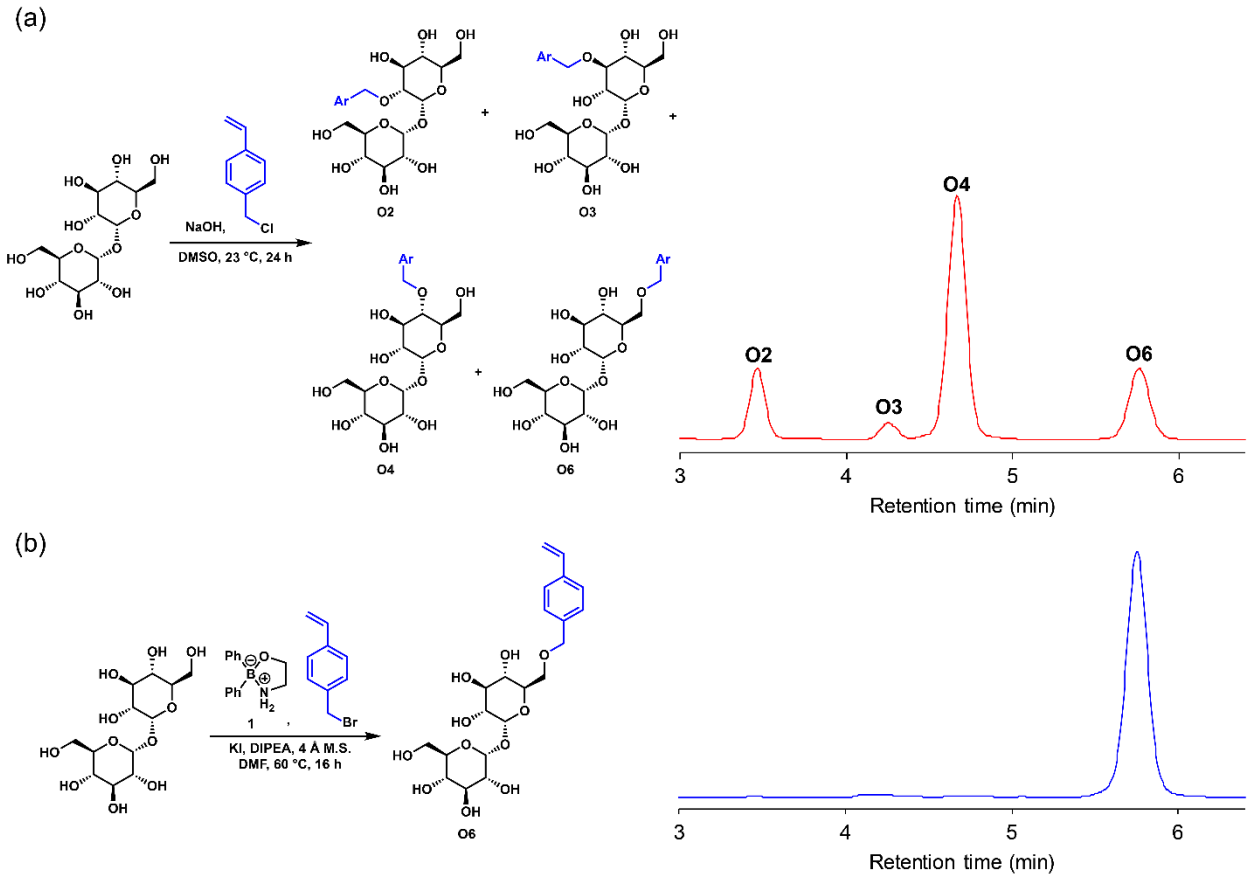

Figure 1-3. Synthesis of vinylbenzyl trehalose monomer using (a) Williamson etherification condition or (b) borinic acid reagent, with HPLC chromatograms of the product mixtures (λ = 280 nm).

Borinic acid catalysis has been reported to give high yield (95%) at 10 mol % loading, although the reaction was conducted in acetonitrile.[24] Under our reaction condition using DMF as

the solvent, the borinic acid turnover number was only 2.2, which suggested the decomposition of the borinic acid or the vinylbenzyl substrate. Borinic acid only showed a single species at 2.1 ppm in DMF as observed by ^{11}B NMR (Experimental Section Figure 1-7), which corresponds to the anionic borate species[30] as expected from the undissociated aminoethanol from the borinic acid. The peak did not show any change after 28 h, and had similar chemical shift as the peak in acetonitrile in which the borinic acid has been reported to be stable.[24] However, the vinylbenzyl substrate subjected to the reaction conditions in the absence of trehalose and the borinic acid showed slight degradation as observed by ^{1}H NMR and some aldehyde species even in deuterated acetonitrile (Experimental Section Figure 1-8). It has been previously reported that alkyl iodide can oxidize benzyl halides to benzaldehydes,[31] and similar mechanism may be in effect. Nevertheless, the reaction seems to proceed fast enough for the desired product to form.

The reaction was optimized by varying the amount of electrophile, KI, and the borinic acid loading (Table 1-1). Increasing the amount of 4-vinylbenzyl bromide from 0.5 to 2 equiv. increased the yield from 0% to 23.6% (entries 1 – 3). It was also found that 4-vinylbenzyl chloride was equally competent substrate and gave 24.4% yield when 1.5 equiv. were used (entry 4) presumably because both benzyl halides (chloride or bromide) needs to be converted to the iodide by KI for reaction with the activated alcohol of trehalose. Since 4-vinylbenzyl chloride is commercially available, it was used for the following experiments unless stated otherwise. When the amount of KI was varied (entries 5 – 11), the yield did not increase past 32% and 0.5 – 1 equiv. of KI was optimal. Increasing both the vinylbenzyl chloride and KI did not result in noticeable increase in the yield, which remained around 30% and decreased to 25.7% at the highest equivalents (4.5 equiv. of vinylbenzyl chloride and 3 equiv. of KI) (entries 12 – 15). Finally, borinic acid loading increased the yield but saturated around 40% (entries 16 – 21).

Table 1-1. Optimization of the reaction condition.

Entry	Screen for electrophile equivalents[a]		Entry	Screen for electrophile/KI equivalents[c]	
	4-Vinylbenzyl halide equiv.	Yield (%)		Equiv. electrophile / KI	Yield (%)
1	0.5 (Br)	0	12	3 / 1	28.8
2	1 (bromide)	12.8	13	3 / 2	28.9
3	2 (bromide)	23.6	14	4.5 / 1	30.3
4	1.5 (chloride)	24.4	15	4.5 / 3	25.7
Entry	Screen for KI equivalents[b]		Entry	Screen for borinic acid equivalents[d]	
	KI Equiv.	Yield (%)		Borinic acid (**1**) (mol %)	Yield (%)
5	0	1.3	16[e]	10	29.6
6	0.25	19.2	17	20	37.7
7	0.5	27.3	18	40	39.7
8	0.75	28.2	19	60	42.8
9	1	29.6	20	80	43.5
10	1.5	26.3	21	100	42.6
11	2	32.0			

[a] 1 equiv. trehalose (0.2 M in DMF), 4-vinylbenzyl bromide (equiv. as designated in the table), 1 equiv. KI, 2.3 equiv. DIPEA, 4 Å molecular sieves. [b] 1 equiv. trehalose (0.2 M in DMF), 1.5 equiv. 4-vinylbenzyl bromide, KI (as designated in the table), 2.3 equiv. DIPEA, 4 Å molecular sieves. [c] 1 equiv. trehalose (0.2 M in DMF), 4-vinylbenzyl bromide (equiv. as designated in the table), KI (as designated in the table), 2.3 equiv. DIPEA, 4 Å molecular sieves. [d] 1 equiv. trehalose (0.2 M in DMF), 1.5 equiv. 4-vinylbenzyl bromide, KI (as designated in the table), 2.3 equiv. DIPEA, 4 Å molecular sieves. [e] Same as entry 9.

Different borinic acids were also screened in an attempt to further increase the yield. One disadvantage of 2-aminoethyl diphenyl borate (**1**) is that the dissociated aminoethanol will react with the electrophile to lower the yield. Other borinic acids such as oxaboraanthracene (**2**) and diphenylborinic anhydride (**3**) that do not have such nucleophilic ligands were thus compared (Table 1-2). Both **2** and **3** can be synthesized in one step using reported procedures.[25, 32, 33] While **1** gave the typical yield of 21.6% (entry 1), the cyclic borinic acid **2** only gave 5.8% of the desired O6-modified trehalose (entry 2), consistent with previous observation that this borinic acid is optimally suited for *cis*-1,2-diol modification.[34] In contrast, the anhydride yielded significantly more product giving 55.0% yield after 14 h (entry 3). Although **1** and **3** have the same active borinic acid species, **3** would release additional borinic acid upon entering the reaction cycle

instead of ethanolamine. Further increasing the amount of borinic acid **3** to 0.4 equiv. did not noticeably enhance the yield (entry 4).

Table 1-2. Screening of borinic acids.

Entry	Borinic acid used / Equiv.	Time (h)	Yield (%)
1[a]	**1** / 0.1	16	21.6
2[a]	**2** / 0.1	16	5.8
3[b]	**3** / 0.2	14	55.0
4[b]	**3** / 0.4	24	57.7

[a] 1 equiv. trehalose (0.2 M in DMF), 1.5 equiv. 4-vinylbenzyl bromide, 1 equiv. KI, 3 equiv. DIPEA, 4 Å molecular sieves.
[b] 1 equiv. 4-vinylbenzyl chloride (0.3 M in DMF), 2 equiv. trehalose, 2 equiv. KI, 0.5 equiv. DIPEA, 4 Å molecular sieves.

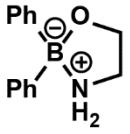

(1)

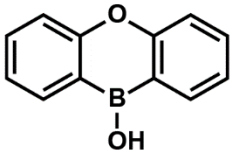

(2)

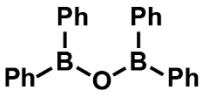

(3)

Although borinic acid proved to be effective in producing styrene-modified trehalose in synthetically useful yields, a method to selectively tosylate trehalose at the O6 hydroxyl would also be valuable for synthesizing various trehalose analogs such as trehalose azides.[11, 35-37] Unfortunately the borinic acid approach did not yield any product for the tosyl chloride substrate, which is more active than the benzyl chloride. Interestingly, the typical tosylation condition (alcohol with tosyl chloride in pyridine) yielded only two isomers with O6-tosylated trehalose in 50.4% yield. Although this is comparable to the borinic acid approach, the presence of other isomer necessitates HPLC purification. Thus, it would be desirable to develop a method to selectively tosylate O6 without generating other isomers. The other isomer could not be conclusively assigned but ^{1}H and ^{13}C NMR spectra showed that it is a single isomer (Experimental Section Figure 1-12).

It was hypothesized that the pyridinium tosylate that is formed as the reactive species poses steric hindrance for modification by other hydroxyl groups, resulting in preferred modification at O6 (Figure 1-4a). It was envisioned that further selectivity may be achieved by using 2,6-lutidine, which forms a much bulkier electrophile that would only be accessible by the primary alcohol O6 (Figure 1-4b).

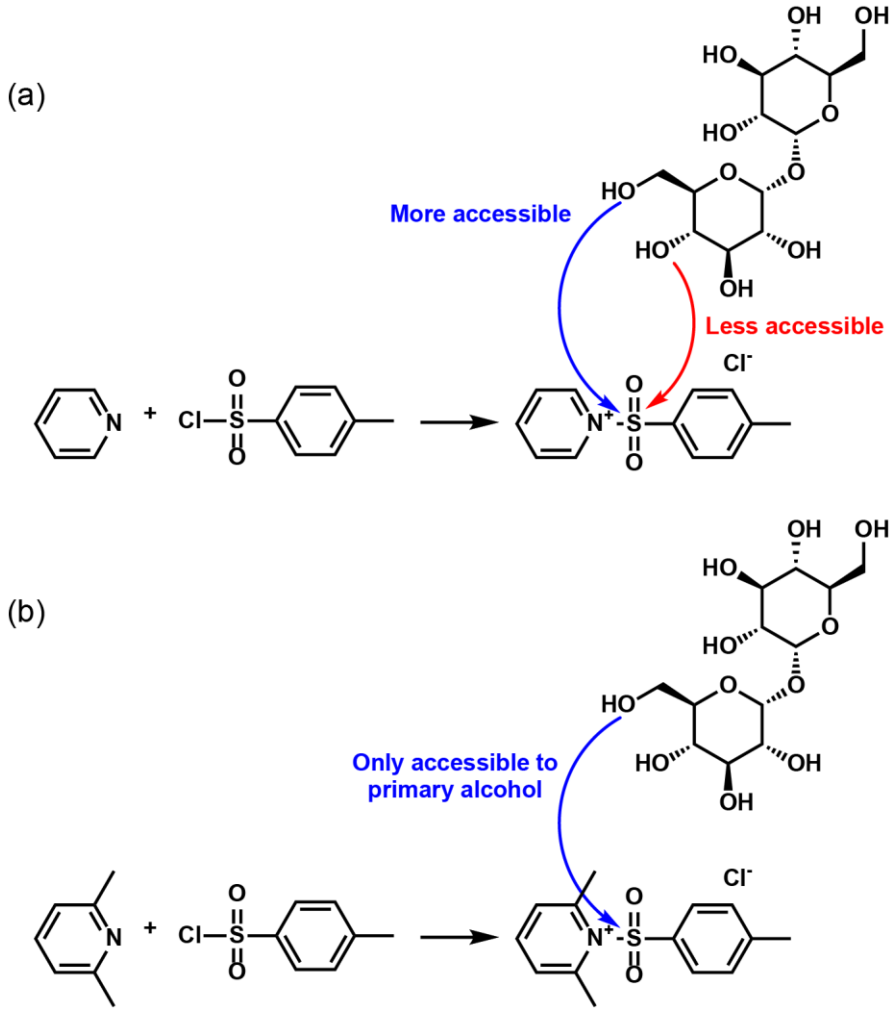

Figure 1-4. Modulation of regioselectivity by steric load around the electrophile.

A cosolvent 1,3-dimethyl-2-imidazolidinone (DMI) was required to solubilize trehalose in the presence of 2,6-lutidine. Although trehalose is soluble in pyridine, a control reaction with

pyridine was conducted in DMI to directly compare the regioselectivity. The reaction using pyridine yielded two isomers, while 2,6-lutidine selectively produced O6 modified product as hypothesized (Figure 1-5). Unfortunately, the added steric hindrance also decreased the reactivity of the tosylate and only resulted in 10.8% yield after 24 h. Although this approach seems promising with regards to its regioselectivity, further optimization of the reaction conditions is required to increase the yield to a useful level.

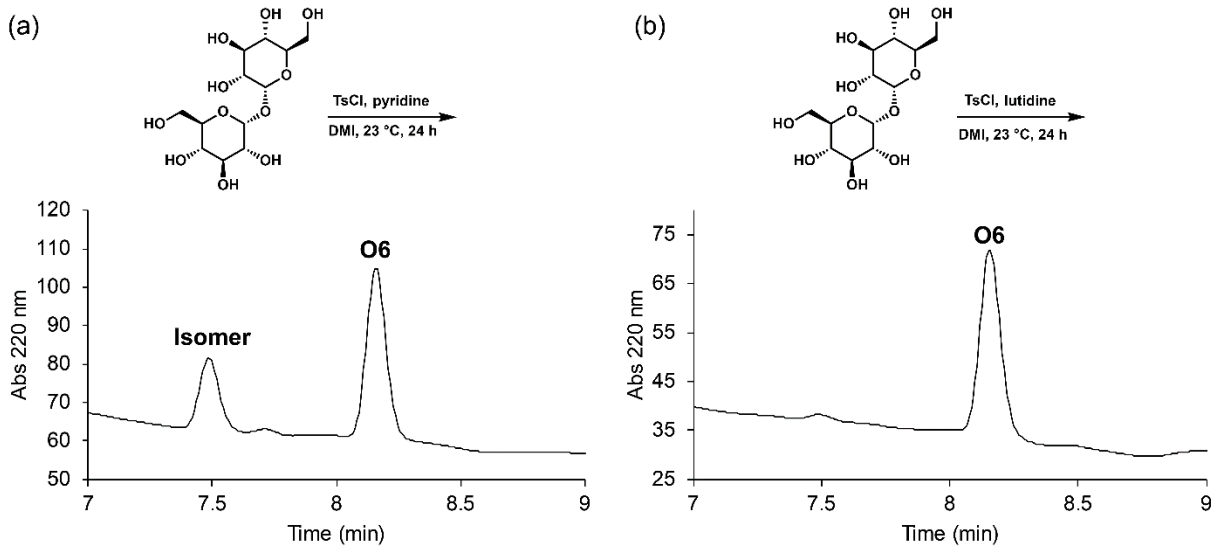

Figure 1-5. Synthesis of tosylated trehalose using (a) pyridine or (b) 2,6-lutidine as the base in 1,3-dimethyl-2-imidazolidinone (DMI).

1.3 Conclusions

A one-step regioselective route to access styrene-type trehalose monomer in synthetically useful 55% yield was established using a borinic acid reagent. Given that other trehalose monomers such as methacrylamide are typically synthesized in 8 steps with 16 – 20% yield, the current methodology involves only a single step, is protecting-group free, and is higher yielding

than our previously reported one step syntheses. Thus, it represents a significant advance in the synthesis of carbohydrate monomers. It is expected that the trehalose monomer synthesis presented in this chapter will greatly facilitate research into trehalose polymers and their diverse applications. In addition, selective tosylation of trehalose was achieved by increasing the steric bulk of the electrophile, but the reaction requires further optimization to enhance the yield to a synthetically useful level.

1.4 Experimental Section

Materials

Trehalose was purchased from The Endowment for Medical Research (Houston, TX) and was azeotropically dried with ethanol and kept under vacuum until use. 2-Aminoethyl diphenyl borate was used as received (Sigma-Aldrich). Oxaboraanthracene[25] and diphenylborinic anhydride[32, 33] were synthesized according to literature procedure.

Analytical Techniques

NMR spectra were recorded on a Bruker DRX 500 MHz or a Bruker AV 500 MHz. HPLC experiments were performed on an Agilent analytical HPLC system (Agilent 1260 Infinity II LC System) connected to Quaternary Pump, Vialsampler, and VWD UV detector using a Phenomenex Luna 5 μm C18(2) 100 Å column (250 x 4.6 mm) with isocratic elution of 25% solvent B over 14 min (solvent A: water + 0.1% trifluoroacetic acid (vol/vol), solvent B: acetonitrile + 0.1% trifluoroacetic acid (vol/vol)) for the vinyl trehalose monomer and elution gradient of 10–100% solvent B over 14 min (solvent A: water + 0.1% trifluoroacetic acid (vol/vol), solvent B: acetonitrile + 0.1% trifluoroacetic acid (vol/vol)) for the tosylated trehalose.

Synthesis of Trehalose Monomers

Representative Procedure: Synthesis of O6-substituted vinylbenzyl ether trehalose using diphenylborinic anhydride. Diphenylborinic anhydride (10.4 mg, 0.03 mmol, 0.2 equiv.), trehalose (103 mg, 0.3 mmol, 2 equiv.), potassium iodide (50 mg, 0.3 mmol, 2 equiv.), *N*,*N*-dimethylformamide (DMF) (0.5 mL), and 4 Å molecular sieves (approximately 96 mg) were added to a dram vial and stirred at 60 °C until trehalose fully dissolved. Then 4-vinylbenzyl chloride (23.5 uL, 0.15 mmol, 1 equiv.) followed by *N*,*N*-diisopropylethylamine (DIPEA) (13 uL, 0.075 mmol, 0.5 equiv.) were added. The reaction was stirred for 14.5 h at 60 °C before removal of the solvent *in vacuo* and dissolution of the solid in 2 mL MilliQ water for HPLC analysis.

Representative Procedure: Synthesis of O6-substituted tosyl trehalose using diphenylborinic anhydride. Trehalose (257 mg, 0.75 mmol, 3 equiv.) was dissolved in 1,3-dimethyl-2-imidazolidinone (DMI, 5 mL) with gentle heating, followed by addition of 2,6-lutidine (1 mL). The solution was cooled to 0 °C, and tosyl chloride (48 mg, 0.25 mmol, 1 equiv.) was added. The mixture was warmed to 23 °C and stirred for 24 h, and then precipitated into 100 mL of 1:1 hexanes:diethyl ether. The solid was dissolved in 9:1 water:methanol (30 mL) and analyzed by HPLC.

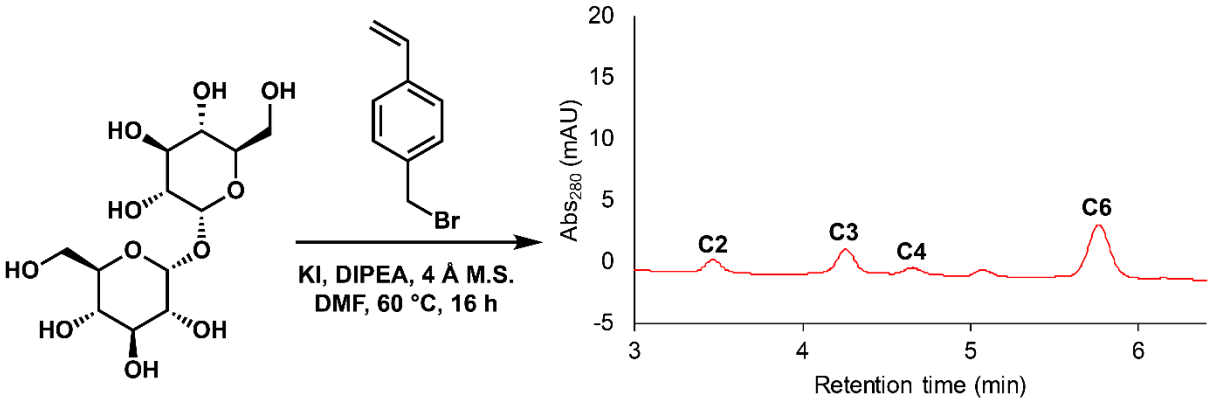

Figure 1-6. Control experiment without borinic acid reagent, showing negligible formation of the product.

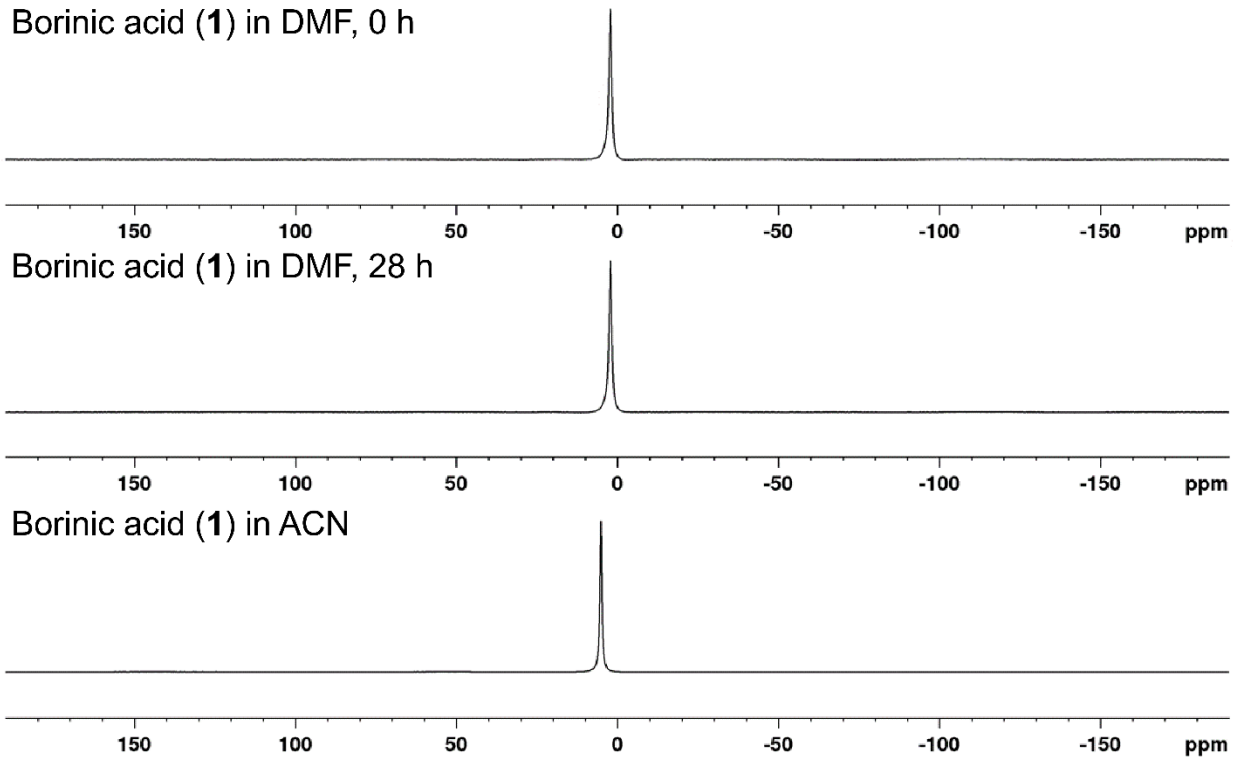

Figure 1-7. ^{11}B NMR spectrum of boric acid in *N*,*N*-dimethylformamide (DMF) or acetonitrile (ACN) (20 mg/mL).

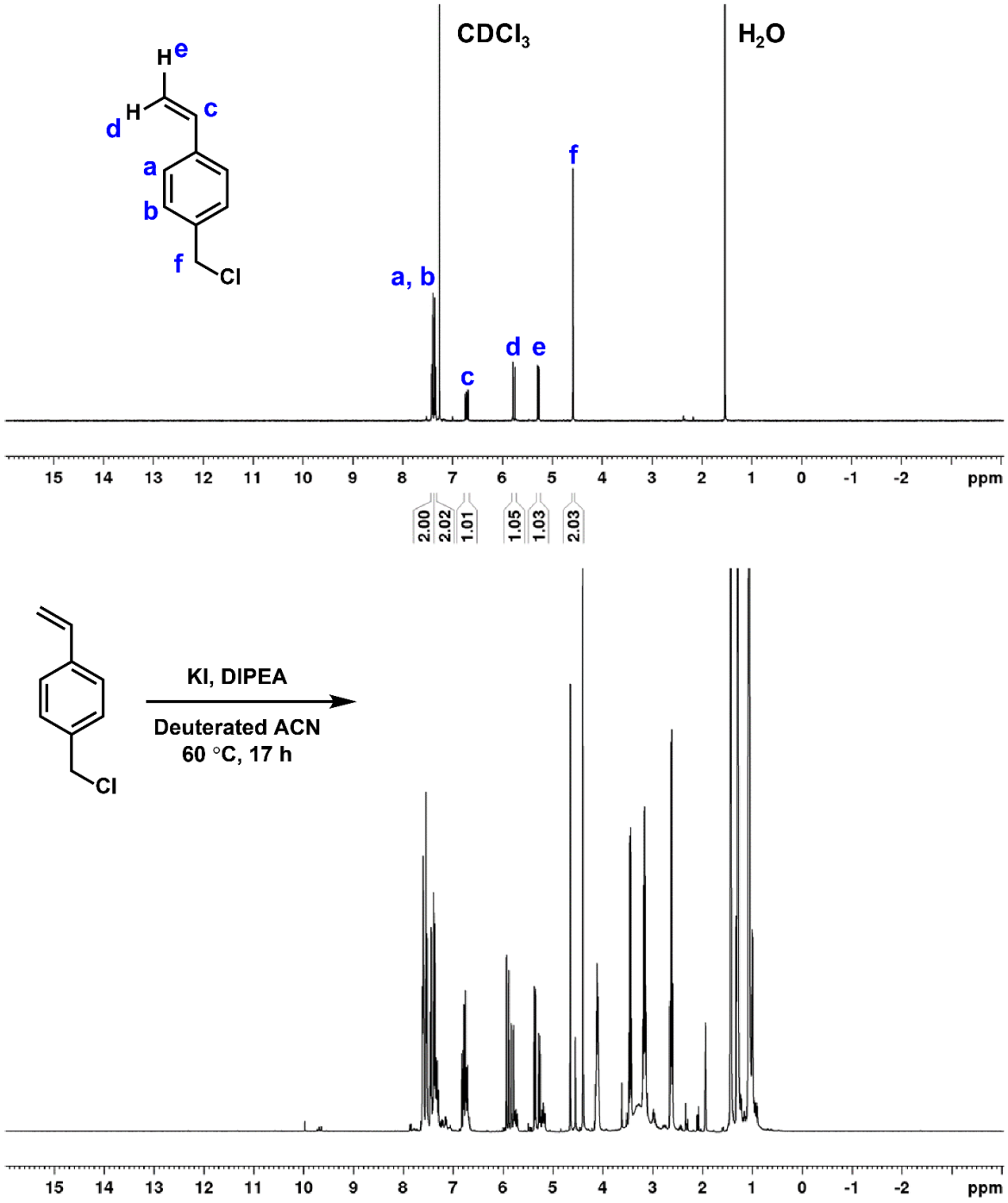

Figure 1-8. ^{1}H NMR spectrum of (top) 4-vinylbenzyl chloride in $CDCl_3$ and (bottom) 4-vinylbenzyl chloride with KI and DIPEA in CD_3CN after 17 h at 60 °C.

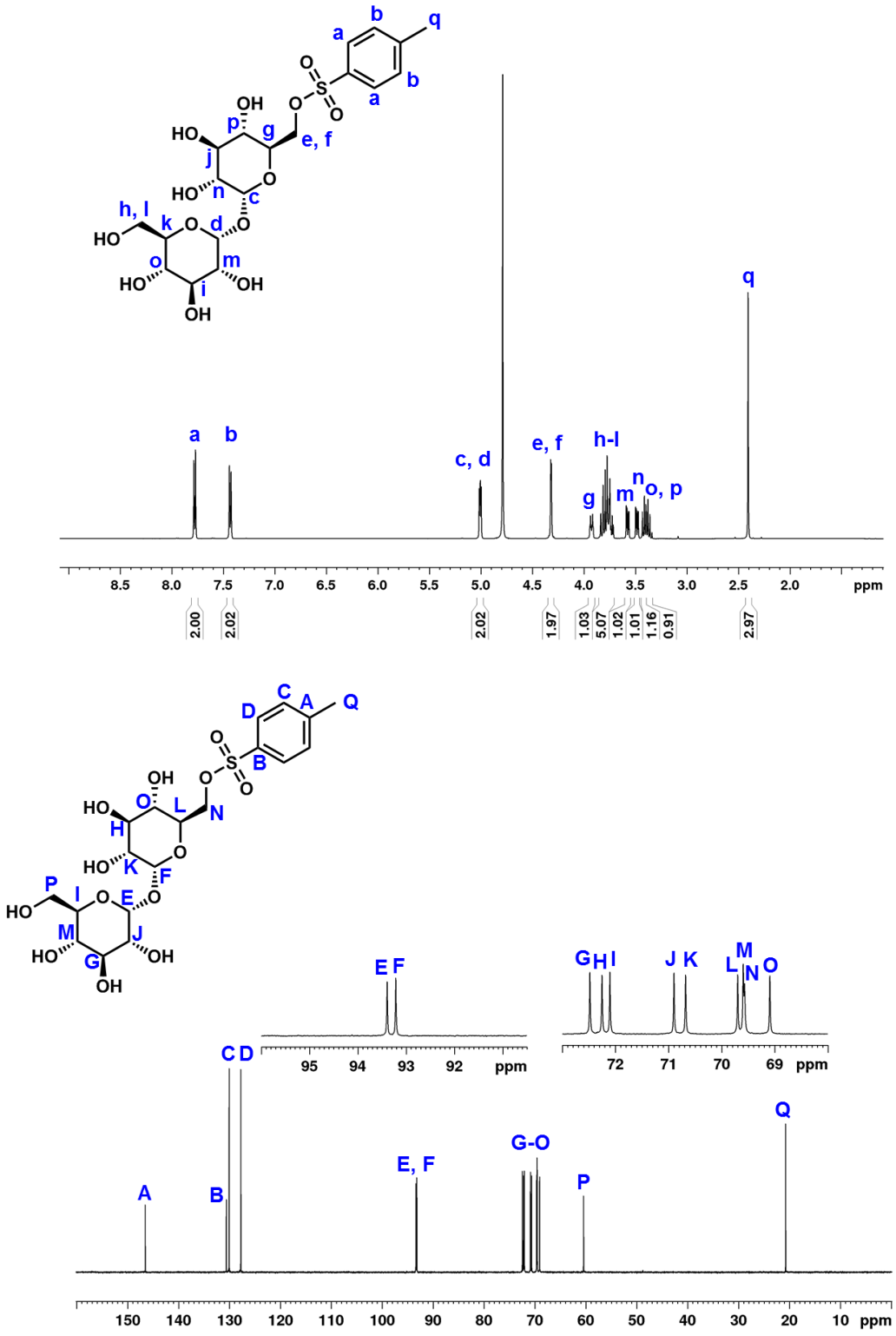

Figure 1-9. ^{1}H (top) and ^{13}C (bottom) NMR spectra of O6-tosyl trehalose (CD_3OD).

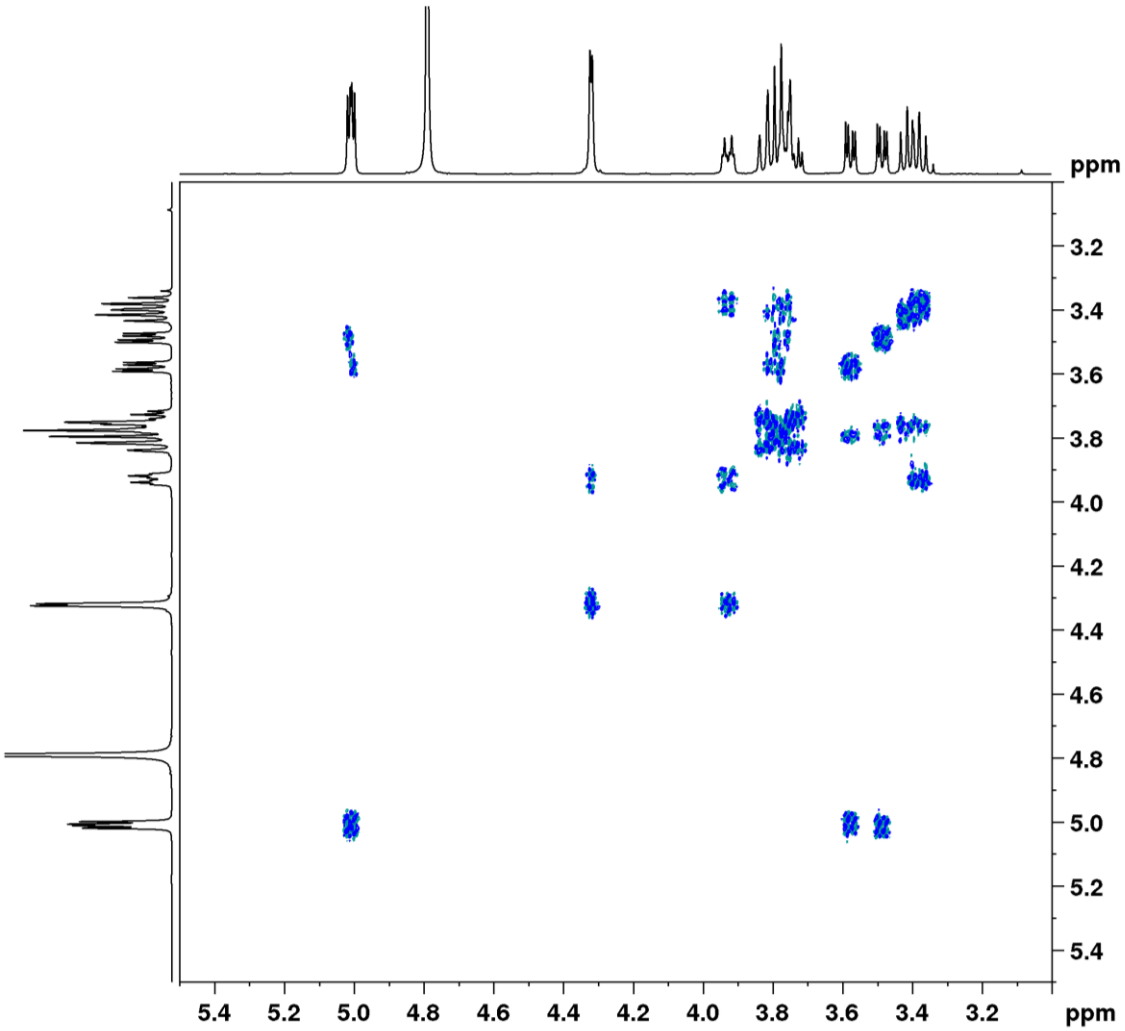

Figure 1-10. COSY NMR spectrum of O6-tosyl trehalose magnified for better visualization of sugar protons (CD_3OD).

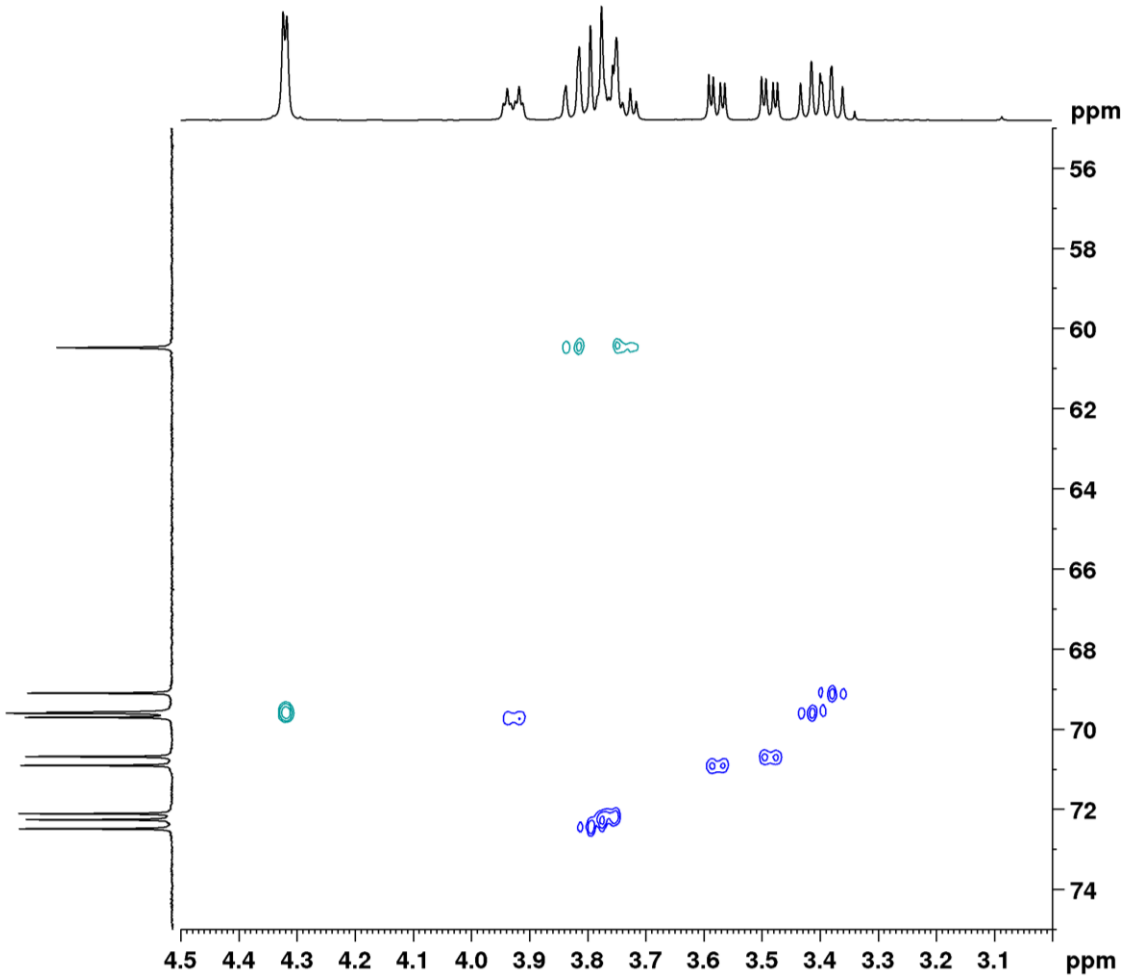

Figure 1-11. HSQC NMR spectrum O6-tosyl trehalose magnified for better visualization of sugar protons (CD_3OD).

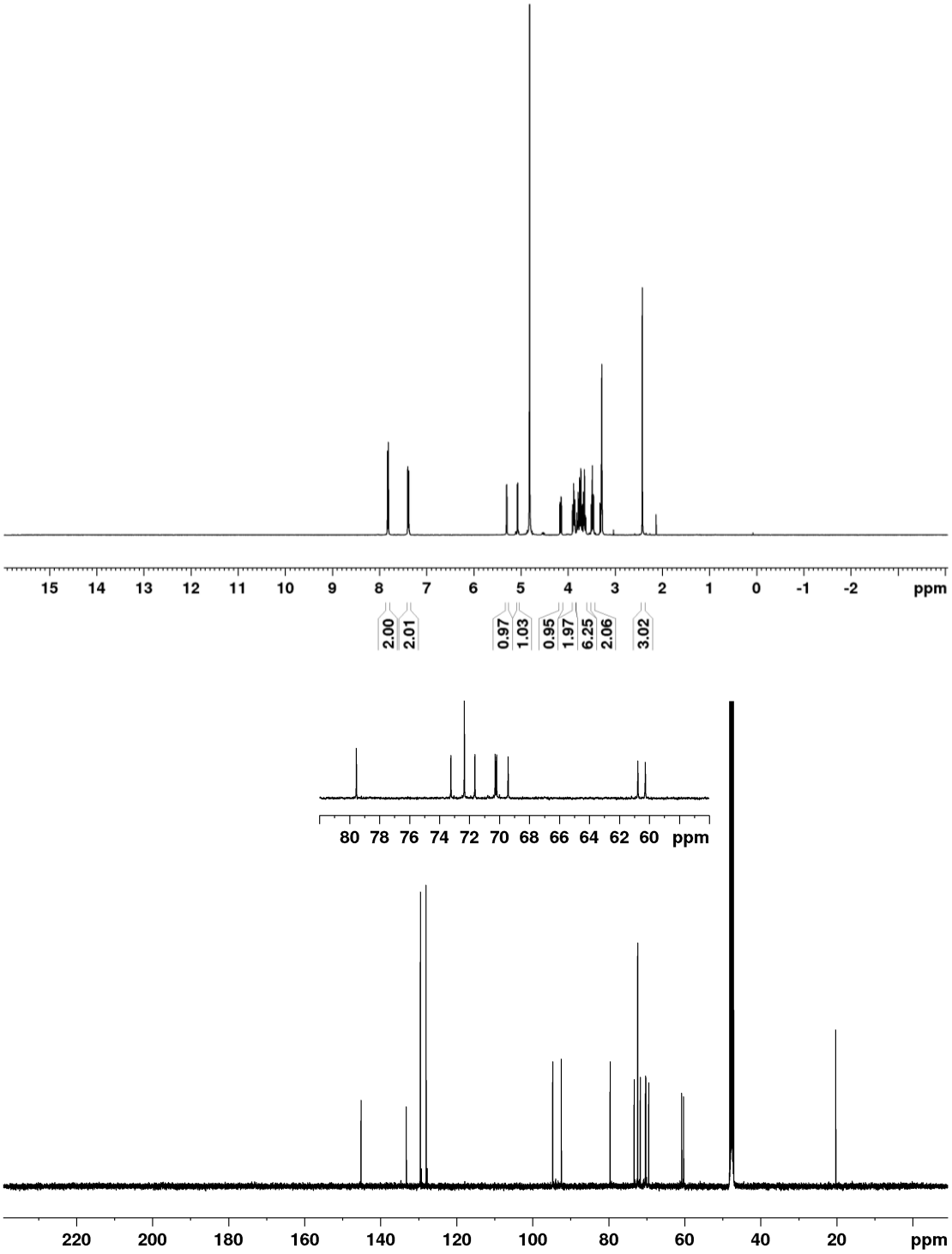

Figure 1-12. ^{1}H (top) and ^{13}C (bottom) NMR spectra of tosyl trehalose regioisomer (CD_3OD).

1.5 References

(1) Sakurai, M., Biological functions of trehalose as a substitute for water. In *Water and Biomolecules*, Springer: 2009; pp 219.

(2) Fedorov, M. V.; Goodman, J. M.; Nerukh, D.; Schumm, S. Self-assembly of trehalose molecules on a lysozyme surface: the broken glass hypothesis. *Phys. Chem. Chem. Phys.* **2011,** *13*, 2294.

(3) Jain, N. K.; Roy, I. Effect of trehalose on protein structure. *Protein Sci.* **2009,** *18*, 24.

(4) Timasheff, S. N. The control of protein stability and association by weak interactions with water: how do solvents affect these processes? *Annu. Rev. Biophys. Biomol. Struct.* **1993,** *22*, 67.

(5) Asakura, S.; Oosawa, F. On interaction between two bodies immersed in a solution of macromolecules. *The Journal of Chemical Physics* **1954,** *22*, 1255.

(6) Lekkerkerker, H. N.; Tuinier, R., *Colloids and the depletion interaction*. Springer: 2011; Vol. 833.

(7) Sola-Penna, M.; Meyer-Fernandes, J. R. Stabilization against thermal inactivation promoted by sugars on enzyme structure and function: why is trehalose more effective than other sugars? *Arch. Biochem. Biophys.* **1998,** *360*, 10.

(8) Kaushik, J. K.; Bhat, R. Why is trehalose an exceptional protein stabilizer? An analysis of the thermal stability of proteins in the presence of the compatible osmolyte trehalose. *J. Biol. Chem.* **2003,** *278*, 26458.

(9) Wada, M.; Miyazawa, Y.; Miura, Y. A specific inhibitory effect of multivalent trehalose toward Aβ (1-40) aggregation. *Polym. Chem.* **2011,** *2*, 1822.

(10) Rajaram, H.; Palanivelu, M. K.; Arumugam, T. V.; Rao, V. M.; Shaw, P. N.; McGeary, R. P.; Ross, B. P. 'Click'assembly of glycoclusters and discovery of a trehalose analogue that retards

Aβ40 aggregation and inhibits Aβ40-induced neurotoxicity. *Bioorg. Med. Chem. Lett.* **2014,** *24*, 4523.

(11) Sizovs, A.; Xue, L.; Tolstyka, Z. P.; Ingle, N. P.; Wu, Y.; Cortez, M.; Reineke, T. M. Poly (trehalose): sugar-coated nanocomplexes promote stabilization and effective polyplex-mediated siRNA delivery. *J. Am. Chem. Soc.* **2013,** *135*, 15417.

(12) Tolstyka, Z. P.; Phillips, H.; Cortez, M.; Wu, Y.; Ingle, N.; Bell, J. B.; Hackett, P. B.; Reineke, T. M. Trehalose-Based Block Copolycations Promote Polyplex Stabilization for Lyophilization and in Vivo pDNA Delivery. *ACS Biomater. Sci. Eng.* **2015,** *2*, 43.

(13) Mancini, R. J.; Lee, J.; Maynard, H. D. Trehalose Glycopolymers for Stabilization of Protein Conjugates to Environmental Stressors. *J. Am. Chem. Soc.* **2012,** *134*, 8474.

(14) Lee, J.; Lin, E.-W.; Lau, U. Y.; Hedrick, J. L.; Bat, E.; Maynard, H. D. Trehalose Glycopolymers as Excipients for Protein Stabilization. *Biomacromolecules* **2013,** *14*, 2561.

(15) Bat, E.; Lee, J.; Lau, U. Y.; Maynard, H. D. Trehalose glycopolymer resists allow direct writing of protein patterns by electron-beam lithography. *Nat. Commun.* **2015,** *6*, 6654.

(16) Lee, J.; Ko, J. H.; Lin, E.-W.; Wallace, P.; Ruch, F.; Maynard, H. D. Trehalose hydrogels for stabilization of enzymes to heat. *Polym. Chem.* **2015,** *6*, 3443.

(17) Liu, Y.; Lee, J.; Mansfield, K. M.; Ko, J. H.; Sallam, S.; Wesdemiotis, C.; Maynard, H. D. Trehalose Glycopolymer Enhances Both Solution Stability and Pharmacokinetics of a Therapeutic Protein. *Bioconj. Chem.* **2017,** *28*, 836.

(18) Messina, M. S.; Ko, J. H.; Yang, Z.; Strouse, M. J.; Houk, K. N.; Maynard, H. D. Effect of trehalose polymer regioisomers on protein stabilization. *Polym. Chem.* **2017,** *8*, 4781.

(19) Pelegri-O'Day, E. M.; Paluck, S. J.; Maynard, H. D. Substituted Polyesters by Thiol-Ene Modification: Rapid Diversification for Therapeutic Protein Stabilization. *J. Am. Chem. Soc.* **2017,** *139*, 1145.

(20) Lee, J.; Ko, J. H.; Mansfield, K. M.; Nauka, P. C.; Bat, E.; Maynard, H. D. Glucose-Responsive Trehalose Hydrogel for Insulin Stabilization and Delivery. *Macromol. Biosci.* **2018,** *18*, 1700372.

(21) O'Shea, T. M.; Webber, M. J.; Aimetti, A. A.; Langer, R. Covalent Incorporation of Trehalose within Hydrogels for Enhanced Long-Term Functional Stability and Controlled Release of Biomacromolecules. *Adv. Healthcare Mater.* **2015,** *4*, 1802.

(22) Kitagawa, M.; Chalermisrachai, P.; Fan, H.; Tokiwa, Y. In *Chemoenzymatic synthesis of biodegradable polymers containing glucobiose branches*, Macromol. Symp., 1999; Wiley Online Library: 1999; pp 247.

(23) Miura, Y.; Wada, N.; Nishida, Y.; Mori, H.; Kobayashi, K. Chemoenzymatic synthesis of glycoconjugate polymers starting from nonreducing disaccharides. *J. Polym. Sci., Part A: Polym. Chem.* **2004,** *42*, 4598.

(24) Lee, D.; Williamson, C. L.; Chan, L.; Taylor, M. S. Regioselective, borinic acid-catalyzed monoacylation, sulfonylation and alkylation of diols and carbohydrates: expansion of substrate scope and mechanistic studies. *J. Am. Chem. Soc.* **2012,** *134*, 8260.

(25) Dimitrijević, E.; Taylor, M. S. 9-Hetero-10-boraanthracene-derived borinic acid catalysts for regioselective activation of polyols. *Chem. Sci.* **2013,** *4*, 3298.

(26) D'Angelo, K. A.; Taylor, M. S. Borinic acid catalyzed stereo-and regioselective couplings of glycosyl methanesulfonates. *J. Am. Chem. Soc.* **2016,** *138*, 11058.

(27) Sawada, Y.; Nanboku, N.; Yanase, E.; Nakatsuka, S.-i. Selective protection of hydroxy group at C6 position of glucose derivatives. *Heterocycl. Commun.* **2010,** *16*, 21.

(28) Ren, B.; Ramström, O.; Zhang, Q.; Ge, J.; Dong, H. An iron (III) catalyst with unusually broad substrate scope in regioselective alkylation of diols and polyols. *Chemistry-A European Journal* **2016,** *22*, 2481.

(29) Martinelli, M. J.; Vaidyanathan, R.; Pawlak, J. M.; Nayyar, N. K.; Dhokte, U. P.; Doecke, C. W.; Zollars, L. M.; Moher, E. D.; Khau, V. V.; Košmrlj, B. Catalytic regioselective sulfonylation of α-chelatable alcohols: scope and mechanistic insight. *J. Am. Chem. Soc.* **2002,** *124*, 3578.

(30) Hermanek, S. Boron-11 NMR spectra of boranes, main-group heteroboranes, and substituted derivatives. Factors influencing chemical shifts of skeletal atoms. *Chem. Rev.* **1992,** *92*, 325.

(31) Kornblum, N.; Jones, W. J.; Anderson, G. J. A new and selective method of oxidation. The conversion of alkyl halides and alkyl tosylates to aldehydes. *J. Am. Chem. Soc.* **1959,** *81*, 4113.

(32) Letsinger, R. L.; Skoog, I. Organoboron Compounds. IV. 1 Aminoethyl Diarylborinates. *J. Am. Chem. Soc.* **1955,** *77*, 2491.

(33) Hosoya, T.; Uekusa, H.; Ohashi, Y.; Ohhara, T.; Kuroki, R. A new photoisomerization process of the 4-cyanobutyl group in a cobaloxime complex crystal observed by neutron diffraction. *Bull. Chem. Soc. Jpn.* **2006,** *79*, 692.

(34) D'Angelo, K. A.; Taylor, M. S. Borinic acid-catalyzed stereo-and site-selective synthesis of β-glycosylceramides. *Chem. Commun.* **2017,** *53*, 5978.

(35) Swarts, B. M.; Holsclaw, C. M.; Jewett, J. C.; Alber, M.; Fox, D. M.; Siegrist, M. S.; Leary, J. A.; Kalscheuer, R.; Bertozzi, C. R. Probing the mycobacterial trehalome with bioorthogonal chemistry. *J. Am. Chem. Soc.* **2012,** *134*, 16123.

(36) Srinivasachari, S.; Liu, Y.; Zhang, G.; Prevette, L.; Reineke, T. M. Trehalose click polymers inhibit nanoparticle aggregation and promote pDNA delivery in serum. *J. Am. Chem. Soc.* **2006,** *128*, 8176.

(37) Backus, K. M.; Boshoff, H. I.; Barry, C. S.; Boutureira, O.; Patel, M. K.; D'hooge, F.; Lee, S. S.; Via, L. E.; Tahlan, K.; Barry III, C. E. Uptake of unnatural trehalose analogs as a reporter for Mycobacterium tuberculosis. *Nat. Chem. Biol.* **2011,** *7*, 228.

Chapter 2.

Regioisomeric Effect of Trehalose Polymers on Protein Stabilization

This chapter contains portions of an edited version of the following published paper:
Messina, M. S.;† Ko, J. H.;† Yang, Z.; Strouse, M. J.; Houk, K. N.; Maynard, H. D. *Polym. Chem.* **2017**, *8*, 4781. († Equal contribution). – Reproduced by permission of The Royal Society of Chemistry.

2.1 Introduction

Proteins are widely used as therapeutics in the pharmaceutical industry, feed-stock additives in the agricultural industry, and biochemical reagents in the laboratory setting. However, many proteins are prone to inactivation when exposed to outside stressors such as heat,[1] pH changes,[2] agitation,[3] and desiccation,[4] and their instability during the production, storage, and transport increases their cost.[5] To prevent denaturation and thereby prolong protein activity, excipients such as sugars and polymers are often added to protein formulations.[6]

Trehalose is a non-reducing disaccharide formed by α,α-1,1-linked glucose units,[7] and is upregulated in lower-level organisms such as tardigrades during long periods of desiccation.[8, 9] This increase in trehalose concentration stabiliizes the organism by protecting the cell membrane and proteins.[10] The mechanism of trehalose protein stabilization is under debate and there exist several different hypotheses.[11-13] The three main hypotheses include water replacement,[13] mechanical entrapment (vitrification),[10] and water entrapment.[14] In the water replacement theory, trehalose forms direct hydrogen bonds with the protein, effectively replacing water molecules and acting as the protein hydration shell. The mechanical entrapment hypothesis suggests that trehalose forms a glassy matrix around the protein, thereby reducing the mobility of the protein and allowing it to retain its tertiary structure. The water entrapment theory states that trehalose molecules trap water molecules around the protein to form a water hydration layer between the protein and trehalose. While the exact mechanism, or the combination of multiple mechanisms, responsible for the stabilization of proteins by trehalose remains to be fully determined,[15] the stability that trehalose imparts on proteins remains clear. It is this feature that has enabled its use as an excipient in a range of protein therapeutic formulations such as Herceptin®, Avastin®, and Advate®.[16] Trehalose has also been effective as an excipient for the stabilization of reverse transcriptase,[17] as

an embedding medium for preserving protein structure during electron crystallography,[18] and as an additive to improve shelf-life of food/pharmaceutical/cosmetic products.[16]

Motivated by these features of trehalose, we developed polymeric materials based on trehalose that stabilize proteins ranging from enzymes,[19-21] growth factors,[22, 23] hormones,[24] and antibodies[22, 25] to various stressors including heat, lyophilization, agitation, and direct electron beam irradiation. Other groups have also used trehalose containing polymers in the prevention of amyloid beta (Aβ) aggregation[26] and small interfering RNA (siRNA) and plasmid DNA (pDNA) delivery.[27, 28] Previously, we have explored the effect of the polymer backbone identity on the overall stabilization properties of trehalose glycopolymers by comparing polystyrene and polymethacrylate backbones as excipients to stabilize horseradish peroxidase (HRP) to heat and β-galactosidase (β-Gal) to lyophilization.[20] Slight differences in stabilizing effect were observed for different polymer backbones at low equivalents of the polymer, but at higher equivalents all of the polymers stabilized the proteins, regardless of polymer backbone.

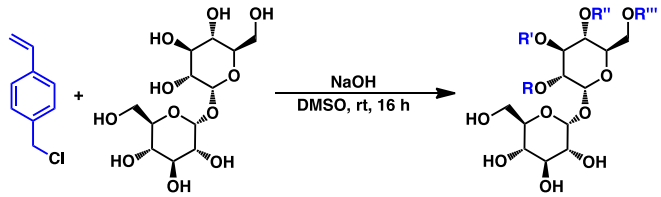

Figure 2-1. Synthesis of trehalose monomer regioisomers.

We were thus motivated to systematically investigate the effect of the point of linkage on trehalose while keeping the polymer backbone the same. To study possible differences between trehalose regioisomers on protein stabilization, we prepared styrenyl trehalose monomers with

trehalose modified at the 2-O, 3-O, 4-O, or 6-O positions (Figure 2-1). The resulting polymers, as well as a polymer containing all of the regioisomers, were then tested as excipients for the stabilization of the model protein insulin to mechanical agitation.

2.2 Results and Discussion

The styrenyl trehalose monomers were synthesized using a single-step Williamson etherification. While the synthetic route does not require protecting group strategies, it does result in four regioisomeric monomers **O2**, **O3**, **O4**, and **O6**. Fortunately, the isomers exhibited significantly different retention times on the HPLC (Table 2-1, top), which allowed us to separate the monomers.

The identity of each regioisomer was assigned after extensive characterization by NMR spectroscopy (COSY, HMBC, and HSQC) (Experimental Section Figure 2-3 through Figure 2-22). Although the regioisomers were expected to exhibit very similar characteristics, the coupling of the geminal benzyl protons in the ^{1}H NMR spectra varied significantly, with **O4** exhibiting strong coupling (10.8 Hz) indicative of nonequivalent geminal protons in significantly different environments and large $\Delta\delta$ (0.16 ppm; Figure 2-2B) and **O2** and **O6** exhibiting similarly strong coupling (Figure 2-2A and C), while **O3** did not show any benzyl proton coupling (Figure 2-8). This spectroscopic data gave us an indication that each monomer likely adopts a different conformation in solution. Direct NMR observation of through-space correlation in aqueous environment was not possible due to the broadening of the trehalose hydroxyl proton signals in water. Therefore, we computationally explored the differences in the aqueous conformation of the regioisomers.

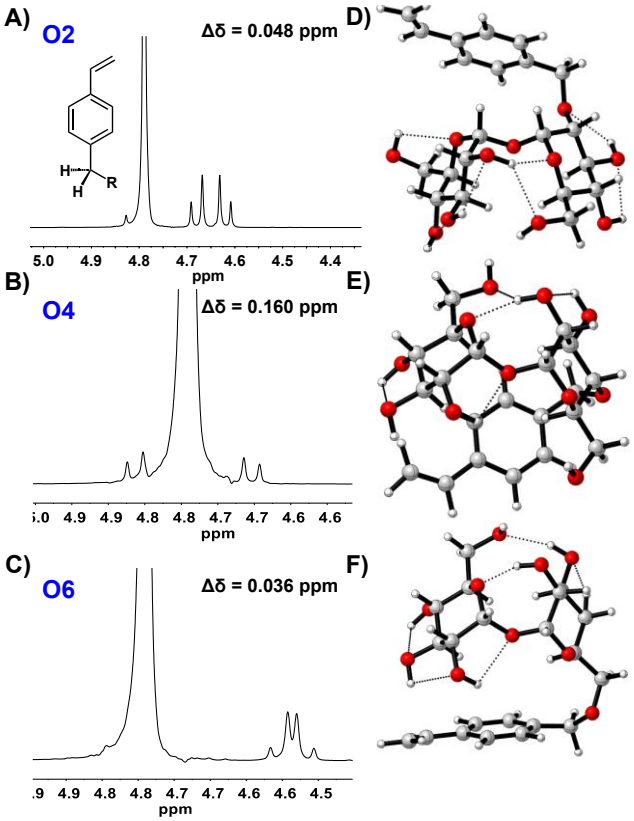

Figure 2-2. Benzyl region of ^{1}H NMR for monomers **O2**, **O4**, and **O6**, and their corresponding lowest energy conformations in aqueous solution.

Table 2-1. HPLC trace and yields for trehalose monomer regioisomers.

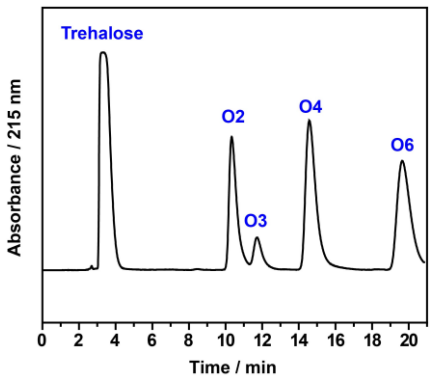

Monomer	Isolated Yield
O2	11%
O3	< 1%
O4	39%
O6	13%
OA	64%

Briefly, for each isomer a conformational search was conducted using Maestro 10.4 and select conformers were optimized by density functional theory (DFT) calculation at B3LYP-D3/6-

31G(d) level of theory in Gaussian 09.[29] As shown by the lowest energy conformers for each isomer (Figure 2-2D-F), all of the isomers retain the so-called clam shell conformation, in which the disaccharide is bent at the anomeric position, bringing the two glucose rings in close proximity that is characteristic for trehalose.[30, 31] All of the stable conformations (defined prior to the calculations as within 2 kcal/mol energy with respect to the most stable conformation) retain the clam shell conformation (Figure 2-23) as opposed to the higher energy more open conformation (Figure 2-24). However, **O6** has a single most stable conformation within 4 kcal/mol (i.e., 99.9 % of the population will be in this conformation at any given time according to Boltzmann distribution), and **O4** has two stable conformations within 2 kcal/mol that only differ by 0.1 kcal/mol in energy. **O2** has multiple stable conformations within 2 kcal/mol. These results suggest that **O6** and **O4** have a relatively rigid conformation while other regioisomers are more flexible and fluctuate among the multiple low energy conformations. This result is reasonable, since **O2** substitution would cause the most steric hindrance to the opposite ring due to the spatial proximity of the vinyl benzyl unit, while **O6** would cause the least hindrance. Furthermore, both of the lowest-energy conformations of **O4** show that one of the benzyl protons is proximal to the oxygen of the adjacent hydroxyl on C3 (2.41 and 1.92 Å for the two lowest energy conformers, (Figure 2-2E), which would explain the exceptionally large $\Delta\delta$ of **O4** benzyl protons in the ^{1}H NMR spectrum (Figure 2-2B).

The yields for all of the regioisomers are provided in Table 2-1; **OA** denotes the combined yield of all of the monomer regioisomers. Interestingly, **O4** was the most favored product. This observed regioselectivity was unexpected, as the primary hydroxyl (**O6**) would be anticipated as the major product in a simple S_N2 reaction such as Williamson etherification. Based on literature reports of metal-trehalose ionic complexation,[32, 33] we hypothesized that ionic complexation of

sodium with trehalose may be responsible for the reduced nucleophilicity of the primary hydroxyl. It has been reported that sugars complex with cations in the following order: $Ca^{2+} > Mg^{2+} > Na^{+} > K^{+}$,[32] and the crystal structure of Ca^{2+} with trehalose indicates that 2-O, 3-O, and 6-O chelate the cation.[33] One would therefore expect that the use of potassium hydroxide in place of sodium hydroxide would result in a relatively looser ion pairing at 6-O and increased modification at the primary hydroxyl due to its intrinsically higher nucleophilicity, if ionic complexation were responsible for the unusual selectivity. Indeed, the yield of **O6** relative to **O4** was increased when potassium hydroxide was used as the base or when less sodium hydroxide was used than in the reaction (Experimental Section Table 2-2). This was further supported by the increased relative yield of **O6** at higher temperature or in water, both of which would attenuate the effect of ionic complexation (Experimental Section Table 2-3). In water **O6** was the major product as expected. However, the absolute yield of the monomers in water was low even in the presence of a phase transfer catalyst, which was likely due to the hydrolysis of the vinylbenzyl chloride.

Modulation of sugar hydroxyl reactivity by intramolecular hydrogen bonds[34] and metal ions[35] has been previously observed. Benzoylation of methyl α-D-glucopyranoside in pyridine showed that hydroxyl reactivity followed the order 6-OH > 2-OH > 3-OH > 4-OH.[34] However, different reaction conditions changed the reactivity, sometimes even favoring the secondary alcohol 2-OH over the primary 6-OH when mannose was methylated in the presence of silver oxide.[34] Miller *et al.* leveraged the calcium complexation of fructose to selectively modify the 3'-OH secondary hydroxyl of the fructose unit in a glycosyl acceptor in the presence of four primary hydroxyls in the donor and the acceptor.[35] Our observation on the interesting chemical reactivity of trehalose adds to the body of work on regioselectivity of sugars.

With the monomer regioisomers assigned, we synthesized polymers from each regioisomer and tested their ability to prevent protein aggregation. Using insulin as a model protein, all polymers added at 10 weight equivalents similarly prevented aggregation of insulin that was agitated at 37 °C with 250 rpm shaking (97 – 100% intact insulin; refer to the publication for polymer synthesis and stabilization data[36]), and none of the polymers stabilized at lower amounts (1 weight equivalent). Since there were no statistical differences in stabilization between polymers at 10 wt. equiv., we conclude that the trehalose monomer regioisomers can be combined to achieve higher monomer yield, and all polymers can be utilized interchangeably, at least with the protein insulin.

The computational studies have shown that while there seem to be differences in conformational flexibility between the monomer regioisomers, all of the stable conformations still possess the clam shell conformation of trehalose (Experimental Section Table 2-2), and it is mostly the vinyl benzyl substituent that moves in the conformations for each isomer. Studies have pointed to the axial α,α-(1→ 1) linkage that results in the clam shell conformation as being important for the protective ability of trehalose.[30, 31] Indeed, we have observed that trehalose polymers have superior protein stabilizing ability over polymers from other sugars such as lactose that have more open conformations.[23] More thorough investigation is needed in the future to conclusively decouple the effects of conformational rigidity and the clam shell conformation on protein stabilization; in other words, more work will need to be done to determine if it is the clam shell conformation and the spatial arrangement of the hydroxyl groups itself or the molecular rigidity that results from the clam shell that is responsible for the stabilization. Nonetheless, we observe that the site of attachment of the trehalose to the polymer backbone does not have significant influence on the stabilizing ability. It should also be noted that the trehalose polymer stabilizes

better than trehalose, likely due to the cluster glycoside effect from increased local concentration[23, 37] and/or the nonionic surfactant character of the hydrophilic sugar side chain attached to the hydrophobic backbone.[20, 23] Together, our findings offer an interesting view on the synthesis of trehalose monomers and provide us with data suggesting that monomer regioisomers can be pooled to increase trehalose polymer yields without reducing protein stabilization ability.

2.3 Conclusions

In conclusion, we synthesized four trehalose regioisomers containing an ether-linked styrene moiety positioned at the 2-O, 3-O, 4-O, or 6-O position of trehalose. The substitution position of each monomer was rigorously identified via NMR spectroscopy. NMR data suggested that each regioisomer adopted a distinct conformation in solution and computational methods were employed to explore this. Calculations gave insight into the relative rigidity of the trehalose regioisomers in solution, with monomers **O6** and **O4** being the least flexible with only one or two stable conformations, and monomer **O2** showing multiple stable conformations suggesting that it is conformationally flexible. Despite the differences in conformational flexibility, all monomer regioisomers retained the native clam shell conformation of trehalose. We then probed the stabilization capability of each trehalose regioisomer in polymeric form. Polymers containing each monomer separately and one containing all monomer regioisomers together were synthesized via free radical polymerization. The stabilization capability of the polymers as excipients against mechanical agitation with moderate heating was then tested using insulin as a model protein. There was no substantial difference in the stabilization capability between each polymer; the different polymers prevented protein aggregation (> 97%) while there was no intact insulin with trehalose itself or free protein. We conclude that different regioisomers may be combined to achieve higher

yields of the polymer material while being able to effectively stabilize proteins, at least insulin, to mechanical stress.

2.4 Experimental Section

Materials

Trehalose was purchased from The Healthy Essential Management Corporation (Houston, TX), dried with ethanol, and stored under vacuum. Azobisisobutyronitrile (AIBN) (98%) was purchased from Sigma-Aldrich and recrystallized from acetone before using. 4-Vinylbenzyl chloride (90%) was purchased from Sigma-Aldrich. Insulin, human recombinant (Cat. No. 91077C; Lot No. 15L255-D) was purchased from Sigma Aldrich. Sodium hydroxide (≥ 97%, Pellets/Certified ACS), *N*,*N*-dimethylformamide (DMF) (≥ 99.8%, Certified ACS), dimethyl sulfoxide (DMSO) (≥ 99.9%, Certified ACS), Eppendorf LoBind® microcentrifuge tubes (0.5 mL and 1.5 mL), and pyridine (≥ 99%, Certified ACS) were purchased from Fisher Scientific. Pyridine was dried via distillation over calcium hydride and stored over 3Å molecular sieves. Spectra/Por® 3 dialysis membrane standard RC tubing (MWCO: 3.5 kDa) was used for dialysis of polymers. Deuterated solvents (Cambridge Isotope Laboratories) for NMR spectroscopic analyses were used as received.

Analytical Techniques

NMR spectra were recorded on Bruker AV 400, 500, or DRX 500 MHz spectrometers. Chemical shifts are reported in ppm relative to the residual signal of the solvent (D_2O: δ 4.79 ppm, $CDCl_3$: δ 7.26 ppm, or $(CD_3)_2SO$: δ 2.50 ppm). ^1H NMR spectra are reported as follows: chemical shift (δ ppm), multiplicity (t= triplet, d= doublet, dd= doublet of doublets, m= multiplet), coupling

constant (Hz), and integration. ^{1}H NMR spectra were acquired with a relaxation of 2 s for small molecules and 30 s for polymers with an acquisition time of 3.27 s and 30° pulse angle. Gel permeation chromatography (GPC) was conducted on a Shimadzu high performance liquid chromatography (HPLC) system with a refractive index RID-10A, one Polymer Laboratories PLgel guard column, and two Polymer Laboratories PLgel 5 μm mixed D columns. Eluent was DMF with LiBr (0.1 M) at 50 °C (flow rate: 0.80 mL/min). Calibration was performed using near-monodisperse pMMA standards from Polymer Laboratories. HPLC purification of trehalose monomers was performed on a Shimadzu HPLC system with a refractive index and UV detector SPD-10A monitoring at λ = 254 and 220 nm, and one Luna 5 μm C18(2) 100 Å LC column (250 x 21.2 mm) with 40% MeOH and 60% H_2O isocratic eluent mixture at a flow rate of 20 mL/min. The same HPLC system, equipped with an analytical Luna 5 μm C18(2) 100 Å column (250 × 4.6 mm), was utilized for detection of insulin with a gradient solvent system (water:acetonitrile = 30:70 to 40:60 + 0.1 % trifluoroacetic acid over 15 min at 1 mL/min). Thermogravimetric analysis (TGA) was performed on a Perkin Elmer Diamond TG/DTA instrument with a ramping rate of 10 °C per minute. Infrared (IR) spectra were obtained with a Perkin-Elmer Spectrum One instrument equipped with a universal attenuated total reflection (ATR) assembly; spectra are reported in wavenumbers ($\tilde{\nu}$). Mass spectra were acquired on a Waters Acquity Ultra Performance Liquid Chromatography (UPLC) connected to a Waters LCT-Premier XE Time of Flight Instrument controlled by MassLynx 4.1 software. The mass spectrometer was equipped with a Multi-Mode Source operated in the electrospray mode. Trehalose samples were separated using an Acquity BEH C18 1.7 μm column (2.1 × 50 mm) and were eluted with a gradient of 5–50% or 10-45% solvent B over 6 min (solvent A: water, solvent B: acetonitrile, both with 0.2% formic acid (vol/vol)). Mass spectra were recorded in the negative ion mode in the m/z range of 70–2000 with

leucine enkephalin (Sigma L9133) as the lock mass standard. Mass spectra were also collected on a Thermo Scientific Exactive Plus mass spectrometer with IonSense Direct Analysis in Real Time (DART-MS) ID-CUBE. Samples of insulin were stressed in a New Brunswick Scientific Excella E24 Incubator Shaker.

Synthesis of Monomers (O2 – O6)

6-O-(4-Vinylbenzyl ether)-α,α-trehalose (**O6**), *4-O-(4-vinylbenzyl ether)-α,α-trehalose* (**O4**), *3-O-(4-vinylbenzyl ether)-α,α-trehalose* (**O3**), *2-O-(4-vinylbenzyl ether)-α,α-trehalose* (**O2**): NaOH (4.44 g, 1.14×10^{-1} mol) was added to DMSO (100 mL) and stirred for 5 min. Trehalose (4.86 g, 1.42×10^{-2} mol) was then added to the reaction flask. Once trehalose dissolved, 4-vinylbenzyl chloride (0.4 mL, 2.55×10^{-3} mol) was added dropwise and reaction turned yellow. The reaction was stirred for 12 hours at 25 °C and was then precipitated in a mixture of cold hexanes (1.6 L) and dichloromethane (400 mL). Precipitate was collected via filtration and dried under reduced pressure to afford a yellow-white solid. The solid was dissolved in H_2O (50 mL) and neutralized with 12 N hydrochloric acid (HCl). Once neutralized, MeOH (50 mL) was added and the solution mixed. The solution was then filtered through a 0.45 µm cellulose acetate filter and purified via preparative HPLC (40% MeOH in H_2O). MeOH was removed under reduced pressure and water was removed via lyophilization to afford compounds **O2**, **O3**, **O4**, and **O6** in 11%, <1%, 39%, and 13% yield, respectively, as fluffy white powders. The combined yield for all the regioisomers was 64%.

O2: HPLC retention time (peak intensity): 10.3 minutes. ^{1}H NMR (500 MHz in D_2O, 298 K): δ = 7.47-7.45 (m, 2H), 7.35-7.33 (m, 2H), 6.77-6.71 (m, 1H), 5.84-5.80 (d, J = 17.69 Hz, 1H), 5.30-

5.28 (d, *J* = 11.42 Hz, 1H), 5.23-5.22 (d, *J* = 3.68 Hz, 1H), 5.14-5.13 (d, *J* = 4.05 Hz, 1H), 4.69-4.61 (m, 2H), 3.91-3.51 (m, 10H), 3.45-3.39 (m, 2H); ^{13}C NMR (125 MHz in D_2O, 298 K): δ = 137.5, 136.6, 136.2, 128.9, 126.4, 114.7, 93.5, 91.4, 78.7, 73.2, 72.4, 72.2, 72.0, 72.0, 71.0, 69.8, 69.2, 60.6, 60.1; IR $\tilde{\nu}$ (cm^{-1}): 3294 (br), 2923, 1635, 1362, 1043, 988, 827, 803; LC-MS (± 1.0) observed (predicted): $[M+HCOO]^-$ 503.1762 (503.1765).

O3: HPLC retention time (peak intensity): 11.7 minutes. ^{1}H NMR (500 MHz in D_2O, 298 K): δ = 7.53-7.45 (q, 4H), 6.83-6.78 (dd, 1H), 5.88-5.85 (d, *J* = 17.86 Hz, 1H), 5.33-5.31 (d, *J* = 11.02 Hz, 1H), 5.20-5.19 (m, 2H), 4.86 (s, 2H), 3.91-3.82 (m, 6H), 3.78-3.73 (m, 3H), 3.67-3.64 (m, 1H), 3.57-3.53 (t, *J* = 9.63 Hz, 1H), 3.47- 3.43 (t, *J* = 9.63 Hz, 1H); ^{13}C NMR (125 MHz in D_2O, 298 K): δ = 137.3, 136.2, 128.9, 126.2, 114.4, 93.2, 93.0, 81.3, 74.8, 72.4, 72.2, 72.1, 70.9, 70.8, 69.6, 69.3, 60.4, 60.3. IR $\tilde{\nu}$ (cm^{-1}): 3301 (br), 2932, 1628, 1512, 1406, 1358, 1285, 1259, 1216, 1146, 1105, 1080, 1027, 986, 943, 910, 827, 802; DART-MS observed (predicted): $[M-H]^-$ 457.17040 (457.17044).

O4: HPLC retention time (peak intensity): 14.6 minutes. ^{1}H NMR (500 MHz in D_2O, 298 K): δ = 7.53-7.41 (q, 4H), 6.83-6.78 (dd, 1H), 5.89-5.85 (d, *J* = 17.73 Hz, 1H), 5.34-5.32 (d, *J* = 10.97 Hz, 1H), 5.19-5.16 (m, 2H), 4.89-4.84 (d, *J* = 10.81 Hz), 4.71-4.69 (d, *J* = 10.81 Hz, 1H), 3.99-3.95 (t, *J* = 9.62, 1H), 3.86-3.79 (m, 5H), 3.76-3.72 (m, 2H), 3.68-3.66 (m, 1H), 3.63-3.59 (m, 1H), 3.54-3.50 (t, *J* = 9.46 Hz, 1H), 3.45-3.41 (t, *J* = 9.62 Hz, 1H); ^{13}C NMR (125 MHz in D_2O, 298 K): δ = 137.5, 136.6, 136.2, 129.2, 126.3, 114.6, 93.2, 93.0, 77.7, 74.6, 72.6, 72.4, 72.0, 71.1, 71.1, 70.9, 69.6, 60.4, 60.2; IR $\tilde{\nu}$ (cm^{-1}): 3234 (br), 2930, 1629, 1360, 1107, 1043, 992, 913, 827, 805; LC-MS (± 1.0) observed (predicted): $[M+HCOO]^-$ 503.1720 (503.1765).

O6: HPLC retention time (peak intensity): 19.7 minutes. ^{1}H NMR (500 MHz in D_2O, 298 K): δ = 7.52-7.38 (q, 4H), 6.82-6.76 (dd, 1H), 5.87-5.84 (d, J = 17.51 Hz, 1H), 5.32-5.30 (d, J = 11.03 Hz, 1H), 5.17-5.15 (m, 2H), 4.62-4.56 (q, 2H), 3.97-3.94 (m, 1H), 3.85-3.79 (m, 5H), 3.76-3.70 (m, 2H), 3.64-3.60 (m, 2H), 3.47-3.41 (q, 2H); ^{13}C NMR (125 MHz in D_2O, 298 K): δ = 137.3, 136.8, 136.2, 128.7, 126.3, 114.5, 93.3, 93.2, 72.6, 72.5, 72.4, 72.1, 70.9, 78.8, 70.7, 69.9, 69.6, 68.6, 60.5; IR $\tilde{\nu}$ (cm^{-1}): 3328 (br), 2928, 1630, 1512, 1407, 1365, 1212, 1147, 1105, 1076, 1032, 987, 942, 909, 826, 805, 718; LC-MS (± 1.0) observed (predicted): $[M+HCOO]^-$ 503.1765 (503.1765).

Synthesis of O2, O3, O4, and O6 Using Different Bases – Representative Example

The reaction was conducted as in the experimental section of the manuscript, with different molar equivalents of base (entry 1 corresponds to the original condition). A representative reaction condition (entry 2) is detailed as follows: Potassium hydroxide (573 mg, 1.02×10^{-2} mol) was suspended in dry dimethyl sulfoxide (9.5 mL) and stirred at room temperature. Trehalose (437 mg, 1.28×10^{-3} mol) was then added and stirred until it dissolved. 4-Vinylbenzyl chloride (40 μL, 2.55×10^{-4} mol) was added dropwise. The reaction was stirred for 12 hours at 25 ˚C and was then precipitated into a mixture of cold hexanes (160 mL) and dichloromethane (40 mL). The precipitate was collected via filtration and dried under reduced pressure, and the resulting solid was analyzed by HPLC (40% MeOH in H_2O).

Table 2-2. Modulation of regioselectivity in monomer synthesis using different hydroxyl bases.

Entry	**Base**		**Regioisomer ratio**
	Base used	**Mol. eq. relative to trehalose**	**O2 : O3 : O4 : O6[a]**
1	NaOH	8	1 : 0.21 : 3.38 : 1.42
2	KOH	8	1 : 0.24 : 1.49 : 1.44
3	NaOH	1	1 : 0.36 : 1.45 : 1.34
4	KOH	1	1 : 0.35 : 1.02 : 1.36

[a] Ratio calculated from HPLC chromatogram AUC.

Synthesis of O2, O3, O4, and O6 in Water or at a Higher Temperature

The reaction was conducted as in the experimental section of the manuscript, except at a different temperature (50 °C) or in water. Briefly, 8 equivalents of NaOH and 1 equivalent of trehalose were dissolved in DMSO (to make 0.15 M trehalose), and 0.2 equivalent of 4-vinylbenzyl chloride was added dropwise and the reaction was allowed to stir for 15 to 21 hours at respective temperature. The reaction was neutralized with dilute hydrochloric acid, and analyzed by LC-MS. The reactions in water was conducted both with (entry 3) and without (entry 2) the phase transfer catalyst (tetrabutylammonium hydrogensulfate) at 0.2 molar equivalents with respect to the added trehalose.

Table 2-3. The effect of solvent and temperature on regioselectivity.

Entry	**Solvent**	**Temperature**	**Additive**	**Regioisomer ratio O2 + O3[a] : O4 : O6[b]**
1	DMSO	50 °C	None	1 : 2.27 : 2.12
2	Water	23 °C	None	1 : 3.78 : 4.61
3	Water	23 °C	Tetrabutylammonium hydrogensulfate	1 : 2.01 : 3.34

[a] Due to the low overall yield and weak signal, O2 and O3 peaks were overlapping.
[b] Ratio calculated from UPLC-MS chromatogram.

Monomer Characterization

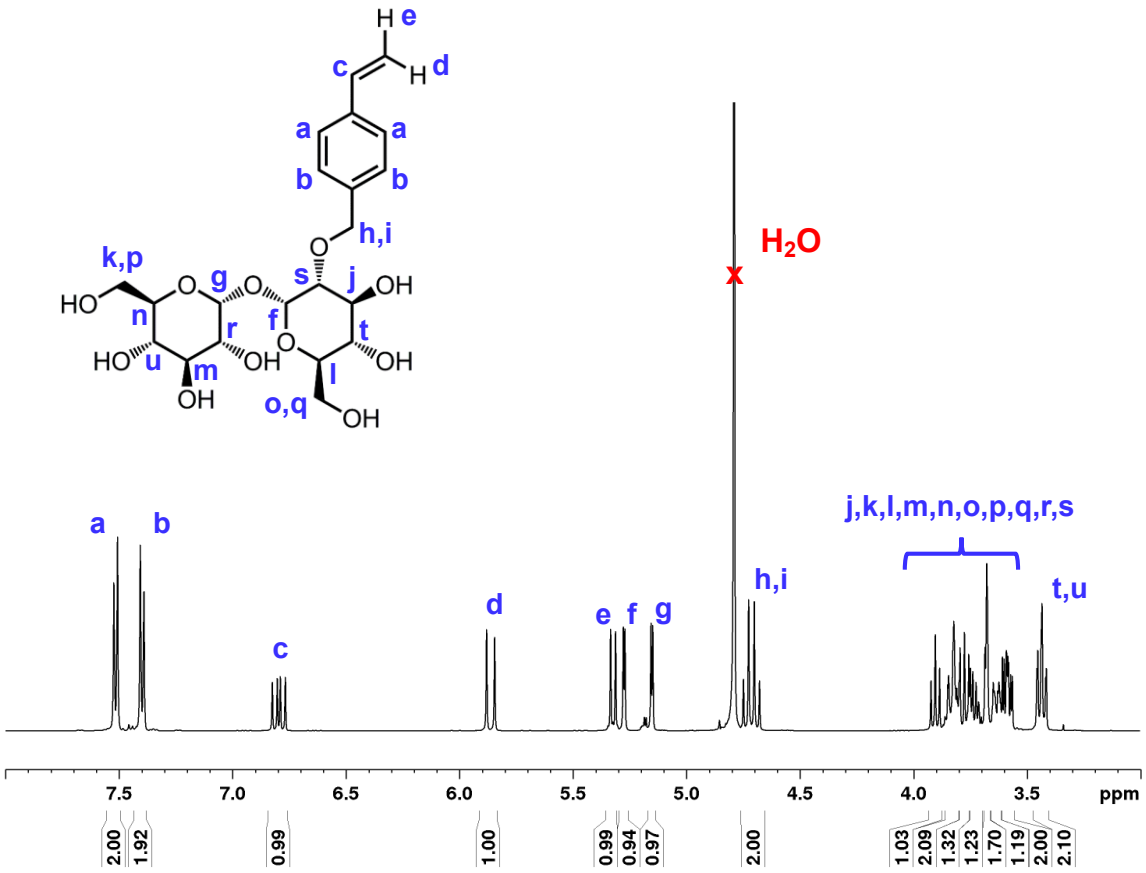

Figure 2-3. ^{1}H NMR spectrum of **O2** (D_2O).

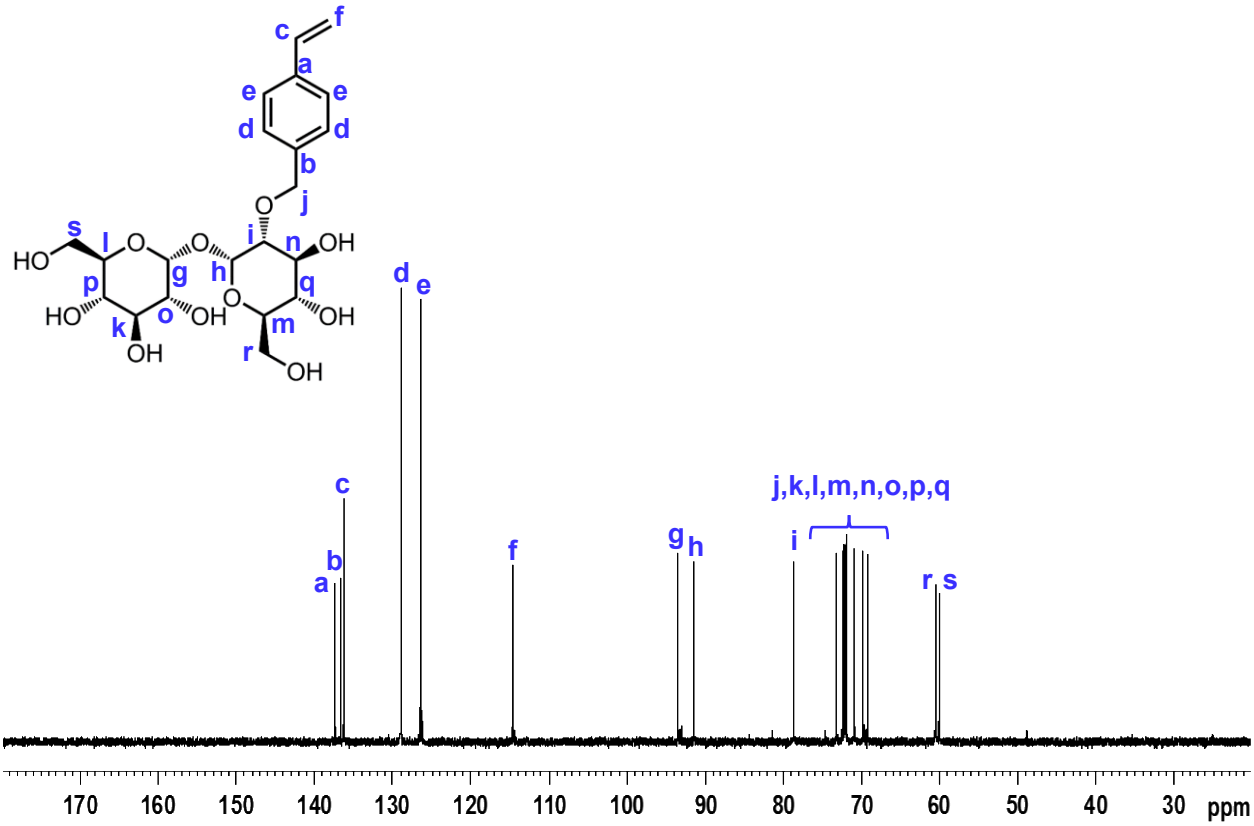

Figure 2-4. ^{13}C NMR spectrum of **O2** (D_2O).

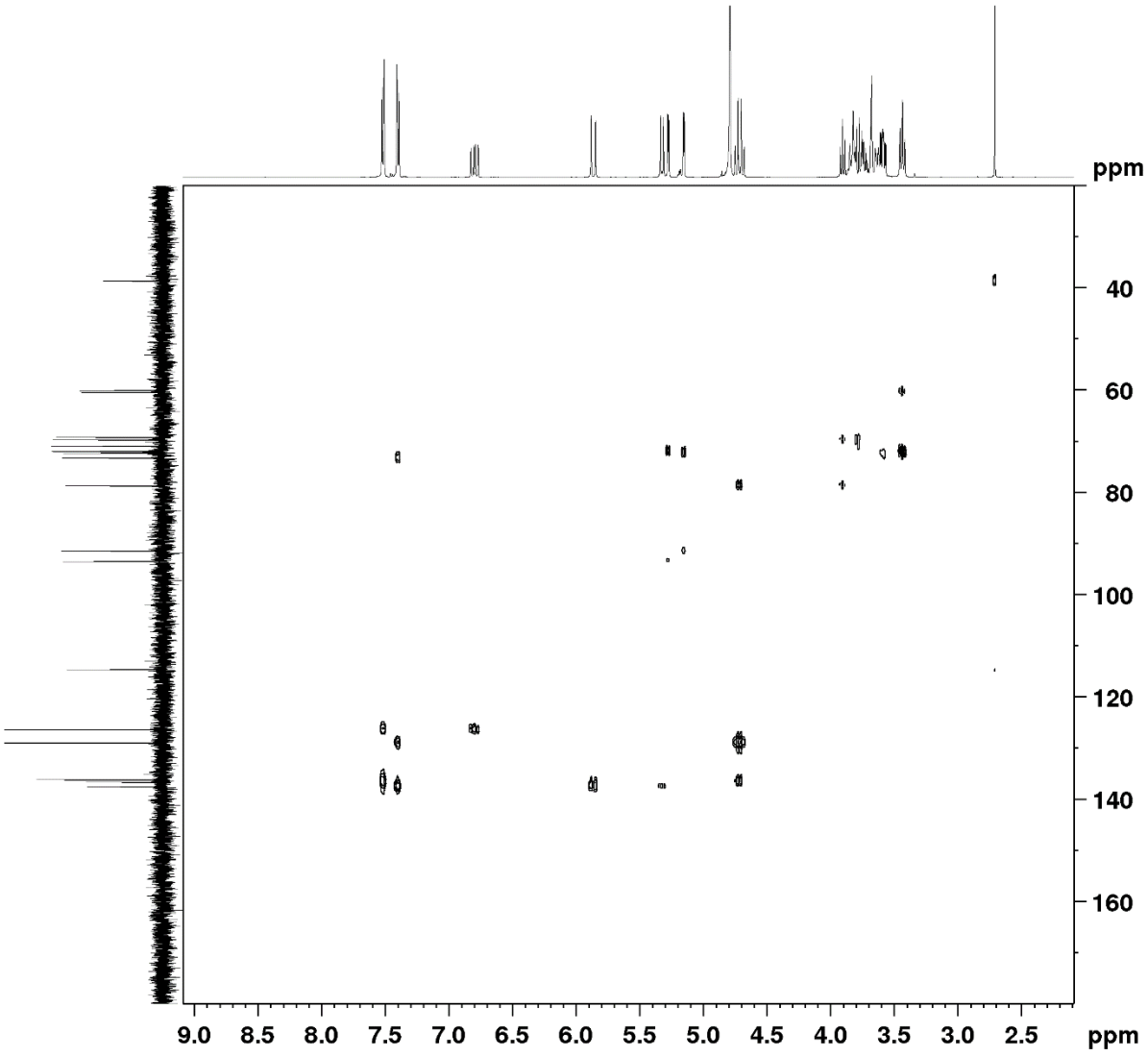

Figure 2-5. HMBC spectrum of **O2** (D_2O).

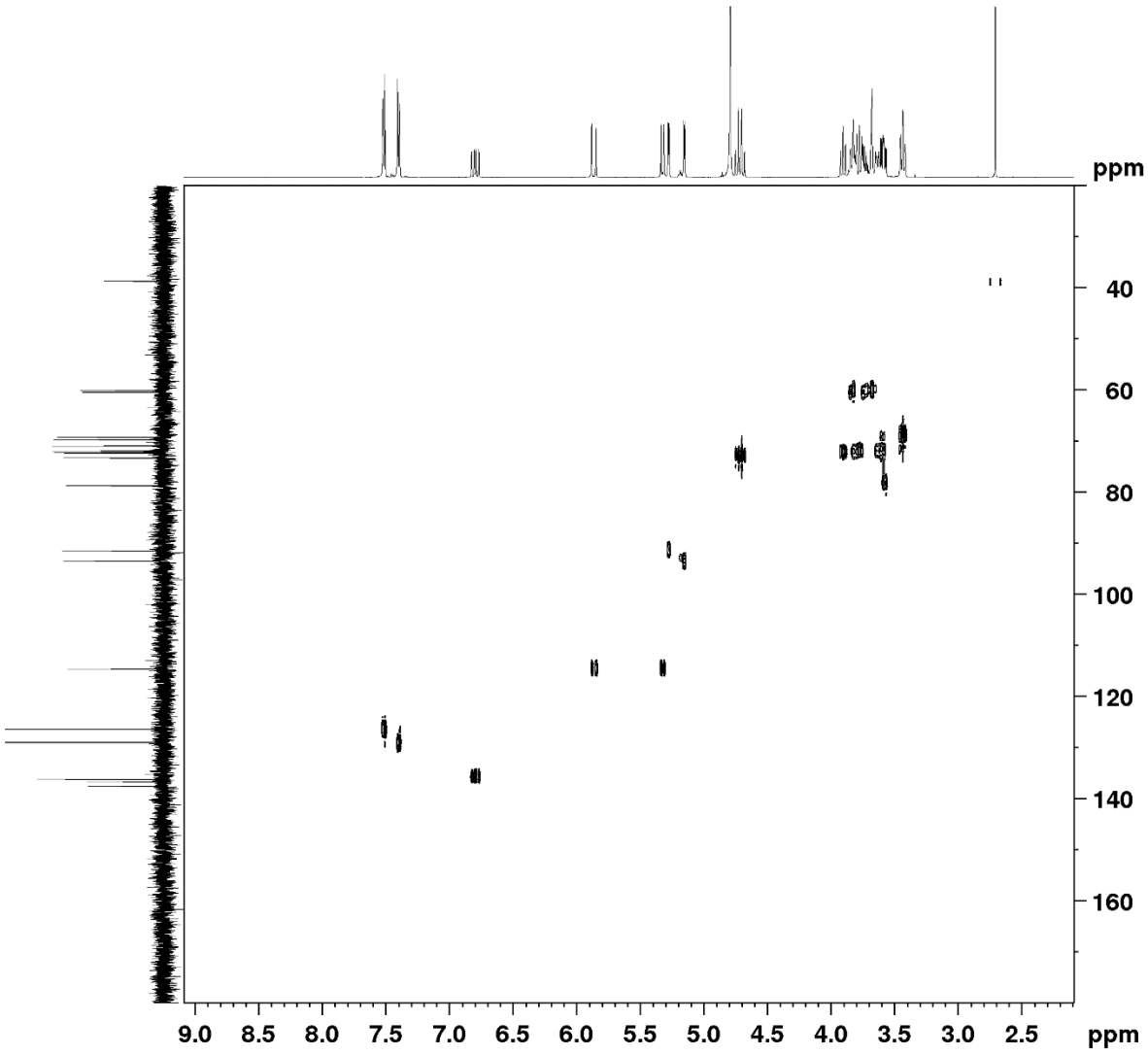

Figure 2-6. HSQC spectrum of **O2** (D_2O).

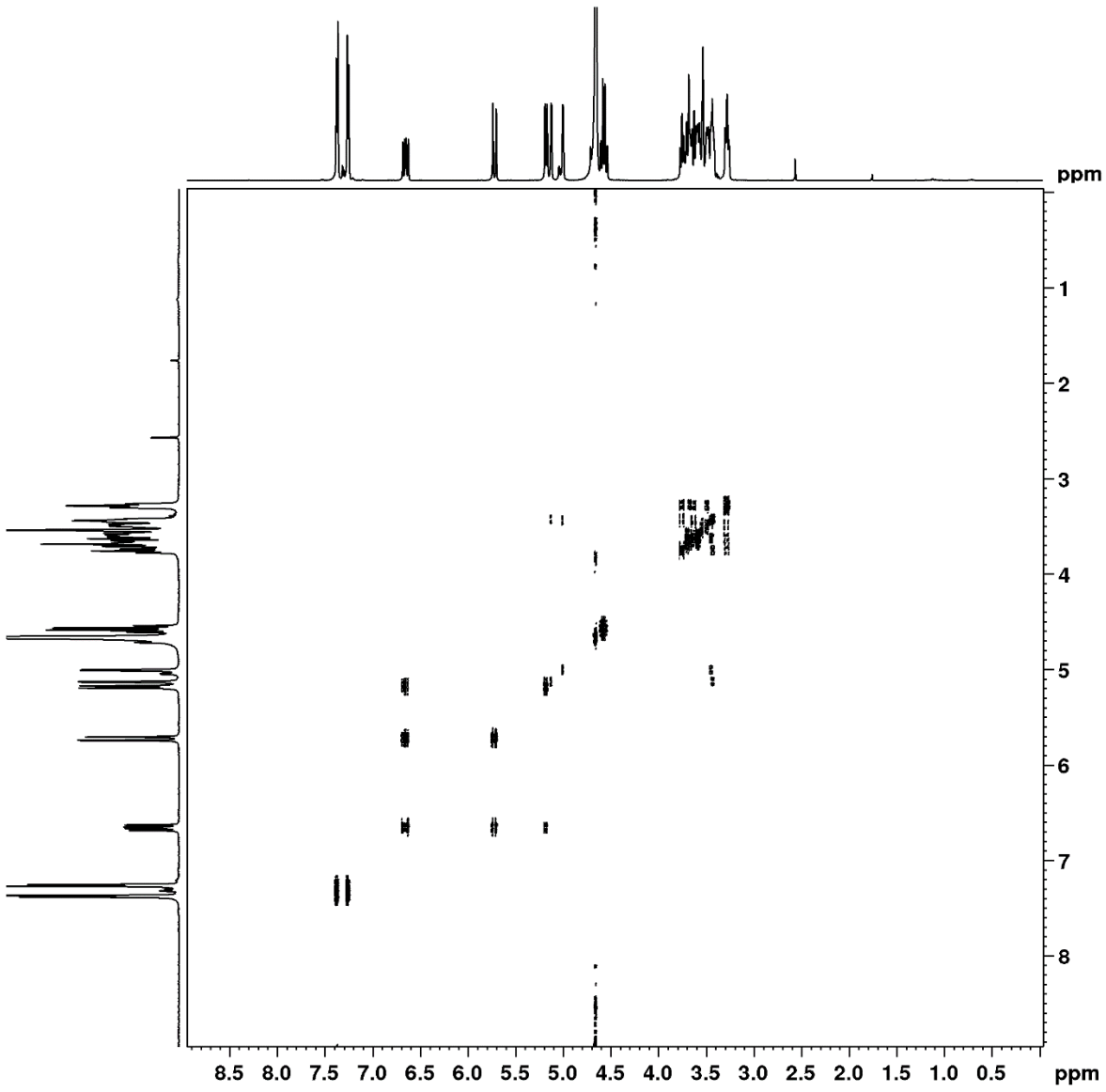

Figure 2-7. COSY spectrum of **O2** (D_2O).

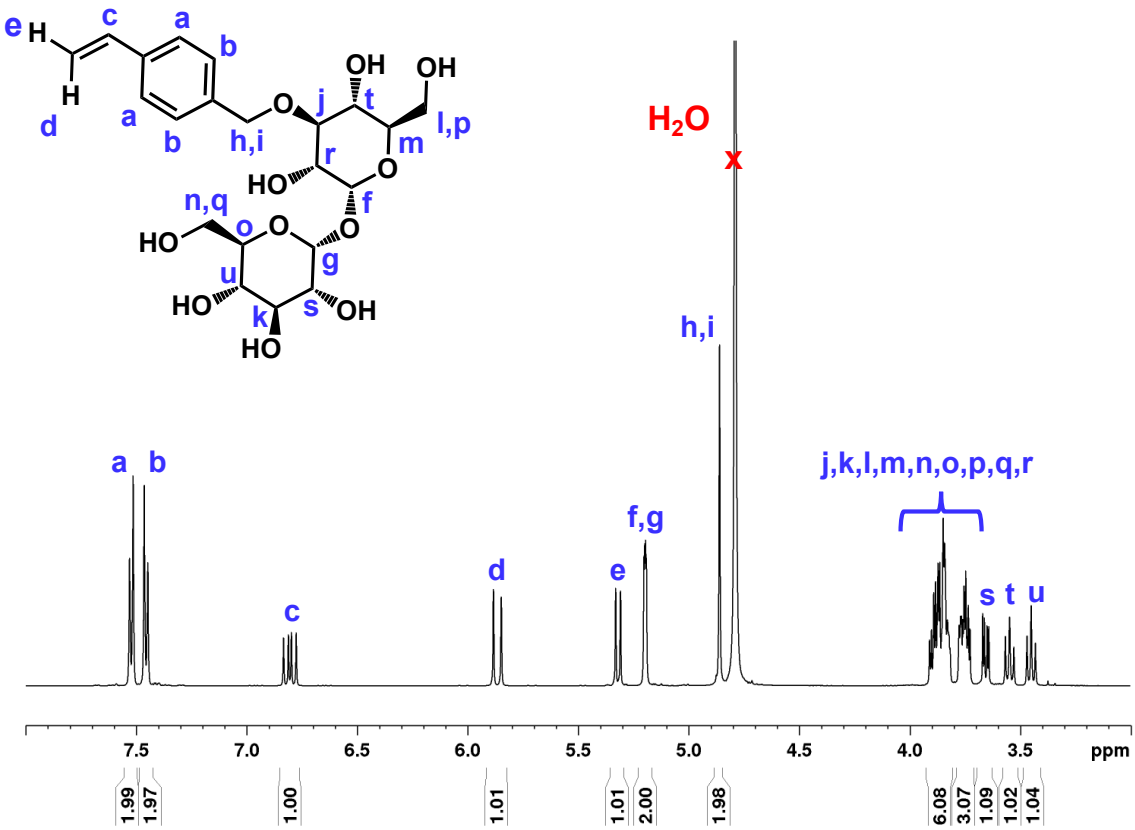

Figure 2-8. ^{1}H NMR spectrum of **O3** (D_2O).

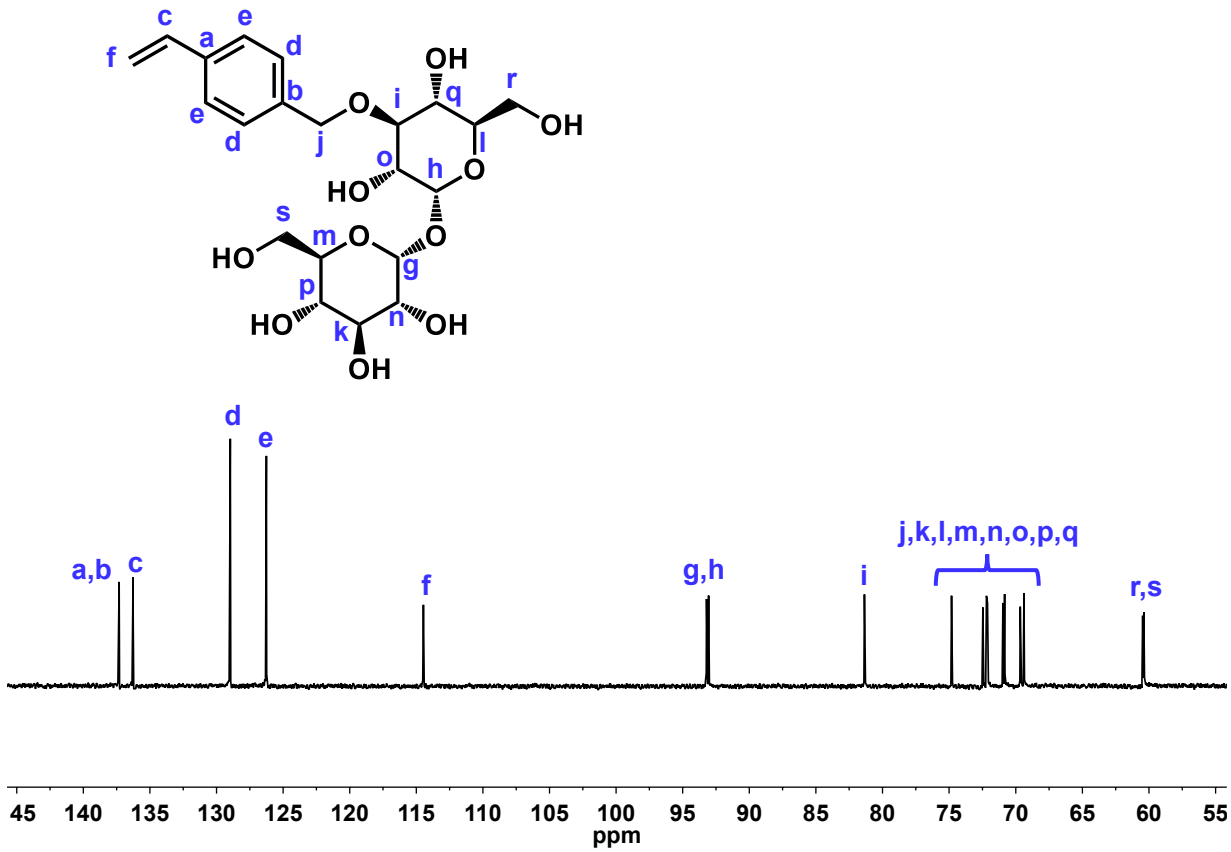

Figure 2-9. ^{13}C NMR spectrum of **O3** (D_2O).

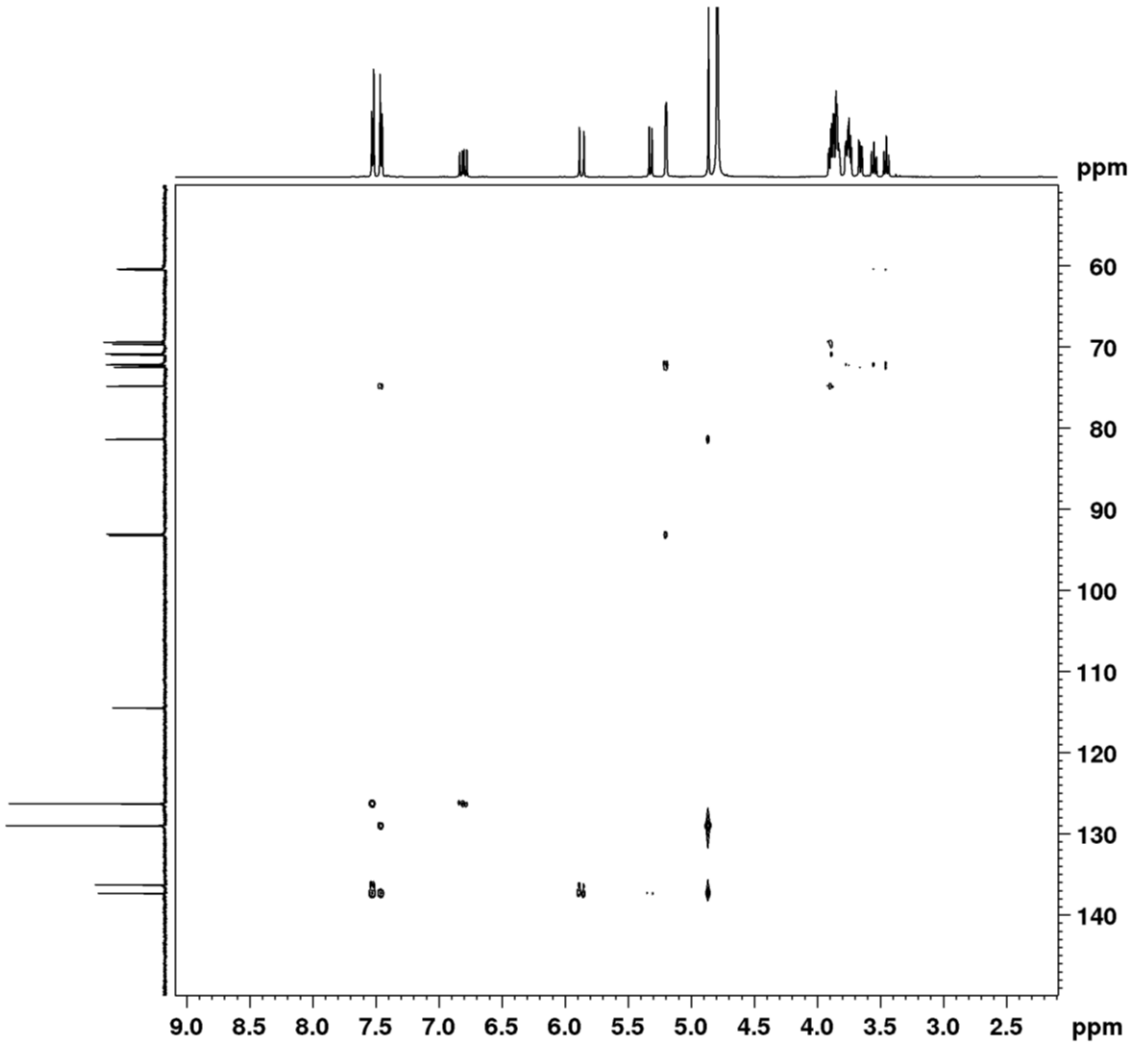

Figure 2-10. HMBC spectrum of **O3** (D_2O).

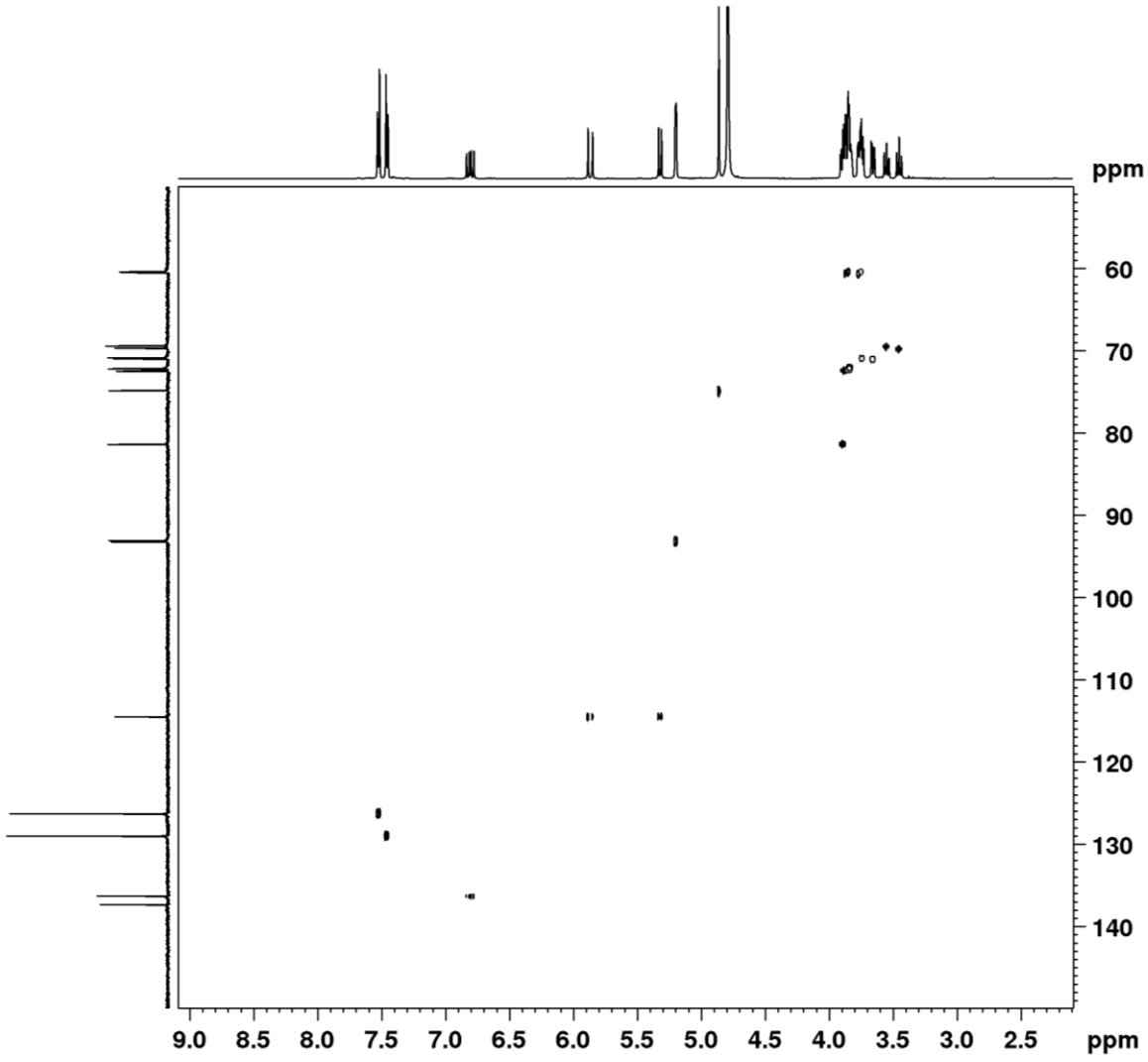

Figure 2-11. HSQC spectrum of **O3** (D_2O).

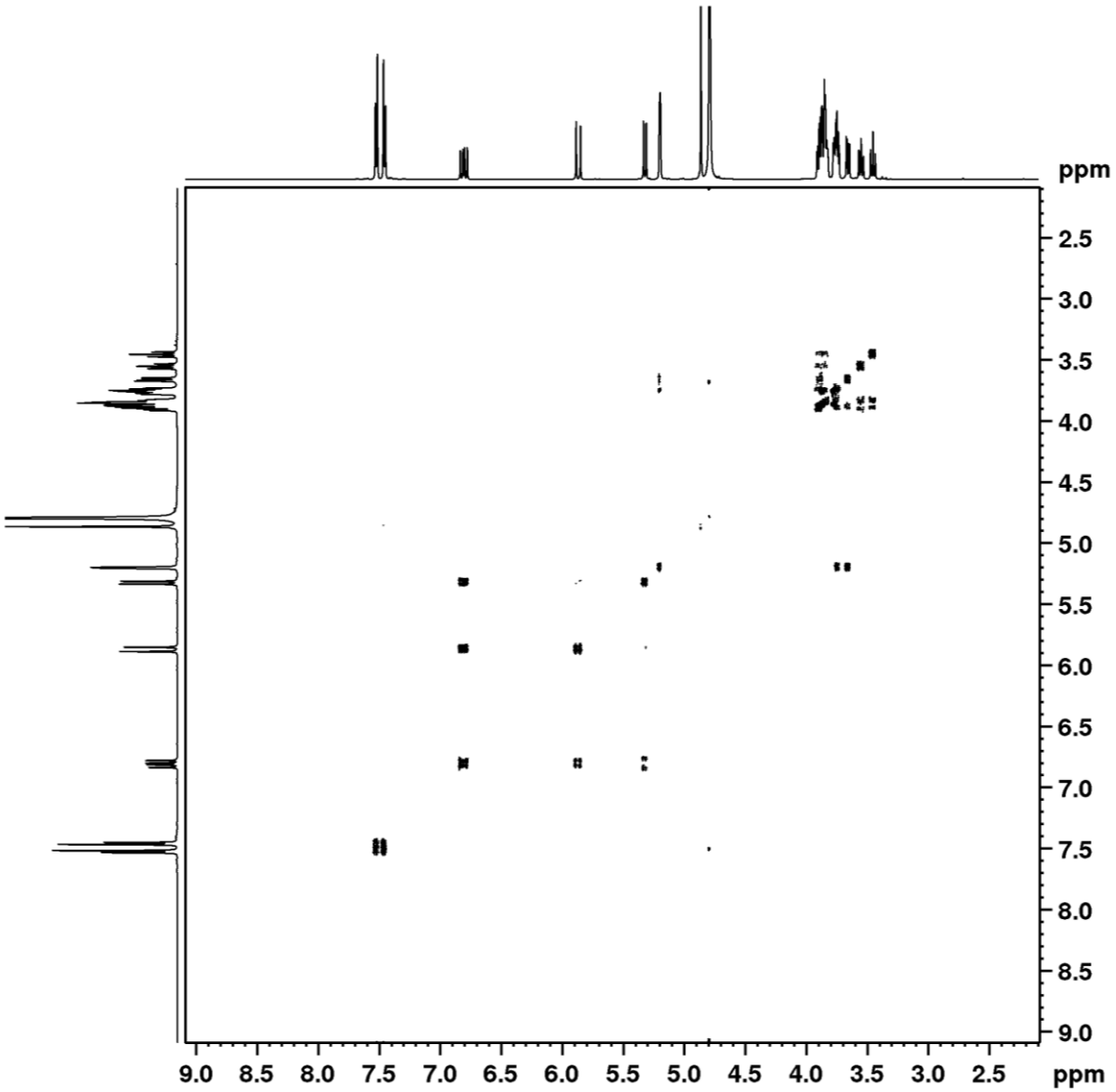

Figure 2-12. COSY spectrum of **O3** (D_2O).

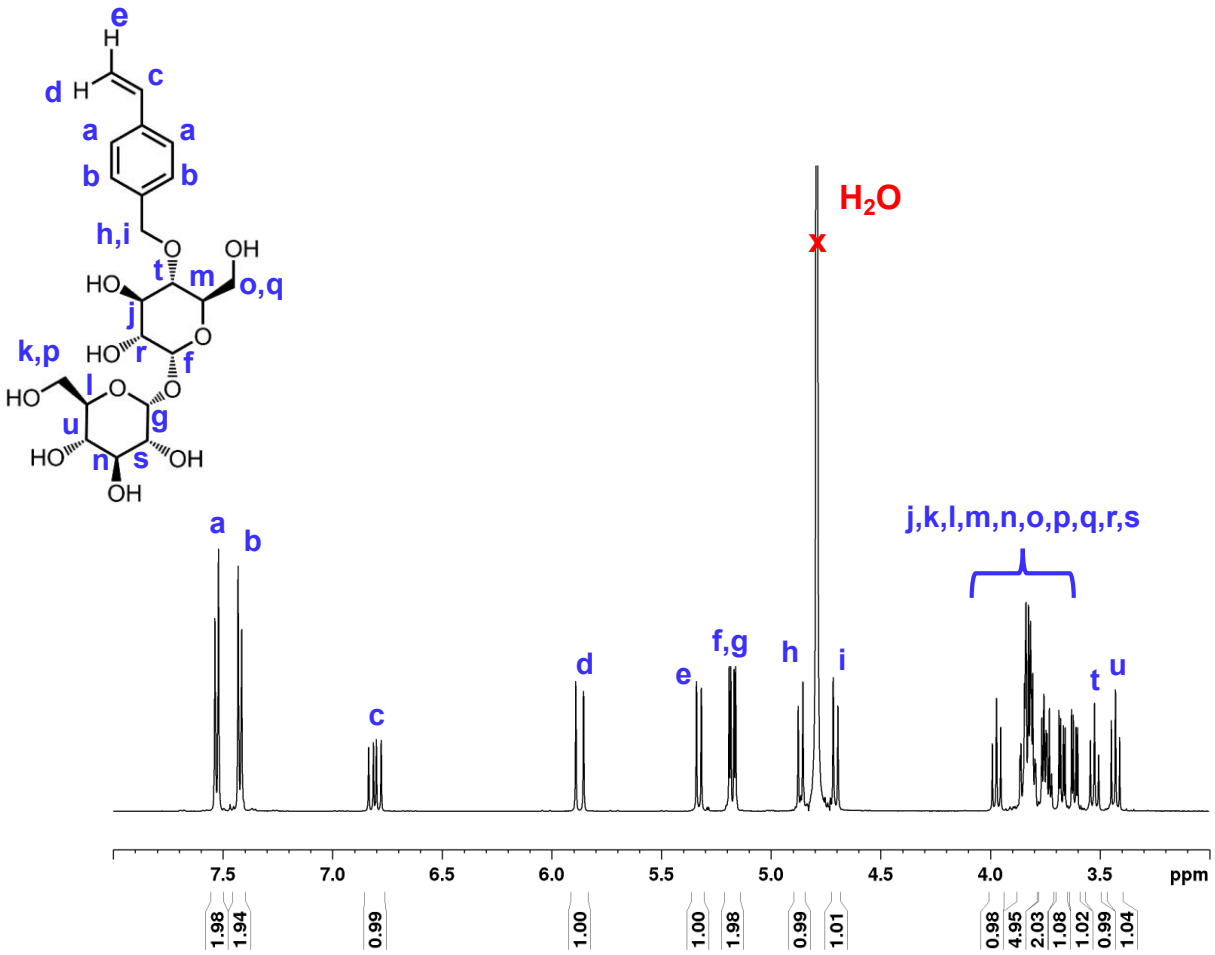

Figure 2-13. ^{1}H NMR spectrum of **O4** (D_2O).

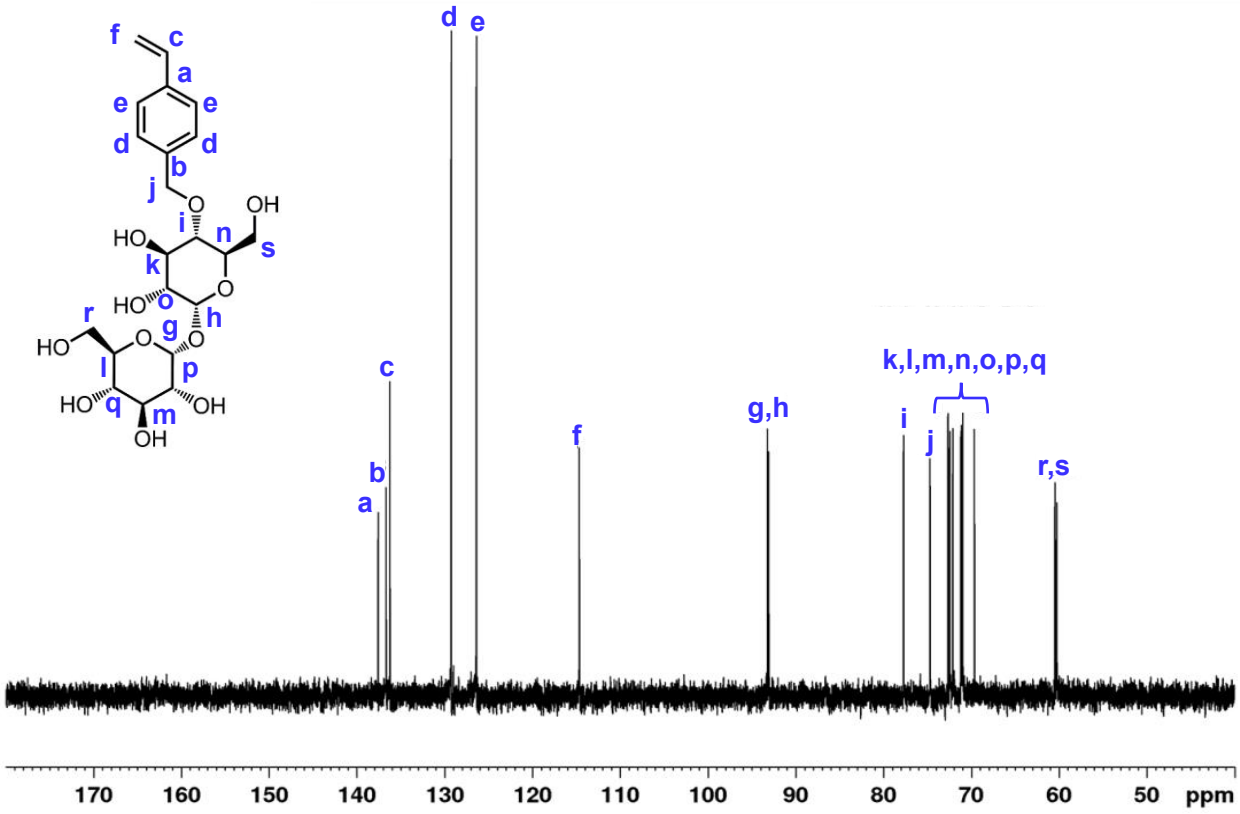

Figure 2-14. ^{13}C NMR spectrum of **O4** (D_2O).

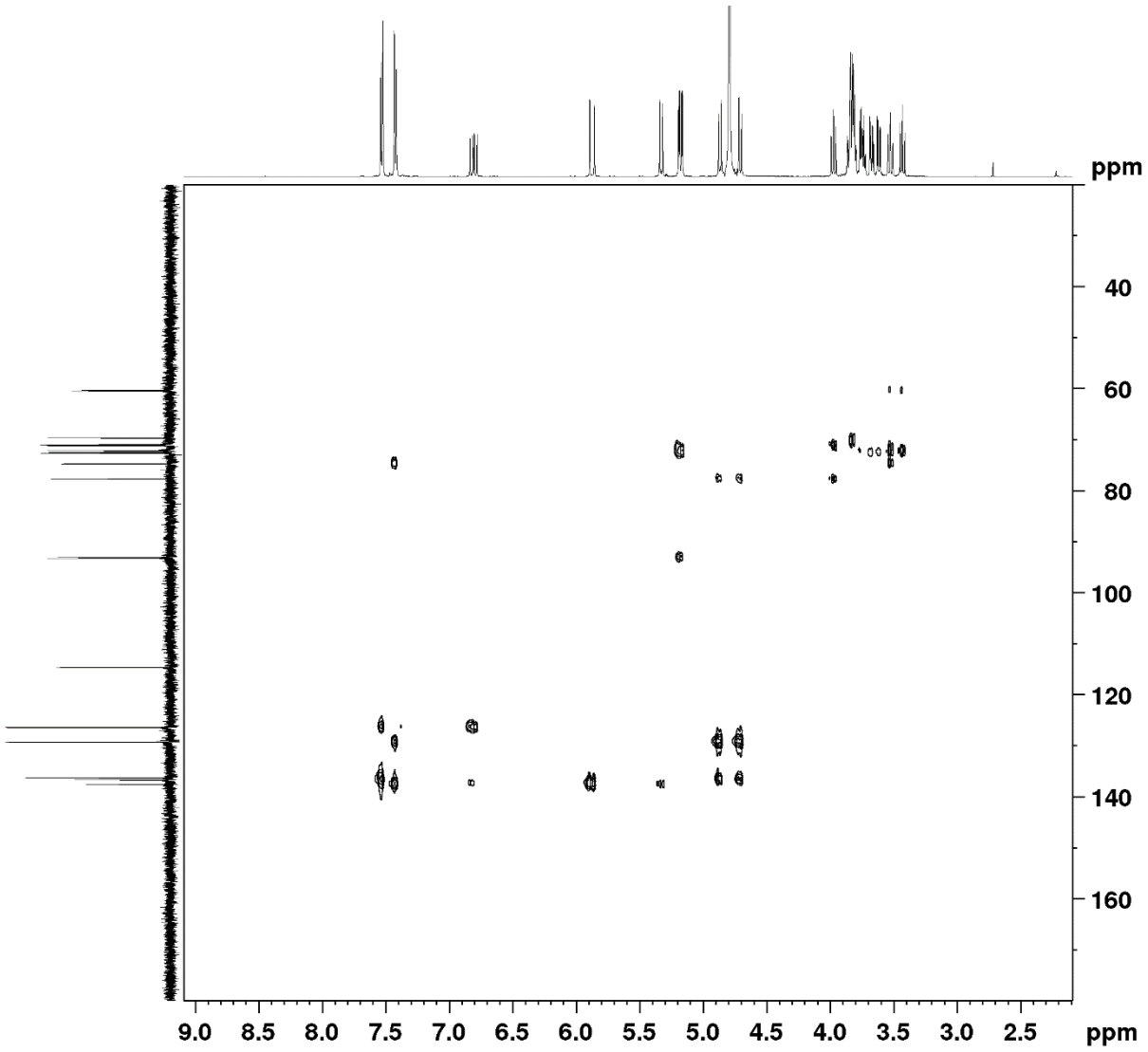

Figure 2-15. HMBC spectrum of **O4** (D_2O).

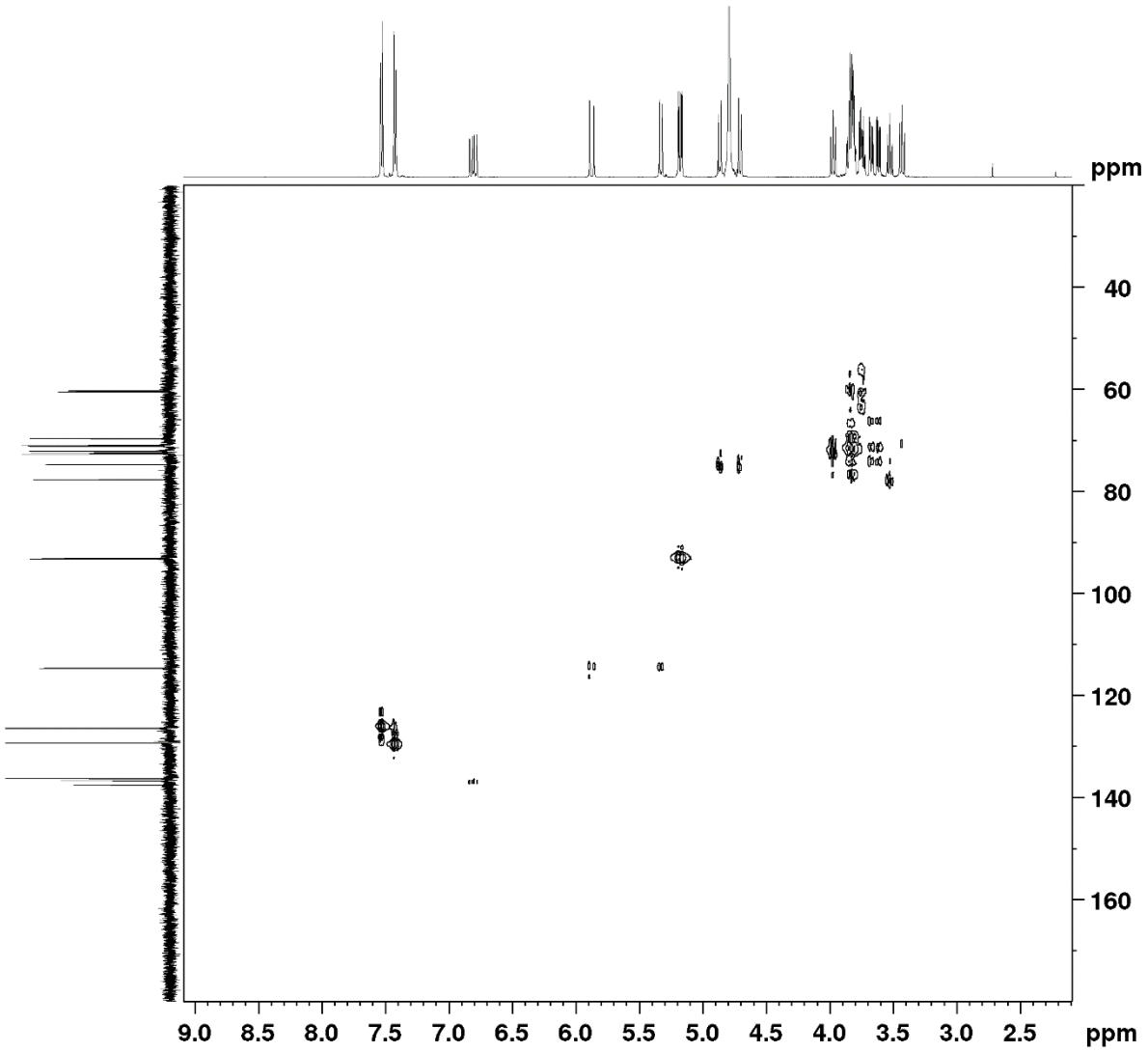

Figure 2-16. HSQC spectrum of **O4** (D_2O).

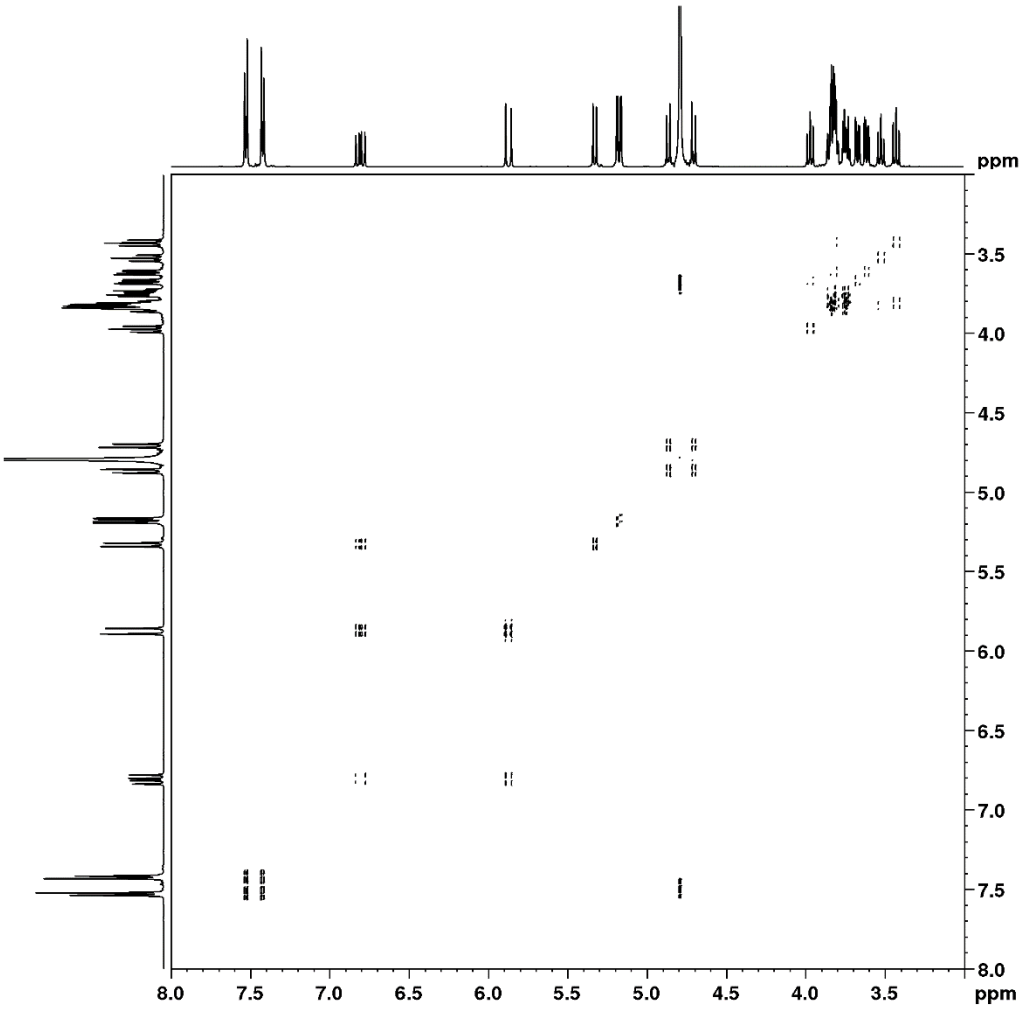

Figure 2-17. COSY spectrum of **O4** (D_2O).

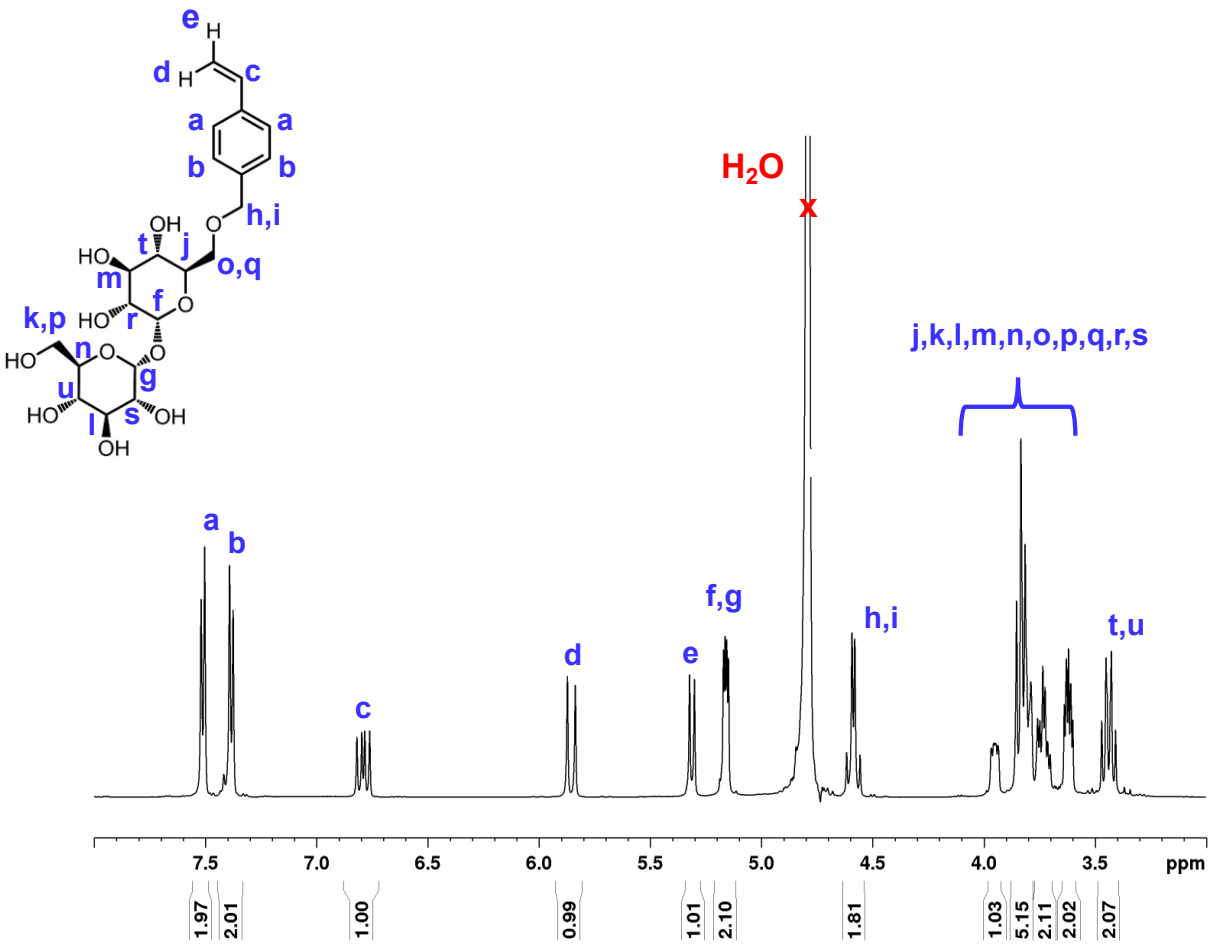

Figure 2-18. ^{1}H NMR spectrum of **O6** (D_2O).

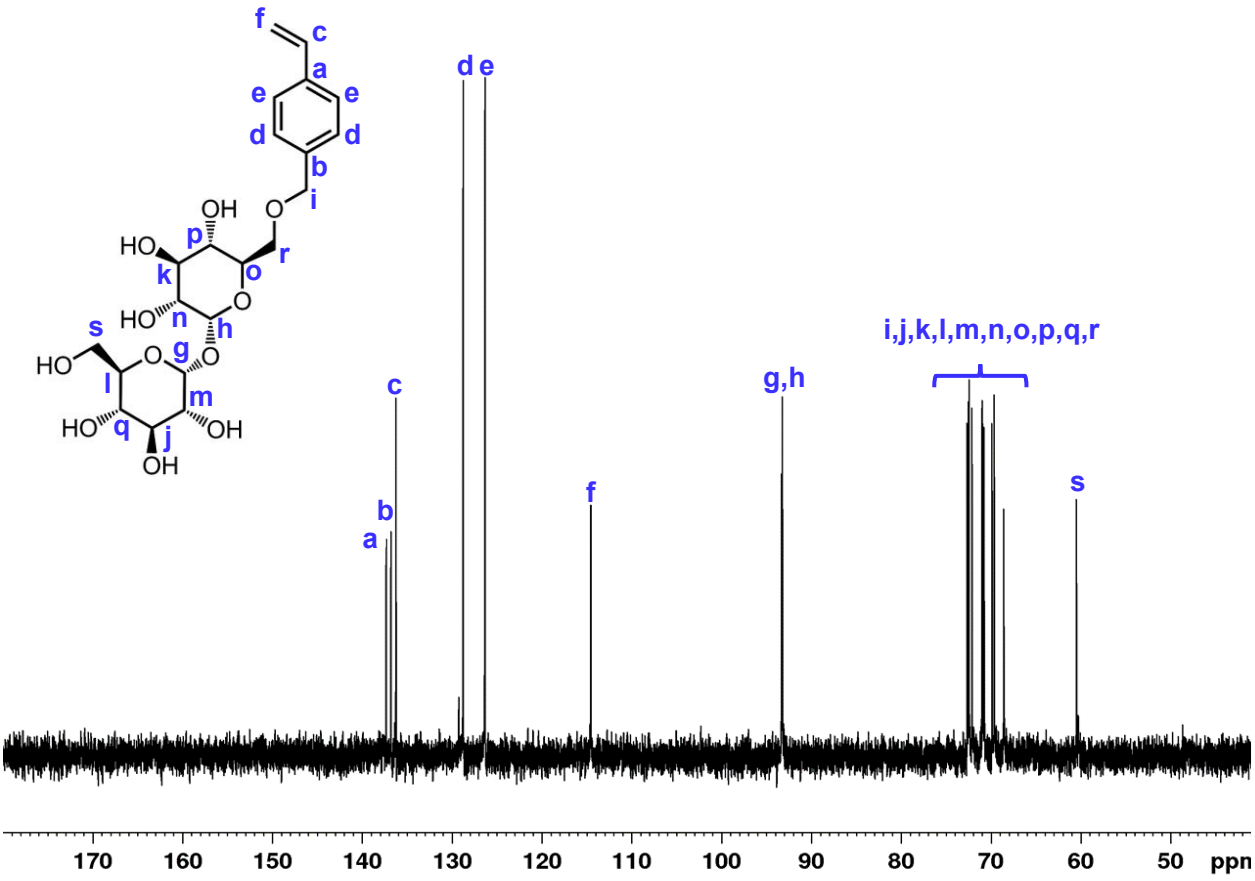

Figure 2-19. ^{13}C NMR spectrum of **O6** (D_2O).

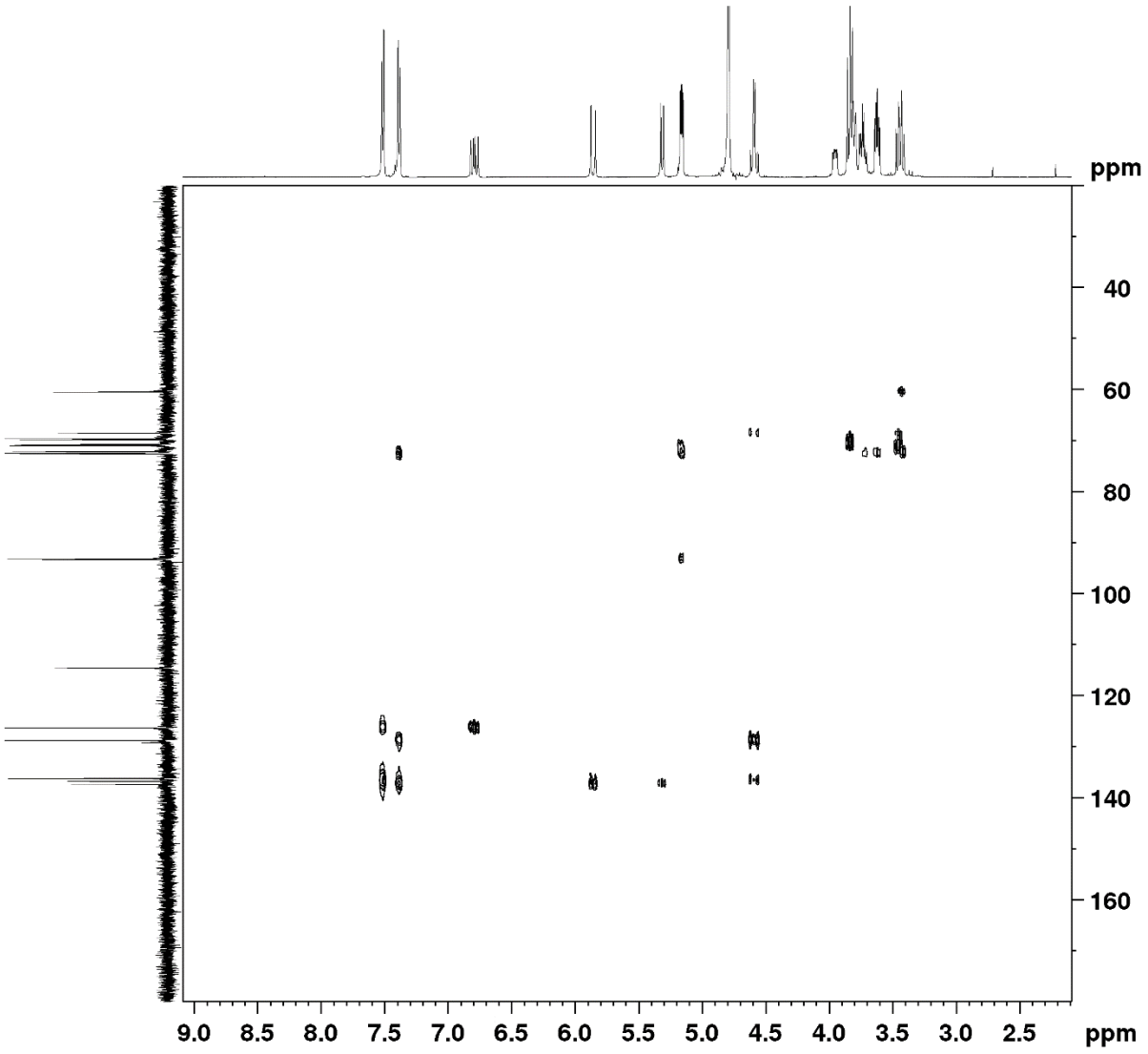

Figure 2-20. HMBC spectrum of **O6** (D_2O).

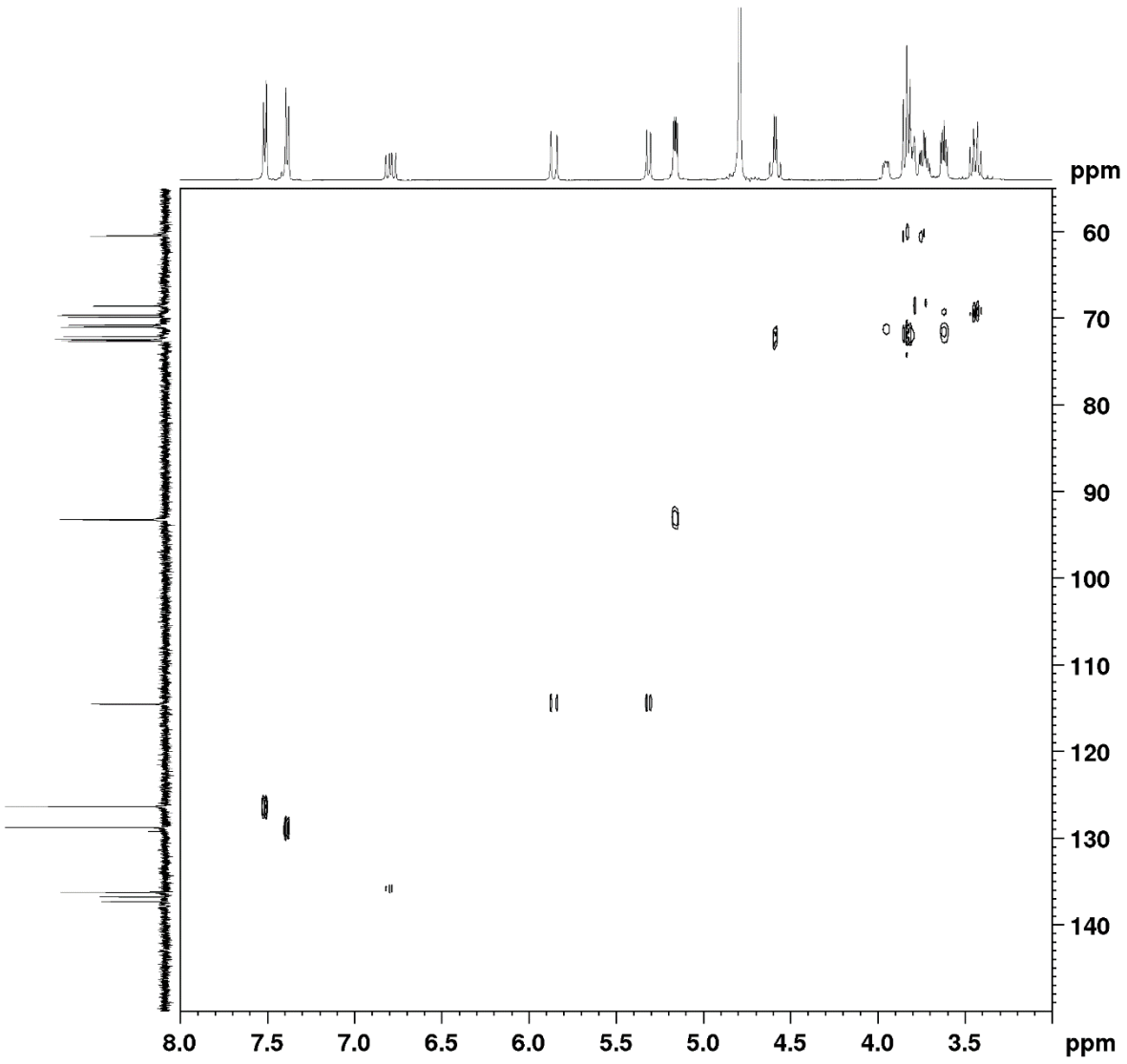

Figure 2-21. HSQC spectrum of **O6** (D_2O).

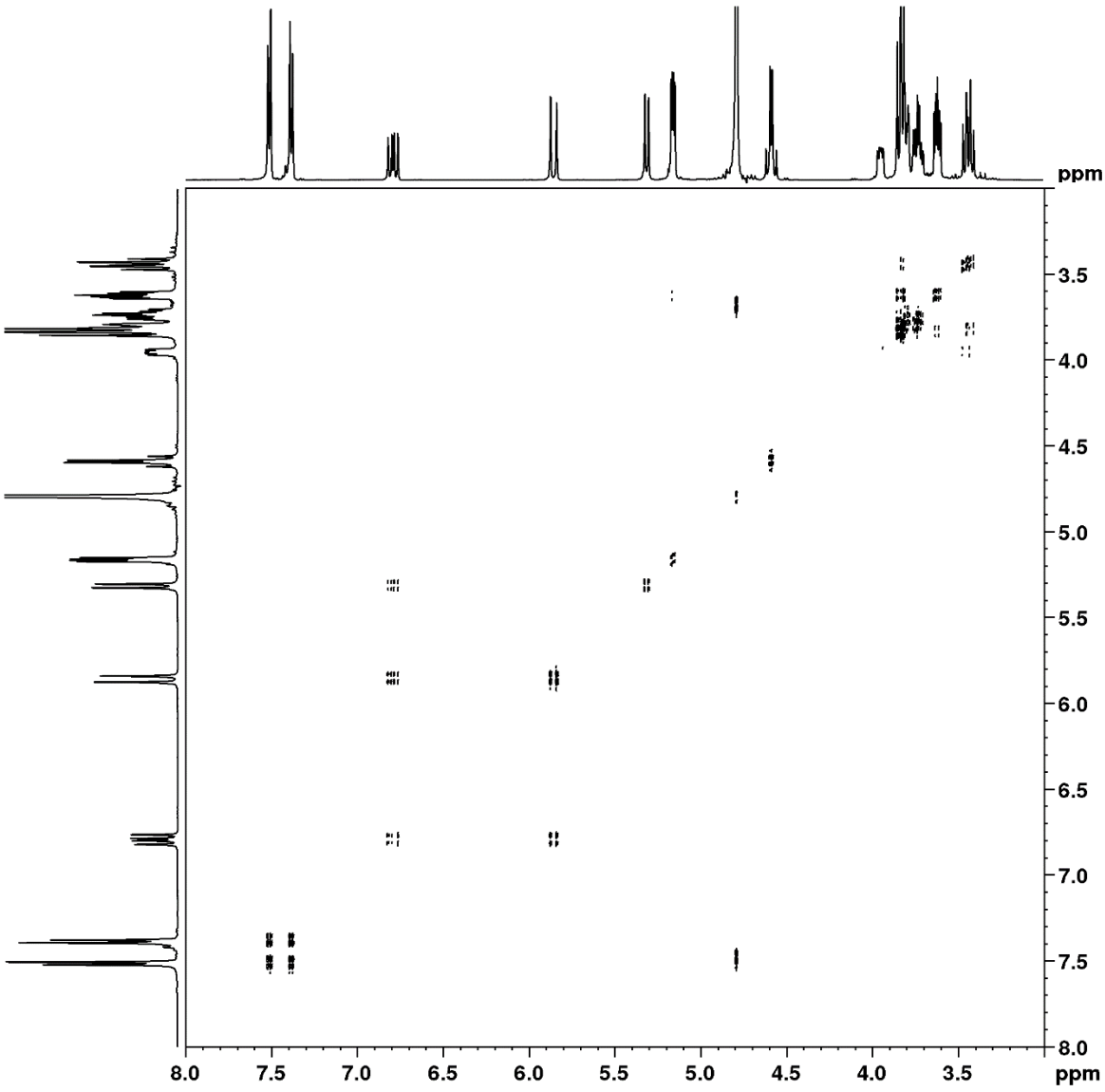

Figure 2-22. COSY spectrum of **O6** (D_2O).

Computational Methods

Conformers for regioisomer **O2**, **O4**, and **O6** were searched by using Maestro 9.4. with OPLS_2015 force field in implicit water. For each regioisomer, the ensemble of conformers consists of those whose energies are within 10 kcal/mol from the lowest one. This ensemble typically includes ~400 structures. The structures were then clustered to 25 representatives for **O2**, 33 for **O4**, and 42 for **O6** using the chemical informatics tool in Maestro 9.4. These structures were then optimized using B3LYP/6-31g(d) with SMD water model in Gaussian 09. Frequency analysis was conducted to confirm that the structures are stationary points on the potential energy surface with no imaginary frequency. Thermal energies are calculated by using simple harmonic oscillator model. The reported energies are Gibbs free energies at 298.15 K and 1 bar.

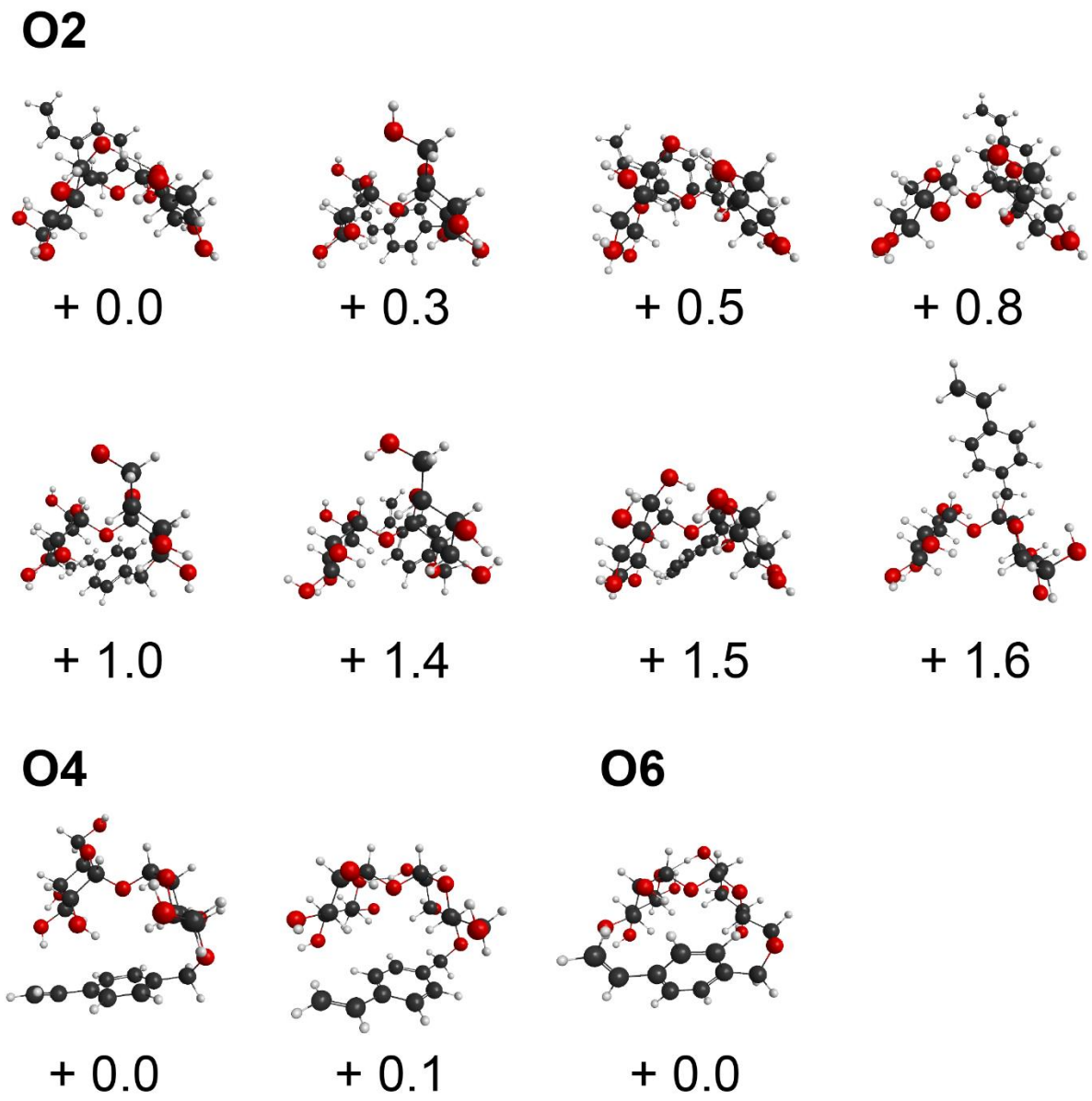

Figure 2-23. Conformers for the regioisomers within 2 kcal/mol of the most stable conformer (energy difference in kcal/mol shown below the structures).

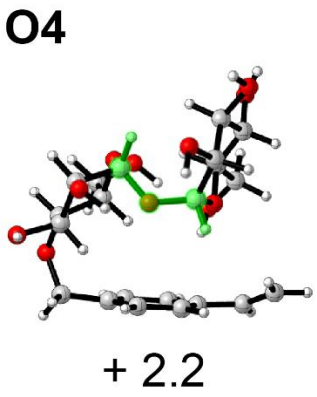

Figure 2-24. Example of conformer with disrupted clam shell conformation (**O4** conformer with 2.2 kcal/mol higher energy than the most stable conformation).

2.5 References

(1) Oobatake, M.; Ooi, T. Hydration and heat stability effects on protein unfolding. *Prog. Biophys. Mol. Biol.* **1993,** *59*, 237.

(2) Chi, E. Y.; Krishnan, S.; Randolph, T. W.; Carpenter, J. F. Physical stability of proteins in aqueous solution: mechanism and driving forces in nonnative protein aggregation. *Pharm. Res.* **2003,** *20*, 1325.

(3) Sluzky, V.; Tamada, J. A.; Klibanov, A. M.; Langer, R. Kinetics of insulin aggregation in aqueous solutions upon agitation in the presence of hydrophobic surfaces. *Proc. Natl. Acad. Sci. U. S. A.* **1991,** *88*, 9377.

(4) Wang, W. Lyophilization and development of solid protein pharmaceuticals. *Int. J. Pharm.* **2000,** *203*, 1.

(5) Kintzing, J. R.; Interrante, M. V. F.; Cochran, J. R. Emerging Strategies for Developing Next-Generation Protein Therapeutics for Cancer Treatment. *Trends Pharmacol. Sci.* **2016,** *37*, 993.

(6) Kamerzell, T. J.; Esfandiary, R.; Joshi, S. B.; Middaugh, C. R.; Volkin, D. B. Protein–excipient interactions: Mechanisms and biophysical characterization applied to protein formulation development. *Adv. Drug Del. Rev.* **2011,** *63*, 1118.

(7) Teramoto, N.; Sachinvala, N. D.; Shibata, M. Trehalose and trehalose-based polymers for environmentally benign, biocompatible and bioactive materials. *Molecules* **2008,** *13*, 1773.

(8) Westh, P.; Ramløv, H. Trehalose accumulation in the tardigrade Adorybiotus coronifer during anhydrobiosis. *J. Exp. Zool.* **1991,** *258*, 303.

(9) Crowe, L. M.; Reid, D. S.; Crowe, J. H. Is trehalose special for preserving dry biomaterials? *Biophys. J.* **1996,** *71*, 2087.

(10) Crowe, J. H.; Carpenter, J. F.; Crowe, L. M. The role of vitrification in anhydrobiosis. *Annu. Rev. Physiol.* **1998,** *60,* 73.

(11) Katyal, N.; Deep, S. Revisiting the conundrum of trehalose stabilization. *Phys. Chem. Chem. Phys.* **2014,** *16*, 26746.

(12) Paul, S.; Paul, S. Molecular insights into the role of aqueous trehalose solution on temperature-induced protein denaturation. *J. Phys. Chem. B* **2015,** *119,* 1598.

(13) Moiset, G.; López, C. A.; Bartelds, R.; Syga, L.; Rijpkema, E.; Cukkemane, A.; Baldus, M.; Poolman, B.; Marrink, S. J. Disaccharides impact the lateral organization of lipid membranes. *J. Am. Chem. Soc.* **2014,** *136*, 16167.

(14) Lins, R. D.; Pereira, C. S.; Hünenberger, P. H. Trehalose–protein interaction in aqueous solution. *Proteins: Struct. Funct. Bioinf.* **2004,** *55*, 177.

(15) Jain, N. K.; Roy, I. Effect of trehalose on protein structure. *Protein Sci.* **2009,** *18*, 24.

(16) Ohtake, S.; Wang, Y. J. Trehalose: current use and future applications. *J. Pharm. Sci.* **2011,** *100*, 2020.

(17) Carninci, P.; Nishiyama, Y.; Westover, A.; Itoh, M.; Nagaoka, S.; Sasaki, N.; Okazaki, Y.; Muramatsu, M.; Hayashizaki, Y. Thermostabilization and thermoactivation of thermolabile enzymes by trehalose and its application for the synthesis of full length cDNA. *Proc. Natl. Acad. Sci. U. S. A.* **1998,** *95*, 520.

(18) Hirai, T.; Murata, K.; Mitsuoka, K.; Kimura, Y.; Fujiyoshi, Y. Trehalose embedding technique for high-resolution electron crystallography: application to structural study on bacteriorhoposin. *J. Electron Microsc.* **1999,** *48*, 653.

(19) Mancini, R. J.; Lee, J.; Maynard, H. D. Trehalose Glycopolymers for Stabilization of Protein Conjugates to Environmental Stressors. *J. Am. Chem. Soc.* **2012,** *134*, 8474.

(20) Lee, J.; Lin, E.-W.; Lau, U. Y.; Hedrick, J. L.; Bat, E.; Maynard, H. D. Trehalose Glycopolymers as Excipients for Protein Stabilization. *Biomacromolecules* **2013,** *14*, 2561.

(21) Lee, J.; Ko, J. H.; Lin, E.-W.; Wallace, P.; Ruch, F.; Maynard, H. D. Trehalose hydrogels for stabilization of enzymes to heat. *Polym. Chem.* **2015,** *6*, 3443.

(22) Bat, E.; Lee, J.; Lau, U. Y.; Maynard, H. D. Trehalose glycopolymer resists allow direct writing of protein patterns by electron-beam lithography. *Nat. Commun.* **2015,** *6*, 6654.

(23) Pelegri-O'Day, E. M.; Paluck, S. J.; Maynard, H. D. Substituted Polyesters by Thiol–Ene Modification: Rapid Diversification for Therapeutic Protein Stabilization. *J. Am. Chem. Soc.* **2017**.

(24) Liu, Y.; Lee, J.; Mansfield, K. M.; Ko, J. H.; Sallam, S.; Wesdemiotis, C.; Maynard, H. D. Trehalose Glycopolymer Enhances Both Solution Stability and Pharmacokinetics of a Therapeutic Protein. *Bioconj. Chem.* **2017,** *28*, 836.

(25) Lau, U. Y.; Saxer, S. S.; Lee, J.; Bat, E.; Maynard, H. D. Direct Write Protein Patterns for Multiplexed Cytokine Detection from Live Cells Using Electron Beam Lithography. *ACS Nano* **2015,** *10*, 723.

(26) Wada, M.; Miyazawa, Y.; Miura, Y. A specific inhibitory effect of multivalent trehalose toward Aβ (1-40) aggregation. *Polym. Chem.* **2011,** *2*, 1822.

(27) Sizovs, A.; Xue, L.; Tolstyka, Z. P.; Ingle, N. P.; Wu, Y.; Cortez, M.; Reineke, T. M. Poly (trehalose): sugar-coated nanocomplexes promote stabilization and effective polyplex-mediated siRNA delivery. *J. Am. Chem. Soc.* **2013,** *135*, 15417.

(28) Tolstyka, Z. P.; Phillips, H.; Cortez, M.; Wu, Y.; Ingle, N.; Bell, J. B.; Hackett, P. B.; Reineke, T. M. Trehalose-Based Block Copolycations Promote Polyplex Stabilization for Lyophilization and in Vivo pDNA Delivery. *ACS Biomater. Sci. Eng.* **2015,** *2*, 43.

(29) Frisch, M. J.; Trucks, G. W.; Schlegel, H. B.; Scuseria, G. E.; Robb, M. A.; Cheeseman, J. R.; Scalmani, G.; Barone, V.; Mennucci, B.; Petersson, G. A.; Nakatsuji, H.; Caricato, M.; Li, X.; Hratchian, H. P.; Izmaylov, A. F.; Bloino, J.; Zheng, G.; Sonnenberg, J. L.; Hada, M.; Ehara, M.; Toyota, K.; Fukuda, R.; Hasegawa, J.; Ishida, M.; Nakajima, T.; Honda, Y.; Kitao, O.; Nakai, H.; Vreven, T.; Montgomery Jr., J. A.; Peralta, J. E.; Ogliaro, F.; Bearpark, M. J.; Heyd, J.; Brothers, E. N.; Kudin, K. N.; Staroverov, V. N.; Kobayashi, R.; Normand, J.; Raghavachari, K.; Rendell, A. P.; Burant, J. C.; Iyengar, S. S.; Tomasi, J.; Cossi, M.; Rega, N.; Millam, N. J.; Klene, M.; Knox, J. E.; Cross, J. B.; Bakken, V.; Adamo, C.; Jaramillo, J.; Gomperts, R.; Stratmann, R. E.; Yazyev, O.; Austin, A. J.; Cammi, R.; Pomelli, C.; Ochterski, J. W.; Martin, R. L.; Morokuma, K.; Zakrzewski, V. G.; Voth, G. A.; Salvador, P.; Dannenberg, J. J.; Dapprich, S.; Daniels, A. D.; Farkas, Ö.; Foresman, J. B.; Ortiz, J. V.; Cioslowski, J.; Fox, D. J. *Gaussian 09*, Gaussian, Inc.: Wallingford, CT, USA, 2009.

(30) Albertorio, F.; Chapa, V. A.; Chen, X.; Diaz, A. J.; Cremer, P. S. The α, α-(1→ 1) linkage of trehalose is key to anhydrobiotic preservation. *J. Am. Chem. Soc.* **2007,** *129*, 10567.

(31) Sakakura, K.; Okabe, A.; Oku, K.; Sakurai, M. Experimental and theoretical study on the intermolecular complex formation between trehalose and benzene compounds in aqueous solution. *J. Phys. Chem. B* **2011,** *115*, 9823.

(32) Oku, K.; Kurose, M.; Kubota, M.; Fukuda, S.; Kurimoto, M.; Tujisaka, Y.; Sakurai, M. Interaction between trehalose and alkaline-earth metal ions. *Biosci., Biotechnol., Biochem.* **2005,** *69*, 7.

(33) Fujimoto, T.; Oku, K.; Tashiro, M.; Machinami, T. Crystal Structure of α, α-Trehalose–Calcium Chloride Monohydrate Complex. *J. Carbohydr. Chem.* **2006,** *25*, 521.

(34) Lawandi, J.; Rocheleau, S.; Moitessier, N. Regioselective acylation, alkylation, silylation and glycosylation of monosaccharides. *Tetrahedron* **2016,** *72*, 6283.

(35) Pelletier, G.; Zwicker, A.; Allen, C. L.; Schepartz, A.; Miller, S. J. Aqueous glycosylation of unprotected sucrose employing glycosyl fluorides in the presence of calcium ion and trimethylamine. *J. Am. Chem. Soc.* **2016,** *138*, 3175.

(36) Messina, M. S.; Ko, J. H.; Yang, Z.; Strouse, M. J.; Houk, K. N.; Maynard, H. D. Effect of trehalose polymer regioisomers on protein stabilization. *Polym. Chem.* **2017,** *8*, 4781.

(37) Lundquist, J. J.; Toone, E. J. The cluster glycoside effect. *Chem. Rev.* **2002,** *102*, 555.

Chapter 3.

Trehalose Hydrogels for Stabilization of Proteins

This chapter contains portions of an edited version of the following published papers:
Lee, J.; Ko, J. H.; Mansfield, K. M.; Nauka, P. C.; Bat, E.; Maynard, H. D. *Macromol. Biosci.* **2018**, *18*, 1700372. – Reproduced by permission of John Wiley and Sons.
Lee, J.;† Ko, J. H.;† Lin, E.-W.; Wallace, P.; Ruch, F.; Maynard, H. D. *Polym. Chem.* **2015**, *6*, 3443. († Equal contribution). – Reproduced by permission of The Royal Society of Chemistry.

Polymeric hydrogels are used for a variety of biomedical applications owing to their hydrophilicity and tunable properties.[1] They can absorb large amounts of water and encapsulate macromolecules such as proteins and even live cells.[2, 3] By choosing appropriate components, the hydrogel can be programmed to protect its cargo and/or release the cargo upon exposure to a desired stimulus.

In particular, hydrogels containing trehalose possess many advantages for protein delivery. As demonstrated by many examples in the other chapters, trehalose stabilizes proteins against many physical stressors. Moreover, the high hydrophilicity of trehalose allows cross-linked trehalose polymers to naturally absorb water and form a hydrogel without the need to incorporate additional hydrophilic monomers. In the first part of this chapter, we combine the protein-stabilizing ability of trehalose with the glucose-responsive property of boronic esters to form a trehalose-boronic acid hydrogel that protects insulin to heat and releases it when glucose level increases, as in diabetic patients after eating meals. The second part of this chapter deals with industrially scalable trehalose hydrogel that stabilizes an enzyme important for the agricultural industry. These examples highlight the versatility of trehalose-based materials in many different applications.

3.1 Glucose-Responsive Trehalose Hydrogel for Insulin Stabilization and Delivery

3.1.1 Introduction

Insulin was the first Food and Drug Administration (FDA)-approved recombinant protein drug, and is one of the most widely used treatment for diabetes.[4] However, one of the challenges associated with insulin therapy is the requirement of repeated injection or insertion of an insulin bolus after each meal in the case of the insulin pump, which may be problematic especially for

children and active young adults.[5] To address these challenges, glucose-responsive insulin delivery systems have been proposed. Early works focused on the sugar binding capability of the lectin, concanavalin A (Con A).[6-8] While some of these systems demonstrated excellent glucose-responsive behavior,[7, 8] the toxicity[9] and potential denaturation[10] of Con A itself were pointed out as inherent problems with the materials. Another popular glucose-responsive material is the enzyme glucose oxidase,[11-13] but delivery systems based on glucose oxidase could also suffer in long term performance due to the instability of the enzyme.

More recently, phenylboronic acid that is non-toxic and durable has been widely used in materials for insulin release.[10, 14] Since boronic acid forms dynamic covalent complexes with 1,2- or 1,3-diols,[15] its incorporation into hydrogels results in glucose-responsive materials. The two main mechanisms of insulin release reported from boronic acid hydrogels are swelling and competitive binding.[10, 14] The swelling mechanism is caused by the shift in the equilibrium of different boronic acid species toward the anionic tetrahedral form upon binding to diols such as those on sugars, which causes osmotic swelling of the hydrogels.[9] Alternatively, boronic acid-based polymers[16-18] can form a hydrogel upon complexation with diol-containing polymers in the presence of insulin, and later be competitively displaced by glucose to dissolve the hydrogel and release insulin.[19]

In addition to controlled release of insulin, the instability of the protein is an important issue that needs to be addressed. Exposure of insulin to changes in temperature during storage often leads to inactivation of the protein resulting in health complications for patients.[20] Instability also contributes to the medical costs of diabetes treatment from drug that is discarded and wasted.[21] While insulin has been modified to increase its half-life *in vivo* (by covalent attachment of a polymer)[22] and to prevent insulin hexamer formation (by mutation of the amino acid sequence),[23]

few studies have reported stabilizing insulin to environmental heat exposure.[24, 25] Peppas and co-workers have used nanospheres composed of poly(N-isopropylacrylamide) and poly(ethylene glycol) (PEG) to enhance thermal and mechanical stability of insulin,[24] but their system lacked a release mechanism. Sunamoto and co-workers have used cholesterol-bearing pullulan nanogels to stabilize insulin against heat and enzymatic degradation, and the nanogel released insulin when exposed to bovine serum albumin (BSA) levels by association of BSA with pullulan.[25] Although this system successfully stabilized insulin, it lacked glucose responsiveness, which is highly desirable in insulin delivery systems. To our knowledge, a hydrogel that is both glucose-responsive and insulin stabilizing has not yet been reported.

Our group has previously shown that trehalose glycopolymers are effective stabilizers for proteins, including insulin, against lyophilization and heat either as conjugates or as excipients.[26-30] We hypothesized that the trehalose glycopolymer, also named PolyProtek, could be used to entrap insulin by complexing with a boronic acid cross-linker and that the resulting hydrogel would also stabilize insulin against environmental stressors, while releasing the hormone upon competitive addition of insulin (Scheme 3-1). Herein, we describe results that demonstrate that the trehalose-boronic acid hydrogel can deliver insulin upon increase in glucose level, while also stabilizing the protein under thermal stress.

3.1.2 Results and Discussion

We designed the three-component glucose-responsive insulin delivery system consisting of trehalose polymer (poly(styrenyl ether trehalose) or poly(SET)), multivalent boronic acid cross-linker (8-arm PEG boronic acid), and insulin (Scheme 3-1). When trehalose and boronic acid polymers are mixed in the presence of insulin, the diols in trehalose polymer should form the

tetrahedral boronate ester with boronic acid moieties and physically entrap insulin within the hydrogel pores. We anticipated that when glucose was added, the 1,2 diols in glucose would competitively displace the 1,3 diols of trehalose to dissolve the hydrogel, leading to insulin release.

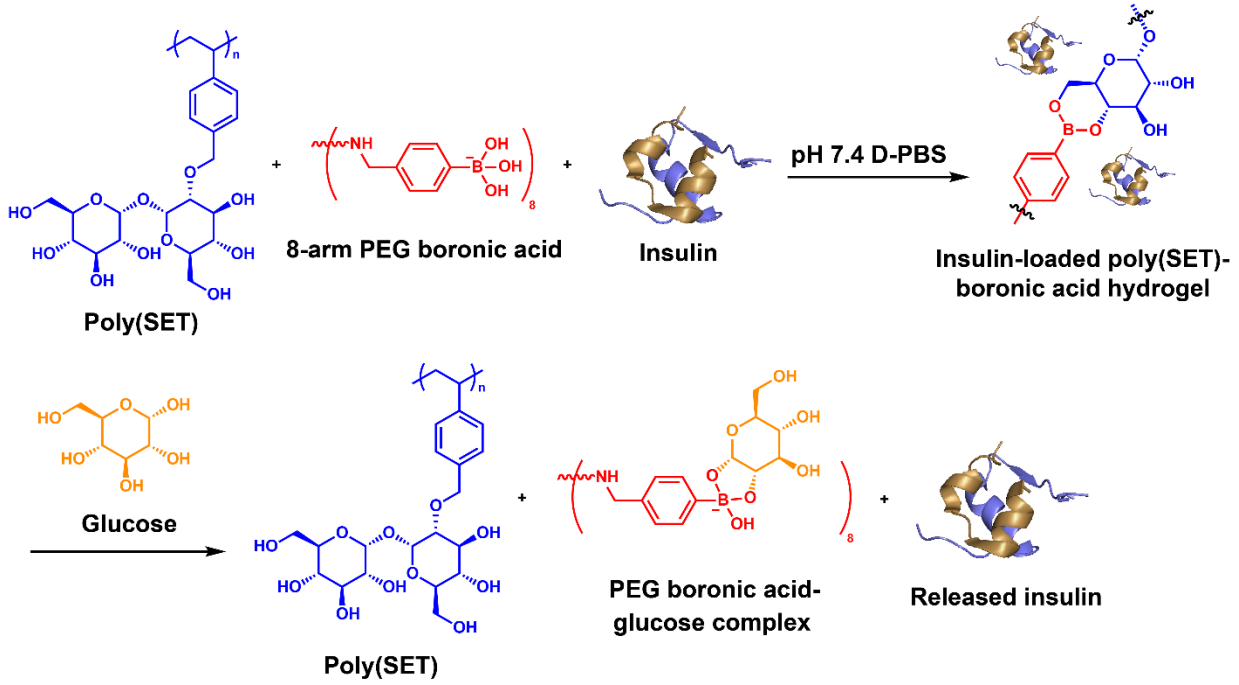

Scheme 3-1. Design for insulin delivery using trehalose-boronic acid hydrogel (insulin PDB ID: 4INS).

Ideally, glucose as the competitive displacer of trehalose polymer should have higher binding to boronic acid in order for the system to exhibit high sensitivity to glucose. Some studies have found no binding affinity between trehalose and boronic acid, limiting its usefulness for applications such as sugar sensing.[31] Yet, other studies have demonstrated weak binding to trehalose.[32] Thus to both confirm trehalose-boronic acid interaction and compare glucose and trehalose binding affinities, we measured the binding constants using a fluorescence-based method (Figure 3-1).[33] Fluorescence of the boronic acid probe was quenched by trehalose in a

concentration-dependent manner at neutral pH, showing that 1,3 diol does indeed bind to boronic acid. Moreover, glucose had 5.4 times higher binding than trehalose (2.57 versus 0.48 M^{-1}), providing support that competitive displacement by glucose was possible. Moreover, we expected the multivalent effect of the polymer to help facilitate gel formation due to an increase in local concentration of diols available to form cross-links.

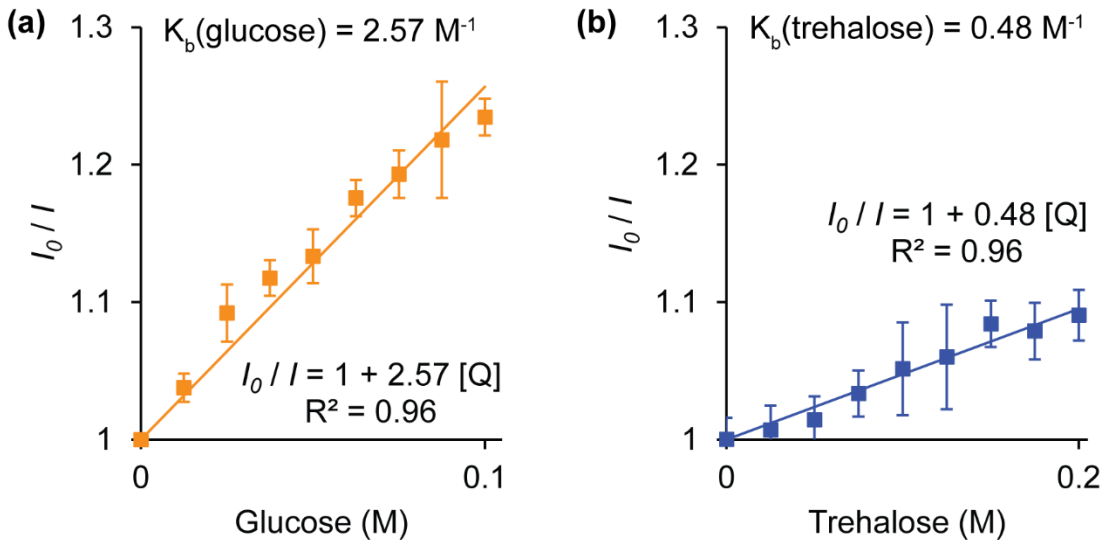

Figure 3-1. Relative fluorescence of boronic acid at pH 7.4 as a function of (a) glucose (n = 3) and (b) trehalose concentration (n = 5 or 6).

With trehalose binding to boronic acid confirmed to be non-zero but weaker than glucose, we then prepared non-covalent hydrogels for study. For the materials, a boronic acid cross-linker was synthesized through reductive amination, using 4-formylphenylboronic acid and 8-arm PEG amine as starting materials. Complete modification of the amine end-groups with phenylboronic acid was confirmed by ^{1}H NMR spectroscopy (Experimental Section Figure 3-4). Next, the trehalose hydrogel was prepared by mixing the 8-arm PEG boronic acid with Poly(SET) at a 1:1

molar ratio of boronic acid to trehalose units (Scheme 3-1) in Dulbecco's phosphate-buffered saline (D-PBS). The gelation occurred instantaneously after mixing the solutions of the two components, thus we envision that the materials may be injected as the hydrogel is fast-forming after mixing.

To test insulin release upon addition of glucose, the poly(SET) boronic acid hydrogels were prepared in the presence of FITC-labeled insulin. 8-Arm PEG boronic acid was dissolved in a buffer containing FITC-labeled insulin and mixed with the poly(SET) to prepare hydrogels, and these were added into D-PBS containing 0, 1, 2, 5, and 10 mg/mL glucose. At first the release at pH 8.0 was tested since boronic acid-diol binding is stronger at basic pH.[9] Aliquots were taken from the solutions at each time point and released insulin was quantified (Experimental Section Figure 3-6). Glucose responsive behavior was observed, with slower release at lower glucose concentrations (1, 2, and 5 mg/mL) and faster release at high glucose concentrations (10 mg/mL). We also conducted the release experiment at pH 7.4 to characterize the glucose-responsive insulin release at a physiological pH (Figure 3-2). We utilized 0, 5, and 10 mg/mL glucose levels since the pH 8 data had demonstrated no statistical differences between 1, 2 and 5 mg/mL. After one hour, the hydrogel in the 10 mg/mL glucose solution was completely dissolved to yield 99 ± 1 % insulin release, while over the same time period 80 ± 9 % and 49 ± 12 % insulin were released in 5 mg/mL and 0 mg/mL glucose solution, respectively. The gel could be completely dissolved with 0.1 M HCl (pH 1); as expected the boronic acid-diol interaction is disrupted at acidic pH.[33] Together, the data shows that the hydrogel was able to release insulin in a glucose-dependent manner, and the system may be fine-tuned in the future to exhibit a more sensitive release profile in accordance with the narrow therapeutic window. For example, the release in more basic buffer (pH 8.0) was slower than at neutral pH suggesting that the pKa of boronic acid may be tailored as

desired for more rapid or delayed insulin delivery. This has been exploited in other systems.[9, 17, 34] Additionally, improved stability of the ester using B-O dative bond formation may be utilized to tune the insulin delivery at neutral pH.[35] Another possible approach to increase the binding affinity and thus decrease the insulin release at low glucose levels is to incorporate a monomer with a cis-1,2 diol into the trehalose polymer chains.

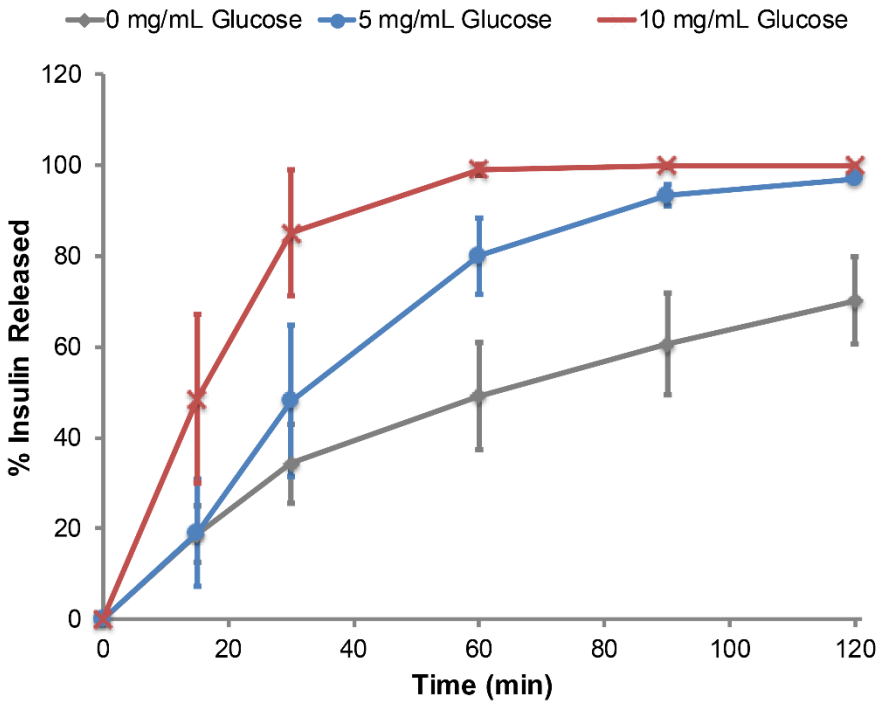

Figure 3-2. Insulin released in D-PBS, pH 7.4, containing 0, 5, and 10 mg/mL glucose (n = 6 per group).

Next, we tested the ability of the trehalose hydrogel to stabilize insulin against heating. Insulin solutions were separately prepared without any additive, with poly(SET), with 8-arm PEG boronic acid, or with the trehalose hydrogel. The samples were heated for 30 min at 90 °C to accelerate heat-induced degradation and then tested with insulin ELISA to confirm the structural

integrity of insulin. A control group with insulin and the trehalose hydrogel stored at 4 °C demonstrated that the hydrogel did not affect the ELISA results (second entry compared to the first entry, Figure 3-3). We have observed that trehalose polymers stabilize proteins to both heat and lyophilization.[26] We hypothesized that the presence of the trehalose network stabilizes insulin in a similar manner.

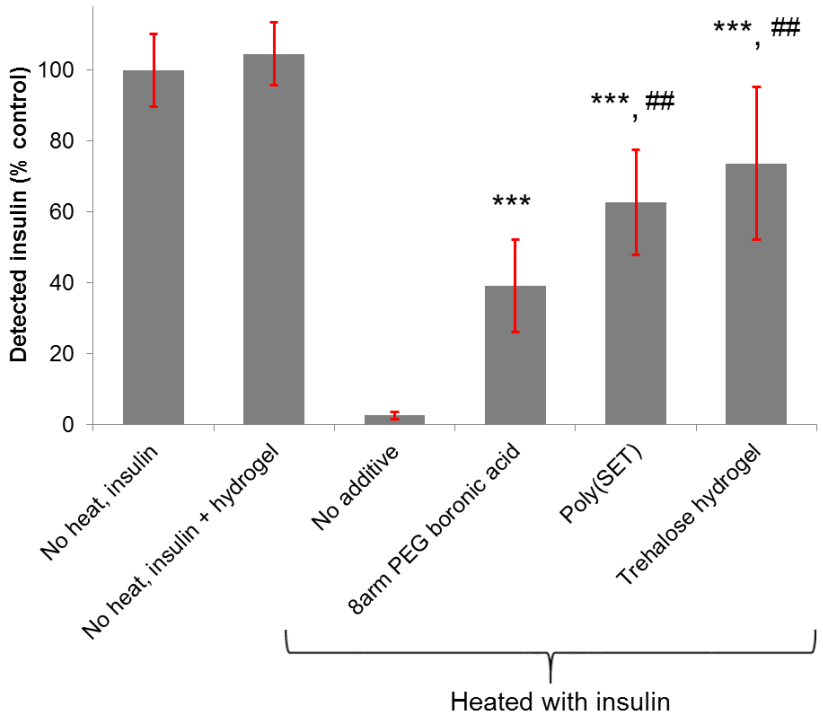

Figure 3-3. ELISA results of insulin (no heat control), insulin with hydrogel (no heat control), insulin with no additive (heated), insulin with 8-arm PEG boronic acid (heated), insulin with trehalose polymer (heated), and insulin with hydrogel (heated). Heating condition was 90 °C for 30 min. *** is $p < 0.001$ relative to no additive, ## is $p < 0.01$ relative to 8-arm PEG boronic acid ($n = 6$).

The data shows that the glucose-responsive trehalose hydrogel is effective at stabilizing insulin against heating stress (Figure 3-3). Insulin without any additive underwent degradation and no longer bound to the antibody upon heating, showing less than 2% signal by ELISA.

Significantly more insulin was detected in the presence of additives. Poly(SET) remarkably stabilized insulin and 63 ± 15 % of the original protein was detected after heating to 90 °C for 30 min. Insulin was also partially stabilized in the presence of the 8-arm PEG boronic acid alone (39 ± 13%). The literature is divided on the effect of PEG on protein stability; it has been suggested that PEG may accelerate protein denaturation at higher temperatures due to the interaction of hydrophobic PEG with the denatured state of protein.[36, 37] However, the specific architecture of PEG polymer may dictate whether PEG stabilizes or destabilizes proteins. For example, Amirgoulova *et al.* have reported that linear PEG interacts with the denatured state of a protein to favor unfolding, and they therefore used star-shaped PEG instead for their surface coating applications.[38] Importantly, the combination of both poly(SET) and branched PEG as a hydrogel resulted in 74 ± 22% stabilization, significantly better than the 8-arm PEG boronic acid ($p < 0.01$) and similar to poly(SET) alone. These results suggest that even though the poly(SET) is partially bound to the 8-arm PEG boronic acid in the gel, the stabilizing properties of the polymer are maintained.

3.1.3 Conclusions

In summary, we have synthesized a glucose-responsive hydrogel based on a trehalose glycopolymer for insulin delivery and stabilization against heat. The results demonstrate that hydrogels can be readily prepared from trehalose polymers and boronic acid cross linkers. The gelation occurred under physiological conditions, and the resulting hydrogel was capable of releasing insulin in a glucose-responsive manner. The addition of glucose led to breaking of the boronate ester bond between the trehalose polymer and the boronic acid cross-linker through competitive displacement by glucose, which has 5.4 times higher binding affinity to boronic acid

than trehalose. As expected, higher glucose concentration in the buffer increased the rate of dissolution of the hydrogel and resulted in faster release of loaded insulin. Additionally, the trehalose hydrogel can effectively protect insulin against extreme heat stress. Since most of the protein drugs must be stored under regulated temperature to maintain their activities, trehalose hydrogels in general may be used to enhance the quality of life of patients by not requiring specialized refrigeration and this is being tested. Also, as boronic acid has been used to create pH-responsive materials,[34] the trehalose boronic-acid hydrogels may have potential applications for delivery of a wider range of protein therapeutics. For example, this has been exploited to release anti-cancer drugs such as therapeutic antibodies at acidic extracellular pH near tumors.[39]

3.1.4 Experimental Section

Materials

All chemicals were purchased from Sigma-Aldrich and Fisher Scientific and were used without purification unless noted otherwise. Recombinant human insulin was purchased from Sigma-Aldrich. Trehalose was purchased from The Healthy Essential Management Corporation (Houston, TX), and was azeotropically dried with ethanol and kept under vacuum until use. Azobisisobutyronitrile (AIBN) was recrystallized from acetone before use. 8-arm PEG amine was purchased from Jenkem Technology (Allen, TX). Human insulin ELISA kit was purchased from Mercodia (Uppsala, Sweden). Styrenyl ether trehalose monomer was prepared using our previously reported procedure.[26]

Analytical Techniques

NMR spectra were recorded on a Bruker DRX 500 MHz spectrometer. Gel permeation chromatography (GPC) was conducted on a Shimadzu HPLC system equipped with a refractive index detector RID-10A and two Polymer Laboratories PLgel 5 μm mixed D columns (with guard column). Lithium bromide (0.1 M) in *N*,*N*-dimethylformamide (DMF) at 40 °C was used as the solvent (flow rate: 0.6 mL/min). Near-monodisperse poly(methyl methacrylate) standards (Polymer Laboratories) were employed for calibration. Infrared spectra were obtained with a Perkin-Elmer Spectrum One instrument equipped with a universal attenuated total reflection (ATR) accessory. Preparatory reverse phase high performance liquid chromatography (HPLC) was carried out on a Shimadzu HPLC system equipped with a UV detector using a Luna 5 μm C18 100 Å column (preparatory: 5 μm, 250 x 21.2 mm) with monitoring at λ = 215 nm and 254 nm. Isocratic solvent system (water:methanol = 50:50) was used as the mobile phase at a flow rate of 10 mL/min. Fluorescence measurement was made on a FlexStation II (Molecular Devices). UV-Vis absorbance was measured using a microplate reader ELx800 (BioTek Instruments, Winooski, VT). Matrix-assisted laser desorption/ionization mass spectrometry (MALDI-MS) analysis of FITC-labeled insulin was performed on a Bruker Ultraflex MALDI-time-of-flight (TOF) mass spectrometer in linear positive ion mode. FITC-labeled insulin (1 mg/mL) in Dulbecco's phosphate-buffered saline (D-PBS) was diluted 10-fold with deionized (Milli-Q filtered) water and mixed 1:1 with sinapinic acid (10 mg/mL) dissolved in 50% acetonitrile with 0.1 % trifluoroacetic acid on the MALDI target plate.

Determination of Boronic Acid Binding Constants

The method was adopted from the report by Deshayes *et al*.[33] Fluorescent boronic acid (2-naphthaleneboronic acid, λ_{ex} = 268 nm, λ_{em} = 344 nm) was dissolved at 335 μM concentration in Dulbecco's phosphate-buffered saline (D-PBS, pH 7.4) containing 2% dimethyl sulfoxide (DMSO), and then 150 μL of the boronic acid solution was mixed with equal volume of D-PBS solution containing trehalose or glucose. Fluorescence quenching was plotted as I_0 / I as a function of sugar concentration, where I_0 is the fluorescence in the absence of any sugar and I is the fluorescence in the presence of sugar. The intercept was fixed at 1, and the slope was taken to be the binding constant K_b according to the Stern-Volmer equation:

$$\boldsymbol{I_0/I = 1 + K_b[\mathrm{quencher}]} \qquad (1)$$

Synthesis of trehalose polymer, poly(SET)

AIBN (5.28 mg, 3.22×10^{-2} mmol) and styrenyl ether trehalose monomer (634 mg, 1.38 mmol) were dissolved in a mixture of DMF (2.31 mL) and H_2O (4.61 mL). Oxygen was removed by three cycles of freeze-pump-thaw and polymerization was initiated at 75 °C. The polymerization was stopped after 8.5 h by immersing the reaction into liquid nitrogen. The polymer was purified by dialysis against H_2O (MWCO 3,500) resulting in a polymer with M_n = 7.0 kDa and $Đ$ = 1.28 (for hydrogel dissolution experiment) and M_n = 7.6 kDa and $Đ$ = 1.33 (for all other experiments). ^{1}H NMR (500 MHz in D_2O) δ: 7.01, 6.45, 5.05, 3.81, 3.71, 3.59, 3.48, 3.36, 1.50.

Synthesis of 8-arm PEG Boronic Acid

8-arm PEG amine (400 mg, 10 kDa, 4×10^{-2} mmol) and 4-formylphenylboronic acid (96 mg, 6.40×10^{-1} mmol) were dissolved in 2.8 mL of MeOH. $NaBH_3CN$ (37.7 mg, 6.00×10^{-1} mmol) was added and the reaction was stirred at 25 °C. After 5 days the reaction solution was purified by dialysis against MeOH for 3 days. The sample was lyophilized and the ^1H NMR spectrum was used to calculate the % modification of the amine end-groups of the PEG. For the aromatic peaks attached at the ends of 8-arm, there are 32 protons (8 arm x 4 aromatic protons per ring). For 10 kDa PEG, there are approximately 10,000 / 44 Da = 227 repeat units (i.e. "n" in the polymer structure is 227 / 8 = 28 per arm), and 227 x 4 protons per repeat unit = 908 protons. This calculation showed that approximately 100 % of the end-groups of the PEG were modified with the boronic acid. ^1H NMR (500 MHz in D_2O) δ: 7.75 (16 H), 7.41 (16 H), 3.69 (908 H). IR: δ = 3390, 2869, 1699, 1456, 1410, 1348, 1297, 1247, 1079, 1041, 986, 947, 839 cm^{-1}.

FITC Labeling of Insulin

Insulin was labeled with fluorescein isothiocyanate isomer I (FITC) by dissolving insulin (0.65 mg, 0.112 μmol) and FITC (3.48 mg, 8.94 μmol) in 0.33 mL of 1 M sodium bicarbonate buffer, pH 8.3. The mixture was stirred for two hours, and free FITC was removed by repeated centrifugation through a membrane using Centriprep™ tubes with molecular weight cut-off (MWCO) of 3 kDa. Typical degree of labeling was approximately 0.7 FITC per insulin as determined by UV absorbance.[40] The MALDI-TOF spectrum (Experimental Section Figure 3-5) confirmed labeling of insulin with 1 or 2 FITC molecules, which is in accordance with the expected reactivity of the three reactive amine groups on insulin (GlyA1, PheB1, and LysB29), with GlyA1 and LysB29 being much more reactive than PheB1.[28]

FITC-Labeled Insulin Release from Trehalose Hydrogel

FITC-labeled insulin (13.22 mg/mL in D-PBS, pH 7.4 or pH 8) was added to the trehalose polymer to make a polymer concentration of 500 mg/mL. The PEG cross-linker was dissolved in D-PBS at 200 mg/mL concentration. Next, 1 µL of the trehalose polymer and FITC-labeled insulin stock solution and 6.84 µL of the PEG cross-linker stock solution were added to an Eppendorf Lo-Bind® centrifuge tube. The tube was agitated on a ThermoShaker (Allsheng Instruments, China) at 1,500 rpm at 21 °C for 1 h. The gels were transferred into a 24-well plate filled with 1 mL D-PBS and left to hydrate for 30 min. Next, the gels were transferred to a 96-well plate that had been blocked with 1% wt/vol BSA in D-PBS to prevent protein adsorption and filled with 0.3 mL of D-PBS containing 0, 5, or 10 mg/mL glucose. At each time point, all the solution was aliquoted and the wells containing the gels were immediately refilled with 0.3 mL of the same buffer. After the last time point, the wells were treated with 0.3 mL of D-PBS containing 100 mg/mL glucose and incubated at 37 °C for 5 min to completely dissolve the gels. All the solution was then transferred for measurement, and fluorescence of the time point aliquots and the residual insulin solutions recovered after gel dissolution was measured.

Trehalose Hydrogel Heating Assay

A stock insulin solution was prepared by first dissolving insulin in D-PBS, pH 7.4 at 1 mg/mL concentration, and then concentrated by centrifugation through a membrane using Centriprep™ tubes with molecular weight cut-off (MWCO) of 3 kDa. The protein concentration was quantified by UV absorbance at 280 nm, and the solution was diluted to 3.93 mg/mL such that the final insulin concentration in the samples was 0.5 mg/mL. Trehalose polymer stock solution was prepared by dissolving poly(SET) in the insulin stock solution at a 500 mg/mL concentration.

The PEG cross-linker was dissolved in D-PBS at 200 mg/mL concentration. The gels were prepared by adding 1 µL of insulin or trehalose polymer stock solution and 6.84 µL of PEG cross-linker stock solution or D-PBS to an Eppendorf Lo-Bind® centrifuge tube, and agitating the tube on a ThermoShaker at 1,500 rpm at 21 °C for 1 h to aid in mixing. The samples were heated at 90 °C for 30 min and the controls were kept at 4 °C. All samples and controls were treated with 1 mL of 100 mg/mL glucose in order to dissolve the hydrogel. The amount of insulin was assayed by ELISA, which was conducted according to manufacturer's instructions. Briefly, 25 µL of the diluted samples were added to the wells pre-coated with the capture antibody. Buffer containing detection antibody was added (100 µL), and the plate was incubated on a rocker at room temperature for 1 h. To prevent residual boronic acid binding to the sugar moieties on horseradish peroxidase used for ELISA,[41, 42] the wells were washed with 350 µL of deionized water acidified with HCl (pH = 3.5) five times after the incubation, and then six times with 350 µL of the wash buffer. These additional washing steps do not affect the ELISA results as confirmed by the controls. 3,3',5,5'-Tetramethylbenzidine (TMB) solution was added (200 µL), and the plate was incubated at room temperature for 15 min before the addition of 50 µL stop solution (1 N H_2SO_4). The amount of insulin detected was quantified by absorbance at 450 nm relative to the standards supplied by the manufacturer.

Statistical Analysis

One-tailed Student's t-test assuming unequal sample variance was used to test the difference between experimental groups. Results were considered significantly different if $p < 0.05$.

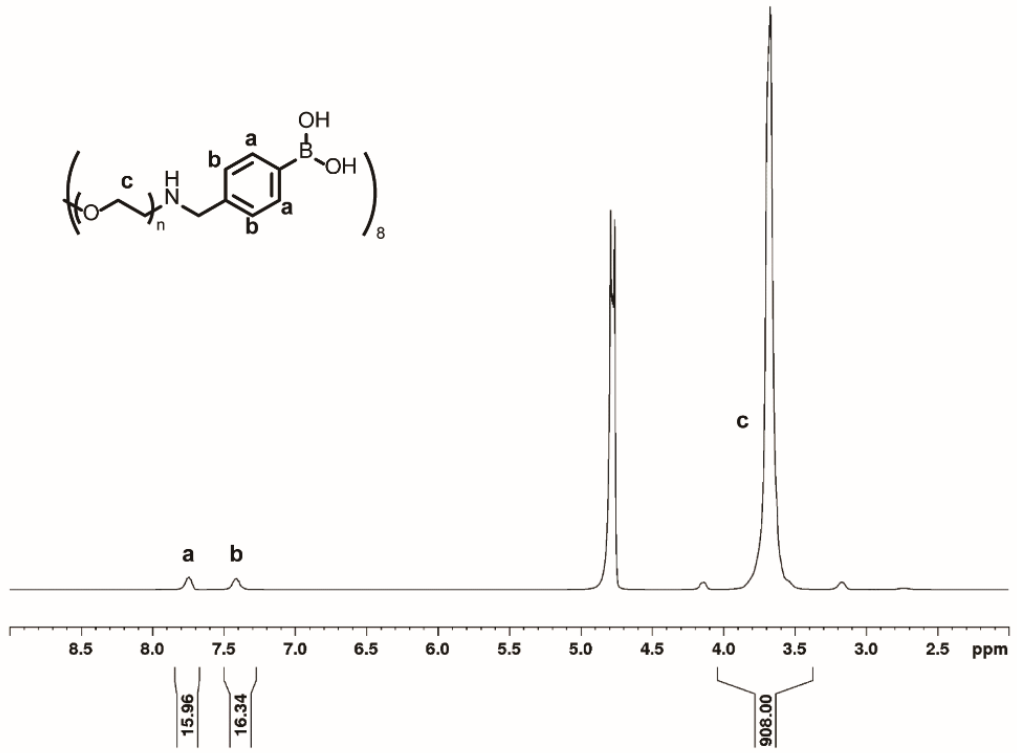

Figure 3-4. ^{1}H NMR spectrum of 8-arm PEG boronic acid (in D_2O). Note that **a**/**b** are the end groups of a ~10,000 Da 8-arm PEG chain indicated as **c**.

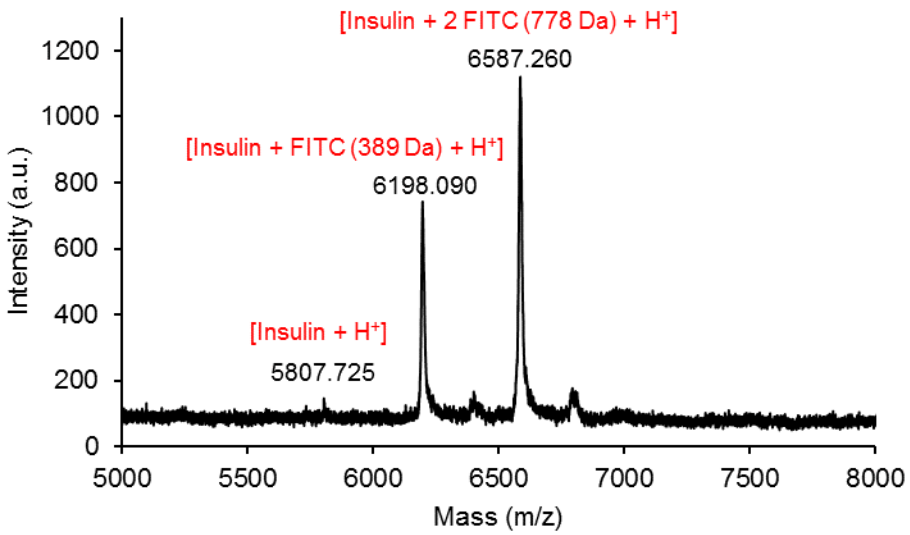

Figure 3-5. MALDI-TOF mass spectrum of FITC-labeled insulin.

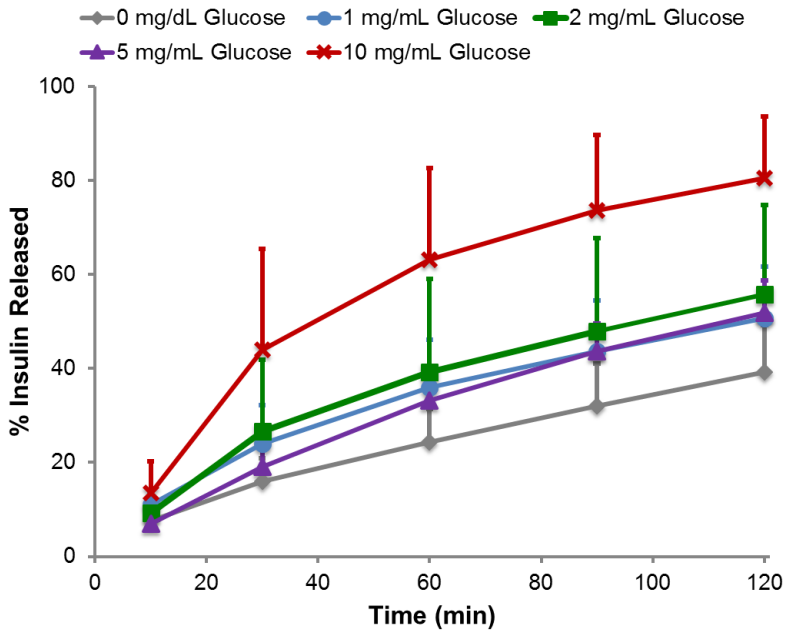

Figure 3-6. Insulin released in D-PBS, pH 8.0, containing 0, 1, 2, 5, and 10 mg/mL glucose (n=3 per group).

3.2 Trehalose Hydrogels for Stabilization of Agricultural Enzymes

3.2.1 Introduction

Enzymes have well-defined three-dimensional structures formed by multiple noncovalent interactions such as hydrogen bonds, salt bridges, and hydrophobic interactions.[43] At high temperatures, enzymes lose their original structure and denature to form insoluble aggregates that are no longer active.[43-45] Because of their high efficiency and selectivity in catalyzing biological processes, enzymes are used for numerous industrial purposes.[44, 46-48] However, this thermal instability of the proteins has negative impact on their applications in the pharmaceutical, food, and biotechnology industries. Many techniques such as chemical modification[49, 50] and protein engineering[51-54] have been developed to address this problem. Additionally, polymers have been used as conjugates or excipients to enhance thermostability of enzymes.[55-59] Yet some of these approaches are too expensive for certain industrial and agricultural applications.

For industrial applications, polymeric hydrogels are especially attractive materials for enzyme stabilization. Enzyme immobilization by hydrogels has been extensively studied in the context of industrial enzyme stabilization, especially to organic solvents.[60] Enzymes can be loaded onto hydrogels without the need of a conjugation reaction, which simplifies the synthesis and stabilization process. And unlike polymer excipients that are difficult to remove from the enzyme solution, the macroscopic hydrogels can be easily separated by filtration or centrifugation. Due to these advantages, hydrogels have been frequently used for stabilization of enzymes as well as other proteins.[61-63] Herein, we propose a novel hydrogel system based on trehalose as an effective excipient for enhancing the stability of enzymes at elevated temperatures.

Trehalose is a non-reducing disaccharide that has been shown to stabilize proteins and cells against stresses such as heat,[64-66] desiccation,[67-69] and freezing.[70-72] Some animals accumulate

trehalose to significant levels in response to environmental stresses,[73, 74] emphasizing the ability of trehalose to stabilize biological molecules. Moreover, trehalose is generally regarded as safe (GRAS)[75] and is used in several pharmaceutical drugs as stabilizers.[76] Our group has previously utilized trehalose-based linear polymers as excipients[77] or conjugates[27] to stabilize proteins and retain their activity against heat and lyophilization. We sought to develop trehalose-based material to stabilize enzymes against heat and focused on hydrogels for the advantages described above.

We chose to study stabilization of phytase because of its importance in the animal feed industry. Phytase is a phosphohydrolytic enzyme that catalyzes the conversion of phosphate in indigestible phytic acid to a highly digestible form.[78-81] The conversion of phytic acid is essential for simple-stomached species such as swine, poultry, and fish to utilize this storage form of phosphate present in common feed grains such as corn, soy, and wheat.[78] In 2011, phytase accounted for approximately 60% of the $550 million global feed enzyme market.[82] Yet, the biggest challenge in the use of phytase in animal feeds is its low thermostability during steam heating of the pelleting process, during which the temperature between 70-90 °C is reached.[78, 83] Despite previous efforts to enhance its heat stability,[78, 83-85] a simple and cost-effective method is still of great interest. As described below, we have found that phytase retains 100% activity when heated to 90 °C in the presence of trehalose hydrogels.

3.2.2 Results and Discussion

Straightforward synthesis, commercially available starting materials, and simple purification steps are some of the most important factors in industrial-scale reactions.[86] Thus, the hydrogel was synthesized in only two steps. First, Williamson etherification using 4-vinylbenzyl chloride and trehalose yielded a crude product mixture that was subsequently precipitated into

DCM. The DCM wash contained mostly DMSO and some trehalose and mono- and di-substituted products, while the precipitate that was used for gelation consisted of unmodified trehalose and vinyl-substituted products (79 % mono-substituted, 16 % di-substituted, and 5 % tri-substituted) as measured by HPLC and LC-MS (Experimental Section Figure 3-11, Figure 3-12, and Table 3-1). We envisioned that the multi-substituted products of the crude monomer reaction mixture could be used as cross-linkers to synthesize a trehalose-based hydrogel directly from the crude reaction mixture (Scheme 3-2). Due to the presence of cross-linkers, polymerization would yield a hydrogel rather than a linear polymer.

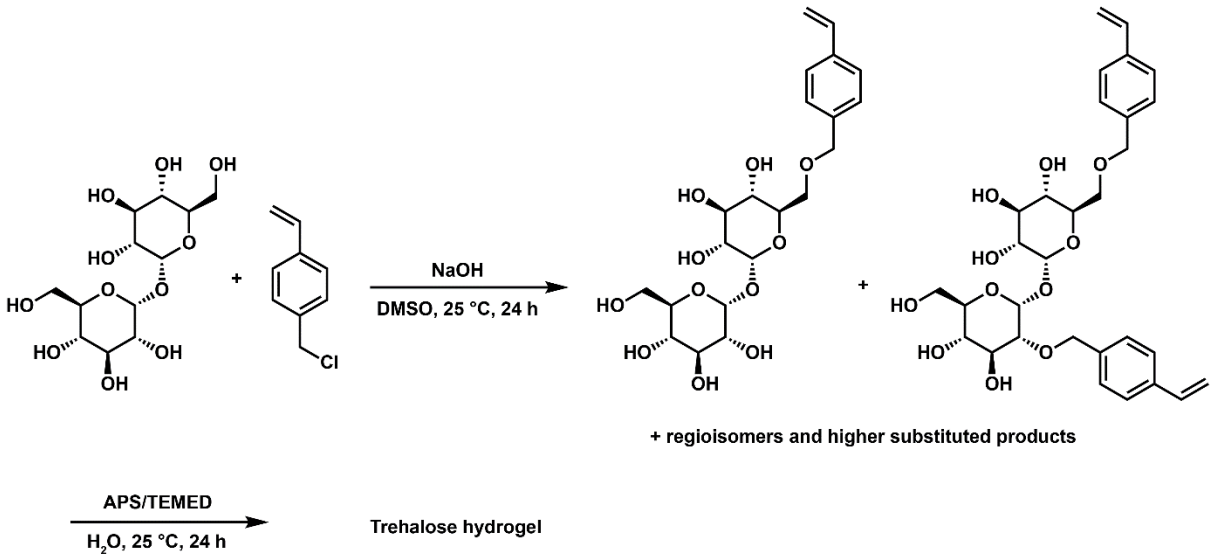

Scheme 3-2. Two-step synthesis of trehalose hydrogel.

The crude mixture was then polymerized by radical polymerization using a redox initiator pair, APS and TEMED. The crude mixture was dissolved in water with TEMED. After the addition of APS, the solution started gelling within 10 min at 25 °C, and the hydrogel network remained intact after lyophilization and rehydration. After 1 day, all of the di- and tri-substituted trehalose

had reacted (Experimental Section Figure 3-13). The crude gel was washed with a Soxhlet extractor for 3 days to remove unreacted monomers, residual initiator and trehalose, yielding a colorless hydrogel. The purified trehalose hydrogel was grounded into a powder with a mortar and pestle for ease of handling and to increase the surface area for internalization of phytase.

The purified hydrogel was characterized by a variable pressure SEM, as shown in Figure 3-7. The images revealed hydrogel architecture with micron-sized pores. Since phytase diameter is approximately 11.1 nm along the major axis as measured from the crystal structure (PDB: 1DKL),[87] phytase was thus expected to be incorporated within the hydrogel. To test this hypothesis, we observed the hydrogel under a confocal microscope after incubation in fluorescein isothiocyanate (FITC)-labeled phytase solution followed by a brief wash in water (Figure 3-8). An even distribution of the fluorophore throughout the gel matrix demonstrated that the phytase was fully internalized into the hydrogel and not simply adsorbed on the hydrogel surface. Because of the pore size, we anticipated that the enzyme would be released from the hydrogel when diluted with water. Indeed, the release profile of FITC-labeled phytase from the hydrogel after lyophilization showed that 78 % of the phytase is released in 6 hours followed by a gradual release (Figure 3-9), providing further evidence that the phytase is internalized inside the hydrogel. Similar release profile was observed when the phytase was released from a hydrated gel (Experimental Section Figure 3-14). This result also demonstrates that the gel can be used to recover enzyme after loading.

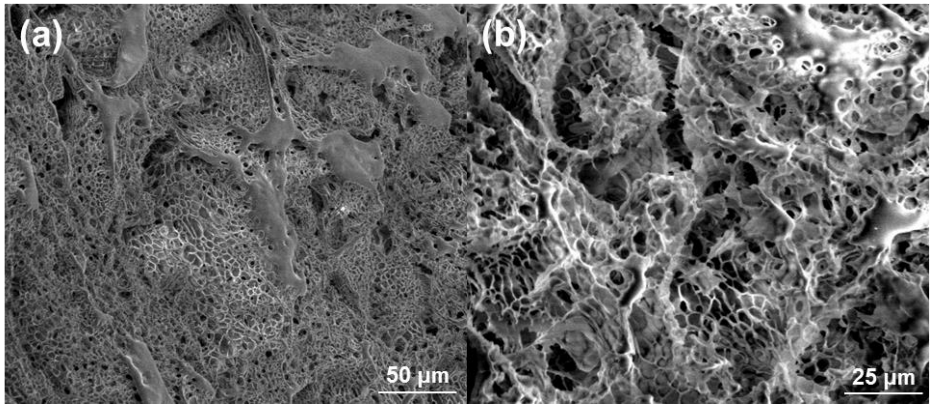

Figure 3-7. SEM images of trehalose hydrogel. (a) Images at 500X magnification and (b) at 1000X magnification.

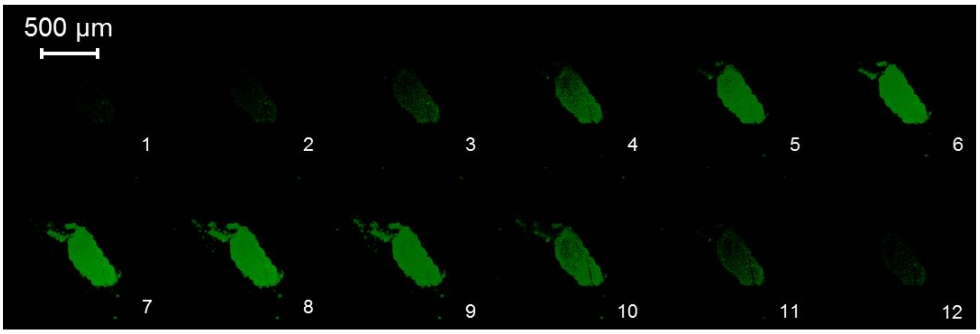

Figure 3-8. Confocal images of trehalose hydrogel incubated overnight in a solution containing FITC-labeled phytase and washed with deionized water. Numbers in the lower right corner indicate transaxial slice indices. Axial resolution = 2 µm.

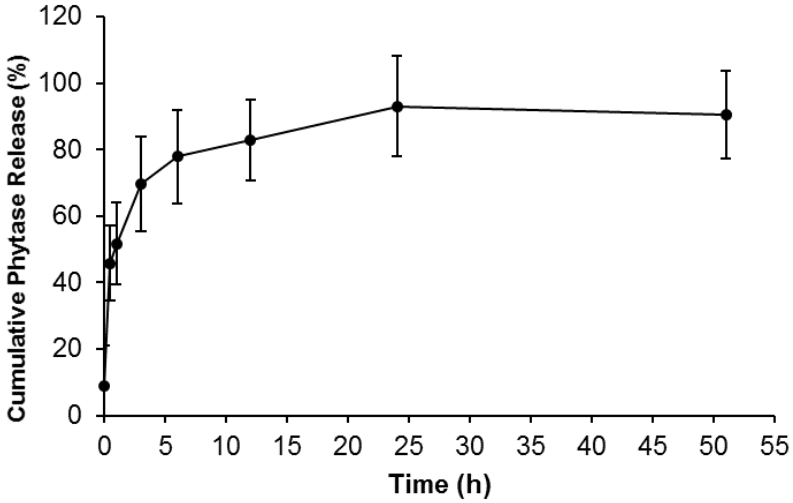

Figure 3-9. Release profile of FITC-labeled phytase from trehalose hydrogel after loading and lyophilization (n=6).

Currently in the animal feed industry, pelleting is the most common process for preparing animal feeds since it improves their efficiency and reduces nutrient excretion compared to mashed forms.[80, 88] Typically temperatures reach 70 - 90 °C for a few minutes during pelleting. For phytase in particular, the dry ingredients including phytase are mixed in a pelleting mill conditioner, reaching a temperature of 80 - 90 °C for 35 - 45 sec , followed by extrusion to produce the desired pellets. Thus, phytase was loaded into the hydrogel and heated in a condition simulating the steam pelleting process (90 °C, 1 min). The phytase solution was added to three different weight equivalents (1, 10, and 40) of lyophilized trehalose hydrogel and incubated for 24 h. The sample was lyophilized again, 53 wt % of water was added to the phytase-loaded trehalose hydrogel, and the gel was incubated for another 24 h to replicate the moisture level of the steam heating process. The water is essential for the pelleting process, but it also expedites denaturation of phytase under the extreme heating.[78, 83] The results showed that phytase heated in the presence of the hydrogel retained significantly higher activity for all weight equivalents tested. Even when only 1 weight equivalent of hydrogel was used, 81% activity was retained compared to the control that had not been heated, and 10 and 40 weight equivalents retained 100% enzyme activity (Figure 3-10). When the hydrogel was absent, only 39% of heated phytase remained active. he average activity indicated that 10 wt equiv of hydrogel to phytase was the optimal amount to completely retain the original phytase activity, while utilizing the minimal amount of hydrogel.

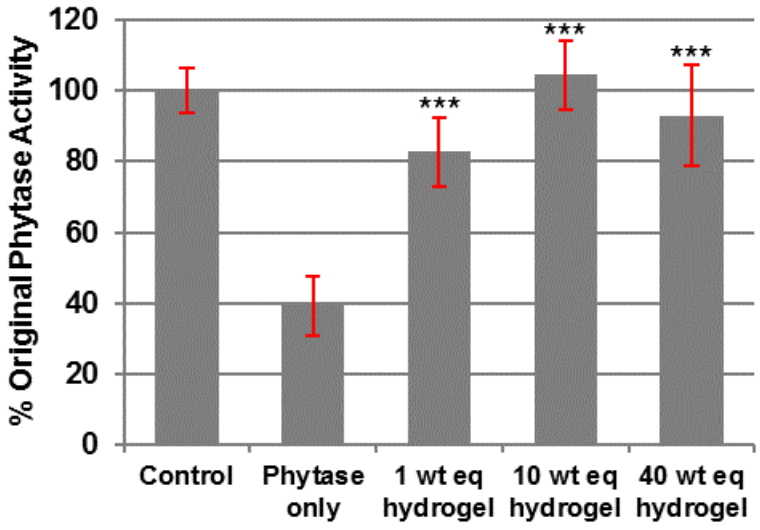

Figure 3-10. Activity of phytase after heating with different weight equivalents of trehalose hydrogel. All the samples except the control were heated for 1 min at 90 °C with 53 wt % of water (n=3). *** = $p < 0.005$ relative to phytase only.

The results demonstrated that the trehalose hydrogel can stabilize phytase against extreme heat conditions. The trehalose hydrogel may be suitable for industrial-scale applications as the synthesis only requires two steps and involves minimal purification that can be easily adapted to a large scale. Specifically, the proposed method uses chromatography-free purification, easily accessible starting materials, protecting group-free chemistry, and a minimal number of steps.[86]

Another advantage of hydrogel formulation is its ease of removal. The release results demonstrate that the protein of interest can be removed from the hydrogel. The release occurred over several hours with 78% release at 6 hours. However, this is with passive diffusion. Since the hydrogel is not soluble in water or organic solvents, it can be separated from the mixture by simple filtration or centrifugation. One can anticipate that by rinsing or pushing water through the system, or with the agitation that occurs in the gastrointestinal tract in the case of phytase-loaded hydrogel,the enzyme would be released faster. This is a potential advantage of the system since the hydrogel could be added and then removed from the protein after stress if so desired.

In addition, despite much research on the genetic engineering of enzymes for improving their thermal stability, multiple optimization iterations or enzyme-specific mutation strategies are usually required, accompanied with a higher cost.[89] Thus, the strategy described herein may be more flexible and cost effective than genetic engineering techniques. Since our group has already demonstrated that linear trehalose polymers stabilize various proteins against heating,[27, 77] the trehalose-based hydrogel hereby described may be readily applicable to thermal stabilization of a wide variety of industrially important enzymes and proteins.

3.2.3 Conclusions

We have detailed the synthesis of a trehalose hydrogel for thermal stabilization of phytase as a model enzyme. This hydrogel can be prepared via simple synthesis and purification steps, which are important considerations in industrial processes. The resulting trehalose hydrogel fully preserved the activity of phytase under temperatures relevant in the pelleting procedure for animal feed preparation. Currently, many enzymes in animal feeds lose the majority of their activity during this steam pelleting process. As demonstrated by the stabilization of phytase in this report, the trehalose hydrogel is a promising material for stabilizing various enzymes and proteins against high-temperature processes.

3.2.4 Experimental Section

Materials

All chemicals were purchased from Sigma-Aldrich and Fisher Scientific and were used without purification unless noted otherwise. All solvents for liquid chromatography mass spectrometry (LC-MS) were purchased from VWR or Fisher Scientific in LC-MS grade. Trehalose

was purchased from The Healthy Essential Management Corporation (Houston, TX), and was azeotropically dried with ethanol and kept under vacuum until use. Phytase was provided by Phytex, LLC.

Analytical Techniques

NMR spectra were recorded on a Bruker DRX 500 MHz spectrometer. LC-MS experiments were carried out on a Waters Acquity UPLC connected to a Waters LCT-Premier XE Time of Flight Instrument controlled by MassLynx 4.1 software. The mass spectrometer was equipped with a Multi-Mode Source operated in the electrospray mode. Trehalose samples were separated using an Acquity BEH C18 1.7 um column (2.1 × 50 mm) and were eluted with a gradient of 5 – 50% solvent B over 6 min (solvent A: water, solvent B: acetonitrile, both with 0.2% formic acid (vol/vol)). Mass spectra were recorded in the negative ion mode in the m/z range of 70–2000 with leucine enkephalin (Sigma L9133) as the lock mass standard. Preparatory reverse phase HPLC was carried out on a Shimadzu HPLC system equipped with a UV detector using a Luna 5 µm C18 100 Å column (preparatory: 5 µm, 250 × 21.2 mm) with monitoring at λ = 215 nm and 254 nm. A linear gradient solvent system (H_2O : methanol = 70:30 to 50:50) was used as the mobile phase at a flow rate of 10 mL/min. Scanning electron microscopy (SEM) images were acquired on a FEI Nova Nano 230 SEM in the UCLA Molecular and Nano Archaeology (MNA) facility under a low vacuum of 50 Pa and high voltage of 5 or 2.5 kV with a spot size of 3.0. Fluorescence images of the hydrogels were acquired using a confocal laser scanning microscope (Leica SP2 1P-FCS, Leica) at the CNSI Advanced Light Microscopy/Spectroscopy Shared Resource Facility at UCLA. Diameter of phytase (PDB: 1DKL)[90] was measured using Swiss-PdbViewer (Swiss Institute of Bioinformatics).[91] Fluorescence measurement was made on a

FlexStation II (Molecular Devices). Light absorbance for phytase activity assay was measured using a Biotek EPOCH microtiter plate reader.

One Pot Reaction for Synthesis of Trehalose Monomers and Cross-Linkers

The one pot reaction for the monomers and cross-linkers was performed by modifying a previously reported literature procedure.[77] Sodium hydroxide (NaOH, 4.44 g, 1.11×10^{-1} mol) was added to dimethyl sulfoxide (DMSO, 96 mL). After stirring for 5 min, trehalose (4.86 g, 1.42×10^{-2} mol) was added to the reaction. After all the trehalose was dissolved, 4-vinylbenzyl chloride (0.4 mL, 2.84×10^{-3} mol) was slowly added to the reaction and was stirred for 24 h at 25 °C. The crude product was then precipitated into 2 L of DCM to remove highly modified trehalose. The resulting solid was dried *in vacuo* and used for gelation without further purification.

Preparation of Phytase-Loaded Trehalose Hydrogel

The crude mixture (3.23 g) from the previous Williamson etherification was dissolved in H_2O (3.23 mL) and then treated with tetramethylethylenediamine (TEMED, 16 μL, 1.07×10^{-4} mol). Next, 807 μL of 10 mg/mL aqueous stock solution of ammonium persulfate (APS, 8.07 mg, 3.54×10^{-5} mol) was added to initiate the gelation. The solution started gelling within 10 min at 25 °C. LC-MS was used to quantify the extent of conversion, by comparing the relative amount of mono-substituted trehalose compared to unmodified trehalose before and after gelation. LC-MS analysis showed that all cross-linkers had reacted after 24 h. After the gelation, the gel was washed with a Soxhlet extractor for 3 days with H_2O to remove unreacted monomers. The hydrogel was lyophilized and then ground into fine powder. 10 μL of phytase solution (40 mg/mL) was added to each dried gel to make phytase : hydrogel ratios of 1:1, 1:10, and 1:40 weight equivalents. The

gels were incubated at 4 °C with the phytase solution for 24 h and lyophilized to yield a white powder for testing in the heat burden study.

Fluorescein Isothiocyanate (FITC) Labeling of Phytase

Phytase (2 mg, 3.57×10^{-2} μmol) and FITC (0.3 mg, 7.71×10^{-1} μmol) were dissolved in 50 mM borate buffer, pH 8.5 (1 mL). The mixture was magnetically stirred at room temperature for an hour. Excess FITC was removed by repeated centrifugation through a 3,000 Da MWCO membrane using 0.5 mL centrifugal filtration tubes until no FITC was detected by UV-Vis in filtrate. Degree of labeling was 0.28 FITC per phytase as determined by UV absorbance.[92]

Release of Phytase from Trehalose Hydrogel

FITC-labeled phytase (74 mg/mL) in 0.1 M sodium acetate buffer (pH 5.0, 10 μL) was added to 4 mg of trehalose hydrogel. The mixture was incubated at 4 °C for 24 h, and then lyophilized. To the gel was added 1000 μL buffer to initiate the passive diffusion of the phytase from the hydrogel. Aliquots (200 μL) were taken at respective time points and the samples were immediately replenished with fresh buffer. The concentrations of the time point aliquots were calculated from the fluorescence measured on a spectrofluorometer using a FITC-labeled phytase calibration curve.

Heat Burden Studies of Phytase

To the dried hydrogel and phytase mixture, 53 wt % of H_2O with respect to the phytase was added. The hydrogel was incubated at 4 °C for 24 h with gentle rocking to evenly distribute

the solution. The hydrogel was then heated at 90 °C for 1 min, and diluted with 0.1 M sodium acetate buffer, pH 5, and incubated for at least 24 h prior to the activity assay.

Phytase Activity Assay

The control and heat treated hydrogels (10 uL) were first diluted in 10 mL of 0.2 M sodium citrate pH 5.5 buffer, and 0.5 mL aliquots of diluted sample were transferred to each of four reaction tubes (1 blank and 3 sample). To all sample tubes, 0.5 mL of 1% phytic acid solution (0.2 M sodium citrate buffer, pH 5.5) was added and the tubes were incubated at 37 °C for 15 minutes. The reactions were then quenched by the addition of 1.0 ml of 15% trichloroacetic acid, and 0.5 mL of phytic acid was added to the blank tubes. Samples (30 uL) were diluted ten-fold with distilled water, and the diluted solutions (150 uL) were treated with 150 uL of 1:3:1 solution of 2.5% ammonium molybdate : 10% sulfuric acid : 10% ascorbic acid in a microtiter plate. The plate was incubated in a 50 °C water bath for 15 minutes, cooled at 4 °C for 15 minutes, and the 820 nm absorbance of individual wells were measured. Phytase activity (FTU) is defined as the amount of enzyme that catalyzes the release of 1.0 micromole of inorganic phosphate per minute from 1% phytic acid in pH 5.5 buffer at 37 °C.

Statistical Analysis

One-tailed Student's t-test assuming unequal sample variance was used. Results were considered significantly different if $p < 0.05$.

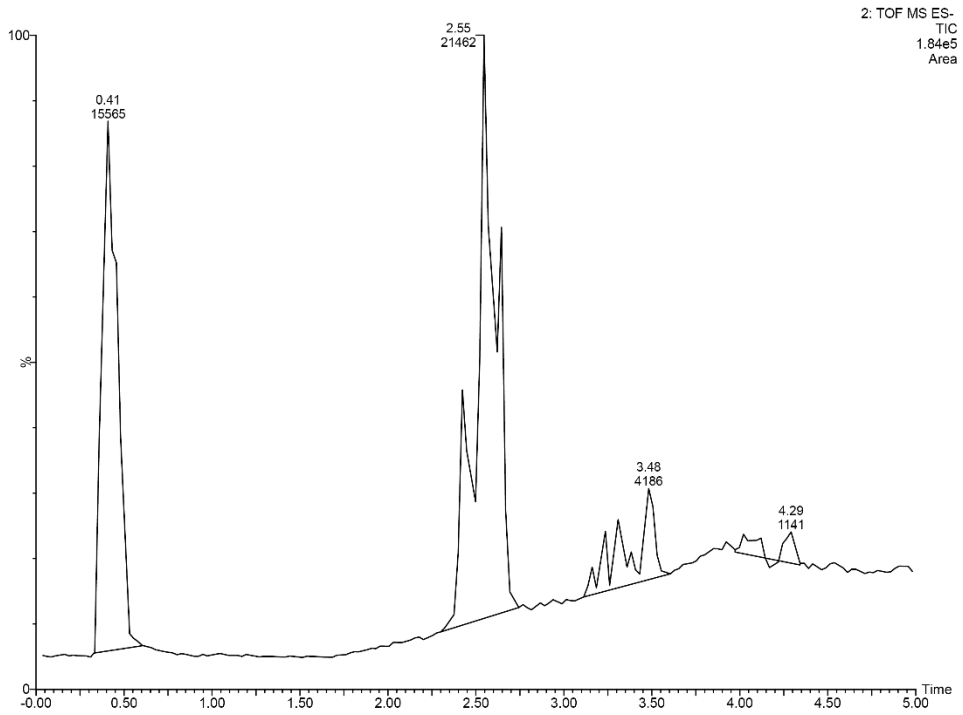

Figure 3-11. LC-MS chromatogram of crude styrenyl ether trehalose mixture after precipitation in DCM.

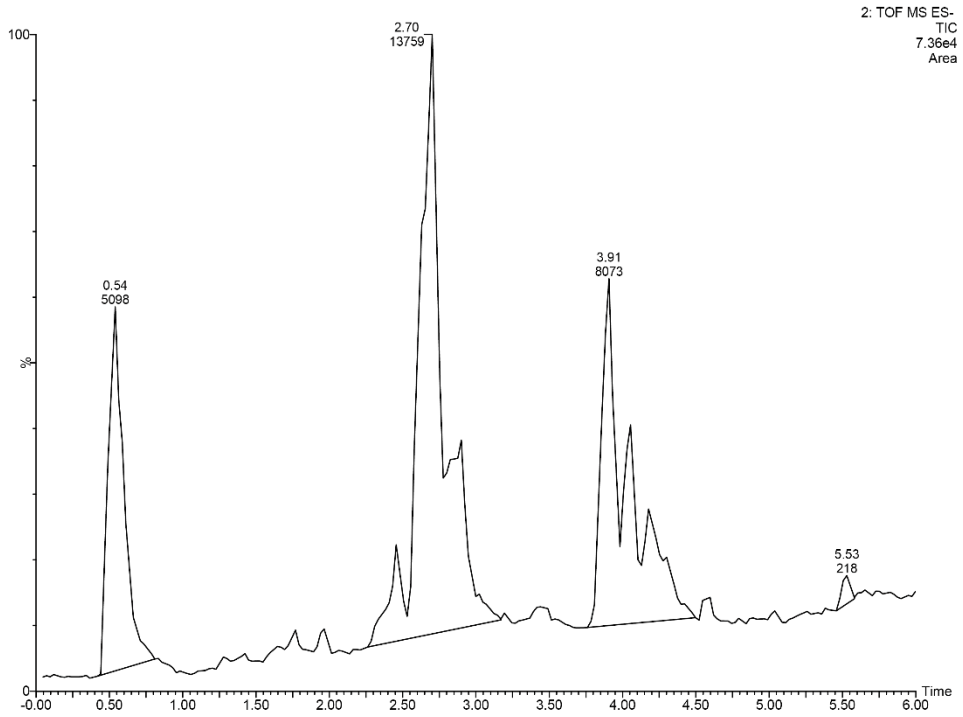

Figure 3-12. LC-MS chromatogram of the DCM wash of the crude styrenyl ether trehalose mixture.

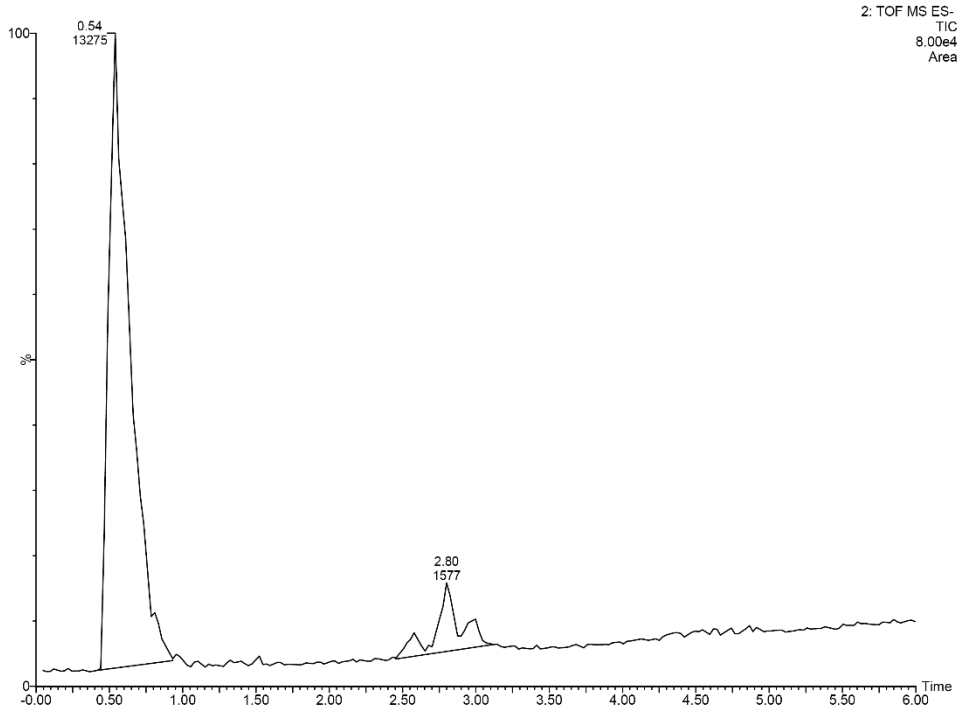

Figure 3-13. LC-MS chromatogram of the trehalose hydrogel reaction mixture after 1 d.

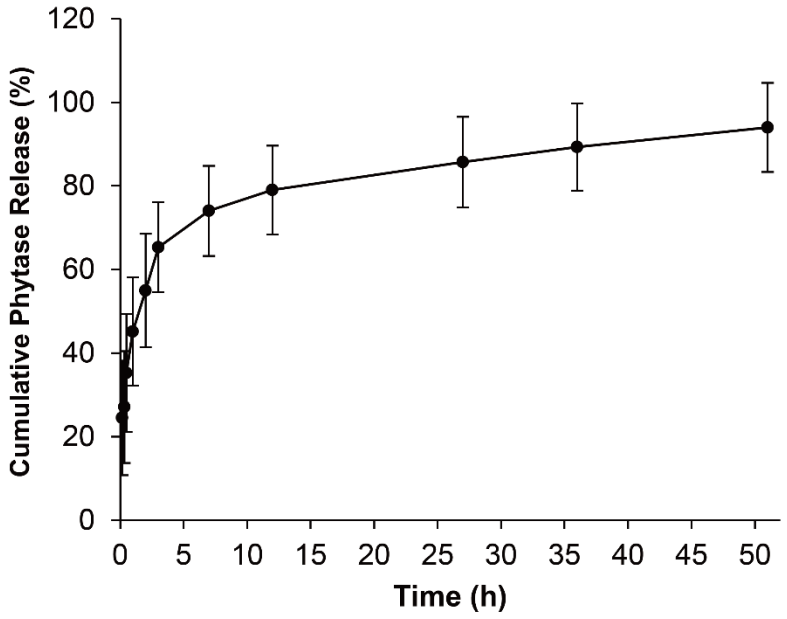

Figure 3-14. Release profile of FITC-labeled phytase from hydrated trehalose hydrogel (n = 6).

Table 3-1. Theoretical and observed masses of $[M+HCOO]^-$ ion of trehalose and its derivatives from LC-MS chromatogram in Figure 3-12.

	Retention time (min)	Theoretical mass (m/z)	Observed mass (m/z)	Δ m/z (ppm)
Trehalose	0.6	387.1139	387.1143	-1.1
Mono-substituted	2.5	503.1765	503.1762	0.5
	2.8	503.1765	503.1720	8.9
	2.9	503.1765	503.1765	-0.1
Di-substituted	4.4	619.2391	619.2369	3.5
Tri-substituted	5.5	735.3017	735.3012	0.6

3.3 References

(1) Hoffman, A. S. Hydrogels for biomedical applications. *Adv. Drug Del. Rev.* **2012,** *64*, 18.

(2) Vermonden, T.; Censi, R.; Hennink, W. E. Hydrogels for protein delivery. *Chem. Rev.* **2012,** *112*, 2853.

(3) Drury, J. L.; Mooney, D. J. Hydrogels for tissue engineering: scaffold design variables and applications. *Biomaterials* **2003,** *24*, 4337.

(4) Brown, L. R. Commercial challenges of protein drug delivery. *Expert Opin. Drug Deliv.* **2005,** *2*, 29.

(5) Burdick, J.; Chase, H. P.; Slover, R. H.; Knievel, K.; Scrimgeour, L.; Maniatis, A. K.; Klingensmith, G. J. Missed insulin meal boluses and elevated hemoglobin A1c levels in children receiving insulin pump therapy. *Pediatrics* **2004,** *113*, e221.

(6) Brownlee, M.; Cerami, A. Glucose-Controlled Insulin-Delivery System - Semi-Synthetic Insulin Bound to Lectin. *Science* **1979,** *206*, 1190.

(7) Kim, J. J.; Park, K. Modulated insulin delivery from glucose-sensitive hydrogel dosage forms. *J. Controlled Release* **2001,** *77*, 39.

(8) Yin, R. X.; Wang, K. M.; Du, S.; Chen, L.; Nie, J.; Zhang, W. J. Design of genipin-crosslinked microgels from concanavalin A and glucosyloxyethyl acrylated chitosan for glucose-responsive insulin delivery. *Carbohydr. Polym.* **2014,** *103*, 369.

(9) Matsumoto, A.; Ishii, T.; Nishida, J.; Matsumoto, H.; Kataoka, K.; Miyahara, Y. A synthetic approach toward a self-regulated insulin delivery system. *Angew. Chem. Int. Ed.* **2012,** *51*, 2124.

(10) Wu, Q.; Wang, L.; Yu, H.; Wang, J.; Chen, Z. Organization of glucose-responsive systems and their properties. *Chem. Rev.* **2011,** *111*, 7855.

(11) Gough, D. A.; Armour, J. C. Development of the implantable glucose sensor: What are the prospects and why is it taking so long? *Diabetes* **1995,** *44*, 1005.

(12) He, C.; Liu, J.; Xie, L.; Zhang, Q.; Li, C.; Gui, D.; Zhang, G.; Wu, C. Activity and thermal stability improvements of glucose oxidase upon adsorption on core− shell PMMA− BSA nanoparticles. *Langmuir* **2009,** *25*, 13456.

(13) Renard, E. Implantable closed-loop glucose-sensing and insulin delivery: the future for insulin pump therapy. *Curr. Opin. Pharm.* **2002,** *2*, 708.

(14) Brooks, W. L. A.; Sumerlin, B. S. Synthesis and Applications of Boronic Acid-Containing Polymers: From Materials to Medicine. *Chem. Rev.* **2016,** *116*, 1375.

(15) Cambre, J. N.; Sumerlin, B. S. Biomedical applications of boronic acid polymers. *Polymer* **2011,** *52*, 4631.

(16) Bapat, A. P.; Roy, D.; Ray, J. G.; Savin, D. A.; Sumerlin, B. S. Dynamic-covalent macromolecular stars with boronic ester linkages. *J. Am. Chem. Soc.* **2011,** *133*, 19832.

(17) Yesilyurt, V.; Webber, M. J.; Appel, E. A.; Godwin, C.; Langer, R. S.; Anderson, D. G. Injectable Self-Healing Glucose-Responsive Hydrogels with pH-Regulated Mechanical Properties. *Adv. Mater.* **2016,** *28*, 86.

(18) Dong, Y.; Wang, W.; Veiseh, O.; Appel, E. A.; Xue, K.; Webber, M. J.; Tang, B. C.; Yang, X.; Weir, G. C.; Langer, R. S. Injectable and Glucose-Responsive Hydrogels Based on Boronic Acid-Glucose Complexation. *Langmuir* **2016,** *32*, 8743.

(19) Wang, Y.; Chai, Z.; Ma, L.; Shi, C.; Shen, T.; Song, J. Fabrication of boronic acid-functionalized nanoparticles via boronic acid-diol complexation for drug delivery. *RSC Advances* **2014,** *4*, 53877.

(20) Pryce, R. Diabetic ketoacidosis caused by exposure of insulin pump to heat and sunlight. *Br. Med. J.* **2009,** *338*, a2218.

(21) Weiss, R. C.; van Amerongen, D.; Bazalo, G.; Aagren, M.; Bouchard, J. R. Economic benefits of improved insulin stability in insulin pumps. *Managed care* **2011,** *20*, 42.

(22) Hinds, K. D.; Kim, S. W. Effects of PEG conjugation on insulin properties. *Adv. Drug Del. Rev.* **2002,** *54*, 505.

(23) Heise, T.; Nosek, L.; Spitzer, H.; Heinemann, L.; Niemoller, E.; Frick, A. D.; Becker, R. H. Insulin glulisine: a faster onset of action compared with insulin lispro. *Diabetes Obes. Metab.* **2007,** *9*, 746.

(24) Leobandung, W.; Ichikawa, H.; Fukumori, Y.; Peppas, N. A. Preparation of stable insulin-loaded nanospheres of poly (ethylene glycol) macromers and N-isopropyl acrylamide. *J. Controlled Release* **2002,** *80*, 357.

(25) Akiyoshi, K.; Kobayashi, S.; Shichibe, S.; Mix, D.; Baudys, M.; Kim, S. W.; Sunamoto, J. Self-assembled hydrogel nanoparticle of cholesterol-bearing pullulan as a carrier of protein drugs: complexation and stabilization of insulin. *J. Controlled Release* **1998,** *54*, 313.

(26) Lee, J.; Lin, E.-W.; Lau, U. Y.; Hedrick, J. L.; Bat, E.; Maynard, H. D. Trehalose Glycopolymers as Excipients for Protein Stabilization. *Biomacromolecules* **2013,** *14*, 2561.

(27) Mancini, R. J.; Lee, J.; Maynard, H. D. Trehalose Glycopolymers for Stabilization of Protein Conjugates to Environmental Stressors. *J. Am. Chem. Soc.* **2012,** *134*, 8474.

(28) Liu, Y.; Lee, J.; Mansfield, K. M.; Ko, J. H.; Sallam, S.; Wesdemiotis, C.; Maynard, H. D. Trehalose Glycopolymer Enhances Both Solution Stability and Pharmacokinetics of a Therapeutic Protein. *Bioconj. Chem.* **2017,** *28*, 836.

(29) Messina, M. S.; Ko, J. H.; Yang, Z.; Strouse, M. J.; Houk, K. N.; Maynard, H. D. Effect of trehalose polymer regioisomers on protein stabilization. *Polym. Chem.* **2017,** *8*, 4781.

(30) Pelegri-O'Day, E. M.; Paluck, S. J.; Maynard, H. D. Substituted Polyesters by Thiol–Ene Modification: Rapid Diversification for Therapeutic Protein Stabilization. *J. Am. Chem. Soc.* **2017,** *139*, 1145.

(31) James, T. D.; Sandanayake, K. R. A. S.; Shinkai, S. Saccharide sensing with molecular receptors based on boronic acid. *Angew. Chem. Int. Ed.* **1996,** *35*, 1910.

(32) Van den Berg, R.; Peters, J. A.; Van Bekkum, H. The Structure and (Local) Stability-Constants of Borate Esters of Monosacchharides and Disaccharides as Studied by B-11 and C-13 Nmr-Spectroscopy. *Carbohydr. Res.* **1994,** *253*, 1.

(33) Deshayes, S.; Cabral, H.; Ishii, T.; Miura, Y.; Kobayashi, S.; Yamashita, T.; Matsumoto, A.; Miyahara, Y.; Nishiyama, N.; Kataoka, K. Phenylboronic acid-installed polymeric micelles for targeting sialylated epitopes in solid tumors. *J. Am. Chem. Soc.* **2013,** *135*, 15501.

(34) Roy, D.; Cambre, J. N.; Sumerlin, B. S. Triply-responsive boronic acid block copolymers: solution self-assembly induced by changes in temperature, pH, or sugar concentration. *Chem. Commun.* **2009**, 2106.

(35) Deng, C. C.; Brooks, W. L. A.; Abboud, K. A.; Sumerlin, B. S. Boronic Acid-Based Hydrogels Undergo Self-healing at Neutral and Acidic pH. *ACS Macro Lett.* **2015,** *4*, 220.

(36) Lee, L. L. Y.; Lee, J. C. Thermal-Stability of Proteins in the Presence of Poly(Ethylene Glycols). *Biochemistry (Mosc.)* **1987,** *26*, 7813.

(37) Senske, M.; Tork, L.; Born, B.; Havenith, M.; Herrmann, C.; Ebbinghaus, S. Protein stabilization by macromolecular crowding through enthalpy rather than entropy. *J. Am. Chem. Soc.* **2014,** *136*, 9036.

(38) Amirgoulova, E. V.; Groll, J.; Heyes, C. D.; Ameringer, T.; Rocker, C.; Moller, M.; Nienhaus, G. U. Biofunctionalized polymer surfaces exhibiting minimal interaction towards immobilized proteins. *ChemPhysChem* **2004,** *5*, 552.

(39) Lee, E. S.; Gao, Z.; Bae, Y. H. Recent progress in tumor pH targeting nanotechnology. *J. Controlled Release* **2008,** *132*, 164.

(40) Schreiber, A. B.; Hoebeke, J.; Bergman, Y.; Haimovich, J.; Strosberg, A. D. A quantitative fluorometric assay for detection and characterization of Fc receptors. *J. Immunol.* **1978,** *121*, 19.

(41) Ye, J.; Chen, Y.; Liu, Z. A boronate affinity sandwich assay: an appealing alternative to immunoassays for the determination of glycoproteins. *Angew. Chem., Int. Ed.* **2014,** *53*, 10386.

(42) Zhang, W.; Liu, W.; Li, P.; Xiao, H.; Wang, H.; Tang, B. A Fluorescence Nanosensor for Glycoproteins with Activity Based on the Molecularly Imprinted Spatial Structure of the Target and Boronate Affinity. *Angew. Chem. Int. Ed.* **2014,** *53*, 12489.

(43) Somero, G. N. PROTEINS AND TEMPERATURE. *Annu. Rev. Physiol.* **1995,** *57*, 43.

(44) Rader, A. J.; Hespenheide, B. M.; Kuhn, L. A.; Thorpe, M. F. Protein unfolding: Rigidity lost. *Proc. Natl. Acad. Sci. U. S. A.* **2002,** *99*, 3540.

(45) Fágáin, C. Ó. Understanding and increasing protein stability. *Biochim. Biophys. Acta* **1995,** *1252*, 1.

(46) Ravindran, V.; Son, J.-H. Feed enzyme technology: present status and future developments. *Recent patents on food, nutrition & agriculture* **2011,** *3*, 102.

(47) Samejima, H.; Kimura, K.; Ado, Y. RECENT DEVELOPMENT AND FUTURE-DIRECTIONS OF ENZYME TECHNOLOGY IN JAPAN. *Biochimie* **1980,** *62*, 299.

(48) Schmid, A.; Dordick, J. S.; Hauer, B.; Kiener, A.; Wubbolts, M.; Witholt, B. Industrial biocatalysis today and tomorrow. *Nature* **2001,** *409*, 258.

(49) DeSantis, G.; Jones, J. B. Chemical modification of enzymes for enhanced functionality. *Curr. Opin. Biotechnol.* **1999,** *10*, 324.

(50) Ryan, O.; Smyth, M. R.; Fagain, C. O. THERMOSTABILIZED CHEMICAL DERIVATIVES OF HORSERADISH-PEROXIDASE. *Enzyme Microb. Technol.* **1994,** *16*, 501.

(51) Frosst, P.; Blom, H. J.; Milos, R.; Goyette, P.; Sheppard, C. A.; Matthews, R. G.; Boers, G. J. H.; Denheijer, M.; Kluijtmans, L. A. J.; Vandenheuvel, L. P.; Rozen, R. A CANDIDATE GENETIC RISK FACTOR FOR VASCULAR-DISEASE - A COMMON MUTATION IN METHYLENETETRAHYDROFOLATE REDUCTASE. *Nat. Genet.* **1995,** *10*, 111.

(52) Matthews, B. W.; Nicholson, H.; Becktel, W. J. ENHANCED PROTEIN THERMOSTABILITY FROM SITE-DIRECTED MUTATIONS THAT DECREASE THE ENTROPY OF UNFOLDING. *Proc. Natl. Acad. Sci. U. S. A.* **1987,** *84*, 6663.

(53) Kumar, S.; Tsai, C. J.; Nussinov, R. Factors enhancing protein thermostability. *Protein Eng.* **2000,** *13*, 179.

(54) Imanaka, T.; Shibazaki, M.; Takagi, M. A NEW WAY OF ENHANCING THE THERMOSTABILITY OF PROTEASES. *Nature* **1986,** *324*, 695.

(55) Gaertner, H. F.; Puigserver, A. J. INCREASED ACTIVITY AND STABILITY OF POLY(ETHYLENE GLYCOL)-MODIFIED TRYPSIN. *Enzyme Microb. Technol.* **1992,** *14*, 150.

(56) Longo, M. A.; Combes, D. Thermostability of modified enzymes: a detailed study. *J. Chem. Technol. Biotechnol.* **1999,** *74*, 25.

(57) Yang, Z.; Domach, M.; Auger, R.; Yang, F. X.; Russell, A. J. Polyethylene glycol-induced stabilization of subtilisin. *Enzyme Microb. Technol.* **1996,** *18*, 82.

(58) Kazan, D.; Erarslan, A. Stabilization of Escherichia coli penicillin G acylase by polyethylene glycols against thermal inactivation. *Appl. Biochem. Biotechnol.* **1997,** *62*, 1.

(59) Tomita, S.; Nagasaki, Y.; Shiraki, K. Different mechanisms of action of poly(ethylene glycol) and arginine on thermal inactivation of lysozyme and ribonuclease A. *Biotechnol. Bioeng.* **2012,** *109*, 2543.

(60) Sheldon, R. A. Enzyme Immobilization: The Quest for Optimum Performance. *Adv. Synth. Catal.* **2007,** *349*, 1289.

(61) Leobandung, W.; Ichikawa, H.; Fukumori, Y.; Peppas, N. A. Preparation of stable insulin-loaded nanospheres of poly(ethylene glycol) macromers and N-isopropyl acrylamide. *J Control Release* **2002,** *80*, 357.

(62) Akiyoshi, K.; Sasaki, Y.; Sunamoto, J. Molecular chaperone-like activity of hydrogel nanoparticles of hydrophobized pullulan: thermal stabilization with refolding of carbonic anhydrase B. *Bioconjug. Chem.* **1999,** *10*, 321.

(63) Wang, Q.; Yang, Z.; Gao, Y.; Ge, W.; Wang, L.; Xu, B. Enzymatic hydrogelation to immobilize an enzyme for high activity and stability. *Soft Matter* **2008,** *4*, 550.

(64) Lippert, K.; Galinski, E. Enzyme stabilization be ectoine-type compatible solutes: protection against heating, freezing and drying. *Appl. Microbiol. Biotechnol.* **1992,** *37*, 61.

(65) Kaushik, J. K.; Bhat, R. Why Is Trehalose an Exceptional Protein Stabilizer?: AN ANALYSIS OF THE THERMAL STABILITY OF PROTEINS IN THE PRESENCE OF THE COMPATIBLE OSMOLYTE TREHALOSE. *Journal of Biological Chemistry* **2003,** *278*, 26458.

(66) Baptista, R. P.; Pedersen, S.; Cabrita, G. J.; Otzen, D. E.; Cabral, J. M.; Melo, E. P. Thermodynamics and mechanism of cutinase stabilization by trehalose. *Biopolymers* **2008,** *89*, 538.

(67) Guo, N.; Puhlev, I.; Brown, D. R.; Mansbridge, J.; Levine, F. Trehalose expression confers desiccation tolerance on human cells. *Nat. Biotechnol.* **2000,** *18*, 168.

(68) Hengherr, S.; Heyer, A. G.; Kohler, H. R.; Schill, R. O. Trehalose and anhydrobiosis in tardigrades--evidence for divergence in responses to dehydration. *FEBS J.* **2008,** *275*, 281.

(69) Crowe, J. H.; Crowe, L. M.; Chapman, D. Preservation of membranes in anhydrobiotic organisms: the role of trehalose. *Science* **1984,** *223*, 701.

(70) Beattie, G. M.; Crowe, J. H.; Lopez, A. D.; Cirulli, V.; Ricordi, C.; Hayek, A. Trehalose: a cryoprotectant that enhances recovery and preserves function of human pancreatic islets after long-term storage. *Diabetes* **1997,** *46*, 519.

(71) Sundaramurthi, P.; Suryanarayanan, R. Trehalose Crystallization During Freeze-Drying: Implications On Lyoprotection. *The Journal of Physical Chemistry Letters* **2009,** *1*, 510.

(72) Duong, T.; Barrangou, R.; Russell, W. M.; Klaenhammer, T. R. Characterization of the tre locus and analysis of trehalose cryoprotection in Lactobacillus acidophilus NCFM. *Appl. Environ. Microbiol.* **2006,** *72*, 1218.

(73) Westh, P.; Ramløv, H. Trehalose accumulation in the tardigrade Adorybiotus coronifer during anhydrobiosis. *J. Exp. Zool.* **1991,** *258*, 303.

(74) Madin, K. A. C.; Crowe, J. H. Anhydrobiosis in nematodes: Carbohydrate and lipid metabolism during dehydration. *J. Exp. Zool.* **1975,** *193*, 335.

(75) Jain, N. K.; Roy, I. Effect of trehalose on protein structure. *Protein science : a publication of the Protein Society* **2009,** *18*, 24.

(76) Ohtake, S.; Wang, Y. J. Trehalose: current use and future applications. *Journal of pharmaceutical sciences* **2011,** *100*, 2020.

(77) Lee, J.; Lin, E. W.; Lau, U. Y.; Hedrick, J. L.; Bat, E.; Maynard, H. D. Trehalose Glycopolymers as Excipients for Protein Stabilization. *Biomacromolecules* **2013,** *14*, 2561.

(78) Lei, X. G.; Weaver, J. D.; Mullaney, E.; Ullah, A. H.; Azain, M. J. Phytase, a New Life for an "Old" Enzyme. *Annual Review of Animal Biosciences* **2013,** *1*, 283.

(79) Kuhn, I.; Partanen, K. Phytase improves apparent total tract digestibility of phosphorus and calcium in piglets fed diets with adequate or reduced phosphorus content. *Journal of Animal Science* **2012,** *90*, 194.

(80) Nahm, K. H. Efficient Feed Nutrient Utilization to Reduce Pollutants in Poultry and Swine Manure. *Crit. Rev. Environ. Sci. Technol.* **2002,** *32*, 1.

(81) Silversides, F. G.; Scott, T. A.; Bedford, M. R. The effect of phytase enzyme and level on nutrient extraction by broilers. *Poult. Sci.* **2004,** *83*, 985.

(82) Adeola, O.; Cowieson, A. J. BOARD-INVITED REVIEW: Opportunities and challenges in using exogenous enzymes to improve nonruminant animal production. *Journal of Animal Science* **2011,** *89*, 3189.

(83) Slominski, B. A.; Davie, T.; Nyachoti, M. C.; Jones, O. Heat stability of endogenous and microbial phytase during feed pelleting. *Livestock Science* **2007,** *109*, 244.

(84) Hughes, K. P.; Soares, J. H., Jr. Efficacy of phytase on phosphorus utilization in practical diets fed to striped bass Morone saxatilis. *Aquacult. Nutr.* **1998,** *4*, 133.

(85) Cao, L.; Wang, W.; Yang, C.; Yang, Y.; Diana, J.; Yakupitiyage, A.; Luo, Z.; Li, D. Application of microbial phytase in fish feed. *Enzyme Microb. Technol.* **2007,** *40*, 497.

(86) Kuttruff, C. A.; Eastgate, M. D.; Baran, P. S. Natural product synthesis in the age of scalability. *Nat. Prod. Rep.* **2014,** *31*, 419.

(87) Oakley, A. J. The structure of Aspergillus niger phytase PhyA in complex with a phytate mimetic. *Biochem. Biophys. Res. Commun.* **2010,** *397*, 745.

(88) Thomas, M.; Van der Poel, A. Physical quality of pelleted animal feed 1. Criteria for pellet quality. *Anim. Feed Sci. Technol.* **1996,** *61*, 89.

(89) Himmel, M. E.; Ding, S. Y.; Johnson, D. K.; Adney, W. S.; Nimlos, M. R.; Brady, J. W.; Foust, T. D. Biomass recalcitrance: engineering plants and enzymes for biofuels production. *Science* **2007,** *315*, 804.

(90) Lim, D.; Golovan, S.; Forsberg, C. W.; Jia, Z. Crystal structures of Escherichia coli phytase and its complex with phytate. *Nat. Struct. Biol.* **2000,** *7*, 108.

(91) Guex, N.; Peitsch, M. C. SWISS-MODEL and the Swiss-PdbViewer: An environment for comparative protein modeling. *Electrophoresis* **1997,** *18*, 2714.

(92) Schreiber, A. B.; Haimovich, J. Quantitative fluorometric assay for detection and characterization of Fc receptors. *Methods Enzymol.* **1983,** *93*, 147.

Chapter 4.

Trehalose Polymer-Protein Drug Conjugates for Therapeutic Applications

This chapter contains portions of an edited version of the following published paper:
Reprinted with permission from Liu, Y.;† Lee, J.;† Mansfield, K. M.; Ko, J. H.; Sallam, S.; Wesdemiotis, C.; Maynard, H. D. *Bioconj. Chem.* **2017**, *28*, 836. († Equal contribution).

Proteins are an important class of therapeutics with growing potential and distinct advantages compared to the traditional small molecule drugs. However, they frequently suffer from physical instability and low pharmacokinetics, which lead to consequences that range from inconvenience and increased financial burden on the patients to medical emergencies from underdosage, if the protein is stable enough to be used as a drug at all. Given that trehalose polymers are excellent protein stabilizers, conjugating the polymers to protein drugs would enhance both their stability by the protective effect of trehalose and serum half-life by decreased renal filtration as well as other elimination pathways.

Insulin is first used as a model drug to test the hypothesis that trehalose polymer conjugation is an effective strategy to enhance solution stability and pharmacokinetics of protein drugs. In the second part of this chapter, the strategy is extended to granulocyte colony-stimulating factor and extensive *in vivo* evaluations of the conjugate including biodistribution, toxicity, and immunogenicity are conducted. Trehalose polymer conjugates of these two model protein drugs demonstrate the great potential of this approach to stabilize a range of therapeutic drugs both inside and outside the body.

4.1 Enhancing Solution Stability and Pharmacokinetics of Insulin by Trehalose Polymer Conjugation

4.1.1 Introduction

Protein drugs have high specificity and potency, and as a result more than 130 proteins or peptides are approved by the FDA.[1] However, proteins also face substantial challenges including short half-lives in the bloodstream, as well as chemical and physical instability upon exposure to environmental stressors leading to short shelf lives.[2-4] Covalent attachment of poly(ethylene glycol) (PEG) to proteins, or PEGylation, is the most widely used polymer conjugation technique to address the pharmacokinetic challenge of proteins, and ten FDA-approved PEGylated proteins are currently on the market.[2, 5-7] However, linear PEG does not necessarily improve the stability of proteins to environmental stressors during storage and transport: close to 80% of all protein drugs need to be refrigerated or frozen even in the presence of PEG or other stabilizing excipients.[1] This lowers patient compliance and quality of life and increases costs due to refrigeration during delivery and storage.[3, 4, 7] More importantly, denaturation of protein drugs as a result of inadequate storage can result in life-threatening events caused by inadequate dosage.

While many PEG alternatives are under development, most have been employed to increase the *in vivo* half-life of protein therapeutics and few have the ability to increase environmental stability.[7, 8] Protein-polymer conjugates with improved *in vivo* half-lives have been successfully prepared with polymers such as poly-(*N*-(2-hydroxypropyl) methacrylamide) (pHPMA),[9-11] polyoxazolines,[12-14] and hydroxyethyl starch (HES).[15, 16] However, conjugating these polymers does not necessarily improve protein stability during storage. There are few recent examples of protein-stabilizing polymers such as zwitterionic carboxybetaine polymer for enzymes,[8, 17] cationic dendrimer for proline-specific endopeptidase (PEP),[18] and branched or

"comb" PEG for oxytocin,[19, 20] but these have been mainly limited to enzyme or small peptide stabilization. There is still a tremendous need and interest in developing new PEG alternatives that can confer both increased half-life and storage stability for a variety of proteins and stressors.

Herein, we describe a trehalose glycopolymer that we call PolyProtek (Figure 4-1) to address protein instability during both storage and use. The polymer has the disaccharide trehalose at the side chains and stabilizes various enzymes and proteins to fluctuations in temperature and lyophilization in solution.[21-23] We have also employed a trehalose glycopolymer as a resist material and demonstrated that the polymer stabilizes proteins to high vacuum and direct electron beam irradiation in solid films.[24, 25] Trehalose is known to stabilize proteins with a mechanism attributed to vitrification, water replacement, and/or water entrapment.[26, 27] Yet, trehalose glycopolymers have outperformed trehalose itself in several studies.[21, 22, 24] This may be a result of both the osmolyte and nonionic surfactant character of the polymer.[22, 28] Others have shown that polymers with trehalose side chains can inhibit amyloid formation and form stable nanoparticles for nucleic acid delivery.[29-31] We hypothesized that trehalose glycopolymers would also stabilize proteins *in vivo* similar to PEG. In this chapter, we demonstrate that the trehalose glycopolymer can maintain the plasma protein concentration within the therapeutic window over an extended period of time and also stabilize a protein therapeutic at elevated temperature and under mechanical stress. Insulin was chosen as a model protein because of its wide clinical usage and well-established structure and bioactivity assays.[32]

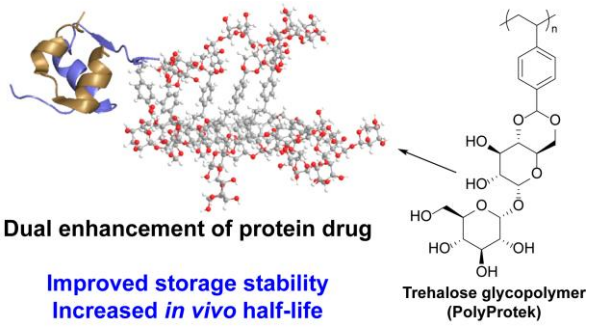

Figure 4-1. Insulin-trehalose glycopolymer conjugate where the polymer improves both the storage stability and *in vivo* plasma half-life (protein structure from the Protein Data Bank 4INS).

4.1.2 Results and Discussion

A protein-reactive trehalose glycopolymer was prepared through reversible addition-fragmentation chain transfer (RAFT) polymerization using a benzaldehyde-functionalized chain transfer agent (M_n = 9.9 kDa and $Đ$ = 1.10 for benzaldehyde end-group polymer) and subsequently conjugated to insulin via reductive amination, which is commonly used to conjugate to amines (Figure 4-2, Experimental Section Figure 4-5 through Figure 4-6).[33, 34] Conjugation was confirmed by native gel (Figure 4-3 and Experimental Section Figure 4-7) and the conjugate was purified via fast protein liquid chromatography (FPLC). Benzaldehyde polymer conjugated with quantitative conversion after 14 hours using 12.5 molar equivalent of the polymer (native polyacrylamide gel electrophoresis (PAGE) in Experimental Section Figure 4-7). PEG aldehyde monomethoxy ether (10 kDa) was also conjugated to insulin as a control (PAGE in Experimental Section Figure 4-8). Characterization of the conjugate by tandem mass spectrometry showed that the trehalose glycopolymer was conjugated to the N-terminal glycine of chain A (GlyA1) and to N-terminal phenylalanine or lysine of chain B (PheB1 or LysB29),[35] consistent with the reported reactivity of these amines followed the order GlyA1 > LysB29 >> PheB1.[36] For the PEG conjugate, MALDI-TOF analysis showed that the PEG conjugate was also mostly mono- and di-substituted

(Experimental Section Figure 4-9), presumably at GlyA1 and LysB29 as previously reported for PEG conjugates.[36] This result also agreed with the PAGE result where two overlapping conjugate species were observed (Experimental Section Figure 4-8). The peaks were separated by roughly 44 m/z, which corresponds to the molecular weight of the PEG repeat unit (Experimental Section Figure 4-9b).

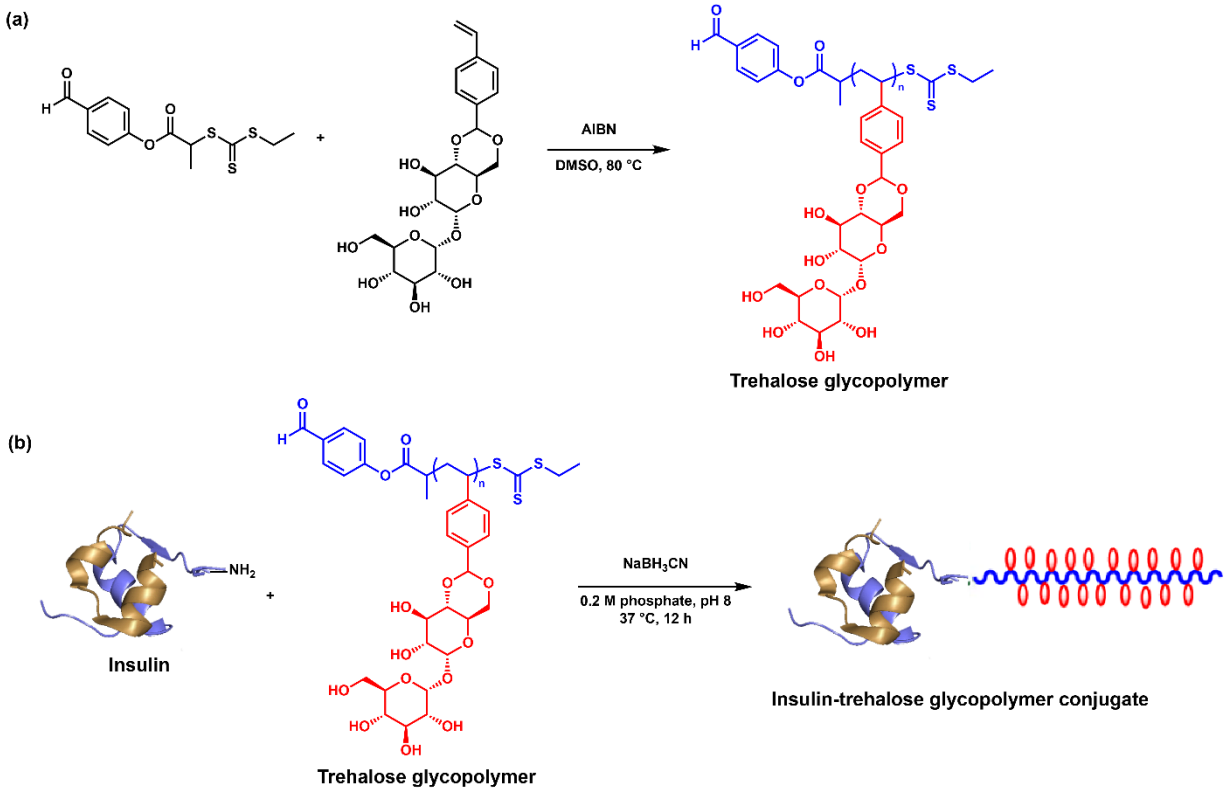

Figure 4-2. Synthesis of insulin trehalose glycopolymer conjugate. (a) RAFT polymerization and (b) subsequent conjugation of trehalose glycopolymer to insulin (PDB: 4INS) by reductive amination.

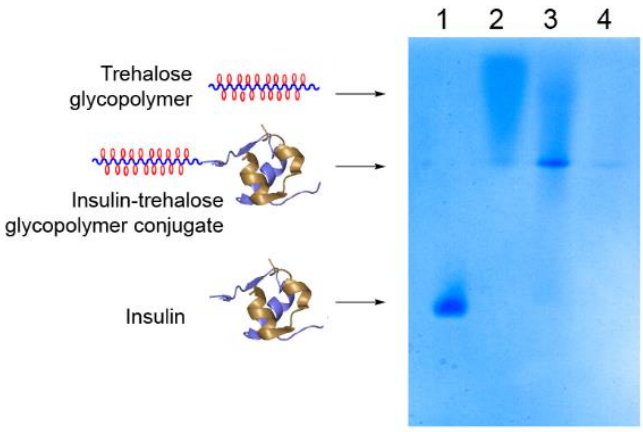

Figure 4-3. Characterization of insulin-trehalose glycopolymer conjugate by Native-PAGE after Coomassie stain (insulin structure PDB: 4INS).

Conjugation of both PEG and trehalose polymer significantly increased the plasma half-life of insulin after intravenous injection into mice.[35] Although the differences in the plasma levels of insulin-trehalose glycopolymer and insulin-PEG conjugates were statistically insignificant at all time points ($p > 0.1$), PEG conjugate showed slightly higher levels. It is interesting to note that the PEG in this instance, even though it was the same molecular weight as the trehalose glycopolymer, had a ten-fold larger degree of polymerization (DP = 227 versus 21.9, respectively). When PEG and trehalose polymer of similar size (20 kDa for PEG and 19 kDa for trehalose polymer) were analyzed by diffusion-ordered spectroscopy (DOSY), hydrodynamic radius of PEG (5.91 Å, Experimental Section Figure 4-10) was twice as large as that of trehalose polymer (2.94 Å, Experimental Section Figure 4-11). Conjugates of PEG with the same molecular weight as trehalose polymer would be expected to have a longer half-life due to its larger hydrated volume, and this should be taken into account for comparing pharmacokinetics of different types of polymers. The slower clearance observed for both conjugates was likely due to reduced renal filtration from the increased hydrodynamic volume,[37] as well as increased protease resistance and

decreased opsonization as is known for PEGylated proteins,[38] and this will be verified along with the effect of degree of polymerization of the trehalose glycopolymer in future studies. Together, this data shows that trehalose glycopolymer conjugation is an effective strategy to extend the half-life of exogenously delivered insulin.

Next, the bioactivities of insulin and the insulin-trehalose glycopolymer conjugate were compared in mice. Generally, conjugation of polymers to proteins results in decreased bioactivity of the protein. Previous reports have shown that attachment of even a relatively small 2 kDa PEG decreases the *in vivo* bioactivity of insulin to about 80% of the original activity, and the effect becomes larger when higher molecular weight PEG is conjugated.[36] In the present work, a loss in activity compared to native insulin was also observed in insulin tolerance tests (ITT) in mice; a five-fold dose of trehalose glycopolymer conjugate (concentration determined by ELISA) was required to achieve equivalent short-term biological activity of native insulin (Figure 4-4a). A similar result has been reported with insulin conjugated to 20 kDa PEG, which had 17-fold lower binding affinity to the insulin receptor than the native protein.[39] This effect may be due to steric hindrance to insulin binding to the receptor as well as prolonged blood circulation and delayed transendothelial transport to tissue of action also observed for the basal insulin analogue insulin detemir.[40] Higher bioactivity may be obtained in the future by site-specific conjugation of the trehalose glycopolymer.[36] Yet, the results did demonstrate that the conjugate was bioactive and able to reduce blood glucose levels in mice.

The heat stability of the conjugate was further investigated *in vivo* by ITT in mice (Figure 4-4b). The results confirmed the HPLC and dynamic light scattering (DLS) data[35] and showed that the protein insulin retained a very low level of activity after heating (17%). In contrast, insulin heated in the presence of 2 molar (10 weight) equivalents of the trehalose glycopolymer added as

an excipient retained 81% of its activity. Importantly, the mice treated with insulin-trehalose glycopolymer conjugate that was heated at 90 °C exhibited full retention of activity relative to the conjugate stored refrigerated, demonstrating that the conjugate was fully active after heating to these conditions.

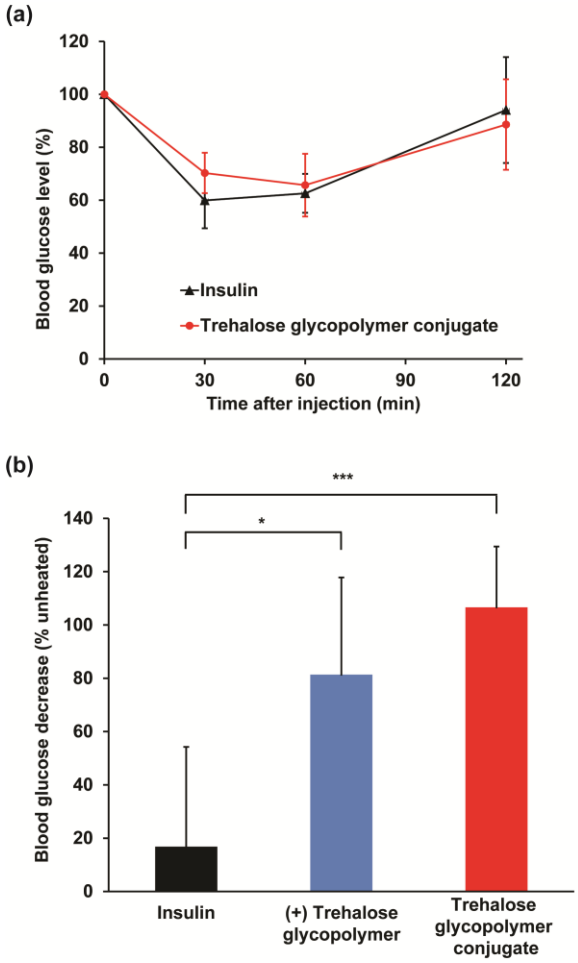

Figure 4-4. Bioactivity study of insulin-trehalose glycopolymer conjugate. (a) Blood glucose levels in fasted mice after i.v. injection with unmodified insulin (16 µg/kg) and insulin-trehalose glycopolymer conjugate (80 µg/kg) (n = 5). (b) Activity of heated insulin, insulin with trehalose glycopolymer excipient (2 molar equivalents), and insulin-trehalose glycopolymer conjugate (90 °C, 30 min) relative to unheated samples during ITT in mice (n = 4, * $p < 0.05$ and *** $p < 0.005$).

With these promising results of the stabilization effect of the trehalose glycopolymer both *in vitro* and *in vivo*, we further tested *in vivo* toxicity of the polymer. We have previously investigated the cytotoxicity in four different cell lines and found that the polymer does not decrease cell viability up to 8 mg/mL.[22] To evaluate the toxicity *in vivo*, hematological parameters were analyzed to assess if the trehalose glycopolymer, as a nonionic surfactant, would cause hemolysis;[41] kidney and liver toxicities were also tested since protein-polymer conjugates are known to be mainly cleared through renal and hepatic pathways.[42] A dosage of 1.6 mg/kg was injected via tail vein into mice. This dosage was selected because it was 100-fold higher dosage than was used in the pharmacokinetic studies and 20-fold higher than used in the bioactivity studies. The animals were monitored for signs of stress and weight loss, which were not observed, and after 48 hours the animals were sacrificed for evaluation of the trehalose glycopolymer toxicity.[43, 44] Liver and kidney enzyme levels for both trehalose glycopolymer and phosphate-buffered saline (PBS) treated groups were both within the normal range (Table 4-1). In addition, hematological parameters including complete blood cell count (CBC) were found to be normal and comparable to the control group of PBS alone, and the histology of all the major organs was normal. These promising results suggest that the polymer is biocompatible at least up to 1.6 mg/kg in mice.

Our results demonstrate that like PEG, trehalose glycopolymer increases the *in vivo* lifetime of a model therapeutic protein. Yet, the trehalose glycopolymer improves upon PEG by also stabilizing the protein to stressors that typically cause aggregation and reduce the activity of the protein. Enhanced pharmacokinetics is desirable because it translates to fewer doses and better dosing regimens, which improves patient compliance and ultimately the therapeutic efficacy of treatment. Stability to external heat and mechanical stress is additionally helpful for longer term

storage of proteins and for better stability during transportation where protein drug solutions can undergo agitation. Thus, this data is the initial work in demonstrating the value of the trehalose glycopolymer (also called PolyProtek) as a potentially superior analog to PEG to enhance both the pharmacokinetics and storage stability of therapeutic proteins. Research along these lines is important to move away from refrigeration of protein therapeutics and to enhance the safety of therapeutics while avoiding the cold chain.

Our study of insulin as a model protein was evaluated only by intravenous injections in mice mainly to test our hypothesis that trehalose glycopolymer could improve the pharmacokinetics of protein drugs. PEG-insulin (Lispro®) has been studied as a once-daily injection for patients with type 1 and type 2 diabetes.[39, 45, 46] Thus, a major application of an analog of PEGylated insulin would be for subcutaneous injection for use as basal insulin. Absorption of insulin from subcutaneous depots is a nonlinear process, which depends on many factors such as the dissolution and diffusion of insulin or insulin conjugates, local blood flow, and local temperature.[47, 48] Intravenous administration of conjugates in the current study helps to rule out these confounding factors to accurately test one of the hypotheses, which is that the trehalose glycopolymer improves blood plasma lifetimes. This was a first test to evaluate whether or not a therapeutic protein could be stabilized *in vivo* with the trehalose glycopolymer. Future studies will entail subcutaneous and muscular injections of the trehalose glycopolymer-insulin conjugate.

We also chose insulin as the model therapeutic protein since insulin instability is clinically relevant and has been reported to cause medical emergencies such as ketoacidosis due to insulin degradation.[49] There has been work on insulin stabilization using modified insulin analogs,[50] small-molecule excipients,[51-53] liposomes,[54] and polymeric vehicles,[55-57] yet due to the large demand of insulin around the world and rapid growth of diabetic population, there is still

significant value in the study of additional approaches. Our research shows that adding trehalose glycopolymer as an excipient can prevent heat and mechanical-induced aggregation and inactivation of insulin, and initial studies show that the polymer is non-toxic in mice. These results indicate that the trehalose glycopolymer should also be further investigated as a potential stabilizer of insulin as an excipient.

The current study also lends support for the further study of the trehalose glycopolymer as a versatile polymer for delivery of various therapeutic proteins. With improved pharmacokinetics and storage stability, protein drugs that are in general prone to degradation and elimination pathways could be stored without special precaution and be delivered with extended bioactivity if stabilized. Currently the most frequent strategy to improve protein stability is through genetic modification of liable amino acid residues. However, this requires *a priori* knowledge of possible degradation pathways. Moreover, modification of even a single amino acid may disrupt the tertiary structure of a protein, making this approach a trial-and-error process that is both time consuming and costly. Trehalose glycopolymers have been shown to be effective stabilizers of various protein classes including enzymes,[21-23] growth factors,[24] antibodies,[24, 25] and insulin as a hormone in this work, to external stressors such as heat, lyophilization, electron beam irradiation, and mechanical agitation. Therefore, we expect that trehalose glycopolymer conjugation will be a generalizable and reliable formulation strategy for stabilizing various proteins of clinical value, and investigation of this hypothesis is underway.

4.1.3 Conclusions

This report presents research on trehalose glycopolymer (PolyProtek) as a polymer that can enhance the stability and pharmacokinetics of a therapeutic protein. Specifically, we describe the

ability of a polymer with pendant trehalose groups to stabilize the model protein insulin to high temperatures and mechanical agitation, and retain its bioactivity by inhibiting protein aggregation. Conjugated to the protein, the polymer increased the concentration of insulin in plasma over time and exhibited bioactivity as shown by the reduction of blood glucose levels even after heating. The *in vivo* toxicity results also suggested that the trehalose glycopolymer is a biocompatible polymer. Together, this research demonstrates that conjugation of the trehalose glycopolymer should be explored as an improvement over PEGylation for protein therapeutics because of its ability to enhance both environmental stability and *in vivo* bioavailability.

4.1.4 Experimental Section

Materials

All chemicals were purchased from Sigma-Aldrich and Fisher Scientific and were used without purification unless noted otherwise. Azobisisobutyronitrile (AIBN) was recrystallized from acetone before use. Trehalose was purchased from The Healthy Essential Management Corporation (Houston, TX) and was azeotropically dried with ethanol and kept under vacuum until use. Recombinant human insulin was purchased from Sigma-Aldrich. Human insulin ELISA kit was purchased from Mercodia (Uppsala, Sweden). 2-(Ethyltrithiocarbonate)propionic acid was synthesized according to a literature procedure.[58] mPEG-propionaldehyde (10.5 kDa by MALDI, Đ = 1.02 by GPC) was purchased from Jenkem Technology (Allen, TX). PEG without end group (20 kDa) was purchased from Sigma-Aldrich. Styrenyl acetal trehalose monomer and trehalose glycopolymer (styrenyl acetal trehalose polymer without end-group synthesized by free radical polymerization, M_n = 29.5 kDa, $Đ$ = 2.11 by GPC) were prepared using previously reported procedure.[22]

Analytical Techniques

Nuclear Magnetic Resonance (NMR) spectra were recorded on a Bruker DRX 500 MHz spectrometer. Gel permeation chromatography (GPC) was conducted on a Shimadzu HPLC system equipped with a refractive index detector RID-10A and two Polymer Laboratories PLgel 5 μm mixed D columns (with guard column). Lithium bromide (0.1 M) in N,N-dimethylformamide (DMF) at 40 °C was used as the eluent (flow rate: 0.6 mL/min). Near-monodisperse poly(methyl methacrylate) standards (Polymer Laboratories) were employed for calibration. Trehalose monomer was purified by preparatory reverse phase HPLC on a Shimadzu HPLC system equipped with a UV detector using a Luna 5 μm C18 100 Å column (preparatory: 5 μm, 250 x 21.2 mm) with monitoring at λ = 215 nm and 254 nm. Isocratic solvent system (water:methanol = 50:50) was used as the mobile phase at a flow rate of 20 mL/min. Matrix-assisted laser desorption/ionization (MALDI)-MS analysis of insulin and the insulin-PEG conjugate was performed on a Voyager DE-STR (Applied Biosystems, Forster City, CA) in linear positive ion mode. Insulin-PEG conjugate was desalted by centriprep ultrafiltration (MWCO 3 kDa) and mixed 1:1 with sinapinic acid dissolved in 50 % acetonitrile with 0.1 % trifluoroacetic acid on the MALDI target plate. Cytochrome *c* was used for the calibration of the insulin-PEG conjugate spectrum and a mixture of angiotensin I, angiotensin II, substance P, neurotensin, and ACTH (18-39) were used for the calibration of the insulin spectrum.

Preparation of Insulin-PEG Conjugate

Insulin (0.50 mg, 8.6×10^{-2} μmol), sodium cyanoborohydride (0.64 mg, 10 μmol), and 10 kDa mPEG-propionaldehyde (45 mg, 4.5 μmol, 52 molar equiv to insulin) were dissolved in 1 mL of 100 mM sodium acetate buffer, pH 4, in a 1.5 mL protein Lo-Bind® tube. The mixture was incubated at 4 ºC for 20 h on a rocker, and the buffer was exchanged to D-PBS, pH 7.4, by centriprep ultrafiltration (MWCO 3 kDa) several times before purification by fast protein liquid chromatography (FPLC). The amount of insulin was assayed by ELISA according to manufacturer's instructions. Briefly, 25 μL of the diluted samples were added to the wells pre-coated with the capture antibody. Buffer containing detection antibody was added (100 μL), and the plate was incubated on a rocker at room temperature (23 °C) for 1 h. The wells were washed six times with 350 μL of the wash buffer. 3,3',5,5'-Tetramethylbenzidine (TMB) solution was added (200 μL), and the plate was incubated at room temperature for 15 min before the addition of 50 μL stop solution. The amount of insulin detected was quantified by absorbance at 450 nm relative to the standards supplied by the manufacturer.

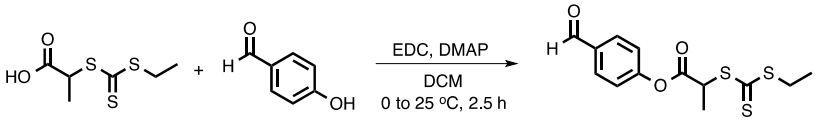

Synthesis of Benzaldehyde End-Functionalized Chain Transfer Agent (CTA)

To the flame-dried flask, 2-(ethyltrithiocarbonate)propionic acid (500 mg, 2.38 mmol) and 4-hydroxybenzaldehyde (377.38 mg, 3.09 mmol) were added and dissolved in DCM (20 mL). The reaction flask was cooled with an ice bath, and 1-ethyl-3-(3-dimethylaminopropyl)carbodiimide (EDC, 911.38 mg, 4.75 mmol) and DMAP (58.08 mg, 4.75×10^{-1} mmol) were added. The reaction was stirred at 0 °C for 30 min and stirred at 25 °C for another 2 h. The reaction was washed with

H_2O three times and the organic layer was collected, dried over $MgSO_4$ and purified by silica gel column chromatography (EtOAc : Hex = 1 : 1) to yield 466.7 mg of yellow CTA2 (62% yield). ^1H NMR (500 MHz in $CDCl_3$) δ: 9.99 (s, 1H), 7.92-7.90 (d, J = 9.47 Hz, 2H), 7.29-2.27 (d, J = 8.84 Hz, 2H), 5.01-4.97 (q, J = 7.18, 7.40 Hz, 1H), 3.42-3.35 (m, 2H), 1.75-1.73 (d, J = 7.41 Hz, 3H), 1.38-1.35 (t, J = 857.62 Hz, 3H), ^{13}C NMR (500 MHz in $CDCl_3$) δ: 221.7, 190.9, 169.3, 155.2, 134.2, 131.3, 122.2, 47.8, 31.8, 16.3, 13.0. IR: ν = 2974, 2925, 2740, 1755, 1698, 1597, 1501, 1449, 1425, 1376, 1298, 1266, 1202, 1151, 1420, 1066, 1032, 1013, 970, 896, 857, 821 cm^{-1}. HRMS (ESI) calculated for $C_{13}H_{14}S_3O_3Na$ ($[M + Na]^+$) 337.0003, found 337.0012.

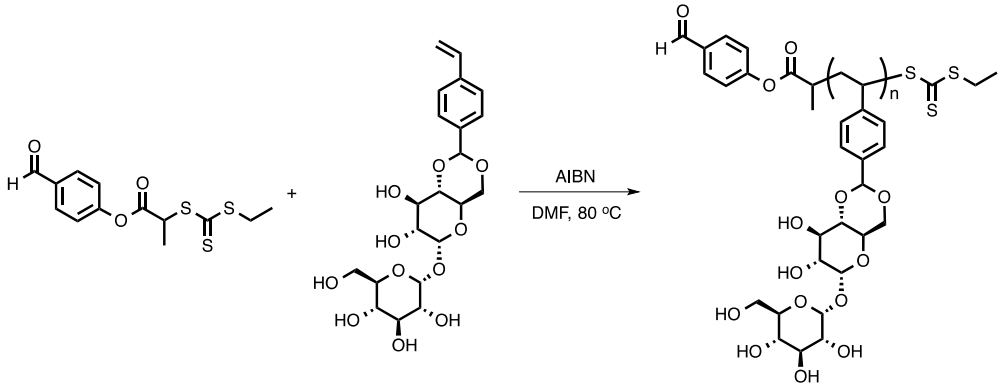

RAFT Polymerization of Trehalose Monomer

CTA (2.35 mg, 7.47×10^{-3} mmol), styrenyl acetal trehalose monomer (92.0 mg, 2.02×10^{-1} mmol), and AIBN (0.49 mg, 2.99×10^{-3} mmol) were dissolved in 0.25 mL of DMF. The solution underwent four cycles of freeze-pump-thaw, and polymerization was initiated by immersing the flask into 80 °C oil bath. The polymerization was stopped at 89 % conversion by ^1H-NMR and purified by dialyzing against H_2O (MWCO 3.5 kDa). ^1H NMR (500 MHz in $CDCl_3$) δ: 9.92, 7.59, 7.15, 6.52, 5.44, 5.17, 4.92, 4.79, 4.37, 4.08, 3.95, 3.75, 3.67, 3.55, 3.46, 3.14, 1.49. M_n = 9.9 kDa (by GPC), Đ = 1.10.

Preparation of Insulin-Trehalose Glycopolymer Conjugate

Insulin (1.5 mg, 2.59×10^{-1} μmol), sodium cyanoborohydride (4 mg, 63.8 μmol), and benzaldehyde end-functionalized trehalose polymer (31 mg, 3.1 μmol, 12 molar equiv to insulin) were dissolved in 1 mL of 200 mM phosphate buffer, pH 8.0, in a 1.5 mL protein Lo-Bind® tube. The mixture was incubated at 37 °C water bath for 12 h, and the buffer was exchanged to Dulbecco's phosphate-buffered saline (D-PBS), pH 7.4, by centriprep ultrafiltration (MWCO 3 kDa) several times before purification by FPLC. The amount of insulin was assayed by ELISA as previously described.

Bioactivity of Insulin and the Insulin-Polymer Conjugates

Bioactivity was determined by the ITT assay using standard protocols.[59] CD1 mice (6-8 wks, female, n = 5, Charles River Laboratories) were fasted for 4-6 hours to reduce variability in baseline blood glucose. Pristine insulin, insulin after heating, insulin with addition of trehalose glycopolymer, insulin-trehalose glycopolymer conjugate, and insulin-trehalose glycopolymer conjugate after heating were intravenously injected at appropriate doses. For the stability assay, insulin formulations were injected at the dose of 40 μg/kg of insulin. To determine the bioactivity of the conjugate, the injection dose was 80 μg/kg and 16 μg/kg of insulin was injected as a control. At each prescribed time point, approximately 2 μL of blood sample was obtained from the tail vein in conscious mice by pricking the tail vein with a needle and sampling the formed blood droplet with a commercially available glucometer to measure the glucose concentration. The percent decrease in blood glucose level was calculated using the following formula:

$$\%\ \text{Blood glucose decrease} = \frac{[\text{Glucose}]_{0\ \text{min, heated}} - [\text{Glucose}]_{30\ \text{min, heated}}}{[\text{Glucose}]_{0\ \text{min, not heated}} - [\text{Glucose}]_{30\ \text{min, not heated}}} \times 100$$

Toxicity Study

CD1 mice (5-6 wks, female, Charles River Laboratories) were injected subcutaneously with either PBS or trehalose glycopolymer (n=5). The animals received one injection of trehalose glycopolymer at a dose of 1.6 mg/kg. After 48 h, 600 μL of blood was collected by cardiac puncture and the major organs were harvested for histology analysis. Complete blood count (CBC) was performed with whole blood to determine the hematological compatibility of the polymer. Serum aspartate (AST) and alanine (ALT) aminotransferase activities were determined to assess liver toxicity; serum creatinine (Creat) and blood urea nitrogen (BUN) levels were determined to assess kidney toxicity. A sample from one animal in the control group (PBS) exhibited hemolysis and was discarded from the dataset. Histology sections of heart, lung, liver, spleen, and kidney were assessed by Dr. Gregory Lawson (Division of Laboratory Animal Medicine, UCLA). They were all found to be normal.

Statistical Analysis

For assessment of the statistical significance of differences, Student's t-test assuming unequal sample variance was employed. Results were considered significantly different if $p < 0.05$.

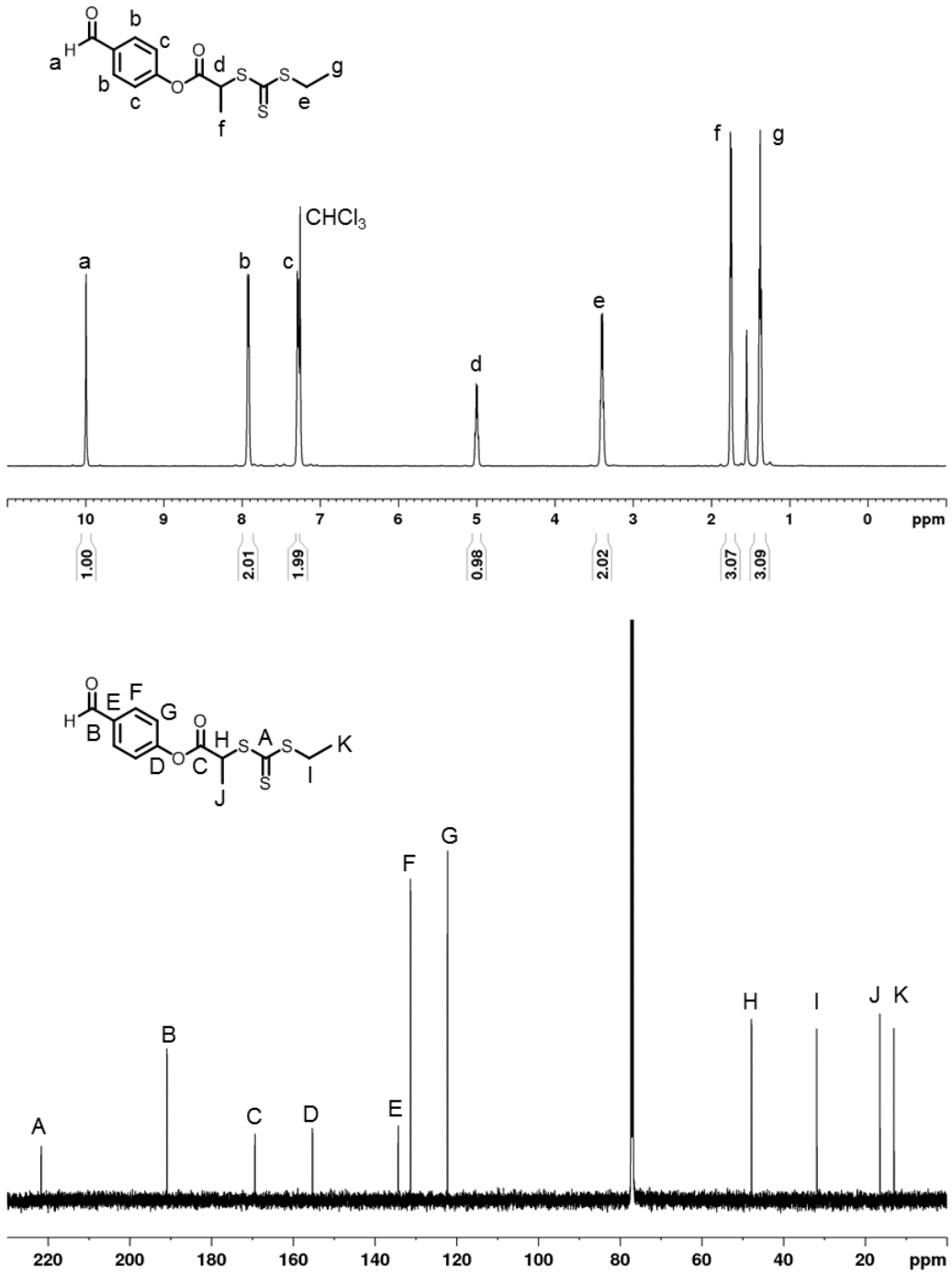

Figure 4-5. ^{1}H (top) and ^{13}C (bottom) NMR spectra of benzaldehyde chain transfer agent ($CDCl_3$).

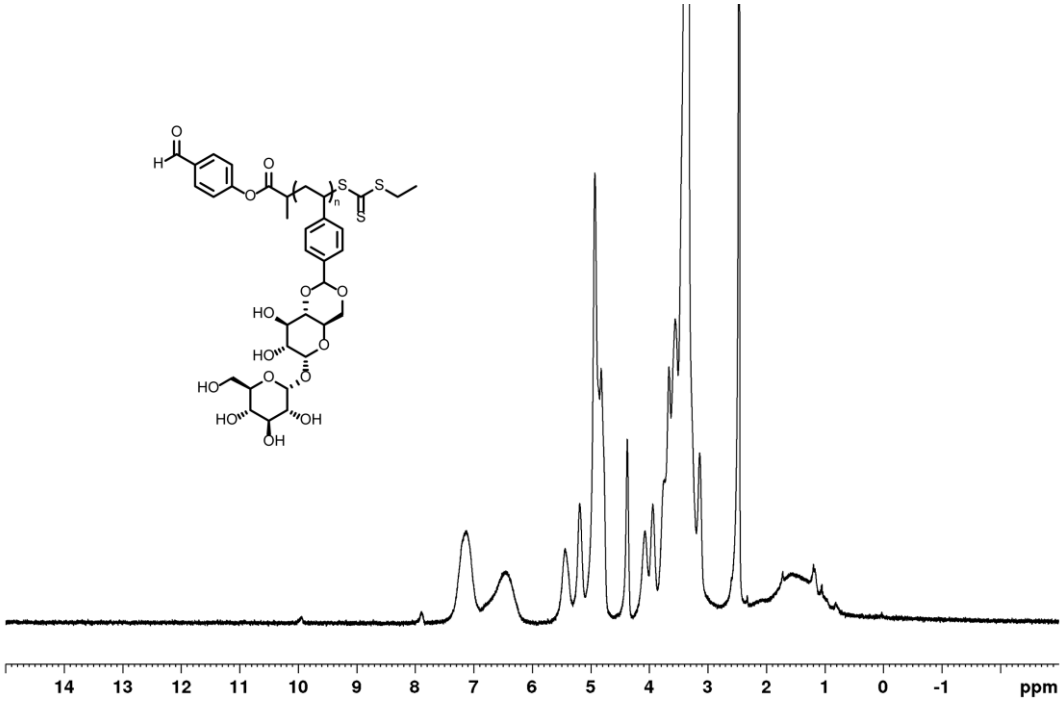

Figure 4-6. ^{1}H NMR spectrum of benzaldehyde end-functionalized trehalose polymer from RAFT polymerization (DMSO-d_6).

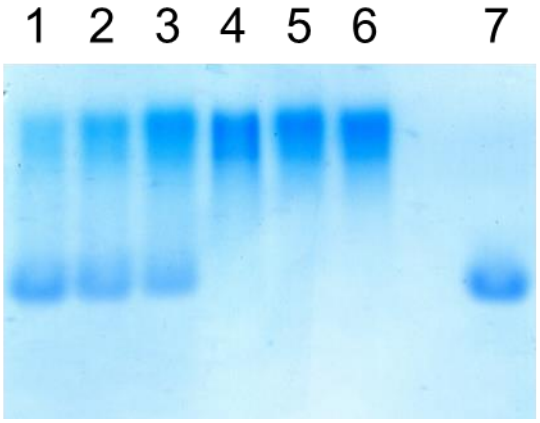

Figure 4-7. Native PAGE of insulin-trehalose glycopolymer conjugation mixture after Coomassie staining (lane 1-3: insulin/trehalose glycopolymer conjugation mixture at 12.5 molar (1), 25 molar (2), and 50 molar (3) equivalents of polymer at the start of conjugation, lane 4-6: insulin/trehalose glycopolymer conjugation mixture at 12.5 molar (4), 25 molar (5), and 50 molar (6) equivalents of polymer after 14 hours, lane 7: insulin).

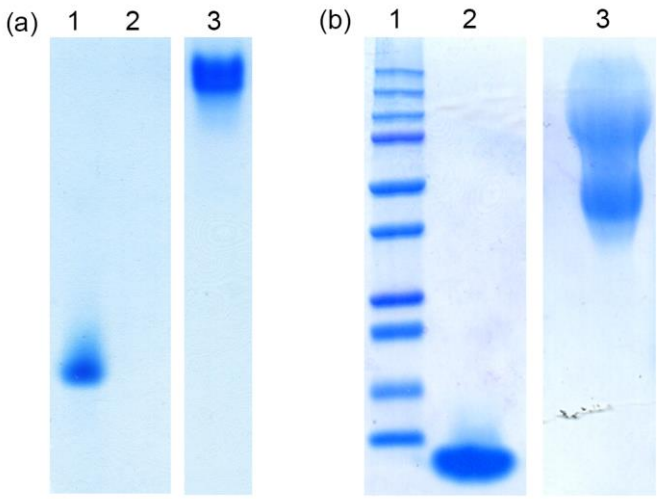

Figure 4-8. PAGE of insulin-PEG conjugate after Coomassie staining. (a) Native PAGE (lane1: insulin, lane2: mPEG-propionaldehyde, lane3: insulin-PEG conjugate after purification) and (b) SDS-PAGE (lane 1: molecular weight ladder, lane 2: insulin, lane 3: insulin-PEG conjugate).

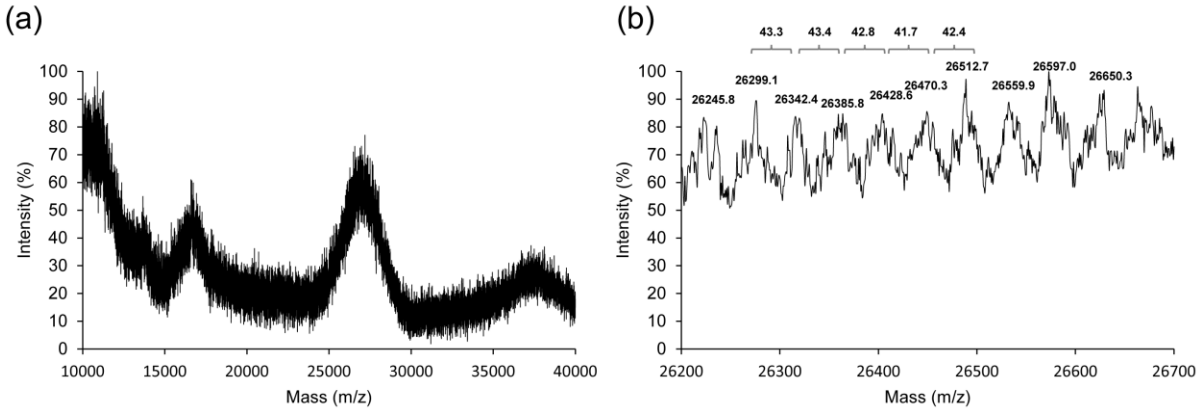

Figure 4-9. MALDI-TOF mass spectrum of insulin-mPEG conjugate. (a) Insulin-PEG conjugate, (b) Zoomed view of insulin-PEG conjugate.

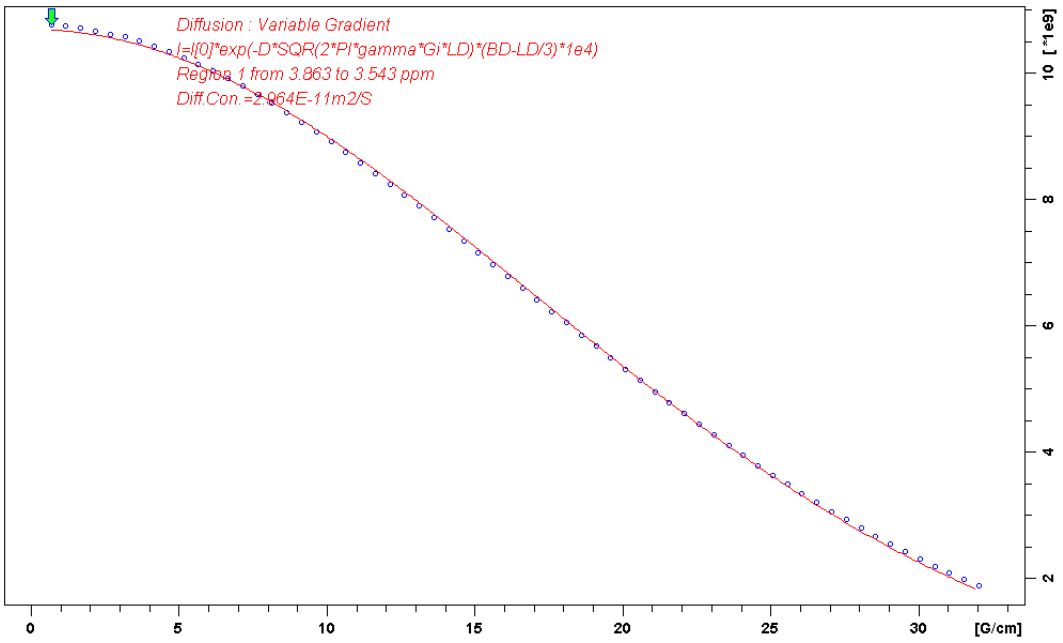

Figure 4-10. Diffusion constant measurement by diffusion-ordered spectroscopy (DOSY) used to calculate the hydrodynamic radius of 20 kDa PEG (D_2O).

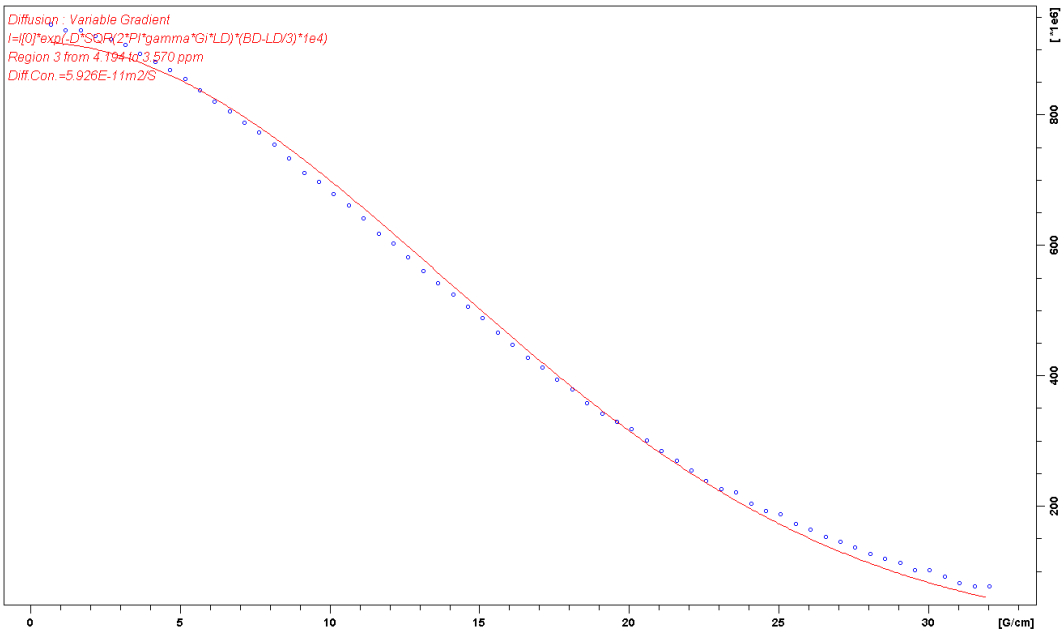

Figure 4-11. Diffusion constant measurement by diffusion-ordered spectroscopy (DOSY) used to calculate the hydrodynamic radius of 18.6 kDa trehalose polymer (D_2O).

Table 4-1. *In vivo* toxicity of trehalose polymer in liver and kidney after acute polymer challenge.

Organ	Test	PBS	Trehalose glycopolymer	Normal Range
Liver	**ALT (U/L)[a]**	51.5 ± 18.9	32.2 ± 7.6	17~77
	AST (U/L)[b]	130.4 ± 52.4	105.2 ± 33.5	54~298
Kidney	**BUN (mg/dL)[c, d]**	25.8 ± 1.3	17.6 ± 2.7	8~33
	Creat (mg/dL)[e]	0.27 ± 0.04	0.25 ± 0.03	0.2~0.9

[a]ALT: alanine transaminase, [b]AST: aspartate transaminase, [c]BUN: blood urea nitrogen, [d]Although BUN in both groups were all within the normal range, it was statistically lower for the trehalose glycopolymer group than the PBS group. The experiment was repeated and BUN evaluated to give 26.0 ± 4.1 for PBS group and 22.2 ± 1.6 for the trehalose glycopolymer group, with $p = 0.11 > 0.05$. [e]Creat: creatinine. (n=4 for PBS and n=5 for the trehalose glycopolymer).

4.2 Synthesis and *In Vivo* Evaluation of Granulocyte Colony-Stimulating Factor-Trehalose Polymer Conjugate

4.2.1 Introduction

Therapeutic proteins have various advantages to traditional small molecule drugs. They are highly specific and typically have fewer side effects,[60] and can act on targets that are often inaccessible by small molecule drugs.[61] These intrinsic benefits of proteins compared to small molecules lead to their higher success rate in clinical trials and subsequent FDA approvals,[62] which make proteins increasingly attractive for the pharmaceutical companies to develop into therapeutic drugs. However, the precise tertiary structure of proteins that enables their high specificity and efficiency also make them susceptible to degradation by physical stresses including heat, agitation, and freezing.

In addition to the physical instability, proteins have poor half-life in the body due to multiple elimination pathways. Proteins smaller than 20 kDa such as insulin ($t_{1/2}$ 4–6 min)[63] are rapidly cleared by renal filtration,[64] but larger proteins such as hyaluronidase (56 kDa) can have an even shorter half-life (2.1 min)[65] due to other clearance mechanisms such as uptake by the liver or the immune system. Increasing the hydrodynamic radius by conjugation of a polymer such as poly(ethylene glycol) is an effective strategy to improve the pharmacokinetics,[5] but it does not necessarily improve the physical stability of the protein.

Our group has used trehalose polymers to stabilize a wide range of proteins that range from enzymes,[21, 23, 24, 66] hormones and growth factors,[24, 35, 67-69] and antibodies.[24, 25] It may be envisioned that conjugating a trehalose polymer that improves physical stability of proteins will also enhance the serum half-life, thereby addressing two major weaknesses of protein therapeutics at once. This approach was shown to be effective using insulin as a model protein drug (see Section 4.1 of this

chapter). The strategy was extended to granulocyte colony-stimulating factor (G-CSF) to establish trehalose conjugation as a generalizable platform for stabilization of protein drugs to both physical stressors and *in vivo* elimination mechanisms, and the work is described in this section. An efficient conjugation method was developed to synthesize G-CSF-trehalose polymer conjugate, and *in vivo* evaluation of bioactivity, biodistribution, toxicity, and immunogenicity was conducted.

4.2.2 Results and Discussion

We have previously synthesized a G-CSF-trehalose polymer conjugate by direct reductive amination between G-CSF and benzaldehyde-functionalized trehalose polymer.[70] This conjugate was shown to exhibit significantly enhanced stability to heat compared to free G-CSF. However, the conjugation efficiency was only modest even when 100 mol. equiv. of the polymer was used, resulting in only 63% modification as assessed by gel densitometry. Even though this conjugation approach has been used by Amgen for G-CSF-PEG conjugate (Neulasta®) and also by our group for insulin-trehalose polymer conjugate, the increased bulk of trehalose polymer compared to PEG as well as the larger size of G-CSF (18.8 kDa) compared to insulin (5.8 kDa) appeared to lower the conjugation yield. We thought to increase the yield by adopting a two-step conjugation approach, in which an alkyne linker will be conjugated to G-CSF by reductive amination that is selective for the N-terminus due to its lower pK_a compared to ε-amino group of lysines, followed by highly efficient copper-catalyzed azide-alkyne cycloaddition (CuAAC) to conjugate G-CSF with azide-functionalized trehalose polymer. First the small-molecule alkyne/benzaldehyde heterobifunctional linker was synthesized using penta(ethylene glycol) as the core since tri(ethylene glycol) was not sufficient to make the linker soluble in water. The alkyne-penta(ethylene glycol)-benzaldehyde linker was synthesized in 6 steps with 25.1% overall yield

(excluding the first desymmetrization step that naturally has low yield, the yield is 49.3%) (Experimental Section Figure 4-20).

The coupling partner azide-functionalized trehalose polymer was synthesized by using reversible addition-fragmentation chain transfer (RAFT) polymerization. The azide group was installed on the polymer by using a chain transfer agent (CTA) connected to an azide via amide linkage to prevent possible hydrolysis. The first CTA (**CTA1**) was synthesized by coupling 2-azidoethanamine to an acid with a methyl at α–position to the trithiocarbonate (colored blue in Figure 4-12). Although an ester-linked benzaldehyde CTA had given good control over the polymerization and narrow dispersity ($Đ$ = 1.10),[70] changing the ester to an amide resulted in both lower conversion (55%) and higher dispersity ($Đ$ = 1.31).

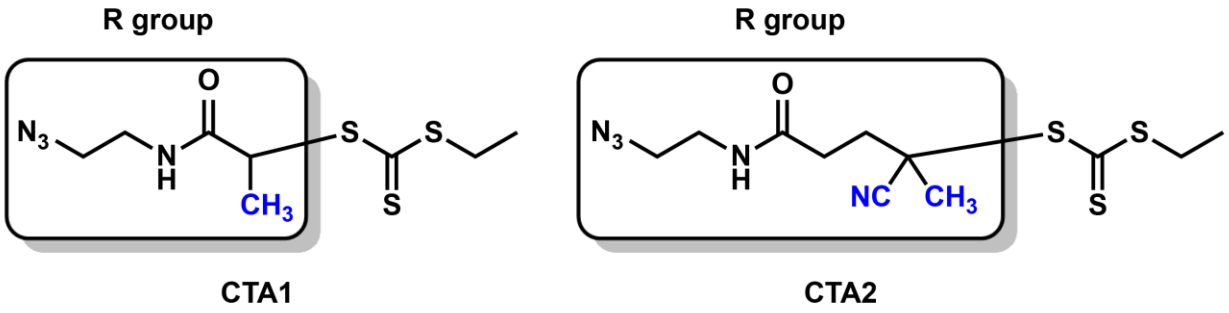

Figure 4-12. Chain transfer agents (CTA) used for the synthesis of azide-functionalized trehalose polymer.

It has been reported that an ester group at the α–position has more favorable chain transfer enthalpy (-29.4 kJ/mol) than an amide group (-14.3 kJ/mol)[71] and may explain the poor performance of the amide **CTA1** compared to the ester CTA previously used. To enhance chain transfer efficiency, **CTA2** was synthesized that had an ethylene linker to move the amide away from the carbon-centered radical that forms during RAFT polymerization, and also contained a

nitrile group at the α–position to further stabilize the radical and promote chain transfer (Figure 4-12). This type of CTA has a very favorable chain transfer enthalpy (-56.6 kJ/mol). Indeed, RAFT polymerization using **CTA2** (Figure 4-13) yielded a polymer that reached a higher conversion (88%) and had lower dispersity ($Đ$ = 1.20). The trithiocarbonate group was removed by aminolysis as confirmed by the loss of the 314 nm trithiocarbonate absorption peak in the UV-vis spectrum (Experimental Section Figure 4-32), and the resulting polymer had an essentially identical SEC elution profile (Experimental Section Figure 4-33) showing that the process was mild and did not affect other functionalities within the polymer.

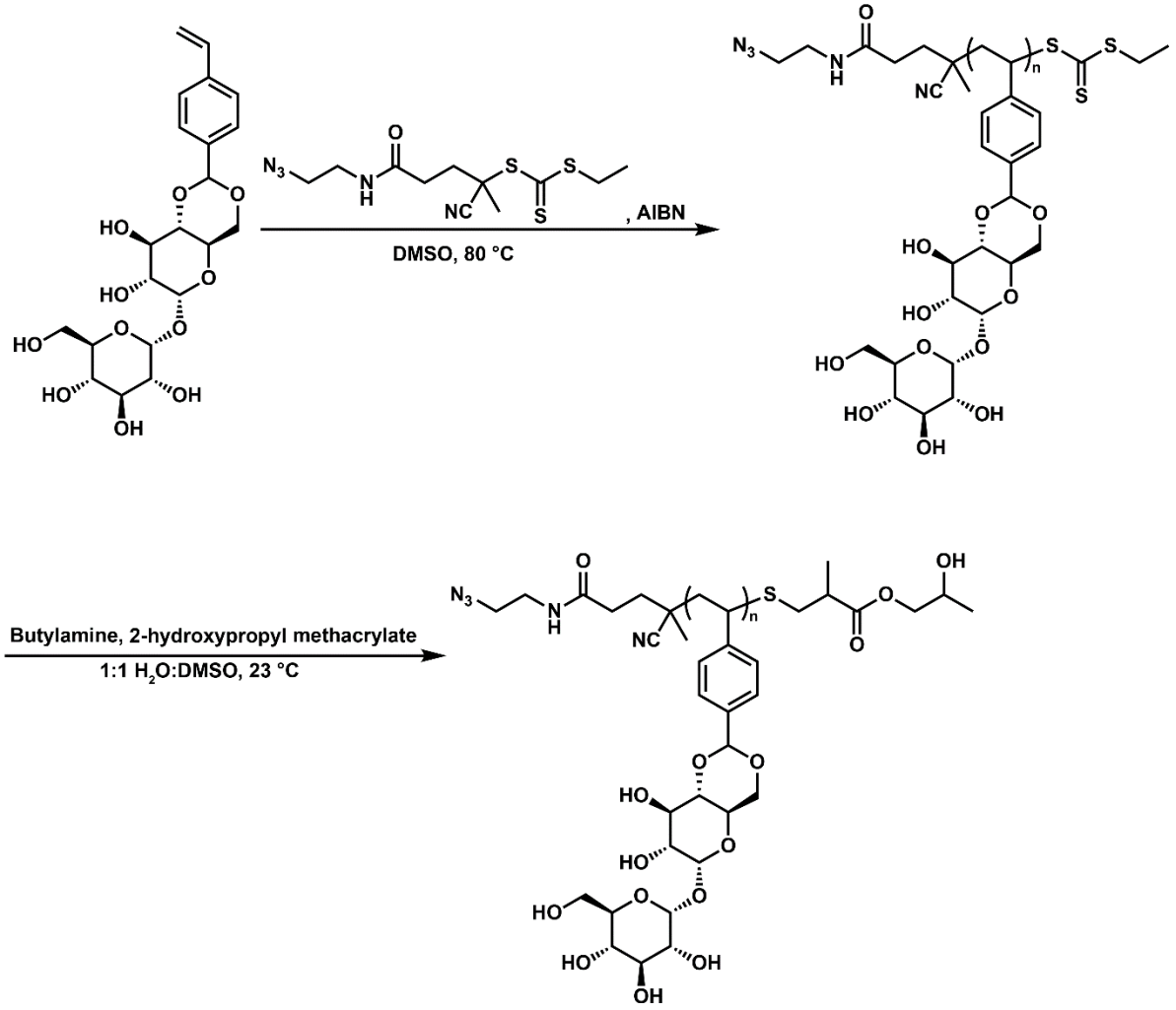

Figure 4-13. Synthesis of azide-functionalized trehalose polymer by reversible addition-fragmentation chain transfer (RAFT) polymerization using **CTA2**.

With both the alkyne linker and the azide polymer in hand, we proceeded with G-CSF conjugation. Since reductive amination at pH 5 is known to selectively modify the N-terminus of G-CSF,[33] the alkyne-penta(ethylene glycol)-benzaldehyde linker was conjugated to G-CSF at pH 5. Matrix-assisted laser desorption/ionization (MALDI) spectrum showed expected m/z shift of 365 Da (Experimental Section Figure 4-34), confirming the conjugation of the linker. Conjugation site was verified by protease digestion of the conjugate followed by liquid chromatography-mass spectrometry (LC-MS) (Table 4-2). We detected the alkyne-modified peptide fragment for only the N-terminus fragment, thereby confirming the N-terminus conjugation. It should be noted that we did not detect the intact fragment for the residues 42 – 175, likely due to the low resolution of high mass species upon deconvolution.

Table 4-2. Peptide fragments detected by LC-MS for determination of conjugation site.

Fragments (residue number)	Expected mass (Da)	Observed mass (Da)
1-17	1788	1786
1-17 + alkyne	2153	2151
18-24	933	933
25-35	1131	1130
36-41	756	756
42-175	14549	None

Azide-functionalized trehalose polymer was conjugated to G-CSF-alkyne by copper-catalyzed azide-alkyne cycloaddition (CuAAC). Using the triazole-type ligand 2-[4-[(bis[(1-*tert*-butyl-1*H*-1,2,3-triazol-4-yl)methyl]amino)methyl]-1*H*-1,2,3-triazol-1-yl]acetic acid (BTTAA)[72] together with copper (II) sulfate, sodium ascorbate, and aminoguanidine[73] yielded G-CSF-trehalose polymer conjugate in 90% yield as estimated by densitometric analysis of the silver-stained gel (Experimental Section Figure 4-36). Copper was removed by the use of

ethylenediaminetetraacetic acid (EDTA) during the purification process, and the residual level was measured by inductively coupled plasma mass spectrometry (ICP-MS) as 1.88 ng copper / μg protein in the conjugate. Given that clinical dose of G-CSF-PEG conjugate (Neulasta®) is 6 mg,[74, 75] the copper level of G-CSF-trehalose polymer conjugate from the current process is 11.3 μg / dose and 30-fold lower than the US Food and Drug Administration (FDA) recommended limit of 340 μg/day.[76]

The bioactivity of G-CSF and G-CSF-trehalose polymer conjugate was evaluated in an *in vivo* model of neutropenia.[77] White blood cell count is decreased in mice by cyclophosphamide injection on days -2 and 0, followed by injection of G-CSF (two injections on days 1 and 2 with 1 mg/kg dose each) or G-CSF-trehalose polymer conjugate (single injection on day 1 with 1 mg/kg dose). The granulocyte count continued to decrease in both groups until day 3, after which the protein promoted granulocyte production and the level started increasing. G-CSF showed a sharp increase in granulocyte count before decreasing again. This is consistent with the short half-life of G-CSF (3.8 h),[78] which necessitates daily injections up to 14 days in the clinic.[74] In contrast, granulocyte count in mice injected with G-CSF-trehalose polymer conjugate continued to increase up to the terminal collection on day 7. This is likely due to the increased serum half-life of the conjugate such that it stimulated granulocyte growth over a longer period even though the same amount of protein was injected at 1 mg/kg (dose is with respect to protein).

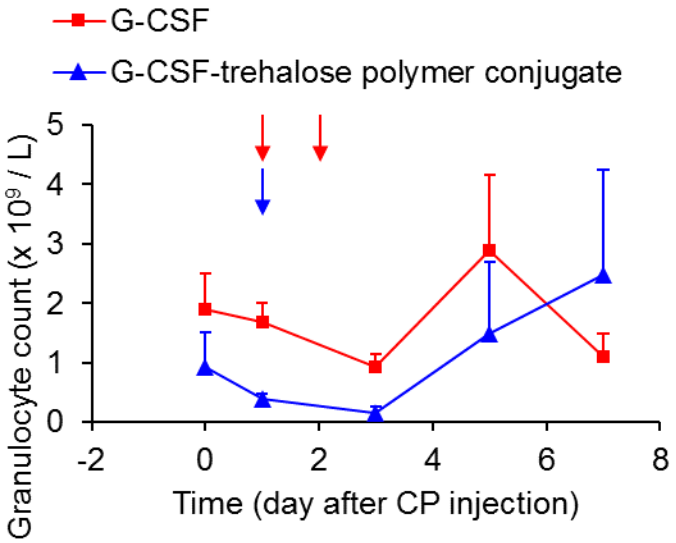

Figure 4-14. Bioactivity of G-CSF (1 mg/kg on days 1 and 2 as denoted by the red arrows) and G-CSF-trehalose polymer conjugate (1 mg/kg on day 1 as denoted by the blue arrow) (n = 4 – 6).

We next investigated the biodistribution of G-CSF and the conjugates by positron emission tomography (PET). Zirconium-89 (^{89}Zr) has a sufficiently long half-life of 3.3 days[79] to observe the extended lifetime of G-CSF conjugates in the body. Deferoxamine (DFO) is the most frequently used chelator for ^{89}Zr, and the commercially available *p*-isothiocyanatobenzyl-DFO was conjugated to G-CSF.[80] The conjugation requires a basic pH condition, but G-CSF precipitated during the conjugation as it is prone to aggregation at higher pH.[81] To circumvent this problem, DFO may be conjugated to a more stable form of G-CSF. G-CSF is expressed in *E. coli* as a maltose-binding protein (MBP) fusion, and this form has significantly increased stability in the solution even at high pH. DFO can be conjugated to the MBP-G-CSF, which would non-selectively modify both the MBP and G-CSF, before cleaving the MBP with tobacco etch virus (TEV) protease. The added benefit of this approach is that MBP is linked at the N-terminus of G-CSF and would block the DFO from modifying at that site, thus acting as a protecting group for the N-terminus and allowing for the polymer to be later installed at the site.

Using this approach, MBP-G-CSF was conjugated with DFO-squaramide (which has been reported to be more water soluble and resistant to ligand exchange[79]) and subsequently cleaved with TEV protease to yield the desired G-CSF-DFO conjugate (Figure 4-15). MALDI spectrum showed unmodified and mono-functionalized G-CSF (Figure 4-16). Even though G-CSF has four lysines available for modification, the absence of higher functionalized species suggests that one lysine is more reactive than others. The conjugation site was not determined since this protein was used only for the biodistribution experiment. Also, PET has high sensitivity and incomplete modification of G-CSF would not pose a problem for the imaging study.

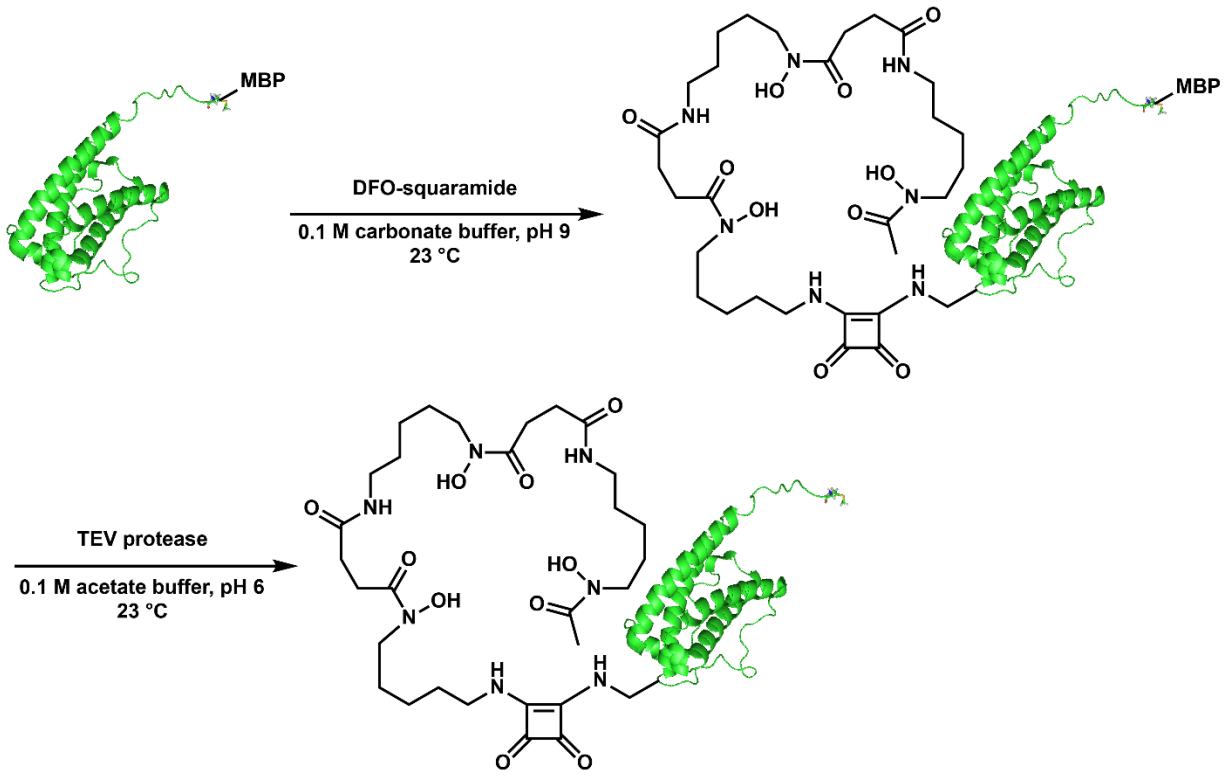

Figure 4-15. Conjugation of DFO to MBP-G-CSF fusion protein and cleavage of MBP with TEV protease.

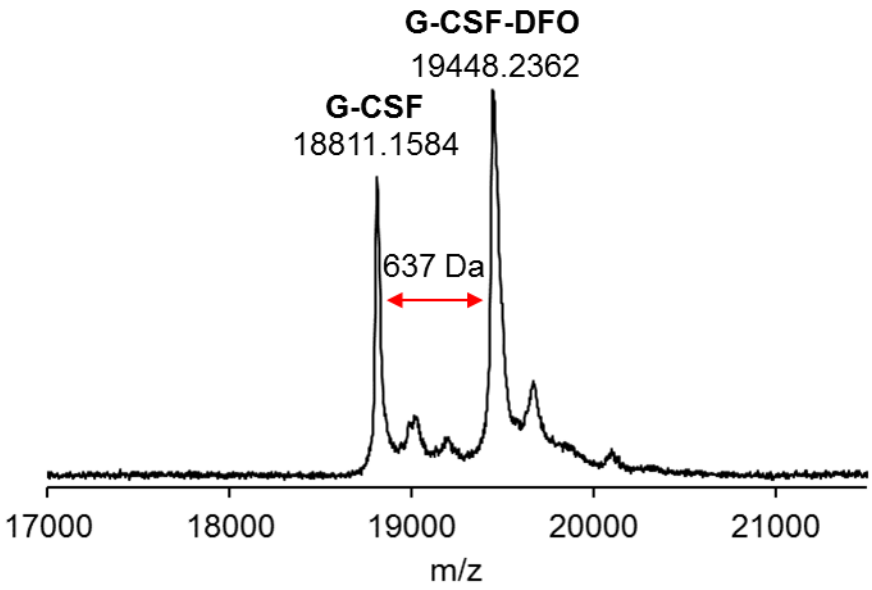

Figure 4-16. MALDI spectrum of G-CSF-DFO, showing 637 Da shift in molecular weight (635 Da expected).

To synthesize the conjugates, G-CSF-DFO was first modified with the alkyne-penta(ethylene glycol)-benzaldehyde linker to yield G-CSF-DFO-alkyne (Experimental Section Figure 4-37), which was then reacted with azide-functionalized trehalose polymer or PEG using CuAAC as described above. SDS-PAGE showed successful formation of the conjugates (Experimental Section Figure 4-38). PEG has 2-fold larger hydrodynamic radius than trehalose polymer with the same molecular weight (see Section 4.1.2 of this chapter) and therefore shows up around 60 kDa instead of the expected 40 kDa molecular weight (19 kDa G-CSF and 20 kDa PEG). MALDI spectrum of G-CSF-DFO-PEG shows a broad signal due to the dispersity of PEG but the distribution is centered at 40 kDa as expected (Experimental Section Figure 4-39). Since trehalose polymer is known to inhibit ionization,[35] G-CSF-DFO-trehalose polymer was not analyzed by MALDI.

G-CSF-DFO was radiolabeled with ^{89}Zr and injected into mice for the biodistribution study.[82] Dynamic PET scans over 1 h (Figure 4-17) showed that intravenously injected G-CSF-DFO-^{89}Zr circulates throughout the body via the heart at earlier time points, but quickly accumulates in the kidneys and bladder as expected for a relatively small protein such as G-CSF. PET scans at extended time points showed residual radioactivity in the kidneys (Figure 4-18a), and this may be from the breakdown of G-CSF and reabsorption as single amino acids.[64, 83] When the mice were euthanized and the organs were analyzed for radioactivity, the liver, spleen, and bone were the major sites of accumulation (Figure 4-18b). Whereas the liver and the spleen are typical organs involved in elimination of proteins, G-CSF has been previously shown to accumulate in the bone marrows[84] to stimulate neutrophil production. In accordance with literature, G-CSF starts accumulating in the bones (around the knee) beginning around 4 h as shown by the scans (Figure 4-18a). ^{89}Zr is also known to be released from the chelator and accumulate in the bone at longer time points[79] and some of the signal from the radioactivity in the bone at 40 h after injection may be attributed to this non-specific accumulation. Biodistribution of the conjugates is currently underway.

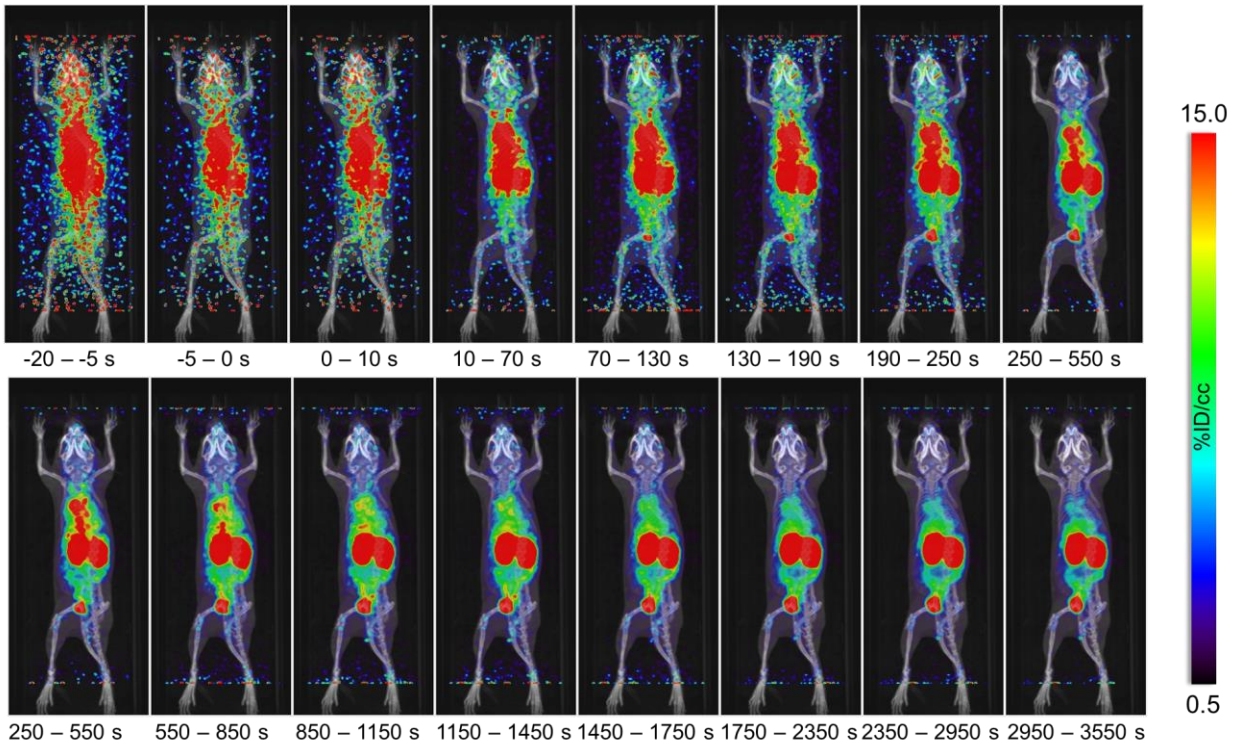

Figure 4-17. Dynamic PET scans of a mouse injected with G-CSF-DFO over 1 h (3600 s).

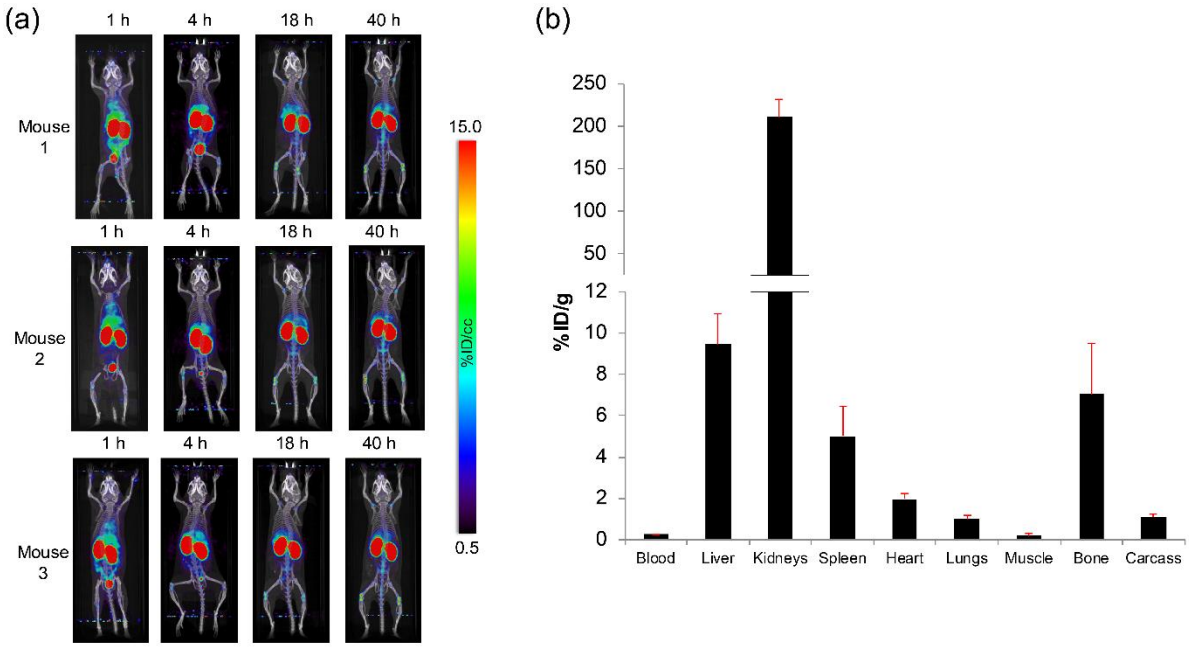

Figure 4-18. (a) PET scans over 40 h after injection with G-CSF-DFO. (b) Biodistribution of radioactivity in the organs 40 h after injection (n = 3).

Finally, *in vivo* safety of the polymer was assessed. Mice were injected with the trehalose polymer at 10 mg/kg, which is 10-fold higher than the therapeutic dose that would be used for G-CSF conjugate. Levels of liver enzymes (alanine transaminase (ALT) and aspartate transaminase (AST)) and kidney metabolites (blood urea nitrogen and creatinine) did not increase relative to the buffer-injected control group (Table 4-3), showing that the polymer did not induce liver or kidney damage. It should be noted that the creatinine level was slightly lower in the polymer treated group (p = 0.0414), but the level was well within the normal range. Immunogenicity of the trehalose polymer was also assessed by measuring cytokine levels after intraperitoneal injection into mice. Whereas lipopolysaccharide as the positive control elicited strong immune response as shown by the elevated levels of multiple cytokines, trehalose polymer injection did not significantly differ from the buffer injection (Figure 4-19) thus showing that the trehalose polymer does not stimulate the innate immune system.

Table 4-3. Liver enzyme and kidney metabolite levels 48 h after acute challenge of trehalose polymer.

	Test	Buffer (control)	Trehalose polymer	Normal Range
Hematology	**WBC (10^3/uL)**	5.92 ± 1.54	5.30 ± 1.90	4.6 ~ 16.2[a]
	RBC (10^6/uL)	9.94 ± 0.44	10.64 ± 0.57	7.2 ~ 11.4[a]
Liver enzymes	**ALT (U/L)**	32 ± 19	26 ± 9	7 ~ 227[b]
	AST (U/L)	135 ± 93	181 ± 66	57 ~ 329[b]
Kidney indices	**BUN (mg/dL)**	24 ± 3	22 ± 3	15 ~ 59[b]
	Creat (mg/dL)	0.45 ± 0.11	0.33 ± 0.06	0.4 ~ 1.6[b]

[a] From the supplier (Charles River CD-1 Mouse Hematology), [b] Loeb, WF and Quimby, FW. 1999. *The Clinical Chemistry of Laboratory Animals*, 2nd ed. Philadelphia: Taylor & Francis USA.), Abbreviations: WBC: white blood cell count, RBC: red blood cell count, ALT: alanine transaminase, AST: aspartate transaminase, BUN: blood urea nitrogen, Creat: creatinine (n = 5 for buffer, n = 6 and 10 mg/kg for trehalose polymer).

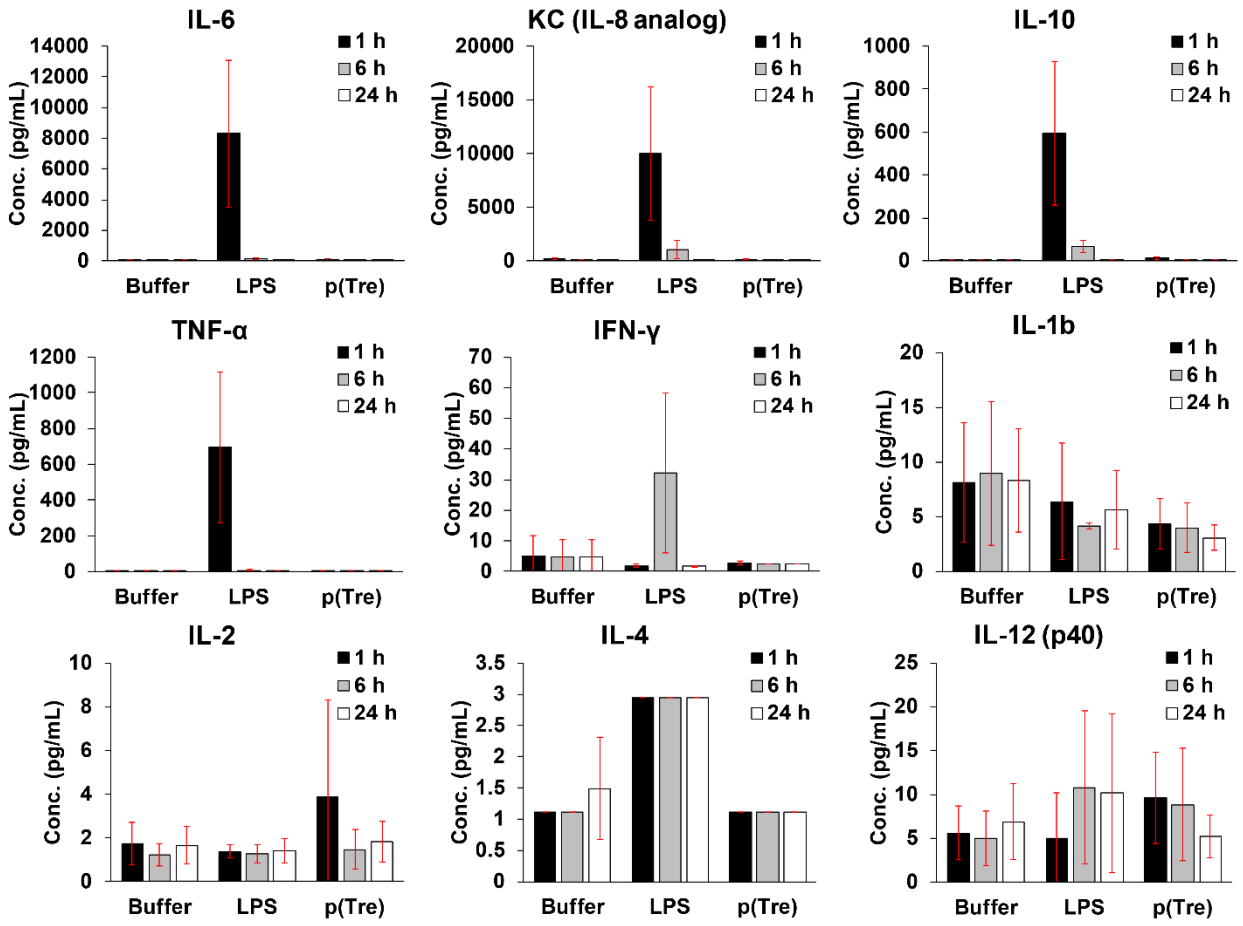

Figure 4-19. Cytokine levels in mice injected with buffer, lipopolysaccharide (20 μg/kg), or trehalose polymer (p(Tre), 10 mg/kg) (n = 5).

4.2.3 Conclusions

We have developed an efficient approach to synthesize G-CSF-trehalose polymer conjugate using CuAAC, with low residual copper levels. The conjugate exhibited extended *in vivo* activity profile compared to the free protein, likely due to the extended serum half-life. We also established a route to modify the unstable G-CSF with a PET chelator by using the MBP fusion protein as both a stabilizing group to prevent G-CSF degradation during conjugation at basic pH and a protecting group for the N-terminus that can be later used for conjugation to polymers. PET imaging of G-CSF showed rapid clearance from the blood, with the kidneys as the

major elimination pathway. The conjugates are expected to significantly reduce this renal elimination pathway, and this will be confirmed by PET imaging of the conjugates. Toxicity and immunological evaluation indicate that the trehalose polymer is non-toxic and non-immunogenic. In the future, the bioactivity of G-CSF and the conjugate will be tested for their stability, and the biodistribution and toxicity experiments will be conducted for the conjugate. Overall, the results strongly suggest that trehalose polymer conjugation to therapeutic proteins is an effective method to improve stability and pharmacokinetics of protein drugs.

4.2.4 Experimental Section

Materials

Trehalose (The Endowment for Medical Research, Houston, TX) was dried by azeotropically drying with ethanol, and was kept under vacuum until use. Azobisisobutyronitrile (AIBN) was recrystallized from acetone before use. 2-[4-[(bis[(1-*tert*-butyl-1*H*-1,2,3-triazol-4-yl)methyl]amino)methyl]-1*H*-1,2,3-triazol-1-yl]acetic acid (BTTAA) was purchased from Ark Pharm and used as received. Endoproteinase Lys-C used for conjugation site analysis was purchased from Thermo Fisher Scientific. Deferoxamine (DFO) (Sigma-Aldrich) and *p*-isothiocyanatobenzyl-DFO (Macrocyclics) were used as received. Trehalose monomer,[21] 2-azido-1-ethylamine,[85] 2-(ethyltrithiocarbonate)propionic acid,[58] 4-cyano-4-(ethylthiocarbonothioylthio)pentanoic acid,[86] and deferoxamine-squaramide[79] were synthesized as previously reported. Trehalose polymer used for toxicity and immunological experiment was synthesized by free radical polymerization (M_n = 33.4 kDa, $Đ$ = 2.56 by DMF SEC).[22] Methoxy poly(ethylene glycol) azide was purchased from Jenkem Technology (Plano, TX) and used as received (M_n = 20.4 Kda, $Đ$ = 1.02). G-CSF was expressed as previously reported,[68] but using

tobacco etch virus (TEV) protease cleavage sequence in place of enterokinase (EK) cleavage sequence. TEV protease was obtained from the Protein Expression Lab at the UCLA-DOE Institute. Ni-NTA resin was purchased from Thermo Fisher Scientific. Endotoxin was removed using Triton-X114 followed by detergent removal using a macroporous hydrophobic resin (Bio-Beads™ SM-2, Bio-Rad),[87] and endotoxin level was measured using ToxinSensor™ Chromogenic LAL Endotoxin Assay Kit (GenScript).

Analytical Techniques

NMR spectra were recorded on a Bruker DRX 500 MHz or a Bruker AV 500 MHz. Silica gel column chromatography was performed on a Biotage Isolera One purification system. Size exclusion chromatography (SEC) was conducted on a Shimadzu HPLC system equipped with a refractive index detector RID-10A and two Polymer Laboratories PLgel 5 μm mixed D columns (with guard column). Lithium bromide (0.1 M) in *N*,*N*-dimethylformamide (DMF) at 50 °C was used as the eluent (flow rate: 0.8 mL/min). Fast protein liquid chromatography (FPLC) was performed on a Bio-Rad BioLogic DuoFlow chromatography system equipped with a GE Healthcare HiTrap Heparin HP column (1 mL) and eluted with 20 mM sodium acetate buffer, pH 5.0 with a salt gradient from 0 M to 1 M NaCl. Infrared (IR) spectra were acquired on a Perkin-Elmer Spectrum One instrument equipped with a universal attenuated total reflection (ATR) assembly. UV-vis absorbance was measured using a microplate reader ELx800 (BioTek Instruments, Winooski, VT). High-resolution mass spectra were obtained on a Thermo Scientific Exactive Plus mass spectrometer with IonSense Direct Analysis in Real Time (DART-MS) ID-CUBE. Matrix-assisted laser desorption/ionization mass spectrometry (MALDI-MS) analysis was performed on a Bruker Ultraflex MALDI-time-of-flight (TOF) mass spectrometer in linear

positive ion mode. Sample was mixed 1:1 with sinapinic acid (10 mg/mL) dissolved in 50% acetonitrile with 0.1 % trifluoroacetic acid on the MALDI target plate. Copper concentration was measured at the UCLA ICP-MS facility by Professor Shane Que Hee.

Synthesis of Small Molecules and Polymers

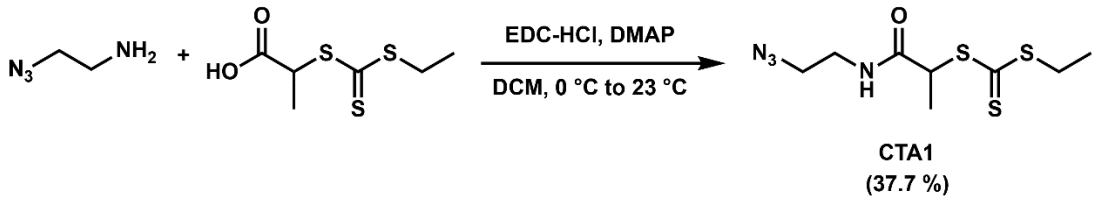

CTA1
(37.7 %)

Synthesis of CTA1. 2-(Ethyltrithiocarbonate)propionic acid (81 mg, 0.39 mmol, 1 equiv.) and 2-azido-1-ethylamine (39 mg, 0.39 mmol, 1 equiv.) were dissolved in 3 mL of dry DCM and cooled to 0 °C. 1-Ethyl-3-(3-dimethylaminopropyl)carbodiimide hydrochloride (EDC-HCl) (148 mg, 0.771 mmol, 2 equiv) and 4-dimethylaminopyridine (DMAP) (9 mg, 0.08 mmol, 0.2 equiv.) were added. The mixture was allowed to warm to 23 °C and stirred for 16 h. The mixture was purified by column chromatography (1:1 hexanes:ethyl acetate) to yield the product (41 mg, 0.15 mmol, 38% yield). ^{1}H NMR (500 MHz in $CDCl_3$) δ: 6.67 (br s, 1H), 4.73 (q, *J* = 7.4 Hz, 1H), 3.43–3.37 (m, 6H), 1.58 (d, *J* = 7.3 Hz, 3H), 1.37 (t, *J* = 7.4 Hz, 3H). ^{13}C NMR (500 MHz in $CDCl_3$) δ: 224.1, 171.0, 50.9, 47.8, 39.3, 32.1, 16.1, 13.0. IR: 3291, 3078, 2972, 2927, 2871, 2095, 1650, 1527, 1446, 1371, 1343, 1300, 1262, 1216, 1077, 1027, 984, 878, 817 cm^{-1}.

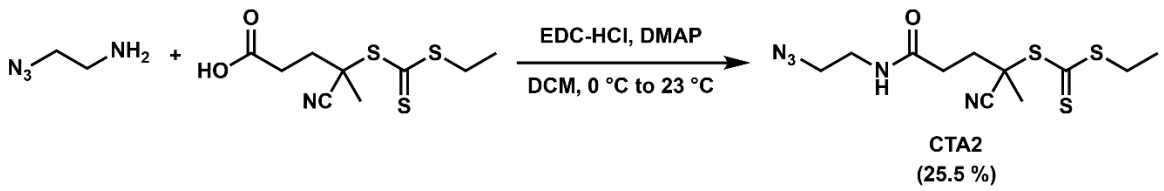

Synthesis of CTA2. 4-cyano-4-(ethylthiocarbonothioylthio)pentanoic acid (338 mg, 1.29 mmol, 1 equiv.), 2-azido-1-ethylamine (130 mg, 1.29 mmol, 1 equiv.) were dissolved in 10 mL of dry DCM and cooled to 0 °C. EDC-HCl (493 mg, 2.57 mmol, 2 equiv) and DMAP (31 mg, 0.26 mmol, 0.2 equiv.) were added. The mixture was allowed to warm to 23 °C and stirred for about 16 h. Solvent was removed in vacuo, and purified by column chromatography (gradient elution of hexanes + 40–50% ethyl acetate) to yield the product (109 mg, 0.329 mmol, 25.5% yield). ^{1}H NMR (500 MHz in $CDCl_3$) δ: 5.79 (br s, 1H), 3.48–3.44 (m, 4H), 3.35 (q, *J* = 7.4 Hz, 2H), 2.57–2.37 (m, 4H), 1.90 (s, 3H), 1.36 (t, *J* = 7.5 Hz, 3H). ^{13}C NMR (500 MHz in $CDCl_3$) δ: 216.9, 171.6, 119.2, 61.2, 46.5, 34.1, 31.5, 30.0, 25.0, 14.3, 12.9. IR: 3292, 3085, 2971, 2929, 2872, 2098, 1649, 1546, 1445, 1375, 1343, 1294, 1260, 1214, 1152, 1115, 1079, 1030, 975, 936, 908, 866, 799 cm^{-1}.

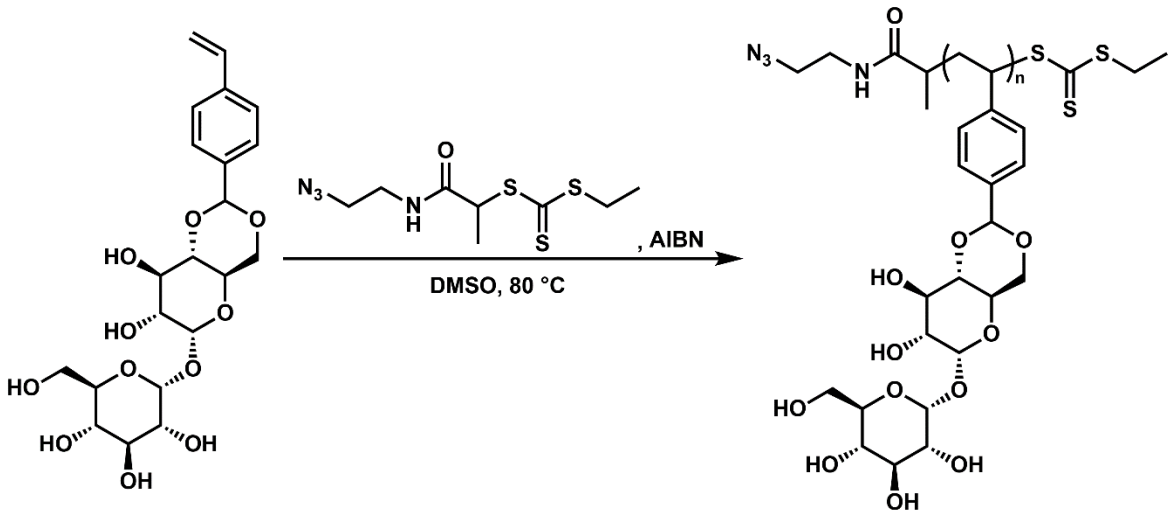

RAFT polymerization of trehalose monomer using CTA1. Trehalose monomer (200 mg, 0.438 mmol, 55 equiv.), **CTA1** (2.22 mg, 0.00797 mmol, 1 equiv.), and AIBN (0.52 mg, 0.0032 mmol, 0.4 equiv) were dissolved in dry DMSO (0.55 mL) and freeze-pump-thawed three times. The polymerization was initiated by immersing the flask into 80 °C oil bath. The polymerization was quenched at 55% conversion by freezing with liquid nitrogen and exposing to air, and dialyzed in deionized water to remove the unreacted monomer (Spectra/Por3® regenerated cellulose membrane, MWCO 3.5 kDa). The water was removed by lyophilization to yield the product. ^{1}H NMR (500 MHz in DMSO-d_6) δ: 7.66–6.91, 6.91–6.05, 5.67–5.32, 5.32–5.11, 5.11–4.88, 4.88–4.69, 4.53–4.31, 4.22–4.05, 4.05–3.89, 3.89–3.76, 3.76–3.67, 3.67–3.53, 3.53–3.46, 3.46–3.39, 3.24–3.09, 2.31–0.61. IR: 3372, 2921, 2875, 2106, 1711, 1638, 1615, 1514, 1418, 1375, 1337, 1307, 1264, 1211, 1145, 1072, 1046, 1016, 983, 928, 824, 799, 720 cm^{-1}. M_n = 11.7 kDa, $Đ$ = 1.31 (DMF SEC).

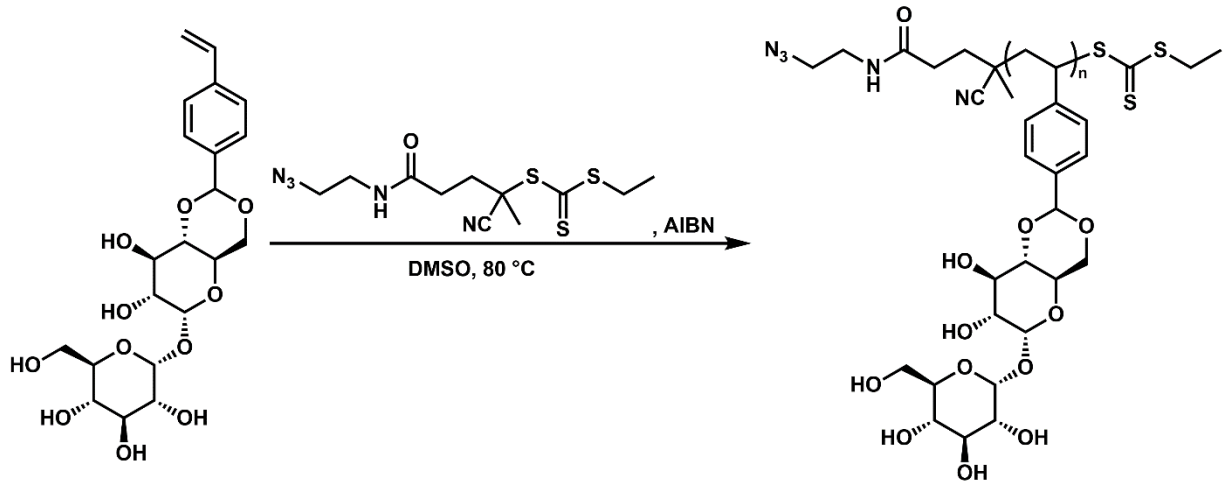

RAFT polymerization of trehalose monomer using CTA2. Trehalose monomer (200 mg, 0.438 mmol, 65 equiv.), **CTA2** (2.22 mg, 0.00797 mmol, 1 equiv.), and AIBN (0.52 mg, 0.0032 mmol, 0.48 equiv) were dissolved in dry DMSO (0.55 mL) and freeze-pump-thawed three times. The polymerization was initiated by immersing the flask into 80 °C oil bath. The polymerization was quenched at 88% conversion by freezing with liquid nitrogen and exposing to air, and dialyzed in deionized water to remove the unreacted monomer (Spectra/Por3® regenerated cellulose membrane, MWCO 3.5 kDa). The water was removed by lyophilization to yield the polymer. ^{1}H NMR (500 MHz in DMSO-d_6) δ: 7.73–6.93, 6.93–6.01, 5.69–5.35, 5.35–5.12, 5.12–4.89, 4.89–4.72, 4.54–4.34, 4.25–4.04, 4.04–3.89, 3.89–3.76, 3.76–3.67, 3.67–3.54, 3.54–3.47, 3.24–3.06, 2.30–0.58. IR: 3362, 2921, 2865, 2111, 1635, 1618, 1514, 1423, 1375, 1271, 1211, 1148, 1110, 1072, 1044, 1016, 976, 928, 826, 799 cm^{-1}. M_n = 15.5 kDa, $Đ$ = 1.20 (DMF SEC). UV-vis spectrum showed trithiocarbonate absorption at λ_{max} = 314 nm.

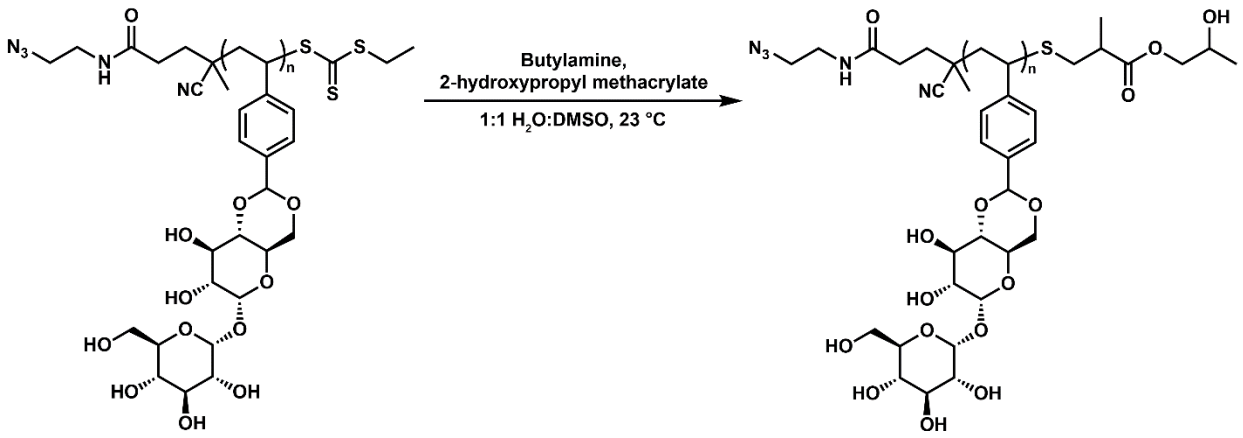

Removal of trithiocarbonate group from the azide-functionalized trehalose polymer by aminolysis. Azide-functionalized polymer (76 mg, 0.0048 mmol, 1 equiv.), *n*-butylamine (94 uL, 0.96 mmol, 200 equiv.), and 2-hydroxypropyl methacrylate (0.13 mL, 0.96 mmol, 200 equiv.) were dissolved in 1:1 water:DMSO (1 mL total) and monitored by UV-vis spectrometer for disappearance of the trithiocarbonate absorption at 314 nm. Cleavage was complete in 3 h. The mixture was diluted with 5 mL of deionized water and dialyzed to remove DMSO before lyophilization to yield the product (72 mg, 95% yield). ^{1}H NMR (500 MHz in DMSO-d_6) δ: 7.53–6.87, 6.87–6.02, 5.70–5.33, 5.33–5.12, 4.88–4.74, 4.47–4.33, 4.27–4.04, 4.04–3.88, 3.88–3.76, 3.76–3.66, 3.66–3.53, 3.53–3.47, 3.47–3.40, 3.24–3.09, 2.20–0.49. M_n = 15.8 kDa, $Đ$ = 1.22 (DMF SEC). UV-vis spectrum showed disappearance of the trithiocarbonate absorption.

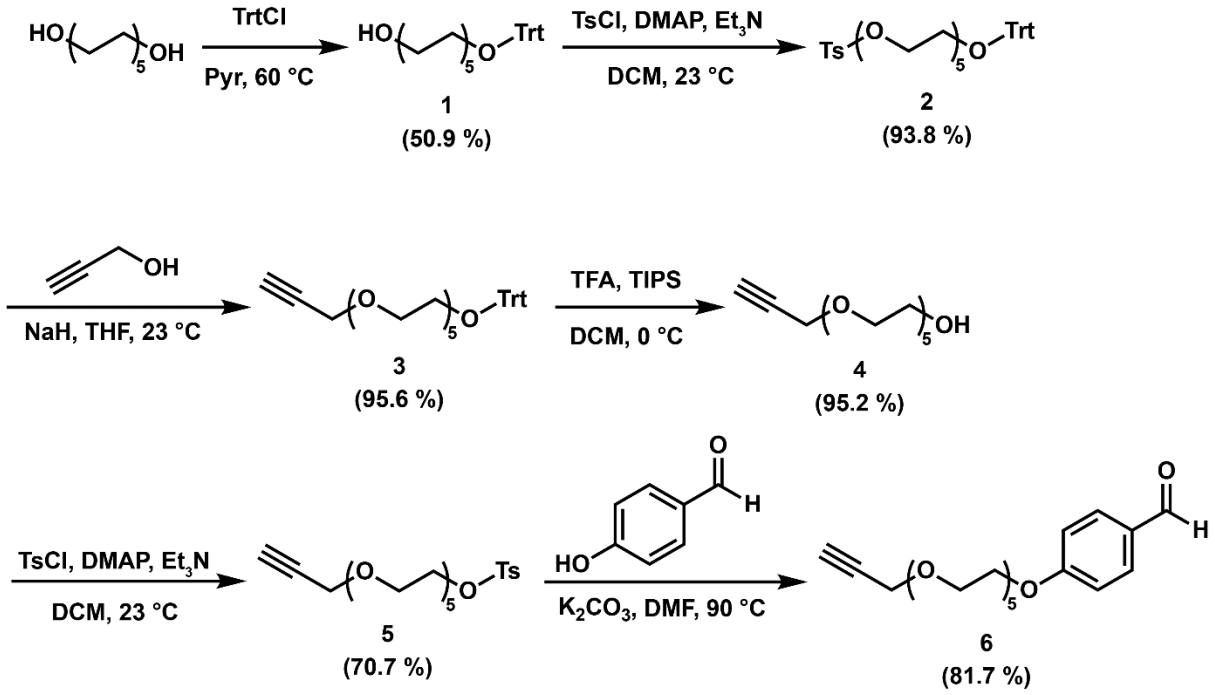

Figure 4-20. Synthesis of alkyne-penta(ethylene glycol)-benzaldehyde linker.

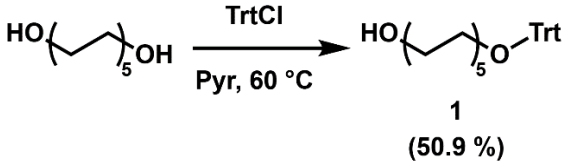

Tritylation of penta(ethylene glycol) (1). Penta(ethylene glycol) (1 g, 4.197 mmol, 2 equiv.) and trityl chloride (585 mg, 2.10 mmol, 1 equiv.) were dissolved in dry pyridine (40 mL) and stirred at 60 °C for 16.5 h. Solvent was removed *in vacuo*, and the solid was extracted with 100 mL of 0.5 M HCl and 100 mL DCM, and the aqueous phase was extracted two more times with 100 mL DCM. The combined organic layer was dried with $MgSO_4$ and added to silica gel and concentrated *in vacuo* for dry load, and purified by column chromatography (ethyl acetate + 0 – 10% MeOH) to yield the product (513 mg, 1.07 mmol, 50.9% yield). ^{1}H NMR (500 MHz in $(CD_3)_2CO$) δ: 7.50 (d, *J* = 7.6 Hz, 6H), 7.33 (t, *J* = 7.7 Hz, 6H), 7.25 (t, *J* = 7.5 Hz, 3H), 3.67 (t, *J* = 5.1 Hz, 2H), 3.64–

3.57 (m, 14H), 3.50 (t, J = 5.1 Hz, 2H), 3.18 (t, J = 5.0 Hz, 2H). ^{13}C NMR (500 MHz in $(CD_3)_2CO$) δ: 145.27, 129.56 128.61, 127.80, 87.21, 73.54, 71.54, 71.36, 71.34, 71.29, 71.27, 71.13, 64.32, 61.98. DART-MS $[C_{29}H_{36}O_6 + NH_4]^+$ calculated 498.2856, observed 498.2858.

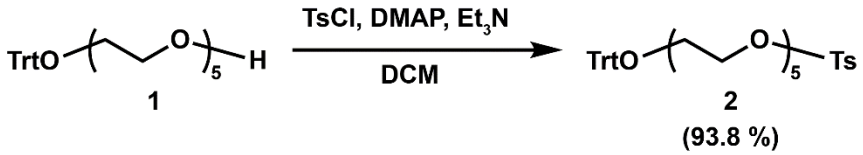

Tosylation of tritylated penta(ethylene glycol) (2). Tritylated penta(ethylene glycol) (2.036 g, 4.236 mmol, 1 equiv.), tosyl chloride (1.615 g, 8.473 mmol, 2 equiv.), and DMAP (104 mg, 0.847 mmol, 0.2 equiv.) were dissolved in DCM (21 mL) and cooled to 0 °C. Triethylamine (1.18 mL, 8.47 mmol, 2 equiv.) was added dropwise, and the mixture was warmed to 23 °C and stirred for 24 h. The mixture was extracted with 100 mL DCM and 100 mL brine, and the aqueous layer was extracted twice with 100 mL DCM. The combined organic layer was dried with $MgSO_4$ and added to silica gel and concentrated *in vacuo* for dry load, and purified by column chromatography (1:1 hexanes:ethyl acetate to 100% ethyl acetate) to yield the product (2.523 g, 3.975 mmol, 93.8% yield). ^{1}H NMR (500 MHz in $CDCl_3$) δ: 7.79 (d, J = 8.3 Hz, 2H) 7.46 (d, J = 7.5 Hz, 6H), 7.33–7.26 (m, 8H), 7.22 (t, J = 7.3 Hz, 3H), 4.13 (t, J = 4.8 Hz, 2H), 3.68–3.60 (m, 12H), 3.57–3.54 (m, 4H), 3.23 (t, J = 5.2 Hz, 2H), 2.43 (s, 3H). ^{13}C NMR (500 MHz in $CDCl_3$) δ: 144.30, 128.85, 127.89, 127.05, 86.65, 79.81, 74.62, 70.94, 70.85, 70.82, 70.81, 70.78, 70.75, 70.71, 70.54, 69.24, 63.46, 58.53. DART-MS $[C_{36}H_{46}NO_8S + NH_4]^+$ calculated 652.2944, observed 652.2947.

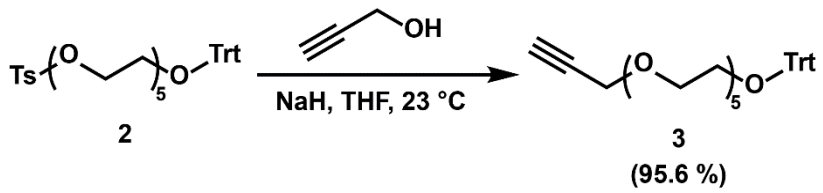

Propargylation of tritylated penta(ethylene glycol) tosylate (3). Sodium hydride (60% dispersion in mineral oil) (630 mg, 15.8 mmol, 10 equiv.) was suspended in dry THF (10 mL) and cooled to 0 °C. Propargyl alcohol (0.92 mL, 16 mmol, 1 equiv.) was added dropwise. The mixture was stirred at 0 °C for 30 min. Tritylated penta(ethylene glycol) tosylate (1 g, 1.575 mmol, 1 equiv.) dissolved in 20 mL of dry THF was added dropwise. The reaction mixture was warmed to 23 °C and stirred for 21.5 h. Solvent was removed *in vacuo*, and the mixture was extracted with 50 mL brine and 50 mL DCM, and the aqueous layer was extracted twice with 50 mL DCM and then with 50 mL ethyl acetate. The combined organic layer was dried with $MgSO_4$ and added to silica gel and concentrated *in vacuo* for dry load, and purified by column chromatography (1:1 hexanes:diethyl ether to 100% diethyl ether) to yield the product (781 mg, 1.51 mmol, 95.6% yield). ^{1}H NMR (500 MHz in $CDCl_3$) δ: 7.46 (d, *J* = 7.7 Hz, 6H), 7.29 (t, *J* = 7.7 Hz, 6H), 7.22 (t, *J* = 7.4 Hz, 3H), 4.19 (d, *J* = 2.3 Hz, 2H), 3.69–3.64 (m, 18H), 3.23 (t, *J* = 5.2 Hz, 2H), 2.41 (t, *J* = 2.2 Hz, 1H). ^{13}C NMR (500 MHz in $CDCl_3$) δ: 144.27, 128.86, 127.90, 127.06, 86.66, 79.82, 74.63, 70.94, 70.86, 70.83, 70.81, 70.78, 70.75, 70.72, 70.54, 69.25, 63.46, 58.54. DART-MS $[C_{32}H_{38}O_6 + NH_4]^+$ calculated 536.3012, observed 536.3012.

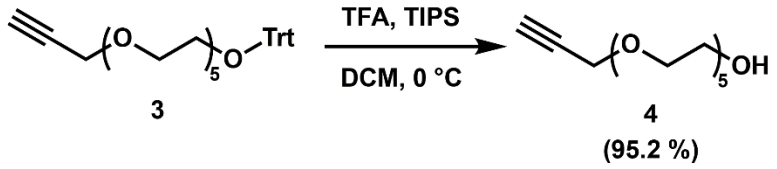

Detritylation of penta(ethylene glycol) alkyne (4). Tritylated penta(ethylene glycol) alkyne (925 mg, 1.78 mmol) and triisopropylsilane (1 mL) were dissolved in 8 mL DCM and cooled to 0 °C. To this mixture was added trifluoroacetic acid (TFA, 1 mL) in 4 mL dropwise. The mixture was stirred at 0 °C for 5 min, after which the reactant was fully consumed as monitored by TLC. Saturated sodium bicarbonate (25 mL) was added dropwise, and the mixture was extracted by adding additional 25 mL of saturated sodium bicarbonate and 50 mL DCM. The aqueous layer was extracted two times with 50 mL DCM. The combined organic layer was dried with $MgSO_4$ and added to silica gel and concentrated *in vacuo* for dry load, and purified by column chromatography (ether + 0 – 10% MeOH) to yield the product (469 mg, 1.70 mmol, 95.2% yield). ^{1}H NMR (500 MHz in $CDCl_3$) δ: 4.19 (d, J = 2.3 Hz, 2H), 3.72–3.59 (m, 20H), 2.87 (br s, 1H), 2.42 (t, J = 2.4 Hz, 1H). ^{13}C NMR (500 MHz in $CDCl_3$) δ: 79.76, 74.64, 72.52, 70.67, 70.63, 70.60, 70.51, 70.39, 69.21, 61.76, 58.50. DART-MS $[C_{13}H_{24}O_6 + NH_4]^+$ calculated 294.1917, observed 294.1917.

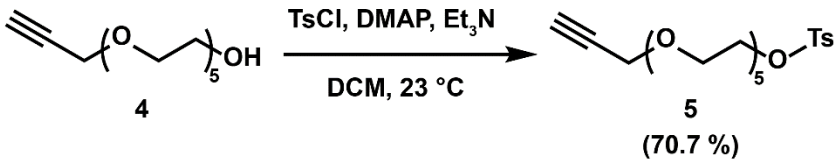

Tosylation of penta(ethylene glycol) alkyne (5). Penta(ethylene glycol) alkyne (468 mg, 1.69 mmol, 1 equiv.), tosyl chloride (646 mg, 3.39 mmol, 2 equiv.), and DMAP (41 mg, 0.34 mmol, 0.2 equiv.) were dissolved in 8.5 mL DCM and cooled to 0 °C. Triethylamine (0.47 mL, 3.4 mmol,

2 equiv.) was added dropwise, and the reaction was allowed to warm to 23 °C and stirred for 25 h. The mixture was exracted with 100 mL DCM and 100 mL brine, and the aqueous layer was extracted twice with 50 mL DCM. The combined organic layer was dried with $MgSO_4$ and concentrated *in vacuo*, and purified by column chromatography (ether + 0 – 70% ethyl acetate) to yield the product (499 mg, 1.20 mmol, 70.7% yield). ^{1}H NMR (500 MHz in $CDCl_3$) δ: 7.80 (d, *J* = 8.2 Hz, 2H), 7.34 (d, *J* = 8.0 Hz, 2H), 4.20 (d, *J* = 2.3 Hz, 2H), 4.16 (t, *J* = 4.8 Hz, 2H), 3.70–3.68 (m, 6H), 3.65–3.61 (m, 8H), 3.58 (s, 4H), 2.45 (s, 3H), 2.42 (t, *J* = 2.3 Hz, 1H). ^{13}C NMR (500 MHz in $CDCl_3$) δ: 144.93, 133.15, 129.98, 128.15, 79.81, 74.66, 70.91, 70.76, 70.72, 70.71, 70.67, 70.55, 69.38, 69.26, 68.83, 58.55, 21.80. DART-MS $[C_{20}H_{30}O_8S + NH_4]$+ calculated 448.2005, observed 448.2006.

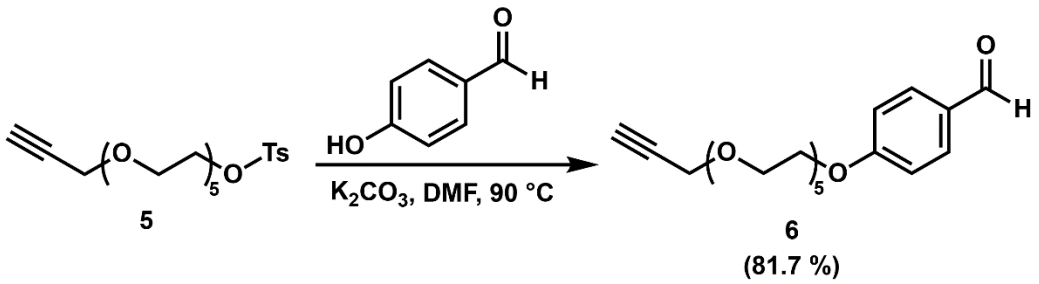

Synthesis of alkyne-penta(ethylene glycol)-benzaldehyde linker (6). Tosylated penta(ethylene glycol) alkyne (496 mg, 1.19 mmol, 1 equiv.), 4-hydroxybenzaldehyde (175 mg, 1.43 mmol, 1.2 equiv.), and potassium carbonate (658 mg, 4.76 mmol, 4 equiv.) were dissolved in 12 mL DMF and stirred at 90 °C for 47 h. The solvent was removed *in vacuo*, and extracted with 250 mL brine and 150 mL DCM. The aqueous layer was extracted twice with 150 mL DCM. The combined organic layer was dried with $MgSO_4$ and added to silica gel and concentrated *in vacuo* for dry load, and purified by column chromatography (ether + 0 – 100% ethyl acetate) to yield the product (370 mg, 0.973 mmol, 81.7% yield). ^{1}H NMR (500 MHz in $CDCl_3$) δ: 9.89 (s, 1H), 7.83 (d, *J* = 8.6 Hz,

2H), 7.02 (d, *J* = 8.6 Hz, 2H), 4.22 (t, *J* = 4.7 Hz, 2H), 4.20 (d, *J* = 2.5 Hz, 2H), 3.89 (t, J = 4.8 Hz, 2H), 3.74–3.72 (m, 2H), 3.71–3.65 (m, 14H), 2.42 (t, *J* = 2.2 Hz, 1H). ^{13}C NMR (500 MHz in $CDCl_3$) δ: IR: 3251, 2866, 2739, 2111, 1684, 1598, 1575, 1510, 1454, 1426, 1393, 1310, 1254, 1216, 1161, 1095, 1054, 1034, 946, 921, 832 cm^{-1}. DART-MS $[C_{20}H_{28}O_7 + NH_4]^+$ calculated 398.2179, observed 398.2179.

Conjugation of Alkyne-Penta(ethylene glycol)-Benzaldehyde Linker to G-CSF

To G-CSF (456 μg in 82 μL of 100 mM sodium acetate buffer, pH 5.0) was added 9.1 μL of alkyne-penta(ethylene glycol)-benzaldehyde dissolved in $NaBH_3CN$ (10 mg/mL of the alkyne and 12.5 mg/mL of $NaBH_3CN$ (5 mg/mL G-CSF, 10 mol equiv. of the alkyne linker, 75 mol equiv. of $NaBH_3CN$). The mixture was incubated at 25 °C with 1250 rpm shaking for 36 h, and the free linker was removed by repeated buffer exchange with Centriprep™ tubes (molecular weight cut-off (MWCO) = 3 kDa). G-CSF-DFO-alkyne was synthesized using the same procedure.

Lys-C Digestion of G-CSF for Conjugation Site Determination

G-CSF-alkyne conjugate (100 μg) was buffer exchanged to 100 mM ammonium bicarbonate, pH 8.0 and concentrated to about 20 μL. Urea (7.2 mg, 6 M) was added and the mixture was sonicated for 10 min. The protein was reduced by adding 0.2 μL of 500 mM tris(2-carboxyethyl)phosphine hydrochloride (TCEP-HCl) (about 20 mM in the mixture) and incubated at 60 °C for 30 min. After warming to 23 °C, 0.2 μL of 500 mM 2-iodoacetamide (about 20 mM in the mixture) was added and the mixture was incubated in the dark at 23 °C for 30 min. After alkylating the cysteines, 40 μL water was added to dilute the urea to 2 M. To this mixture was added 2 μL Lys-C (1 mg/mL, 1:50 ratio compared to the G-CSF conjugate), and the sample was incubated at 60 °C for 13 h before LC-MS analysis (Dr. Julian Whitelegge, The Pasarow Mass Spectrometry Laboratory, The NPI-Semel Institute, UCLA David Geffen School of Medicine).

Conjugation of Polymers to G-CSF-Alkyne

Representative Procedure: Trehalose polymer conjugation to G-CSF. To G-CSF-alkyne (203 μg in 25 μL of 25 mM sodium acetate buffer, pH 4.0) was added azide-functionalized trehalose

polymer (3.4 mg, 220 nmol, 20 mol equiv.). The mixture was mixed by pipetting and centrifuged for 1 min to remove any air bubbles. To this mixture was added 1.35 μL of $CuSO_4$/BTTAA (15 mM $CuSO_4$ and 90 mM of BTTAA), 1.35 μL of 150 mM aminoguanidine, and 1.35 μL of 300 mM sodium ascorbate (final concentrations: 0.5 mM $CuSO_4$, 3 mM BTTAA, 5 mM aminoguanidine, and 10 mM sodium ascorbate). The mixture was incubated at 23 °C for 23 h, and then exchanged to 20 mM sodium acetate buffer, pH 5 with 10 mM EDTA and purified by cation exchange chromatography on FPLC using a heparin column. Residual unmodified G-CSF was removed by repeated centrifuge cycles using Centriprep™ tubes with MWCO of 30 kDa. PEG conjugate was synthesized using the same procedure, except using PEG-azide instead of trehalose polymer.

Conjugation of Deferoxamine (DFO) to G-CSF

Maltose binding protein (MBP)-G-CSF fusion protein (17.2 mg of total protein content) in 3.1 mL of 0.1 M carbonate-bicarbonate buffer, pH 9 was mixed with 344 μL of 5 mg/mL DFO-squaramide in 10% DMSO. The mixture was incubated at 23 °C for 58 h, and then buffer exchanged into 0.1 M sodium acetate, pH 6 using 30 kDa MWCO Centriprep™ tubes to remove unreacted DFO. MBP was cleaved from G-CSF by digestion with TEV protease (1.72 mg, 10:1 weight ratio of protein:protease) at 23 °C for 7 h. G-CSF-DFO and free G-CSF were purified from MBP by Ni-nitrilotriacetic acid (NTA) affinity chromatography.

Animal Usage

All animal experiments were conducted according to the protocol approved by the UCLA Animal Research Committee (ARC).

In Vivo Bioactivity of G-CSF and G-CSF-Trehalose Polymer Conjugate

CD1 mice (female, 6 wks, n = 6) were intraperitoneally injected with cyclophosphamide (150 mg/kg each) at days -2 and 0 to induce neutropenia (second injection date is day 0 by convention). Drinking water was treated with enrofloxacin (0.25 mg/mL) as a prophylactic antibiotic to prevent infection during neutropenia. The mice were either administered with G-CSF (1 mg/kg on days 1 and 2) or G-CSF-trehalose polymer conjugate (1 mg/kg based on the protein concentration on day 1) by subcutaneous injection. Blood (around 40 μL) was collected into EDTA-coated tubes by saphenous bleed on days 0, 1, 3, and 5. On day 7, the mice were euthanized and the blood was collected by cardiac puncture. Samples were analyzed for blood cell counts by the Pathology and Laboratory Medicine Services, UCLA Division of Laboratory Animal Medicine (DLAM).

PET Imaging of G-CSF-DFO

Radiolabelling and PET/CT imaging were conducted by the UCLA Crump Institute for Molecular Imaging. Briefly, C57BL/6 mice (female, 8-12 wks, n = 3) were injected intravenously with G-CSF-DFO that has been radiolabeled with ^{89}Zr using a literature procedure[82] (around 11 μCi radioactivity or 13 μg of protein). Briefly, 89Zr-oxalate and G-CSF-DFO were incubated at pH 7.0 at room temperature for 1 h, and radiolabeling efficiency was measured using instant thin layer chromatography (Biodex Medical Systems) with a Wizard 3" 1480 Automatic Gamma Counter (Perkin-Elmer). The protein was purified from the free ^{89}Zr by BioRad6 Spin columns (Bio-Rad). The mice were observed by PET for 40 h, and then euthanized for analysis of radioactivity in each organ.

Toxicological Evaluation of Trehalose Polymer

CD1 mice (female, 6 wks, n = 6) were intravenously injected with trehalose polymer synthesized by free radical polymerization (10 mg/kg). After 48 h, the mice were euthanized and blood was collected by cardiac puncture. Blood for liver enzyme (ALT and AST) and kidney metabolite (blood urea nitrogen and creatinine) analysis was collected into the silica clot activator tubes (BD Vacutainer®), and blood for hematology was collected into EDTA-coated tubes. Serum and blood samples were analyzed by the Pathology and Laboratory Medicine Services, UCLA Division of Laboratory Animal Medicine (DLAM).

Immunological Evaluation of Trehalose Polymer

CD1 mice (female, 6 wks, n = 5) were intraperitoneally injected with a trehalose polymer synthesized by free radical polymerization (10 mg/kg). The negative control group was injected with buffer (Dulbecco's phosphate buffered saline (D-PBS)), and the positive control group was injected with lipopolysaccharide (20 μg/kg). Blood was collected from alternate sides by retro-orbital bleeding at 1 h and 6 h after the injection. At 24 h, the mice were euthanized and the blood was collected by cardiac puncture. Blood was collected into the silica clot activator tubes (BD Vacutainer®), and serum was separated by centrifuging at 2000 × g for 10 min at 4 °C. IL1b, IL2, IL4, IL6, KC (IL8 murine analog), IL10, IL12, IFNγ, and TNFα were measured using the multiplexed ELISA-type assay (Luminex xMAP) at the UCLA Immune Assessment Core (Dept. Pathology and Laboratory Medicine).

Statistical Analysis

Student's t-test assuming unequal sample variance was used to test the difference between experimental groups. Results were considered significantly different if $p < 0.05$.

NMR Spectra

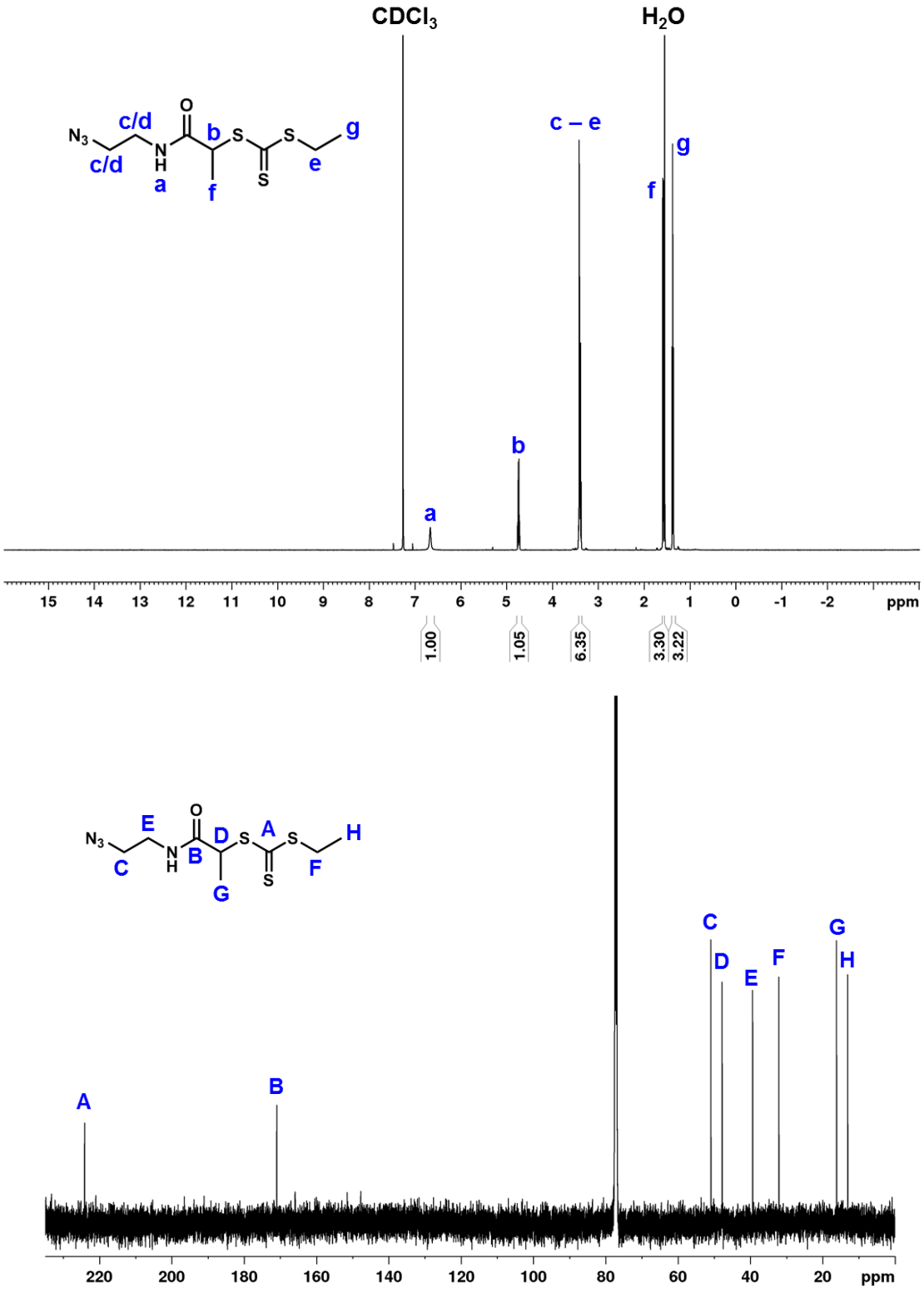

Figure 4-21. ^{1}H (top) and ^{13}C (bottom) NMR spectra of **CTA1** ($CDCl_3$).

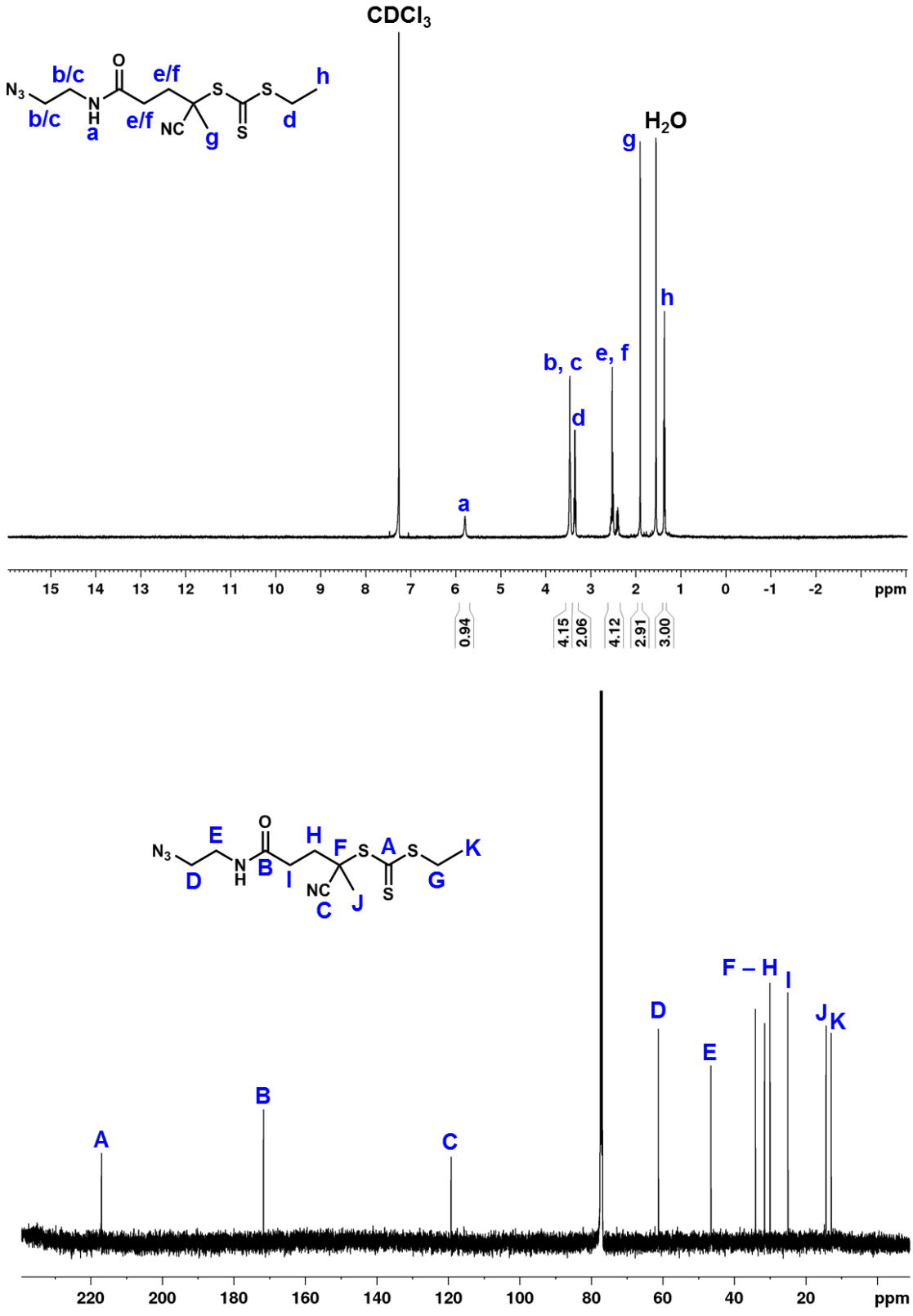

Figure 4-22. ^{1}H (top) and ^{13}C (bottom) NMR spectra of **CTA2** ($CDCl_3$).

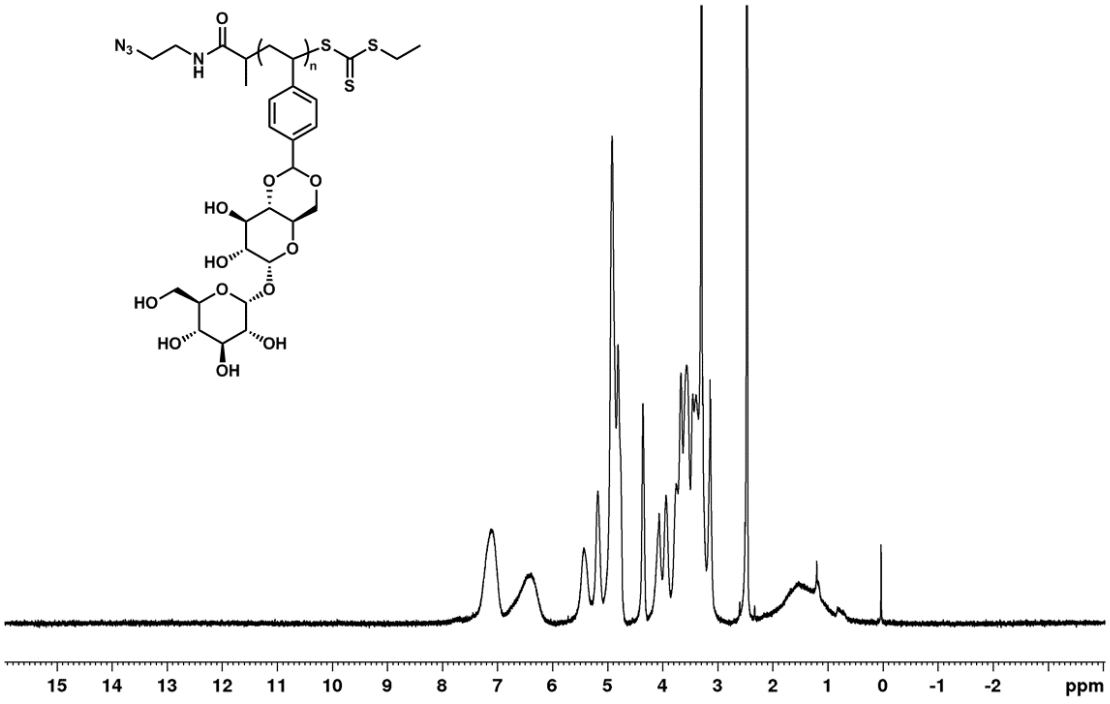

Figure 4-23. ^{1}H NMR spectrum of trehalose polymer from RAFT polymerization using **CTA1** (DMSO-d_6).

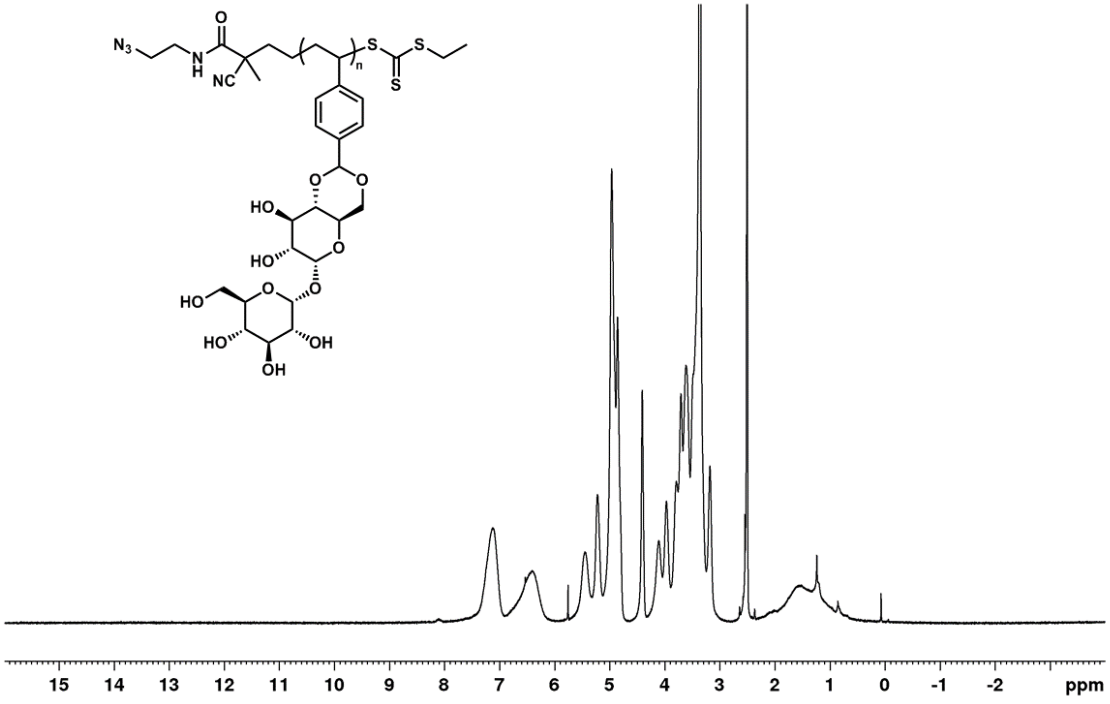

Figure 4-24. ^{1}H NMR spectrum of trehalose polymer from RAFT polymerization using **CTA2** (DMSO-d_6).

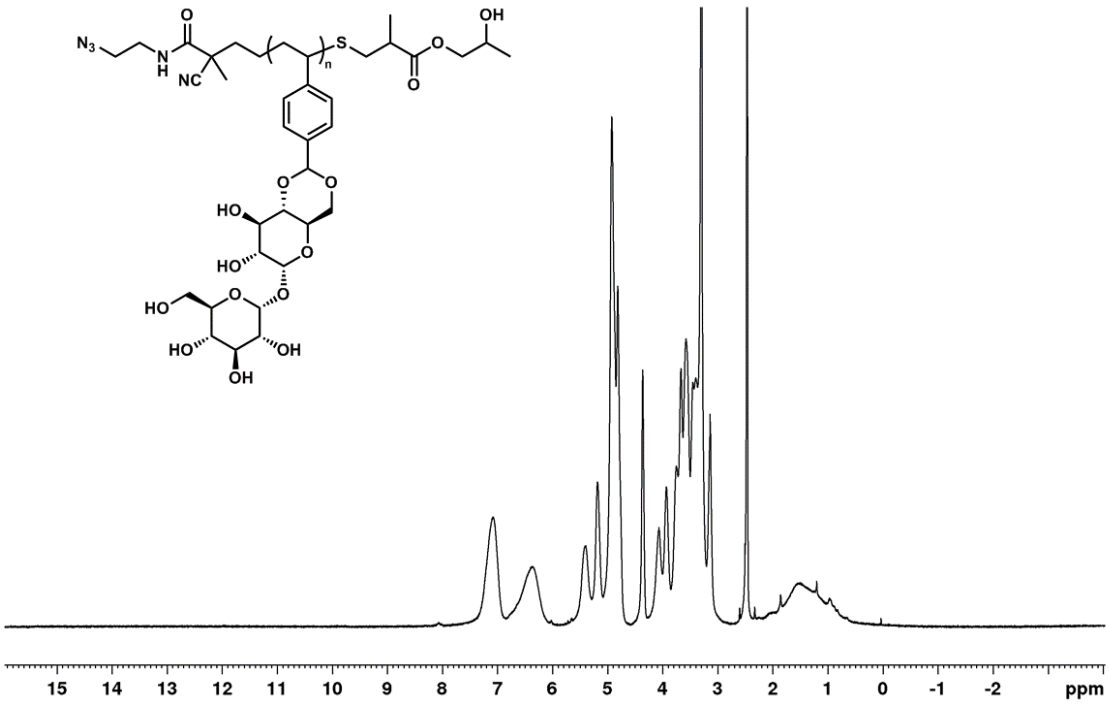

Figure 4-25. ^{1}H NMR spectrum of azide-functionalized trehalose polymer (from **CTA2**) after removal of the trithiocarbonate group (DMSO-d_6).

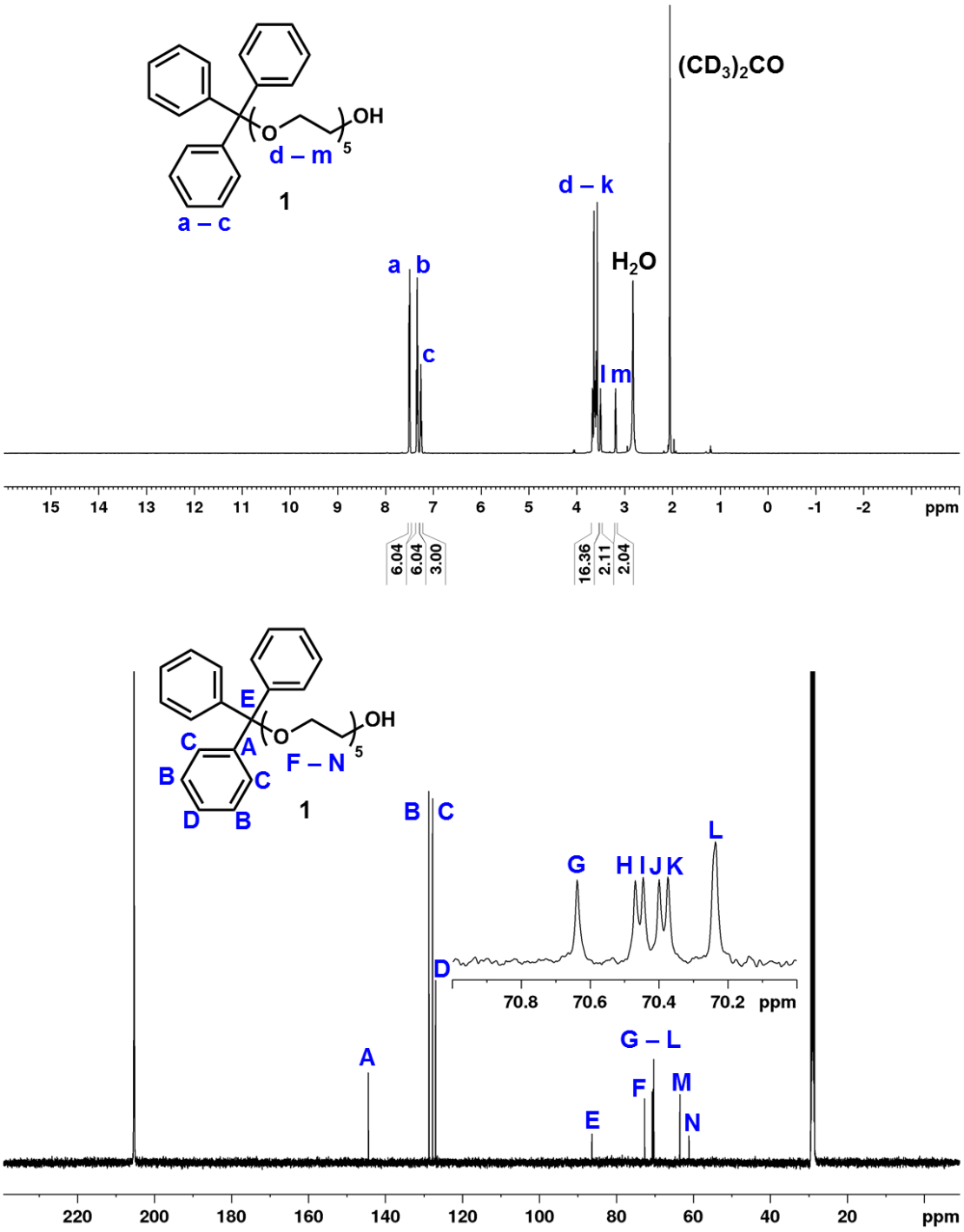

Figure 4-26. ^{1}H (top) and ^{13}C (bottom) spectra of tritylated penta(ethylene glycol) **1** ($(CD_3)_2CO$).

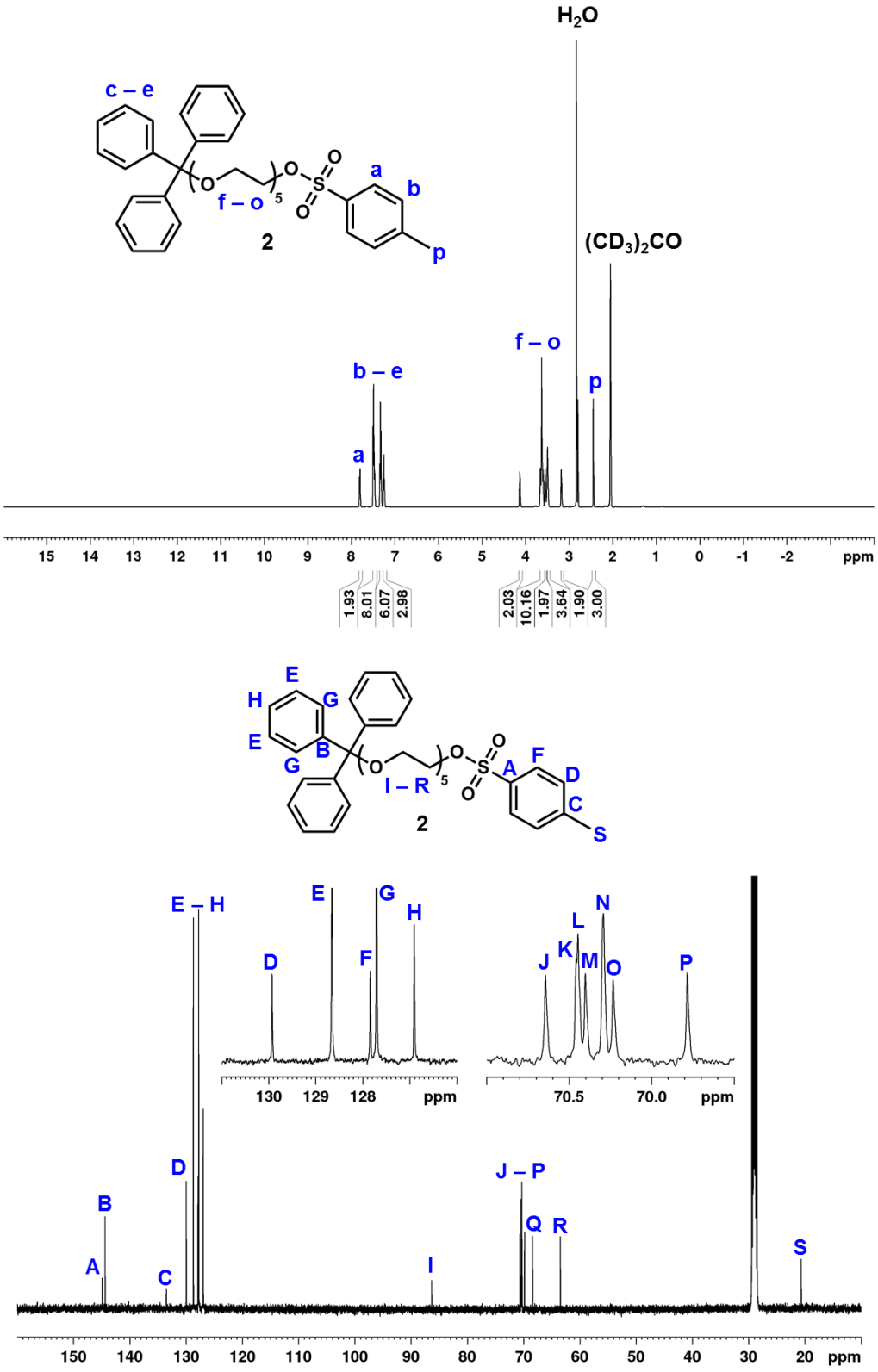

Figure 4-27. ^{1}H (top) and ^{13}C (bottom) spectra of tritylated penta(ethylene glycol) tosylate **2** ($(CD_3)_2CO$).

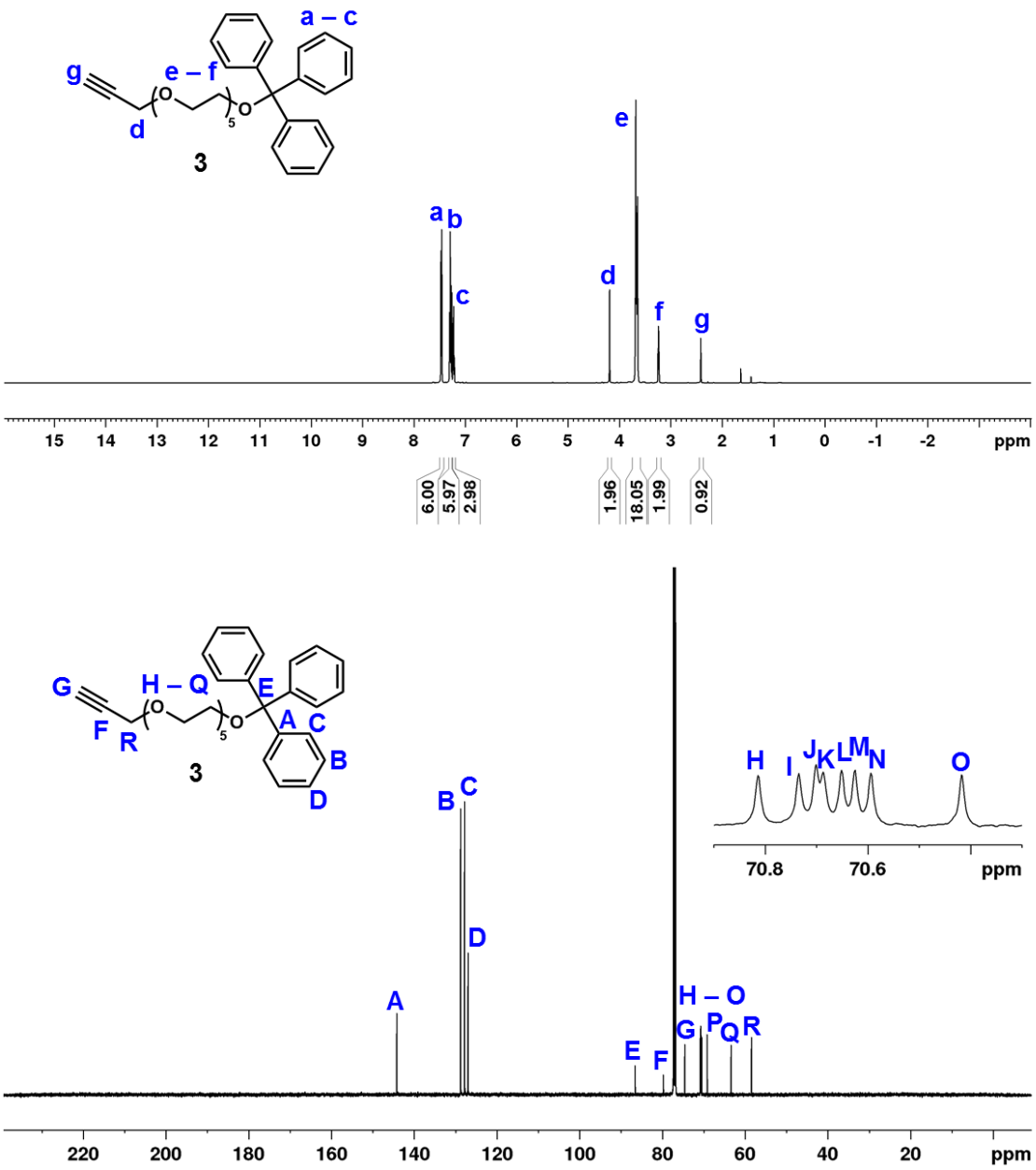

Figure 4-28. ^{1}H (top) and ^{13}C (bottom) spectra of tritylated penta(ethylene glycol) alkyne **3** ($CDCl_3$).

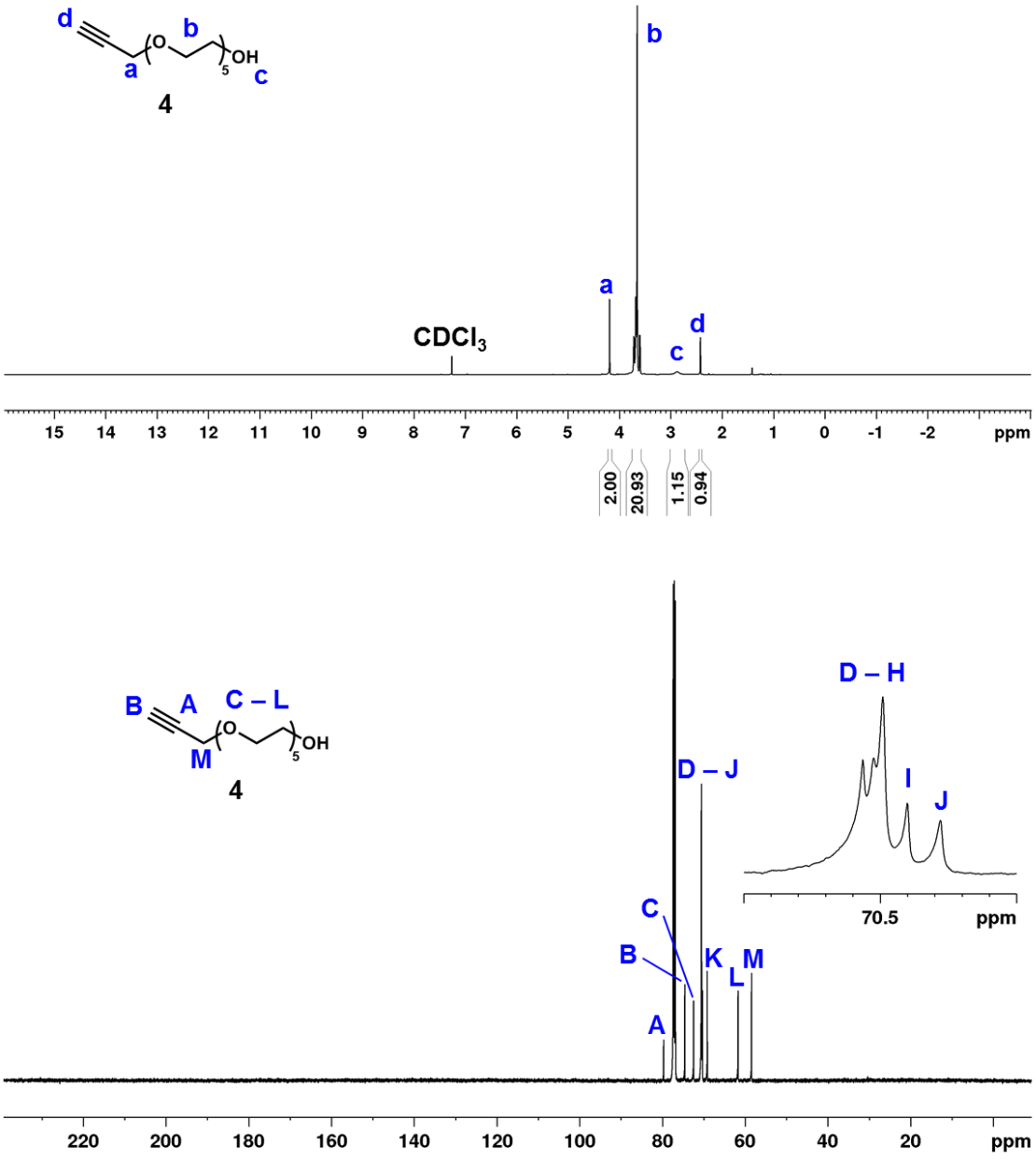

Figure 4-29. ^{1}H (top) and ^{13}C (bottom) spectra of penta(ethylene glycol) alkyne **4** ($CDCl_3$).

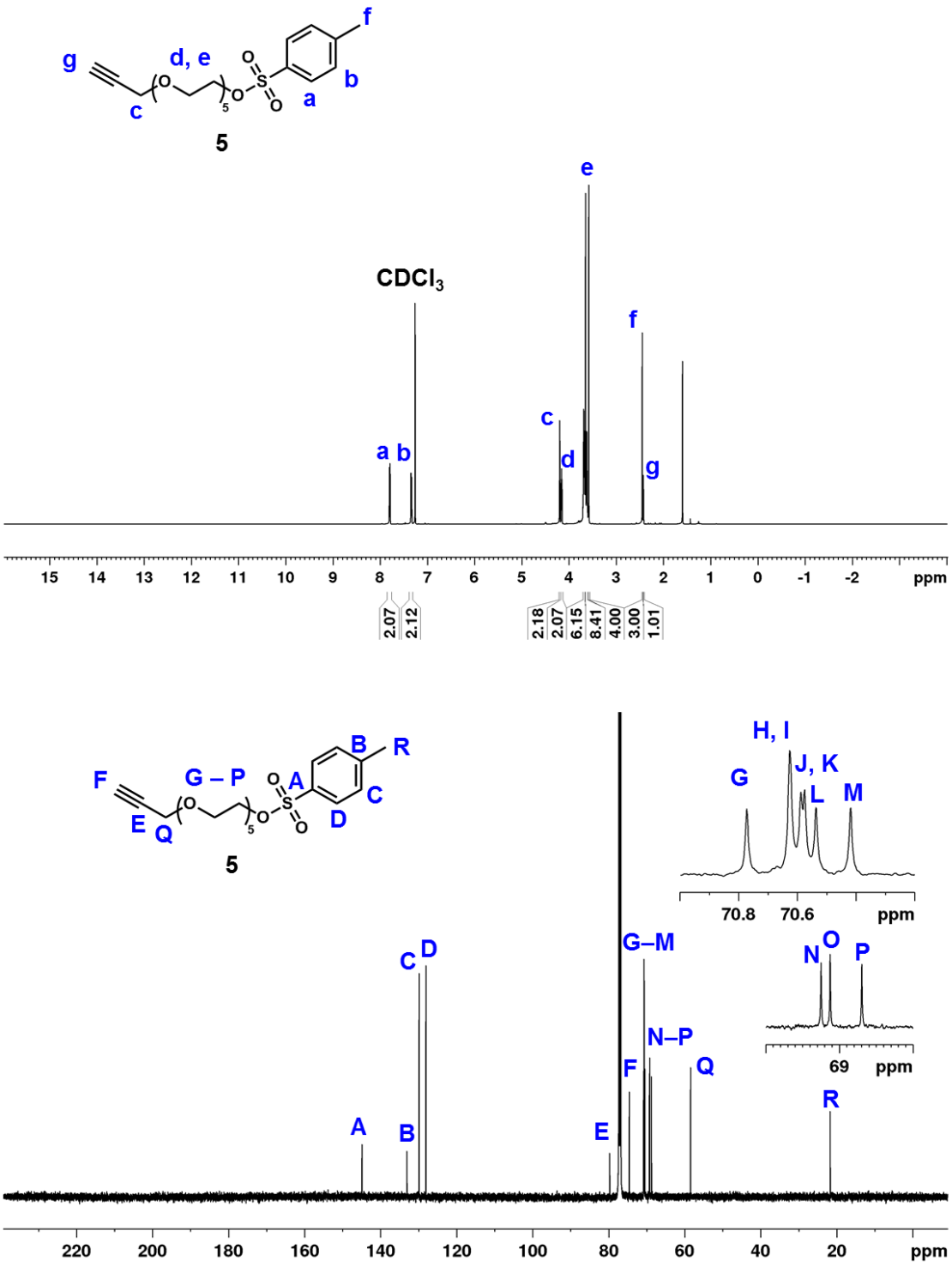

Figure 4-30. ^{1}H (top) and ^{13}C (bottom) spectra of tosylated penta(ethylene glycol) alkyne **5** ($CDCl_3$).

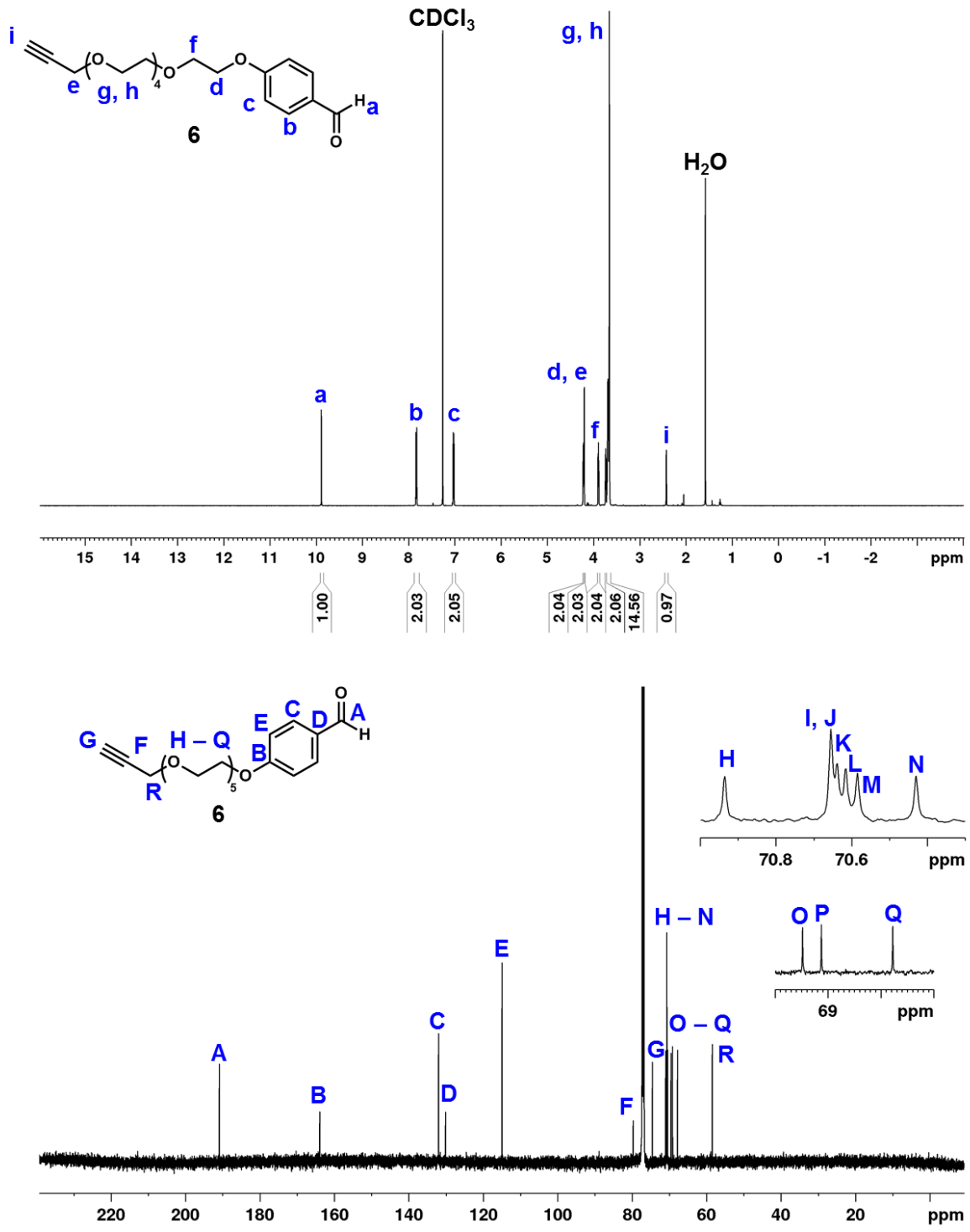

Figure 4-31. ^{1}H (top) and ^{13}C (bottom) spectra of alkyne-penta(ethylene glycol)-benzaldehyde linker **6** ($CDCl_3$).

Additional Figures

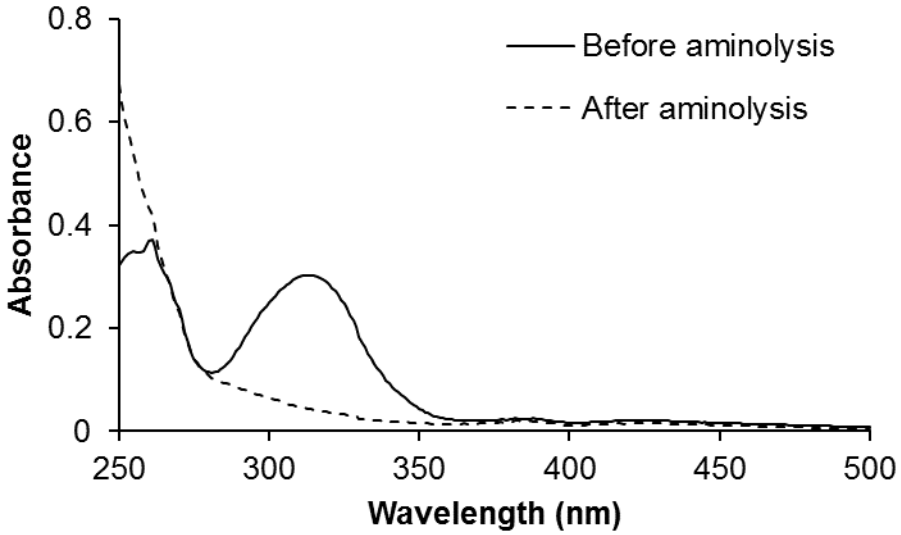

Figure 4-32. UV-vis spectrum of azide-functionalized trehalose polymer before (solid) and after (dashed) aminolysis to remove the trithiocarbonate end-group.

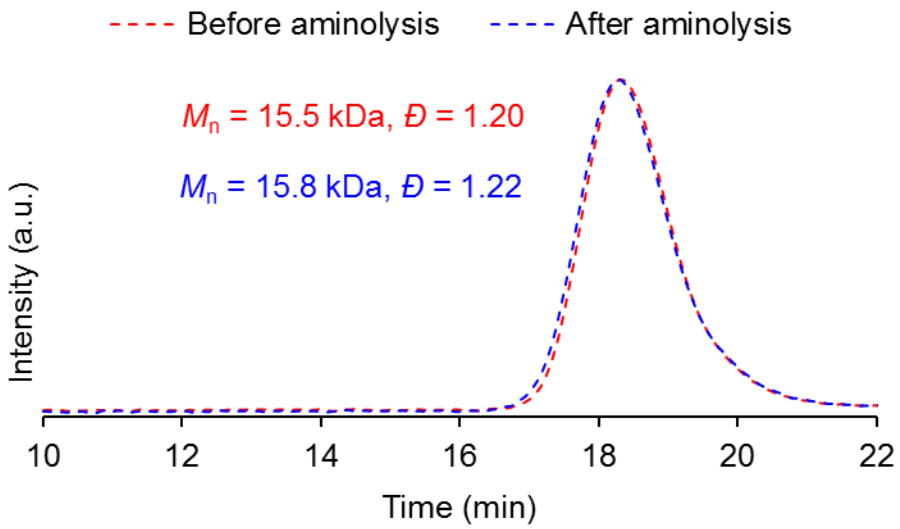

Figure 4-33. SEC chromatogram of azide-functionalized trehalose polymer before (red) and after (blue) aminolysis.

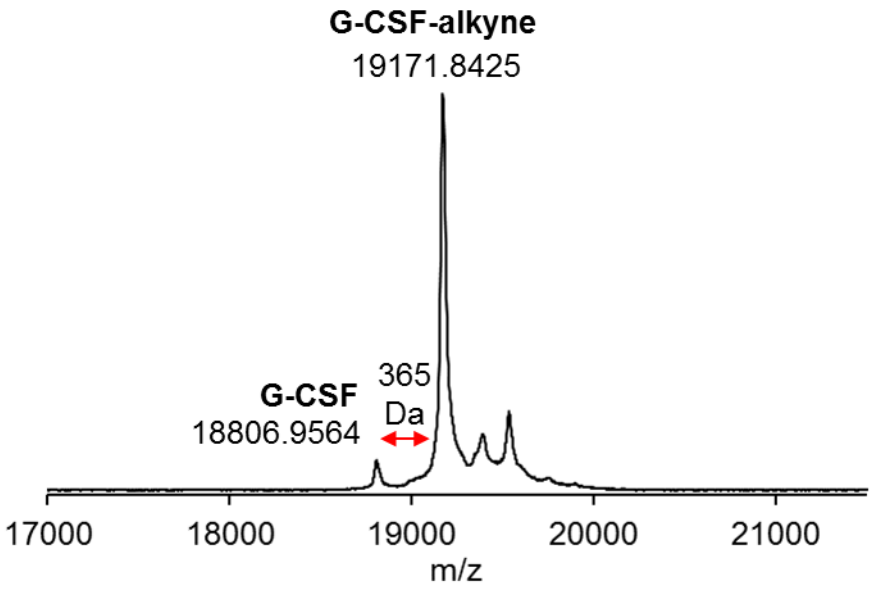

Figure 4-34. MALDI spectrum of G-CSF-alkyne.

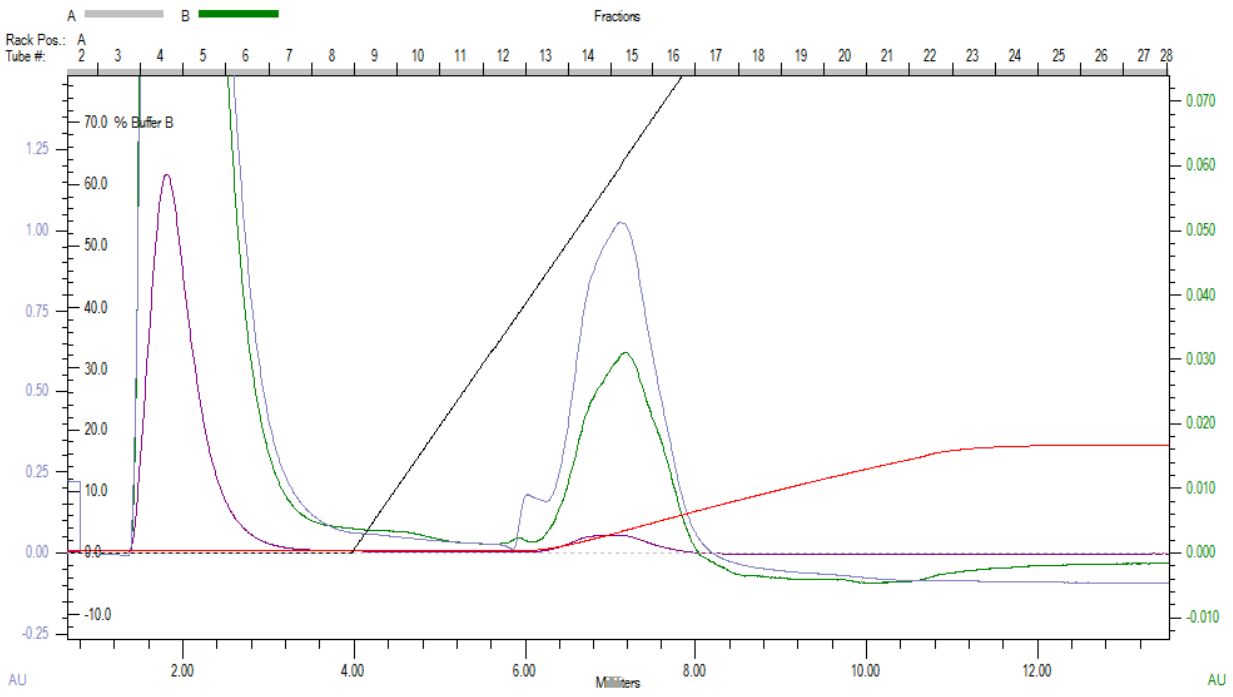

Figure 4-35. Fast protein liquid chromatography (FPLC) chromatogram of G-CSF-trehalose polymer mixture.

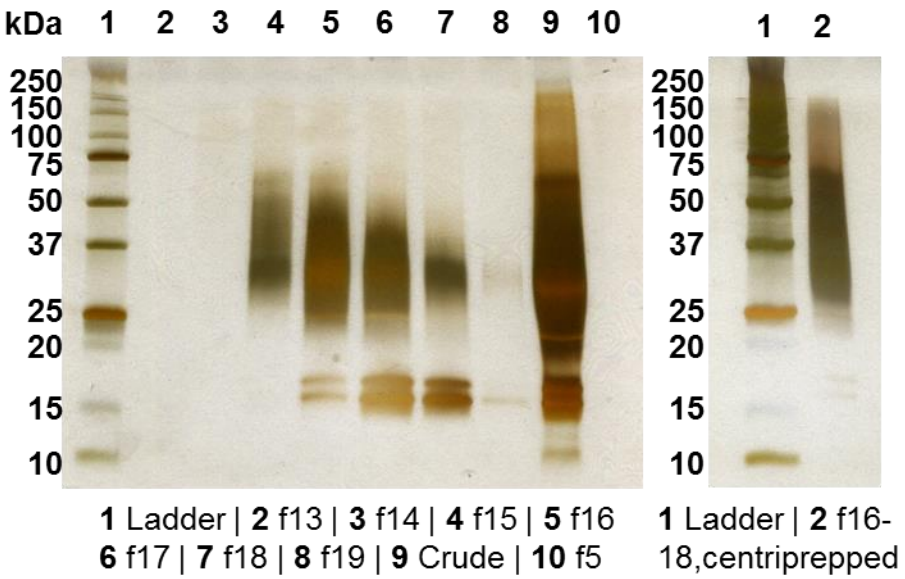

Figure 4-36. SDS-PAGE of FPLC fractions from Figure 4-35 with silver stain.

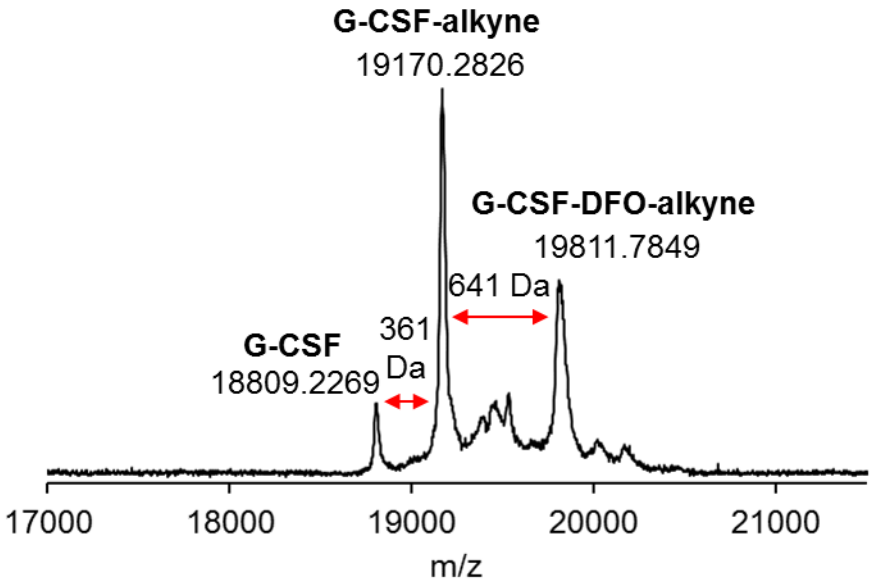

Figure 4-37. MALDI spectrum of G-CSF-DFO-alkyne.

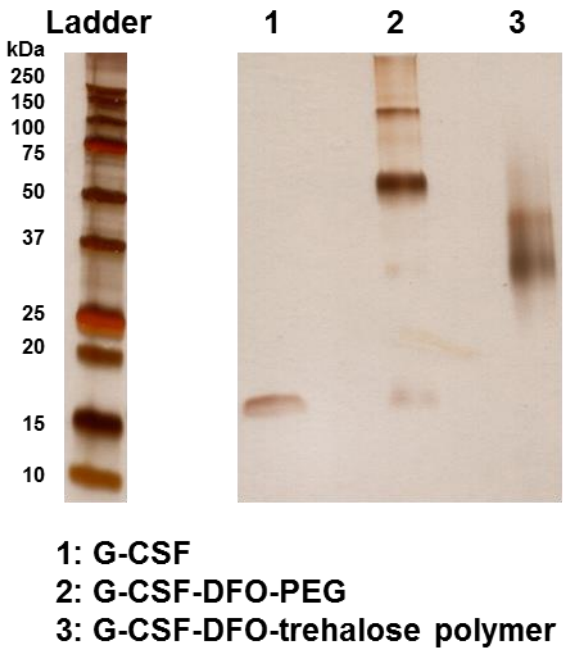

Figure 4-38. SDS-PAGE of G-CSF-DFO conjugates.

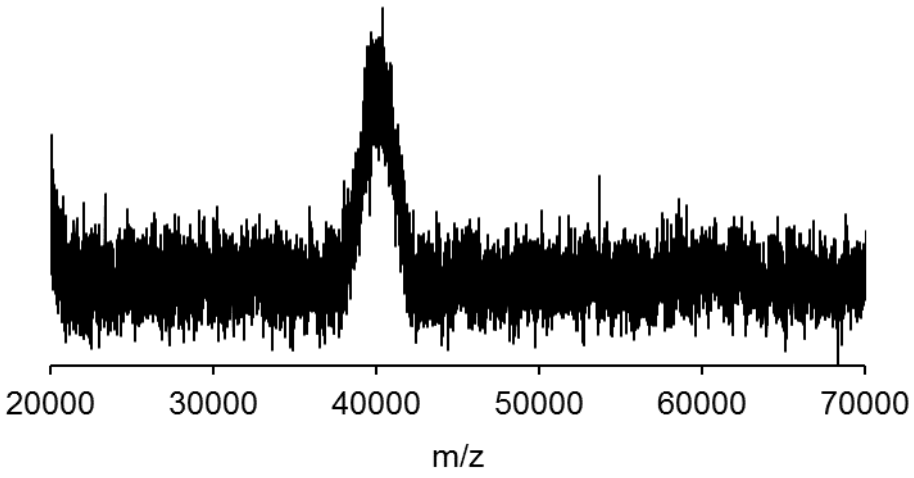

Figure 4-39. MALDI spectrum of G-CSF-DFO-PEG.

4.3 References

(1) Leader, B.; Baca, Q. J.; Golan, D. E. Protein therapeutics: a summary and pharmacological classification. *Nat. Rev. Drug Discovery* **2008,** *7*, 21.

(2) Harris, J. M.; Chess, R. B. Effect of pegylation on pharmaceuticals. *Nat. Rev. Drug Discovery* **2003,** *2*, 214.

(3) Frokjaer, S.; Otzen, D. E. Protein drug stability: A formulation challenge. *Nat. Rev. Drug Discovery* **2005,** *4*, 298.

(4) Manning, M. C.; Chou, D. K.; Murphy, B. M.; Payne, R. W.; Katayama, D. S. Stability of Protein Pharmaceuticals: An Update. *Pharm. Res.* **2010,** *27*, 544.

(5) Alconcel, S. N. S.; Baas, A. S.; Maynard, H. D. FDA-approved poly(ethylene glycol)-protein conjugate drugs. *Polym. Chem.* **2011,** *2*, 1442.

(6) Pfister, D.; Morbidelli, M. Process for protein PEGylation. *J. Controlled Release* **2014,** *180*, 134.

(7) Pelegri-O'Day, E. M.; Lin, E.-W.; Maynard, H. D. Therapeutic Protein–Polymer Conjugates: Advancing Beyond PEGylation. *J. Am. Chem. Soc.* **2014,** *136*, 14323.

(8) Zhang, P.; Sun, F.; Tsao, C.; Liu, S.; Jain, P.; Sinclair, A.; Hung, H. C.; Bai, T.; Wu, K.; Jiang, S. Zwitterionic gel encapsulation promotes protein stability, enhances pharmacokinetics, and reduces immunogenicity. *Proc. Natl. Acad. Sci. U. S. A.* **2015,** *112*, 12046.

(9) Tao, L.; Davis, T. P. Branched Polymer-Protein Conjugates Made From Mid-Chain-Functional P(HPMA). *Biomacromolecules* **2009,** *10*, 2847.

(10) Tao, L.; Liu, J.; Xu, J.; Davis, T. P. Synthesis and bioactivity of poly(HPMA)-lysozyme conjugates: the use of novel thiazolidine-2-thione coupling chemistry. *Org. Biomol. Chem.* **2009,** *7*, 3481.

(11) Tao, L.; Chen, G.; Zhao, L.; Xu, J.; Huang, E.; Liu, A.; Marquis, C. P.; Davis, T. P. Protein Release from Biodegradable PolyHPMA-Lysozyme Conjugates Resulting in Bioactivity Enhancement. *Chemistry an Asian Journal* **2011,** *6*, 1398.

(12) Mero, A.; Fang, Z.; Pasut, G.; Veronese, F. M.; Viegas, T. X. Selective conjugation of poly(2-ethyl 2-oxazoline) to granulocyte colony stimulating factor. *J. Controlled Release* **2012,** *159*, 353.

(13) Viegas, T. X.; Bentley, M. D.; Harris, J. M.; Fang, Z.; Yoon, K.; Dizman, B.; Weimer, R.; Mero, A.; Paust, G.; Veronese, F. M. Polyoxazoline: Chemistry, Properties, and Applications in Drug Delivery. *Bioconj. Chem.* **2011,** *22*, 976.

(14) Tong, J.; Yi, X.; Luxenhofer, R.; Banks, W. A.; Jordan, R.; Zimmerman, M. C.; Kabanov, A. V. Conjugates of Superoxide Dismutase 1 with Amphiphilic Poly(2-oxazoline) Block Copolymers for Enhanced Brain Delivery: Synthesis, Characterization and Evaluation in Vitro and in Vivo. *Mol. Pharm.* **2013,** *10*, 360.

(15) Liebner, R.; Meyer, M.; Hey, T.; Winter, C.; Besheer, A. Head to Head Comparison of the Formulation and Stability of Concentrated Solutions of HESylated versus PEGylated Anakinra. *J. Pharm. Sci.* **2015,** *104*, 515.

(16) Liebner, R.; Mathaes, R.; Meyer, M.; Hey, T.; Winter, C.; Besheer, A. Protein HESylation for half-life extension: Synthesis, characterization and pharmacokinetics of HESylated anakinra. *Eur. J. Pharm. Biopharm.* **2014,** *87*, 378.

(17) Keefe, A. J.; Jiang, S. Poly(zwitterionic)protein conjugates offer increased stability without sacrificing binding affinity or bioactivity. *Nat. Chem.* **2012,** *4*, 59.

(18) Fuhrmann, G.; Grotzky, A.; Lukić, R.; Matoori, S.; Luciani, P.; Yu, H.; Zhang, B.; Walde, P.; Schlüter, A. D.; Gauthier, M. A. Sustained gastrointestinal activity of dendronized polymer–enzyme conjugates. *Nat. Chem.* **2013,** *5*, 582.

(19) Collins, J.; Kempe, K.; Wilson, P.; Blindaur, C. A.; McIntosh, M. P.; Davis, T. P.; Whittaker, M. R.; Haddleton, D. M. Stability Enhancing N-Terminal PEGylation of Oxytocin Exploiting Different Polymer Architectures and Conjugation Approaches. *Biomacromolecules* **2016,** *17*, 2755.

(20) Collins, J.; Tanaka, J.; Wilson, P.; Kempe, K.; Davis, T. P.; McIntosh, M. P.; Whittaker, M. R.; Haddleton, D. M. In Situ Conjugation of Dithiophenol Maleimide Polymers and Oxytocin for Stable Reversible Polymer-Peptide Conjugates. *Bioconj. Chem.* **2015,** *26*, 633.

(21) Mancini, R. J.; Lee, J.; Maynard, H. D. Trehalose Glycopolymers for Stabilization of Protein Conjugates to Environmental Stressors. *J. Am. Chem. Soc.* **2012,** *134*, 8474.

(22) Lee, J.; Lin, E. W.; Lau, U. Y.; Hedrick, J. L.; Bat, E.; Maynard, H. D. Trehalose Glycopolymers as Excipients for Protein Stabilization. *Biomacromolecules* **2013,** *14*, 2561.

(23) Lee, J.; Ko, J. H.; Lin, E.-W.; Wallace, P.; Ruch, F.; Maynard, H. D. Trehalose hydrogels for stabilization of enzymes to heat. *Polym. Chem.* **2015,** *6*, 3443.

(24) Bat, E.; Lee, J.; Lau, U. Y.; Maynard, H. D. Trehalose glycopolymer resists allow direct writing of protein patterns by electron-beam lithography. *Nat. Commun.* **2015,** *6*, 6654.

(25) Lau, U. Y.; Saxer, S. S.; Lee, J.; Bat, E.; Maynard, H. D. Direct Write Protein Patterns for Multiplexed Cytokine Detection from Live Cells Using Electron Beam Lithography. *ACS Nano* **2015,** *10*, 723.

(26) Lins, R. D.; Pereira, C. S.; Hunenberger, P. H. Trehalose-protein interaction in aqueous solution. *Proteins: Struct. Funct. Bioinf.* **2004,** *55*, 177.

(27) Sakurai, M., Biological functions of trehalose as a substitute for water. In *Water and Biomolecules*, Springer: 2009; pp 219.

(28) Kale, S. S.; Akamanchi, K. G. Trehalose monooleate: a potential anti-aggregation agent for stabilization of proteins. *Mol. Pharm.* **2016**.

(29) Wada, M.; Miyazawa, Y.; Miura, Y. A specific inhibitory effect of multivalent trehalose toward A beta(1-40) aggregation. *Polym. Chem.* **2011,** *2*, 1822.

(30) Sizovs, A.; Xue, L.; Tolstyka, Z. P.; Ingle, N. P.; Wu, Y.; Cortez, M.; Reineke, T. M. Poly (trehalose): sugar-coated nanocomplexes promote stabilization and effective polyplex-mediated siRNA delivery. *J. Am. Chem. Soc.* **2013,** *135*, 15417.

(31) Tolstyka, Z. P.; Phillips, H.; Cortez, M.; Wu, Y.; Ingle, N.; Bell, J. B.; Hackett, P. B.; Reineke, T. M. Trehalose-Based Block Copolycations Promote Polyplex Stabilization for Lyophilization and in Vivo pDNA Delivery. *ACS Biomater. Sci. Eng.* **2015,** *2*, 43.

(32) Pickup, J. C. Insulin-Pump Therapy for Type 1 Diabetes Mellitus. *New Engl. J. Med.* **2012,** *366*, 1616.

(33) Kinstler, O. B.; Brems, D. N.; Lauren, S. L.; Paige, A. G.; Hamburger, J. B.; Treuheit, M. J. Characterization and stability of N-terminally PEGylated rhG-CSF. *Pharm. Res.* **1996,** *13*, 996.

(34) Dou, H.; Zhang, M.; Zhang, Y.; Yin, C. Synthesis and Purification of Mono-PEGylated Insulin. *Chemical biology & drug design* **2007,** *69*, 132.

(35) Liu, Y.; Lee, J.; Mansfield, K. M.; Ko, J. H.; Sallam, S.; Wesdemiotis, C.; Maynard, H. D. Trehalose Glycopolymer Enhances Both Solution Stability and Pharmacokinetics of a Therapeutic Protein. *Bioconj. Chem.* **2017,** *28*, 836.

(36) Uchio, T.; Baudys, M.; Liu, F.; Song, S. C.; Kim, S. W. Site-specific insulin conjugates with enhanced stability and extended action profile. *Adv. Drug Del. Rev.* **1999,** *35*, 289.

(37) Caliceti, P.; Veronese, F. M. Pharmacokinetic and biodistribution properties of poly(ethylene glycol)–protein conjugates. *Adv. Drug Delivery Rev.* **2003,** *55*, 1261.

(38) Owens, D. E., 3rd; Peppas, N. A. Opsonization, biodistribution, and pharmacokinetics of polymeric nanoparticles. *Int. J. Pharm.* **2006,** *307*, 93.

(39) Madsbad, S. LY2605541--a preferential hepato-specific insulin analogue. *Diabetes* **2014,** *63*, 390.

(40) Hamilton-Wessler, M.; Ader, M.; Dea, M.; Moore, D.; Jorgensen, P. N.; Markussen, J.; Bergman, R. N. Mechanism of protracted metabolic effects of fatty acid acylated insulin, NN304, in dogs: retention of NN304 by albumin. *Diabetologia* **1999,** *42*, 1254.

(41) Zaslavsky, B. Y.; Ossipov, N. N.; Krivich, V. S.; Baholdina, L. P.; Rogozhin, S. V. Action of surface-active substances on biological membranes. II. Hemolytic activity of nonionic surfactants. *Biochimica et Biophysica Acta (BBA)-Biomembranes* **1978,** *507*, 1.

(42) Webster, R.; Didier, E.; Harris, P.; Siegel, N.; Stadler, J.; Tilbury, L.; Smith, D. PEGylated proteins: evaluation of their safety in the absence of definitive metabolism studies. *Drug Metab. Dispos.* **2007,** *35*, 9.

(43) Chen, Y.; Zhang, W.; Huang, Y.; Gao, F.; Sha, X.; Lou, K.; Fang, X. The therapeutic effect of methotrexate-conjugated Pluronic-based polymeric micelles on the folate receptor-rich tumors treatment. *Int. J. Nanomedicine* **2015,** *10*, 4043.

(44) De Jong, W. H.; Borm, P. J. Drug delivery and nanoparticles:applications and hazards. *Int. J. Nanomedicine* **2008,** *3*, 133.

(45) Eli Lily and Company. *A Study of Insulin Peglispro (LY2605541) in Participants With Type 2 Diabetes Mellitus*, <https://clinicaltrials.gov/ct2/show/NCT02106364?term=peglispro&rank=5>.

(46) Caparrotta, T. M.; Evans, M. PEGylated insulin Lispro, (LY2605541)—a new basal insulin analogue. *Diabetes Obes. Metab.* **2014,** *16*, 388.

(47) Brange, J.; Owens, D. R.; Kang, S.; Volund, A. Monomeric insulins and their experimental and clinical implications. *Diabetes Care* **1990,** *13*, 923.

(48) Hinds, K. D.; Kim, S. W. Effects of PEG conjugation on insulin properties. *Adv Drug Deliv Rev* **2002,** *54*, 505.

(49) Pryce, R. Diabetic ketoacidosis caused by exposure of insulin pump to heat and sunlight. *Brit. Med. J.* **2009,** *338*.

(50) Karas, J. A.; Patil, N. A.; Tailhades, J.; Sani, M. A.; Scanlon, D. B.; Forbes, B. E.; Gardiner, J.; Separovic, F.; Wade, J. D.; Hossain, M. A. Total Chemical Synthesis of an Intra-A-Chain Cystathionine Human Insulin Analogue with Enhanced Thermal Stability. *Angew. Chem. Int. Ed.* **2016**.

(51) Hovgaard, L.; Mack, E. J.; Kim, S. W. Insulin stabilization and GI absorption. *J. Controlled Release* **1992,** *19*, 99.

(52) Hovgaard, L.; Jacobs, H.; Mazer, N. A.; Kim, S. W. Stabilization of insulin by alkylmaltosides. A. Spectroscopic evaluation. *Int. J. Pharm.* **1996,** *132*, 107.

(53) Sluzky, V.; Klibanov, A. M.; Langer, R. Mechanism of insulin aggregation and stabilization in agitated aqueous solutions. *Biotechnol. Bioeng.* **1992,** *40*, 895.

(54) Park, S.-J.; Choi, S. G.; Davaa, E.; Park, J.-S. Encapsulation enhancement and stabilization of insulin in cationic liposomes. *Int. J. Pharm.* **2011,** *415*, 267.

(55) Leobandung, W.; Ichikawa, H.; Fukumori, Y.; Peppas, N. A. Preparation of stable insulin-loaded nanospheres of poly (ethylene glycol) macromers and N-isopropyl acrylamide. *J. Controlled Release* **2002,** *80*, 357.

(56) Chalasani, K. B.; Russell-Jones, G.; Yandrapu, S. K.; Diwan, P. V.; Jain, S. K. A novel vitamin B 12-nanosphere conjugate carrier system for peroral delivery of insulin. *J. Controlled Release* **2007,** *117*, 421.

(57) Akiyoshi, K.; Kobayashi, S.; Shichibe, S.; Mix, D.; Baudys, M.; Kim, S. W.; Sunamoto, J. Self-assembled hydrogel nanoparticle of cholesterol-bearing pullulan as a carrier of protein drugs: complexation and stabilization of insulin. *J. Controlled Release* **1998,** *54*, 313.

(58) Wood, M. R.; Duncalf, D. J.; Rannard, S. P.; Perrier, S. Selective One-Pot Synthesis of Trithiocarbonates, Xanthates, and Dithiocarbamates for Use in RAFT/MADIX Living Radical Polymerizations. *Org. Lett.* **2006,** *8*, 553.

(59) Ayala, J. E.; Samuel, V. T.; Morton, G. J.; Obici, S.; Croniger, C. M.; Shulman, G. I.; Wasserman, D. H.; McGuinness, O. P. Standard operating procedures for describing and performing metabolic tests of glucose homeostasis in mice. *Disease Models & Mechanisms* **2010,** *3*, 525.

(60) Craik, D. J.; Fairlie, D. P.; Liras, S.; Price, D. The future of peptide-based drugs. *Chemical biology & drug design* **2013,** *81*, 136.

(61) Gurevich, E. V.; Gurevich, V. V., Therapeutic potential of small molecules and engineered proteins. In *Arrestins-Pharmacology and Therapeutic Potential*, Springer: 2014; pp 1.

(62) Hay, M.; Thomas, D. W.; Craighead, J. L.; Economides, C.; Rosenthal, J. Clinical development success rates for investigational drugs. *Nat. Biotechnol.* **2014,** *32*, 40.

(63) Duckworth, W. C.; Bennett, R. G.; Hamel, F. G. Insulin degradation: progress and potential. *Endocr. Rev.* **1998,** *19*, 608.

(64) Maack, T.; Johnson, V.; Kau, S. T.; Figueiredo, J.; Sigulem, D. Renal filtration, transport, and metabolism of low-molecular-weight proteins: a review. *Kidney Int.* **1979,** *16*, 251.

(65) Menzel, E.; Farr, C. Hyaluronidase and its substrate hyaluronan: biochemistry, biological activities and therapeutic uses. *Cancer Lett.* **1998,** *131*, 3.

(66) Lee, J.; Lin, E.-W.; Lau, U. Y.; Hedrick, J. L.; Bat, E.; Maynard, H. D. Trehalose Glycopolymers as Excipients for Protein Stabilization. *Biomacromolecules* **2013,** *14*, 2561.

(67) Messina, M. S.; Ko, J. H.; Yang, Z.; Strouse, M. J.; Houk, K. N.; Maynard, H. D. Effect of trehalose polymer regioisomers on protein stabilization. *Polym. Chem.* **2017,** *8*, 4781.

(68) Pelegri-O'Day, E. M.; Paluck, S. J.; Maynard, H. D. Substituted Polyesters by Thiol-Ene Modification: Rapid Diversification for Therapeutic Protein Stabilization. *J. Am. Chem. Soc.* **2017,** *139*, 1145.

(69) Lee, J.; Ko, J. H.; Mansfield, K. M.; Nauka, P. C.; Bat, E.; Maynard, H. D. Glucose-Responsive Trehalose Hydrogel for Insulin Stabilization and Delivery. *Macromol. Biosci.* **2018,** *18*, 1700372.

(70) Lau, U. Y. Trehalose Glycopolymers for Protein and Cell Stabilization. Ph.D. Dissertation, University of California, Los Angeles, 2016.

(71) Krenske, E. H.; Izgorodina, E. I.; Coote, M. L., An Ab Initio Guide to Structure—Reactivity Trends in Reversible Addition Fragmentation Chain Transfer Polymerization. ACS Publications: 2006.

(72) Besanceney-Webler, C.; Jiang, H.; Zheng, T.; Feng, L.; Soriano del Amo, D.; Wang, W.; Klivansky, L. M.; Marlow, F. L.; Liu, Y.; Wu, P. Increasing the efficacy of bioorthogonal click reactions for bioconjugation: a comparative study. *Angew. Chem. Int. Ed.* **2011,** *50*, 8051.

(73) Hong, V.; Presolski, S. I.; Ma, C.; Finn, M. Analysis and Optimization of Copper-Catalyzed Azide–Alkyne Cycloaddition for Bioconjugation. *Angew. Chem. Int. Ed.* **2009,** *48*, 9879.

(74) Green, M.; Koelbl, H.; Baselga, J.; Galid, A.; Guillem, V.; Gascon, P.; Siena, S.; Lalisang, R.; Samonigg, H.; Clemens, M. A randomized double-blind multicenter phase III study of fixed-

dose single-administration pegfilgrastim versus daily filgrastim in patients receiving myelosuppressive chemotherapy. *Ann. Oncol.* **2003,** *14*, 29.

(75) Yang, B.-B.; Morrow, P. K.; Wu, X.; Moxness, M.; Padhi, D. Comparison of pharmacokinetics and safety of pegfilgrastim administered by two delivery methods: on-body injector and manual injection with a prefilled syringe. *Cancer Chemother. Pharmacol.* **2015,** *75*, 1199.

(76) US Food and Drug Administration. Q3D Elemental Impurities Guidance for Industry. **2015**.

(77) Scholz, M.; Ackermann, M.; Engel, C.; Emmrich, F.; Loeffler, M.; Kamprad, M. A pharmacokinetic model of filgrastim and pegfilgrastim application in normal mice and those with cyclophosphamide-induced granulocytopaenia. *Cell proliferation* **2009,** *42*, 813.

(78) Cohen, A. M.; Zsebo, K. M.; Inoue, H.; Hines, D.; Boone, T. C.; Chazin, V. R.; Tsai, L.; Ritch, T.; Souza, L. M. In vivo stimulation of granulopoiesis by recombinant human granulocyte colony-stimulating factor. *Proc. Natl. Acad. Sci. U. S. A.* **1987,** *84*, 2484.

(79) Rudd, S. E.; Roselt, P.; Cullinane, C.; Hicks, R. J.; Donnelly, P. S. A desferrioxamine B squaramide ester for the incorporation of zirconium-89 into antibodies. *Chem. Commun.* **2016,** *52*, 11889.

(80) Vosjan, M. J.; Perk, L. R.; Visser, G. W.; Budde, M.; Jurek, P.; Kiefer, G. E.; Van Dongen, G. A. Conjugation and radiolabeling of monoclonal antibodies with zirconium-89 for PET imaging using the bifunctional chelate p-isothiocyanatobenzyl-desferrioxamine. *Nat. Protoc.* **2010,** *5*, 739.

(81) Ricci, M. S.; Sarkar, C. A.; Fallon, E. M.; Lauffenburger, D. A.; Brems, D. N. pH Dependence of structural stability of interleukin-2 and granulocyte colony-stimulating factor. *Protein Sci.* **2003,** *12*, 1030.

(82) Tavaré, R.; McCracken, M. N.; Zettlitz, K. A.; Salazar, F. B.; Olafsen, T.; Witte, O. N.; Wu, A. M. ImmunoPET of murine T cell reconstitution post-adoptive stem cell transplant using anti-CD4 and anti-CD8 cys-diabodies. *J. Nucl. Med.* **2015,** *56*, 1258.

(83) Emmanouel, D.; Lindheimer, M.; Katz, A. Role of the kidney in hormone metabolism and its implications in clinical medicine. *Klin. Wochenschr.* **1980,** *58*, 1005.

(84) Kuwabara, T.; Kobayashi, S.; Sugiyama, Y. Pharmacokinetics and pharmacodynamics of a recombinant human granulocyte colony-stimulating factor. *Drug Metab. Rev.* **1996,** *28*, 625.

(85) Hannant, J.; Hedley, J. H.; Pate, J.; Walli, A.; Al-Said, S. A. F.; Galindo, M. A.; Connolly, B. A.; Horrocks, B. R.; Houlton, A.; Pike, A. R. Modification of DNA-templated conductive polymer nanowires via click chemistry. *Chem. Commun.* **2010,** *46*, 5870.

(86) Tao, L.; Liu, J.; Davis, T. P. Branched Polymer− Protein Conjugates Made From Mid-Chain-Functional P (HPMA). *Biomacromolecules* **2009,** *10*, 2847.

(87) Teodorowicz, M.; Perdijk, O.; Verhoek, I.; Govers, C.; Savelkoul, H. F.; Tang, Y.; Wichers, H.; Broersen, K. Optimized Triton X-114 assisted lipopolysaccharide (LPS) removal method reveals the immunomodulatory effect of food proteins. *PLoS One* **2017,** *12*, e0173778.

Chapter 5.

Traceless Conjugation to Primary Alkyl Amines with Potential Application in Protein Conjugation

5.1 Introduction

Biomolecules such as proteins are commonly modified with synthetic small molecules and polymers to improve their properties or for novel functions. For example, polymers have been conjugated to proteins to enhance their stability[1, 2] and pharmacokinetics,[3] while antibody-drug conjugates are used clinically to deliver anti-cancer drugs selectively to the tumor while minimizing off-target effects.[4] However, such modifications very frequently reduce the activity of the protein. Site-specific conjugation[5] to an amino acid distal to the active site or binding motif can minimize such an effect, but the decrease in activity often cannot be completely avoided.

An alternative strategy is to use a reversible conjugation chemistry such that the small molecule or polymer remains attached to the protein until a desired stimulus is encountered, after which the small molecule or polymer releases itself to regenerate the native protein. Referred to as traceless conjugation, common release mechanisms include 1,6-elimination, disulfide exchange, and photoresponsive linkers.[6] The most frequently used linker is the benzyl carbamate linkage[7] that is formed with amines that are abundant in proteins and can release the protein via 1,6-elimination upon uncapping of the phenol (Figure 5-1). The quinone methide by-product is immediately trapped by the solvent (water) to generate a 4-hydroxybenzyl alcohol by-product that has minimal toxicity.[6]

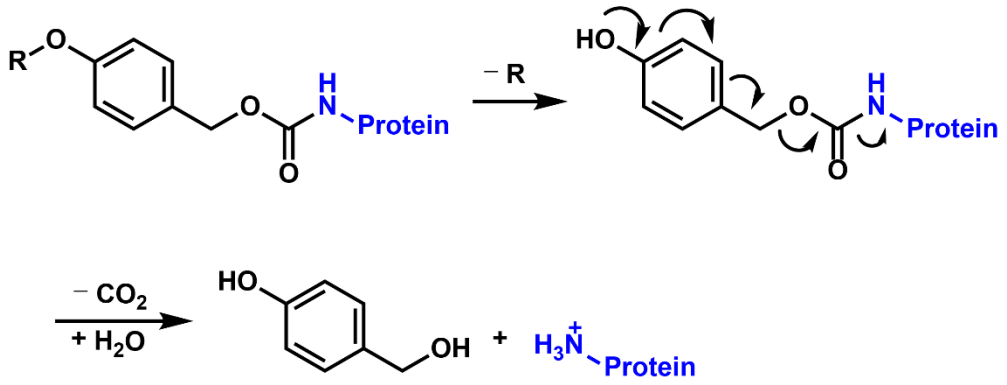

Figure 5-1. Mechanism of 1,6-elimination by benzyl carbamate linker.

This linker has proven to be effective and used for many antibody-drug conjugates,[8] but there are some limitations (Figure 5-2). First, the conjugation optimally proceeds at basic pH, since sufficient amounts of the nucleophilic amine of the protein should be deprotonated for the S_N2 reaction with the electrophile on the synthetic molecule. However, this conjugation condition is not compatible with proteins that are unstable at high pH such as granulocyte-colony stimulating factor (G-CSF).[9] Second, the benzylic position of the linker must be activated in order to form the carbamate linkage. This has negative consequences such as additional synthetic steps, the instability of the reagent, and limited functional group tolerance during the synthesis of the molecules. Finally, the formed conjugate loses the positive charge on the amine as it is transformed into a carbamate, and a loss of charge may lead to protein destabilization.[10]

A complementary and potentially superior approach for traceless conjugation would be to directly couple the protein and the synthetic molecule via reductive amination using benzaldehyde derivatives (Figure 5-2). Reductive amination occurs in the mildly acidic to mildly basic pH (5 – 8), which is complementary to the neutral to basic pH range (7 – 10) required for the traditional linker. Moreover, commercially available benzaldehydes can be used as starting materials without

the need for additional activation. In addition, compared with the activated carbonyl, benzaldehydes are more tolerant to nucleophiles and are not subject to hydrolysis. Finally, the conjugate formed from reductive amination retains the positive charge on the secondary amine at a neutral pH, which renders the conjugate more similar to the native protein and help improve the stability of the conjugate.[10]

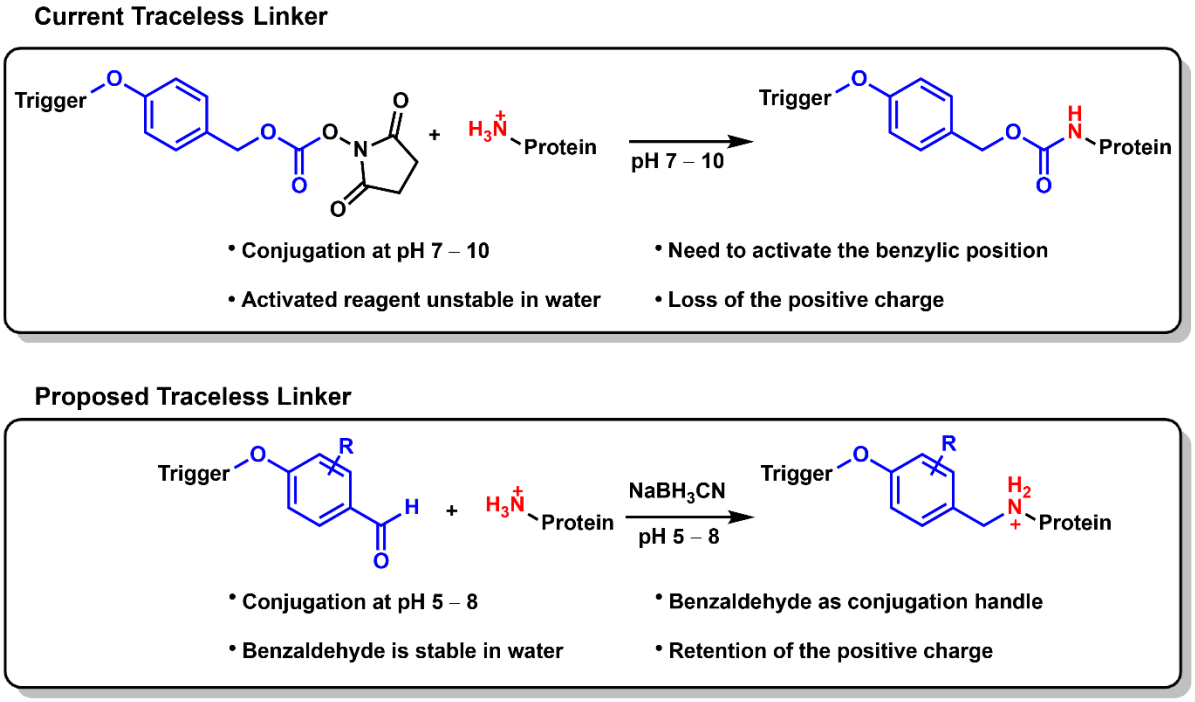

Figure 5-2. Comparison of benzyl linkers for traceless conjugation to proteins.

It was recently reported that tertiary and heteroaryl amines conjugated at the benzylic position of this linker can undergo 1,6-elimination to release small molecule amine-containing drugs.[11] However, the conjugation of the amine with the linker required the use of thionyl chloride in *N*,*N*-dimethylformamide, precluding any potential use in protein conjugation. Moreover, the report does not discuss primary alkyl amines, which are presumably not activated enough to

undergo 1,6-elimination. We hypothesized that increasing the density in the aromatic system by adding electron-donating groups may lower the activation energy to allow release of alkyl amines.

In this chapter, we will present a linker design that allows for traceless conjugation of synthetic molecules to alkyl amines, similar to those in proteins, under mild conditions that would be suitable for biomolecules. This simple methodology is complementary to the existing benzyl carbamate approach widely used in both the academia and the industry, and may provide easier access to traceless conjugates and offer advantages for proteins unstable at high pH.

5.2 Results and Discussion

Given that only tertiary and heteroaryl amines are capable of undergoing 1,6-elimination from the benzyl position, we hypothesized that electron donating groups would stabilize the intermediate and allow the reaction to proceed at an appreciable rate for alkyl amines. Since the proposed quinone methide intermediate resulting from the 1,6-elimination is a positively charged species, electron-donating groups would lower the activation barrier.[12] Hammett parameters for hydrogen ($\sigma_{para} = 0.00$), methyl ($\sigma_{para} = -0.17$) and methoxy ($\sigma_{para} = -0.27$) groups [13] suggested that the rate of 1,6-elimination would increase in the following order: H < Me < OMe. We designed the linker to contain two electron donating groups at the ortho position to maximally accelerate 1,6-elimination (Figure 5-3). Density-functional theory (DFT) calculations showed that 1,6-elimination occurs with a monotonous increase in energy towards the product (i.e., no transition state along the reaction coordinate) (courtesy of Dr. Zhongyue Yang from Professor Ken Houk's research group). Moreover, the calculated free energy change correlated with the trend expected from the Hammett parameters.

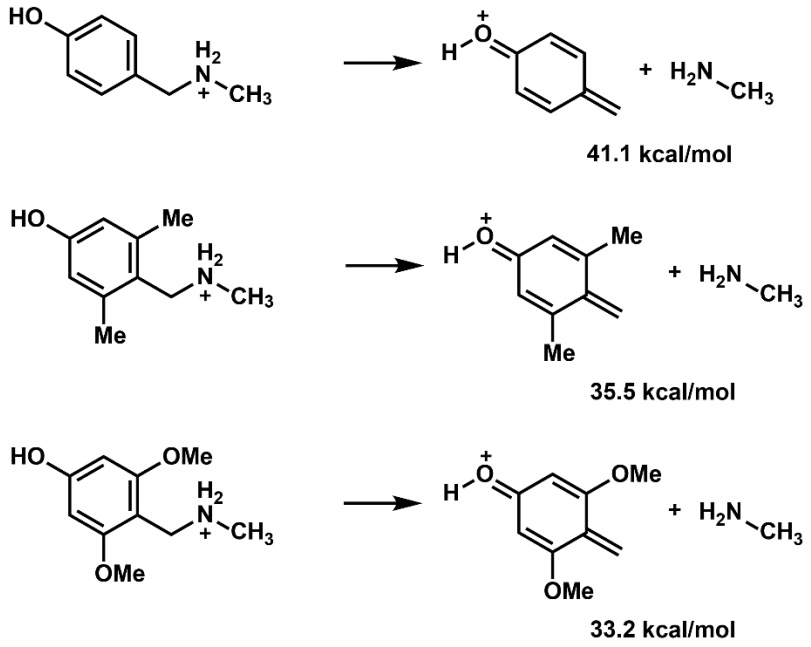

Figure 5-3. Computed structures to study the electronic effect on the 1,6-elimination of benzyl amines (structures optimized using B3LYP/6-31g(d) with SMD water model in GAMESS[14]).

With the computational results supporting the hypothesis, the silyl-protected benzyl amines were used as a model system to show the feasibility of alkyl amine release from the benzyl linker (Figure 5-4). A silyl protecting group was chosen because it has been previously used to cap the phenolic oxygen for benzyl carbonates,[15] and the silyl deprotection with a fluoride source such as tetrabutylammonium fluoride (TBAF) is selective and rapid. We chose 2-(2-aminoethyl)pyridine as the model alkyl amine; its pyridine ring allows for UV measurement during the high-performance liquid chromatography (HPLC) and also improves water solubility of the silyl-protected benzylamine substrates.

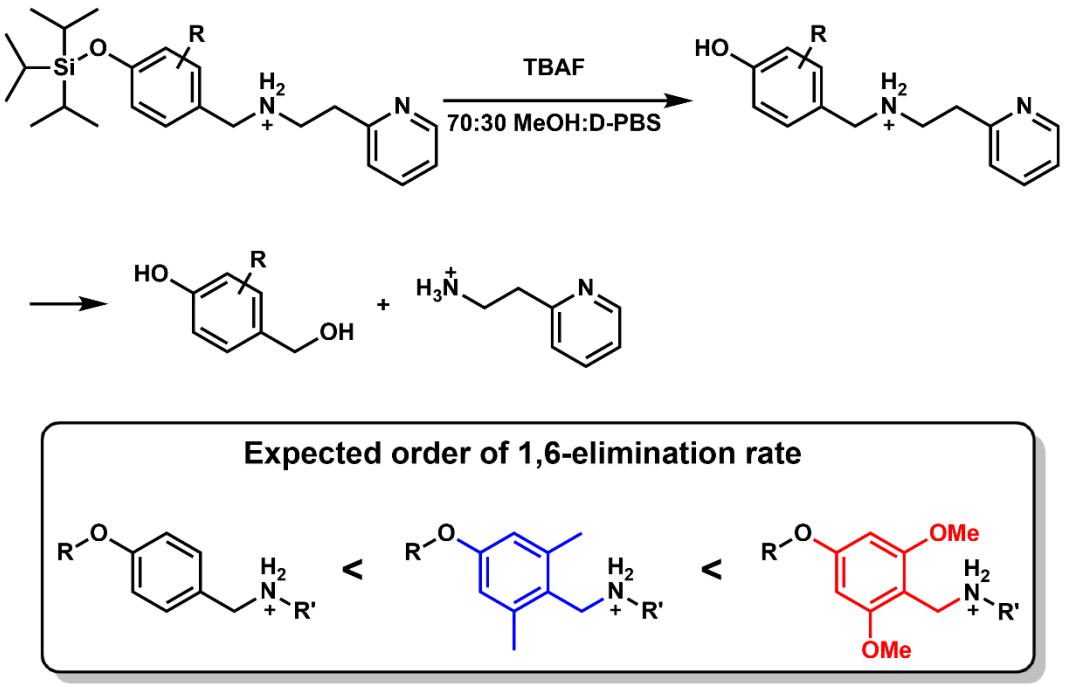

Figure 5-4. Model system for measuring the kinetics of a model amine release.

Silyl-protected benzyl amines were dissolved in 70:30 methanol:buffer (Dulbecco's buffered saline (D-PBS), pH 7.4) with 0.3 M TBAF. The kinetics of amine release was quantified using HPLC calibration curve of known concentrations of 2-(2-aminoethyl)pyridine. According to the assumed mechanism, the kinetics should be approximately first-order since the initial silyl deprotection is fast and the fluoride reagent is in great excess (0.3 M) compared to the tested compounds (5 – 7 μM). The rate of amine released followed the expected trend H < Me < OMe (Figure 5-5). The control experiments without TBAF showed slow but noticeable release for the dimethyl and dimethoxy linkers (Experimental Section Figure 5-19), which was attributed to the hydrolysis of the TIPS group. Indeed, when the phenol of the dimethoxy linker is methylated (trimethoxy in the figure) the background release is suppressed.

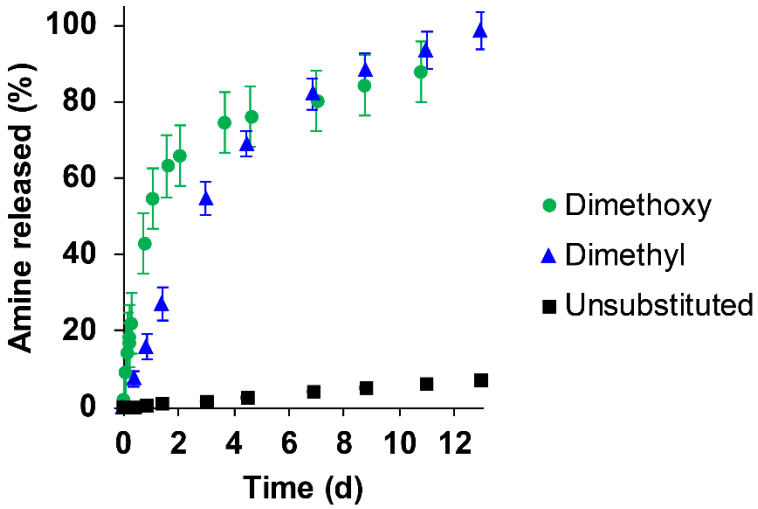

Figure 5-5. Kinetics of amine release for different traceless linkers (n = 3).

In accordance with the unimolecular reaction mechanism for the 1,6-elimination, the logarithmic plot was linear for the unsubstituted and the dimethyl substituted linker. It should be noted that the slight deviation at very high conversion (98%) of the dimethyl substituted linker was due to the amplification of error close to 100% on the logarithmic plot (Experimental Section Figure 5-18). In contrast, the dimethoxy linker was only linear for the initial time points. At this time, we presume that strong electron donation from the dimethoxy substituents stabilizes the quinone methide, intermediate that had been previously assumed to be immediately quenched by the solvent.[6] The quinone methide may reversibly add to the amine, forming a shunt pathway that slows down the reaction once enough quinone methide has accumulated (Figure 5-6).

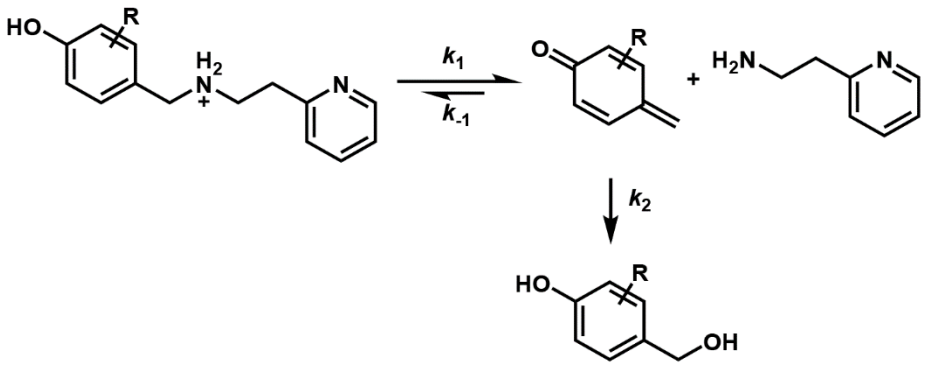

Figure 5-6. Proposed pathway responsible for delayed amine release at high conversion.

Having confirmed that increased electron density around the ring accelerates the 1,6-elimination, we thought to further accelerate the kinetics. The first approach was to substitute the –OH with $–NH_2$ at the para position. Because corresponding anilines were not commercially available, the three differently substituted 4-hydroxybenzaldehydes were converted to aniline by reacting with 2-bromopropionamide followed by *in situ* Smiles rearrangement (Figure 5-7).[16] However, the resulting anilines had poor solubility in organic solvents and were difficult to derivatize, and this route was abandoned.

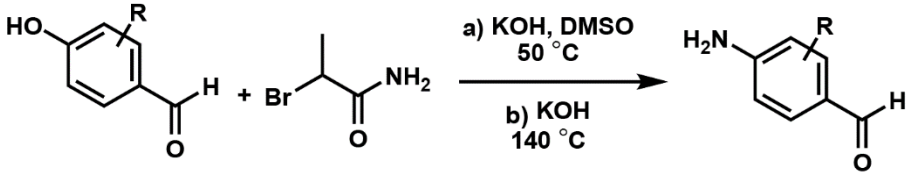

Figure 5-7. Conversion of 4-hydroxybenzaldehydes to corresponding anilines.

The second approach was to install a dimethylamino group, which has a very large Hammett constant (σ_{para} = -0.83). Since 4-hydroxybenzaldehyde with ortho-dimethylamino substitution was not commercially available, 2-hydroxybenzaldehyde with para-dimethylamino

substitution that can undergo analogous 1,4-elimination was selected for the study instead. It was reported that 1,4-elimination occurs in the same manner as 1,6-elimination albeit at a slightly diminished rate.[17] Even with only a single substitution, the large Hammett constant for dimethylamino suggested that it will release amine faster than the doubly-substituted dimethoxy linker (OCH_3 σ_{para} = -0.27). The DFT calculation supported this hypothesis and predicted that the energy for amine release will be 4.5 kcal/mol more favorable for the dimethylamino linker compared to the dimethoxy linker.

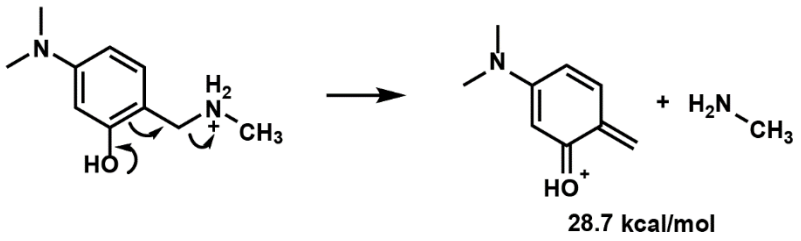

Figure 5-8. Dimethylamino linker undergoing 1,4-elimination (structures optimized using B3LYP/6-31g(d) with SMD water model in GAMESS).

While we were synthesizing the silyl-protected dimethylamino linker, we found that the TIPS deprotected compound (Figure 5-9) was able to be isolated as a cyanoborohydride salt. The solvent used in the previous kinetic experiments was 70:30 methanol:D-PBS with 0.3 M TBAF to deprotect the phenol to initiate the release, but since this compound has a free phenol it was dissolved in 70:30 methanol:D-PBS without TBAF. This linker exhibited even faster amine release, with more than 50% release occurring within the first 5 hours, whereas the dimethoxy linker took 1 day and the dimethyl linker took 3 days to release 50% amine. The log plot (Experimental Section Figure 5-18) deviated from linearity as it did for dimethoxy linker, likely due to the stabilization of the quinone methide intermediate, which potentially creates a shunt pathway as discussed earlier.

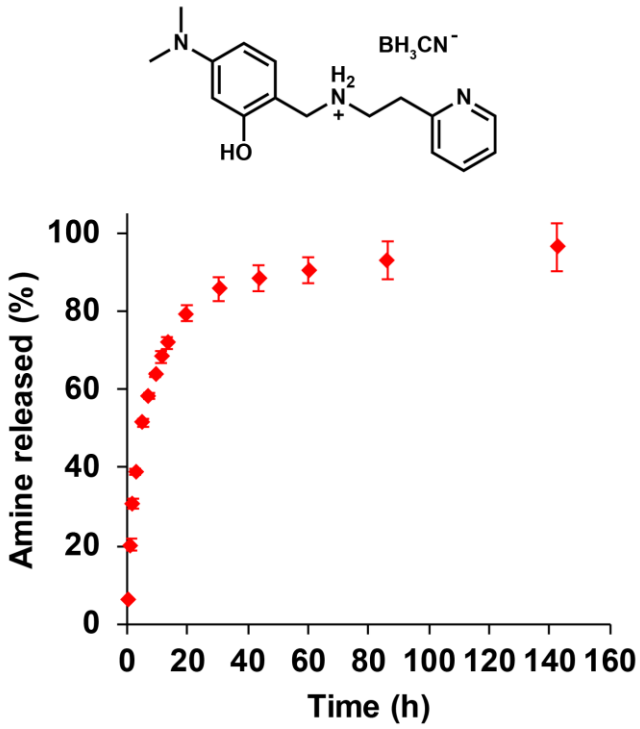

Figure 5-9. Kinetics of amine release from the dimethylamino linker (n = 3).

The slope of the linear portions of the log plots (Experimental Section Figure 5-18) gives the first-order rate constants (Table 5-1). General trend of the rate constant follows the electron donating ability of the substituent as denoted by the Hammett parameter, with the most electron-donating dimethylamino linker having a rate constant that is 368-times larger than that of the unsubstituted linker. Although the 1,6-elimination of amine from the benzyl position is reminiscent of reactions explained by the Hammett equation, the rate constant does not follow a linear free energy relationship and increases much slower than predicted by the Hammett parameters even within only the 1,6-elimination series (H, dimethyl, and dimethoxy). Steric effects from ortho position as well as the double substitution would contribute to the deviation. In addition, the dimethoxy linker was shown to form a hydrogen bond (2.109 Å) between the ammonium hydrogen

and the methoxy oxygen, and the benzyl amine arm is tilted to the left side (Experimental Section Figure 5-20). In contrast, unsubstituted and dimethyl substituted linkers do not have such hydrogen bonds and show near σ_v symmetry except for the phenol hydrogen. The stabilization of the reactant by hydrogen bonding increases the energy barrier to product formation, and partially offsets the electronic acceleration from the dimethoxy substitution. Similarly, the dimethylamino linker has a hydrogen bond between the amine and the phenolic oxygen (2.069 Å). Future efforts at further accelerating the amine release may involve disrupting this hydrogen bond.

Table 5-1. Electronic effect on the rate constants.

Ring substituent	k (s^{-1})	Hammett parameter (σ_{para})
H	6.65×10^{-8}	0.00
CH_3 (doubly substituted)	2.86×10^{-6}	-0.17
OCH_3 (doubly substituted)	7.24×10^{-6}	-0.27
$N(CH_3)_2$	2.45×10^{-5}	-0.83

5.3 Conclusions

A new traceless conjugation strategy was developed using commercially available benzaldehydes to couple to primary amines via reductive amination. The key to the success of this approach was to stabilize the cationic quinone methide intermediate by increasing the electron density around the aromatic ring. The rate of amine release followed the Hammett parameter trends, although it significantly deviated from the linear free energy relationship likely due to the steric effects as well as internal hydrogen bonding observed for several linkers. Dimethylamino substitution enabled the release of 52% amine in 5 hours, while the linker with no substitution would require ~120 days to reach the same level of release. Unlike the benzyl carbamate linker,

this conjugation strategy does not require a separate activation step for modification at the benzylic site. Moreover, the benzaldehyde moiety has higher functional group tolerance than activated carbonates used for the benzyl carbamate linker and is more stable. The reductive amination for conjugation of primary alkyl amine occurs at a pH range (pH 5 – 8) that is complementary to the basic pH (pH 7 – 10) used for the conjugation via carbamate linker, which would be beneficial for proteins that are unstable at high pH. Another advantage of this method is that the resulting conjugate retains the positive charge on the amine, which has been reported to help with protein stability. These benefits suggest that the newly developed traceless methodology will find many applications in conjugation of polymers as well as small molecules to proteins.

5.4 Experimental Section

Materials

4-Hydroxybenzaldehyde (Sigma-Aldrich), 4-hydroxy-2,6-dimethylbenzaldehyde (Ark Pharm), 4-hydroxy-2,6-dimethoxybenzaldehyde (Combi-Blocks), 4-(dimethylamino)salicylaldehyde (Combi-Blocks), 2-(2-aminoethyl)pyridine (Oakwood Chemical), sodium cyanoborohydride (Strem Chemicals), triisopropylchlorosilane (Oakwood Chemical), and 2-bromopropionamide (Sigma-Aldrich) were used as received.

Analytical Techniques

NMR spectra were recorded on a Bruker AV 400 MHz, a Bruker DRX 500 MHz, or a Bruker AV 500 MHz. Silica gel column chromatography was performed on a Biotage Isolera One purification system. Substituted benzyl amines were purified on a Shimadzu preparative high-performance liquid chromatography (HPLC) system connected to two LC-8A pumps and a SPD-10A UV

detector using a Phenomenex Luna 5 μm C18(2) 100 Å LC column (250 x 21.2 mm, AXIA packed) (flow rate: 20 mL/min). The kinetic experiments were performed on an Agilent analytical HPLC system (Agilent 1260 Infinity II LC System) connected to Quaternary Pump, Vialsampler, and VWD UV detector using a Phenomenex Luna 5 μm C18(2) 100 Å column (250 x 4.6 mm) with elution gradient of 10–95% solvent B over 14 min (solvent A: water + 0.1% trifluoroacetic acid (vol/vol), solvent B: methanol). Infrared (IR) spectra were acquired on a Perkin-Elmer Spectrum One instrument equipped with a universal attenuated total reflection (ATR) assembly. High-resolution mass spectra were obtained on a Thermo Scientific Exactive Plus mass spectrometer with IonSense Direct Analysis in Real Time (DART-MS) ID-CUBE.

TIPS-protection of Benzaldehydes

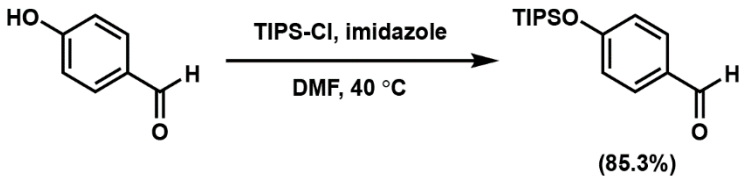

Representative Procedure: TIPS-protected 4-hydroxybenzaldehyde. 4-Hydroxybenzaldehyde (250 mg, 2.05 mmol, 1 equiv), triisopropylchlorosilane (0.66 mL, 3.1 mmol, 1.5 equiv), and imidazole (348 mg, 5.12 mmol, 2.5 equiv) were dissolved in 0.5 mL of *N*,*N*-dimethylformamide (DMF) dried and stored with 4 Å molecular sieves under argon. The reaction mixture was stirred at 40 °C for 15 h, and extracted with 50 mL water and 50 mL dichloromethane (DCM) three times. The combined organic layer was dried with $MgSO_4$, concentrated *in vacuo*, and purified by column chromatography (95:5 hexanes:ethyl acetate) to yield the product (486 mg, 85.3% yield). ^{1}H NMR (500 MHz in $CDCl_3$) δ: 9.88 (s, 1H), 7.78 (d, J = 8.5 Hz, 2H), 6.98 (d, J = 8.5 Hz, 2H), 1.30 (sept,

J = 7.6 Hz, 3H), 1.11 (d, *J* = 7.6 Hz, 18H). ^{13}C NMR (500 MHz in $CDCl_3$) δ: 191.0, 162.1, 132.1, 130.3, 120.5, 18.0, 12.8. DART-MS $[C_{16}H_{26}O_2Si + H]^+$ calculated 279.1780, observed 279.1750.

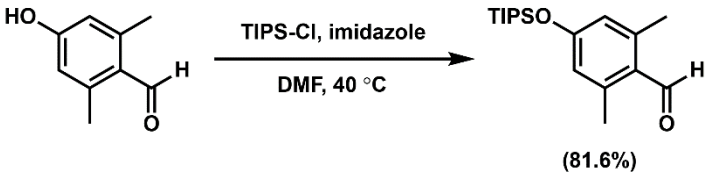

(81.6%)

TIPS-protected 4-hydroxy-2,6-dimethylbenzaldehyde. The reaction was conducted as in the representative procedure to yield the product (416 mg, 81.6% yield). ^{1}H NMR (500 MHz in $CDCl_3$) δ: 10.47 (s, 1H), 6.56 (s, 2H), 2.57 (s, 6H), 1.28 (sept, *J* = 7.6 Hz, 3H), 1.11 (d, *J* = 7.5 Hz, 18 H). ^{13}C NMR (500 MHz in $CDCl_3$) δ: 191.9, 160.2, 144.5, 126.4, 120.9, 21.1, 18.0, 12.9. DART-MS $[C_{18}H_{30}O_2Si + H]^+$ calculated 307.2093, observed 307.2087.

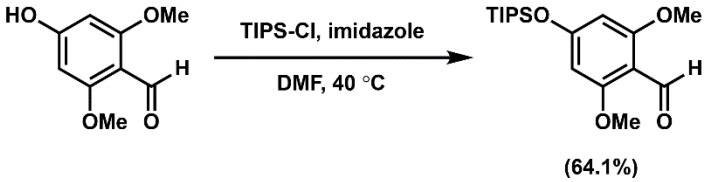

(64.1%)

TIPS-protected 4-hydroxy-2,6-dimethoxybenzaldehyde. The reaction was conducted as in the representative procedure to yield the product (298 mg, 64.1% yield). ^{1}H NMR (500 MHz in $CDCl_3$) δ: 10.35 (s, 1H), 6.06 (s, 2H), 3.85 (s, 6H), 1.29 (sept, *J* = 7.4 Hz, 3H), 1.13 (d, *J* = 7.4 Hz, 18H). ^{13}C NMR (500 MHz in $CDCl_3$) δ: 188.0, 164.1, 163.6, 109.2, 96.2, 56.1, 18.0, 12.9.

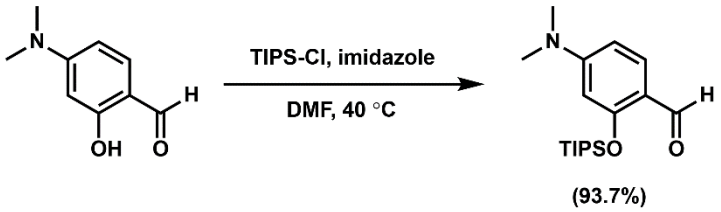

TIPS-protected 4-(dimethylamino)salicylaldehyde. The reaction was conducted as in the representative procedure to yield the product (456 mg, 93.7% yield). ^{1}H NMR (500 MHz in $CDCl_3$) δ: 10.26 (s, 1H), 7.71 (d, *J* = 8.9 Hz, 1H), 6.33 (dd, *J* = 8.9, 1.9 Hz, 1H), 6.02 (d, *J* = 2.0 Hz, 1H), 3.03 (s, 6H), 1.34 (sept, *J* = 7.5 Hz, 3H), 1.14 (d, *J* = 7.5 Hz, 18H). ^{13}C NMR (500 MHz in $CDCl_3$) δ: 188.1, 161.4, 155.9, 129.8, 116.8, 105.7, 100.8, 40.2, 18.2, 13.2. IR: 2962, 2936, 2886, 2865, 2825, 2749, 2658, 1673, 1646, 1587, 1547, 1524, 1486, 1441, 1416, 1373, 1327, 1284, 1244, 1218, 1158, 1112, 1067, 983, 920, 880, 834, 816, 796, 766 cm^{-1}.

Reductive Amination of TIPS-protected Benzaldehydes

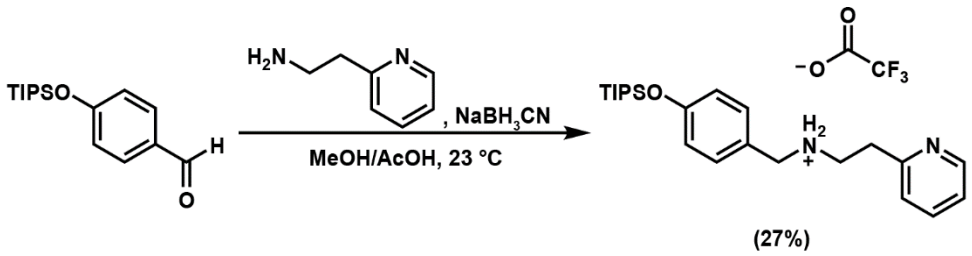

Representative Procedure: Reductive amination of TIPS-protected 4-hydroxybenzaldehyde. TIPS-protected benzaldehyde (200 mg, 0.72 mmol, 1 equiv), 2-(2-aminoethyl)pyridine (0.10 mL, 0.86 mmol, 1.2 equiv), and acetic acid (0.16 mL, 2.9 mmol, 4 equiv) were dissolved in 2 mL methanol and stirred in a dram vial for 30 min. The mixture was then cooled to 0 °C, and sodium cyanoborohydride (90 mg, 1.4 mmol, 2 equiv) in 2 mL methanol was added dropwise at °C. The mixture was stirred at 23 °C for 5 h, and quenched by addition of 4 mL saturated aqueous

ammonium chloride and stirring for around 12 h. To this mixture was added 10 mL methanol and 2 mL water to make 70% methanol solution, which was filtered and purified by preparative HPLC (70% methanol isocratic) to yield the product (98 mg, 27% yield). ^{1}H NMR (400 MHz in CD_3OD) δ: 8.52 (d, *J* = 4.9 Hz, 1H), 7.80 (t, *J* = 8.0 Hz, 1H), 7.40 (d, *J* = 8.4 Hz, 2H), 7.36–7.31 (m, 2H), 6.97 (d, *J* = 8.4 Hz, 2H), 4.22 (s, 2H), 3.42 (t, *J* = 6.9 Hz, 2H), 3.18 (t, *J* = 6.9 Hz, 2H), 1.29 (sept, J = 7.4 Hz, 3H), 1.12 (d, J = 7.4 Hz, 18H). ^{13}C NMR (500 MHz in CD_3OD) δ: 158.7, 158.6, 150.1, 139.0, 132.6, 125.1, 124.9, 123.8, 121.6, 51.6, 47.2, 33.3, 18.3, 13.9. ^{19}F NMR (400 MHz in CD_3OD) δ -74.5. DART-MS $[C_{23}H_{36}N_2OSi + H]^+$ calculated 385.2675, observed 385.2666.

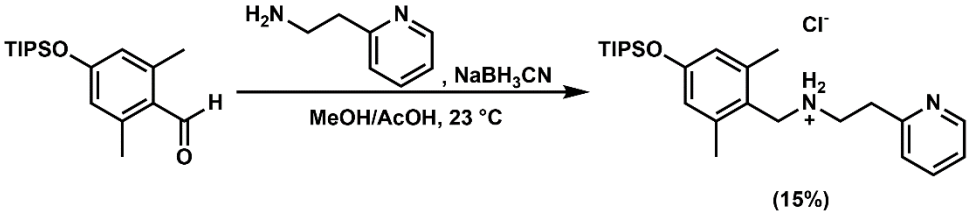

Reductive amination of TIPS-protected 4-hydroxy-2,6-dimethylbenzaldehyde. The reaction was conducted as in the representative procedure to yield the product (43 mg, 15% yield). ^{1}H NMR (400 MHz in CD_3OD) δ: 8.50 (d, *J* = 4.9 Hz, 1H), 7.82 (td, *J* = 7.7, 1.8 Hz, 1H), 7.39–7.32 (m, 2H), 6.69 (s, 2H), 4.35 (s, 2H), 3.58 (t, *J* = 6.3 Hz, 2H), 3.25 (t, 6.4 Hz, 2H), 2.45 (s, 6H), 1.28 (sept, *J* = 7.2 Hz, 3H), 1.11 (d, *J* = 7.3 Hz, 18H). ^{13}C NMR (500 MHz in CD_3OD) δ: 159.2, 158.2, 149.9, 141.3, 139.1, 125.0, 123.9, 122.5, 121.3, 48.2, 46.2, 32.4, 20.0, 18.3, 13.9. DART-MS $[C_{25}H_{40}N_2OSi + H]^+$ calculated 413.2988, observed 413.2975.

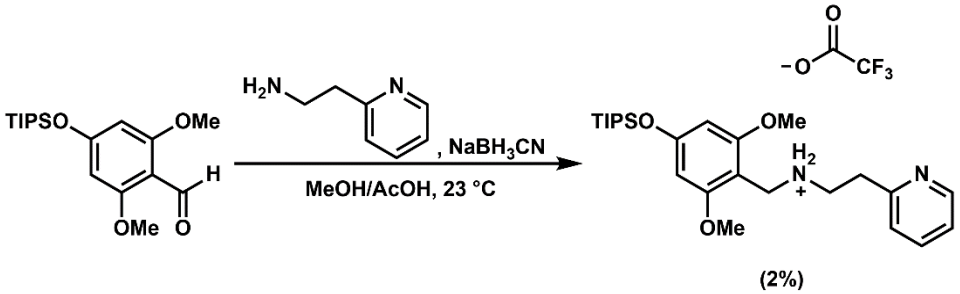

Reductive amination of TIPS-protected 4-hydroxy-2,6-dimethoxybenzaldehyde. The reaction was conducted as in the representative procedure and purified by preparative HPLC with elution gradient of 65–90% solvent B over 20 min (solvent A: water, solvent B: methanol) to yield the product (4 mg, 2% yield). ^{1}H NMR (400 MHz in CD_3OD) δ: 8.51 (d, *J* = 5.0 Hz, 1H), 7.80 (td, *J* = 7.7, 1.7 Hz, 1H) 7.35–7.31 (m, 2H), 6.23 (s, 2H), 4.26 (s, 2H), 3.86 (s, 6H), 3.40 (t, *J* = 6.5 Hz, 2H), 3.19 (t, *J* = 6.4 Hz, 2H), 1.32 (sept, *J* = 7.3 Hz, 3H), 1.14 (d, *J* = 7.3 Hz, 18H). ^{13}C NMR (500 MHz in CD_3OD) δ: 161.1, 160.9, 159.2, 149.9, 139.0, 124.9, 123.7, 101.3, 97.3, 56.5, 47.2, 40.9, 32.6, 18.4, 13.9. ^{19}F NMR (400 MHz in CD_3OD) δ -72.7. DART-MS $[C_{25}H_{40}N_2O_3Si + H]^+$ calculated 445.2887, observed 445.2878.

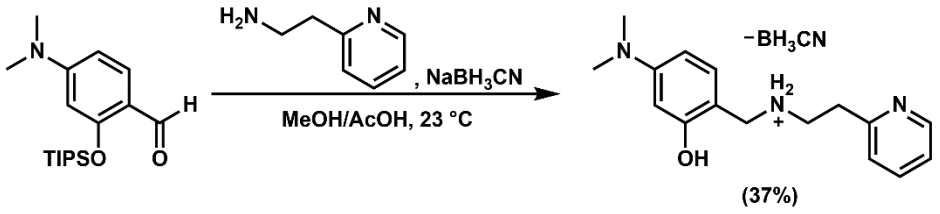

Reductive amination of TIPS-protected 4-(dimethylamino)salicylaldehyde. The reaction was conducted as in the representative procedure, and the major product collected was the TIPS-deprotected compound that was purified by preparative HPLC with elution gradient of 10–95% solvent B over 20 min (solvent A: water, solvent B: methanol) to yield the product (71 mg, 37% yield). ^{1}H NMR (400 MHz in CD_3OD) δ: 8.51 (d, *J* = 4.8 Hz, 1H), 7.79 (td, *J* = 7.7, 1.8 Hz, 1H),

7.34–7.31 (m, 2H), 7.1 (d, *J* = 8.1 Hz, 1H), 6.29–6.27 (m, 2H), 4.14 (s, 2H), 3.40 (t, *J* = 6.5 Hz, 2H), 3.18 (t, *J* = 6.5 Hz, 2H), 2.93 (s, 6H), 0.41 (q and septet, J = 88.0, 29.1 Hz, 3H). ^{13}C NMR (500 MHz in CD_3OD) δ: 159.1, 158.3, 154.7, 149.9, 138.9, 133.0, 124.8, 123.7, 106.4, 105.4, 99.8, 48.4, 46.9, 40.5, 32.8. IR: 3356, 3083, 3017, 2951, 2805, 2318, 2172, 1676, 1618, 1595, 1577, 1529, 1476, 1438, 1362, 1319, 1279, 1246, 1221, 1203, 1173, 1150, 1115, 1062, 1024, 998, 978, 940, 897, 859, 824, 776, 756, 718 cm^{-1}.

Release of Alkyl Amine from Traceless Linkers

TIPS-protected traceless linkers conjugated with pyridyl amine (1.5 mg) were dissolved in 0.15 mL of Dulbecco's phosphate buffered saline (D-PBS, pH 7.4) and 0.3 mL of methanol. Kinetic experiment was initiated by addition of 3 M TBAF in 0.05 mL MeOH. For the dimethylamino linker that has a free phenol, kinetic experiment was initiated by dissolving the compound in 7:3 methanol:D-PBS without TBAF. Kinetics of amine release was monitored by analytical HPLC, and percent amine released was quantified using a calibration curve of 2-(2-aminoethyl)pyridine.

NMR Spectra

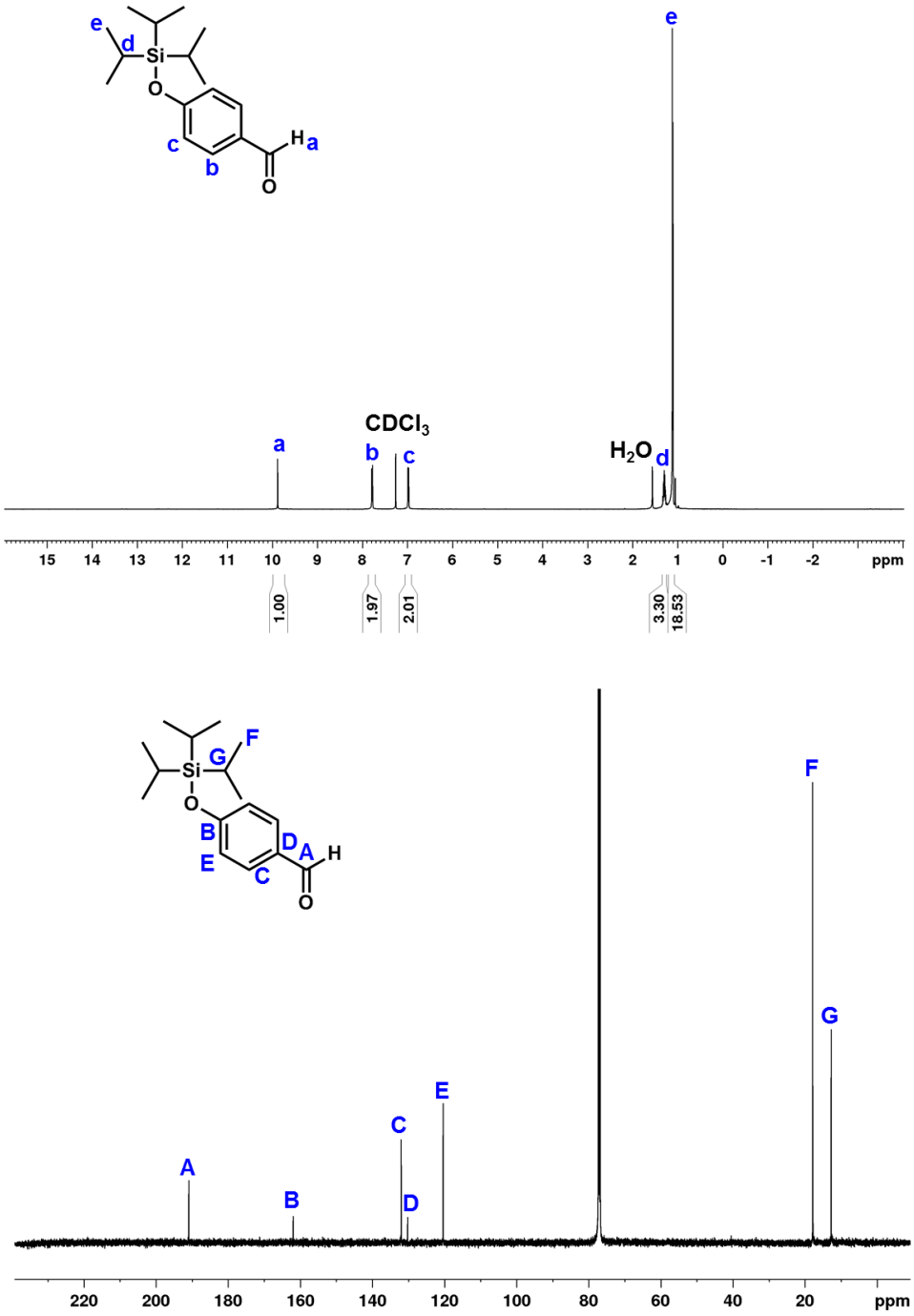

Figure 5-10. ^{1}H (top) and ^{13}C (bottom) NMR spectra of TIPS-protected 4-hydroxybenzaldehyde ($CDCl_3$).

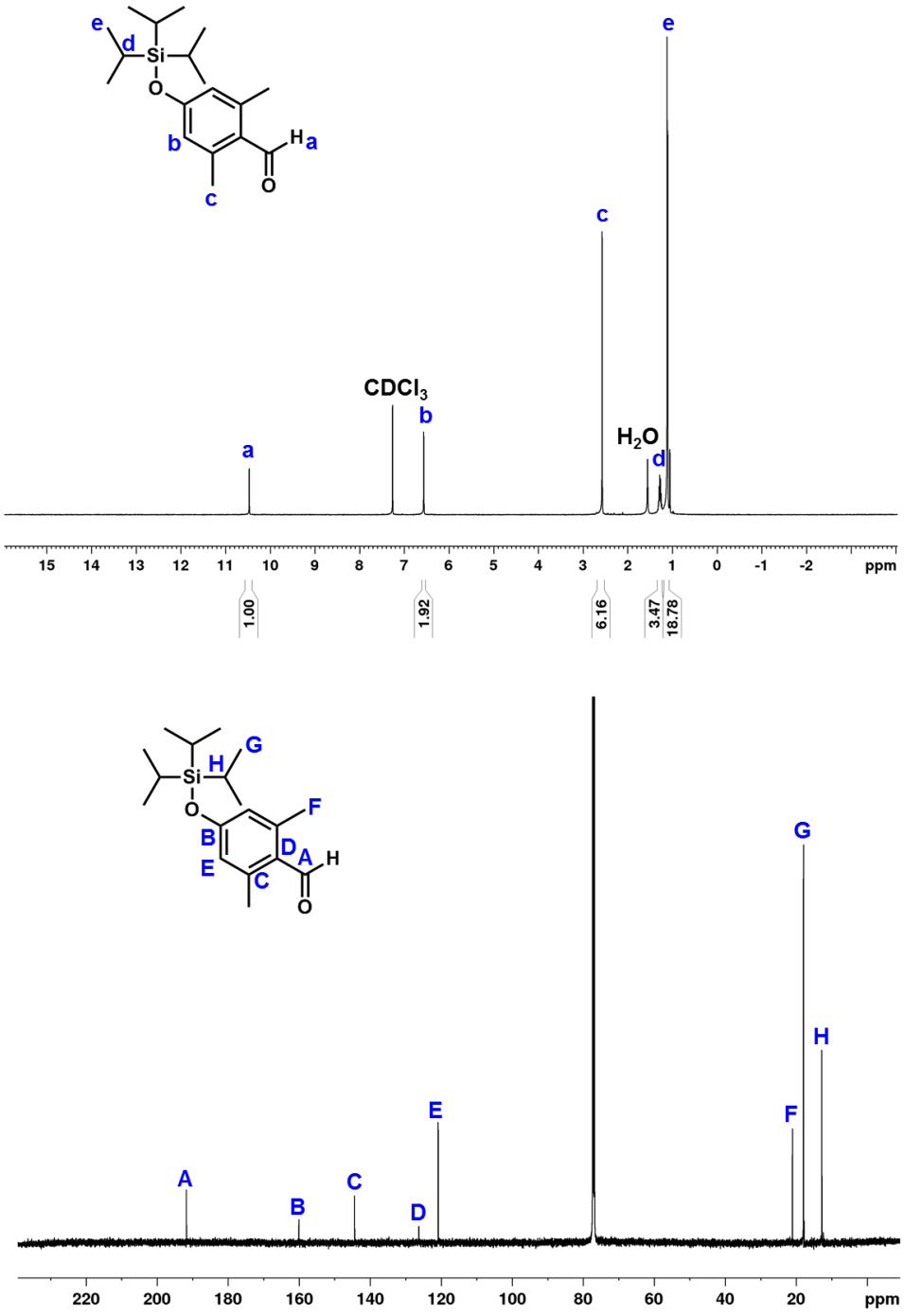

Figure 5-11. ^{1}H (top) and ^{13}C (bottom) NMR spectra of TIPS-protected 4-hydroxy-2,6-dimethylbenzaldehyde ($CDCl_3$).

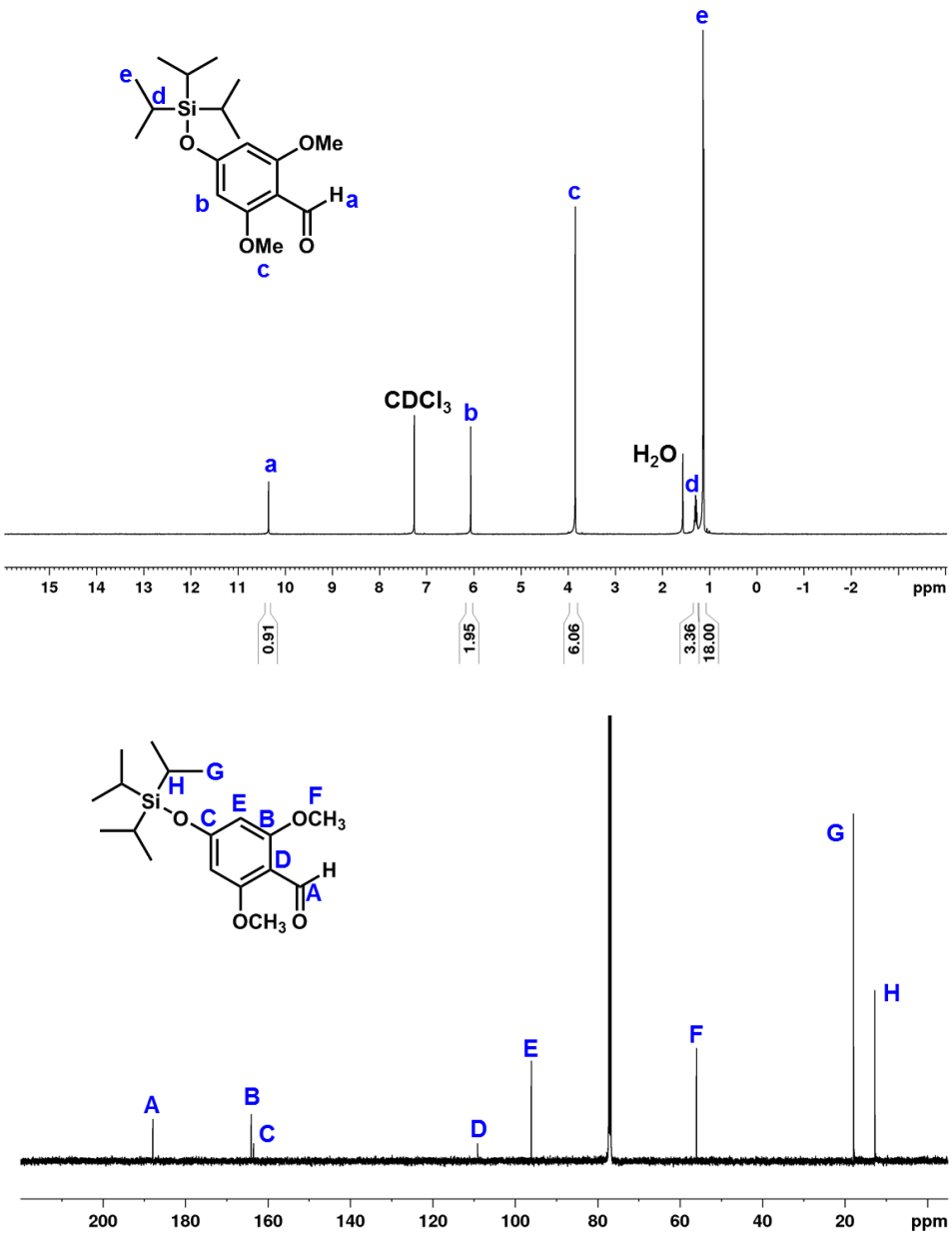

Figure 5-12. ^{1}H (top) and ^{13}C (bottom) NMR spectra of TIPS-protected TIPS-protected 4-hydroxy-2,6-dimethoxybenzaldehyde ($CDCl_3$).

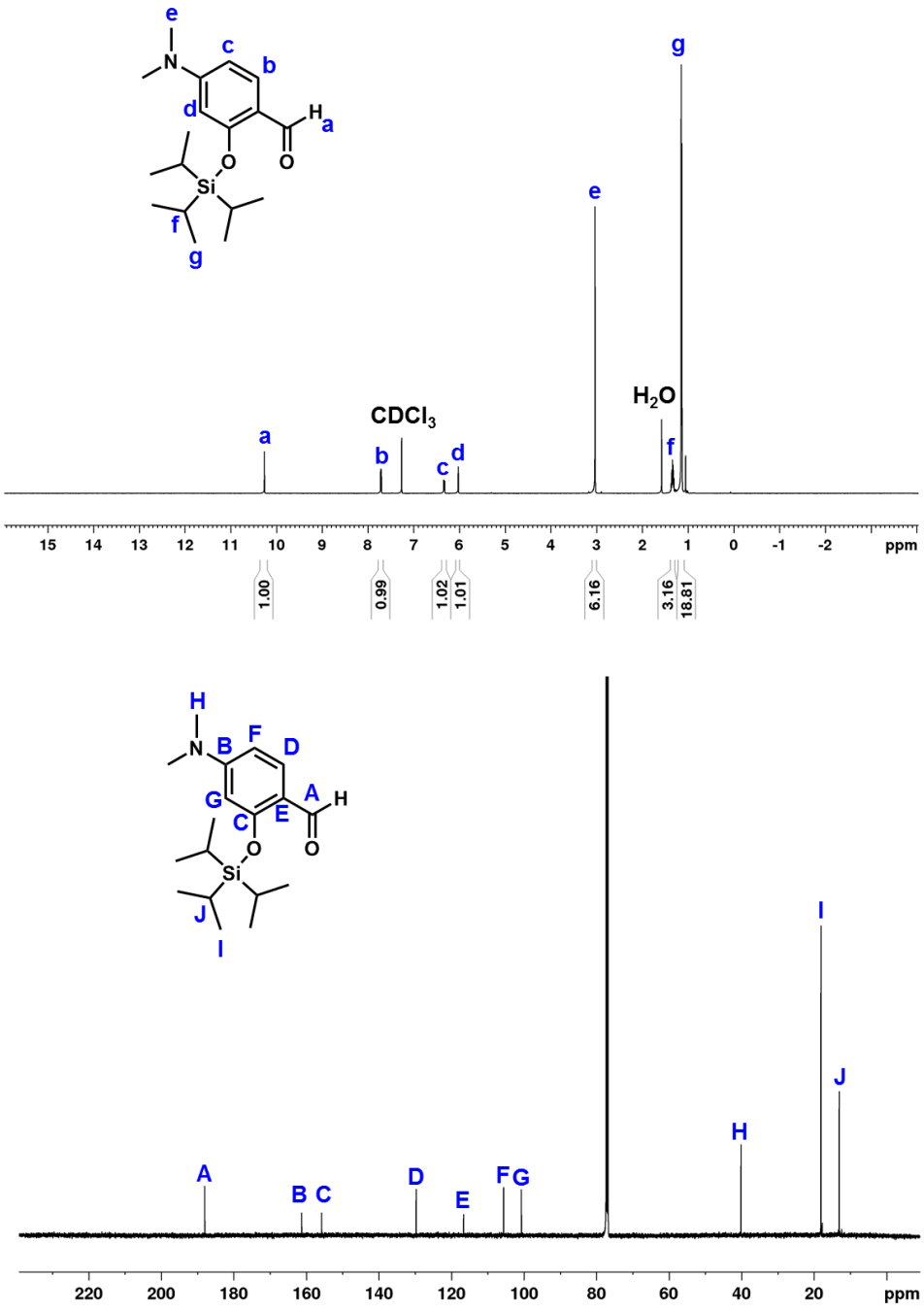

Figure 5-13. ^{1}H (top) and ^{13}C (bottom) NMR spectra of TIPS-protected 4-(dimethylamino)salicylaldehyde ($CDCl_3$).

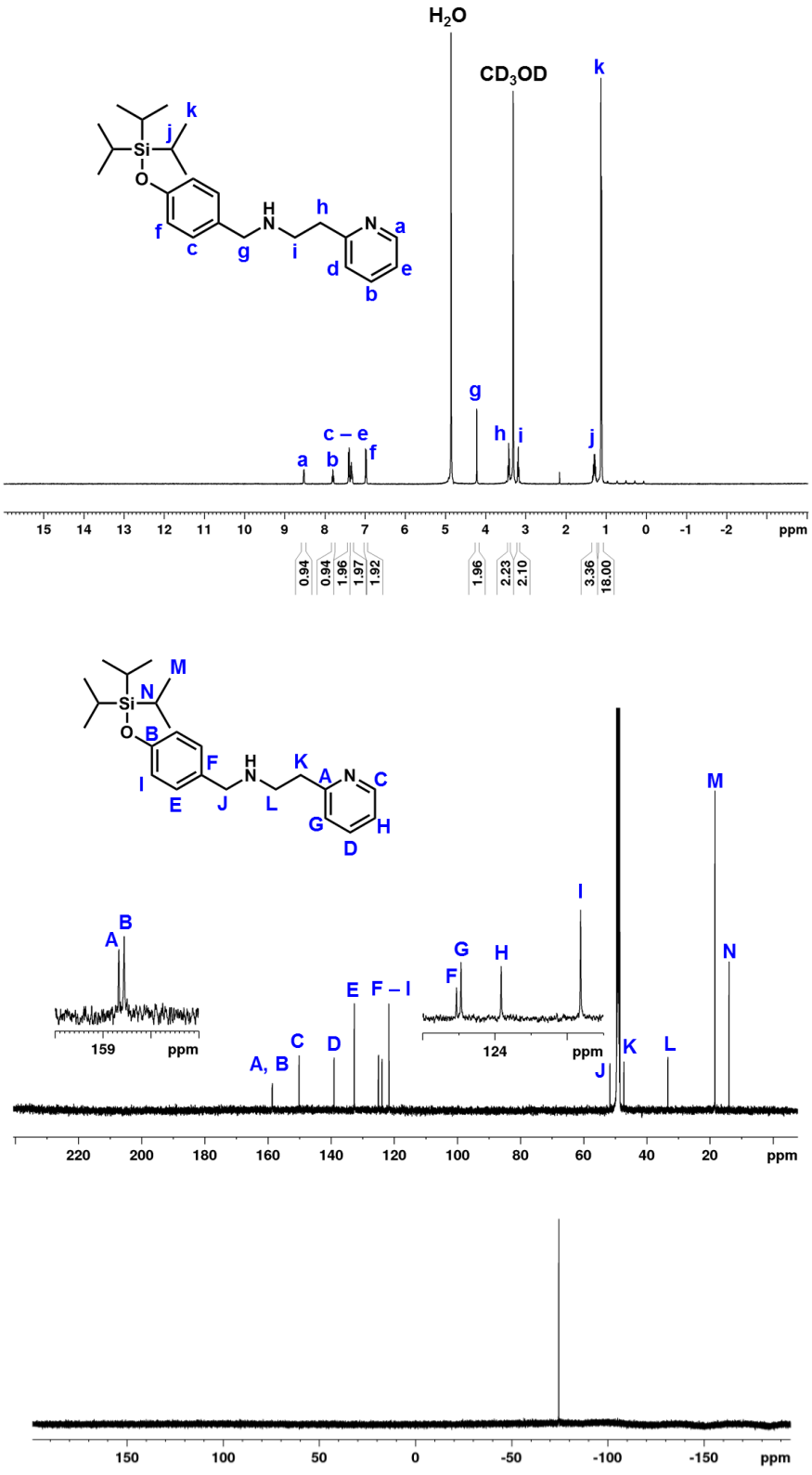

Figure 5-14. ^{1}H (top), ^{13}C (middle), and ^{19}F (bottom) NMR spectra of unsubstituted linker conjugated to 2-(2-aminoethyl)pyridine (CD_3OD).

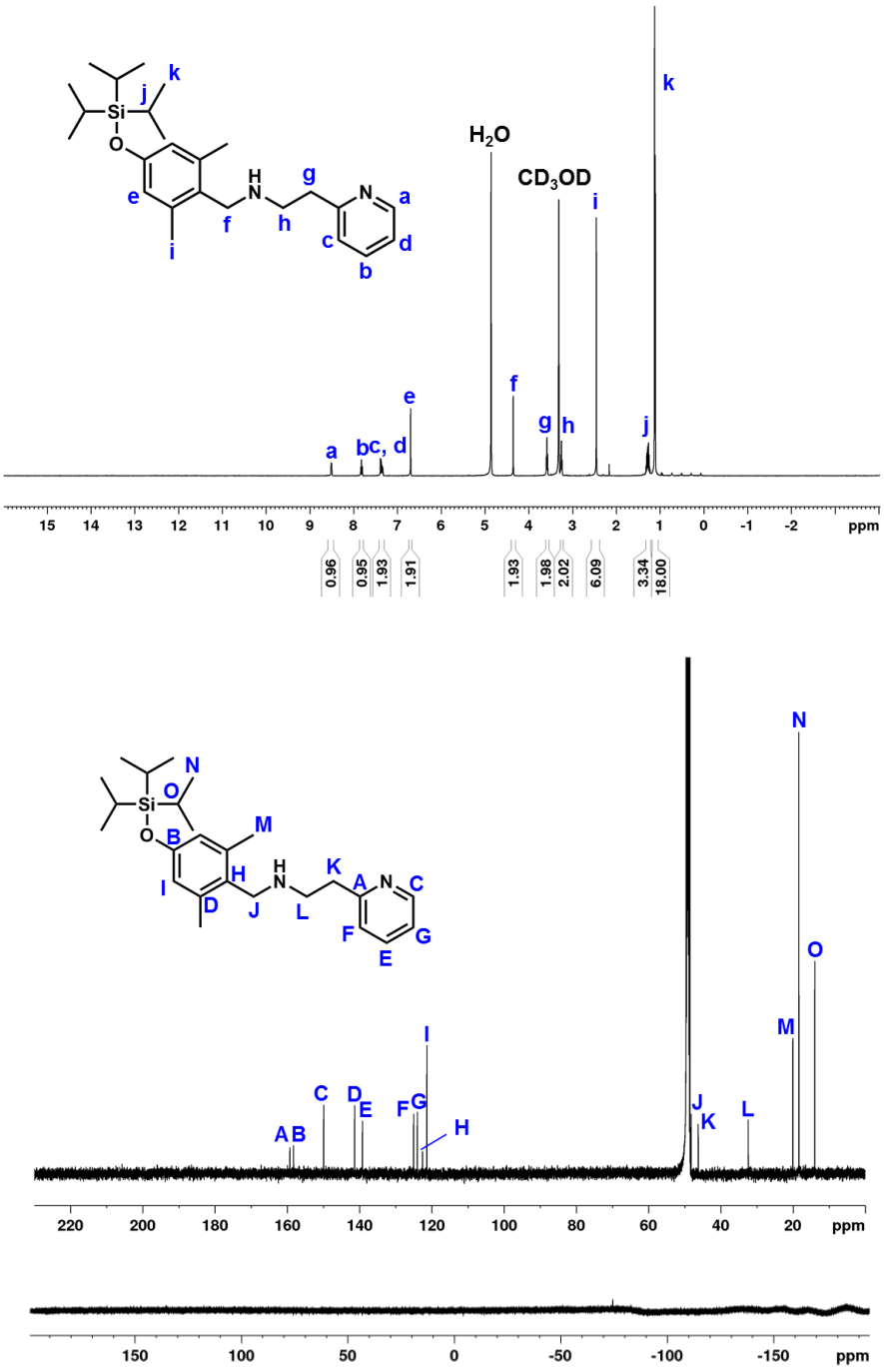

Figure 5-15. ^{1}H (top), ^{13}C (middle), and ^{19}F (bottom) NMR spectra of dimethyl linker conjugated to 2-(2-aminoethyl)pyridine (CD_3OD).

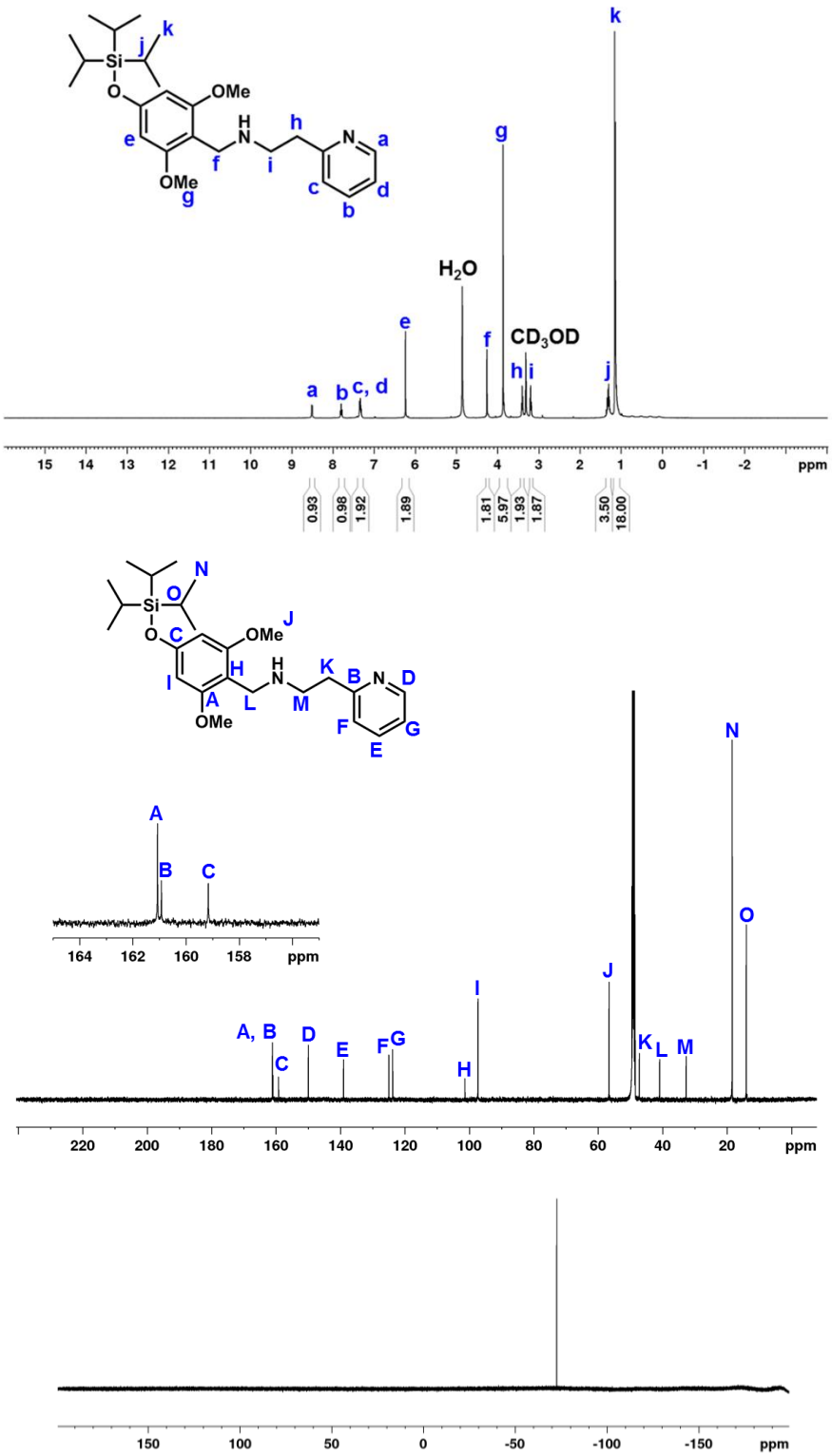

Figure 5-16. ^{1}H (top), ^{13}C (middle), and ^{19}F (bottom) NMR spectra of dimethoxy linker conjugated to 2-(2-aminoethyl)pyridine (CD_3OD).

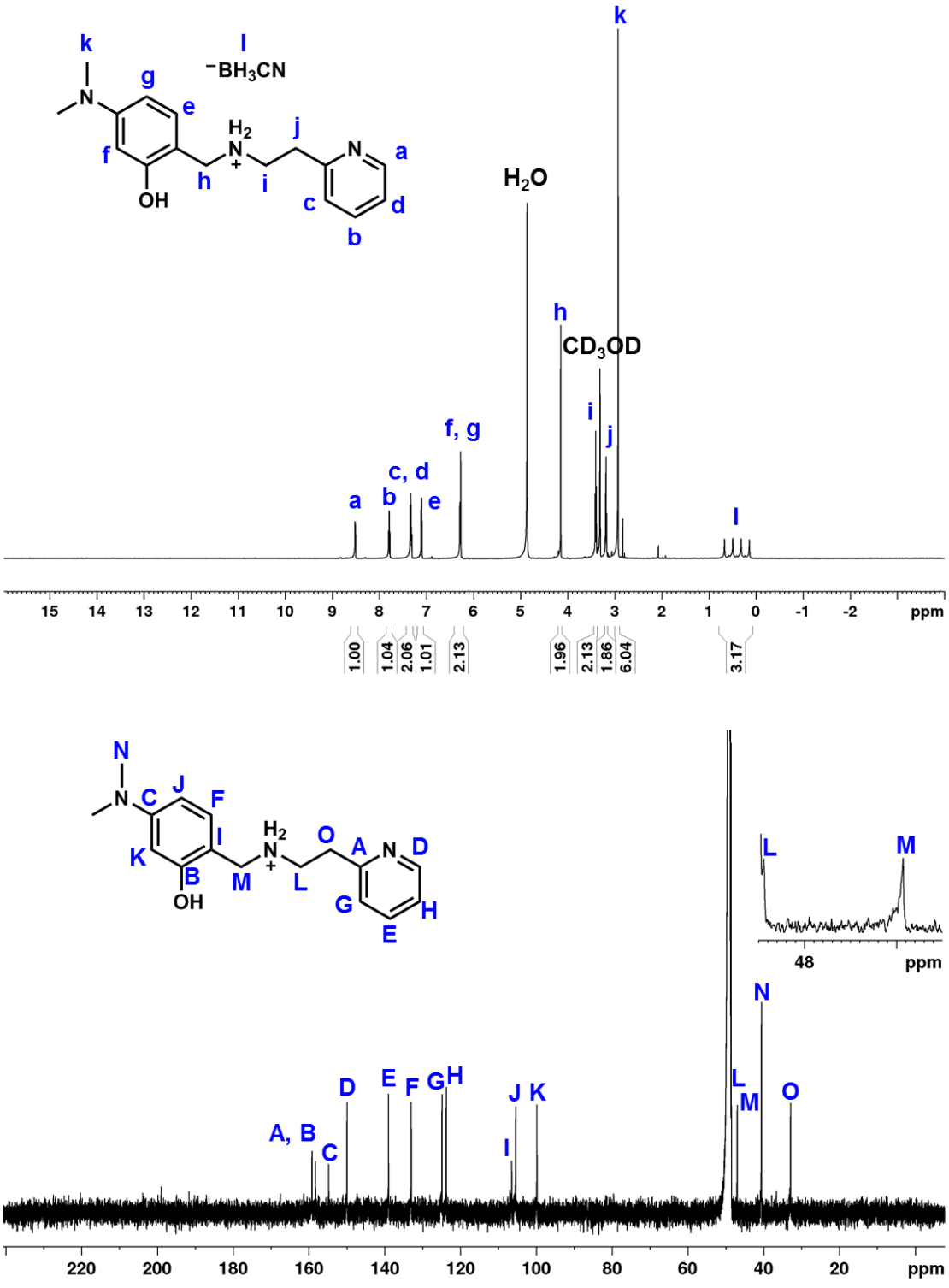

Figure 5-17. ^{1}H (top) and ^{13}C (bottom) NMR spectra of dimethylamino linker conjugated to 2-(2-aminoethyl)pyridine (CD_3OD).

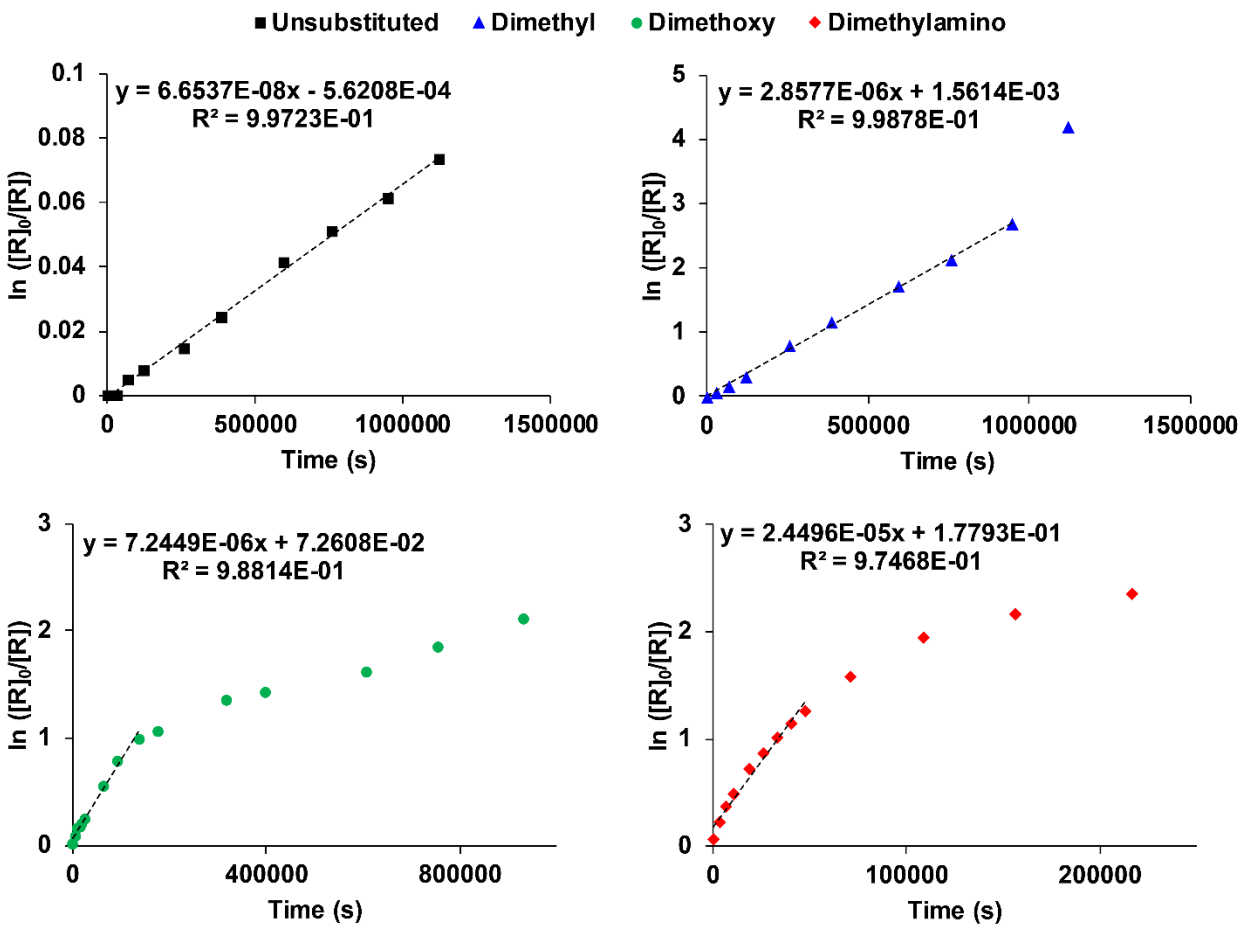

Figure 5-18. Logarithmic plots for the amine release from traceless linkers. Reactant concentration [R] is calculated as (100% - % amine released), and the slope of the linear region is taken as the rate.

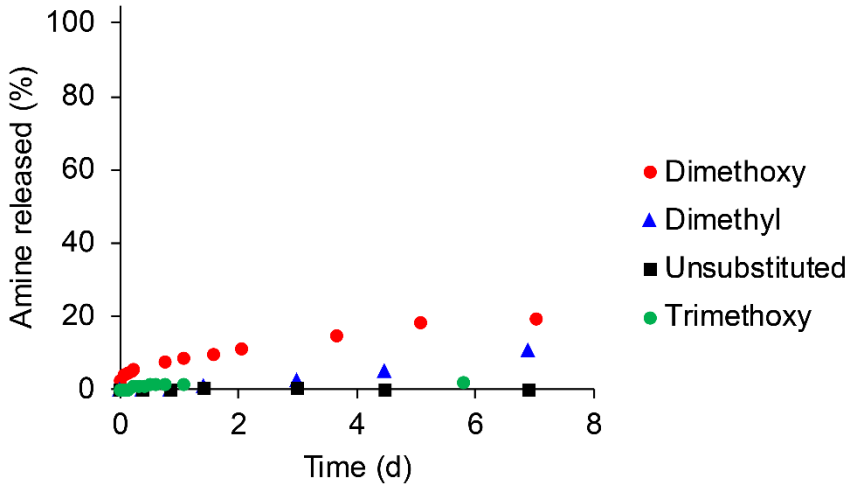

Figure 5-19. Control experiments for amine release kinetics (n = 1). Dimethoxy, dimethyl, and unsubstituted linkers are TIPS-protected compounds dissolved in 30:70 methanol:D-PBS without TBAF, while trimethoxy is the methylated version of the dimethoxy linker.

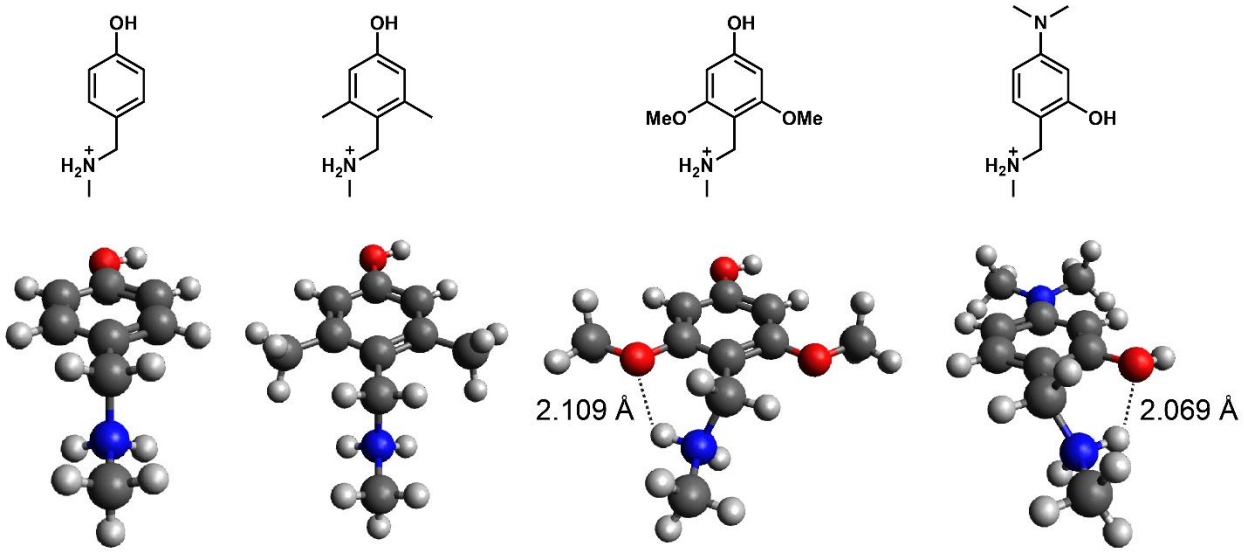

Figure 5-20. DFT optimized structures showing hydrogen bonding for dimethoxy and dimethylamino substituted linkers (structures optimized using B3LYP/6-31g(d) with SMD water model in GAMESS[14]).

5.5 References

(1) Mancini, R. J.; Lee, J.; Maynard, H. D. Trehalose Glycopolymers for Stabilization of Protein Conjugates to Environmental Stressors. *J. Am. Chem. Soc.* **2012,** *134*, 8474.

(2) Liu, Y.; Lee, J.; Mansfield, K. M.; Ko, J. H.; Sallam, S.; Wesdemiotis, C.; Maynard, H. D. Trehalose Glycopolymer Enhances Both Solution Stability and Pharmacokinetics of a Therapeutic Protein. *Bioconj. Chem.* **2017,** *28*, 836.

(3) Alconcel, S. N.; Baas, A. S.; Maynard, H. D. FDA-approved poly (ethylene glycol)–protein conjugate drugs. *Polym. Chem.* **2011,** *2*, 1442.

(4) Doronina, S. O.; Toki, B. E.; Torgov, M. Y.; Mendelsohn, B. A.; Cerveny, C. G.; Chace, D. F.; DeBlanc, R. L.; Gearing, R. P.; Bovee, T. D.; Siegall, C. B. Development of potent monoclonal antibody auristatin conjugates for cancer therapy. *Nat. Biotechnol.* **2003,** *21*, 778.

(5) Stephanopoulos, N.; Francis, M. B. Choosing an effective protein bioconjugation strategy. *Nat. Chem. Biol.* **2011,** *7*, 876.

(6) Gong, Y.; Leroux, J.-C.; Gauthier, M. A. Releasable conjugation of polymers to proteins. *Bioconj. Chem.* **2015,** *26*, 1172.

(7) Carl, P. L.; Chakravarty, P. K.; Katzenellenbogen, J. A. A novel connector linkage applicable in prodrug design. *J. Med. Chem.* **1981,** *24*, 479.

(8) Nolting, B., Linker Technologies for Antibody–Drug Conjugates. In *Antibody-Drug Conjugates*, Ducry, L., Ed. Humana Press: Totowa, NJ, 2013; pp 71.

(9) Ricci, M. S.; Sarkar, C. A.; Fallon, E. M.; Lauffenburger, D. A.; Brems, D. N. pH Dependence of structural stability of interleukin-2 and granulocyte colony-stimulating factor. *Protein Sci.* **2003,** *12*, 1030.

(10) Kinstler, O. B.; Brems, D. N.; Lauren, S. L.; Paige, A. G.; Hamburger, J. B.; Treuheit, M. J. Characterization and stability of N-terminally PEGylated rhG-CSF. *Pharm. Res.* **1996,** *13*, 996.

(11) Staben, L. R.; Koenig, S. G.; Lehar, S. M.; Vandlen, R.; Zhang, D.; Chuh, J.; Yu, S.-F.; Ng, C.; Guo, J.; Liu, Y. Targeted drug delivery through the traceless release of tertiary and heteroaryl amines from antibody–drug conjugates. *Nat. Chem.* **2016,** *8*, 1112.

(12) Alouane, A.; Labruere, R.; Le Saux, T.; Schmidt, F.; Jullien, L. Self-Immolative Spacers: Kinetic Aspects, Structure–Property Relationships, and Applications. *Angew. Chem. Int. Ed.* **2015,** *54*, 7492.

(13) Hansch, C.; Leo, A.; Taft, R. A survey of Hammett substituent constants and resonance and field parameters. *Chem. Rev.* **1991,** *91*, 165.

(14) Gordon, M. S.; Michael, W. S., Advances in electronic structure theory: GAMESS a decade later. In *Theory and Applications of Computational Chemistry: the first forty years*, Dykstra, C. E., Frenking, G., Kim, K. S., Scuseria, G. E., Eds. Elsevier: Amsterdam, 2005; pp 1167.

(15) Lee, H. Y.; Jiang, X.; Lee, D. Kinetics of self-immolation: faster signal relay over a longer linear distance? *Org. Lett.* **2009,** *11*, 2065.

(16) Xie, Y.-S.; Vijaykumar, B.; Jang, K.; Shin, H.-H.; Zuo, H.; Shin, D.-S. One-pot conversion of phenols to anilines via Smiles rearrangement. *Tetrahedron Lett.* **2013,** *54*, 5151.

(17) Erez, R.; Shabat, D. The azaquinone-methide elimination: comparison study of 1, 6-and 1, 4-eliminations under physiological conditions. *Org. Biomol. Chem.* **2008,** *6*, 2669.

Chapter 6.

Amphiphilic Random Copolymers for Encapsulation of a Fluorinated Agrochemical

This chapter contains portions of an edited version of a paper submitted as:
Ko, J. H.; Bhattacharya, A.; Terashima, T.; Sawamoto, M.; Maynard, H. D. *J. Polym. Sci., Part A: Polym. Chem.*, provisionally accepted.

6.1 Introduction

Amphiphilic copolymers with hydrophilic and hydrophobic units exhibit different self-assembly behavior depending on various factors including the solvent interaction (χ) of the two units,[1] their spatial arrangement,[2, 3] as well as molecular weight distribution[4] and stereochemistry.[5] While block copolymers have dominated the self-assembly research, amphiphilic random copolymers have recently been found to exhibit self-folding behavior in which a single polymer chain forms a core-shell structure where the core is composed of hydrophobic units and the shell is composed of hydrophilic units.[6-10] Polymers with alkyl pendants as the hydrophobic unit self-folded only in water, whereas polymers with fluorinated pendants as the hydrophobic unit self-folded in water, organic solvent, and fluorous solvent[10] due to the unique immiscibility and partitioning of fluorinated compounds from both aqueous and organic solvents.[11]

The previous studies on self-assembly of amphiphilic random copolymers have mostly focused on polyethylene glycol (PEG) as the hydrophilic unit. Since the change in the hydrophobic unit resulted in significantly different properties as described above, we were interested in observing the effect of the hydrophilic unit identity on the properties of the resulting polymer. Even though PEG is water soluble, it has amphiphilic character and intermediate polarity. Strongly polar molecules such as sugars are interesting candidates as the hydrophilic unit. An amphiphilic polymer with strongly hydrophilic sugar units and strongly hydrophobic fluorinated units may possess different self-assembly properties, but at the same time also presents a unique synthetic challenge.

Moreover, fluorinated amphiphilic polymers have been previously used to sequester and encapsulate fluorinated small molecules.[12, 13] Although these examples used star polymers with cross-linked cores, the self-folded amphiphilic polymers are expected to possess similar ability to

encapsulate fluorinated molecules. Especially of interest are fluorinated agrochemicals as many agrochemicals contain one or more fluorines and there is a need for efficient formulation of these molecules for their use.[14, 15] Amphiphilic polymers encapsulating these fluorinated agrochemicals would be useful for their formulation and use for agriculture.

In this chapter, we optimized the copolymerization of a sugar-modified methacrylate as the hydrophilic monomer and a fluorinated methacrylate as the hydrophobic monomer, and compared the encapsulation of a fluorinated agrochemical by polymers possessing PEG and/or sugar units, as well as their self-assembly behavior in solution.

6.2 Results and Discussion

Synthesis of Polymers

Previously we synthesized amphiphilic random copolymer using poly(ethylene glycol) methyl ether methacrylate (PEGMA) as the hydrophilic unit while the hydrophobic unit was varied from alkyl monomers such as dodecyl methacrylate[6] to fluorinated monomers such as 1*H*,1*H*,2*H*,2*H*-perfluorooctyl methacrylate (13FOMA).[10] To study the effect of changing the hydrophilic unit, we chose a methacrylate modified with trehalose. Trehalose is a naturally occurring disaccharide that is non-toxic and has interesting properties in stabilizing biomolecules such as proteins and DNA.[16] We and others have synthesized polymeric versions and observed that the polymer retains the protective properties of trehalose.[17-23]

The copolymerization of acetylated trehalose methacrylate (AcTreMA) and 13FOMA was conducted using the ruthenium indenyl catalyst ($Ru(Ind)Cl(PPh_3)_2$) with the chloride initiator (ethyl-2-chloro-2-phenylacetate, ECPA) (Figure 6-1). The polymerization was initially undertaken in toluene, which led to a polymer with relatively high dispersity of $Đ$ = 1.55 (**P1**, Table 6-1) even

though both monomers were consumed at equal rates (Figure 6-2). The polymer did not visibly precipitate during the polymerization at 80 °C, but did precipitate out of toluene after quenching and cooling the reaction to room temperature. Given that trehalose substitution greatly increases the polarity of the methacrylate, toluene may poorly solvate the growing polymer chain and/or may induce self-assembly of the growing polymer chain resulting in low mobility or partial burying of the chain ends; this could lead to non-uniform activation and the observed molecular weight dispersity.[24]

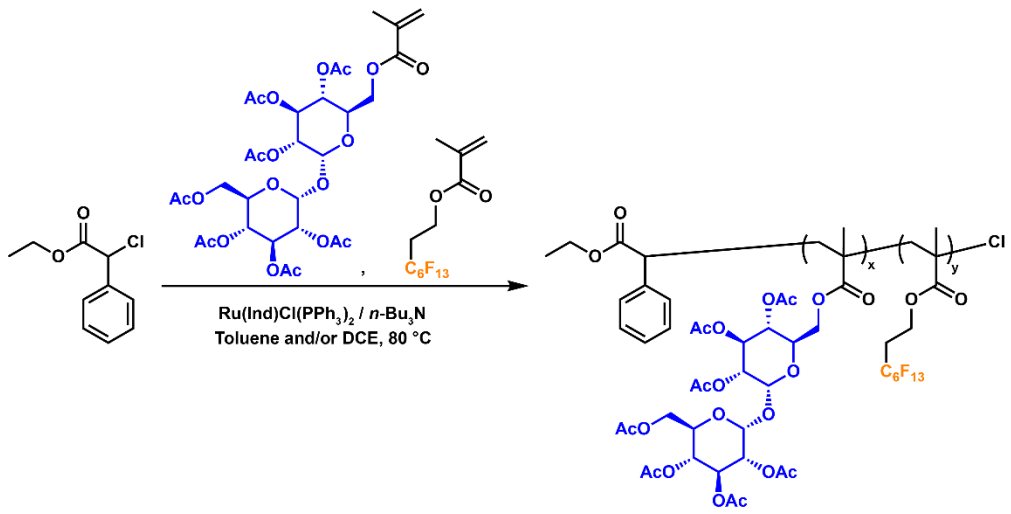

Figure 6-1. Ruthenium-catalyzed living radical polymerization of AcTreMA and 13FOMA.

Table 6-1. Copolymerization of AcTreMA and 13FOMA.

Polymer	AcTreMA: 13FOMA	Time (h)	Conv. (%)[a]	M_n (kDa)	$Đ$
P1[b]	50:50	30	87 / 83	37.5	1.55
P2[c]	50:50	96.5	74 / 94	30.3	1.27
P3	70:30	56	81 / 82	39.2	1.35
P4	90:10	46.3	77 / 82	36.9	1.37
P5[d]	30:70	40.5	78 / 89	N/A	N/A

[Monomer]/[ECPA]/[Ru(Ind)Cl(PPh_3)$_2$]/[*n*-Bu_3N] = 500/4/2/20 mM in 6:4 toluene:DCE at 80 °C. [a] AcTreMA conv. / 13FOMA conv. [b] Toluene instead of 6:4 toluene:DCE. [c] DCE instead of 6:4 toluene:DCE. [d] Insoluble so molecular weight could not be determined.

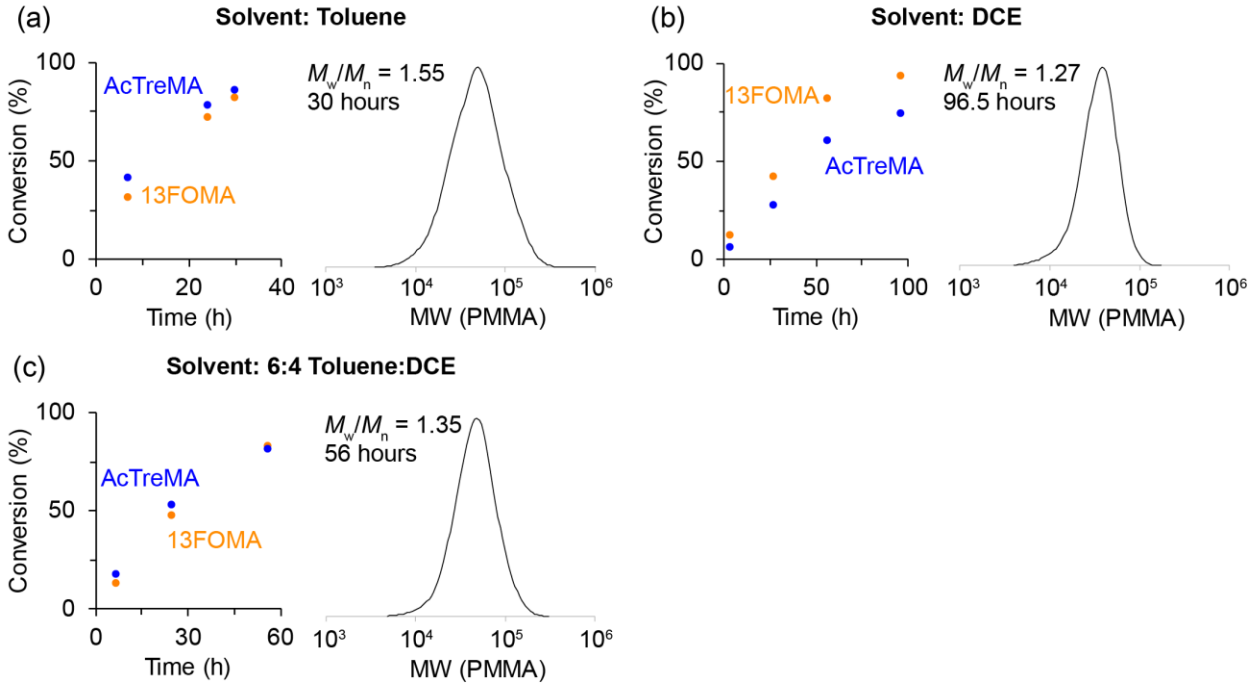

Figure 6-2. Effect of solvent on copolymerization of AcTreMA and 13FOMA. Left column: conversion plot, right column: SEC chromatogram. Polymerizations were conducted in (a) toluene, (b) DCE, or (c) 6:4 toluene:DCE. For (a) and (b), AcTreMA:13FOMA = 50:50. For (c), AcTreMA:13FOMA = 70:30.

Switching the polymerization solvent to more polar 1,2-dichloroethane (DCE) resulted in lower dispersity ($Đ$ = 1.27) (**P2**, Table 6-1). The polymerization time increased from 30 h to 96.5 h when the solvent was changed from toluene to DCE, which was also previously observed for the $Cp^*RuCl(PPh_3)_2$ catalyst.[25] However, the two monomers were consumed at significantly different rates and the monomer conversion differed by 20 % at the end of the polymerization (Figure 6-2b). The two experiments suggested that toluene promotes equal reactivity of both monomers while DCE helps to keep the dispersity low. Thus, 6:4 toluene:DCE mixture was chosen as the polymerization solvent. Using this condition, polymers with different AcTreMA:13FOMA ratios were synthesized. The 70:30 AcTreMA:13FOMA (**P3**, Table 6-1) and 90:10 AcTreMA:13FOMA (**P4**, Table 6-1) were relatively well controlled ($Đ$ = 1.35 – 1.37) and both monomers were consumed at comparable rates. The more fluorinated 30:70 AcTreMA:13FOMA (**P5**, Table 6-1) was insoluble in DMF, and the molecular weight could not be analyzed.

The polymers with acetylated trehalose units were deacetylated using hydrazine hydrate.[19] Removal of the acetyl groups was confirmed by the loss of the sharp peak centered at 2.0 ppm in the ^{1}H NMR spectrum (see SI). Under these relatively mild conditions, cleavage of the backbone methacrylate ester was not observed in the IR spectra, as shown by the lack of the broad carboxylic acid O-H stretch centered around 3000 cm^{-1} (Experimental Section Figure 6-22 through Figure 6-28).

The large polarity difference between TreMA and 13FOMA in p(TreMA-*co*-13FOMA) led to moderate dispersity ($Đ$ ~ 1.35) even after optimization of polymerization conditions. To address this issue, PEGMA was added as a comonomer with intermediate polarity that may mitigate the unfavorable interaction between the TreMA and 13FOMA. The random terpolymer p(AcTreMA-*co*-PEGMA-*co*-13FOMA) was readily synthesized under the condition previously

optimized for p(AcTreMA-*co*-13FOMA) (Figure 6-3). With addition of PEGMA to help solubilize the growing chain, the dispersity decreased to 1.26 (**P6**, Table 6-2) when all monomers were added in equimolar amounts. When AcTreMA content was increased to 56% and PEGMA content was decreased to 18%, the dispersity returned to moderate level ($Đ$ = 1.34, **P7**, Table 6-2). The polymer with equimolar amounts of TreMA and PEGMA but lower 13FOMA content (26%) again showed lower dispersity at 1.27 (**P8**, Table 6-2).

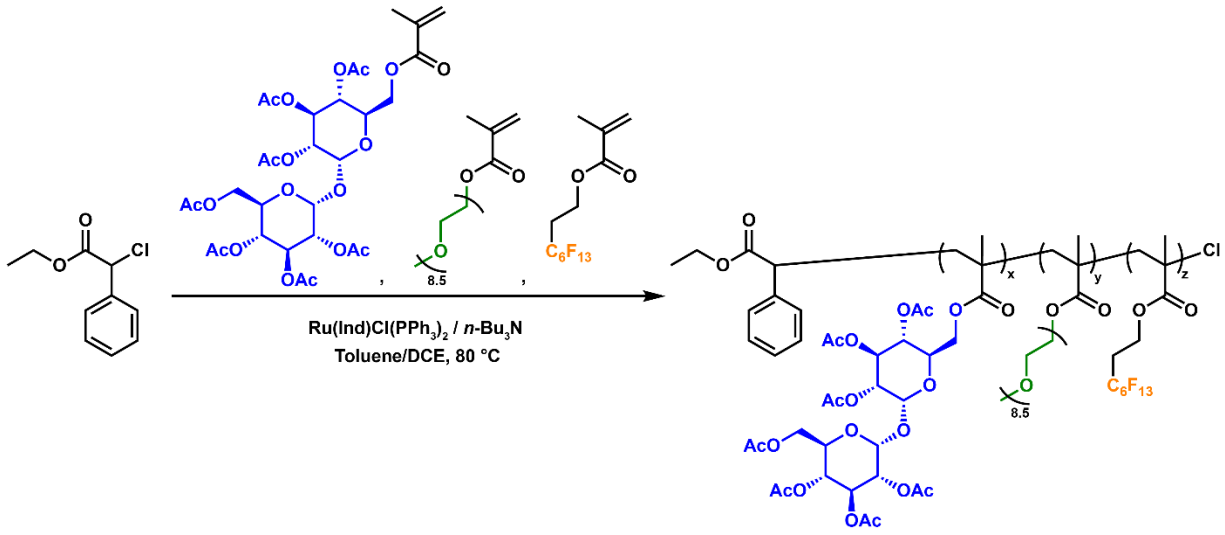

Figure 6-3. Ruthenium-catalyzed living radical polymerization of AcTreMA, PEGMA, and 13FOMA.

Table 6-2. Copolymerization of AcTreMA, PEGMA, and 13FOMA.

Polymer	AcTreMA: PEGMA: 13FOMA	Conv. (%)[a]	M_n (kDa)	$Đ$
P6[b]	33:33:33	86 / 83 / 84	39.8	1.26
P7[c]	56:18:26	85 / 86 / 74	26.4	1.34
P8[c]	37:37:26	72 / 68 / 74	28.3	1.27

[ECPA]/[$Ru(Ind)Cl(PPh_3)_2$]/[*n*-Bu_3N] = 4/2/20 mM in 6:4 toluene:DCE at 80 °C. Combined monomer concentrations are listed below. [a] AcTreMA conv. / PEGMA conv. / 13FOMA conv. [b] [Monomer] = 510 mM, [c] [Monomer] = 448 mM.

The evidence for incorporation of all three types of monomer in the same polymer chain was as follows. First, the monomers were consumed at comparable rates and reached similar conversion, suggesting copolymerization. Second, p(TreMA-*co*-13FOMA) that lack PEGMA were not soluble in fluoroalcohols at any compositions, while the terpolymers with lower trehalose content and PEGMA (**P6** and **P8**) were soluble in fluoroalcohols dodecafluoroheptanol and hexafluoroisopropanol. Third, ^{1}H diffusion-ordered NMR spectroscopy of **P8** showed that peaks corresponding to TreMA and PEGMA (13FOMA peak is too broad to be observed by ^{1}H NMR) have the same diffusion constants (Figure 6-17) as expected if TreMA and PEGMA were on the same chain.

Encapsulation of a Fluorinated Agrochemical

As a potential application for the use of the amphiphilic fluorinated polymers, p(PEGMA-*co*-13FOMA), p(TreMA-*co*-13FOMA), and p(TreMA-*co*-PEGMA-*co*-13FOMA) were tested for their ability to encapsulate fluorinated agrochemicals. Many agrochemicals are fluorinated; for

example, around 25% of herbicides are reported to be fluorinated.[15] However, fluorination decreases the aqueous solubility and as a result, formulation is non-trivial. For example, novaluron is a pesticide that is co-formulated with the organic solvent *N*-methyl-2-pyrrolidone (NMP).[26] Replacing this organic solvent with a polymeric material may be beneficial with regard to toxicity concerns. p(PEGMA-*co*-13FOMA) is noncytotoxic[27] and trehalose polymers have been tested to be safe *in vivo*.[28] Given that amphiphilic star polymers with fluorinated core have been shown to sequester fluorinated compounds in water,[12, 13] we hypothesized that amphiphilic random copolymers with PEGMA, TreMA, or combination of both as the hydrophilic unit may be capable of encapsulating fluorinated agrochemicals such as novaluron.

To encapsulate novaluron, p(PEGMA-*co*-13FOMA) (**P0**, 60:40 PEGMA:13FOMA), p(TreMA-*co*-13FOMA) (**P3**, 70:30 TreMA:13FOMA and **P4**, 90:10 TreMA:13FOMA), or p(TreMA-*co*-PEGMA-*co*-13FOMA) (**P8**, 37:37:26 TreMA:PEGMA:13FOMA) were dissolved in DMSO in the presence of novaluron, and nanoprecipitated into water. After dialysis to remove DMSO, the novaluron-polymer mixture was lyophilized and redissolved in deuterated DMSO-d_6 to calculate percent encapsulation. Note that redissolution in D_2O led to disappearance of peaks corresponding to novaluron due to its encapsulation within the polymer and reduced mobility that led to significant peak broadening[29] (Experimental Section Figure 6-18 through Figure 6-21), suggesting that the sharp peak observed in DMSO-d_6 is from the free novaluron released from the polymer chain. At a polymer:pesticide ratio of 10:1, the percent encapsulation was 34.9 ± 6.9 % (n = 5) for p(PEGMA-*co*-13FOMA) (**P0**) and 31.1 ± 6.4 % (n = 5) for p(TreMA-*co*-PEGMA-*co*-13FOMA) (**P8**). Trehalose polymers without PEGMA (**P3** and **P4**) did not fully redissolve in DMSO and the percent encapsulation was low at 10.7 ± 3.5 % for **P3** and 14.2 ± 17.0 % for **P4** (n = 5 each). DLS showed significant amount of large aggregates for **P3** (d > 1000 nm) (Figure 6-29)

but not for **P4** or any other polymers (Experimental Section Figure 6-30 through Figure 6-32). A control experiment with nanoprecipitation of novaluron alone in the absence of any polymer led to visible precipitation, and dialysis followed by filtration as done for polymer-containing samples (see the Experimental Section) showed negligible amounts of novaluron at 1.9 ± 0.8 % (n = 3). Increasing the novaluron loading to 5:1 polymer:pesticide resulted in even higher loading at 44.7 ± 7.6 % (n = 5) for p(TreMA-*co*-PEGMA-*co*-13FOMA) (**P8**). However, highly variable loading (32.9 ± 15.7 %, n = 6) was observed for p(PEGMA-*co*-13FOMA) (**P0**) possibly due to the excess hydrophobicity from the pesticide and 13FOMA, making the polymer more prone to aggregation. As with 10:1 polymer:pesticide ratio, trehalose polymers without PEGMA showed low and variable encapsulation efficiencies of 20.6 ± 10.6 (**P3**) and 21.5 ± 12.4 (**P4**) (n = 5 each). Further increase in loading to 1:1 polymer:pesticide led to visible precipitation for all polymers and the encapsulation efficiency was not quantified. Table **6-3** provides a summary of all the encapsulation data. These experiments show that PEGMA/13FOMA amphiphilic polymer and TreMA/PEGMA/13FOMA terpolymer are the most efficient at encapsulating novaluron in water at an appropriate polymer:pesticide ratio and provide a benchmark for future design of fluorinated amphiphilic polymers for encapsulation of fluorinated agrochemicals.

Table 6-3. Encapsulation efficiency of agrochemical novaluron inside amphiphilic random copolymers.

Polymer	Polymer:novaluron (average ± std. dev.)	
	10:1	5:1
P0[a]	34.9 ± 6.9%	32.9 ± 15.7%
P3[b]	10.7 ± 3.5%	20.6 ± 10.6%
P4[c]	14.2 ± 17.0%	21.5 ± 12.4%
P8[d]	31.1 ± 6.4%	44.7 ± 7.6%
Control[e]	1.9 ± 0.8 %	

6.3 Conclusions

Amphiphilic random copolymers with PEG and/or trehalose as the hydrophilic units were synthesized, and used to encapsulate novaluron as a model fluorinated agrochemical. The challenging copolymerization of highly polar TreMA and fluorous 13FOMA required solvent optimization as well as the addition of PEGMA as the comonomer with intermediate polarity to improve the dispersities of the resulting polymers. The PEG and trehalose/PEG polymers were the most efficient at encapsulating novaluron, and provide a benchmark to explore fluorous amphiphilic polymers to replace the organic solvent used for formulation of novaluron.

6.4 Experimental Section

Materials

All commercially obtained reagents were used as received unless otherwise specified. Novaluron was obtained from AdipoGen Life Sciences and used as received. Acetylated trehalose methacrylate (AcTreMA) was synthesized as reported previously.[18] Ethyl-2-chloro-2-phenylacetate (ECPA, Aldrich) was purified by distillation under reduced pressure.

$Ru(Ind)Cl(PPh_3)_2$ (Aldrich) was used as received and handled in a glove box under a moisture- and oxygen-free argon atmosphere (H_2O < 1 ppm, O_2 < 1 ppm). Poly(ethylene glycol) methyl ether methacrylate (PEGMA, Aldrich, M_n = 475 (n = 8.5)) and 1*H*,1*H*,2*H*,2*H*-perfluorooctyl methacrylate (13FOMA, Wako) were purified by column chromatography charged with inhibitor remover (Aldrich) and purged by argon before use. The co-catalyst tributylamine (*n*-Bu_3N, TCI) was degassed by reduced pressure. Tetralin (TCI), used as the internal standard for calculating monomer conversion by ^1H NMR, was purified by drying over calcium chloride overnight and distilling from calcium hydride. Toluene (Kishida Chemical) was purified by passing through a purification column (Glass Contour Solvent Systems, Nikko Hansen & Co., Ltd.) and sparged with nitrogen gas. 1,2-Dichloroethane (DCE, TCI) was dehydrated with molecular sieves (4 Å) and sparged with nitrogen gas. The polymer p(PEGMA-*co*-13FOMA) (referred to as **P0** in the text, PEGMA:13FOMA = 60:40, M_n = 50.9 kDa, $Đ$ = 1.18 by size exclusion chromatography (SEC) in *N*,*N*-dimethylformamide (DMF)) was synthesized as reported previously.[10]

Analytical Techniques

NMR spectra were recorded on a Bruker AV 400 MHz, a Bruker DRX 500 MHz, or a JEOL JNM-ECA500 spectrometer with a relaxation delay of 10 s. Analytical size exclusion chromatography (SEC) was conducted in *N*,*N*-dimethylformamide (DMF) containing 10 mM lithium bromide at 40 °C (flow rate: 1 mL/min) on three linear-type polystyrene gel columns (Shodex KF-805L) connected to a Jasco PU-2080 precision pump, a Jasco RI-2031 refractive index detector, and a Jasco UV-2075 UV/Vis detector set at 270 nm. Near-monodisperse poly(methyl methacrylate) standards (Polymer Laboratories) were employed for the SEC calibration. Preparative SEC was conducted in chloroform at room temperature on a polystyrene

gel column (Shodex K-5003) that was connected to a Jasco PU-2086 precision pump, a Jasco RI-2031 refractive index detector, and a Jasco UV-2075 UV/vis detector set at 250 nm. Dynamic light scattering (DLS) measurements were conducted on a Malvern ZetaSizer Nano or an Otsuka Photal ELSZ-0 at 10 mg/mL polymer concentration. Infrared (IR) spectra were acquired on a Perkin-Elmer Spectrum One instrument equipped with a universal ATR assembly.

Synthesis of Polymers

Representative Procedure: Co-polymerization of AcTreMA, PEGMA, and 13FOMA (ratio = 33:33:33) (P8). Inside a glove box, Ru(Ind)Cl(PPh_3)$_2$ (1.54 mg, 1.98×10^{-3} mmol) was weighed out into a Schlenk flask equipped with three-way stopcock. To this flask under argon were added AcTreMA (117 mg, 1.66×10^{-1} mmol), PEGMA (75 μL, 1.7×10^{-1} mmol), 13FOMA (50 μL, 1.7×10^{-1} mmol), 41.7 mM toluene solution of ECPA (95 μL, 4.0×10^{-3} mmol), tetralin (15 μL, 1.1×10^{-1} mmol), and 400 mM toluene solution of *n*-Bu_3N (50 μL, 2.0×10^{-2} mmol), toluene (0.43 mL), and DCE (0.29 mL) were added under argon (total volume: 1.01 mL). This corresponds to the following reagent concentrations: [AcTreMA] / [PEGMA] / [13FOMA] / [ECPA] / [Ru(Ind)Cl(PPh_3)$_2$] / [*n*-Bu_3N] = 165 / 170 / 172 / 4 / 2 / 20 mM. The flask was immersed in an oil bath maintained at 80 °C over a magnetic stirrer, and approximately 50 μL aliquots were taken to measure monomer conversion. The polymerization was quenched after 22.5 h by cooling the mixture to -78 °C and exposing it to air (AcTreMA conversion 86%, PEGMA conversion 83%, and 13FOMA conversion 84% by ^{1}H NMR). The polymer was purified by preparative size exclusion chromatography in chloroform. ^{1}H NMR (500 MHz in $CDCl_3$) δ: 5.58–4.86, 4.41–3.89, 3.72–3.56, 3.56–3.46, 3.42–3.31, 2.68–2.33, 2.33–1.68, 1.22–0.60 ppm. ^{19}F NMR (500 MHz in $CDCl_3$ with TFA at δ = -76.5 ppm as an internal standard) δ: -81.4–82.5, -113.6–115.7, -122.5–

123.5, -123.5–124.3, -124.3–125.3, -126.7–127.2 ppm. Number average molecular weight (M_n) = 39.8 kDa, dispersity ($Đ$) = 1.26 (DMF SEC).

p(AcTreMA-*co*-13FOMA), AcTreMA:13FOMA = 50:50 (polymerized in toluene, P1 in Table 7-1). Polymerization was conducted as in the representative procedure above, with the following reagent concentrations: [AcTreMA] / [13FOMA] / [ECPA] / [Ru(Ind)Cl(PPh_3)$_2$] / [*n*-Bu_3N] = 250 / 250 / 4 / 2 / 20 mM. Polymerization was quenched after 30 h. ^{1}H NMR (500 MHz in $CDCl_3$) δ: 5.57–4.82, 4.45–3.66, 2.66–2.32, 2.32–1.72, 1.21–0.54 ppm. ^{19}F NMR (500 MHz in $CDCl_3$ with TFA at δ = -76.5 ppm as an internal standard) δ: -81.4–82.9, -113.5–116.6, -122.6–123.7, -123.7–124.5, -124.5–125.4, -126.9–128.0 ppm. M_n = 37.5 kDa, $Đ$ = 1.55 (DMF SEC).

This polymer was deprotected as described below. ^{1}H NMR (500 MHz in DMSO-d_6) δ: 5.31–4.18, 4.18–3.85, 3.85–3.39, 3.20–2.82, 1.35–0.25 ppm. ^{19}F NMR (500 MHz in DMSO-d_6 with TFA at δ = -76.5 ppm as an internal standard) δ: -80.1–85.8, -111.4–117.6, -121.1–123.7, -123.7–126.3, -126.3–129.8 ppm. IR: δ = 3387.34, 2936.70, 1729.49, 1446.34, 1431.17, 1390.73, 1362.92, 1317.41, 1233.98, 1188.48, 1142.97, 1077.24, 1041.85, 1021.62, 988.76, 940.73, 842.13, 804.21, 746.06, 730.89, 708.14, 698.03 cm^{-1}.

p(AcTreMA-*co*-13FOMA), AcTreMA:13FOMA = 50:50 (polymerized in DCE, P2 in Table 7-1). Polymerization was conducted as in the representative procedure above, with the following reagent concentrations: [AcTreMA] / [13FOMA] / [ECPA] / [Ru(Ind)Cl(PPh_3)$_2$] / [*n*-Bu_3N] = 248 / 249 / 4 / 2 / 20 mM. Polymerization was quenched after 96.5 h. ^{1}H NMR (500 MHz in $CDCl_3$) δ: 5.66–4.83, 4.47–3.68, 2.71–2.33, 2.33–1.69, 1.29–0.60 ppm. ^{19}F NMR (500 MHz in $CDCl_3$ with

TFA at δ = -76.5 ppm as an internal standard) δ: -81.2–82.6, -113.4–116.3, -122.6–123.6, -123.6–124.4, -124.4–125.5, -126.8–128.1 ppm. M_n = 30.3 kDa, $Đ$ = 1.27 (DMF SEC).

This polymer was deprotected as described below. ^{1}H NMR (500 MHz in DMSO-d_6) δ: 5.39–3.82, 3.82–3.40, 3.20–2.96, 2.06–1.51, 1.30–0.43 ppm. ^{19}F NMR (500 MHz in DMSO-d_6 with TFA at δ = -76.5 ppm as an internal standard) δ: -80.4–84.6, -111.9–117.3, -121.6–123.7, -123.7–126.3, -126.3–129.3 ppm. IR: δ = 3367.08, 2936.70, 1726.96, 1641.01, 1451.40, 1390.73, 1365.44, 1319.94, 1233.98, 1188.48, 1142.97, 1122.75, 1077.24, 1044.38, 1024.15, 988.76, 943.25, 842.13, 806.74, 746.06, 730.89, 708.14, 698.03 cm^{-1}.

p(AcTreMA-*co*-13FOMA), AcTreMA:13FOMA = 70:30 (P3 in Table 7-1). Polymerization was conducted as in the representative procedure above, with the following reagent concentrations: [AcTreMA] / [13FOMA] / [ECPA] / [Ru(Ind)Cl(PPh_3)$_2$] / [*n*-Bu_3N] = 360 / 153 / 4 / 2 / 21 mM. Polymerization was quenched after 56 h. ^{1}H NMR (500 MHz in $CDCl_3$) δ: 5.66–4.76, 4.50–3.69, 2.73–2.33, 2.33–1.72, 1.26–0.50 ppm. ^{19}F NMR (500 MHz in $CDCl_3$ with TFA at δ = -76.5 ppm as an internal standard) δ: -81.2–82.8, -113.0–116.4, -122.5–123.6, -123.6–124.4, -124.4–125.6, -126.6–128.1 ppm. M_n = 39.2 kDa, $Đ$ = 1.35 (DMF SEC).

This polymer was deprotected as described below. ^{1}H NMR (500 MHz in DMSO-d_6) δ: 5.44–4.24, 4.24–3.85, 3.85–3.37, 3.20–2.84, 2.04–1.50, 1.31–0.42 ppm. ^{19}F NMR (500 MHz in DMSO-$d_6$with TFA at δ = -76.5 ppm as an internal standard) δ: -80.0–84.7, -111.3–117.3, -121.0–123.4, -123.4–125.9, -125.9–129.0 ppm. IR: δ = 3362.02, 2931.64, 1721.91, 1646.06, 1448.87, 1388.20, 1362.92, 1319.94, 1233.98, 1191.01, 1142.97, 1074.71, 1044.38, 1024.15, 986.23, 940.73, 842.13, 804.21, 746.06, 730.89, 705.61, 695.50 cm^{-1}.

p(AcTreMA-*co*-13FOMA), AcTreMA:13FOMA = 90:10 (P4 in Table 7-1). Polymerization was conducted as in the representative procedure above, with the following reagent concentrations: [AcTreMA] / [13FOMA] / [ECPA] / [Ru(Ind)Cl(PPh_3)$_2$] / [*n*-Bu_3N] = 444 / 48 / 4 / 2 / 20 mM. Polymerization was quenched after 46.3 h. ^{1}H NMR (500 MHz in $CDCl_3$) δ: 5.79–4.67, 4.67–3.27, 2.47–1.69, 1.23–0.36 ppm. ^{19}F NMR (500 MHz in $CDCl_3$ with TFA at δ = -76.5 ppm as an internal standard) δ: -81.2–82.4, -82.9–83.5, -113.5–116.5, -122.3–123.4, -123.4–124.3, -124.3–125.2, -125.2–125.8, -126.5–127.7, -127.8–128.5 ppm. Note that the residual 13FOMA monomer is not removed even with prep GPC and two-time DMF dialysis of the deprotected polymer below. This is likely due to the large polarity difference of TreMA and 13FOMA, the residual 13FOMA strongly interacts with the polymer 13FOMA side-chains. M_n = 36.9 kDa, $Đ$ = 1.37 (DMF SEC).

This polymer was deprotected as described below. ^{1}H NMR (500 MHz in DMSO-d_6) δ: 5.46–4.27, 4.27–3.86, 3.86–3.42, 3.22–2.88, 2.06–1.53, 1.28–0.39 ppm. ^{19}F NMR (500 MHz in DMSO-$d_6$with TFA at δ = -76.5 ppm as an internal standard) δ: -79.5–82.7, -111.8–115.1, -121.0–122.7, -122.7–125.0, -125.6–127.7 ppm. IR: δ = 3367.08, 2931.64, 1716.85, 1643.53, 1448.87, 1362.92, 1332.58, 1239.04, 1142.97, 1105.05, 1074.71, 1041.85, 1024.15, 986.23, 940.73, 842.13, 804.21, 746.06, 730.89, 698.03 cm^{-1}.

p(AcTreMA-*co*-13FOMA), AcTreMA:13FOMA = 30:70 (P5 in Table 7-1). Polymerization was conducted as in the representative procedure above, with the following reagent concentrations: [AcTreMA] / [13FOMA] / [ECPA] / [Ru(Ind)Cl(PPh_3)$_2$] / [*n*-Bu_3N] = 150 / 347 / 4 / 2 / 20 mM. Polymerization was quenched after 40.5 h. ^{1}H NMR (500 MHz in $CDCl_3$) δ: 5.62–4.84, 4.42–3.68, 2.63–2.29, 2.22–1.69, 1.19–0.64 ppm. ^{19}F NMR (500 MHz in $CDCl_3$ with TFA at δ = -76.5 ppm

as an internal standard) δ: -81.3–83.1, -113.6–116.4, -122.5–123.7, -123.7–124.6, -124.6–125.6, -127.0–128.2 ppm. M_n and $Đ$ were unable to be measured due to insolubility.

p(AcTreMA-*co*-PEGMA-*co*-13FOMA), AcTreMA:PEGMA:13FOMA = 33:33:33 (P6 in Table 7-2). This polymerization is listed as the representative procedure above with the corresponding spectral data.

This polymer was deprotected as described below. ^{1}H NMR (500 MHz in DMSO-d_6) δ: 5.19–4.49, 4.49–3.82, 3.82–3.37, 3.27–3.18, 3.18–2.99, 2.15–1.47, 1.19–0.48 ppm. ^{19}F NMR (500 MHz in DMSO-d_6 with TFA at δ = -76.5 ppm as an internal standard) δ: -80.2–84.2, -111.8–116.0, -121.6–123.4, -123.4–125.7, -125.7–128.6 ppm. IR: δ = 3387.34, 2916.45, 2875.94, 1726.96, 1635.95, 1451.40, 1385.67, 1350.28, 1236.51, 1191.01, 1140.44, 1102.52, 1077.24, 1044.38, 1029.21, 988.76, 943.25, 842.13, 806.74, 746.06, 730.89, 708.14, 695.50 cm^{-1}.

p(AcTreMA-*co*-PEGMA-*co*-13FOMA), AcTreMA:PEGMA:13FOMA = 56:18:26 (P7 in Table 7-2). Polymerization was conducted as in the representative procedure above, with the following reagent concentrations: [AcTreMA] / [PEGMA] / [13FOMA] / [ECPA] / [Ru(Ind)Cl(PPh_3)$_2$] / [*n*-Bu_3N] = 246 / 83 / 120 / 4 / 2 / 20 mM. Polymerization was quenched after 18.6 h. M_n = 26.4 kDa, $Đ$ = 1.34 (DMF SEC). The crude polymerization mixture was directly subject to deacetylation as described below.

^{1}H NMR (500 MHz in DMSO-d_6) δ: 5.26–4.48, 4.48–3.77, 3.77–3.40, 3.24–3.15, 3.15–2.99, 2.19–1.41, 1.20–0.45 ppm. ^{19}F NMR (500 MHz in DMSO-d_6 with TFA at δ = -76.5 ppm as an internal standard) δ: -79.8–84.1, -111.7–116.2, -121.3–123.5, -123.5–125.5, -125.9–128.7 ppm. IR: δ = 3372.15, 2921.51, 2881.01, 1726.96, 1646.06, 1451.40, 1388.20, 1350.28, 1236.51,

1193.53, 1142.97, 1102.52, 1074.71, 1044.38, 1024.15, 988.76, 940.73, 842.13, 804.21, 746.06, 730.89, 705.61, 698.03 cm^{-1}.

p(AcTreMA-*co*-PEGMA-*co*-13FOMA), AcTreMA:PEGMA:13FOMA = 37:37:26 (P8 in Table 7-2). Polymerization is listed as the representative procedure above, with the following reagent concentrations: [AcTreMA] / [PEGMA] / [13FOMA] / [ECPA] / [Ru(Ind)Cl(PPh_3)$_2$] / [*n*-Bu_3N] = 165 / 166 / 117 / 4 / 2 / 20 mM. Note that for this polymerization, inadvertent oxygen oxidized the catalyst, and the polymerization was quenched at 23.3 h and then resumed by addition of more Ru catalyst. Polymerization was quenched after total 47.3 h. M_n = 28.3 kDa, $Đ$ = 1.27 (DMF SEC). The crude polymerization mixture was directly subject to deacetylation as described below.

^{1}H NMR (500 MHz in DMSO-d_6) δ: 5.16–4.52, 4.52–3.85, 3.85–3.46, 3.46–3.40, 3.26–3.20, 3.20–3.04, 2.25–1.38, 1.38–0.43 ppm. ^{19}F NMR (400 MHz in DMSO-d_6 with TFA at δ = -76.5 ppm as an internal standard) δ: -80.1–83.0, -111.5–115.6, -121.5–122.8, -122.8–124.9, -125.6–127.7 ppm. IR: δ = 3377.21, 2921.51, 2875.94, 1726.96, 1646.06, 1451.40, 1388.20, 1350.28, 1236.51, 1191.01, 1140.44, 1102.52, 1077.24, 1044.38, 1026.68, 988.76, 940.73, 842.13, 804.21, 746.06, 730.89, 705.51, 695.50 cm^{-1}.

Deacetylation of p(AcTreMA-co-13FOMA) and p(AcTreMA-co-PEGMA-co-13FOMA)

The acetyl groups from AcTreMA were removed either from the purified polymer or from the crude polymerization mixture. For the purified polymer p(AcTreMA-*co*-13FOMA), 56 mg of the polymer (0.345 mmol of acetyl protecting groups) was dissolved in 1 mL DMF and to this mixture was dropwise added hydrazine hydrate (98 μL, 5.8 mol equiv. with respect to the acetyl

groups). After stirring at room temperature for 22 h, the reaction was quenched with 0.1 mL acetone and the polymer was purified by dialysis in a regenerated cellulose membrane (Spectra/Por 3, MWCO 3.5 kDa) with water for 24 hours with 5 times change of water. Water was removed by lyophilization.

Deprotection can be simplified by treating the crude polymerization mixture directly with hydrazine to remove the acetyl groups. The p(AcTreMA-*co*-PEGMA-*co*-13FOMA) polymerization mixture (**P8**, Table **6-2**) was dried *in vacuo* to remove toluene and DCE, and the solid (1.78 g of total monomer mass in the original polymerization mixture, 1.28 g estimated from % conv.) was redissolved in 21 mL dimethyl sulfoxide (DMSO) and hydrazine hydrate (2.04 mL, 6.9 molar equiv. with respect to hydroxyl group estimated from % conv.) was added dropwise. After stirring at room temperature for 16 h, the reaction was quenched with 3.5 mL acetone and the polymer was purified by dialysis in a regenerated cellulose membrane (Spectra/Por 3, MWCO 3.5 kDa) with DMF for 12 hours then with water for 12 hours. Water was removed by lyophilization.

Encapsulation of the Agrochemical by the Amphiphilic Copolymers

The fluorinated agrochemical novaluron was dissolved in DMSO (1 mg/mL), and the solution was used to dissolve p(PEGMA-*co*-13FOMA) or p(TreMA-*co*-PEGMA-*co*-13FOMA) at 10 mg/mL (polymer:agrochemical = 10:1 by weight). This final solution (0.5 mL) was added to deionized water (1 mL) dropwise with rapid stirring for nanoprecipitation. The mixture was rapidly stirred for 30 min, and dialyzed in regenerated cellulose membrane (Spectra/Por 3, MWCO 3.5 kDa) for 1 day with frequent water change. The dialyzed solution was filtered with a 0.45 μm syringe filter (cellulose acetate) and lyophilized.

Percent encapsulation was calculated by ^{1}H NMR integration of the aromatic proton of novaluron ortho to the chloride (7.98 ppm) compared to the aldehyde peak (9.71 ppm) in the 4-hydroxybenzaldehyde standard added to the DMSO-d_6 stock solution (0.3 mg/mL, 0.6 mL used to dissolve each sample).

NMR Spectra

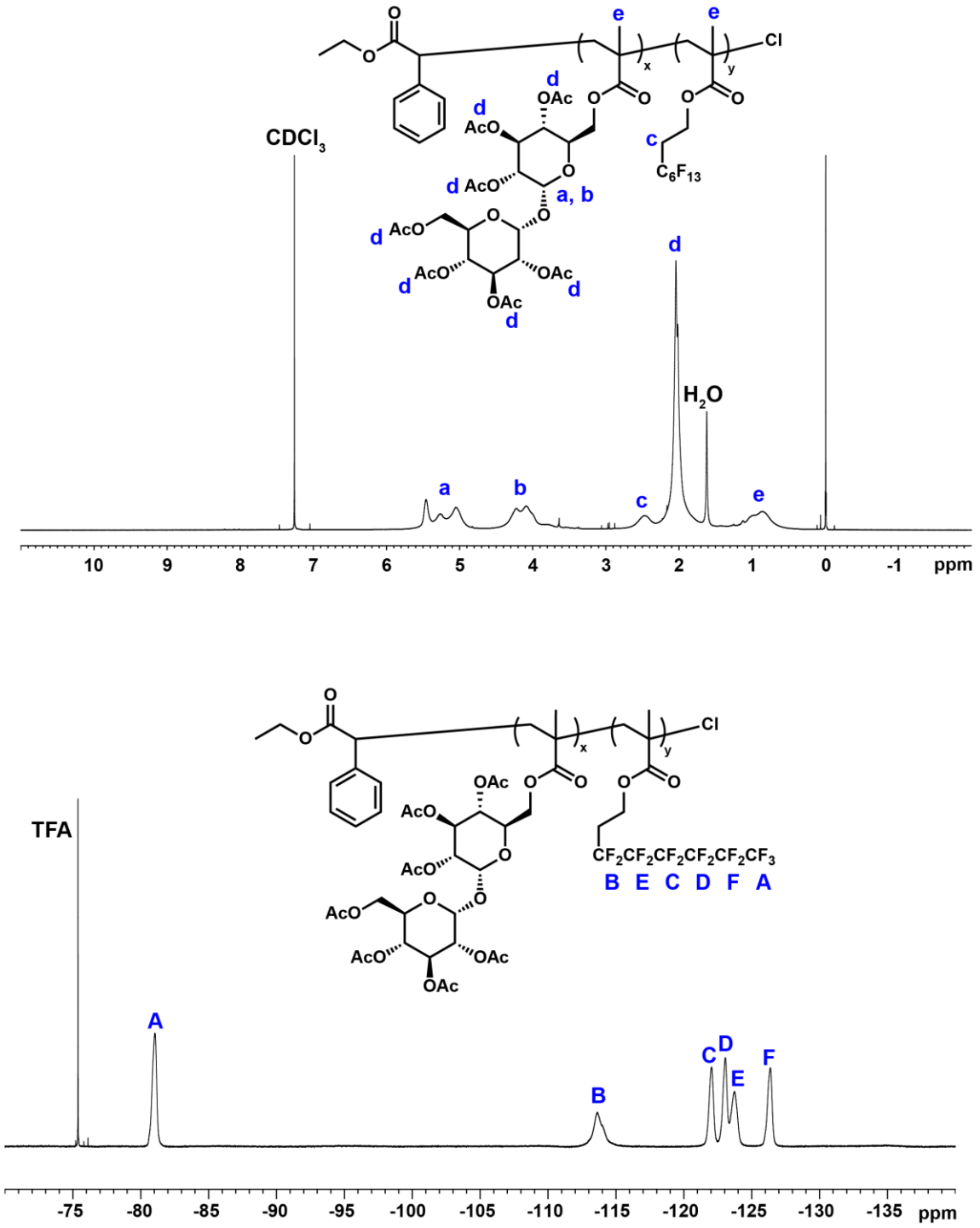

Figure 6-4. ^{1}H (top) and ^{19}F (bottom) NMR spectra of p(AcTreMA-*co*-13FOMA) (**P1**, AcTreMA:13FOMA = 50:50) ($CDCl_3$ for ^{1}H, $CDCl_3$ with TFA capillary for ^{19}F).

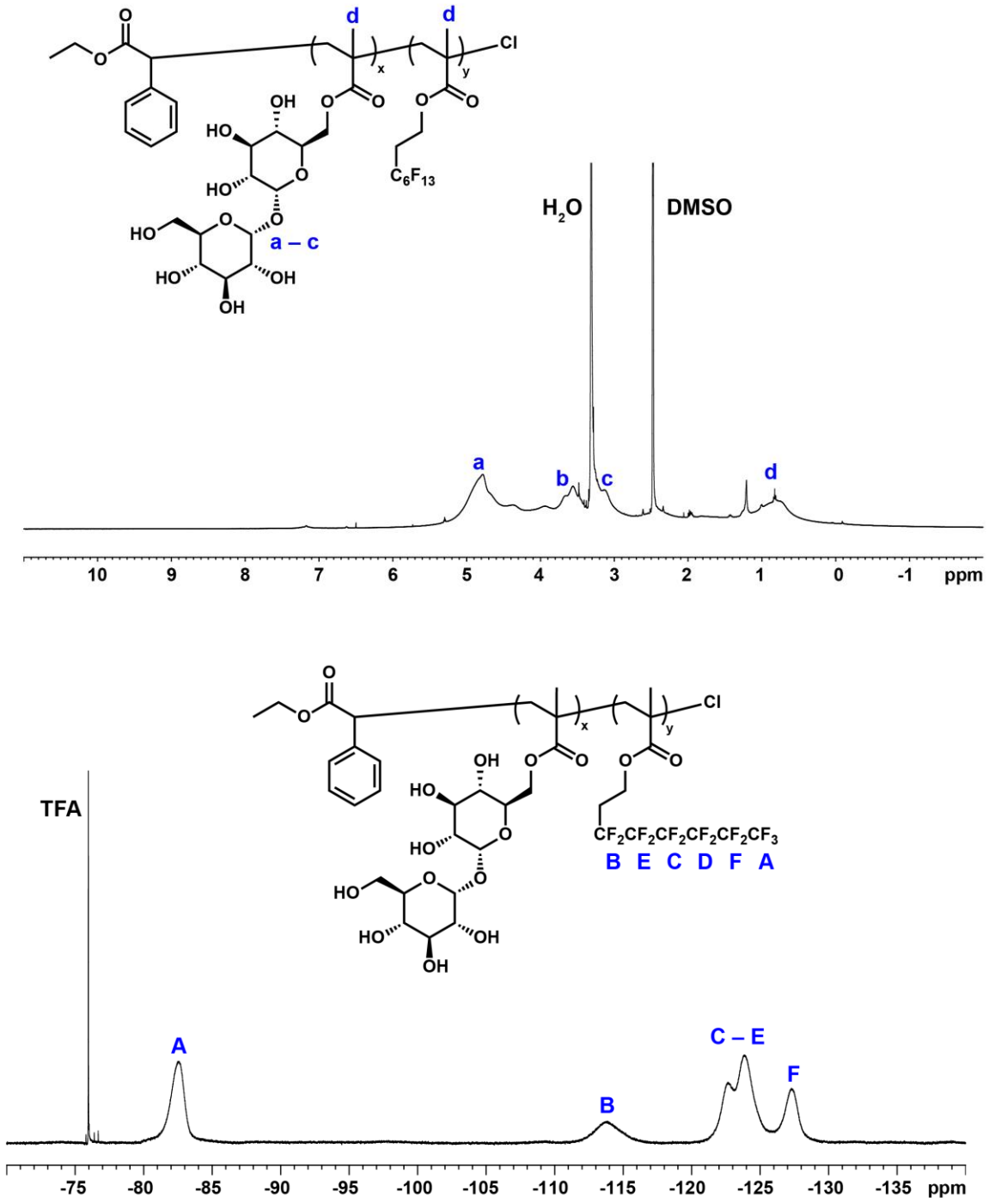

Figure 6-5. ^{1}H (top) and ^{19}F (bottom) NMR spectra of deacetylated p(TreMA-*co*-13FOMA) (**P1**, AcTreMA:13FOMA = 50:50) (DMSO-d_6 for ^{1}H, DMSO-d_6 with TFA capillary for ^{19}F).

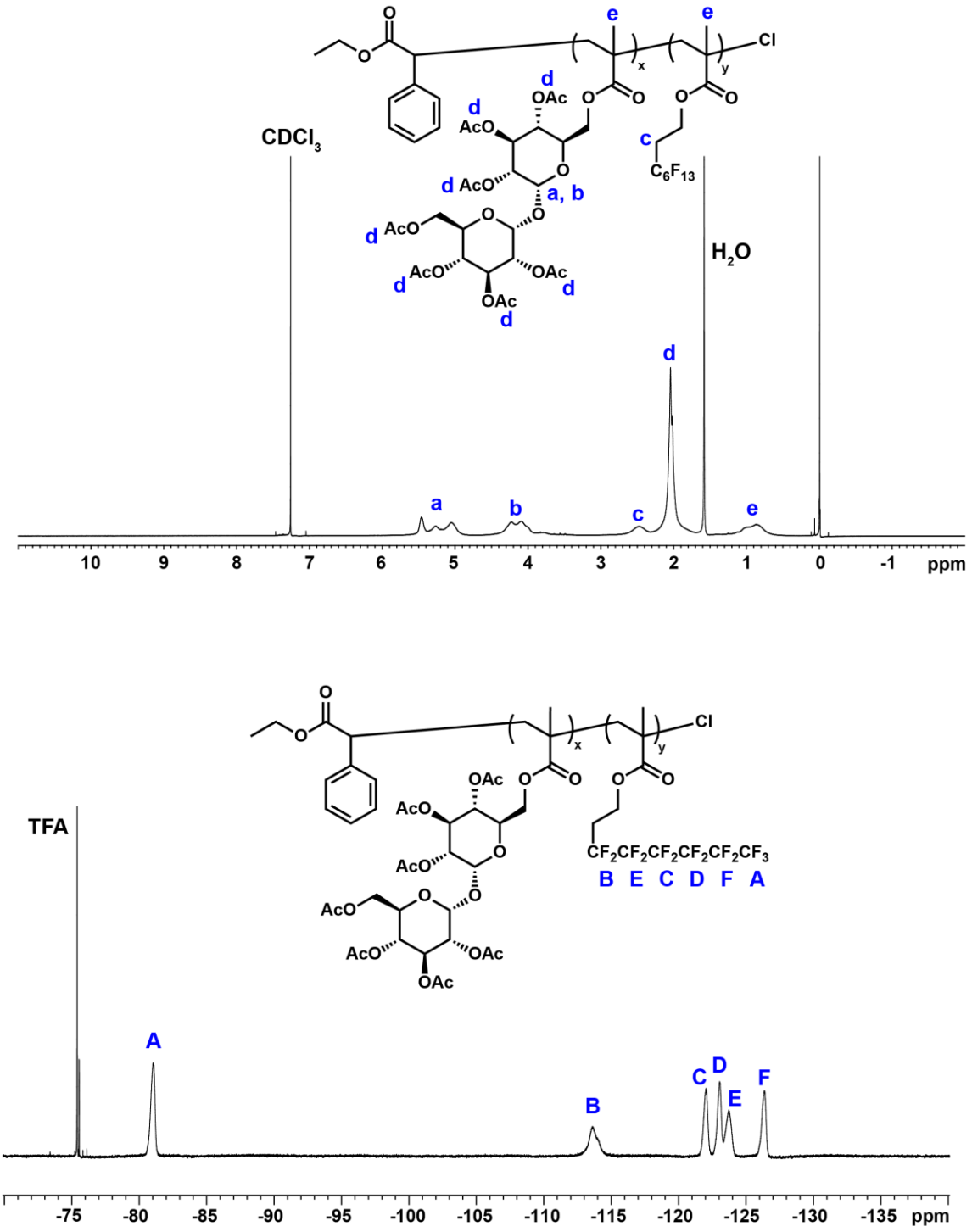

Figure 6-6. ^{1}H (top) and ^{19}F (bottom) NMR spectra of p(AcTreMA-*co*-13FOMA) (**P2**, AcTreMA:13FOMA = 50:50) ($CDCl_3$ for ^{1}H, $CDCl_3$ with TFA capillary for ^{19}F).

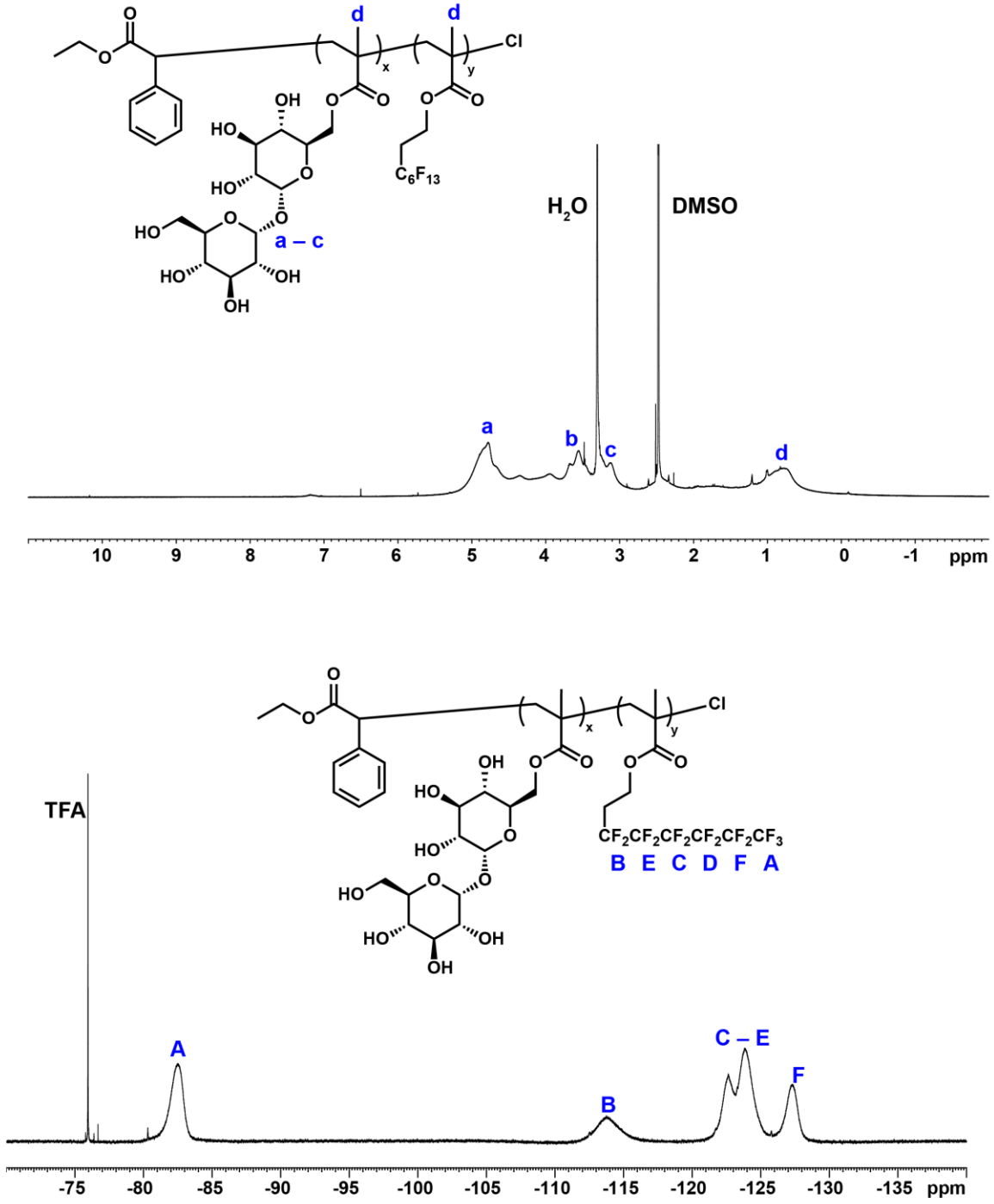

Figure 6-7. ^{1}H (top) and ^{19}F (bottom) NMR spectra of deacetylated p(TreMA-*co*-13FOMA) (**P2**, AcTreMA:13FOMA = 50:50) (DMSO-d_6 for ^{1}H, DMSO-d_6 with TFA capillary for ^{19}F).

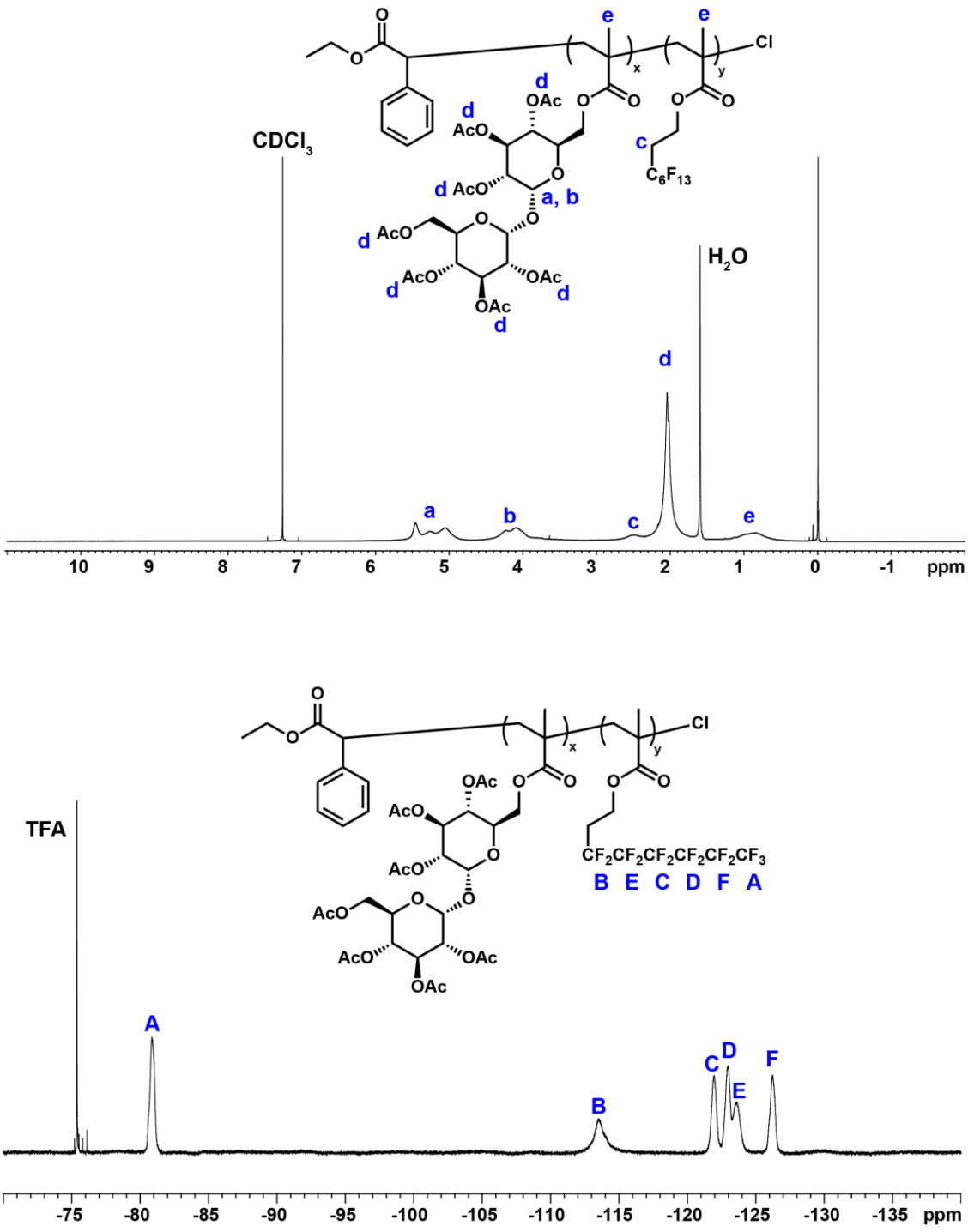

Figure 6-8. ^{1}H (top) and ^{19}F (bottom) NMR spectra of p(AcTreMA-*co*-13FOMA) (**P3**, AcTreMA:13FOMA = 70:30) ($CDCl_3$ for ^{1}H, $CDCl_3$ with TFA capillary for ^{19}F).

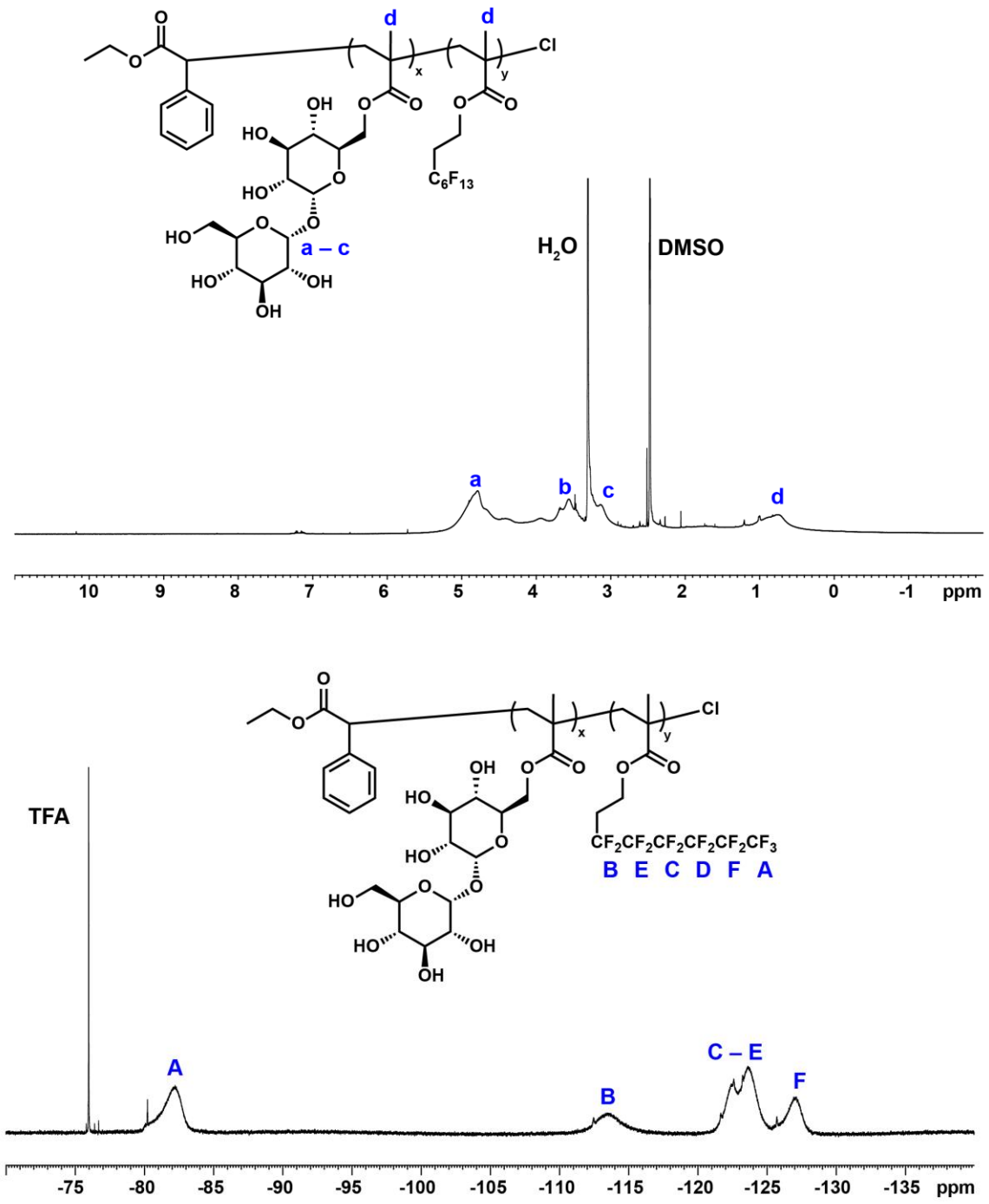

Figure 6-9. ^{1}H (top) and ^{19}F (bottom) NMR spectra of deacetyated p(TreMA-*co*-13FOMA) (**P3**, AcTreMA:13FOMA = 70:30) (DMSO-d_6 for ^{1}H, DMSO-d_6 with TFA capillary for ^{19}F).

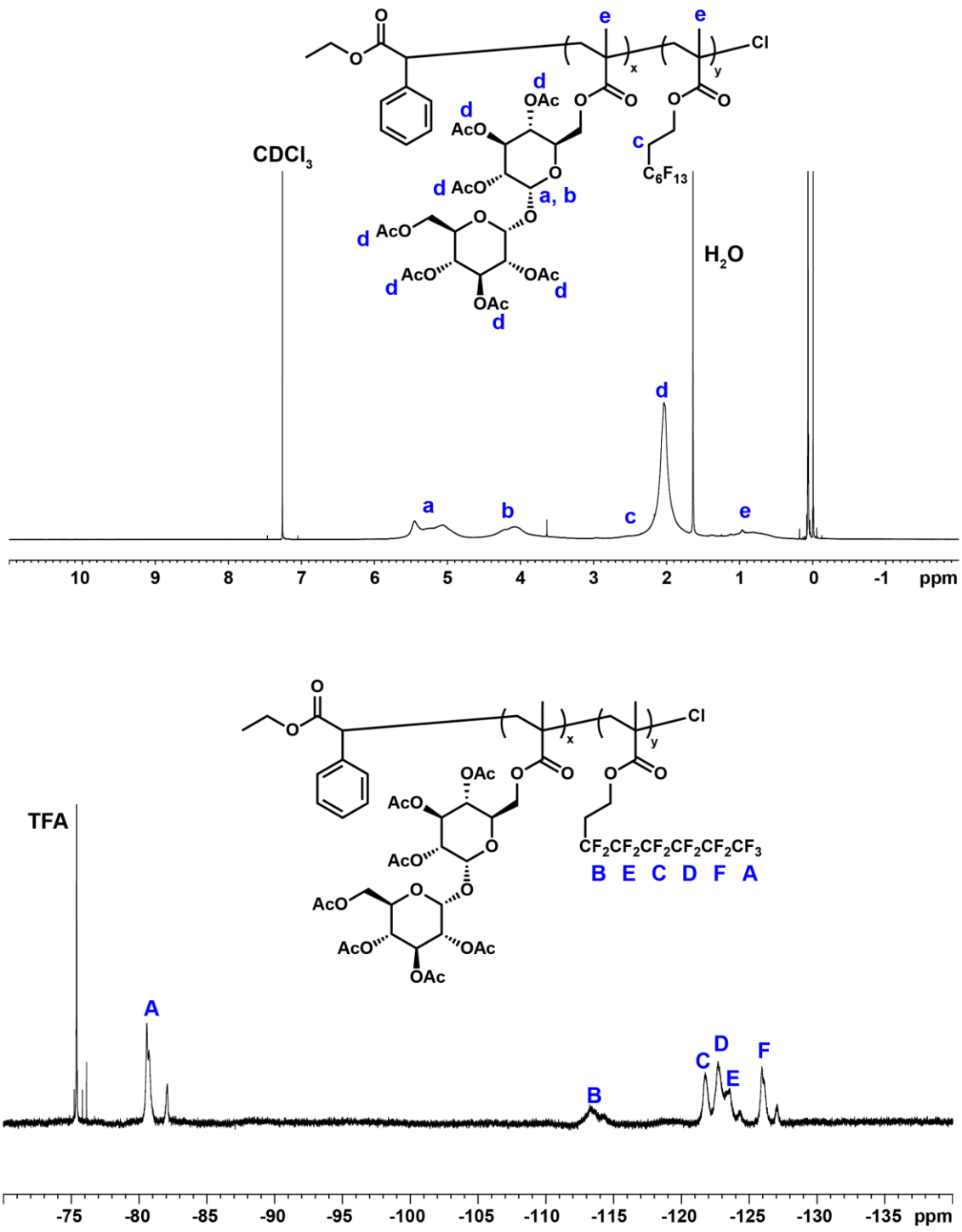

Figure 6-10. ^{1}H (top) and ^{19}F (bottom) NMR spectra of p(AcTreMA-*co*-13FOMA) (**P4**, AcTreMA:13FOMA = 90:10) ($CDCl_3$ for ^{1}H, $CDCl_3$ with TFA capillary for ^{19}F).

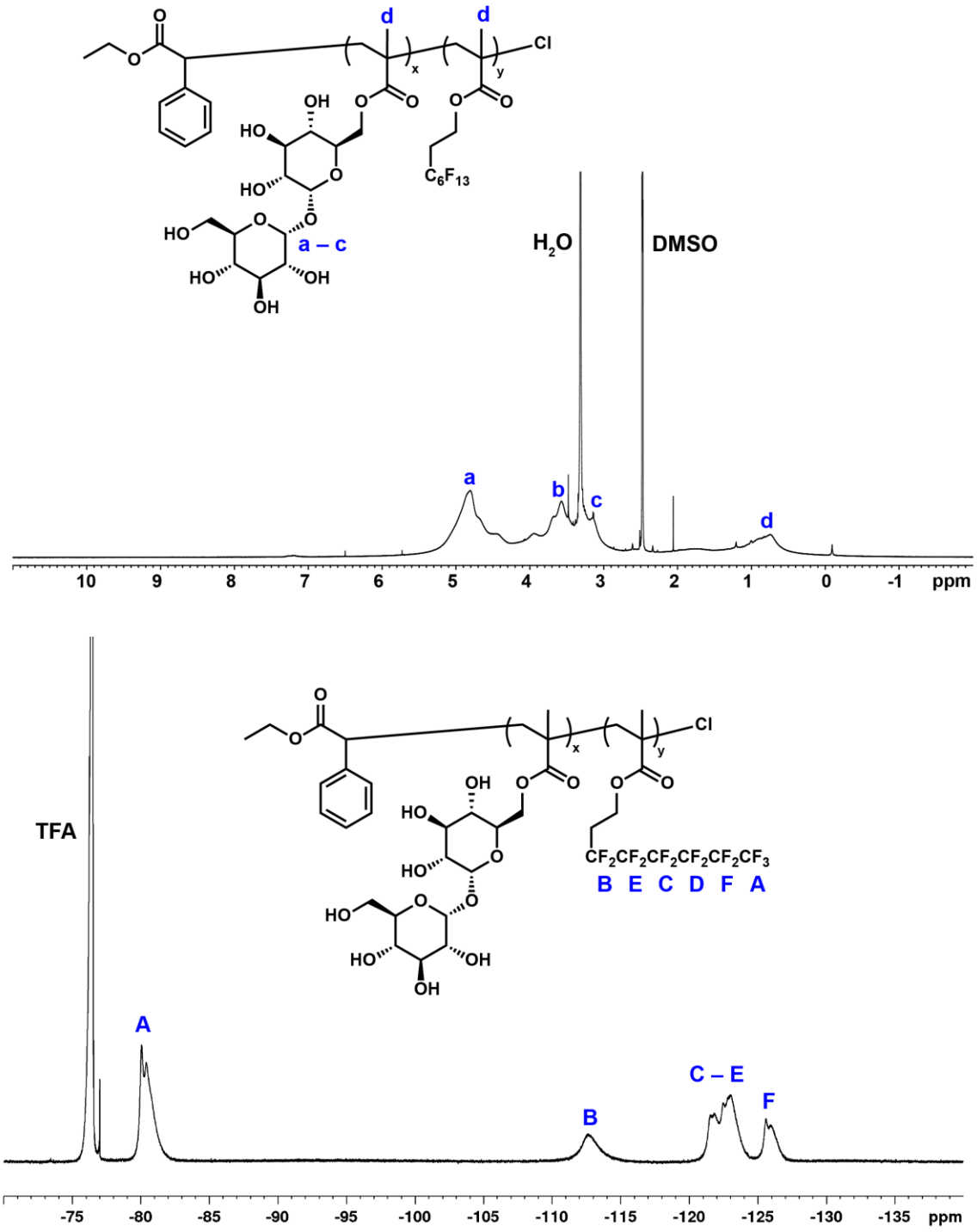

Figure 6-11. ^{1}H (top) and ^{19}F (bottom) NMR spectra of deacetyated p(TreMA-*co*-13FOMA) (**P4**, AcTreMA:13FOMA = 90:10) (DMSO-d_6 for ^{1}H, DMSO-d_6 with TFA capillary for ^{19}F).

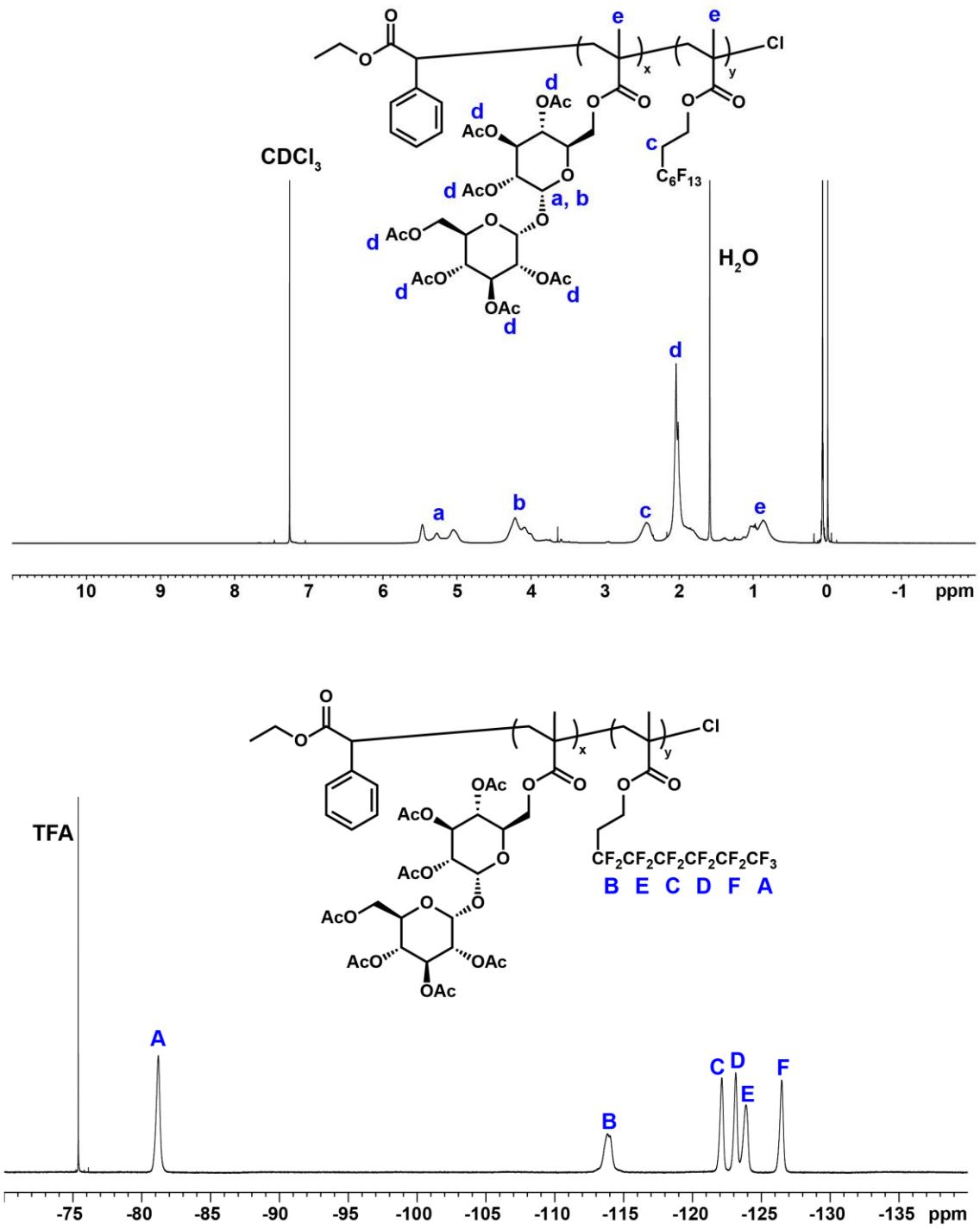

Figure 6-12. ^{1}H (top) and ^{19}F (bottom) NMR spectra of p(AcTreMA-*co*-13FOMA) (**P5**, AcTreMA:13FOMA = 30:70) ($CDCl_3$ for ^{1}H, $CDCl_3$ with TFA capillary for ^{19}F).

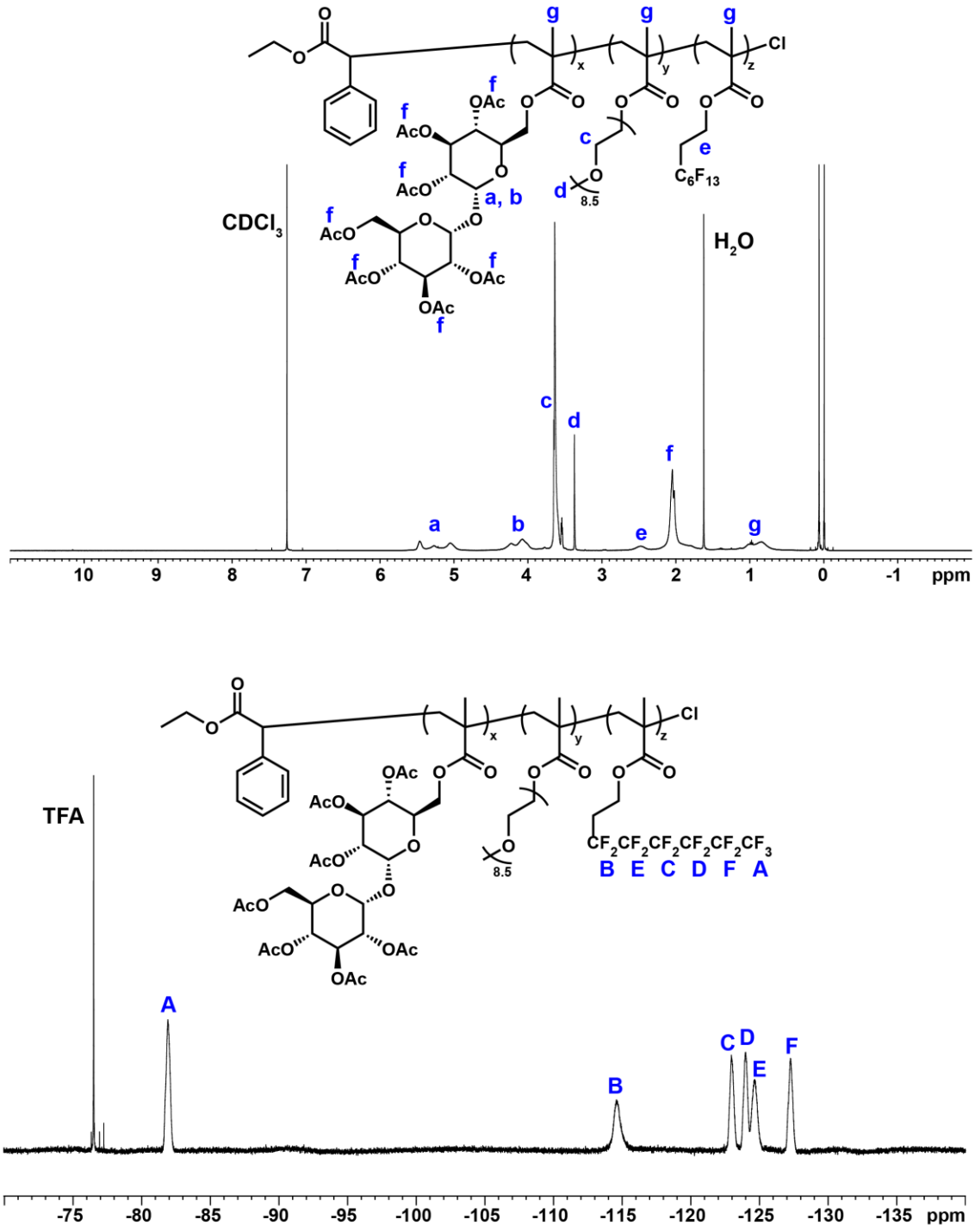

Figure 6-13. ^{1}H (top) and ^{19}F (bottom) NMR spectra of p(AcTreMA-*co*-PEGMA-*co*-13FOMA) (**P6**, AcTreMA:PEGMA:13FOMA = 33:33:33) ($CDCl_3$ for ^{1}H, $CDCl_3$ with TFA capillary for ^{19}F).

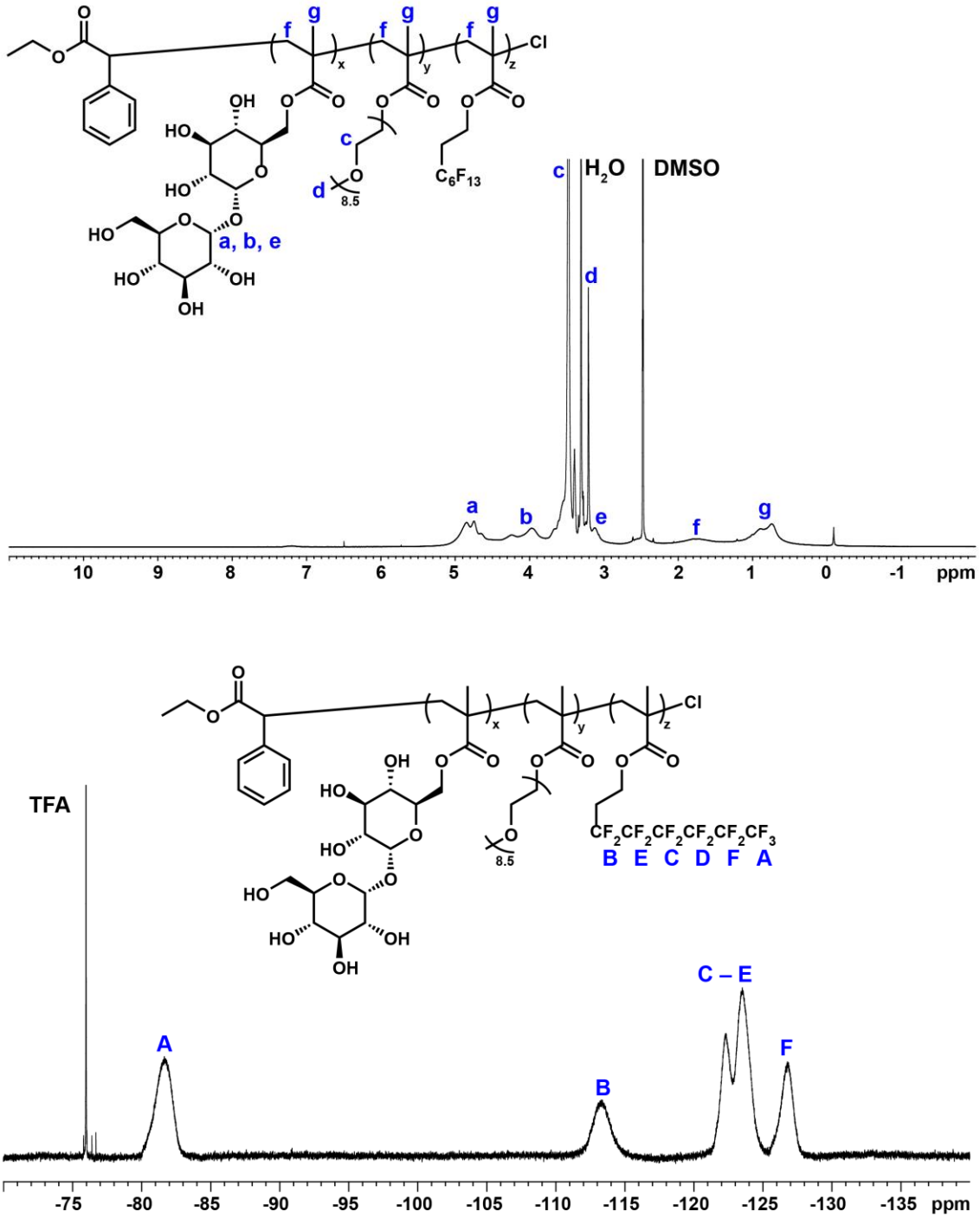

Figure 6-14. ^{1}H (top) and ^{19}F (bottom) NMR spectra of deacetyated p(TreMA-*co*-PEGMA-*co*-13FOMA) (**P6**, TreMA:PEGMA:13FOMA = 33:33:33) (DMSO-d_6 for ^{1}H, DMSO-d_6 with TFA capillary for ^{19}F).

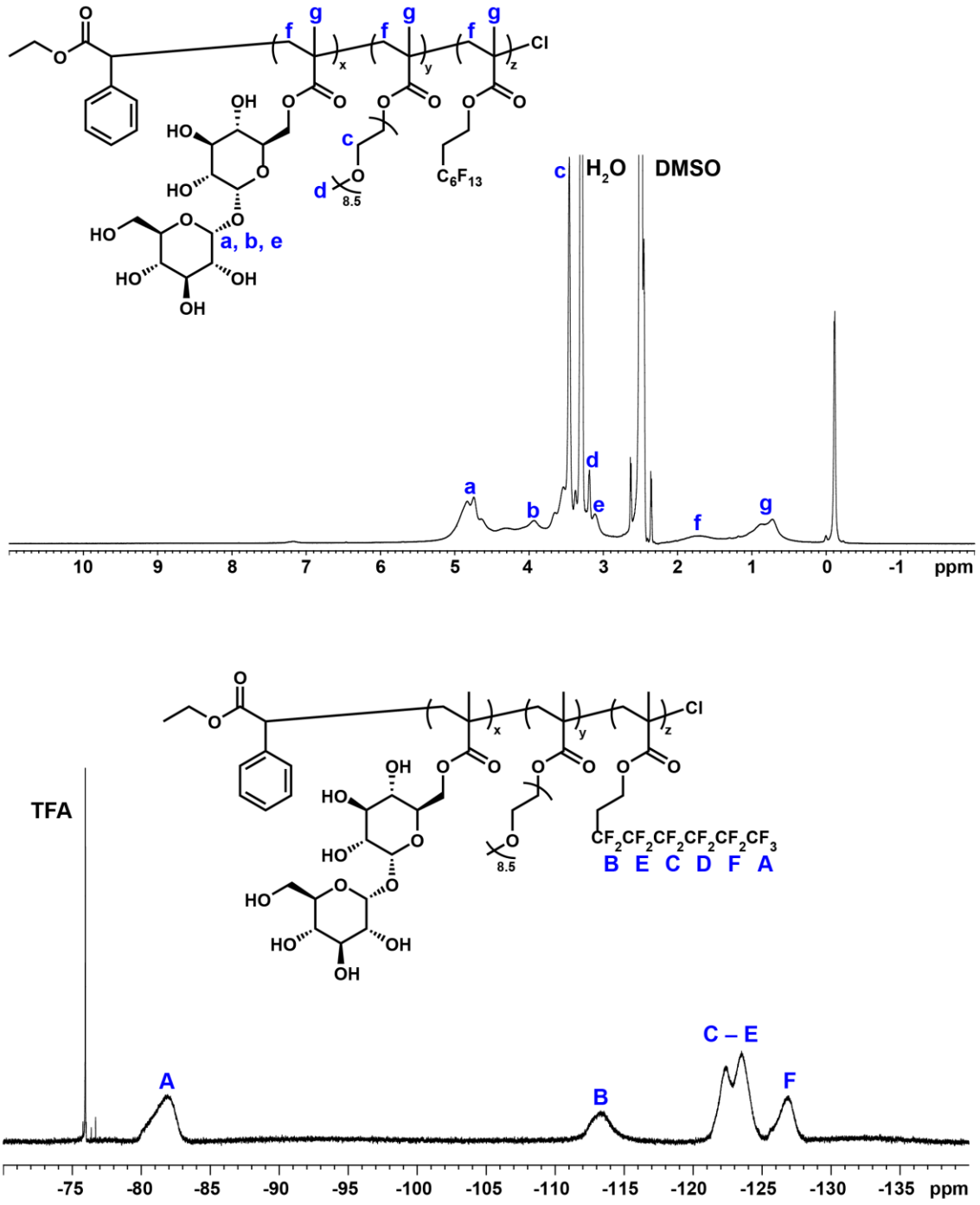

Figure 6-15. ^{1}H (top) and ^{19}F (bottom) NMR spectra of deacetyated p(TreMA-*co*-PEGMA-*co*-13FOMA) (**P7**, TreMA:PEGMA:13FOMA = 56:18:26) (DMSO-d_6 for ^{1}H, DMSO-d_6 with TFA capillary for ^{19}F).

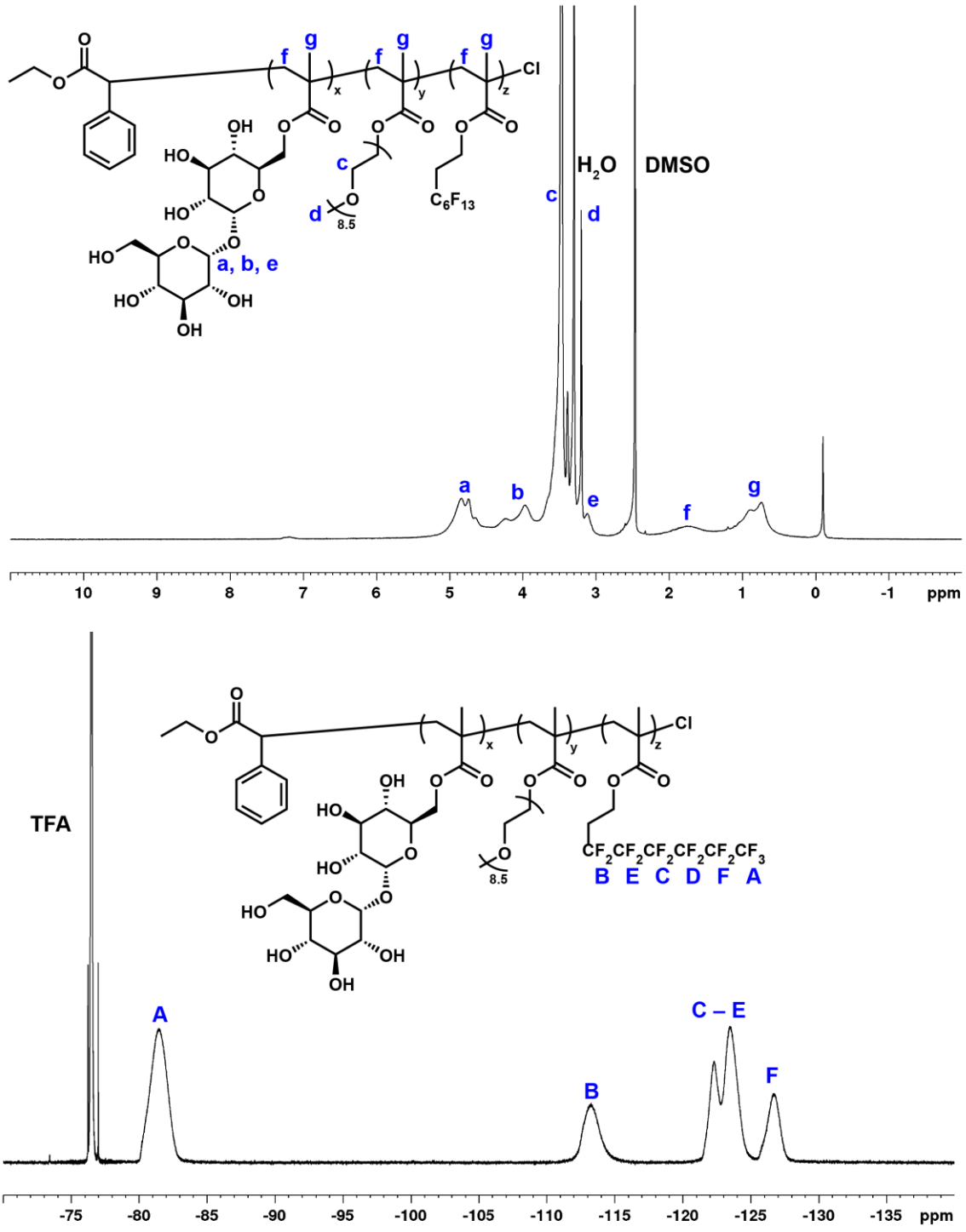

Figure 6-16. ^{1}H (top) and ^{19}F (bottom) NMR spectra of deacetyated p(TreMA-*co*-PEGMA-*co*-13FOMA) (**P8**, TreMA:PEGMA:13FOMA = 37:37:26) (DMSO-d_6 for ^{1}H, DMSO-d_6 with TFA capillary for ^{19}F).

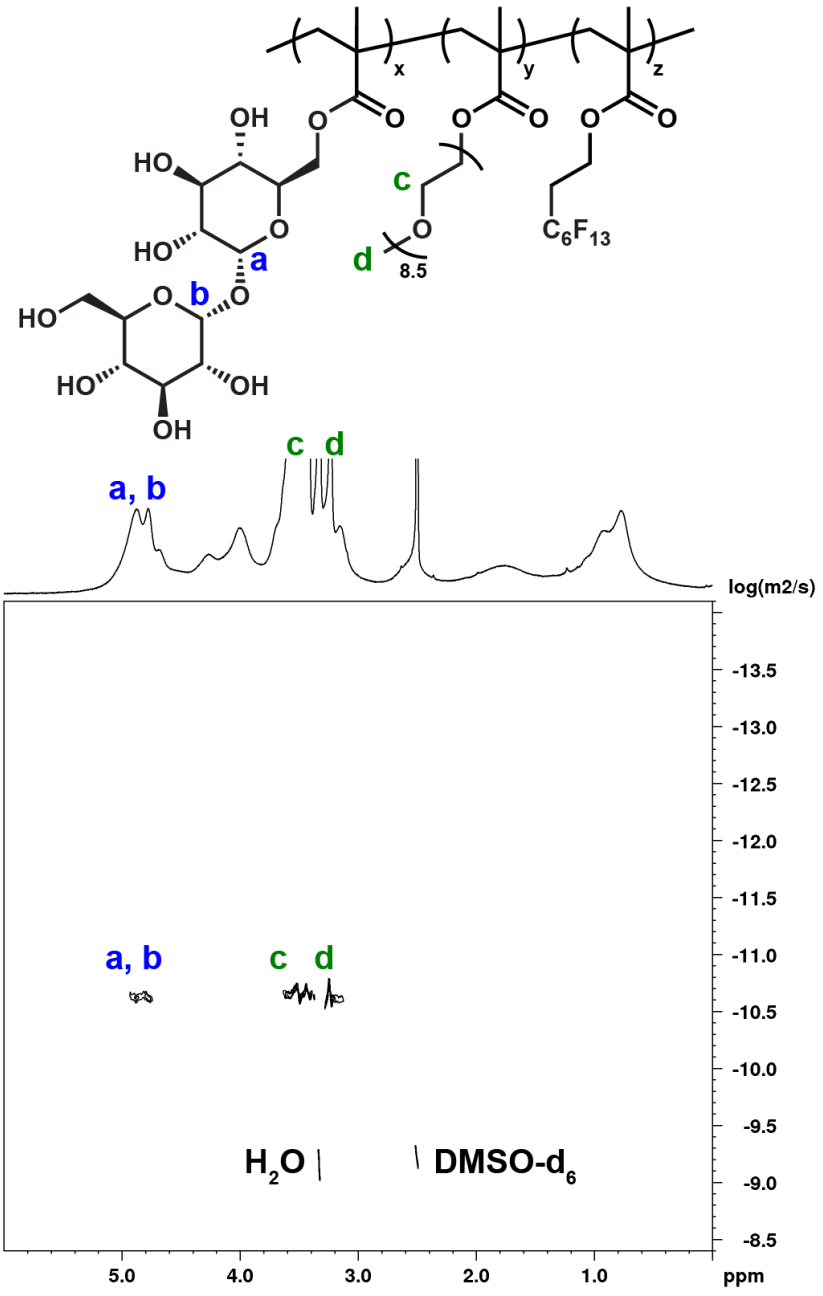

Figure 6-17. DOSY spectrum of p(TreMA-*co*-PEGMA-*co*-13FOMA) (**P8**, TreMA:PEGMA:13FOMA = 37:37:26) showing peaks corresponding to TreMA and PEGMA.

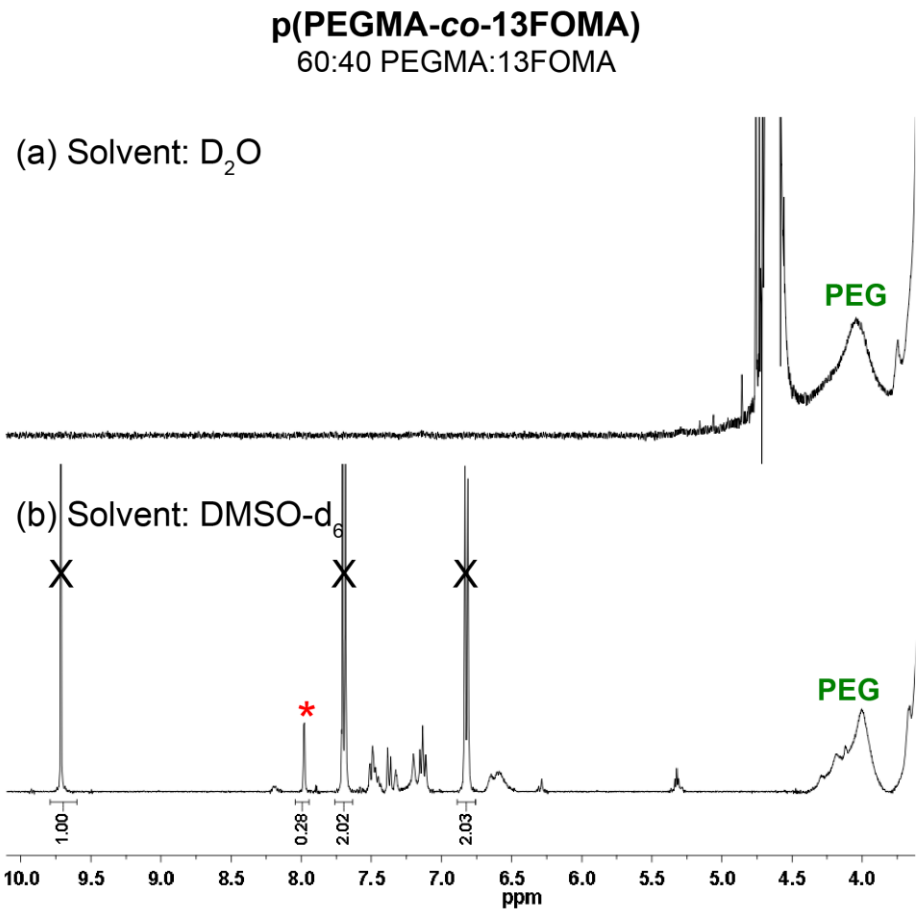

Figure 6-18. ^{1}H NMR spectra of p(PEGMA-*co*-13FOMA) nanoprecipitated with novaluron (polymer:novaluron = 10:1) in (a) D_2O and (b) DMSO-d_6**.** Samples analyzed in DMSO-d_6 contain 4-hydroxybenzaldehyde as an internal standard (denoted by X in the spectra). Red asterisk denotes the peak (corresponding to the proton ortho to the chlorine in novaluron) used for the quantification of encapsulation efficiency. The standard is present at 1.47×10^{-6} mol (0.18 mg), and the integration ratio leads to 4.13×10^{-7} mol of the novaluron. Comparing with novaluron added (0.5 mg, 1.01×10^{-6} mol), the percent encapsulation is 40.7 % for this sample. Following the same procedure for 4 other independently prepared samples, the average encapsulation efficiency was 34.9 ± 6.9 % (n = 5).

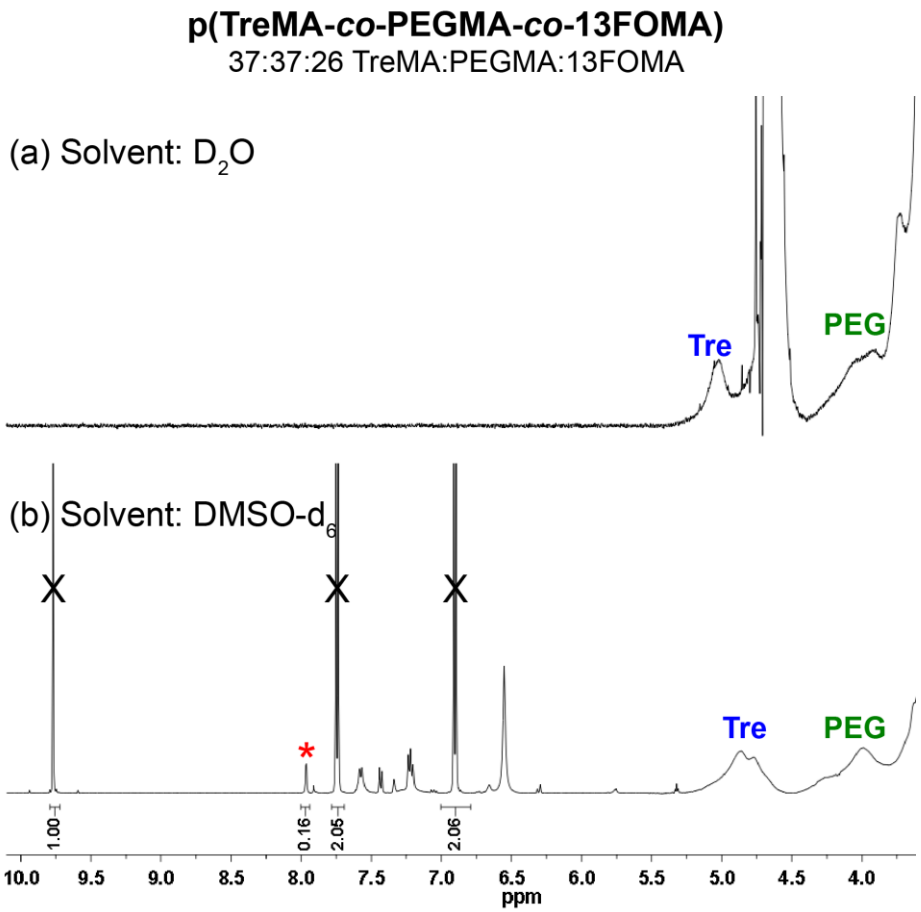

Figure 6-19. ^{1}H NMR spectra of p(TreMA-*co*-PEGMA-*co*-13FOMA) nanoprecipitated with novaluron (polymer:novaluron = 10:1) in (a) D_2O and (b) DMSO-d_6**.** Samples analyzed in DMSO-d_6 contain 4-hydroxybenzaldehyde as an internal standard (denoted by X in the spectra). Red asterisk denotes the peak (corresponding to the proton ortho to the chlorine in novaluron) used for the quantification of encapsulation efficiency. The standard is present at 1.47×10^{-6} mol (0.18 mg), and the integration ratio leads to 2.36×10^{-7} mol of the novaluron. Comparing with novaluron added (0.5 mg, 1.01×10^{-6} mol), the percent encapsulation is 23.2 % for this sample. Following the same procedure for 4 other independently prepared samples, the average encapsulation efficiency was 31.1 ± 6.4 % (n = 5).

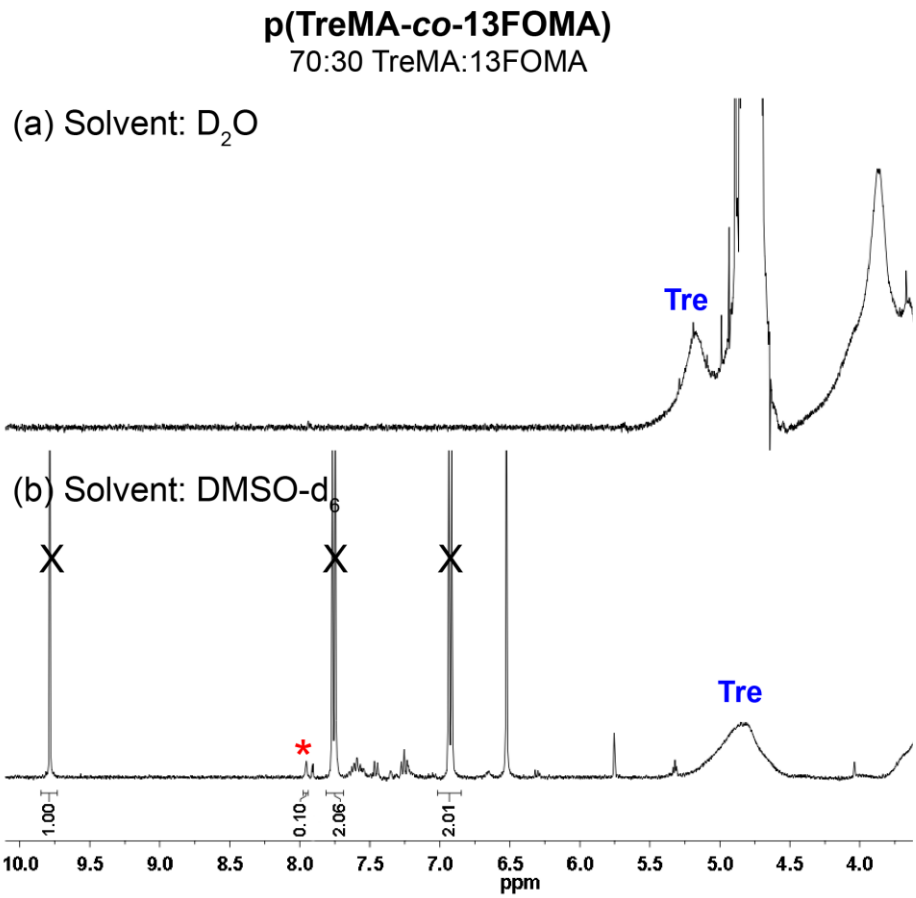

Figure 6-20. ^{1}H NMR spectra of p(TreMA-*co*-13FOMA) (70:30 TreMA:13FOMA) nanoprecipitated with novaluron (polymer:novaluron = 10:1) in (a) D_2O and (b) DMSO-d_6**.** Samples analyzed in DMSO-d_6 contain 4-hydroxybenzaldehyde as an internal standard (denoted by X in the spectra). Red asterisk denotes the peak (corresponding to the proton ortho to the chlorine in novaluron) used for the quantification of encapsulation efficiency. The standard is present at 1.47×10^{-6} mol (0.18 mg), and the integration ratio leads to 1.47×10^{-7} mol of the novaluron. Comparing with novaluron added (0.5 mg, 1.01×10^{-6} mol), the percent encapsulation is 14.5 % for this sample. Following the same procedure for 4 other independently prepared samples, the average encapsulation efficiency was 10.7 ± 3.5 % (n = 5).

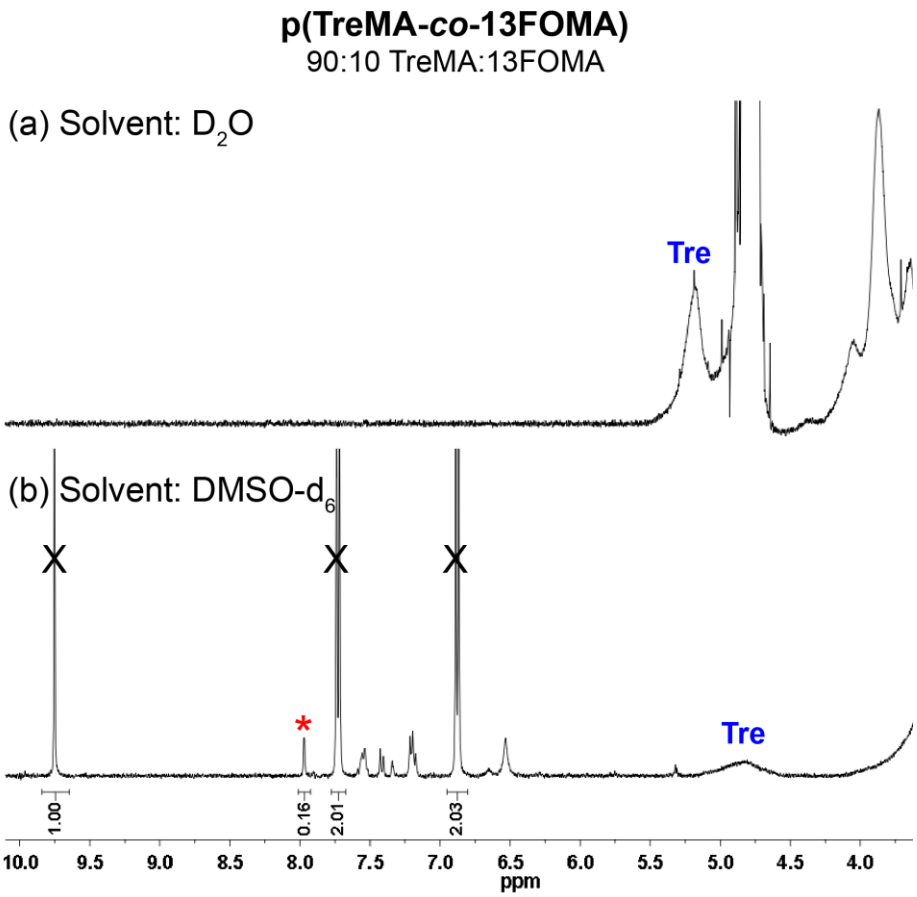

Figure 6-21. ^{1}H NMR spectra of p(TreMA-*co*-13FOMA) (90:10 TreMA:13FOMA) nanoprecipitated with novaluron (polymer:novaluron = 5:1) in (a) D_2O and (b) DMSO-d_6**.** Samples analyzed in DMSO-d_6 contain 4-hydroxybenzaldehyde as an internal standard (denoted by X in the spectra). Red asterisk denotes the peak (corresponding to the proton ortho to the chlorine in novaluron) used for the quantification of encapsulation efficiency. The standard is present at 1.47×10^{-6} mol (0.18 mg), and the integration ratio leads to 2.36×10^{-7} mol of the novaluron. Comparing with novaluron added (0.5 mg, 1.01×10^{-6} mol), the percent encapsulation is 23.2 % for this sample. Following the same procedure for 4 other independently prepared samples, the average encapsulation efficiency was 14.2 ± 17.0 % (n = 5).

IR Spectra

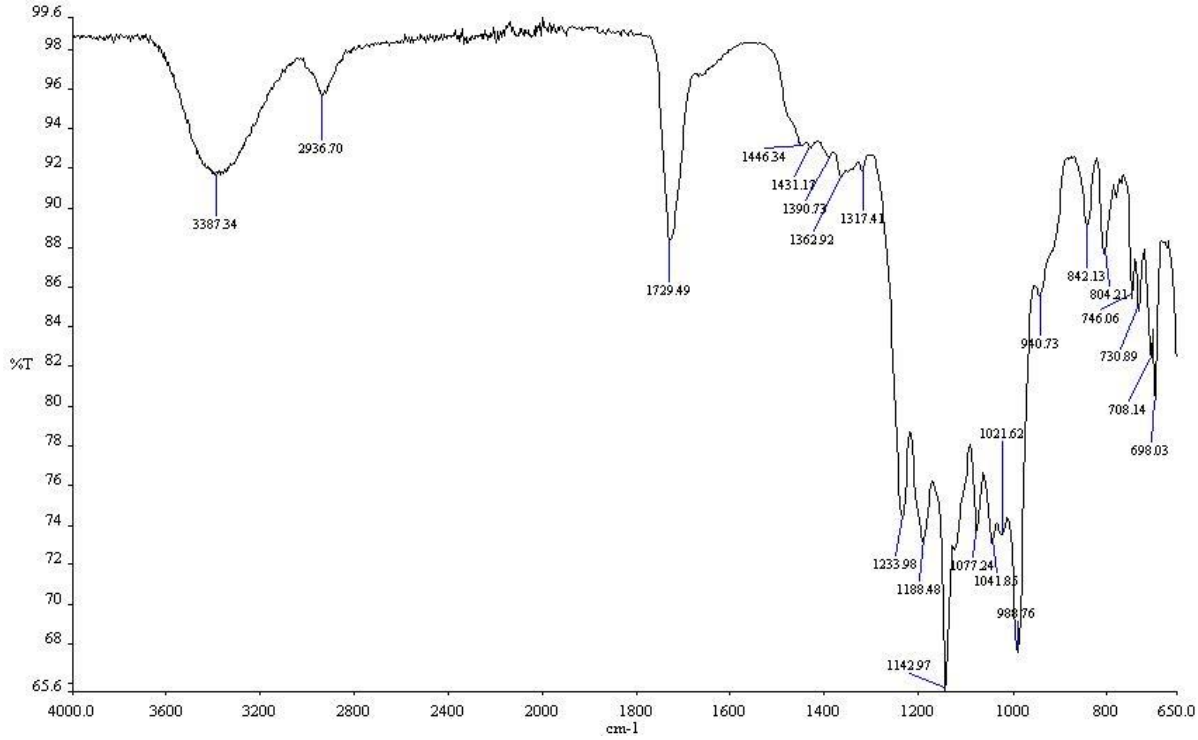

Figure 6-22. IR spectrum of p(TreMA-*co*-13FOMA) (**P1**, TreMA:13FOMA = 50:50).

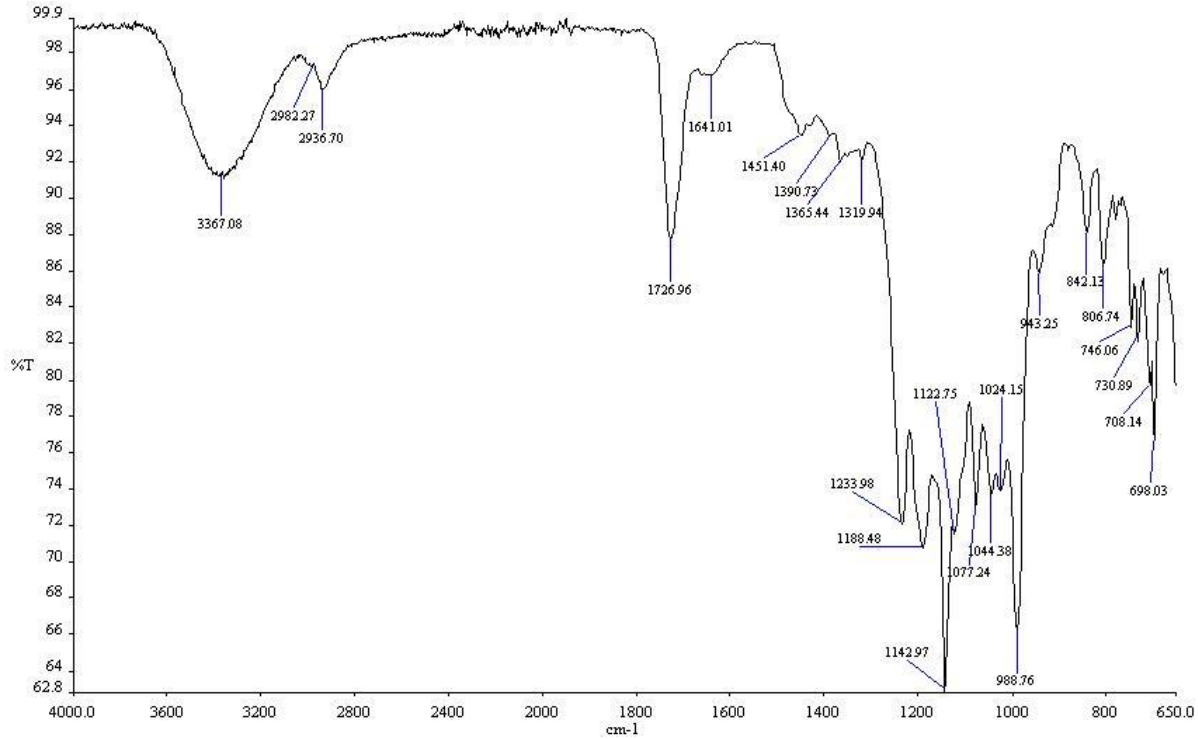

Figure 6-23. IR spectrum of p(TreMA-*co*-13FOMA) (**P2**, TreMA:13FOMA = 50:50).

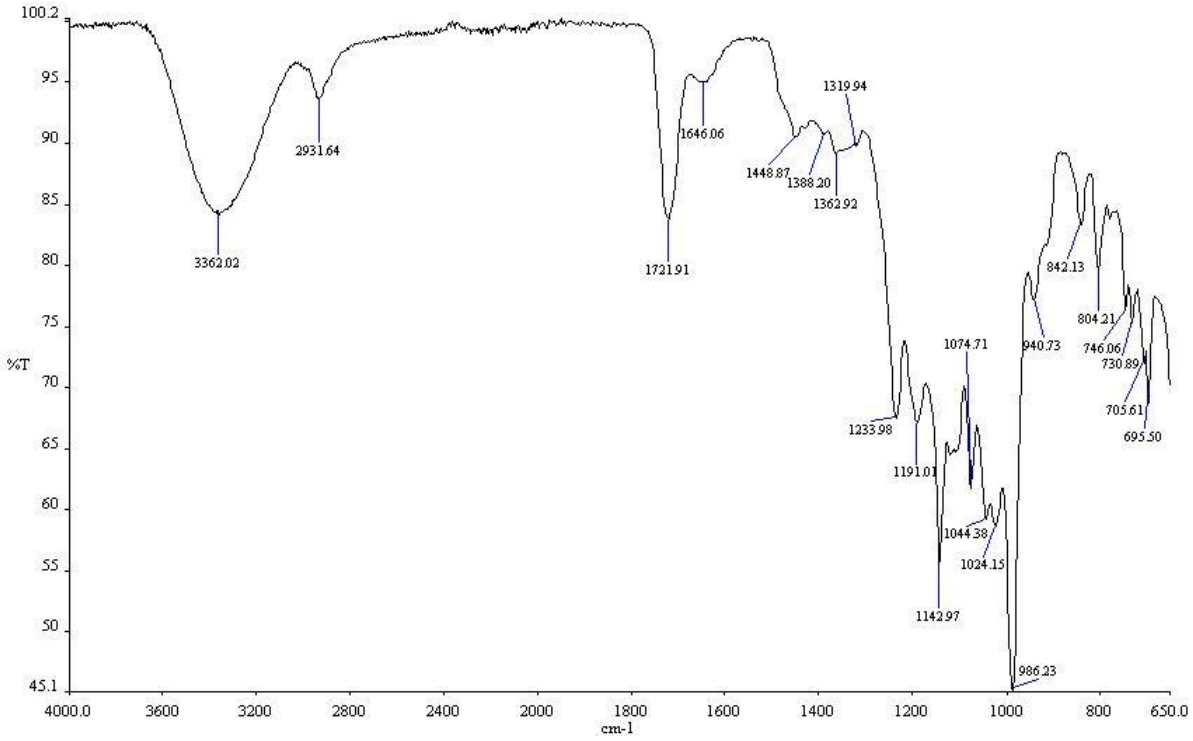

Figure 6-24. IR spectrum of p(TreMA-*co*-13FOMA) (**P3**, TreMA:13FOMA = 70:30.

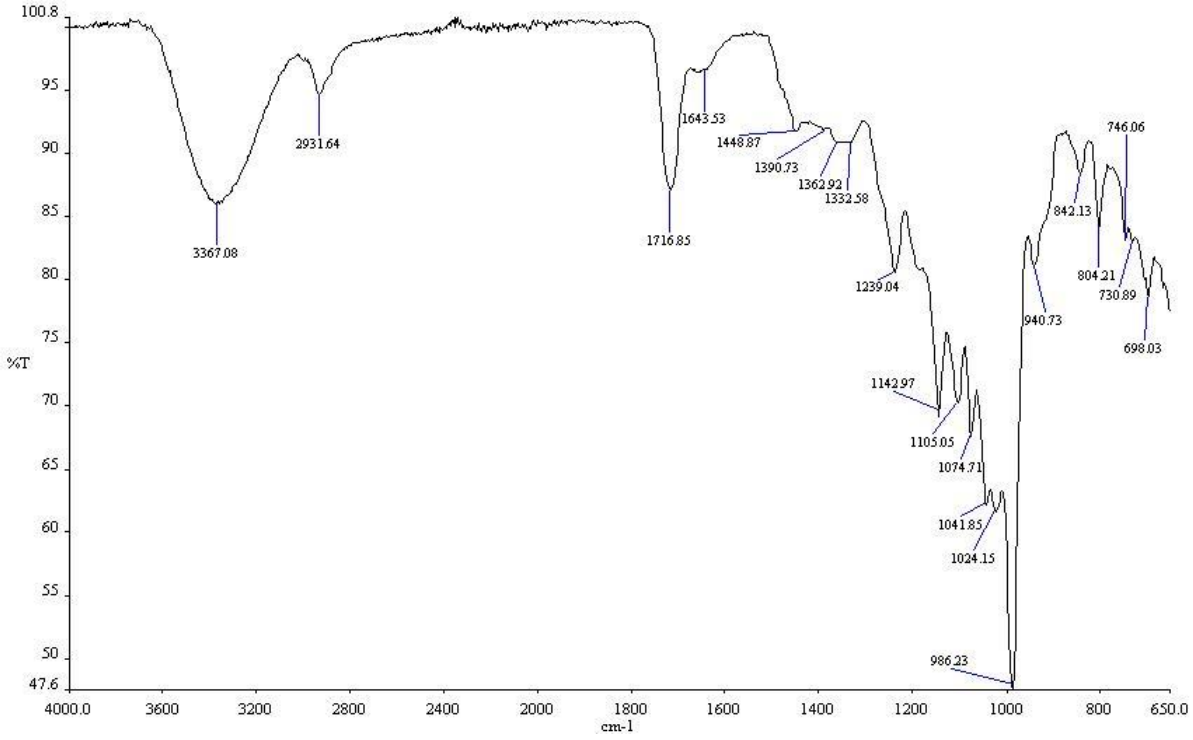

Figure 6-25. IR spectrum of p(TreMA-*co*-13FOMA) (**P4**, TreMA:13FOMA = 90:10).

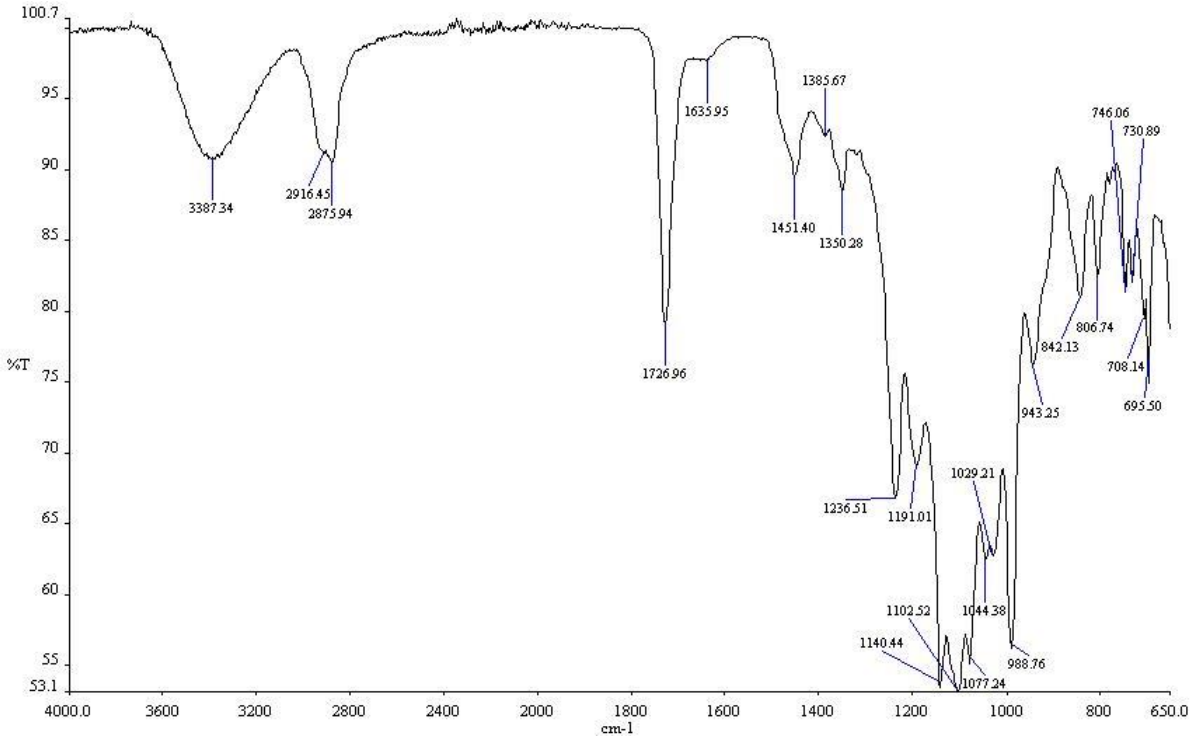

Figure 6-26. IR spectrum of p(TreMA-*co*-PEGMA-*co*-13FOMA) (**P6**, TreMA:PEGMA:13FOMA = 33:33:33).

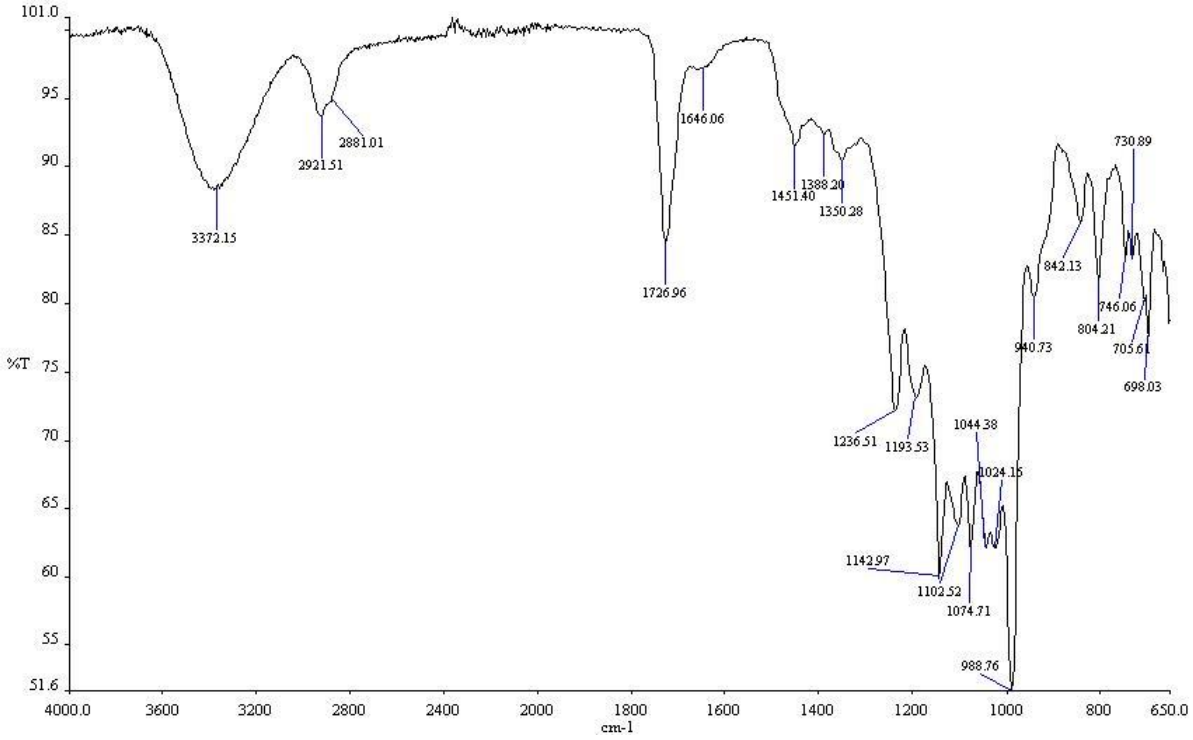

Figure 6-27. IR spectrum of p(TreMA-*co*-PEGMA-*co*-13FOMA) (**P7**, TreMA:PEGMA:13FOMA = 56:18:26).

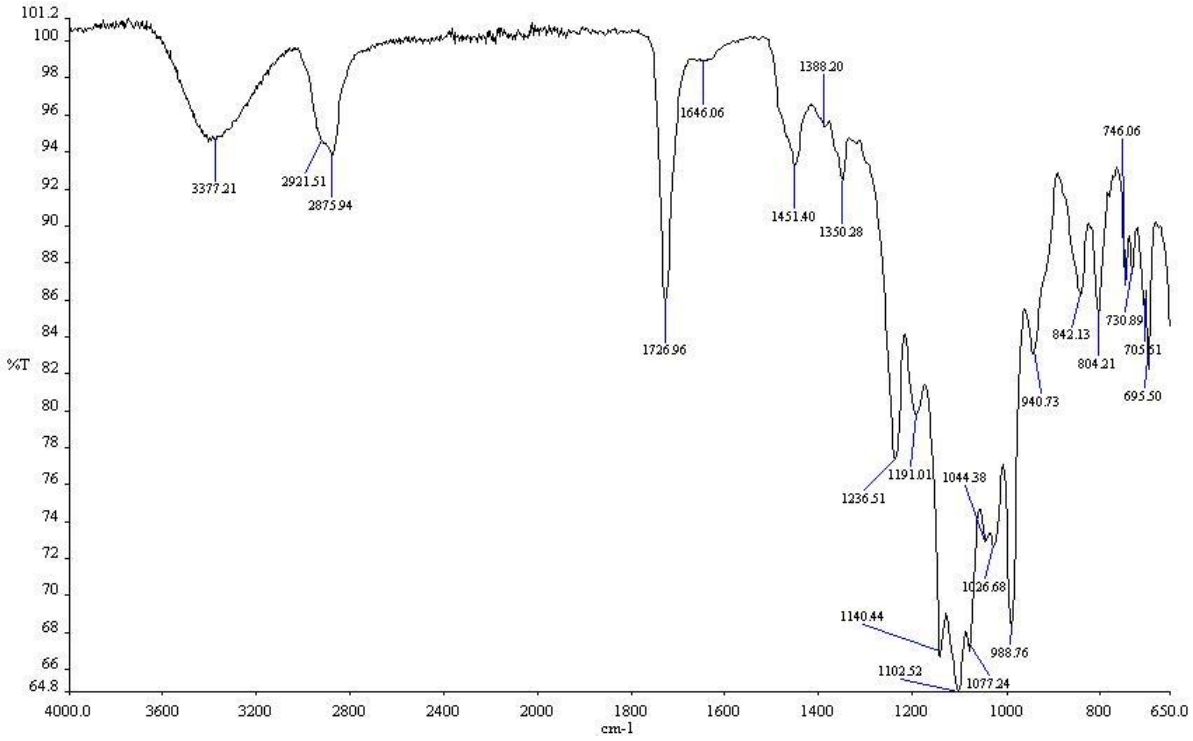

Figure 6-28. IR spectrum of p(TreMA-*co*-PEGMA-*co*-13FOMA) (**P8**, TreMA:PEGMA:13FOMA = 37:37:26).

DLS Spectra

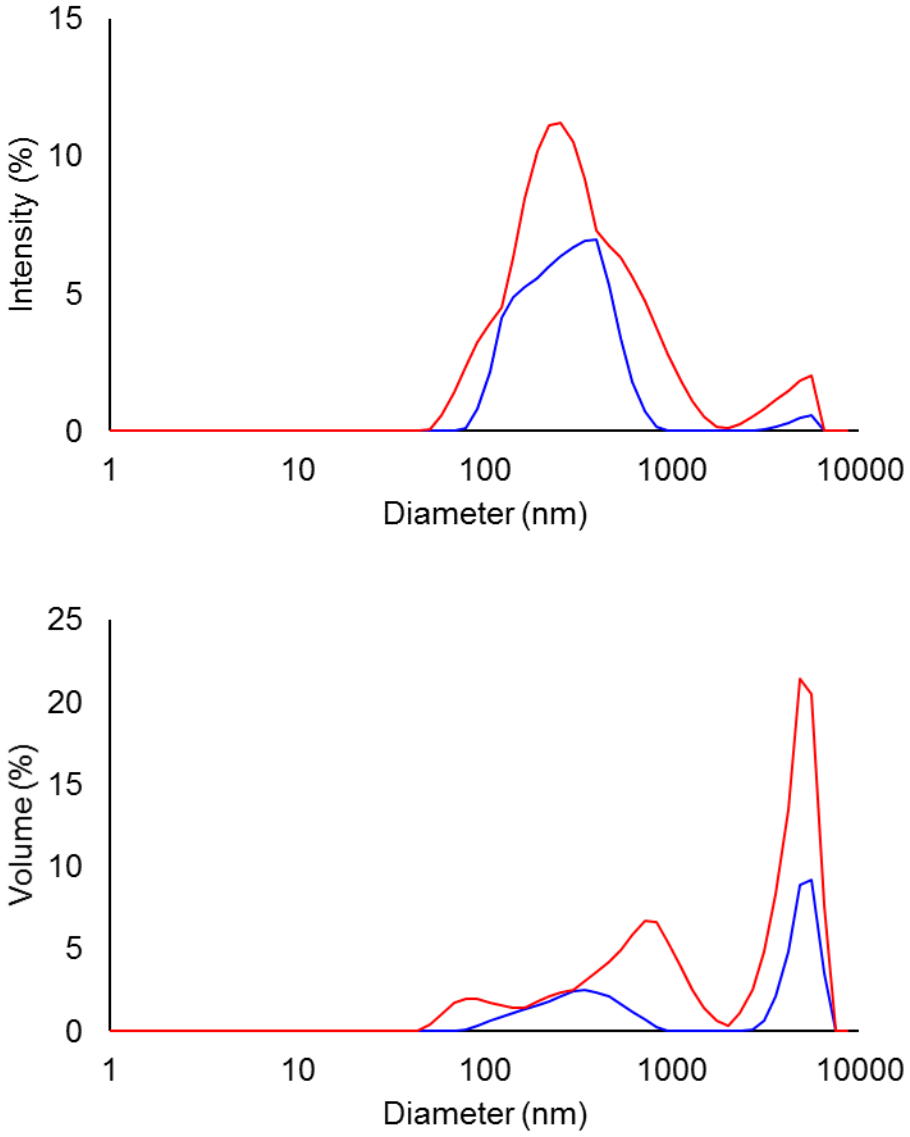

Figure 6-29. DLS intensity (top) and volume (bottom) distribution of p(TreMA-*co*-13FOMA) (**P3**, TreMA:13FOMA = 70:30) nanoprecipitated with novaluron at polymer:novaluron = 10:1. Maximum (red) and minimum (blue) values from repeated measurements (n = 3).

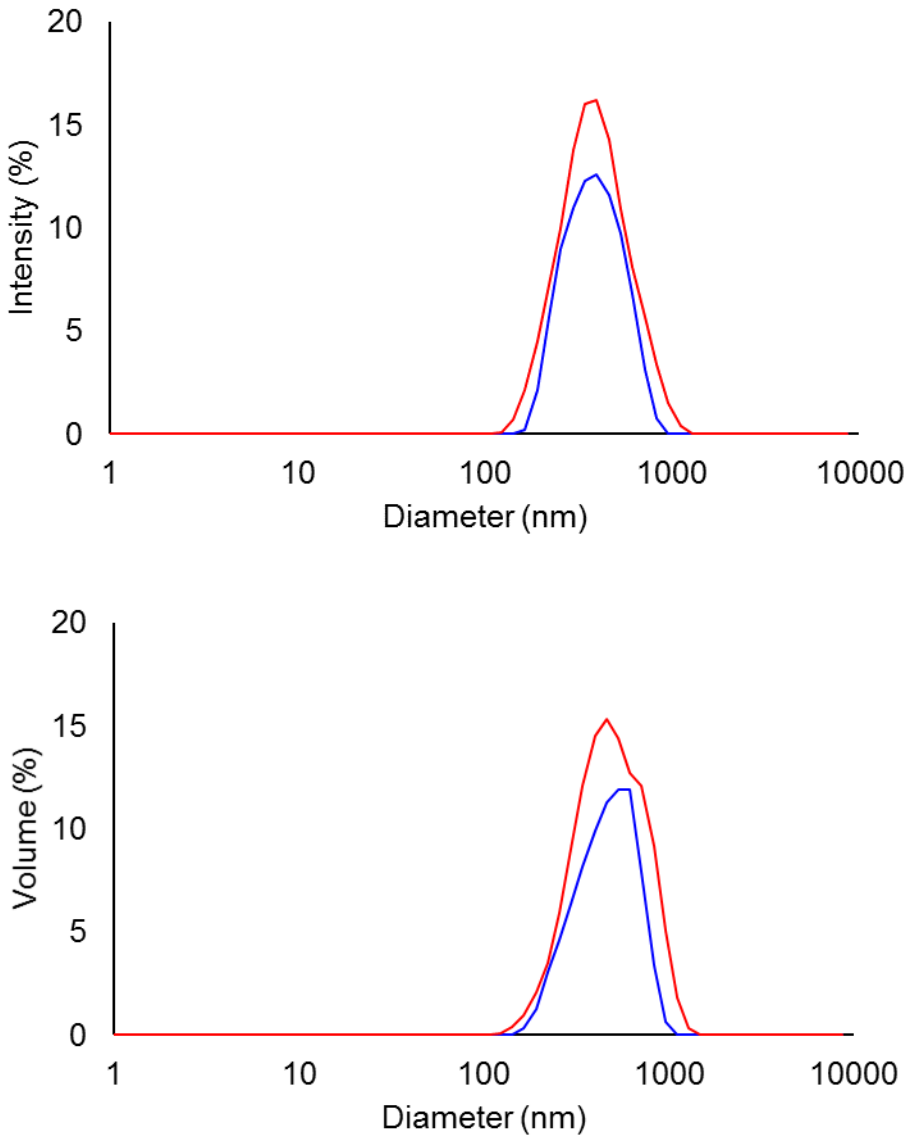

Figure 6-30. DLS intensity (top) and volume (bottom) distribution of p(PEGMA-*co*-13FOMA) (**P0**, PEGMA:13FOMA = 60:40) nanoprecipitated with novaluron at polymer:novaluron = 10:1. Maximum (red) and minimum (blue) values from repeated measurements (n = 3).

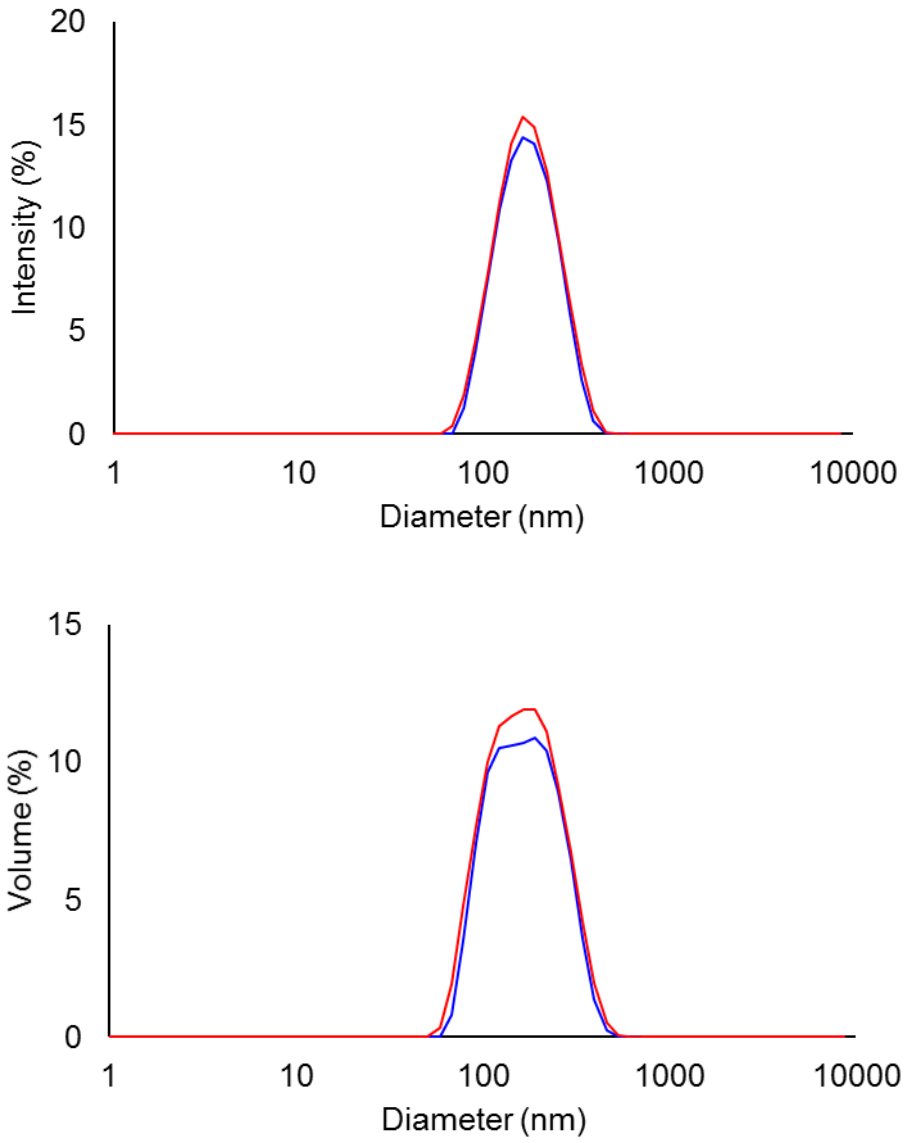

Figure 6-31. DLS intensity (top) and volume (bottom) distribution of p(TreMA-*co*-13FOMA) (**P4**, TreMA:13FOMA = 90:10) nanoprecipitated with novaluron at polymer:novaluron = 10:1. Maximum (red) and minimum (blue) values from repeated measurements (n = 3).

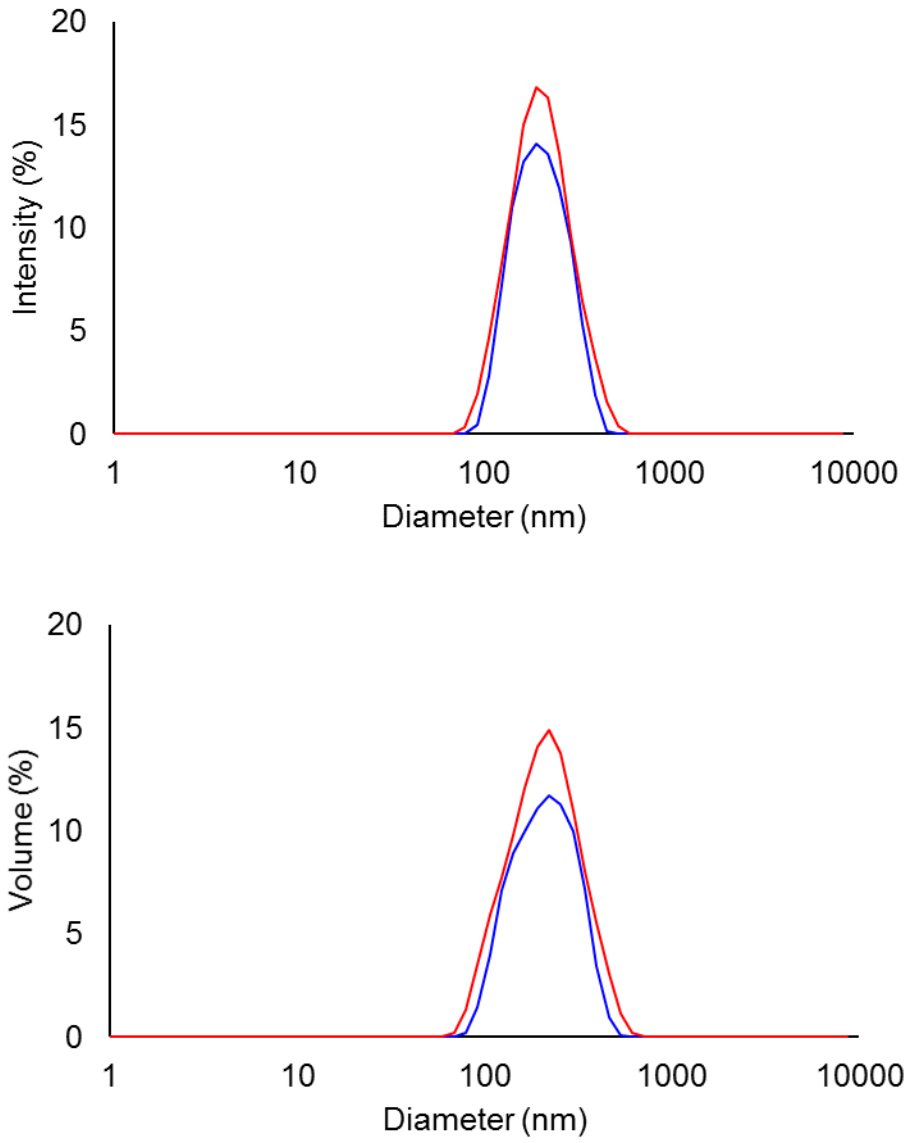

Figure 6-32. DLS intensity (top) and volume (bottom) distribution of p(TreMA-*co*-PEGMA-*co*-13FOMA) (**P8**, TreMA:PEGMA:13FOMA = 37:37:26) in water with maximum (red) and minimum (blue) values from repeated measurements (n = 3).

6.5 References

(1) Hillmyer, M. A.; Lodge, T. P. Synthesis and self-assembly of fluorinated block copolymers. *J. Polym. Sci., Part A: Polym. Chem.* **2002,** *40*, 1.

(2) Discher, D. E.; Ahmed, F. Polymersomes. *Annu. Rev. Biomed. Eng.* **2006,** *8*, 323.

(3) Chang, A. B.; Lin, T.-P.; Thompson, N. B.; Luo, S.-X.; Liberman-Martin, A. L.; Chen, H.-Y.; Lee, B.; Grubbs, R. H. Design, Synthesis, and Self-Assembly of Polymers with Tailored Graft Distributions. *J. Am. Chem. Soc.* **2017,** *139*, 17683.

(4) Gentekos, D. T.; Jia, J.; Tirado, E. S.; Barteau, K. P.; Smilgies, D.-M.; DiStasio Jr, R. A.; Fors, B. P. Exploiting Molecular Weight Distribution Shape to Tune Domain Spacing in Block Copolymer Thin Films. *J. Am. Chem. Soc.* **2018,** *140*, 4639.

(5) Golder, M. R.; Jiang, Y.; Teichen, P. E.; Nguyen, H. V.-T.; Wang, W.; Milos, N.; Freedman, S. A.; Willard, A. P.; Johnson, J. A. Stereochemical Sequence Dictates Unimolecular Diblock Copolymer Assembly. *J. Am. Chem. Soc.* **2018**.

(6) Terashima, T.; Sugita, T.; Fukae, K.; Sawamoto, M. Synthesis and single-chain folding of amphiphilic random copolymers in water. *Macromolecules* **2014,** *47*, 589.

(7) Terashima, T.; Sugita, T.; Sawamoto, M. Single-chain crosslinked star polymers via intramolecular crosslinking of self-folding amphiphilic copolymers in water. *Polym. J.* **2015,** *47*, 667.

(8) Sugita, T.; Matsumoto, K.; Terashima, T.; Sawamoto, M. Synthesis of Amphiphilic Three-Armed Star Random Copolymers via Living Radical Polymerization and their Unimolecular Folding Properties in Water. *Macromol. Symp.* **2015,** *350*, 76.

(9) Matsumoto, M.; Terashima, T.; Matsumoto, K.; Takenaka, M.; Sawamoto, M. Compartmentalization Technologies via Self-Assembly and Crosslinking of Amphiphilic Random Block Copolymers in Water. *J. Am. Chem. Soc.* **2017,** *139*, 7164.

(10) Koda, Y.; Terashima, T.; Sawamoto, M. Multimode Self-Folding Polymers via Reversible and Thermoresponsive Self-Assembly of Amphiphilic/Fluorous Random Copolymers. *Macromolecules* **2016,** *49*, 4534.

(11) Sletten, E. M.; Swager, T. M. Fluorofluorophores: fluorescent fluorous chemical tools spanning the visible spectrum. *J. Am. Chem. Soc.* **2014,** *136*, 13574.

(12) Koda, Y.; Terashima, T.; Sawamoto, M. Fluorous microgel star polymers: selective recognition and separation of polyfluorinated surfactants and compounds in water. *J. Am. Chem. Soc.* **2014,** *136*, 15742.

(13) Koda, Y.; Terashima, T.; Takenaka, M.; Sawamoto, M. Star Polymer Gels with Fluorinated Microgels via Star–Star Coupling and Cross-Linking for Water Purification. *ACS Macro Lett.* **2015,** *4*, 377.

(14) Theodoridis, G. Fluorine-containing agrochemicals: an overview of recent developments. *Advances in fluorine science* **2006,** *2*, 121.

(15) Fujiwara, T.; O'Hagan, D. Successful fluorine-containing herbicide agrochemicals. *J. Fluorine Chem.* **2014,** *167*, 16.

(16) Crowe, J. H.; Crowe, L. M.; Oliver, A. E.; Tsvetkova, N.; Wolkers, W.; Tablin, F. The trehalose myth revisited: introduction to a symposium on stabilization of cells in the dry state. *Cryobiology* **2001,** *43*, 89.

(17) Mancini, R. J.; Lee, J.; Maynard, H. D. Trehalose Glycopolymers for Stabilization of Protein Conjugates to Environmental Stressors. *J. Am. Chem. Soc.* **2012,** *134*, 8474.

(18) Lee, J.; Lin, E.-W.; Lau, U. Y.; Hedrick, J. L.; Bat, E.; Maynard, H. D. Trehalose Glycopolymers as Excipients for Protein Stabilization. *Biomacromolecules* **2013,** *14*, 2561.

(19) Pelegri-O'Day, E. M.; Paluck, S. J.; Maynard, H. D. Substituted Polyesters by Thiol–Ene Modification: Rapid Diversification for Therapeutic Protein Stabilization. *J. Am. Chem. Soc.* **2017,** *139*, 1145.

(20) Sizovs, A.; Xue, L.; Tolstyka, Z. P.; Ingle, N. P.; Wu, Y.; Cortez, M.; Reineke, T. M. Poly (trehalose): sugar-coated nanocomplexes promote stabilization and effective polyplex-mediated siRNA delivery. *J. Am. Chem. Soc.* **2013,** *135*, 15417.

(21) Tolstyka, Z. P.; Phillips, H.; Cortez, M.; Wu, Y.; Ingle, N.; Bell, J. B.; Hackett, P. B.; Reineke, T. M. Trehalose-Based Block Copolycations Promote Polyplex Stabilization for Lyophilization and in Vivo pDNA Delivery. *ACS Biomater. Sci. Eng.* **2015,** *2*, 43.

(22) O'Shea, T. M.; Webber, M. J.; Aimetti, A. A.; Langer, R. Covalent Incorporation of Trehalose within Hydrogels for Enhanced Long-Term Functional Stability and Controlled Release of Biomacromolecules. *Adv. Healthcare Mater.* **2015,** *4*, 1802.

(23) Wada, M.; Miyazawa, Y.; Miura, Y. A specific inhibitory effect of multivalent trehalose toward Aβ (1-40) aggregation. *Polym. Chem.* **2011,** *2*, 1822.

(24) Ouchi, M.; Terashima, T.; Sawamoto, M. Transition metal-catalyzed living radical polymerization: toward perfection in catalysis and precision polymer synthesis. *Chem. Rev.* **2009,** *109*, 4963.

(25) Hibi, Y.; Tokuoka, S.; Terashima, T.; Ouchi, M.; Sawamoto, M. Design of AB divinyl "template monomers" toward alternating sequence control in metal-catalyzed living radical polymerization. *Polym. Chem.* **2011,** *2*, 341.

(26) Fine, J. D.; Mullin, C. A.; Frazier, M. T.; Reynolds, R. D. Field Residues and Effects of the Insect Growth Regulator Novaluron and Its Major Co-Formulant N-Methyl-2-Pyrrolidone on Honey Bee Reproduction and Development. *J. Econ. Entomol.* **2017,** *110*, 1993.

(27) Koda, Y.; Terashima, T.; Sawamoto, M.; Maynard, H. D. Amphiphilic/fluorous random copolymers as a new class of non-cytotoxic polymeric materials for protein conjugation. *Polym. Chem.* **2015,** *6*, 240.

(28) Liu, Y.; Lee, J.; Mansfield, K. M.; Ko, J. H.; Sallam, S.; Wesdemiotis, C.; Maynard, H. D. Trehalose Glycopolymer Enhances Both Solution Stability and Pharmacokinetics of a Therapeutic Protein. *Bioconj. Chem.* **2017,** *28*, 836.

(29) Spěváček, J.; Hanyková, L. 1H NMR relaxation study of polymer-solvent interactions during thermotropic phase transition in aqueous solutions. *Macromol. Symp.* **2003,** *203*, 229.

Chapter 7.

Modulation of Cyclic Ketene Acetal Reactivity and Vinyl Polymer Degradation Using Fluorous Co-Monomer

This chapter is an edited version of a published paper:
Reprinted with permission from Ko, J. H.; Terashima, T.; Sawamoto, M.; Maynard, H. D. *Macromolecules* **2017**, *50*, 9222.

7.1 Introduction

Fluorinated compounds have widespread utility as durable coating materials,[1, 2] agrochemicals,[3, 4] fuel cell membranes,[5] therapeutic drugs,[4, 6, 7] and radiotracers for positron emission tomography (PET).[7-9] In addition, interest in using fluorinated compounds for medical applications has been steadily increasing,[4, 6, 7] with fluorinated polymers emerging as a promising platform for drug delivery for fluorinated drugs and imaging reagents.[10-14] Fluorinated polymers possess unique properties such as high chemical resistance,[1, 2] preference for fluorous phase over both aqueous and organic phases,[15] enhanced cell membrane permeability,[13, 16] and self-assembly in water.[17, 18] However, most fluorinated polymers are non-degradable, and the use of non-degradable polymers *in vivo* may lead to build up in the body and environment causing undesired side-effects in the long term.[19] Therefore, there is a need for fundamental understanding of the synthesis and properties of degradable fluorinated polymers; yet very few studies on the subject exist.[13, 20, 21]

We envisioned that co-polymerization of a fluorinated vinyl monomer and cyclic ketene acetal using ruthenium-catalyzed living radical polymerization would enable easy access to degradable fluorous polymers. Along with other controlled polymerization techniques such as nitroxide-mediated polymerization (NMP),[22] reversible addition-fragmentation chain-transfer (RAFT) polymerization,[23] and ring-opening metathesis polymerization (ROMP),[24] metal-catalyzed living radical polymerization enables synthesis of well-defined and highly functional polymeric materials. More recently, we have studied the behavior of amphiphilic fluorous polymethacrylates synthesized by various ruthenium catalysts and demonstrated the ability of the polymers to recognize and segregate fluorous compounds in water[25-27] and also form single-chain nanoparticle via intra-molecular folding of fluorous side chains.[17]

Such fluorous vinyl polymers may be made degradable by the incorporation of degradable units into the backbone. Cyclic ketene acetals are well-characterized monomers that co-polymerize with common vinyl monomers, such as methacrylates, to impart degradability to the resulting polymer.[28-30] Upon radical addition to the double bond of a cyclic ketene acetal, its ring strain causes the structure to open and produce a hydrolytically degradable ester linkage in the polymer backbone. Cyclic ketene acetals typically contain a radical-stabilizing aromatic ring adjacent to the ketene acetal to facilitate ring opening, such as in 5,6-benzo-2-methylene-1,3-dioxepane (BMDO). In particular, BMDO undergoes quantitative ring opening with vinyl monomers[31] and its degradation product has shown to be cell compatible and non-cytotoxic,[32] making it one of the most popular ketene acetals used.

We set out to develop degradable fluorous polymers from poly(ethylene glycol methyl ether methacrylate) (PEGMA), fluorinated methacrylates, and the cyclic ketene acetal BMDO. We decided to use PEGMA as a co-monomer to solubilize the resulting polymer in aqueous media. We have previously shown that PEGMA co-polymerizes well with fluorinated methacrylates to form self-folded assemblies that can be conjugated to proteins[33] and can be also used to stabilize proteins in fluorous solvent.[34] Moreover, PEGMA and fluorous methacrylates have been shown to produce polymers that are biocompatible and non-cytotoxic to cells at least up to 1 mg/mL.[33]

In this chapter, we report the synthesis of co-polymers of cyclic ketene acetal with both hydrophilic and fluorous methacrylates by ruthenium-catalyzed living radical polymerization. The technique allowed us to create a series of well-defined polymers with varying fluorous contents, which was used to establish the relationship between the monomer feed ratios and the resulting co-polymerization properties and polymer degradation kinetics. We anticipate that by combining

the findings in this study with powerful living radical polymerization techniques, researchers will be able to design well-defined degradable fluorous materials for a variety of applications.

7.2 Results and Discussion

Given the limited examples of degradable fluorous polymers, we were interested in exploring the co-polymerization of BMDO and fluorous methacrylates as a facile route to degradable fluorous polymers. BMDO is known to co-polymerize slowly with activated monomers[35, 36] due to its high electron density. We hypothesized that the fluorous methacrylates (R_FMA) with electron-withdrawing side chains will have better orbital overlap with BMDO than alkyl-substituted methacrylates, allowing the BMDO incorporation to be modulated by the amount of the R_FMA in the random co-polymer of BMDO, R_FMA, and PEGMA. The report by Yamago and Mishima provides quantitative support for this hypothesis.[37] In their study, various acrylates and methacrylates were more readily co-polymerized with vinyl ether monomers when the acrylate/methacrylate contained the electron-withdrawing CF_3 pendant group. Their density functional theory (DFT) calculations suggested that the CF_3 acts to lower the singly occupied molecular orbital (SOMO) energy of the acrylate/methacrylate radical interacting with the highest occupied molecular orbital (HOMO) energy of electron-rich vinyl ether.

We adopted the analysis of Yamago and Mishima to gain a theoretical insight into our hypothesis. Our DFT calculation (at UB3LYP/6-31G(d) level of theory using GAMESS[38, 39]) of BMDO and R_FMAs leads to a similar conclusion (Figure 7-1). It has been previously demonstrated that 1*H*,1*H*,2*H*,2*H*-perfluorooctyl methacrylate (13FOMA) exhibits high fluorous property, which directs the folding behavior in p(PEGMA-*co*-13FOMA)[17] and was thus chosen for our study. Since poor polymer solubility was expected at high 13FOMA feed ratio, 1*H*,1*H*,2*H*,2*H*,3*H*,3*H*-

perfluoropentyl methacrylate (5FPMA)[40] was also employed for the high fluorous monomer feed ratios. The calculations show that fluorinated substituents lower the SOMO energy of methacrylate by 6 kcal/mol for the 13FOMA analog with ethyl spacer and 4 kcal/mol for the 5FPMA analog with propyl linker, which bring the SOMO energies closer to the HOMO energy of BMDO. In this instance, the perfluorinated chain of R_FMA was substituted with CF_3 to decrease the calculation time. This result encouraged us that both 13FOMA and 5FPMA will exhibit enhanced reactivity with BMDO.

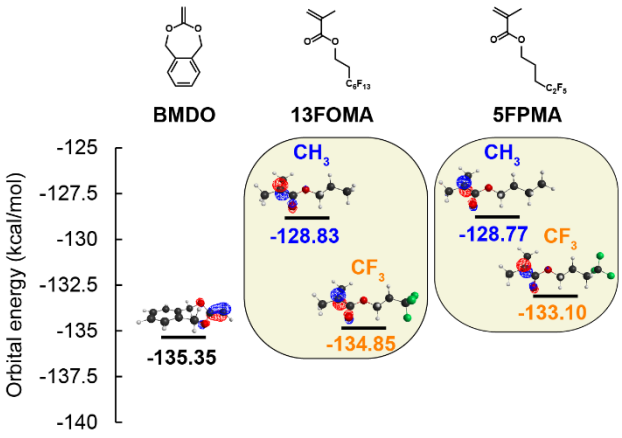

Figure 7-1. Structures of monomers utilized in this study. HOMO energy of BMDO, and SOMO energies of fluorous methacrylate radicals representing 13FOMA and 5FPMA, and corresponding alkyl methacrylate radicals are shown below the structures. Structures were optimized by DFT calculation at UB3LYP/6-31G(d) level of theory in GAMESS[38, 39] and visualized by MacMolPlt.[41]

Optimization of Polymerization Condition. Although BMDO has previously been co-polymerized with acrylates and methacrylates using reversible addition-fragmentation chain-transfer (RAFT) polymerization,[42, 43] nitroxide-mediated polymerization (NMP),[36, 44] and atom transfer radical polymerization (ATRP) via copper catalysis,[45-47] the use of ruthenium complexes for BMDO co-polymerization with vinyl monomers has not been explored to date. Ruthenium catalysts have excellent functional group tolerance and large coordination sphere, which allow

them to accommodate ligands with various electronic and steric properties and achieve fine control over the polymerization of various monomers.[48] Therefore, we set out to initially optimize the conditions for Ru-catalyzed polymerization of BMDO with methacrylates, using PEGMA as a model methacrylate (Scheme 7-1). The half-metallocene indenyl complex $Ru(Ind)Cl(PPh_3)_2$ is a versatile catalyst that produces polymers with a narrow molecular weight distribution for a wide range of monomers[48, 49] and was used for the experiment. The chloride initiator ethyl 2-chloro-2-phenylacetate (ECPA) is particularly well-suited for polymerization of methacrylates using $Ru(Ind)Cl(PPh_3)_2$ and was employed for the first set of polymerizations (Table 7-1, entries 2 through 4). Polymerizations proceeded smoothly at low BMDO feed (20 mol %) but became sluggish at higher feed ratios; the polymerization only reached 58 % conversion after 86 hours using 60 mol % of BMDO compared to 77 % conversion after 24 hours with 20 mol % of BMDO. Moreover, the size exclusion chromatography (SEC) trace was asymmetrical and indicated some low molecular weight tailing (Figure 7-2, red). The asymmetry of the SEC traces was quantified using asymmetry factor (A_s), which is a chromatographic index[50, 51] recently used by the Fors group to analyze molecular weight distribution change with controlled initiator addition.[52] When A_s is greater than 1, the SEC peak exhibits tailing towards the low molecular weight region. As a control, a well-defined p(PEGMA-*co*-13FOMA) polymer that did not contain BMDO exhibited relatively low $A_s = 1.45$ (entry 1). However, the polymers synthesized using ECPA had large $A_s \geq 2$ (entries 2 and 3) demonstrating that addition of BMDO inhibits chain growth and causes the tailing with this initiator. At very high BMDO content (60 mol%), low monomer conversion resulted in the calculation of a smaller A_s (entry 4). It should also be noted that the current difficulty of co-polymerization of cyclic ketene acetal with activated vinyl monomers is the moderate control ($Đ$

= 1.3 – 1.7) due to the limited reactivity of cyclic ketene acetal,[32, 42, 43, 53] and our data are comparable to previous results obtained by copper-mediated ATRP, RAFT, and NMP.

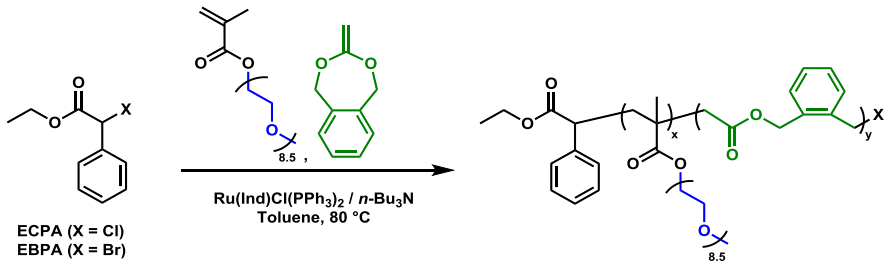

Scheme 7-1. Ruthenium-catalyzed living radical polymerization of poly(ethylene glycol) methyl ether methacrylate (PEGMA) and 5,6-benzo-2-methylene-1,3-dioxepane (BMDO) using chloride and bromide initiators.

Table 7-1. Molecular weight data and asymmetry factor of p(PEGMA-*co*-BMDO) polymers synthesized with chloride or bromide initiator.

Entry	Initiator	PEGMA: BMDO	Time (h)	PEGMA conv. (%)	M_n (kDa)	$Đ$	A_s
1	Control (ECPA, Cl)[a]	N/A	49	80.6	50.9	1.18	1.45
2		80:20	24	76.9	34.1	1.43	2.38
3	ECPA (Cl)[b]	60:40	48	69.4	28.4	1.66	2.00
4		40:60	86	58.2	17.9	1.61	1.39
5		80:20	18	80.7	21.6	1.53	1.55
6	EBPA (Br)[c]	60:40	23	69.4	26.0	1.60	1.57
7		40:60	34	77.6	19.0	1.54	1.60

[a] [PEGMA]:[13FOMA] = 60:40. [b] [PEGMA + BMDO] / [ECPA] / [Ru(Ind)Cl(PPh_3)$_2$] / [*n*-Bu_3N] = 500 / 4 / 2 / 20 mM in toluene at 80 °C. [c] [PEGMA] / [BMDO] / [EBPA] / [Ru(Ind)Cl(PPh_3)$_2$] / [*n*-Bu_3N] = 400 / 100 or 267 or 600 / 4 / 2 / 20 mM in toluene at 80 °C.

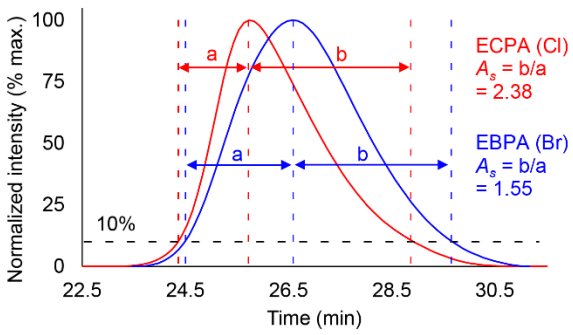

Figure 7-2. Comparison of SEC chromatogram peak asymmetry for p(PEGMA-*co*-BMDO) (20% BMDO) synthesized using Cl (red, Table 7-1, entry 2) or Br initiator (blue, Table 7-1, entry 5).

To explain the chain growth inhibition by BMDO when using the chloride initiator, we turned our attention to the disparity between the C-Cl bond strengths for BMDO (69.4 kcal/mol for the benzylic C-Cl) and methyl methacrylate (MMA) (66.9 kcal/mol for the methacrylic C-Cl).[54] Once BMDO adds to the chain end, the polymer has 2.5 kcal/mol higher thermodynamic barrier for C-Cl bond cleavage to form the active chain compared to polymers with PEGMA at the chain ends. As a result, the PEGMA-end chains will continue to polymerize while BMDO-end chains will remain mainly dormant. In contrast, the more scissile C-Br bond has energies that are more comparable for both BMDO (60.2 kcal/mol) and MMA (58.9 kcal/mol),[54] which suggests that the bromide initiator ethyl 2-bromo-2-phenylacetate (EBPA) may reduce tailing. Indeed, EBPA-initiated polymerizations yielded polymers with $A_s \leq 1.6$ and reduced tailing (Figure 7-2, blue). Yet the $Đ$ values are similar to the chloride initiator likely due to the innate BMDO reactivity with PEGMA. To accelerate polymerization at high BMDO contents, the monomer concentrations were increased by 1.3 fold for 40 mol % and 2 fold for 60 mol % BMDO, which effectively led to decreased polymerization time and high conversion even at 60 mol % (77.6 % at 34 h) (Table 7-1, entry 7).

Using this bromide initiator, PEGMA and BMDO were then co-polymerized with 13FOMA and 5FPMA at various fluorous methacrylate ratios (Scheme 7-2). BMDO feed amount was fixed at 40 % for all polymerizations as our aim was to study the effect of fluorous content on polymerization and resulting material properties. When PEGMA and BMDO were co-polymerized in the absence of 13FOMA, BMDO incorporation was only 8.6 % (Table 7-2). This BMDO incorporation is comparable to our previous result using RAFT to co-polymerize BMDO and PEGMA (between 9 and 10.5 % at 50 % BMDO feed ratio).[42] At higher 13FOMA feed ratios, significantly more BMDO was incorporated into the polymer (Figure 7-3 and Table 7-2), with 13.4 % BMDO being incorporated at the highest 13FOMA feed ratio (entry 4). However, the molecular weight could not be measured by SEC at this feed ratio since the *dn/dc* was nearly zero due to the very low polarizability of fluorine leading to a low refractive index.[55] We have previously reported a similar decrease in the polymer *dn/dc* with increasing R_FMA content.[17] In addition, the polymerization time was extended to 52 hours in order to maintain the monomer conversion at around 75 % as in other polymerizations; the increased polymerization time was presumably due to increased BMDO incorporation. To study p(PEGMA-*co*-R_FMA-*co*-BMDO) at high R_FMA content, the less fluorous monomer 5FPMA was used in place of 13FOMA for co-polymerization with PEGMA and BMDO. To compensate for the decreased polymerization rate at high fluorous monomer content, 5FPMA polymerizations were conducted at a slightly higher concentration (25 % more concentrated). As a result, high conversion was reached in 24 hours and at the same time the *dn/dc* remained positive for the 5FPMA polymers allowing for SEC analysis.

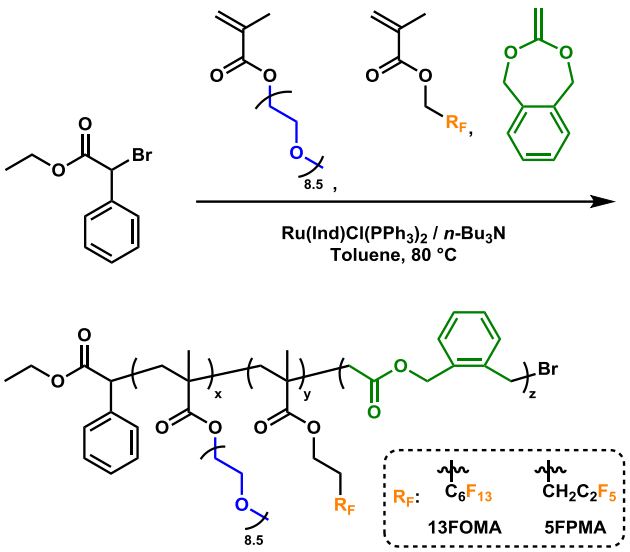

Scheme 7-2. Ruthenium-catalyzed living radical polymerization of PEGMA, perfluoroalkyl methacrylates (R_FMA: 13FOMA, 5FPMA), and BMDO.

Table 7-2. Degradable fluorous polymers synthesized by ruthenium-catalyzed living radical polymerization.

Entry	R_FMA	PEGMA: R_FMA	Time (h)	PEGMA conv. (%)	M_n (kDa)	$Đ$	% BMDO
1	None[a]	100:0	23	69.4	26.0	1.60	8.6
2	13FOMA[b]	80:20	31.5	74.9	22.6	1.46	10.6
3		60:40	47.5	75.9	21.3	1.50	12.1
4		40:60	52	73.3	N/A[c]	N/A[c]	13.4
5	5FPMA[d]	40:60	24	75.0	20.0	1.37	12.7
6		20:80	24	73.7	16.8	1.34	13.5

[a] Reproduced from Table 7-1 (EBPA, PEGMA:BMDO = 60:40) for easy comparison. [b] [PEGMA + 13FOMA] / [BMDO] / [EBPA] / [Ru(Ind)Cl(PPh$_3$)$_2$] / [*n*-Bu$_3$N] = 400 / 267 / 4 / 2 / 20 mM in toluene at 80 °C. [c] SEC trace was not observable due to near-zero *dn/dc* at this composition.[17] [d] [PEGMA + 5FPMA] / [BMDO] / [EBPA] / [Ru(Ind)Cl(PPh$_3$)$_2$] / [*n*-Bu$_3$N] = 500 / 333 / 5 / 2.5 / 25 mM in toluene at 80 °C.

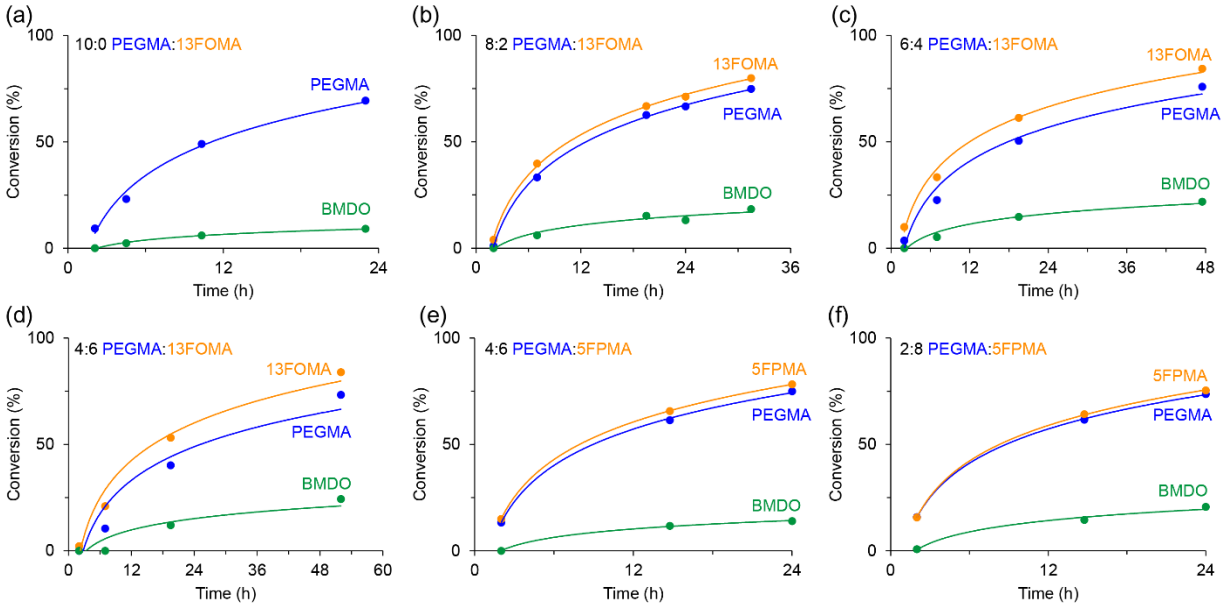

Figure 7-3. Polymerization kinetics of p(PEGMA-*co*-R_FMA-*co*-BMDO) polymers at fixed BMDO feed ratio (40% BMDO with respect to combined methacrylates). (a) 10:0 PEGMA:R_FMA, (b) 8:2 PEGMA:13FOMA, (c) 6:4 PEGMA:13FOMA, (d) 4:6 PEGMA:13FOMA, (e) 4:6 PEGMA:5FPMA , and (f) 2:8 PEGMA:5FPMA (orange: R_FMA, blue: PEGMA, green: BMDO).

R_FMA Content Modulates BMDO Incorporation. When BMDO incorporation was plotted as a function of R_FMA content, a highly linear relationship was observed for both 13FOMA and 5FPMA (Figure 7-4). This result supports the hypothesis that the increased electrophilicity of R_FMA improves the incorporation of BMDO. DFT calculation showed that the orbital energy gap between the methacrylate and BMDO decreases from 6.5 kcal/mol for alkyl methacrylates to 0.5 kcal/mol for 13FOMA and 2.3 kcal/mol for 5FPMA (Figure 7-1). The slightly smaller orbital energy gap for 13FOMA may be responsible for the larger slope for 13FOMA compared to 5FPMA, although the difference is not pronounced. It is possible that the higher BMDO incorporation was caused by the solvent or polar effects from the presence of the fluorous unit at the chain end. However, such through-space field effects of fluorine are expected to show greater discrepancy in the % BMDO incorporation between 13FOMA and 5FPMA than the observed

result since 13FOMA contains 2.6 times more fluorine atoms per repeat unit than 5FPMA. The combined data suggests that the higher BMDO incorporation is indeed due to the increased electrophilicity of the R_FMAs from the inductive electron withdrawal by the fluorous side chain. Finding that electron-deficient fluorinated methacrylates better react with BMDO may give insights into strategies for improving the control of cyclic ketene acetal co-polymerizations in future studies.

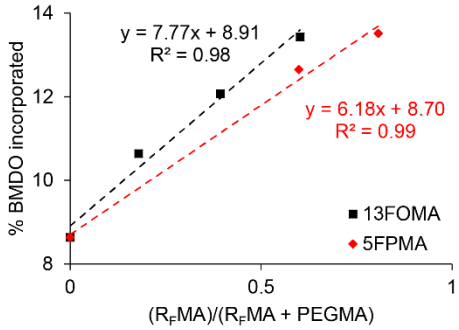

Figure 7-4. BMDO incorporation as a function of R_FMA content in the polymer (black: 13FOMA, red: 5FPMA).

Degradation Rate is Controlled by R_FMA Content. Given the effect of fluorous monomer content on BMDO incorporation, it was also reasonable to expect that fluorous content would affect the polymer degradation kinetics. To examine this relationship, the polymers with different R_FMA content were exposed to hydrolysis in a basic aqueous media. All polymers were soluble in water except 80 % 5FPMA, which required 10 % DMSO for solubilization. Thus, to make the test condition comparable across the polymers, the degradation was carried out in the presence of 10 % DMSO.

Degradation of the polymers was monitored over 24 hours by measuring polymer molecular weight by SEC (Figure 7-5). Polymer without any fluorous unit quickly degraded and exhibited a drastic shift in the SEC chromatogram for the first time point at 15 min. The rate of

chromatogram shift corresponding to the degradation decreased as R_FMA content increased. When the molecular weights are plotted as % original molecular weight (Figure 7-6a), the trend of faster degradation for lower fluorous content polymer is clear. This is despite the fact that the more fluorous polymer contains more degradable units (Table 7-2). A control polymer p(PEGMA-*co*-13FOMA) without any degradable unit did not show significant shift in the SEC chromatogram after 24 hours under the same hydrolysis condition (Figure 7-5f), confirming that the observed shifts were due to degradation of the BMDO units and not due to the cleavage of methacrylate side chains. The SEC chromatograms qualitatively confirmed that the degradation rate continuously decreases with increased hydrophobicity from the fluorous units.

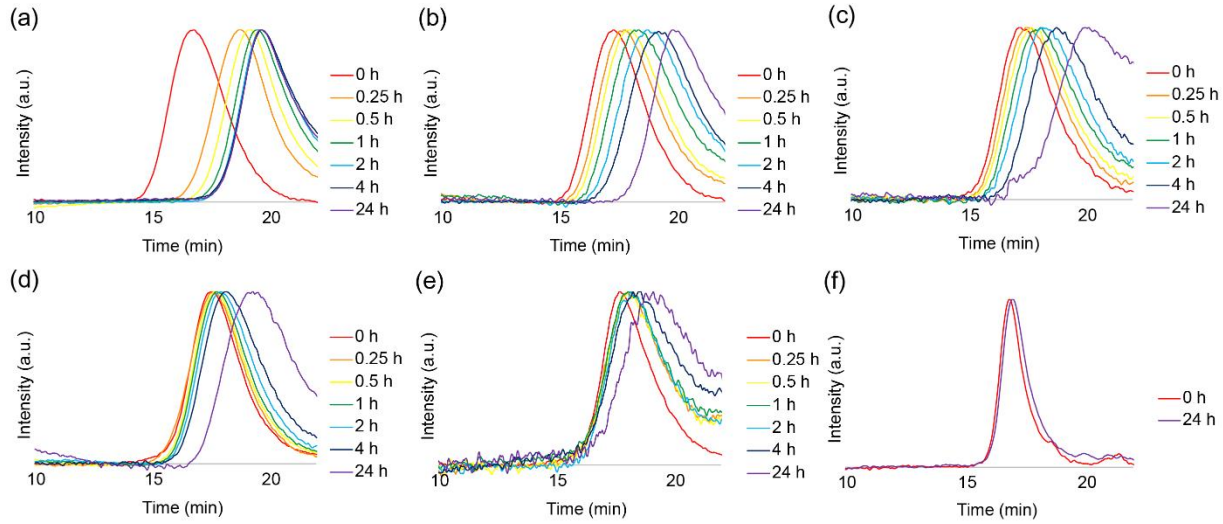

Figure 7-5. SEC chromatogram of p(PEGMA-*co*-R_FMA-*co*-BMDO) polymers in 4.5% KOH + 10% DMSO. (a) 0% R_FMA, (b) 20% 13FOMA, (c) 40% 13FOMA, (d) 60% 5FPMA, (e) 80% 5FPMA, and (f) control polymer without BMDO (p(PEGMA-*co*-13FOMA) with 60:40 PEGMA:13FOMA).

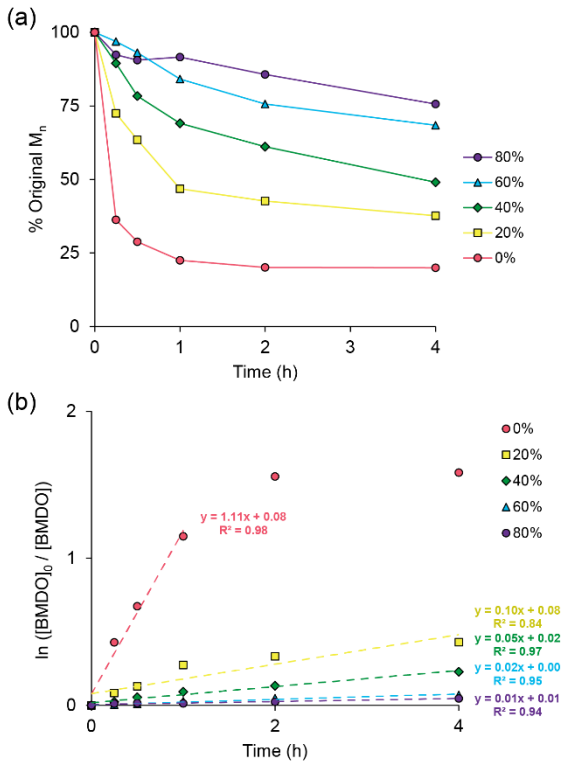

Figure 7-6. Degradation kinetics of p(PEGMA-*co*-R_FMA-*co*-BMDO) polymers. (a) Percent molecular weight over time and (b) pseudo-first order reaction kinetics of BMDO unit over time. Red: 0%, yellow: 20%, green: 40%, blue: 60%, and purple: 80% R_FMA with respect to total methacrylate content.

Modeling the Degradation Rate. To gain a quantitative understanding of the effect of fluorous content on degradation rate, we sought to convert the molecular weight information into the number of hydrolyzed BMDO units. Towards this goal, we modeled the degradation kinetics as a pseudo-first order reaction of BMDO hydrolysis with large excess of hydroxide ions. Recognizing that hydrolysis of each BMDO unit will increase the number of polymer chains by 1 and the total mass of all the polymers does not change, for the degradation of a single polymer chain, the relationship between the average molecular weight of degraded polymer chains and the number of hydrolyzed BMDO (*n*) at any time can be expressed as MW(degraded) = MW(original)

/ (n + 1). Rearranging this equation gives n = [MW(original)/ MW(degraded)] – 1 as the expression for the number of hydrolyzed or reacted BMDO in terms of molecular weight data from SEC. A Monte Carlo simulation was used to validate the extension of this model from a single polymer chain to a polymer ensemble (see Experimental Section for details). The simulation used the reported reactivity ratio of MMA and BMDO[35] to generate 1,000 polymer chains, which showed a gradient polymer with higher BMDO distribution near the polymer tail as would be predicted from its lower reactivity (Experimental Section Figure 7-26). When BMDO units in these polymers were randomly degraded, the simulation agreed perfectly with the analytical solution from the equation validating our degradation model (Experimental Section Figure 7-27).

The degradation model was used to generate a pseudo-first order reaction plot (Figure 7-6b). The plot showed good linearity at early time points, but deviation was observed at longer times (see Experimental Section Figure 7-20). This deviation from linearity is likely due to the model assumption that all BMDO units are susceptible to hydrolysis with equal probability regardless of their position in the polymer or chain length. Nevertheless, the model provides a platform for quantitative comparison of degradation rates and shows good linearity for the first four hours. The slope of each plot for the first four hours (except for 0% R_FMA, which reaches complete degradation in 2 hours) was converted to a rate constant (Table 7-3). The degradation rate spans two orders of magnitude with different fluorous monomer contents. The most drastic decrease is observed when R_FMA content is increased from 0 % to 20 %, as the rate constant decreases by 11-fold. It should also be noted that the decreasing rate trend of 13FOMA (20 and 40 %) continues for 5FPMA (60 and 80 %), suggesting that it is the number of fluorous units and not the number of fluorine atoms that has the largest impact on the degradation rate.

Table 7-3. Rate constant for degradation for different fluorous monomer contents.

% R_FMA	$k \times 10^3$ (M^{-1} min^{-1})
0	23.07
20	2.08
40	1.14
60	0.38
80	0.22

Self-Folding of the Polymers in Aqueous Media. Next, the aggregation state of polymers in aqueous solution (10% DMSO in water) was investigated by dynamic light scattering (DLS) (Figure 7-7). Although we typically conduct these studies in pure water,[17] DMSO was added to solubilize the 80% fluorous content polymer in order to make direct comparisons to the degradation data, which was undertaken in the same media. We have previously studied the self-folding behavior of p(PEGMA-*co*-13FOMA) in water, and observed that the polymer folds into a single-chain aggregate (or "unimer micelle") at fluorous contents up to 40 mol % 13FOMA and forms larger micelles at higher fluorous content.[17] By DLS intensity distribution, polymers with low fluorous content exhibited similar distributions of unimer micelles and multi-chain aggregates (Figure 7-7a – c) while polymers with higher fluorous content assembled into larger multi-chain particles (Figure 7-7d and e). Note that larger particles dominate the intensity distribution,[56] and by volume distribution the polymers with low fluorous contents (0-40% R_FMA) were mostly unimer micelles (8~10 nm, > 99.5% volume fraction) (Experimental Section Figure 7-21a – c) whereas multi-chain micelles were observed at higher fluorous contents (60-80 % R_FMA) (Experimental Section Figure 7-21d – e).

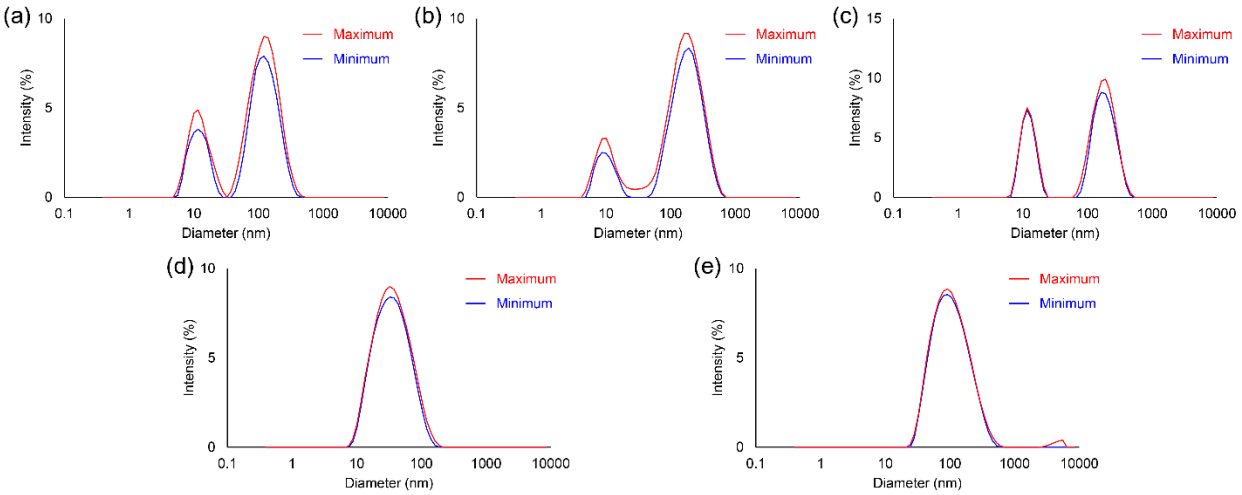

Figure 7-7. DLS intensity distribution in water + 10 % DMSO with maximum (red) and minimum (blue) values from independent sample repeats (n = 3). (a) 0% R_FMA, (b) 20% 13FOMA, (c) 40% 13FOMA, (d) 60% 5FPMA, and (e) 80% 5FPMA.

We were interested to determine if the modulation of degradation kinetics stems from the multi-chain micelles observed at higher fluorous content being better able to protect BMDO from hydrolytic degradation. If the self-assembled structures were directly responsible for the degradation rate, then the polymers with more unimer micelle population would degrade faster while the polymers with more multi-chain aggregate population would degrade slower. However, all polymers with low fluorous content (0-40 % R_FMA) exhibit similar size distributions (Figure 7-7a – c) yet have very different degradation rates (Table 7-3). Since unimer micelles also have a fluorous/hydrophobic core, both the single-chain (~10 nm) and multi-chain (40~200 nm) particles would be able to slow the degradation of BMDO. Therefore, the primary factor for hindering degradation seems to be the presence of R_FMA in the vicinity of BMDO units (local proximity).

Decreased Degradation Rate is Due to Shielding by the Fluorous Side Chains. Comparison of ^{1}H NMR spectra of the polymers in organic and aqueous media further reinforced the view that the water-repelling microenvironment of the polymer modulates the degradation rate (Figure 7-8). We have previously demonstrated that the NMR signal of fluorous side chain broadens with increasing solvent polarity and completely disappears in D_2O[17] due to the line broadening of less mobile aggregated side chains at the core of unimer micelles.[57] It was anticipated that if BMDO units are indeed shielded by the fluorous core, BMDO peak broadening in water would increase with fluorous content. Polymer without any fluorous units showed only slight broadening for the BMDO peak (peaks *a* and *b* in Figure 7-8f compared to Figure 7-8a) in aqueous media. As the fluorous content increases, PEG peaks *e* and *f* that interact with water molecules remain mostly sharp while BMDO peaks *a* and *b* gradually broaden until they nearly disappear for 80 % R_FMA (Figure 7-8j). Other peaks corresponding to hydrophobic protons in the fluorous methacrylates (*c*) and near the backbone (*d*, *g-j*) also broaden and features of the hydrophobic backbone peak (*j*) progressively become indistinguishable as the fluorous content increases. NMR data shows that the ester backbone of BMDO is in a more water-repelling environment likely because of the hydrophobic and fluorous core at higher R_FMA content, and thus more resistant to degradation by hydroxide ions.

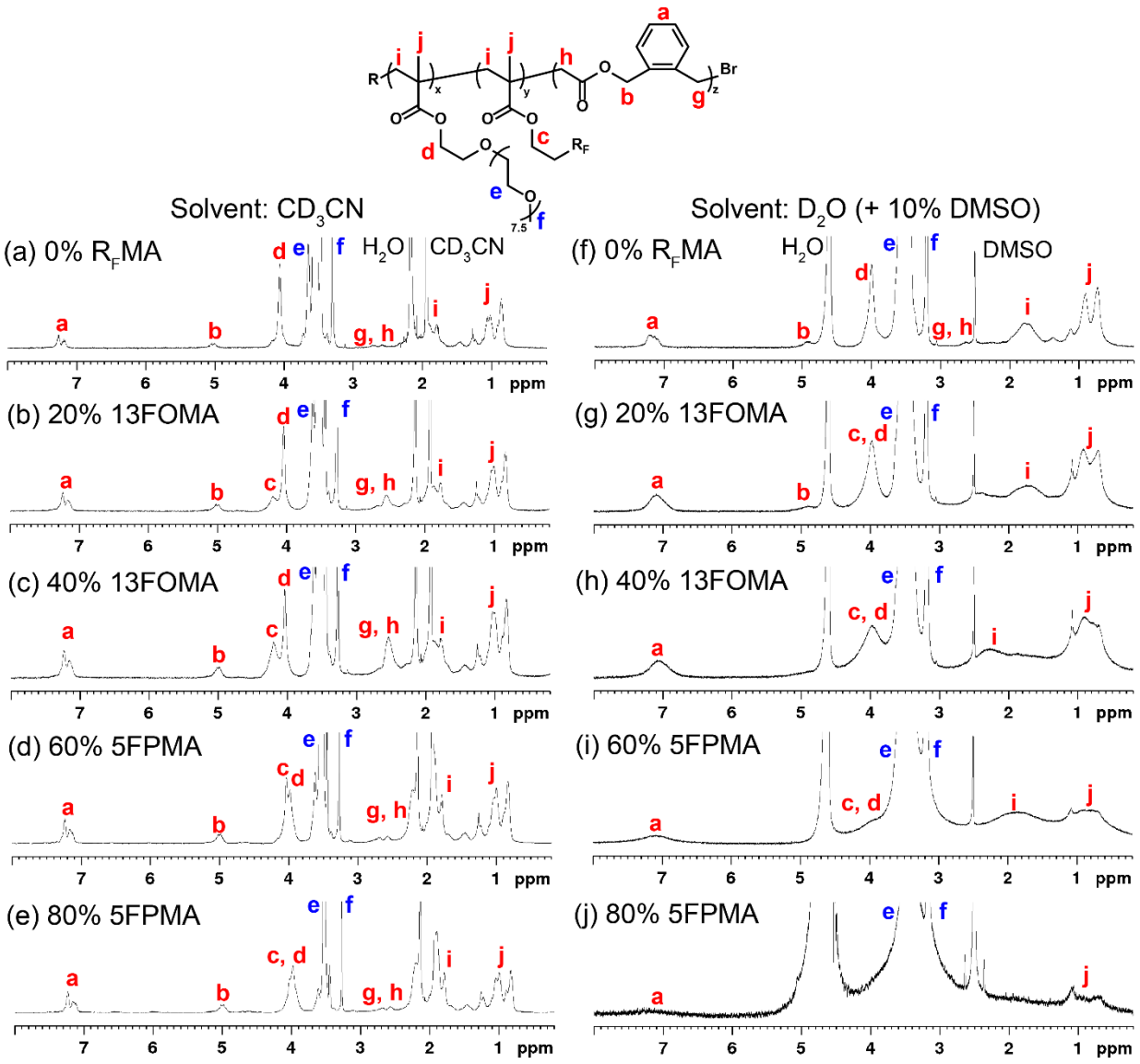

Figure 7-8. ^{1}H NMR of p(PEGMA-*co*-R_FMA-*co*-BMDO) polymers in (a-e) CD_3CN and (f-j) D_2O + 10% DMSO-d_6. Hydrophilic peaks are colored in blue and hydrophobic peaks are colored in red. Note that y-axis is enlarged at higher fluorous contents to facilitate viewing of the broadened BMDO peak.

The present study establishes the fundamental understanding of chemistry and properties of degradable fluorous polymers. We have discovered that fluorous methacrylates can modulate both the reactivity of propagating chain end to enhance the incorporation of BMDO and the

degradation kinetics by shielding BMDO within the water-repelling environment, likely provided by the self-assembly of fluorous side chains. With growing interest in the use of fluorous polymers for therapeutic and other applications, routes to various degradable fluorous polymers would be highly valuable. The knowledge on degradable polymer synthesis garnered by the polymer chemistry field in the past couple decades will undoubtedly help us make progress towards this goal. One approach would be to incorporate labile linkages such as disulfide, acetal, and orthoester within a monomer containing fluorous molecule and assemble the units by methods such as polycondensation, as done by Tang and co-workers in a recent publication.[13] Some limitations to this approach include the difficulty in controlling the size and dispersity of the polymer, and the limited functionalities available when compared to vinyl monomers. The alternative route delineated herein, which combines the metal-catalyzed radical polymerization technique with advances in degradable vinyl monomer, is attractive in that it yields polymers with controllable size, and allows the use of numerous vinyl monomers that can be easily functionalized with various side chains. The metal catalyst would be efficiently removed by various methods[58-60] prior to use in biological systems.

7.3 Conclusions

We have demonstrated that ruthenium-catalyzed living radical polymerization enables the straightforward synthesis of degradable fluorous polymers. By judicious choice of polymerization conditions, the degradable BMDO monomer can be readily incorporated into a methacrylic polymer. Co-polymerization of BMDO with hydrophilic PEGMA and fluorous methacrylate (13FOMA or 5FPMA) yields water-soluble and degradable fluorous polymers. It was found that increased electrophilicity of fluorous methacrylates help lower the SOMO-HOMO gap with

BMDO to improve the reactivity of BMDO with the methacrylates, while the fluorous/hydrophobic core of the polymers in solution provides a varying degree of protection for the BMDO towards hydrolytic degradation. Using a simulation-validated degradation model, the degradation rate was quantified to span two orders of magnitude depending on the fluorous content of the polymer. Spectroscopic data suggests that the microenvironment of unimer micelle and multi-chain micelle is responsible for the delayed BMDO hydrolysis at higher fluorous contents. Our findings provide at once a practical route to a series of degradable fluorous polymers and insight into the effect of fluorous monomers on polymer reactivity and degradation rate.

7.4 Experimental Section

Materials

Ethyl-2-chloro-2-phenylacetate (ECPA, Aldrich) and ethyl-2-bromo-2-phenylacetate (EBPA, Aldrich) were purified by distillation under reduced pressure. Ru(Ind)Cl(PPh_3)$_2$ (Aldrich) was used as received and handled in a glove box under a moisture- and oxygen-free argon atmosphere (H_2O < 1 ppm, O_2 < 1 ppm). Poly(ethylene glycol) methyl ether methacrylate (PEGMA, Aldrich, M_n = 475 (l = 8.5)) and 1H,1H,2H,2H-perfluorooctyl methacrylate (13FOMA, Wako) were purified by column chromatography charged with inhibitor remover (Aldrich) and purged by argon before use. 1*H*,1*H*,2*H*,2*H*,3*H*,3*H*-Perfluoropentyl methacrylate (5FPMA)[40] and 5,6-benzo-2-methylene-1,3-dioxepane (BMDO)[42] were synthesized as previously reported. The co-catalyst tributylamine (*n*-Bu_3N, TCI) was degassed by reduced pressure. Tetralin (TCI), used as the internal standard for calculating monomer conversion by ^{1}H NMR, was purified by drying over calcium chloride overnight and distilling from calcium hydride. Toluene (Kishida Chemical) was purified by passing through a purification column (Glass Contour Solvent Systems by SG

Water, USA) and sparged with nitrogen gas. The control polymer p(PEGMA-*co*-13FOMA) (PEGMA:13FOMA = 60:40, M_n = 50.9 kDa, $Đ$ = 1.18 by DMF SEC) was prepared using a previously reported procedure.[17]

Analytical Techniques

NMR spectra were recorded on a Bruker AV 400 MHz, a Bruker DRX 500 MHz, or a JEOL JNM-ECA500 spectrometer with a relaxation delay of 10 s. Size exclusion chromatography (SEC) for polymer characterization was conducted in *N*,*N*-dimethylformamide (DMF) containing 10 mM lithium bromide (flow rate: 1 mL/min) on three linear-type polystyrene gel columns (Shodex KF-805L) connected to a Jasco PU-2080 precision pump, a Jasco RI-2031 refractive index detector, and a Jasco UV-2075 UV/vis detector set at 270 nm. SEC for polymer degradation was conducted on a Shimadzu HPLC system equipped with a refractive index detector RID-10A and two Polymer Laboratories PLgel 5 μm mixed D columns (with guard column). Lithium bromide (0.1 M) in DMF at 50 °C was used as the eluent (flow rate: 0.8 mL/min). Near-monodisperse poly(methyl methacrylate) standards (Polymer Laboratories) were employed for the calibration of both systems. Dynamic light scattering (DLS) measurements were conducted on a Malvern ZetaSizer Nano, and intensity size distribution is reported. Infrared (IR) spectra were acquired on a Perkin-Elmer Spectrum One instrument equipped with a universal ATR assembly.

Synthesis of Polymers

Representative Procedure: Co-polymerization of PEGMA, 13FOMA, and BMDO (PEGMA:13FOMA = 80:20). Inside a glove box, $Ru(Ind)Cl(PPh_3)_2$ was weighed out into a Schlenk flask equipped with three-way stopcock, and toluene was added to the flask under argon

to make 2.05 mg/mL concentration of the catalyst. In a separate Schlenk flask equipped with a magnetic stir bar, BMDO (100 mg, 6.2×10^{-1} mmol) was added. To this flask, the ruthenium catalyst stock solution (1.75 mL, 4.62×10^{-3} mmol catalyst), PEGMA (325 μL, 7.39×10^{-1} mmol), 13FOMA (55 μL, 1.9×10^{-1} mmol), 287 mM toluene solution of EBPA (32 μL, 9.2×10^{-3} mmol), tetralin (35 μL, 2.6×10^{-1} mmol), and 400 mM toluene solution of *n*-Bu_3N (115 μL, 4.6×10^{-2} mmol) were added under argon (total volume: 2.31 mL). This corresponds to the following reagent concentrations: [PEGMA] / [13FOMA] / [BMDO] / [EBPA] / [$Ru(Ind)Cl(PPh_3)_2$] / [*n*-Bu_3N] = 320 / 82 / 267 / 4 / 2 / 20 mM. The flask was immersed in an oil bath maintained at 80 °C over a magnetic stirrer, and approximately 50 μL aliquots were taken to measure monomer conversion. After 31.5 h, the polymerization was terminated by cooling the mixture to -78 °C and exposing it to air (PEGMA conversion 75%, 13FOMA conversion 80%, BMDO conversion 18% by ^1H NMR). The polymer was purified by dialysis in a regenerated cellulose membrane (Spectra/Por® 3, MWCO 3.5 kDa) in DMF for 2 days followed by solvent exchange to water for 2 days, and water was removed by lyophilization. Percent BMDO incorporated was calculated using ^1H NMR spectrum integrations of the characteristic benzyl/ester CH_2 peak at approximately 5.0 ppm and the PEGMA CH_3 peak around 3.3 ppm. ^1H NMR (500 MHz in CD_3CN) δ: 7.57–7.02, 5.31–4.86, 4.42–3.84, 3.81–3.36, 3.35–3.20, 2.80–2.38, 2.38–1.61, 1.54–0.70 ppm. ^{19}F NMR (400 MHz in CD_3CN with TFA at δ = -76.5 ppm as an internal standard) δ: -80.8–81.5, -112.9–113.8, -121.6–122.2, -122.6–123.2, -123.4–124.0, -125.9–126.6 ppm. IR: δ = 2865.82, 1726.96, 1651.12, 1451.40, 1347.75, 1254.21, 1239.04, 1094.94, 1024.15, 948.31, 852.24, 799.15, 748.59, 695.50 cm^{-1}. M_n = 22.6 kDa, $Đ$ = 1.46 (DMF SEC).

p(PEGMA-*co*-13FOMA-*co*-BMDO), PEGMA:13FOMA = 60:40

Polymerization was conducted as in the representative procedure above, with the following reagent concentrations: [PEGMA] / [13FOMA] / [BMDO] / [EBPA] / [Ru(Ind)Cl(PPh_3)$_2$] / [*n*-Bu_3N] = 241 / 159 / 266 / 4 / 2 / 20 mM. Polymerization was terminated after 47.5 h. ^{1}H NMR (500 MHz in CD_3CN) δ: 7.53–6.99, 5.29–4.88, 4.43–3.83, 3.83–3.36, 3.36–3.20, 2.83–2.36, 2.36–1.60, 1.55–0.68 ppm. ^{19}F NMR (400 MHz in CD_3CN with TFA at δ = -76.5 ppm as an internal standard) δ: -80.9–81.9, -113.0–114.0, -121.7–122.5, -122.8–123.5, -123.5–124.2, -126.1–126.8 ppm. IR: δ = 2865.82, 1729.49, 1451.40, 1350.28, 1236.51, 1196.06, 1140.44, 1097.47, 1021.62, 950.84, 844.66, 801.68, 746.06, 733.42, 708.14, 695.50 cm^{-1}. M_n = 21.3 kDa, $Đ$ = 1.50 (DMF SEC).

p(PEGMA-*co*-13FOMA-*co*-BMDO), PEGMA:13FOMA = 40:60

Polymerization was conducted as in the representative procedure above, with the following reagent concentrations: [PEGMA] / [13FOMA] / [BMDO] / [EBPA] / [Ru(Ind)Cl(PPh_3)$_2$] / [*n*-Bu_3N] = 163 / 240 / 267 / 4 / 2 / 20 mM. Polymerization was terminated after 52 h. ^{1}H NMR (500 MHz in CD_3CN) δ: 7.59–6.96, 5.27–4.83, 4.47–3.82, 3.82–3.35, 3.35–3.18, 2.83–2.24, 2.24–1.61, 1.61–0.66 ppm. ^{19}F NMR (400 MHz in CD_3CN with TFA at δ = -76.5 ppm as an internal standard) δ: -81.2–82.0, -113.8–114.8, -122.2–122.9, -123.2–123.9, -123.9–124.7, -126.5–127.2 ppm. IR: δ = 3002.53, 2870.88, 1729.49, 1453.93, 1350.28, 1233.98, 1191.01, 1140.44, 1120.22, 1100.00, 1024.15, 950.84, 844.66, 801.68, 748.59, 705.61, 695.50 cm^{-1}. M_n and $Đ$ were unable to be measured due to low *dn/dc*.

p(PEGMA-*co*-5FPMA-*co*-BMDO), PEGMA:5FPMA = 40:60

Polymerization was conducted as in the representative procedure above, with the following reagent concentrations: [PEGMA] / [5FPMA] / [BMDO] / [EBPA] / [Ru(Ind)Cl(PPh_3)$_2$] / [*n*-Bu_3N] = 197 / 291 / 334 / 5 / 2.5 / 25 mM. Polymerization was terminated after 24 h. ^{1}H NMR (500 MHz in

CD_3CN) δ: 7.52–7.01, 5.26–4.86, 4.30–3.82, 3.75–3.35, 3.35–3.21, 2.90–2.47, 2.47–1.61, 1.61–0.66 ppm. ^{19}F NMR (400 MHz in CD_3CN with TFA at δ = -76.5 ppm as an internal standard) δ: -85.4–86.1, -117.9–118.6 ppm. IR: δ = 2951.89, 2870.88, 1726.96, 1451.40, 1388.20, 1347.75, 1259.26, 1239.04, 1191.01, 1092.41, 1016.57, 1001.40, 945.78, 854.77, 801.68, 756.17, 715.73 cm^{-1}. M_n = 20.0 kDa, $Đ$ = 1.37 (DMF SEC).

p(PEGMA-*co*-5FPMA-*co*-BMDO), PEGMA:5FPMA = 20:80

Polymerization was conducted as in the representative procedure above, with the following reagent concentrations: [PEGMA] / [5FPMA] / [BMDO] / [EBPA] / [Ru(Ind)Cl(PPh_3)$_2$] / [*n*-Bu_3N] = 100 / 398 / 332 / 5 / 2.5 / 25 mM. Polymerization was terminated after 24 h. ^1H NMR (500 MHz in CD_3CN) δ: 7.55–7.01, 5.28–4.81, 4.26–3.82, 3.72–3.35, 3.35–3.21, 2.89–2.47, 2.47–1.59, 1.59–0.64 ppm. ^{19}F NMR (400 MHz in CD_3CN with TFA at δ = -76.5 ppm as an internal standard) δ: -85.5–86.2, -118.0–118.6 ppm. IR: δ = 2956.96, 2875.94, 1726.96, 1471.62, 1451.40, 1388.20, 1347.75, 1314.88, 1259.26, 1236.51, 1191.01, 1135.39, 1092.41, 1016.57, 998.87, 862.35, 799.15, 753.65, 715.73 cm^{-1}. M_n = 16.8 kDa, $Đ$ = 1.34 (DMF SEC).

p(PEGMA-*co*-BMDO), PEGMA:BMDO = 80:20, ECPA initiated

Polymerization was conducted as in the representative procedure above, with the following reagent concentrations: [PEGMA] / [BMDO] / [ECPA] / [Ru(Ind)Cl(PPh_3)$_2$] / [*n*-Bu_3N] = 402 / 100 / 4 / 2 / 20 mM. Polymerization was terminated after 24 h. ^1H NMR (500 MHz in CD_3CN) δ: 7.40–7.10, 5.12–4.95, 4.23–3.93, 3.79–3.35, 3.35–3.24, 1.92–1.65, 1.56–0.69 ppm. IR: δ = 2870.88, 1729.49, 1474.15, 1451.40, 1347.75, 1249.15, 1110.11, 1036.79, 948.31, 852.24 cm^{-1}. M_n = 34.1 kDa, $Đ$ = 1.43 (DMF SEC).

p(PEGMA-*co*-BMDO), PEGMA:BMDO = 60:40, ECPA initiated

Polymerization was conducted as in the representative procedure above, with the following reagent concentrations: [PEGMA] / [BMDO] / [ECPA] / [Ru(Ind)Cl(PPh_3)$_2$] / [*n*-Bu_3N] = 304 / 202 / 4 / 2 / 20 mM. Polymerization was terminated after 48 h. ^{1}H NMR (500 MHz in CD_3CN) δ: 7.48–7.10, 5.19–4.93, 4.27–3.89, 3.80–3.34, 3.34–3.22, 2.81–2.53, 1.91–1.65, 1.56–0.74 ppm. IR: δ = 2865.82, 1726.96, 1453.93, 1347.75, 1289.60, 1249.15, 1107.58, 1036.79, 991.29, 948.31, 854.77, 748.59 cm^{-1}. M_n = 28.4 kDa, $Đ$ = 1.66 (DMF SEC).

p(PEGMA-*co*-BMDO), PEGMA:BMDO = 40:60, ECPA initiated

Polymerization was conducted as in the representative procedure above, with the following reagent concentrations: [PEGMA] / [BMDO] / [ECPA] / [Ru(Ind)Cl(PPh_3)$_2$] / [*n*-Bu_3N] = 204 / 302 / 4 / 2 / 20 mM. Polymerization was terminated after 86 h. ^{1}H NMR (500 MHz in CD_3CN) δ: 7.46–7.04, 5.22–4.91, 4.27–3.89, 3.78–3.34, 3.34–3.23, 2.99–2.51, 1.90–1.65, 1.59–0.76 ppm. IR: δ = 2865.82, 1726.96, 1451.40, 1347.75, 1287.07, 1246.62, 1097.47, 1034.26, 993.82, 945.78, 852.24, 758.70 cm^{-1}. M_n = 17.9 kDa, $Đ$ = 1.61 (DMF SEC).

p(PEGMA-*co*-BMDO), PEGMA:BMDO = 80:20, EBPA initiated

Polymerization was conducted as in the representative procedure above, with the following reagent concentrations: [PEGMA] / [BMDO] / [EBPA] / [Ru(Ind)Cl(PPh_3)$_2$] / [*n*-Bu_3N] = 400 / 100 / 4 / 2 / 20 mM. Polymerization was terminated after 18 h. ^{1}H NMR (500 MHz in CD_3CN) δ: 7.50–7.09, 5.20–4.89, 4.30–3.93, 3.79–3.35, 3.35–3.22, 1.90–1.68, 1.56–0.72 ppm. IR: δ = 2865.82, 1726.96, 1641.01, 1453.93, 137.75, 1244.10, 1100.00, 1036.79, 993.82, 945.78, 917.97, 852.24, 748.59 cm^{-1}. M_n = 21.6 kDa, $Đ$ = 1.53 (DMF SEC).

p(PEGMA-*co*-BMDO), PEGMA:BMDO = 60:40, EBPA initiated

Polymerization was conducted as in the representative procedure above, with the following reagent concentrations: [PEGMA] / [BMDO] / [EBPA] / [Ru(Ind)Cl(PPh_3)$_2$] / [*n*-Bu_3N] = 400 / 267 / 4 / 2 / 20 mM. Polymerization was terminated after 23 h. ^{1}H NMR (500 MHz in CD_3CN) δ: 7.36–7.07, 5.23–4.88, 4.28–3.92, 3.80–3.35, 3.35–3.21, 2.79–2.51, 1.91–1.72, 1.54–0.73 ppm. IR: δ = 2865.82, 1726.96, 1643.53, 1453.93, 1385.67, 1347.75, 1325.00, 1282.02, 1246.62, 1097.47, 1034.26, 993.82, 945.78, 852.24, 751.12 cm^{-1}. M_n = 26.0 kDa, $Đ$ = 1.60 (DMF SEC).

p(PEGMA-*co*-BMDO), PEGMA:BMDO = 40:60, EBPA initiated

Polymerization was conducted as in the representative procedure above, with the following reagent concentrations: [PEGMA] / [BMDO] / [EBPA] / [Ru(Ind)Cl(PPh_3)$_2$] / [*n*-Bu_3N] = 400 / 600 / 4 / 2 / 20 mM. Polymerization was terminated after 34 h. ^{1}H NMR (500 MHz in CD_3CN) δ: 7.46–7.10, 5.18–4.90, 4.26–3.88, 3.79–3.34, 3.34–3.20, 2.87–2.27, 1.88–1.64, 1.57–0.78 ppm. IR: δ = 2865.82, 1726.96, 1641.01, 1453.93, 1385.67, 1347.75, 1325.00, 1284.55, 1246.62, 1094.94, 1034.26, 991.29, 945.78, 852.24, 758.70 cm^{-1}. M_n = 19.0 kDa, $Đ$ = 1.54 (DMF SEC).

Degradation of Fluorous Polymers

Polymer was weighed into a dram vial and then dissolved in aqueous solution containing 10% DMSO and 4.5% KOH to make the final polymer concentration of 1 mg/mL for the most fluorous 20:80 PEGMA:5FPMA polymer (Table 7-1, entry 6) for dissolution or 5 mg/mL for all other polymers. At pre-determined time points (0.25, 0.5, 1, 2, 4, and 24 h), 2 mL was taken out for the most fluorous polymer and 0.4 mL was taken out for all others. Hydrolysis was quenched by approximately 15 drops (for 2 mL aliquot) or 3 drops (for 0.4 mL aliquot) of acetic acid, and the polymer was extracted with 10 mL brine and 5 mL THF (for the 2:8 PEGMA:5FPMA polymer)

or 2 mL brine and 2 mL THF (for all others), and aqueous layer was extracted two more times with THF. The combined organic fractions were dried *in vacuo*, dissolved in 55 uL of DMF, filtered with 0.45 μm PTFE filter, and analyzed by DMF SEC.

Model for Degradation Kinetics

For each polymer chain, *n* degradation events from BMDO hydrolysis leads to *n* + 1 chain fragments (Experimental Section Figure 7-22). Therefore, the number-average molecular weight for degraded chain fragments from a single polymer chain can be expressed as the following.

$$M_{\mathrm{n}}(\mathrm{degraded}) = \frac{M_{\mathrm{n}}(\mathrm{original})}{(n+1)}$$

This expression relates the molecular weight data observable by SEC to the number of BMDO units that have degraded (*n*) at each time point. The equation can be rearranged as

$$n = \frac{M_{\mathrm{n}}(\mathrm{original})}{M_{\mathrm{n}}(\mathrm{degraded})} - 1 \qquad \text{Eq. 1}$$

To validate the equation for an ensemble of polymers, Monte Carlo simulation was used to first generate 1000 polymer chains using the reported reactivity ratios of MMA and BMDO,[35] and then the chains were degraded. The simulation provided both the "true value" for *n*, and the M_{n} of degrading polymer ensemble at each time point that could be used with Eq. 1 to calculate *n*. The true value and the calculated value were compared to validate the equation. The true value and calculated value agreed very closely and their difference was less than 0.9% for all iterations (Experimental Section Figure 7-27), thereby validating Eq. 1. Flowcharts of the simulation are given in Experimental Section Figure 7-23 through Figure 7-25, and the simulation codes written in R[61] using pracma package[61] are included below.

Calculation of Asymmetry Factor (A_s)[50-52]

From the SEC trace, the time for the peak to increase from 10% intensity to maximum intensity was defined as *a*, and the time for the peak to decrease from maximum intensity back down to 10% intensity was defined as *b*. The asymmetry factor was given as the ratio of *b* to *a* ($A_s = b/a$). Refer to Figure 7-2 for the graphical representation of the calculation.

Figures and Tables

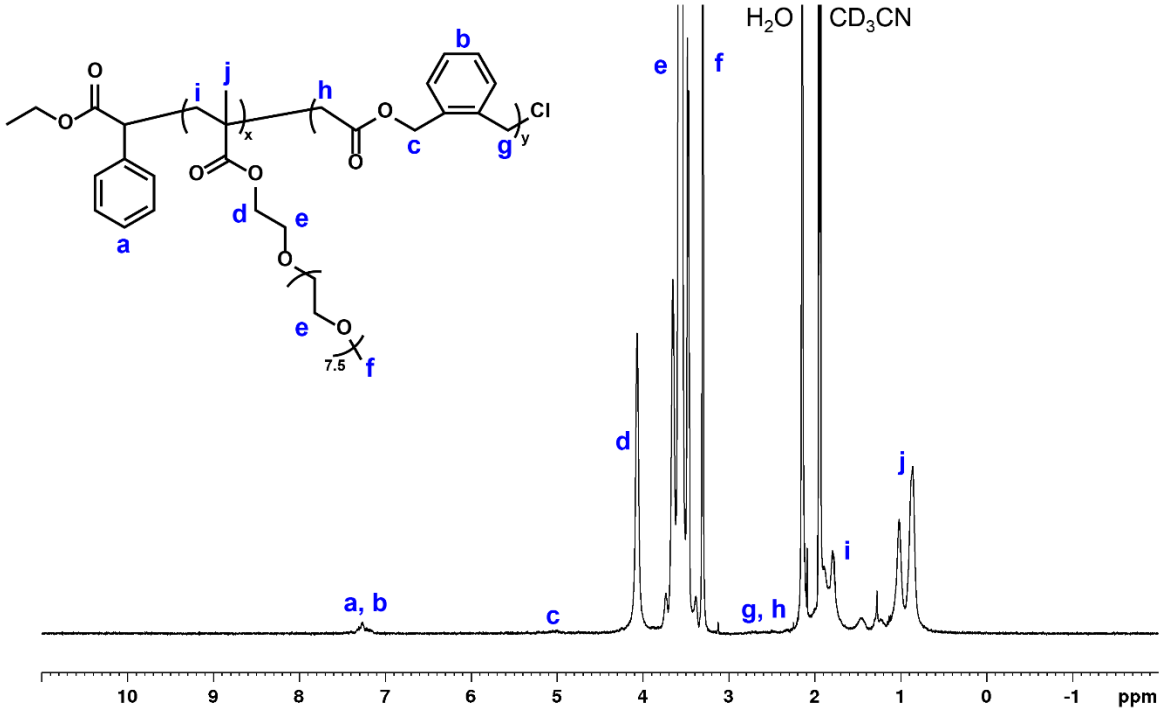

Figure 7-9. ^{1}H NMR spectrum of p(PEGMA-*co*-BMDO) synthesized with chloride initiator at PEGMA:BMDO = 80:20 (CD_3CN).

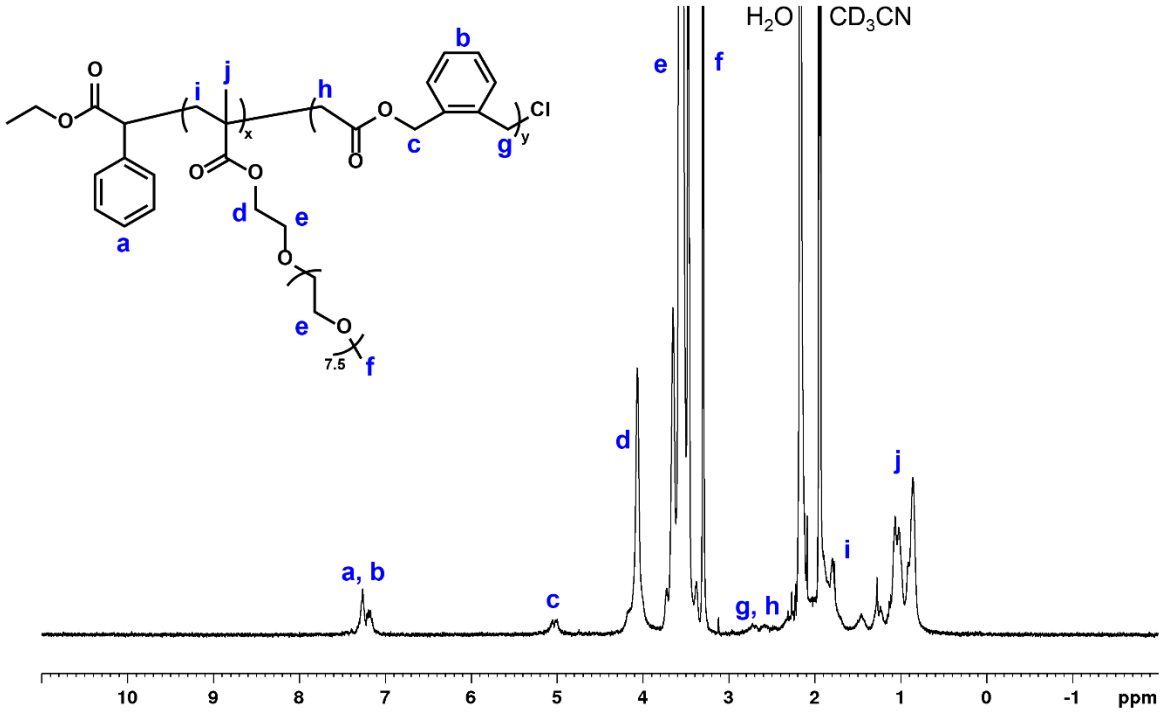

Figure 7-10. ^{1}H NMR spectrum of p(PEGMA-*co*-BMDO) synthesized with chloride initiator at PEGMA:BMDO = 60:40 (CD_3CN).

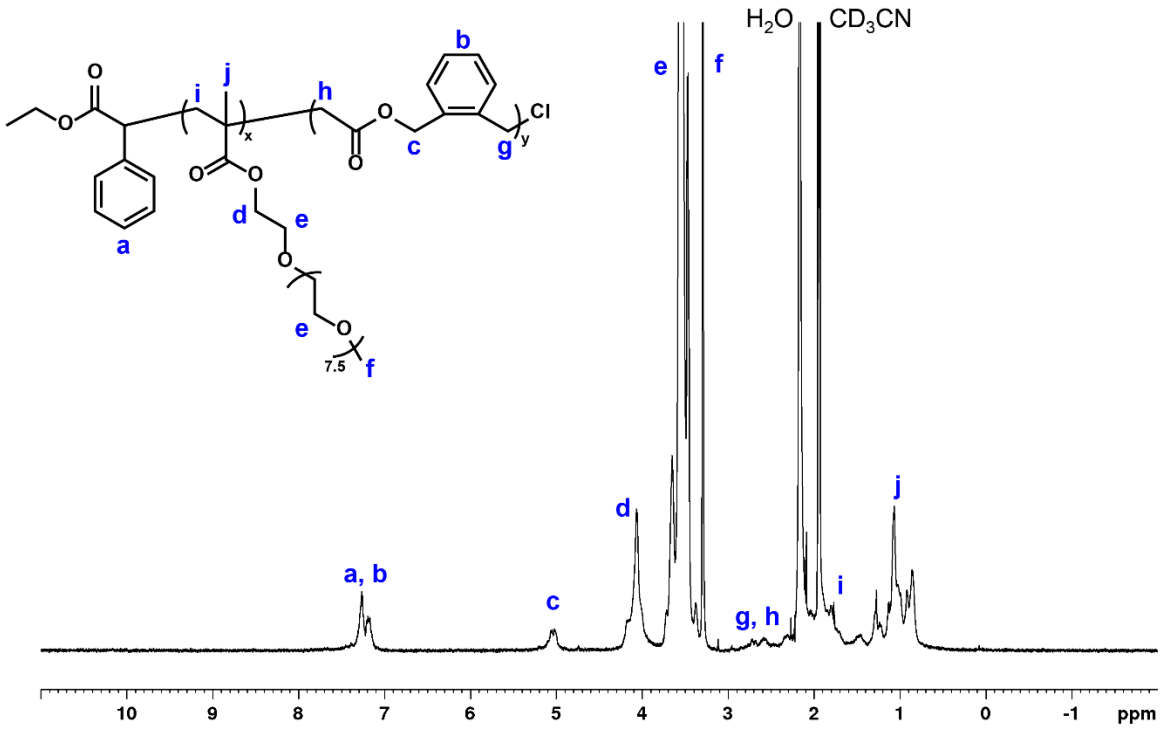

Figure 7-11. ^{1}H NMR spectrum of p(PEGMA-*co*-BMDO) synthesized with chloride initiator at PEGMA:BMDO = 40:60 (CD_3CN).

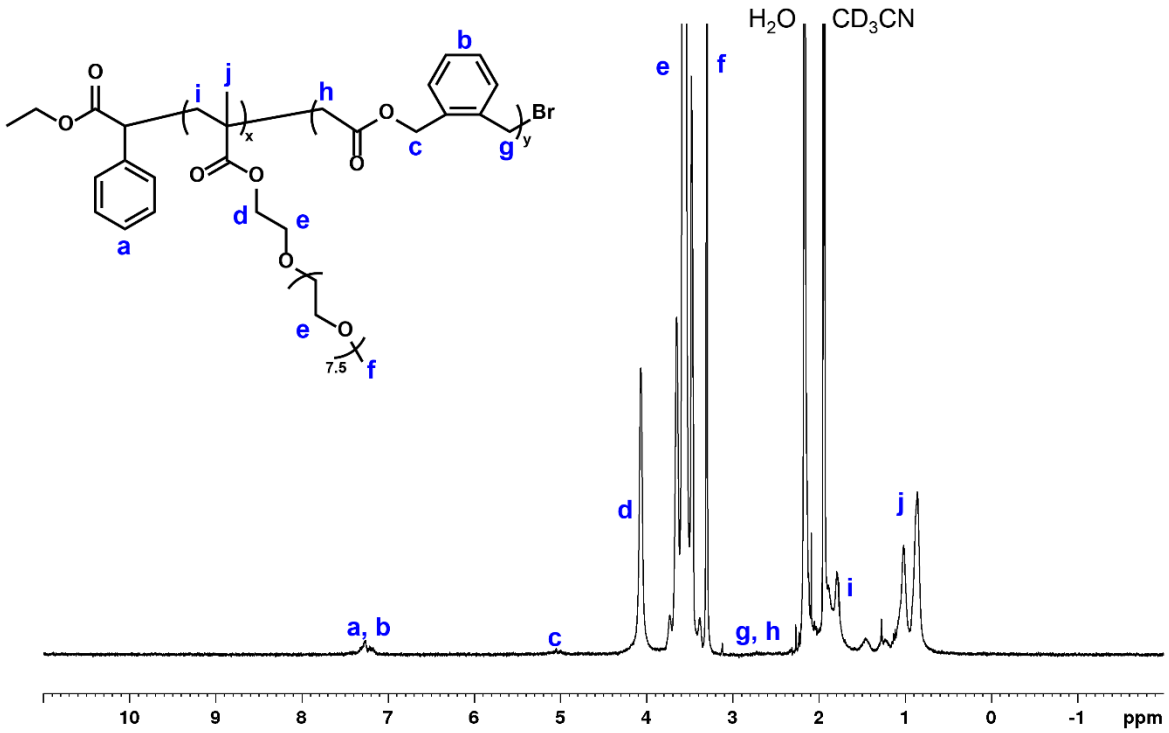

Figure 7-12. ^{1}H NMR spectrum of p(PEGMA-*co*-BMDO) synthesized with bromide initiator at PEGMA:BMDO = 80:20 (CD_3CN).

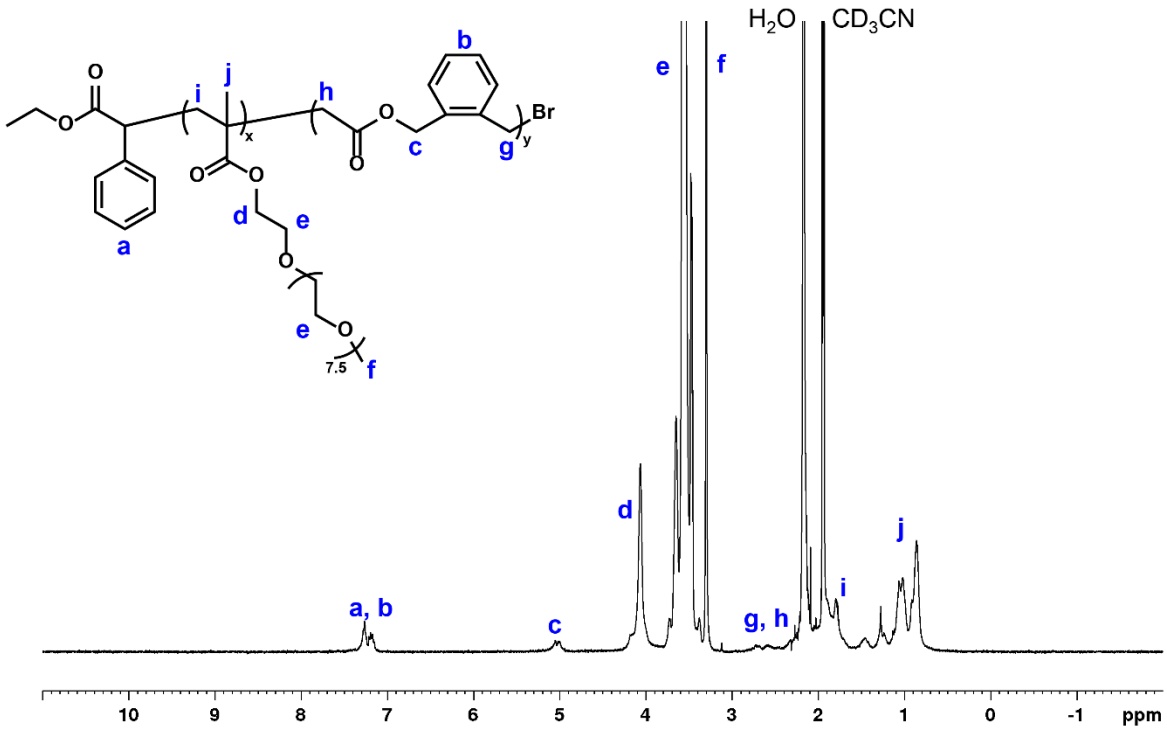

Figure 7-13. ^{1}H NMR spectrum of p(PEGMA-*co*-BMDO) synthesized with bromide initiator at PEGMA:BMDO = 60:40 (CD_3CN).

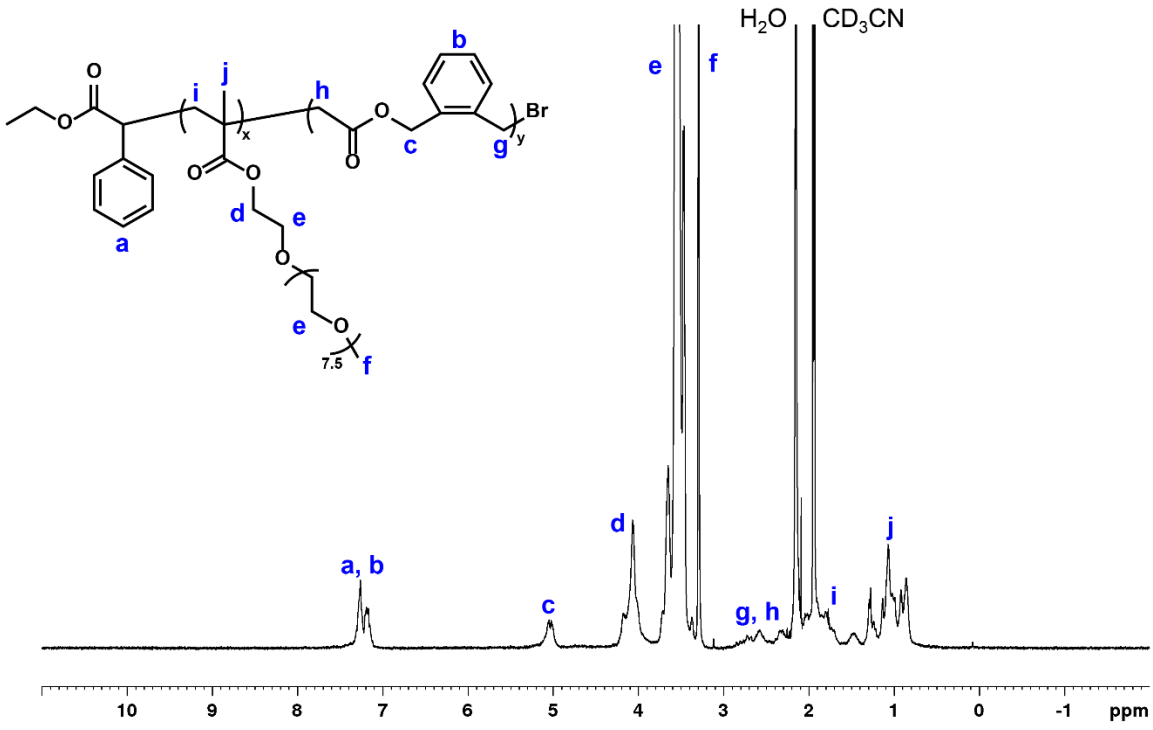

Figure 7-14. ^{1}H NMR spectrum of p(PEGMA-*co*-BMDO) synthesized with bromide initiator at PEGMA:BMDO = 40:60 (CD_3CN).

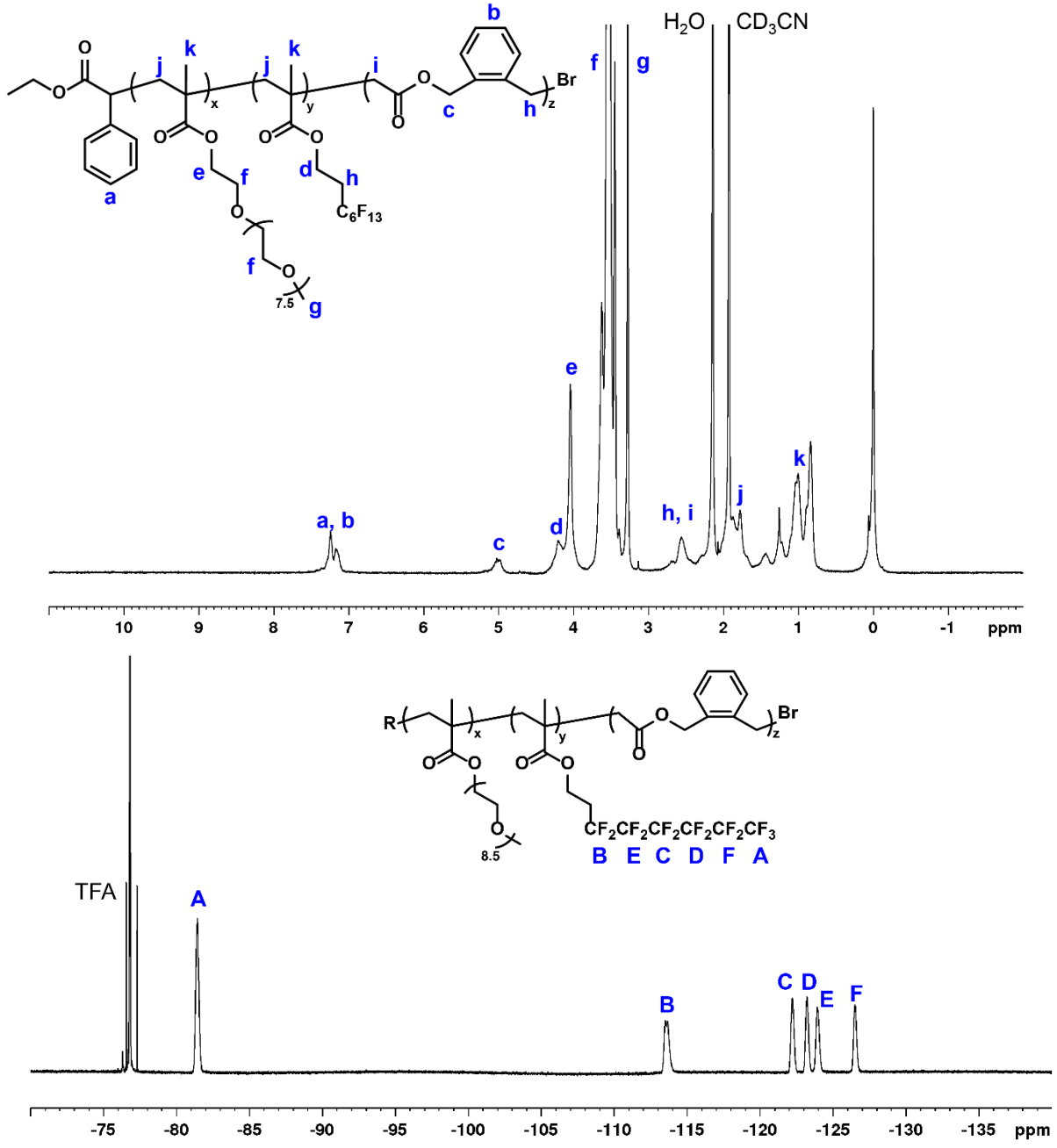

Figure 7-15. ^{1}H (top) and ^{19}F (bottom) NMR spectra of p(PEGMA-*co*-13FOMA-*co*-BMDO) (PEGMA:13FOMA = 8:2, methacrylate:BMDO = 6:4) (CD_3CN for ^{1}H, $CDCl_3$ with TFA capillary for ^{19}F).

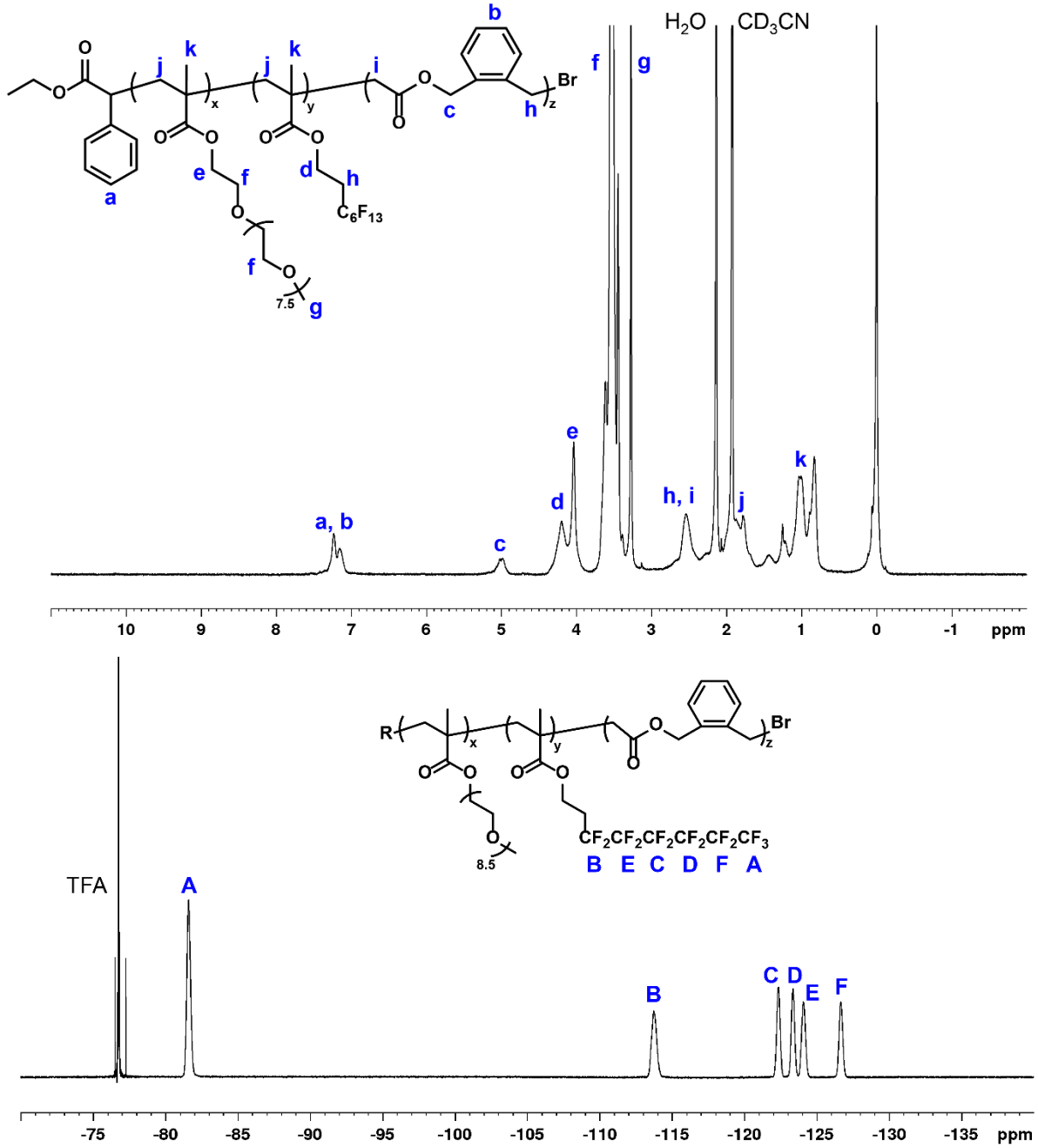

Figure 7-16. ^{1}H (top) and ^{19}F (bottom) NMR spectra of p(PEGMA-*co*-13FOMA-*co*-BMDO) (PEGMA:13FOMA = 6:4, methacrylate:BMDO = 6:4) (CD_3CN for ^{1}H, $CDCl_3$ with TFA capillary for ^{19}F).

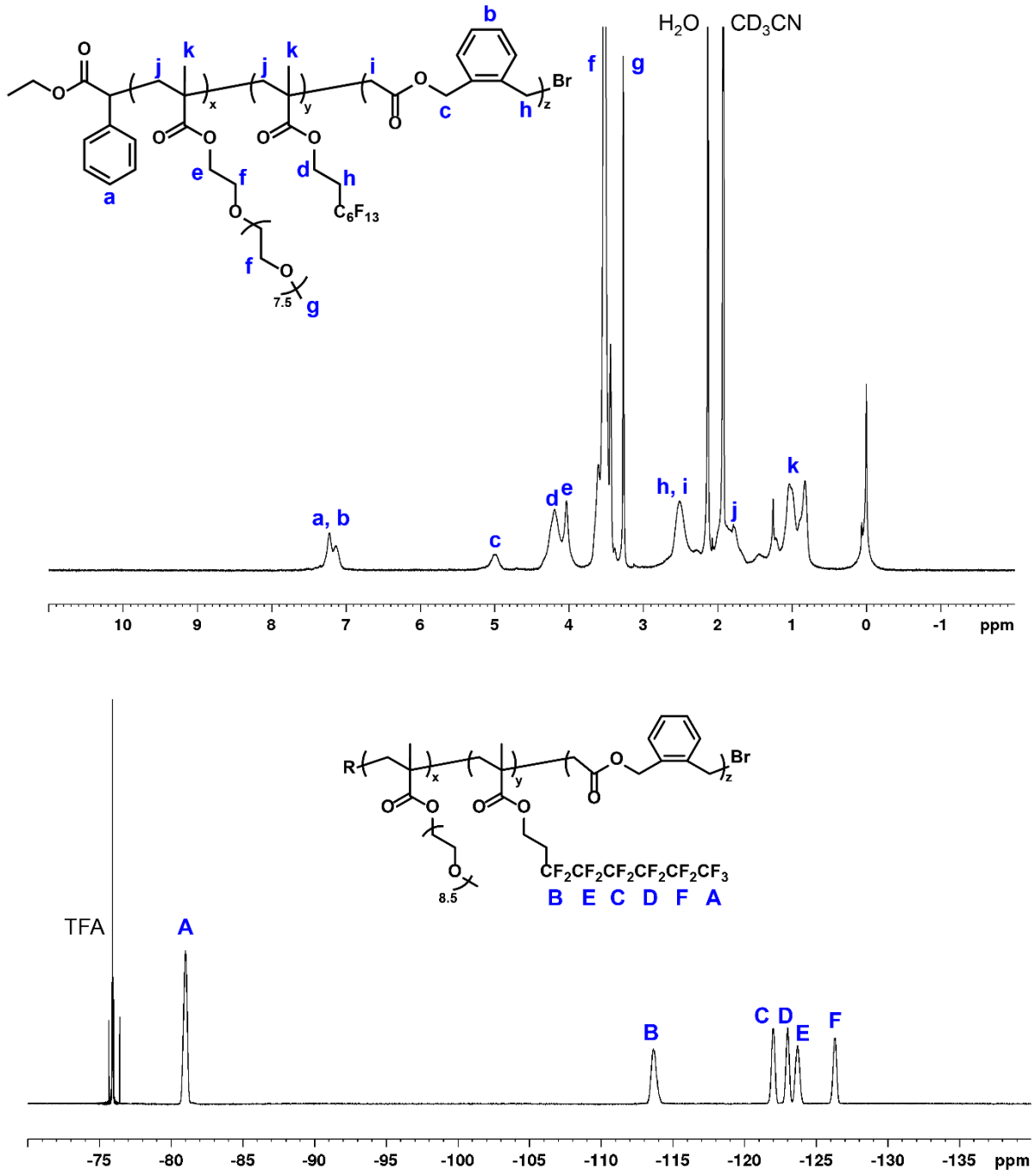

Figure 7-17. ^{1}H (top) and ^{19}F (bottom) NMR spectrum of p(PEGMA-*co*-13FOMA-*co*-BMDO) (PEGMA:13FOMA = 4:6, methacrylate:BMDO = 6:4) (CD_3CN for ^{1}H, $CDCl_3$ with TFA capillary for ^{19}F).

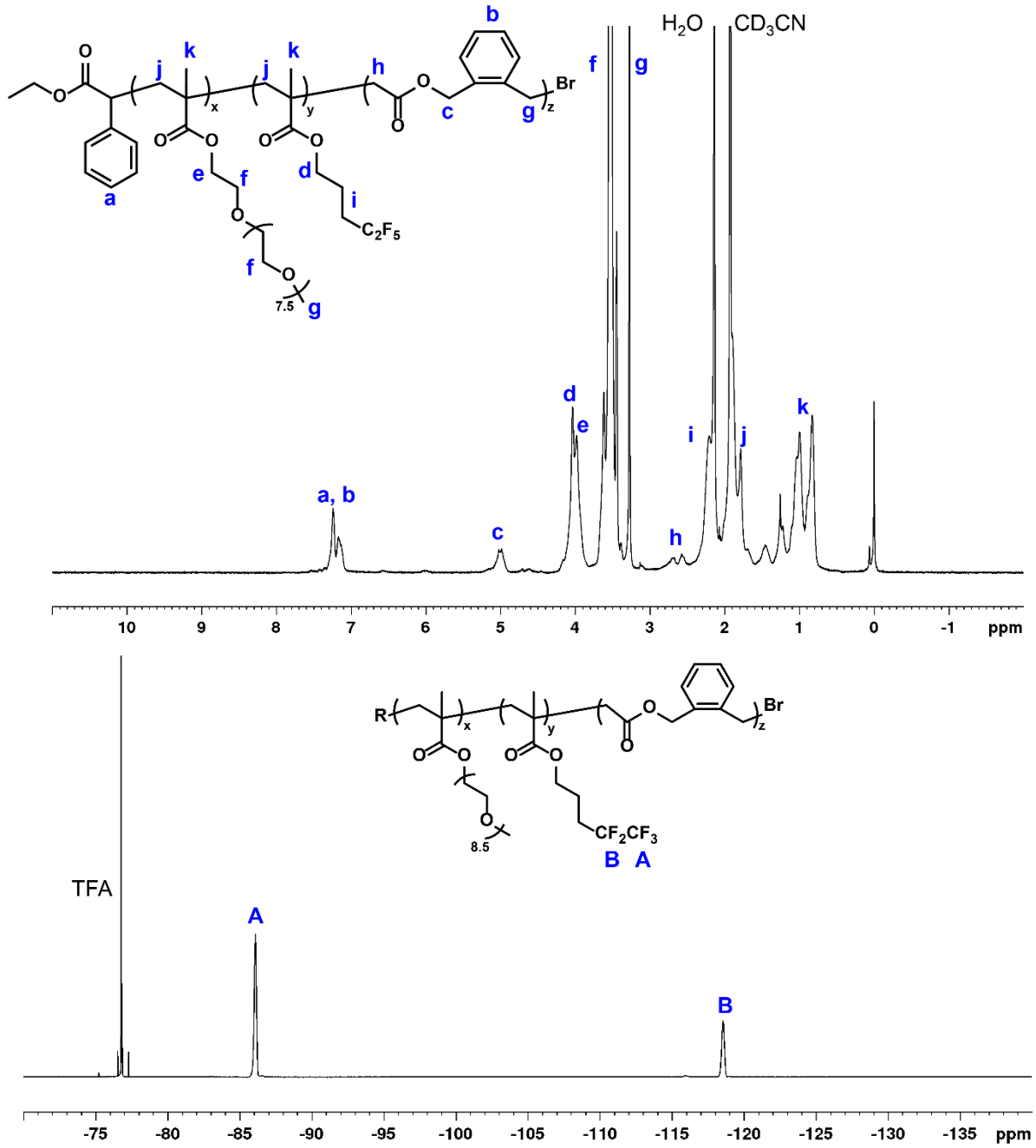

Figure 7-18. ^{1}H (top) and ^{19}F (bottom) NMR spectra of p(PEGMA-*co*-5FPMA-*co*-BMDO) (PEGMA:5FPMA = 4:6, methacrylate:BMDO = 6:4) (CD_3CN for ^{1}H, $CDCl_3$ with TFA capillary for ^{19}F).

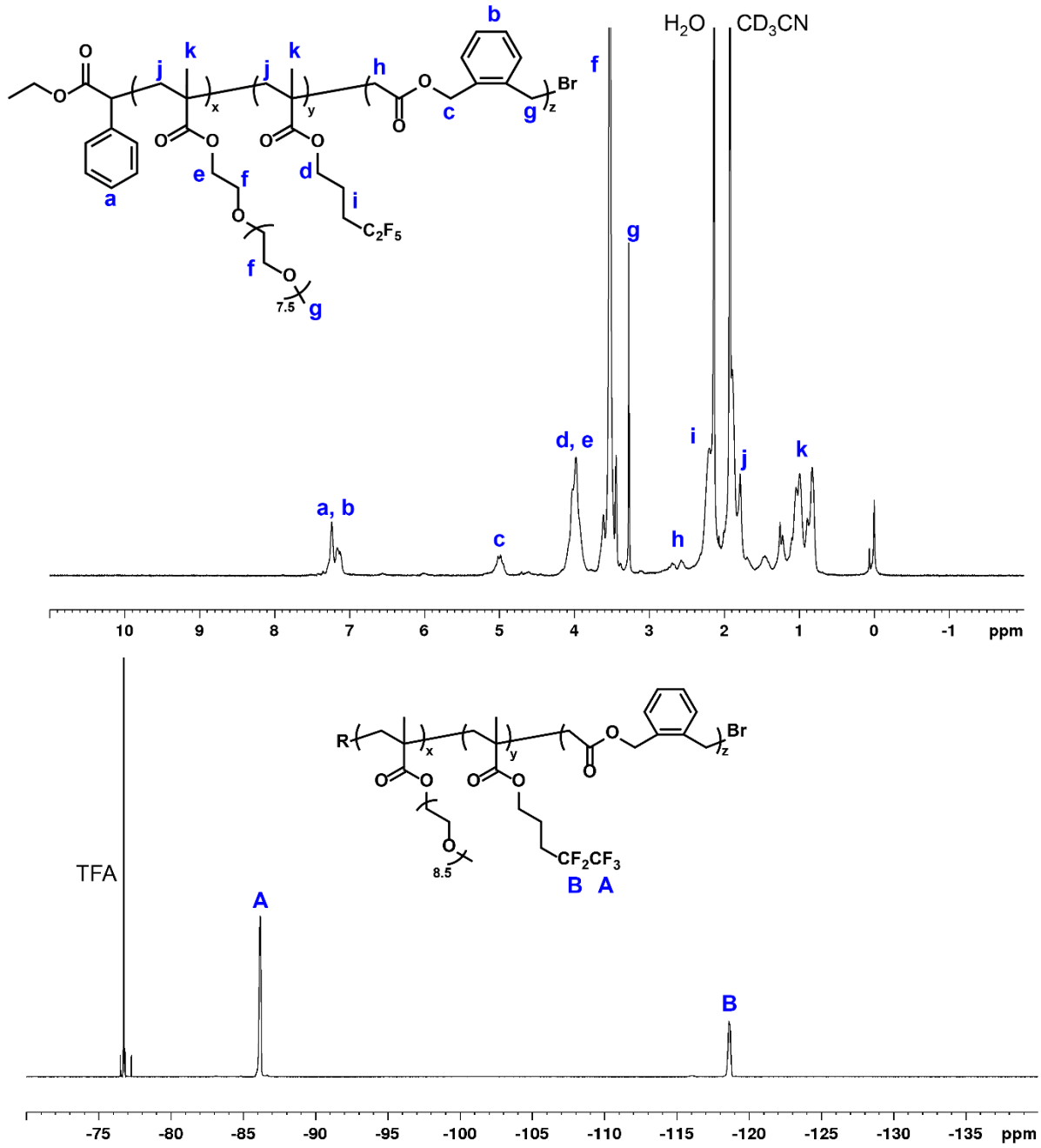

Figure 7-19. ^{1}H (top) and ^{19}F (bottom) NMR spectra of p(PEGMA-*co*-5FPMA-*co*-BMDO) (PEGMA:5FPMA = 2:8, methacrylate:BMDO = 6:4) (CD_3CN for ^{1}H, $CDCl_3$ with TFA capillary for ^{19}F).

Table 7-4. Percent BMDO incorporated in p(PEGMA-*co*-BMDO) polymers synthesized with chloride or bromide initiator.

Entry	Initiator	PEGMA:BMDO	% BMDO
1		80:20	3.1
2	ECPA (Cl)	60:40	9.4
3		40:60	14.8
4		80:20	3.6
5	EBPA (Br)	60:40	8.6
6		40:60	19.4

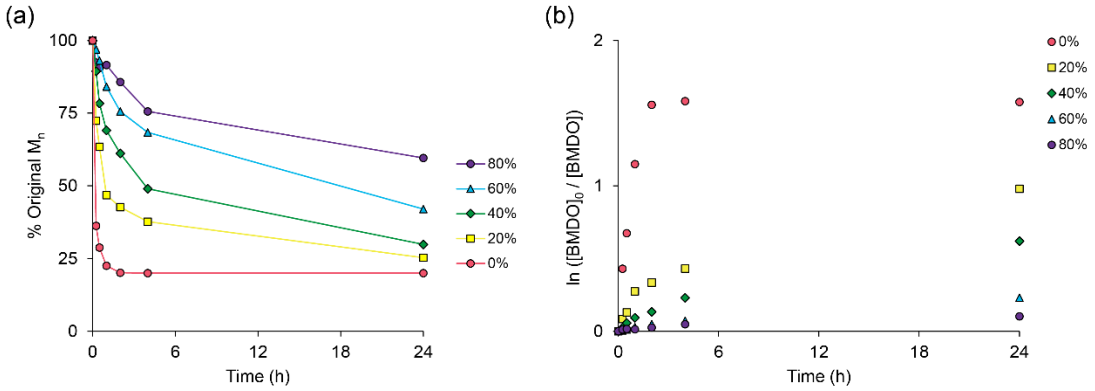

Figure 7-20. Extended degradation kinetics of p(PEGMA-*co*-R_FMA-*co*-BMDO) polymers. (a) Percent molecular weight over time and (b) pseudo-first order reaction kinetics of BMDO unit over time.

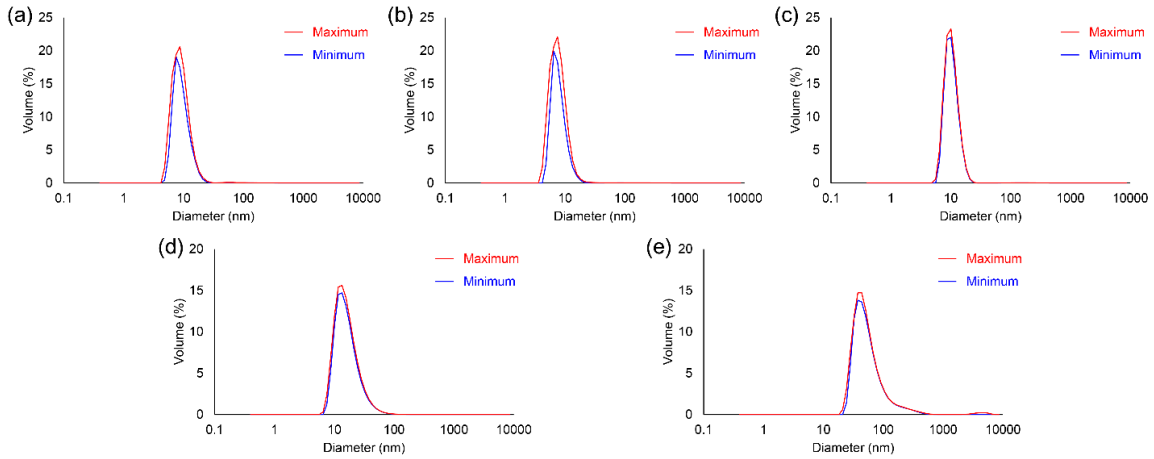

Figure 7-21. DLS volume distribution in water + 10 % DMSO with maximum (red) and minimum (blue) values from independent sample repeats (n = 3). (a) 0% R_FMA (d = 9.2 nm), (b) 20% 13FOMA (d = 8.2 nm), (c) 40% 13FOMA (d = 10.6 nm), (d) 60% 5FPMA (d = 17.6 nm), and (e) 80% 5FPMA (d = 63.6 nm).

Simulation of Polymer Degradation

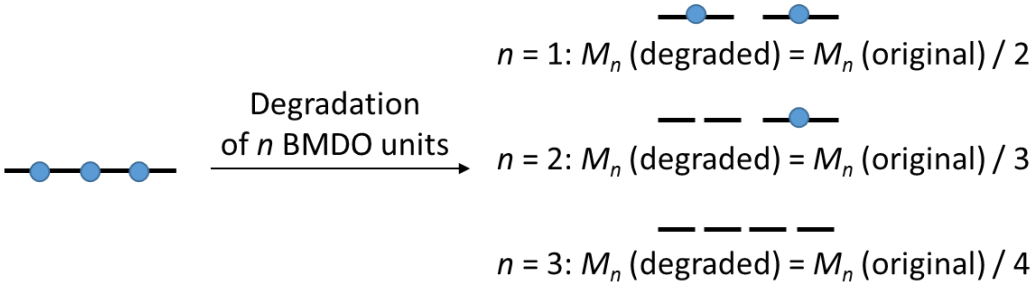

Figure 7-22. Schematic representation of the relationship between the number of degraded BMDO units and the polymer number-average molecular weight.

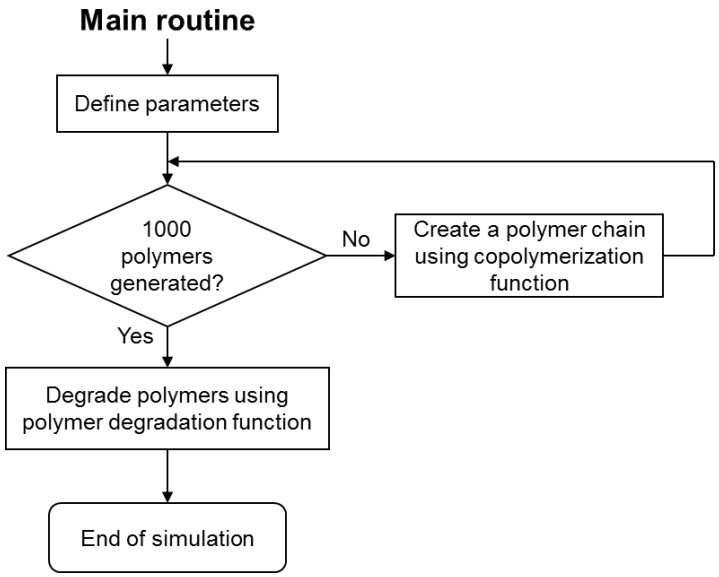

Figure 7-23. Flowchart for the simulation main routine.

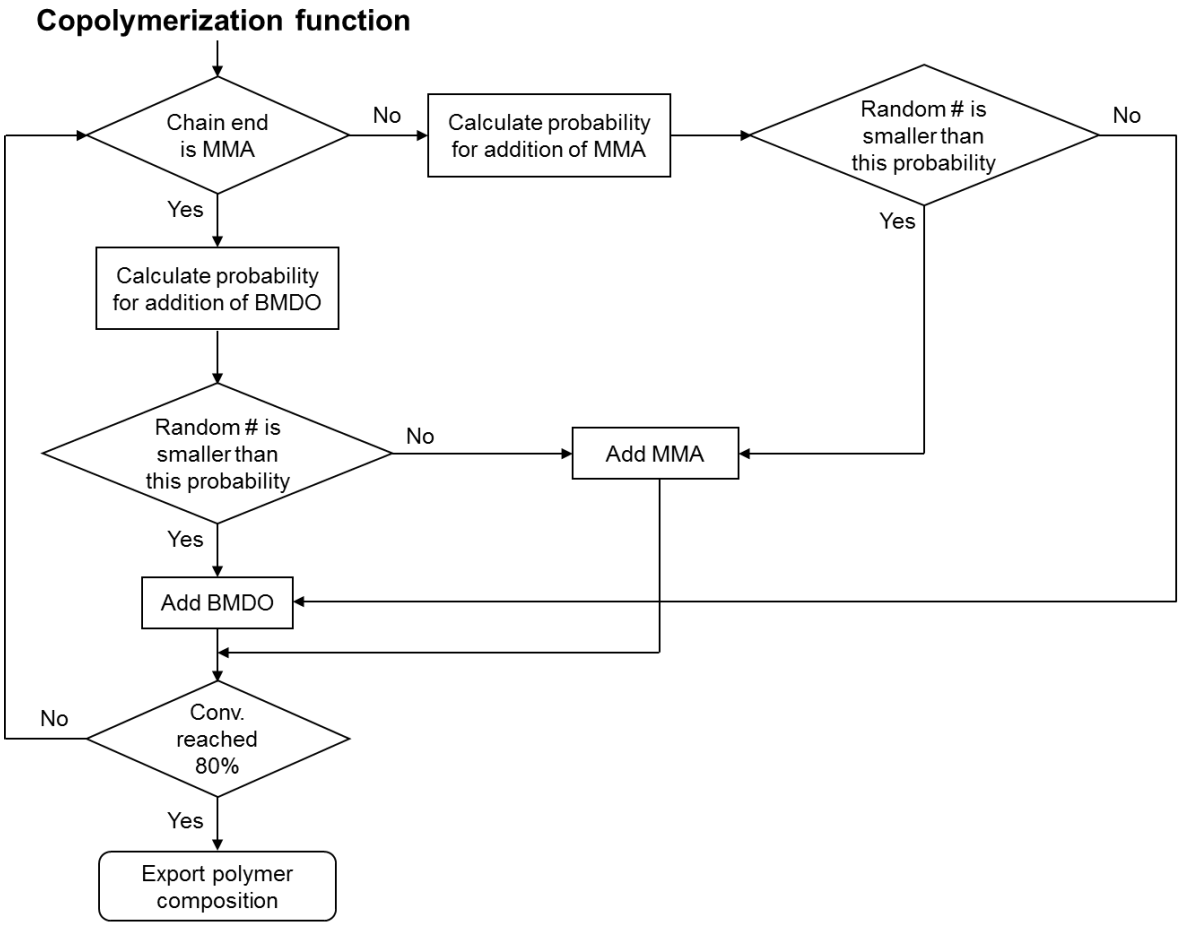

Figure 7-24. Flowchart for the copolymerization function.

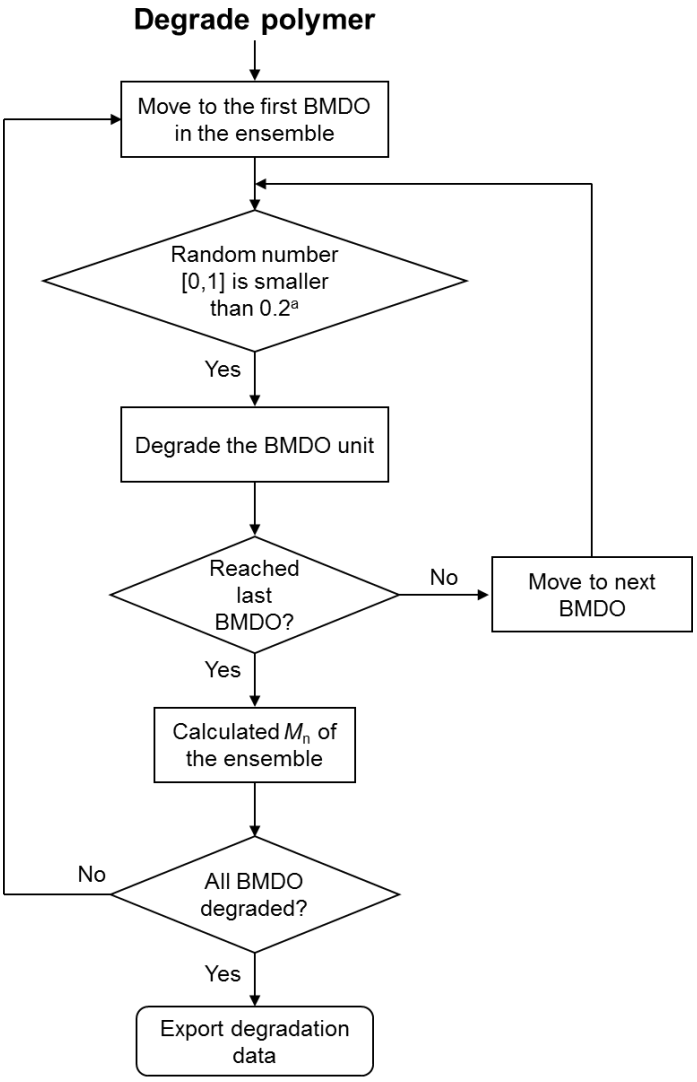

Figure 7-25. Flowchart for the polymer degradation function. [a] The arbitrary threshold for BMDO hydrolysis is set to 20% to introduce randomness to the system. The threshold can be increased or decreased to change sparsity of the sampled data without affecting the trend. Alternative stochastic model of choosing a single BMDO from all of the polymer chains to be degraded per iteration gave identical result, but it involved approximately 15-fold more iterations and thus required more computation time than the model presented here.

In the copolymerization function, the probability of propagating chain with either PEGMA or BMDO chain end to react with respective monomer was derived as follows, based on the terminal model.[62]

Co-polymerization can be represented by the following four reactions:

$$M_1^* + M_1 \xrightarrow{k_{11}} M_1 M_1^*$$

$$M_1^* + M_2 \xrightarrow{k_{12}} M_1 M_2^*$$

$$M_2^* + M_2 \xrightarrow{k_{22}} M_2 M_2^*$$

$$M_2^* + M_1 \xrightarrow{k_{21}} M_2 M_1^*$$

where M_1 and M_2 are monomers and M_1^* and M_2^* are polymers with M_1 and M_2 at chain ends, respectively.

Let $M_{1\to1}^*$ be a polymer with M_1 chain end that derived from M_1^*, and $M_{1\to2}^*$ be a polymer with M_2 chain end that also derived from M_1^*.

$$\frac{d[M_{1\to1}^*]}{dt} = k_{11}[M_1][M_1^*]$$

$$\frac{d[M_{1\to2}^*]}{dt} = k_{12}[M_2][M_1^*]$$

Then at any instant the probability that a given M_1^* will react with M_1 is

$$\frac{k_{11}[M_1][M_1^*]}{k_{11}[M_1][M_1^*] + k_{12}[M_2][M_1^*]} = \frac{k_{11}[M_1]}{k_{11}[M_1] + k_{12}[M_2]} = \frac{1}{1 + \frac{[M_2]}{r_1[M_1]}}$$

and the probability that a given M_1^* will react with M_2 is

$$\frac{k_{12}[M_2][M_1^*]}{k_{11}[M_1][M_1^*] + k_{12}[M_2][M_1^*]} = \frac{k_{12}[M_2]}{k_{11}[M_1] + k_{12}[M_2]} = \frac{1}{r_1\frac{[M_1]}{[M_2]} + 1}$$

Similarly, probability for M_2^* to react with M_1 is

$$\frac{k_{21}[M_1][M_2^*]}{k_{21}[M_1][M_2^*] + k_{22}[M_2][M_2^*]} = \frac{k_{21}[M_1]}{k_{21}[M_1] + k_{22}[M_2]} = \frac{1}{1 + r_2\frac{[M_2]}{[M_1]}}$$

and the probability that M_2^* will react with M_2 is

$$\frac{k_{22}[M_2][M_2^*]}{k_{21}[M_1][M_2^*] + k_{22}[M_2][M_2^*]} = \frac{k_{22}[M_2]}{k_{21}[M_1] + k_{22}[M_2]} = \frac{1}{\frac{[M_1]}{r_2[M_2]} + 1}$$

where $r_1 = \frac{k_{11}}{k_{12}}$ and $r_2 = \frac{k_{22}}{k_{21}}$

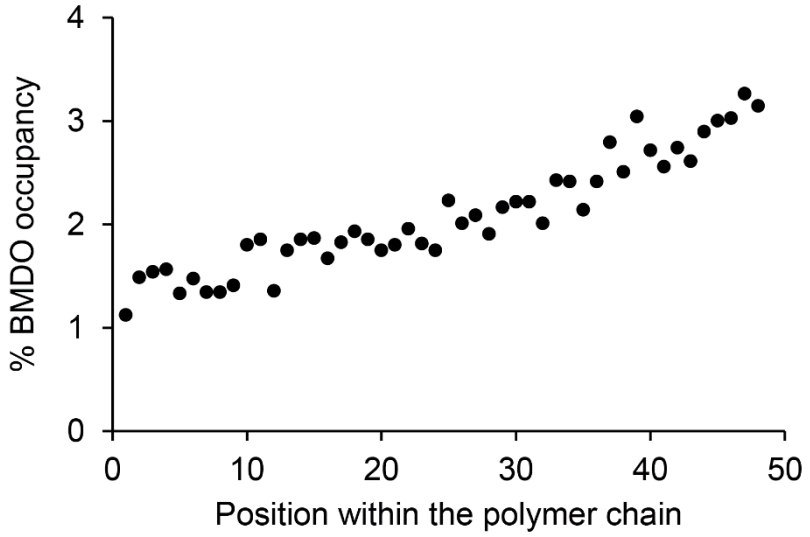

Figure 7-26. Normalized BMDO occupancy at each position in the polymer chain (position 1 corresponds to the initiating chain end).

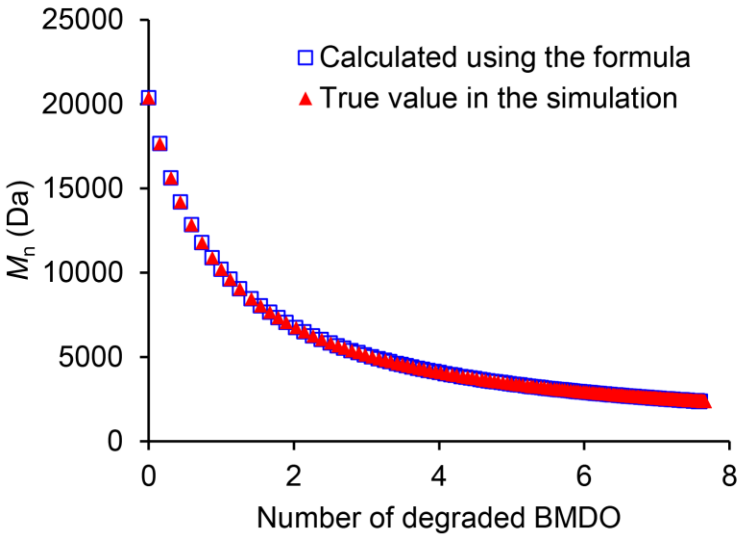

Figure 7-27. Molecular weight as a function of number of degraded BMDO units from the Monte Carlo simulation.

R Codes Used for Simulation

```
########################################
# p(PEGMA-co-BMDO) degradation simulation (main routine)
#
# Written by Jeong Hoon Ko (JK)
# Maynard Research Group
# Dept. of Chemistry and Biochemistry
# University of California, Los Angeles
#
# April 28, 2017
########################################

# Legend
# M1: Number of monomer 1 - PEGMA
# M2: Number of monomer 2 - BMDO
# r1: Reactivity ratio of monomer 1, r1 = k11/k12
# r2: Reactivity ratio of monomer 2, r2 = k21/k22

# Clear workspace
rm(list = ls());

# Load function
source("copolymerization.r");

# Monomer feed - 60:40 PEGMA:BMDO
M1 = 60;
```

```
M2 = 40;

# MMA/BMDO reactivity ratio from Junkers et al.
# Stephan Kobben, Anitha Ethirajan, Thomas Junkers, J. Polym. Sci. A, 2014, 52, 1633.
r1 = 6.0; # PEGMA (MMA)
r2 = 0.33; # BMDO
L = (0.8 * M1)+1; # 80% PEGMA conversion; add 1 for initiator (which will be
subtracted below)

# Run the copolymerization function
n = 1000;
out = matrix(0,n,L)
for (i in 1:n) {
       temp <- copolymerization(M1, M2, r1, r2, L)
       out[i,] = temp;
}

# Substract the initiator
out = out[,2:L];
L = L-1;

# Export degradable unit composition (inds_all)
df2 <- data.frame(Pos=1:ncol(out),DegradeSum=colSums(out));
write.table(df2, "Pos_gradient.txt", sep="\t")

#######################################

# Load function
source("degrade_polymer.r");

# Indices of BMDO units
inds_all = which(t(out)!=0,arr.ind = T);

n = 1000;
prob = 0.02; # Threshold for degradation; higher value leads to faster calculation
MW_PEGMA = 475;
MW_BMDO = 162.19;
out2 <- degrade_polymer(L,n,inds_all,prob,MW_PEGMA,MW_BMDO)

N_degraded = out2[,2]; # Number of degraded units
Mn = out2[,1]; # Number average chain length

# Make dataframe
df <- data.frame(round=1:nrow(out2),chainlen=c(Mn));

# Save current data
df2 <- data.frame(N_degraded=c(N_degraded),Mn=c(Mn));
write.table(df2, "Mn_degradation.txt", sep="\t")
```

```
########################################
# Copolymerization
#
# Written by Jeong Hoon Ko (JK)
# Maynard Research Group
# Dept. of Chemistry and Biochemistry
# University of California, Los Angeles
#
# April 28, 2017
########################################

# Legend
# 0: Monomer unit M1
# 1: Monomer unit M2

copolymerization <- function(M1, M2, r1, r2, L) {

	out = rep(0,L); # Initialize output vector (polymer chain)
	out[1] = 0;  # Treat initiator as PEGMA so that r1 can be used for first
monomer addition

	for (i in 2:L) {
		if (out[i-1] == 0){ # If previous monomer is M1
			M2_prob = 1 / (r1*M1/M2 + 1); # Probability that M2 adds
			if (runif(1) < M2_prob) { # If below threshold, add M2
				out[i] = 1;
				M2 = M2 - 1;
			} else { # If not, add M1
				out[i] = 0;
				M1 = M1 - 1;
			}
		} else if (out[i-1] == 1) { # If previous monomer is M2
			M1_prob = 1 / (r2*M2/M1 + 1); # Probability that M1 adds
			if (runif(1) < M1_prob) { # If below threshold, add M1
				out[i] = 0;
				M1 = M1 - 1;
			} else { # If not, add M2
				out[i] = 1;
				M2 = M2 - 1;
			}
		}
	}

	# Return output
	return(out)
}
```

```
########################################
# Polymer degradation
#
# Written by Jeong Hoon Ko (JK)
# Maynard Research Group
# Dept. of Chemistry and Biochemistry
# University of California, Los Angeles
#
# April 28, 2017
########################################

# Legend
# 0: Regular monomer unit
# 1: Intact degradable monomer unit
# 2: Degraded monomer unit
# L: Initial polymer length
# n: Total number of polymers to be simulated
# inds: Indices of degradable units
# prob: Degradation probability, between 0 and 1
# MW1: MW of regular monomer unit
# MW2: MW of degradable monomer unit

degrade_polymer <- function(L, n, inds, prob, MW1, MW2) {

	# Load pracma package
	library('pracma');

	# Degraded BMDO fragment MWs
	frag1 = 59.04; # Acid fragment
	frag2 = 121.16; # Benzyl alcohol fragment

	########################################
	# Create the starting polymer matrix

	# Create empty polymer chain ensemble
	master_mat = matrix(0,n,L);

	# Place degradable units
	for (i in 1:nrow(inds)){
		master_mat[inds[i,2],inds[i,1]] = 1;
	}

	num_deg = nrow(inds);
	########################################

	########################################
	# Start degradation routine
	count = num_deg; # Counter to keep track when the chain has fully degraded
	out <- vector(mode="numeric", length=0); # Initialize output vector
	deg_count <- vector(mode="numeric", length=0); # Counter for number of degraded
units

	# Skip first iteration to store MW of initial polymer chain
	first_iter = 1;
```

```
	while(count) {
		# Single iteration, go through each degradable unit and cleave the chain
		# if a random number is smaller than the probability threshold

		if (first_iter == 1){
			first_iter = 0;
		} else {
			for (k in 1:num_deg){
				i=inds[k,2]; # Polymer chain ID (1 through n)
				j=inds[k,1]; # BMDO position within the polymer
				if (master_mat[i,j] < 2){
					if (runif(1) < prob){ # Generate random number from
uniform distribution and compare to prob
						master_mat[i,j] = 2;
						count = count - 1; # Decrease counter by 1 BMDO
degradaed
					}
				}
			}
		}
		# Store molecular weights of each chain
		MW_now = 0; # Initialize MW_now
		for (i in 1:n) {
			for (j in 1:L){
				if (master_mat[i,j] == 0){ # If monomer unit is 0, add MW1
to MW_now
					MW_now[length(MW_now)] = MW_now[length(MW_now)] + MW1;
				} else if (master_mat[i,j] == 1) { # If monomer unit is 1,
add MW2 to MW_now
					MW_now[length(MW_now)] = MW_now[length(MW_now)] + MW2;
				} else{ # If monomer unit has degraded, add frag1 for current
chain, store current chain length, and add frag2 for the next chain
					MW_now[length(MW_now)]  =  MW_now[length(MW_now)]  +
frag1;
					MW_now[length(MW_now)+1] = frag2;
				}
			}
			MW_now[length(MW_now)+1] = 0;
		}
		# Store Mn
		out[length(out)+1] = sum(MW_now) / length(MW_now);
		deg_count[length(deg_count)+1] = num_deg/1000 * n - count;
	}
	out = cbind(out,deg_count)
	# Return output
	return(out)
	########################################
}
```

7.5 References

(1) Teng, H. Overview of the Development of the Fluoropolymer Industry. *Appl. Sci.* **2012,** *2*, 496.

(2) Boday, D. J., The State of Fluoropolymers. In *Advances in Fluorine-Containing Polymers*, American Chemical Society: 2012; Vol. 1106, pp 1.

(3) Fujiwara, T.; O'Hagan, D. Successful fluorine-containing herbicide agrochemicals. *J. Fluorine Chem.* **2014,** *167*, 16.

(4) Müller, K.; Faeh, C.; Diederich, F. Fluorine in pharmaceuticals: looking beyond intuition. *Science* **2007,** *317*, 1881.

(5) Kusoglu, A.; Weber, A. Z. New Insights into Perfluorinated Sulfonic-Acid Ionomers. *Chem. Rev.* **2017,** *117*, 987.

(6) Wang, J.; Sánchez-Roselló, M.; Aceña, J. L.; del Pozo, C.; Sorochinsky, A. E.; Fustero, S.; Soloshonok, V. A.; Liu, H. Fluorine in pharmaceutical industry: fluorine-containing drugs introduced to the market in the last decade (2001–2011). *Chem. Rev.* **2013,** *114*, 2432.

(7) Purser, S.; Moore, P. R.; Swallow, S.; Gouverneur, V. Fluorine in medicinal chemistry. *Chem. Soc. Rev.* **2008,** *37*, 320.

(8) Phelps, M.; Huang, S.; Hoffman, E.; Selin, C.; Sokoloff, L.; Kuhl, D. Tomographic measurement of local cerebral glucose metabolic rate in humans with (F-18) 2-fluoro-2-deoxy-D-glucose: validation of method. *Ann. Neurol.* **1979,** *6*, 371.

(9) Couturier, O.; Luxen, A.; Chatal, J.-F.; Vuillez, J.-P.; Rigo, P.; Hustinx, R. Fluorinated tracers for imaging cancer with positron emission tomography. *Eur. J. Nucl. Med. Mol. Imag.* **2004,** *31*, 1182.

(10) DeSimone, J. M.; Mecham, S. J.; Farrell, C. L. Organic Polymer Chemistry in the Context of Novel Processes. *ACS Cent. Sci.* **2016,** *2*, 588.

(11) Wallat, J. D.; Czapar, A. E.; Wang, C.; Wen, A. M.; Wek, K. S.; Yu, X.; Steinmetz, N. F.; Pokorski, J. K. Optical and Magnetic Resonance Imaging Using Fluorous Colloidal Nanoparticles. *Biomacromolecules* **2016**.

(12) Johnson, M. E.; Shon, J.; Guan, B. M.; Patterson, J. P.; Oldenhuis, N. J.; Eldredge, A. C.; Gianneschi, N. C.; Guan, Z. Fluorocarbon Modified Low-Molecular-Weight Polyethylenimine for siRNA Delivery. *Bioconj. Chem.* **2016,** *27*, 1784.

(13) Yan, G.; Wang, J.; Zhang, P.; Hu, L.; Wang, X.; Yang, G.; Fu, S.; Cheng, X.; Tang, R. Tunable dynamic fluorinated poly (ortho ester)-based drug carriers for greatly enhanced chemotherapeutic efficacy. *Polym. Chem.* **2017,** *8*, 2063.

(14) Sletten, E. M.; Swager, T. M. Fluorofluorophores: fluorescent fluorous chemical tools spanning the visible spectrum. *J. Am. Chem. Soc.* **2014,** *136*, 13574.

(15) Bergbreiter, D. E.; Franchina, J. G. A soluble fluorous phase polymer support. *Chem. Commun.* **1997**, 1531.

(16) Ma, S.; Zhou, J.; Zhang, Y.; He, Y.; Jiang, Q.; Yue, D.; Xu, X.; Gu, Z. Highly stable fluorinated nanocarriers with iRGD for overcoming the stability dilemma and enhancing tumor penetration in an orthotopic breast cancer. *ACS Appl. Mater. Interfaces* **2016,** *8*, 28468.

(17) Koda, Y.; Terashima, T.; Sawamoto, M. Multimode Self-Folding Polymers via Reversible and Thermoresponsive Self-Assembly of Amphiphilic/Fluorous Random Copolymers. *Macromolecules* **2016,** *49*, 4534.

(18) Hillmyer, M. A.; Lodge, T. P. Synthesis and self-assembly of fluorinated block copolymers. *J. Polym. Sci., Part A: Polym. Chem.* **2002,** *40*, 1.

(19) Pelegri-O'Day, E. M.; Lin, E.-W.; Maynard, H. D. Therapeutic protein–polymer conjugates: advancing beyond PEGylation. *J. Am. Chem. Soc.* **2014,** *136*, 14323.

(20) Agarwal, S. Radical ring opening and vinyl copolymerization of 2, 3, 4, 5, 6-pentafluorostyrene with 5, 6-Benzo-2-methylene-1, 3-dioxepane: synthesis and structural characterization using 1D and 2D NMR techniques. *J. Polym. Res.* **2006,** *13*, 403.

(21) Borkar, S.; Sen, A.; Shallenberger, J. R. Alternating polyester/fluoroalkene copolymers: Combining high hydrophobicity with degradability. *J. Polym. Sci., Part A: Polym. Chem.* **2006,** *44*, 1225.

(22) Hawker, C. J.; Bosman, A. W.; Harth, E. New polymer synthesis by nitroxide mediated living radical polymerizations. *Chem. Rev.* **2001,** *101*, 3661.

(23) Moad, G.; Rizzardo, E.; Thang, S. H. Living radical polymerization by the RAFT process–a second update. *Aust. J. Chem.* **2009,** *62*, 1402.

(24) Bielawski, C. W.; Grubbs, R. H. Living ring-opening metathesis polymerization. *Prog. Polym. Sci.* **2007,** *32*, 1.

(25) Koda, Y.; Terashima, T.; Nomura, A.; Ouchi, M.; Sawamoto, M. Fluorinated microgel-core star polymers as fluorous compartments for molecular recognition. *Macromolecules* **2011,** *44*, 4574.

(26) Koda, Y.; Terashima, T.; Sawamoto, M. Fluorous microgel star polymers: selective recognition and separation of polyfluorinated surfactants and compounds in water. *J. Am. Chem. Soc.* **2014,** *136*, 15742.

(27) Koda, Y.; Terashima, T.; Takenaka, M.; Sawamoto, M. Star Polymer Gels with Fluorinated Microgels via Star–Star Coupling and Cross-Linking for Water Purification. *ACS Macro Lett.* **2015,** *4*, 377.

(28) Delplace, V.; Nicolas, J. Degradable vinyl polymers for biomedical applications. *Nat. Chem.* **2015,** *7*, 771.

(29) Tardy, A.; Nicolas, J.; Gigmes, D.; Lefay, C.; Guillaneuf, Y. Radical Ring-Opening Polymerization: Scope, Limitations, and Application to (Bio) Degradable Materials. *Chem. Rev.* **2017,** *117*, 1319.

(30) Agarwal, S. Chemistry, chances and limitations of the radical ring-opening polymerization of cyclic ketene acetals for the synthesis of degradable polyesters. *Polym. Chem.* **2010,** *1*, 953.

(31) Bailey, W. J.; Ni, Z.; Wu, S. R. Free radical ring-opening polymerization of 4, 7-dimethyl-2-methylene-1, 3-dioxepane and 5, 6-benzo-2-methylene-1, 3-dioxepane. *Macromolecules* **1982,** *15*, 711.

(32) Siegwart, D. J.; Bencherif, S. A.; Srinivasan, A.; Hollinger, J. O.; Matyjaszewski, K. Synthesis, characterization, and in vitro cell culture viability of degradable poly (N-isopropylacrylamide-co-5, 6-benzo-2-methylene-1, 3-dioxepane)-based polymers and crosslinked gels. *J. Biomed. Mater. Res., Part A* **2008,** *87*, 345.

(33) Koda, Y.; Terashima, T.; Sawamoto, M.; Maynard, H. D. Amphiphilic/fluorous random copolymers as a new class of non-cytotoxic polymeric materials for protein conjugation. *Polym. Chem.* **2015,** *6*, 240.

(34) Koda, Y.; Terashima, T.; Maynard, H. D.; Sawamoto, M. Protein storage with perfluorinated PEG compartments in a hydrofluorocarbon solvent. *Polym. Chem.* **2016,** *7*, 6694.

(35) Kobben, S.; Ethirajan, A.; Junkers, T. Synthesis of degradable poly (methyl methacrylate) star polymers via RAFT copolymerization with cyclic ketene acetals. *J. Polym. Sci., Part A: Polym. Chem.* **2014,** *52*, 1633.

(36) Delplace, V.; Harrisson, S.; Tardy, A.; Gigmes, D.; Guillaneuf, Y.; Nicolas, J. Nitroxide-Mediated Radical Ring-Opening Copolymerization: Chain-End Investigation and Block Copolymer Synthesis. *Macromol. Rapid Commun.* **2014,** *35*, 484.

(37) Mishima, E.; Yamago, S. Controlled random and alternating copolymerization of (meth) acrylates, acrylonitrile, and (meth) acrylamides with vinyl ethers by organotellurium-, organostibine-, and organobismuthine-mediated living radical polymerization reactions. *J. Polym. Sci., Part A: Polym. Chem.* **2012,** *50*, 2254.

(38) Schmidt, M. W.; Baldridge, K. K.; Boatz, J. A.; Elbert, S. T.; Gordon, M. S.; Jensen, J. H.; Koseki, S.; Matsunaga, N.; Nguyen, K. A.; Su, S. General atomic and molecular electronic structure system. *J. Comput. Chem.* **1993,** *14*, 1347.

(39) Gordon, M. S.; Michael, W. S., Advances in electronic structure theory: GAMESS a decade later. In *Theory and Applications of Computational Chemistry: the first forty years*, Dykstra, C. E., Frenking, G., Kim, K. S., Scuseria, G. E., Eds. Elsevier: Amsterdam, 2005; pp 1167.

(40) Ogura, Y.; Terashima, T.; Sawamoto, M. Synthesis of fluorinated gradient copolymers via in situ transesterification with fluoroalcohols in tandem living radical polymerization. *Polym. Chem.* **2017,** *8*, 2299.

(41) Bode, B. M.; Gordon, M. S. MacMolPlt: a graphical user interface for GAMESS. *J. Mol. Graphics Model.* **1998,** *16*, 133.

(42) Decker, C. G.; Maynard, H. D. Degradable PEGylated protein conjugates utilizing RAFT polymerization. *Eur. Polym. J.* **2015,** *65*, 305.

(43) Ganda, S.; Jiang, Y.; Thomas, D. S.; Eliezar, J.; Stenzel, M. H. Biodegradable Glycopolymeric Micelles Obtained by RAFT-controlled Radical Ring-Opening Polymerization. *Macromolecules* **2016,** *49*, 4136.

(44) Delplace, V.; Tardy, A.; Harrisson, S.; Mura, S.; Gigmes, D.; Guillaneuf, Y.; Nicolas, J. Degradable and comb-like PEG-based copolymers by nitroxide-mediated radical ring-opening polymerization. *Biomacromolecules* **2013,** *14*, 3769.

(45) Yuan, J.-Y.; Pan, C.-Y.; Tang, B. Z. “Living” Free Radical Ring-Opening Polymerization of 5, 6-Benzo-2-methylene-1, 3-dioxepane Using the Atom Transfer Radical Polymerization Method. *Macromolecules* **2001,** *34*, 211.

(46) Lutz, J.-F.; Andrieu, J.; Üzgün, S.; Rudolph, C.; Agarwal, S. Biocompatible, thermoresponsive, and biodegradable: simple preparation of “all-in-one” biorelevant polymers. *Macromolecules* **2007,** *40*, 8540.

(47) Huang, J.; Gil, R.; Matyjaszewski, K. Synthesis and characterization of copolymers of 5, 6-benzo-2-methylene-1, 3-dioxepane and n-butyl acrylate. *Polymer* **2005,** *46*, 11698.

(48) Ouchi, M.; Terashima, T.; Sawamoto, M. Transition metal-catalyzed living radical polymerization: toward perfection in catalysis and precision polymer synthesis. *Chem. Rev.* **2009,** *109*, 4963.

(49) Takahashi, H.; Ando, T.; Kamigaito, M.; Sawamoto, M. Half-Metallocene-Type Ruthenium Complexes as Active Catalysts for Living Radical Polymerization of Methyl Methacrylate and Styrene 1. *Macromolecules* **1999,** *32*, 3820.

(50) Pápai, Z.; Pap, T. L. Analysis of peak asymmetry in chromatography. *J. Chromatogr.* **2002,** *953*, 31.

(51) Foley, J. P.; Dorsey, J. G. Equations for calculation of chromatographic figures of merit for ideal and skewed peaks. *Anal. Chem* **1983,** *55*, 730.

(52) Kottisch, V.; Gentekos, D. T.; Fors, B. P. “Shaping” the Future of Molecular Weight Distributions in Anionic Polymerization. *ACS Macro Lett.* **2016,** *5*, 796.

(53) Tran, J.; Guégain, E.; Ibrahim, N.; Harrisson, S.; Nicolas, J. Efficient synthesis of 2-methylene-4-phenyl-1, 3-dioxolane, a cyclic ketene acetal for controlling the NMP of methyl methacrylate and conferring tunable degradability. *Polym. Chem.* **2016,** *7*, 4427.

(54) Gillies, M. B.; Matyjaszewski, K.; Norrby, P.-O.; Pintauer, T.; Poli, R.; Richard, P. A DFT Study of R− X Bond Dissociation Enthalpies of Relevance to the Initiation Process of Atom Transfer Radical Polymerization. *Macromolecules* **2003,** *36*, 8551.

(55) Smart, B. E. Fluorine substituent effects (on bioactivity). *J. Fluorine Chem.* **2001,** *109*, 3.

(56) Chicea, D. Revealing Fe3O4 nanoparticles aggregation dynamics using dynamic light scattering. *Optoelectron. Adv. Mater., Rapid Commun.* **2009,** *3*, 1299.

(57) Spěváček, J.; Hanyková, L. 1H NMR relaxation study of polymer-solvent interactions during thermotropic phase transition in aqueous solutions. *Macromol. Symp.* **2003,** *203*, 229.

(58) Ouchi, M.; Ito, M.; Kamemoto, S.; Sawamoto, M. Highly Active and Removable Ruthenium Catalysts for Transition-Metal-Catalyzed Living Radical Polymerization: Design of Ligands and Cocatalysts. *Chem. - Asian J.* **2008,** *3*, 1358.

(59) Mueller, L.; Matyjaszewski, K. Reducing copper concentration in polymers prepared via atom transfer radical polymerization. *Macromol. React. Eng.* **2010,** *4*, 180.

(60) Anastasaki, A.; Haddleton, A. J.; Zhang, Q.; Simula, A.; Droesbeke, M.; Wilson, P.; Haddleton, D. M. Aqueous Copper-Mediated Living Radical Polymerisation of N-Acryloylmorpholine, SET-LRP in Water. *Macromol. Rapid Commun.* **2014,** *35*, 965.

(61) Borchers, H. W. 2016; pracma: Practical Numerical Math Functions. R package version 1.9.5. https://CRAN.R-project.org/package=pracma.

(62) Hiemenz, P. C.; Lodge, T. P., *Polymer Chemistry*. CRC press: 2007.

Chapter 8.

Air-Stable Benzonorbornadiene Polymers

Enabled by Aryne Chemistry

This chapter is an edited version of a paper published as:
Medina, J. M.;† Ko, J. H.;† Maynard, H. D.; Garg, N. K. *Macromolecules* **2017**, *50*, 580. († Equal contribution).

8.1 Introduction

Since its original discovery, ring-opening metathesis polymerization (ROMP) has enabled ready access to well-defined polymers for numerous industrial applications including drug delivery,[1, 2] electronic materials,[3, 4] and nanostructures.[5, 6] This process typically relies on strained monomers, such as norbornene and cyclopentene, to provide the thermodynamic driving force necessary to achieve ring opening and promote polymerization. In particular, norbornene and its related analogues have proven to be ideal substrates for ROMP. The energy stored as ring strain (~27.2 kcal / mol) allows for facile ring opening and promotes the subsequent polymerization, while substituents prevent the secondary metathesis of the polymer backbone.[7] In fact, norbornenes are the most frequently used substrates for ROMP.[8]

Despite the widespread utility of norbornenes in various synthetic applications, norbornadienes fused to a benzene ring, or benzonorbornadienes, have been rarely investigated. As a result, the potential utility of the resulting polymers have been largely overlooked. El-Saafin and Feast first reported the synthesis of poly(benzonorbornadiene) (**1**, Figure 8-1) in 1982.[9, 10] In their study, this polymer was found to be susceptible to oxidation under ambient conditions. Molecular oxygen was thought to facilitate oxidation of the benzylic / allylic position, which then led to intermolecular cross-linking, chain scission, and the ultimate formation of ill-defined materials. Similar studies on related systems by the groups of Grubbs[11] and Schrock[12, 13] further suggested that polymers containing a C–H bond at the readily oxidized benzylic / allylic position undergo rapid decomposition, rendering the polymers unstable and of limited utility.

To evade the problem of poly(benzonorbornadiene) stability, one approach is to chemically alter the resulting polymer to essentially mask the troublesome functional groups, thus avoiding the undesired reactivity (Figure 8-1, *Solution A*). In fact, the Swager group opted to hydrogenate

the olefins in the benzonorbornadiene polymer backbone to give **2**, in order to prevent oxidation and improve polymer solubility.[14] This strategy proved effective for further electrochemical polymerization and cross-linking of the polymers to form conducting materials. However, the hydrogenation reaction was shown to change the polymer properties such as glass transition temperatures and oxidation onset values.

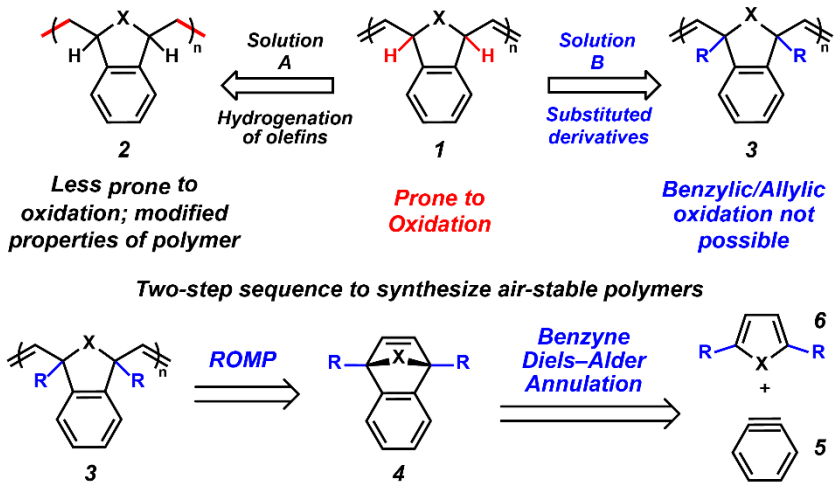

Figure 8-1. Possible solutions to poly(benzonorbornadiene) oxidation problem

An alternative solution for the synthesis of air-stable poly(benzonorbornadiene) involves substituting the benzylic / allylic position that is otherwise prone to oxidation with an unreactive substituent (R = alkyl group) (Figure 8-1, *Solution B*). Ideally, the substituents would be introduced prior to ROMP, thus allowing for the synthesis of polymers without further chemical modification. Such a strategy would not only complement the approach taken by Swager, but could also allow for the potential utilization of the intact double bonds for post-polymerization modification.[15-18] To test this general strategy, we envisioned accessing substituted polymers **3** (Figure 8-1) via

ROMP of monomers **4**. The success of this approach hinged on the development of an efficient route to access various monomers **4**. For this purpose, we sought to utilize the Diels–Alder trapping of benzyne (**5**) with cyclic dienes **6**. Although historically avoided due to their high reactivity, arynes have been recently employed in chemical synthesis,[19-42] albeit with only limited applications in polymer chemistry.[43-46] In this chapter, we report the use of a benzyne annulation / ROMP reaction sequence to furnish well-defined poly(benzonorbornadiene) derivatives, including two that are stable to oxidation.

8.2 Results and Discussion

The benzonorbornadiene monomers **M1**–**M4** were easily synthesized using the commercially available benzyne precursor **7**,[47] as summarized in Table 8-1. Whereas **M3** and **M4** would later be used to access air-stable polymers, the less substituted monomers, **M1** and **M2**, were targeted for comparative purposes. Silyltriflate **7** was exposed to CsF in the presence of cyclic diene trapping partners in acetonitrile at 60 °C. This simple protocol promotes an elimination reaction to give the benzyne intermediate (**5**), which is subsequently trapped in Diels–Alder cycloadditions to give monomers **M1**–**M4** in excellent yields. Several features of this approach should be noted: (a) the reactions are operationally trivial to perform and generally do not require the rigorous exclusion of water or oxygen; (b) the benzyne trapping allows for the formation of two new carbon–carbon bonds and two tertiary stereocenters in a single transformation, and (c) purification of the desired monomers is straightforward using chromatography.

Table 8-1. Benzonorbornadiene monomers **M1**–**M4** synthesized by aryne chemistry.

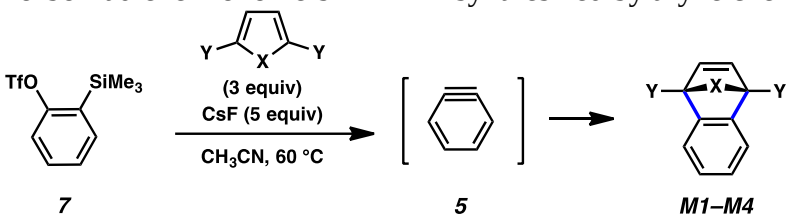

7 *5* *M1–M4*

Entry	*Trapping agent*	*Product*		*Yield*
1			*M1*	99%
2			*M2*	94%
3	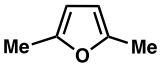	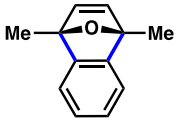	*M3*	99%
4	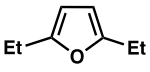	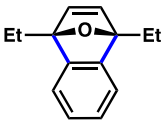	*M4*	91%

The results of polymerization studies are shown in Table 8-2. Monomers **M1**–**M3** were readily polymerized using the first-generation Grubbs catalyst in toluene at room temperature (entries 1–9) at various monomer to catalyst ratios. Initially we observed that ROMP of benzonorbornadiene **M1** resulted in polymers **P1** with moderate dispersities (Đ = 1.60 – 1.73, Experimental Section Figure 8-5b). Based on the aforementioned precedents, we suspected that polymers **P1** were highly sensitive to molecular oxygen and readily oxidized at the benzylic / allylic position when exposed to air. Since the polymers were stored in the freezer and thus exposed to ambient oxygen prior to analysis, we theorized that this was the origin of the observed molecular weight distributions. To test this hypothesis, we took freshly polymerized samples directly from the glove box and dissolved them in chloroform immediately before analyzing by

gel permeation chromatography (GPC). Even with this precaution, the traces of **P1** exhibited shoulder peaks (Figure 8-2a); however the dispersities of the polymers (Đ = 1.15 – 1.20, Table 8-2) were much smaller than those of the stored samples. It is also interesting to observe that the molecular weight of **P1** decreased after incubation in air (Experimental Section Table 8-4) suggesting chain scission. El-Saafin and Feast had postulated that molecular oxygen reacts at the benzylic / allylic of poly(benzonorbornadiene) to produce peroxy radical and that oxidation of the polymer both degrades and cross-links the polymer;[9] the GPC data for **P1** supports this hypothesis.

Table 8-2. ROMP of monomers **M1**–**M4** using Grubbs catalysts.

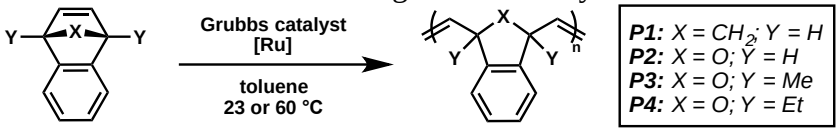

M1–M4 *P1–P4*

P1: *X = CH_2; Y = H*
P2: *X = O; Y = H*
P3: *X = O; Y = Me*
P4: *X = O; Y = Et*

Entry	*Catalyst*	*Monomer*	*[M] / [I]*	*M_n (theo)*	*M_n*	*Đ*
1	G1	M1	50	7.1 kDa	11.8 kDa	1.16
2	G1	M1	150	21.3 kDa	31.6 kDa	1.15
3	G1	M1	300	42.6 kDa	53.0 kDa	1.20
4	G1	M2	50	7.2 kDa	15.7 kDa[a]	1.83[a]
5	G1	M2	150	21.6 kDa	38.4 kDa[a]	1.86[a]
6	G1	M2	300	43.3 kDa	50.6 kDa[a]	2.00[a]
7	G1	M3	50	8.6 kDa	5.4 kDa	1.14
8	G1	M3	150	25.8 kDa	25.2 kDa	1.14
9	G1	M3	300	51.7 kDa	54.0 kDa	1.17
10	G3	M4	50	10.0 kDa	17.4 kDa	1.11
11	G3	M4	150	30.0 kDa	46.4 kDa	1.12
12	G3	M4	300	60.1 kDa	162.0 kDa	1.07

[a] Major peak calculated from RI trace

Grubbs 1
G1

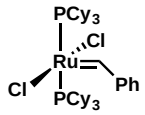

Grubbs 3
G3

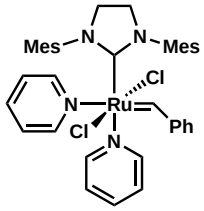

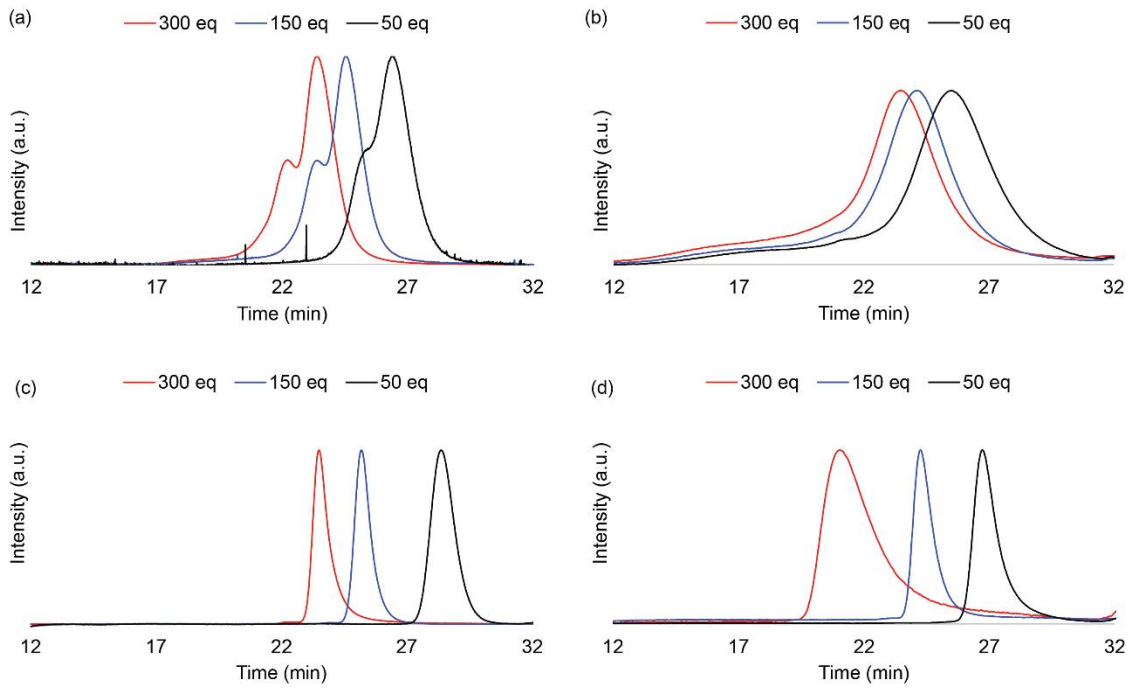

Figure 8-2. SEC-MALS Chromatograms of unsubstituted polymers (a) **P1** and (b) **P2** show broad overlapping peaks. Chromatograms of substituted polymers (c) **P3** and (d) **P4** show well-defined peaks.

The oxygen-containing analogue **M2** resulted in ill-defined polymers with high dispersities even when analyzed right after polymerization (Experimental Section Figure 8-5c). The light scattering (LS) trace significantly differed from the refractive index (RI) trace and showed larger molecular weight species that eluted prior to the main peak (Experimental Section Figure 8-5c). It should be noted that LS is more sensitive to higher molecular weight species than RI,[48-50] and thus the high molecular weight shoulder is more pronounced in the LS trace. Continued exposure of the sample to air resulted in further deformation of the LS trace, and a second distinct peak appeared near the 10 min mark on the chromatogram (Experimental Section Figure 8-5d). Comparison of **P1** and **P2** GPC traces suggested that **P2** underwent more significant oxidation (Experimental Section Figure 8-5a vs. c), suggesting that **P2** is especially prone to oxidation and will likely oxidize immediately upon contact with air. To compare the relative oxidation potentials

of **P1** and **P2**, energies of monomer units were computed by density functional theory (DFT) calculations.[51] Results show that the oxidation potential of **P2** is 0.238 V higher than that of **P1**, which supports the experimental observation that **P2** oxidizes more readily than **P1** (see Calculation of Oxidation Potential section in the Experimental Section).

It was also noted that the main peaks from the **P2** chromatogram had higher dispersity values (Figure 8-2b, Đ = 1.83 – 2.00) than those observed for fresh **P1** (Figure 8-2a, Đ = 1.15 – 1.20). It has been previously reported that monomer **M2** is roughly 19 times more reactive than monomer **M1**.[52] Assuming similar rate of initiation (k_i) for the first-generation Grubbs catalyst in the ROMP of **M1** and **M2**, this increased reactivity likely leads to high propagation rate (k_p) and low k_i / k_p ratio that consequently results in the observed higher dispersities for **M2**.

Whereas the unsubstituted polymers **P1** and **P2** were highly susceptible to oxidation, polymers **P3** and **P4** (bearing alkyl substituents at the benzylic / allylic positions) did not exhibit such discrepancy between RI and LS traces, suggesting that benzylic substitution effectively prevents oxidation. For the dimethyl-substituted monomer **M3**, the substitution attenuates the reactivity of the system, allowing for well-controlled polymerizations with narrow dispersity (Đ = 1.14 – 1.17) for all molecular weights tested (Figure 8-2c). Effective polymerization of monomer **M4** required the use of the more reactive third-generation Grubbs catalyst and higher reaction temperatures (60 ^{o}C) (Table 8-2, entries 10–12) to give polymers with low dispersity values (Figure 8-2d, $Đ$ = 1.07 – 1.12).

In order to verify that alkyl substitution at the benzylic / allylic positions results in polymers that are stable to oxidation, we analyzed polymers **P1**–**P4** by elemental analysis (Table 8-3). Benzonorbornadiene polymer **P1** was detected to contain 0.37 oxygen atoms per repeat unit. This represents direct evidence for the incorporation of oxygen to the polymer once it is exposed to air.

Similarly, oxabenzonorbornadiene polymer **P2** was found to contain 1.32 oxygen atoms per repeat unit. The instrumental error in the measurement of oxygen is 0.30%. The data indicates that both unsubstituted polymers have higher oxygen-content than we would normally expect (>30% more oxygen). In stark contrast, polymers **P3** and **P4** both contained the expected number of oxygen atoms per repeat unit, suggesting that substitution at the benzylic / allylic positions successfully suppressed the oxidation pathway.

Table 8-3. Elemental analysis data for polymers **P1**–**P4**.

Polymer	*Element*	*% observed*	*# of atoms per unit observed*	*# of atoms per unit theoretical*
P1	Carbon	88.70	11	11
	Hydrogen	7.27	10.74	10
	Oxygen	3.96	0.37	0
P2	Carbon	80.38	10	10
	Hydrogen	5.58	8.27	8
	Oxygen	14.14	1.32	1
P3	Carbon	83.54	12	12
	Hydrogen	7.09	12.14	12
	Oxygen	9.46	1.02	1
P4	Carbon	83.89	14	14
	Hydrogen	7.93	15.77	16
	Oxygen	8.08	1.01	1

To further confirm the oxidation of **P1** and **P2**, the polymer samples were subjected to Fourier-transform infrared spectroscopy (FT-IR) analysis (Figure 8-3). Upon oxidation and incorporation of an OH group, the FT-IR spectrum is expected to show a broad alcohol or peroxide O–H stretch in the 3600–3200 cm^{-1} range. Polymer **P1** shows a small broad peak at 3400 cm^{-1} (Figure 8-3a), in good agreement with the IR spectrum previously reported for the poly(benzonorbornadiene).[10] The same indicative stretch (3400 cm^{-1}) is more pronounced in polymer **P2** (Figure 3b), and it is completely absent in the cases of polymers **P3** and **P4** (Figure

8-3c and d). Taken together with the elemental analysis data, these experimental findings confirm that benzonorbornadiene monomers with benzylic / allylic substitution give air-stable polymers.

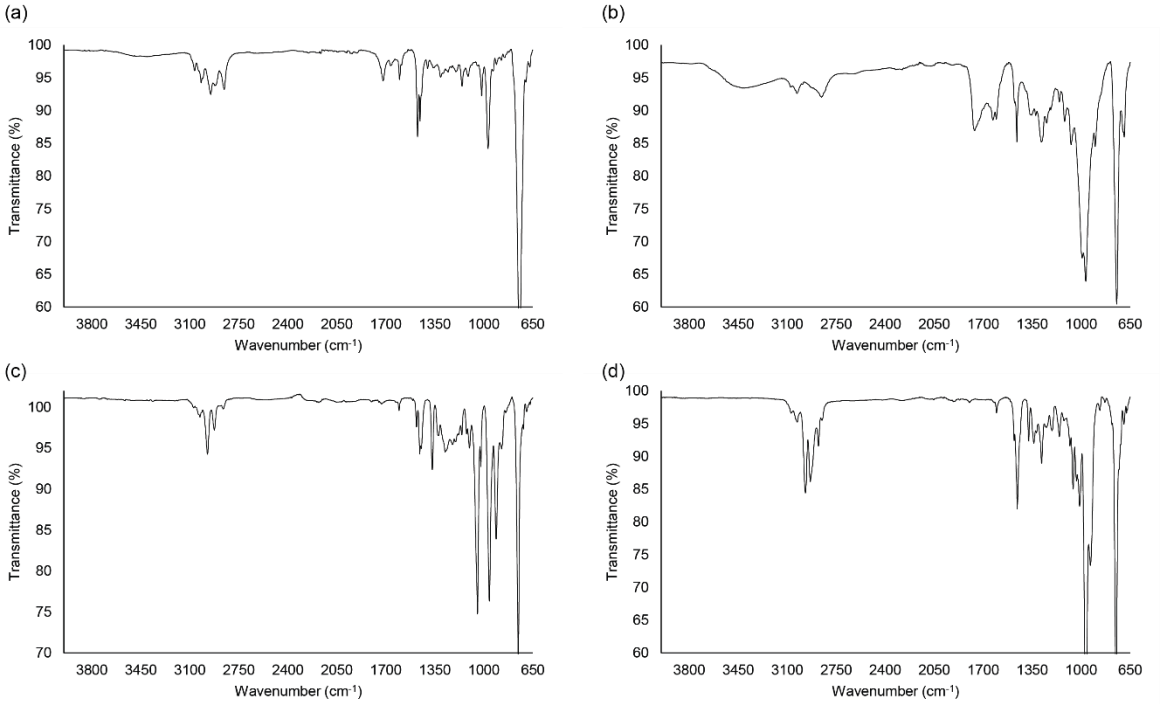

Figure 8-3. FT–IR spectra: (a) **P1**, (b) **P2**, (c) **P3**, and (d) **P4**.

Having determined the relative stability to oxygen of non-substituted (**P1** and **P2**) and substituted (**P3** and **P4**) polymers, we measured the glass transition temperatures (T_g) by dynamic scanning calorimetry (DSC) (Figure 8-4). Polymers **P1** and **P3** each have a high T_g (**P1**: 155.40 °C and **P2**: 151.99 °C), whereas the diethyl-substituted polymer **P4** has a lower T_g (93.58 °C). This drastic decrease in glass transition temperature, related to the longer alkyl substituent (methyl vs. ethyl), has been previously attributed to the internal plasticization effect.[53, 54] Longer alkyl substituents are thought to disrupt intermolecular interactions between polymer chains, thereby reducing the thermal barrier required to reach the glass transition threshold. For polymer **P2** (Figure 8-4b), Schrock and coworkers have previously reported a T_g of 167 °C.[13] Interestingly, we

do not observe a T_g in the –50 to 250 °C range. We suspect that the polymer cross-linked through the oxidation pathway prior to analysis, which would restrict polymer chain motion that causes the onset of glass transition.[55] As cross-linking would make the microstructure of the polymer highly heterogeneous, the glass transition of the polymer may be altered to different extents, ultimately leading to broadening of T_g such that it is not detectable.

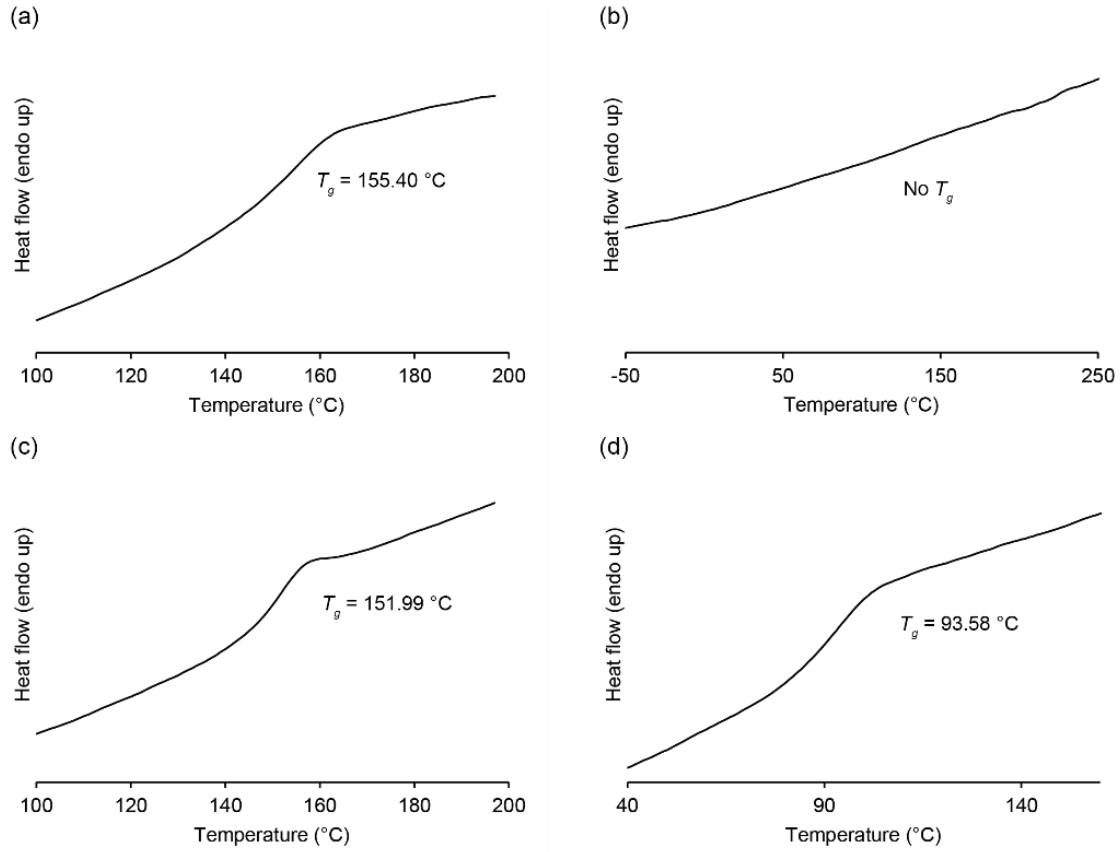

Figure 8-4. DSC curves for polymers **P1**–**P4**, (a) **P1**, (b) **P2** (not detected), (c) **P3**, and (d) **P4**.

8.3 Conclusions

We have successfully demonstrated an efficient approach for the synthesis of air-stable benzonorbornadiene polymers. Monomers were synthesized in high yields using benzyne Diels–

Alder reactions involving a commercially available benzyne precursor. Subsequently, ruthenium-based Grubbs catalysts were used to promote ROMP, giving polymers with good control over molecular weight dispersity. This approach complements more commonly used strategies for handling unstable materials, such as post-polymerization modifications. We anticipate that this report will enable research of the synthesis and properties of benzonorbornadiene polymers, and also stimulate further efforts to utilize arynes in the synthesis of polymers.

8.4 Experimental Section

Materials and Methods

Unless stated otherwise, reactions were conducted in flame-dried glassware under an atmosphere of nitrogen using anhydrous solvents (freshly distilled or passed through activated alumina columns). All commercially obtained reagents were used as received unless otherwise specified. Cesium fluoride (CsF) was obtained from Strem Chemicals and stored on the bench-top at ambient temperature under an N_2 atmosphere. 2-(Trimethylsilyl)phenyl trifluoromethanesulfonate, dicyclopentadiene, and 2,5-dimethylfuran were obtained from Sigma Aldrich. Furan was obtained from Alfa Aesar. First-generation and second-generation Grubbs catalysts were obtained from Materia Inc. Third-generation Grubbs catalyst was synthesized from second-generation catalyst according to literature.[56] Reaction temperatures were controlled using an IKAmag temperature modulator and, unless stated otherwise, reactions were performed at room temperature (rt, approximately 23 °C). Thin-layer chromatography (TLC) was conducted with EMD gel 60 F254 pre-coated plates (0.25 mm) and visualized using a combination of UV light and potassium permanganate staining. Silicycle Siliaflash P60 (particle size 0.040–0.063 mm) was used for flash column chromatography. ^{1}H NMR spectra were recorded on Bruker spectrometers

(at 400 MHz, or 500 MHz) and are reported relative to deuterated solvent signals. Data for ^{1}H NMR spectra are reported as follows: chemical shift (δ ppm), multiplicity, coupling constant (Hz) and integration. ^{13}C NMR spectra were recorded on Bruker spectrometers (at 125 MHz) and are reported relative to deuterated solvent signals. Data for ^{13}C NMR spectra are reported in terms of chemical shift and, when necessary, multiplicity, and coupling constant (Hz). IR spectra were recorded on a Perkin-Elmer 100 spectrometer and are reported in terms of frequency of absorption (cm^{-1}). High-resolution mass spectra were obtained on Waters LCT Premier with ACQUITY LC and Thermo Scientific™ Exactive Mass Spectrometers with DART ID-CUBE.

Analytical Techniques

Gel permeation chromatography (GPC) was conducted on a Shimadzu HPLC Prominence-i system equipped with a UV detector, Wyatt DAWN Heleos-II Light Scattering detector, Wyatt Optilab T-rEX RI detector, one MZ-Gel SDplus guard column, and two MZ-Gel SDplus 100 Å 5 μm 300 x 8.0 mm columns. Chloroform ($CHCl_3$) at 40 °C was used as the eluent (flow rate: 0.70 mL/min). For polymers **P1**, **P3**, and **P4**, dn/dc was calculated by the Astra 6.0 software and used for calculation of molecular weights. For **P2**, near-monodisperse poly(styrene) standards (Polymer Laboratories) were employed for calibration and molecular weights were calculated from refractive index. Infrared absorption spectra were recorded on a PerkinElmer FT-IR equipped with an ATR accessory. Elemental analysis was conducted through Midwest Microlab, Inc., on an Exeter Analytical CE-440. For each polymer series, equal amounts of samples were combined from all equivalents (50, 150, and 300 equiv) and submitted for analysis. The samples were vacuum dried overnight prior to the elemental analysis. Differential scanning calorimetry was conducted on a DSCQ200 calorimeter (TA Instruments) equipped with a RSC 90 electric freezing

machine, using approximately 5 mg of dried polymer sample (150 equiv as the representative sample) in an aluminum pan under a dry nitrogen flow at a heating/cooling rate of 10 °C/min, with a total of two cycles from –80 to 200 °C.

Synthesis of Monomers M1–M4

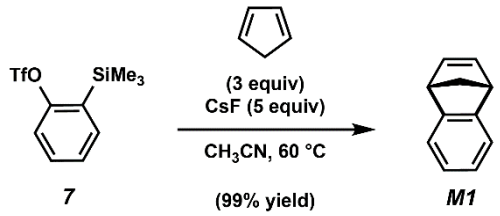

Representative Procedure: Cyclopentadiene Diels-Alder monomer M1. Cyclopentadiene was purified as follows: a 250 mL round bottom flask containing a stir bar was attached to a Vigreux column. The Vigreux column was fitted with a short-path distillation head, which in turn, was connected to a Schlenk tube. The apparatus was flame-dried, and then the 250 mL round bottom flask was charged with dicyclopentadiene (100 mL). The apparatus was purged with N_2, and the 250 mL round bottom flask was heated to 220 °C. After several hours, approximately 50 mL of cyclopentadiene was collected in the Schlenk tube, which was submerged in a –78 °C bath (acetone/dry ice). The distillate was stored at –80 °C.

To a stirred solution of silyltriflate **7** (500 mg, 1.68 mmol) and cyclopentadiene (705 µL, 8.38 mmol, 5 equiv) in CH_3CN (17 mL) was added CsF (1.3 g, 8.38 mmol, 5 equiv). The reaction vessel was sealed and placed in an aluminum heating block maintained at 60 °C for 16 h. After cooling to 23 °C, the reaction mixture was filtered over silica gel (EtOAc eluent). Evaporation under reduced pressure afforded the crude **M1**. The crude residue was further purified by column

chromatography (hexanes) to afford **M1** (239 mg, 99% yield) as a colorless oil: Spectral data matched those previously reported.[57]

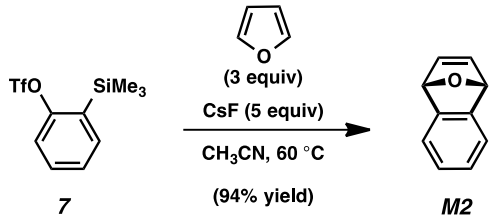

Furan Diels-Alder monomer M2. To a stirred solution of silyltriflate **7** (500 mg, 1.68 mmol) and furan (370 µL, 5.03 mmol, 3 equiv) in CH_3CN (17 mL) was added CsF (1.3 g, 8.38 mmol, 5 equiv). The crude residue was purified by column chromatography (95:5 hexanes:EtOAc) to afford **M2** (227 mg, 94% yield) as a colorless oil: Spectral data matched those previously reported.[58]

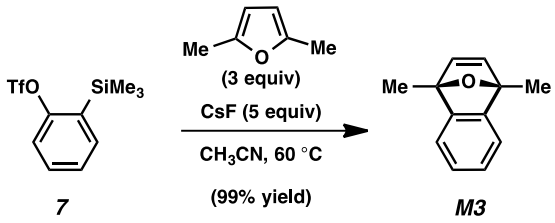

2,5-Dimethylfuran Diels-Alder monomer M3. To a stirred solution of silyltriflate **7** (500 mg, 1.68 mmol) and 2,5-dimethylfuran (555 µL, 5.03 mmol, 3 equiv) in CH_3CN (17 mL) was added CsF (1.3 g, 8.38 mmol, 5 equiv). The crude residue was purified by column chromatography (95:5 hexanes:EtOAc) to afford **M3** (289 mg, 99% yield) as a faint yellow oil: Spectral data matched those previously reported.[59]

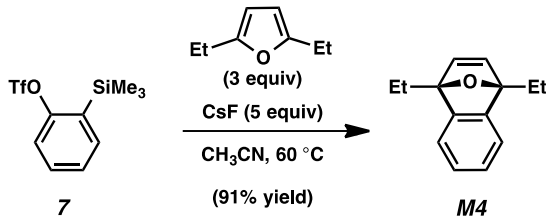

2,5-Diethylfuran Diels-Alder monomer M4. To a stirred solution of silyltriflate **7** (500 mg, 1.68 mmol) and 2,5-diethylfuran (625 mg, 5.03 mmol, 3 equiv) in MeCN (17 mL) was added CsF (1.3 g, 8.38 mmol, 5 equiv). The crude residue was purified by column chromatography (99:1 hexanes:EtOAc) to afford **M4** (305 mg, 91% yield) as a faint orange oil. **M4**: R_f 0.63 (9:1 hexanes:EtOAC); ^{1}H NMR (500 MHz, $CDCl_3$): δ 7.15–7.10 (m, 2H), 6.99–6.93 (m, 2H), 6.79 (s, 2H), 2.40–2.32 (m, 2H), 2.30–2.22 (m, 2H), 1.19 (t, J = 7.53, 6H); ^{13}C NMR (125 MHz, $CDCl_3$): δ 152.6, 146.0, 124.7, 119.0, 92.5, 22.5, 9.2; IR (film): 3069, 2970, 2937, 1452, 1379, 1291 cm^{-1}; HRMS-ESI (m/z) $[M + H]^+$ calcd for $C_{14}H_{17}O$, 201.12739; found, 201.12732.

Synthesis of Polymers P1–P4

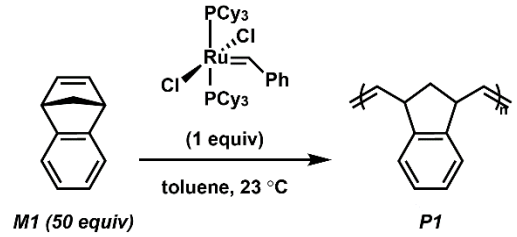

Representative Procedure: Polymerization P1 (50 equiv) (Table 2, Entry 1). A 1-dram vial containing a magnetic stir bar was flame-dried under reduced pressure, and then allowed to cool under N_2. The vial was charged with monomer **M1** (20.0 mg, 0.14 mmol, 50 equiv), and the vial was flushed with N_2. The vial was taken into a glove box and the monomer was dissolved in toluene (100 µL).

In the glovebox, a separate vial was charged with Grubbs first-generation catalyst (5.9 mg) and toluene (230 µL). A 90 µL aliquot of the resulting solution (2.3 mg Grubbs 1st gen. cat., 2.8 µmol, 1 equiv) was then added to the monomer **M1** solution while stirring vigorously. The reaction mixture was allowed to stir at 23 °C for 24 h. The vial was then removed from the glove box and the reaction was quenched with ethyl vinyl ether (10 µL, 0.1 mmol). The polymer was then precipitated by dropwise addition into a scintillation vial containing 15 mL of MeOH kept at –20 °C. The precipitated polymer was recovered and freeze-dried from benzene to afford **P1** (50 equiv). ^{1}H NMR (400 MHz, CD_2Cl_2) δ: 7.56–6.93 (4H), 5.88–5.41 (2H), 4.35–4.09 (1H), 3.93–3.60 (1H), 2.74–2.43 (1H), 1.92–1.64 (1H). M_n (MALS): 5.8 kDa, $Đ$ = 1.73.

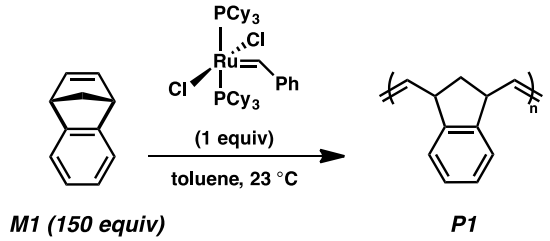

P1 (150 equiv) (Table 2, Entry 2). ^{1}H NMR (400 MHz, CD_2Cl_2) δ: 7.66–7.04 (4H), 5.85–5.43 (2H), 4.33–4.00 (1H), 3.92–3.55 (1H), 2.74–2.39 (1H), 1.89–1.61 (1H). M_n (MALS): 10.8 kDa, $Đ$ = 1.62.

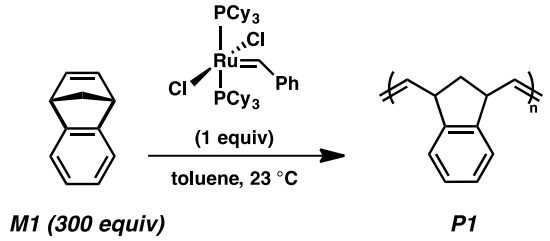

P1 (300 equiv) (Table 2, Entry 3). ^{1}H NMR (400 MHz, CD_2Cl_2) δ: 7.41–7.09 (4H), 5.80–5.46 (2H), 4.32–4.04 (1H), 3.92–3.59 (1H), 2.74–2.38 (1H), 1.90–1.61 (1H). M_n (MALS): 17.4 kDa, $Đ$ = 1.60.

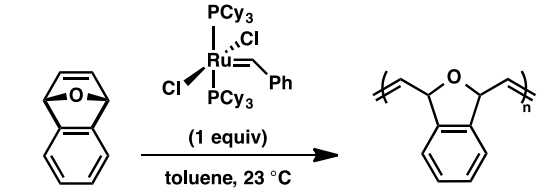

M2 (50 equiv) *P2*

P2 (50 equiv) (Table 2, Entry 4). ^{1}H NMR (400 MHz, CD_2Cl_2) δ: 7.45–7.11 (4H), 6.27–5.91 (2H), 5.89–5.54 (2H). M_n (PS standards): 15.7 kDa, $Đ$ = 1.83.

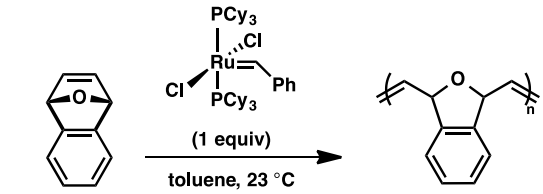

M2 (150 equiv) *P2*

P2 (150 equiv) (Table 2, Entry 5). ^{1}H NMR (400 MHz, CD_2Cl_2) δ: 7.45–7.08 (4H), 6.28–5.94 (2H), 5.91–5.56 (2H). M_n (PS standards): 38.4 kDa, $Đ$ = 1.86.

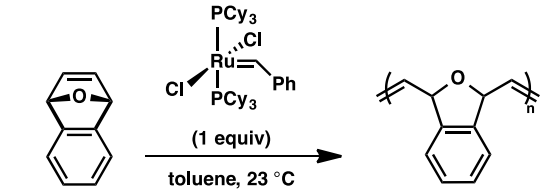

M2 (300 equiv) *P2*

P2 (300 equiv) (Table 2, Entry 6). ^{1}H NMR (400 MHz, CD_2Cl_2) δ: 7.44–7.09 (4H), 6.33–5.93 (2H) 5.92–5.54 (2H). M_n (PS standards): 50.6 kDa, $Đ$ = 2.00.

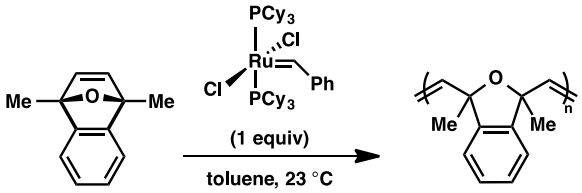

M3 (50 equiv) *P3*

P3 (50 equiv) (Table 2, Entry 7). ^{1}H NMR (400 MHz, CD_2Cl_2) δ: 7.35–6.89 (4H), 6.13–5.84 (2H), 1.70–1.40 (6H). M_n (MALS): 5.4 kDa, $Đ$ = 1.14.

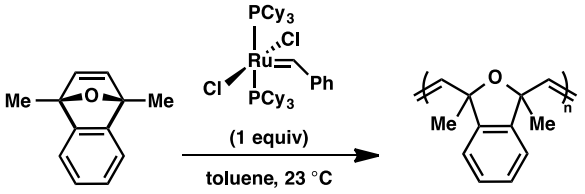

M3 (150 equiv) *P3*

P3 (150 equiv) (Table 2, Entry 8). ^{1}H NMR (400 MHz, CD_2Cl_2) δ: 7.35–6.90 (4H), 6.10–5.86 (2H), 1.67–1.40 (6H). M_n (MALS): 25.2 kDa, $Đ$ = 1.14.

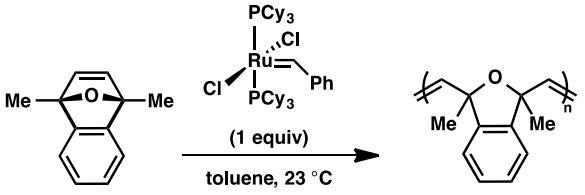

M3 (300 equiv) *P3*

P3 (300 equiv) (Table 2, Entry 9). ^{1}H NMR (400 MHz, CD_2Cl_2) δ: 7.37–6.87 (4H), 6.08–5.88 (2H), 1.69–1.46 (6H). M_n (MALS): 54.0 kDa, $Đ$ = 1.17.

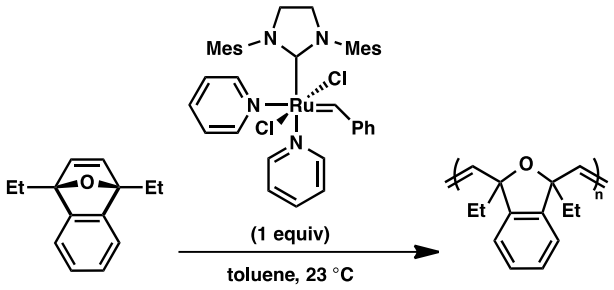

M4 (50 equiv) *P4*

P4 (50 equiv) (Table 2, Entry 10). ^{1}H NMR (400 MHz, CD_2Cl_2) δ: 7.25–7.01 (2H), 7.01–6.82 (2H), 6.13–5.85 (2H), 1.99–1.80 (2H), 1.80–1.62 (2H), 1.02–0.77 (6H). M_n (MALS): 17.4 kDa, $Đ$ = 1.11.

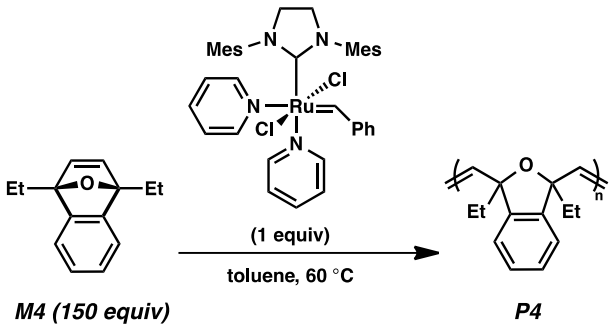

P4 (150 equiv) (Table 2, Entry 11). A 1-dram vial containing a magnetic stir bar was flame-dried under reduced pressure, and then allowed to cool under N_2. The vial was charged with monomer **M4** (20.2 mg, 0.10 mmol, 150 equiv), and the vial was flushed with N_2. The vial was taken into a glovebox.

In the glovebox, a separate vial was charged with Grubbs third-generation catalyst (4.5 mg) and toluene (560 µL). A 60 µL aliquot of the resulting solution (0.48 mg Grubbs 3rd gen. cat., 0.67 µmol, 1 equiv) was then added to the monomer **M4** (neat) while stirring vigorously. The reaction mixture was allowed to stir at 60 °C for 24 h. The vial was then removed from the glovebox and the reaction was quenched with ethyl vinyl ether (10 µL, 0.1 mmol). The polymer was then precipitated by dropwise addition into a scintillation vial containing 15 mL of MeOH kept at –20 C. The precipitated polymer was recovered and freeze-dried from benzene to afford **P4** (150 equiv). ^{1}H NMR (400 MHz, CD_2Cl_2) δ: 7.14–6.99 (2H), 6.99–6.84 (2H), 6.09–5.92 (2H), 1.94–1.80 (2H), 1.80–1.65 (2H), 0.97–0.79 (6H). M_n (MALS): 46.4 kDa, $Đ$ = 1.12.

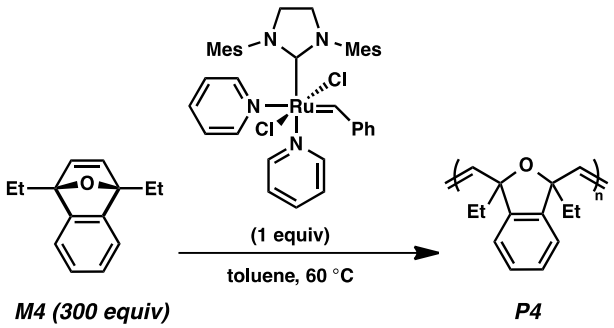

P4 (300 equiv) (Table 2, Entry 12). A 1-dram vial containing a magnetic stir bar was flame-dried under reduced pressure, and then allowed to cool under N_2. The vial was charged with monomer **M4** (20.4 mg, 0.10 mmol, 300 equiv), and the vial was flushed with N_2. The vial was taken into a glovebox.

In the glovebox, a separate vial was charged with Grubbs third-generation catalyst (3.2 mg) and toluene (800 µL). A 60 µL aliquot of the resulting solution (0.24 mg Grubbs 3rd gen. cat., 0.33 µmol, 1 equiv) was then added to the monomer **M4** (neat) while stirring vigorously. The reaction mixture was allowed to stir at 60 °C for 24 h. The vial was then removed from the glovebox and the reaction was quenched with ethyl vinyl ether (10 µL, 0.1 mmol). The polymer was then precipitated by dropwise addition into a scintillation vial containing 15 mL of MeOH kept at –20 C. The precipitated polymer was recovered and freeze-dried from benzene to afford **P4** (300 equiv). ^{1}H NMR (400 MHz, CD_2Cl_2) δ: 7.13–7.02 (2H), 7.01–6.84 (2H), 6.05–5.92 (2H), 1.94–1.78 (2H), 1.78–1.64 (2H), 0.95–0.77 (6H). M_n (MALS): 162 kDa, $Đ$ = 1.07.

Figures and Tables

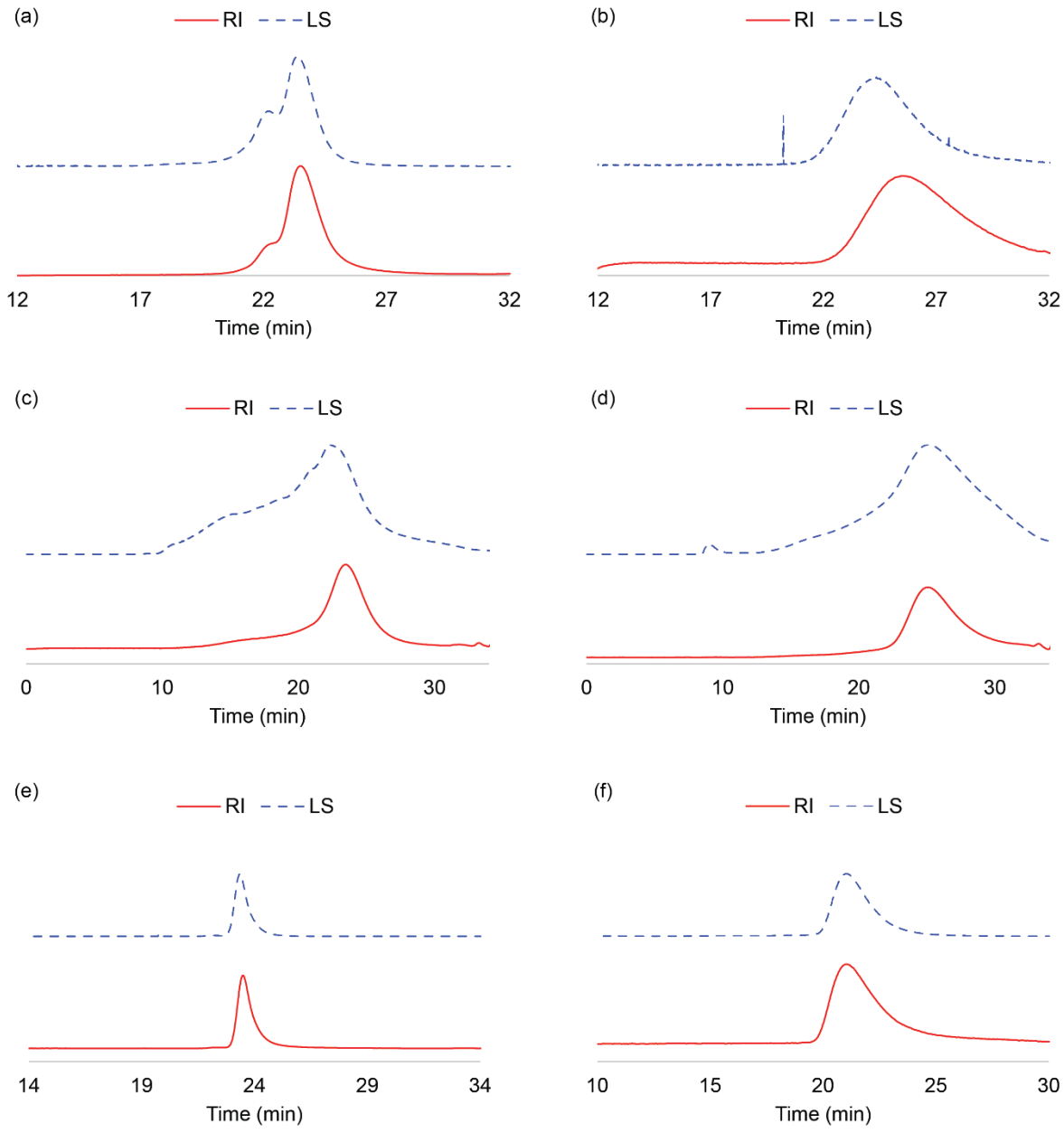

Figure 8-5. Comparison of RI and LS traces of benzonorbornadiene polymers. (a) **P1** immediately after polymerization, (b) **P1** after incubation in air, (c) **P2** immediately after polymerization, (d) **P2** after incubation in air, (e) **P3**, and (f) **P4**.

Table 8-4. Molecular weight of **P1** after incubation in air.

[M] / [I]	M_n *(theo)*	M_n	*Đ*
50	7.1 kDa	5.8 kDa	1.73
150	21.3 kDa	10.8 kDa	1.62
300	42.6 kDa	17.4 kDa	1.60

Calculation of Oxidation Potential

Oxidation potential calculation for **P1** and **P2** were calculated as reported by Nicewicz and co-workers.[51] Briefly, neutral and cation radical structures for respective model compounds **P1'** and **P2'** were optimized using B3LYP/6-31+G(d,p) in the gas phase with Gaussian 09 and their energies were computed.

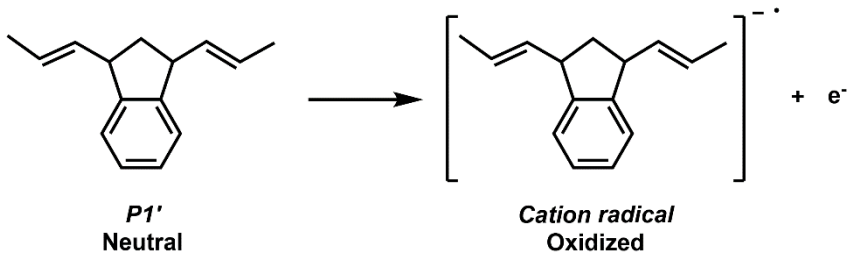

G_{298}(neutral) = –581.928047 Hartree

G_{298}(oxidized) = –581.626248 Hartree

$\Delta G^0_{1/2}$ = (–581.928047 – (–581.626248 Hartree)) × 627.5 kcal mol^{-1} Hartree^{-1} = –189.4 kcal mol^{-1}

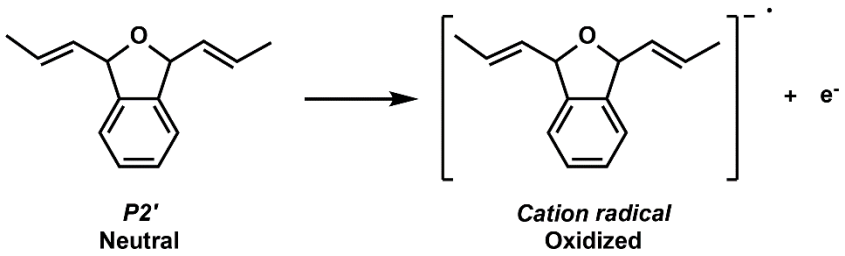

G_{298}(neutral) = –617.841918 Hartree

G_{298}(oxidized) = –617.531377 Hartree

$\Delta G^0_{1/2}$ = (–617.841918 – (–617.531377 Hartree)) × 627.5 kcal mol^{-1} Hartree^{-1} = –194.9 kcal mol^{-1}

The obtained free energies were transformed into oxidation potential by the following equation:

$$E^{0,\mathrm{calc}}_{1/2} = -\frac{\Delta G^0_{1/2}}{n_e \mathcal{F}} - E^{0,\mathrm{SHE}}_{1/2} + E^{0,\mathrm{SCE}}_{1/2}$$

where n_e = number of electrons (one electron in the oxidation of interest), $\mathcal{F}$ = Faraday's constant (23.061 kcal mol^{-1} V^{-1}), $E^{0,\mathrm{SHE}}_{1/2}$ and $E^{0,\mathrm{SCE}}_{1/2}$ are the potential of the standard hydrogen electrode and the saturated calomel electrode, respectively.

Taking the difference in oxidation potential of **P1'** and **P2'** cancels out the electrode potentials $E^{0,\mathrm{SHE}}_{1/2}$ and $E^{0,\mathrm{SCE}}_{1/2}$ to yield the following expression:

$$\Delta E^{0,\mathrm{calc}}_{\frac{1}{2}} = E^{0,\mathrm{calc}}_{\frac{1}{2}}(\mathbf{P2'}) - E^{0,\mathrm{calc}}_{\frac{1}{2}}(\mathbf{P1'})$$

$$= -\frac{\Delta G^0_{\frac{1}{2}}(\mathbf{P2'}) - \Delta G^0_{\frac{1}{2}}(\mathbf{P1'})}{n_e \mathcal{F}} = -\frac{-194.9 - (-189.4)\ \mathrm{kcal\ mol^{-1}}}{1 \times 23.061\ \mathrm{kcal\ mol^{-1}\ V^{-1}}} = 0.238\ \mathrm{V}$$

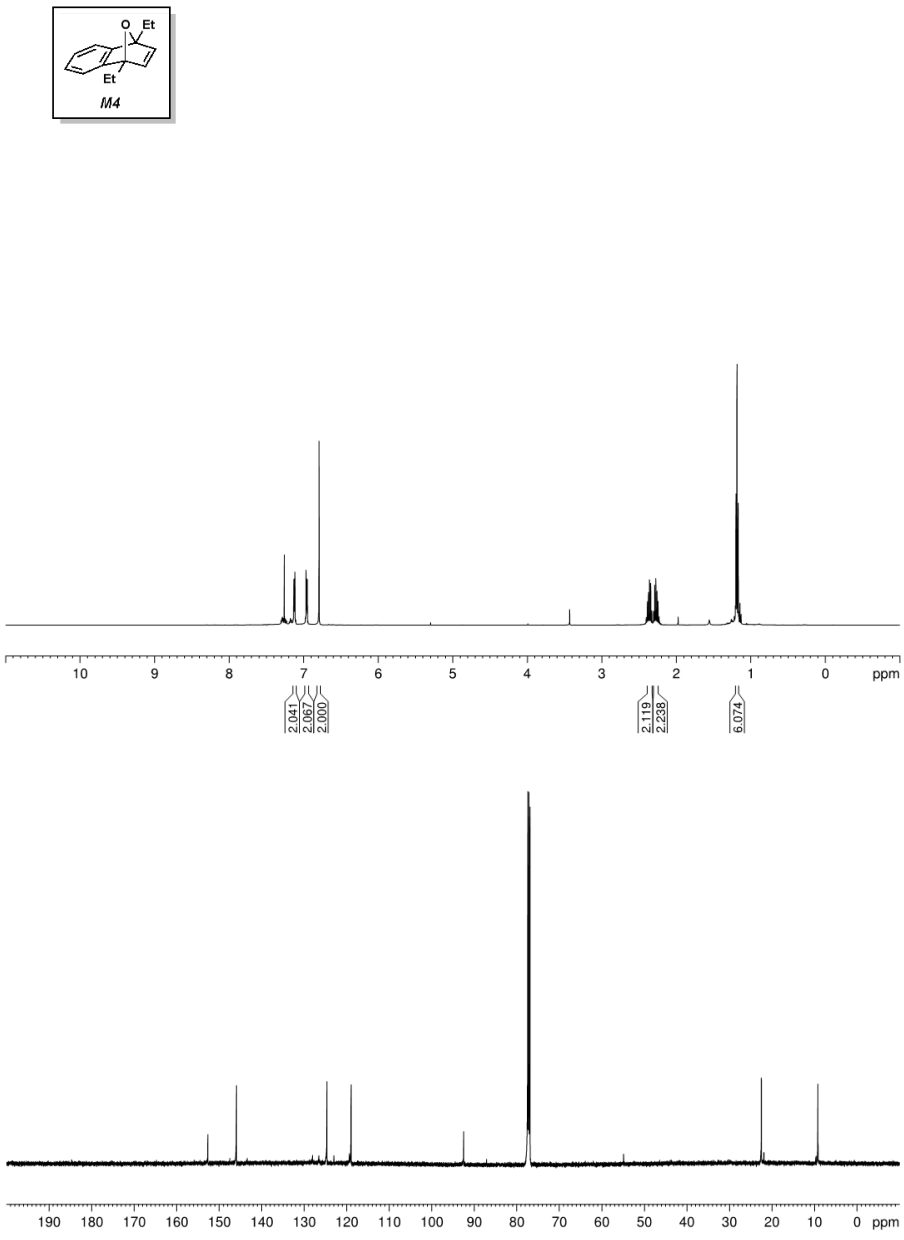

Figure 8-6. ^{1}H (top) and ^{13}C NMR spectra of **M4** ($CDCl_3$).

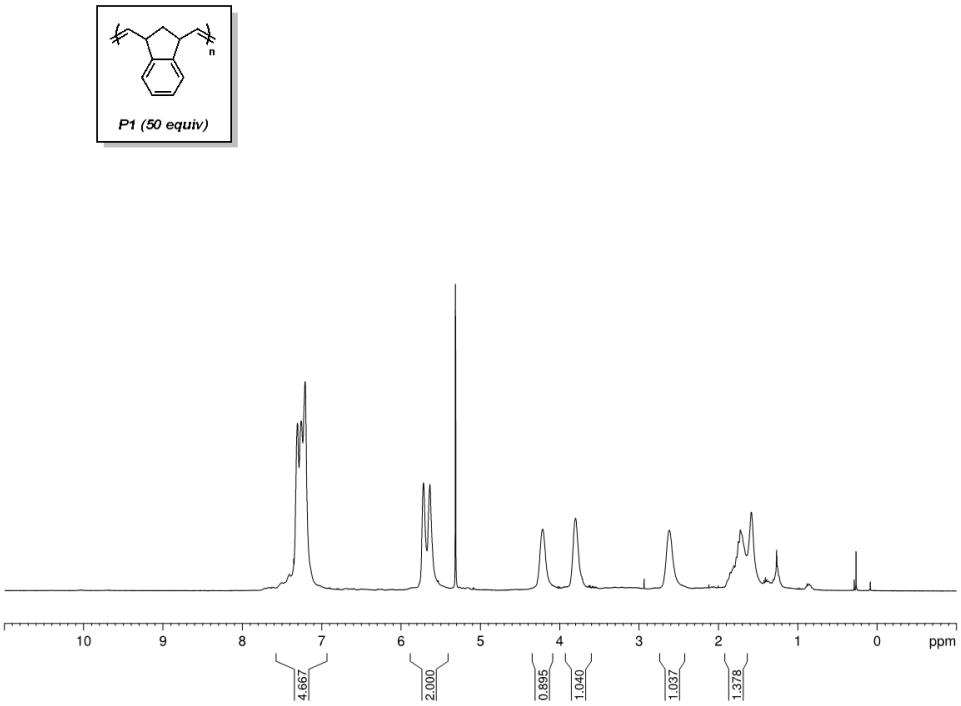

Figure 8-7. ^{1}H NMR spectrum of **P1** (50 equiv) (CD_2Cl_2).

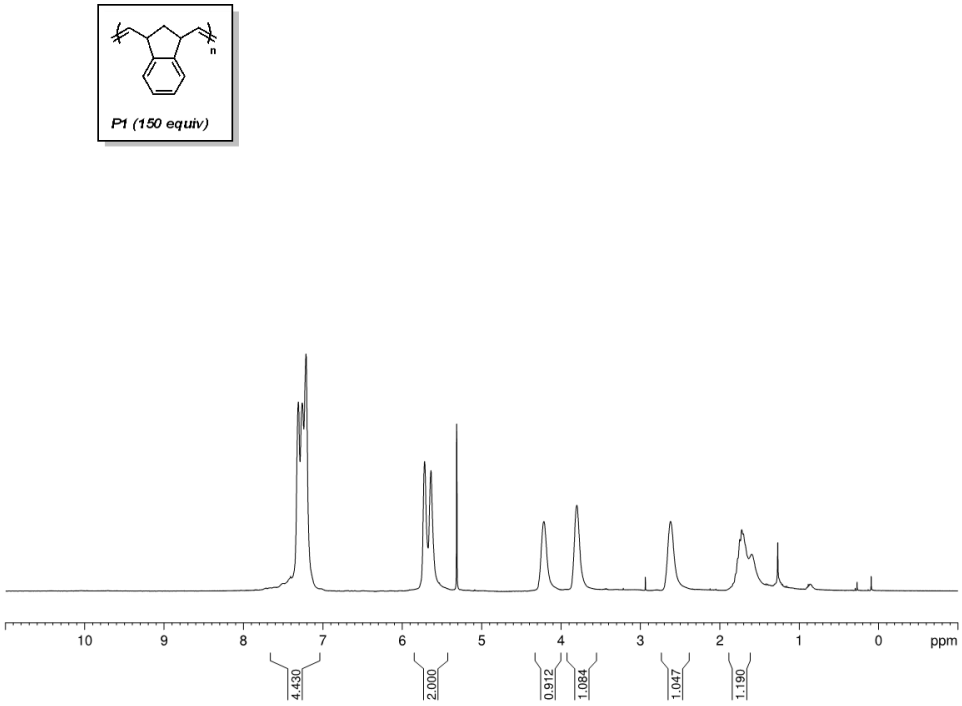

Figure 8-8. ^{1}H NMR spectrum of **P1** (150 equiv) (CD_2Cl_2).

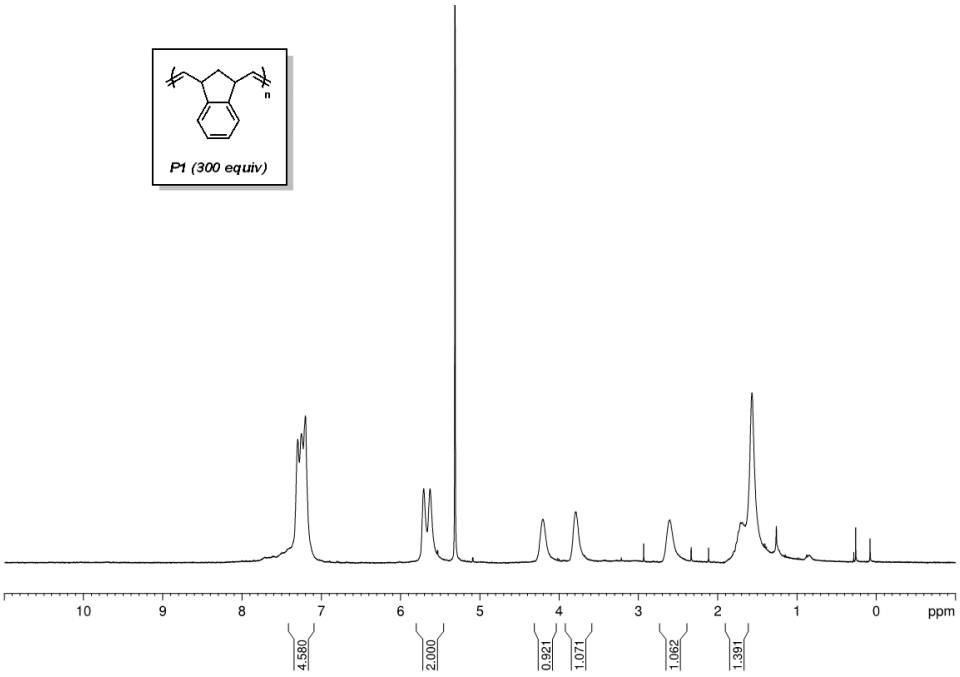

Figure 8-9. ^{1}H NMR spectrum of **P1** (300 equiv) (CD_2Cl_2).

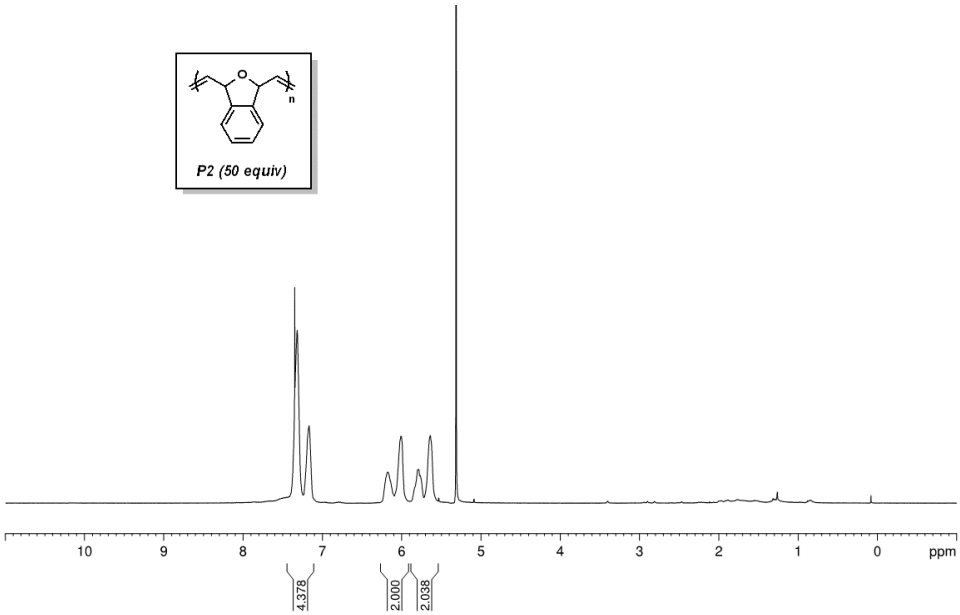

Figure 8-10. ^{1}H NMR spectrum of **P2** (50 equiv) (CD_2Cl_2).

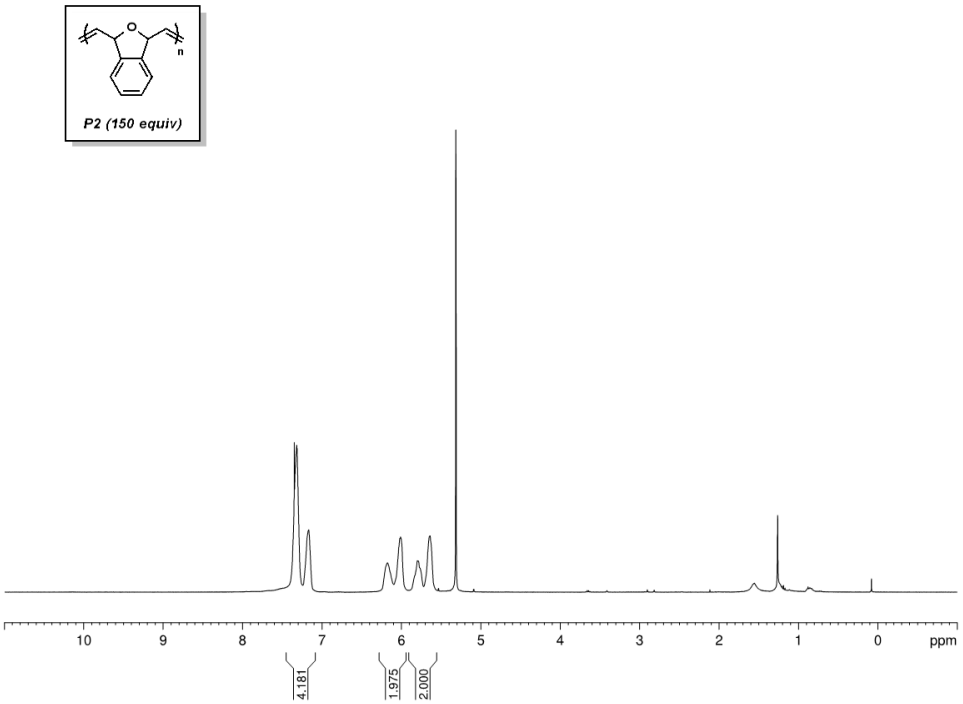

Figure 8-11. ^{1}H NMR spectrum of **P2** (150 equiv) (CD_2Cl_2).

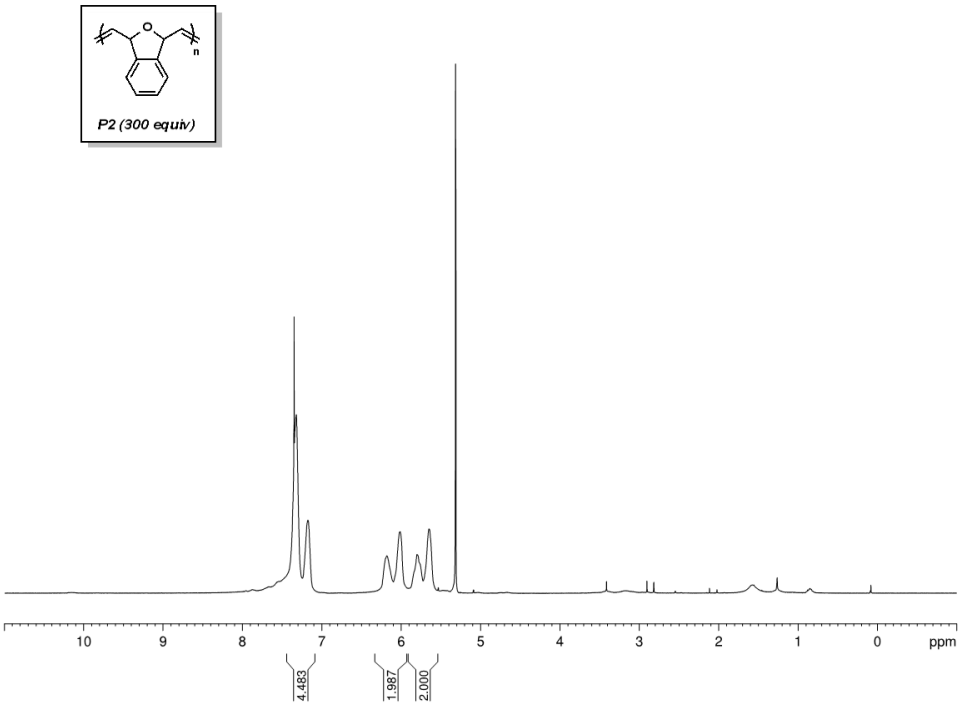

Figure 8-12. ^{1}H NMR spectrum of **P2** (300 equiv) (CD_2Cl_2).

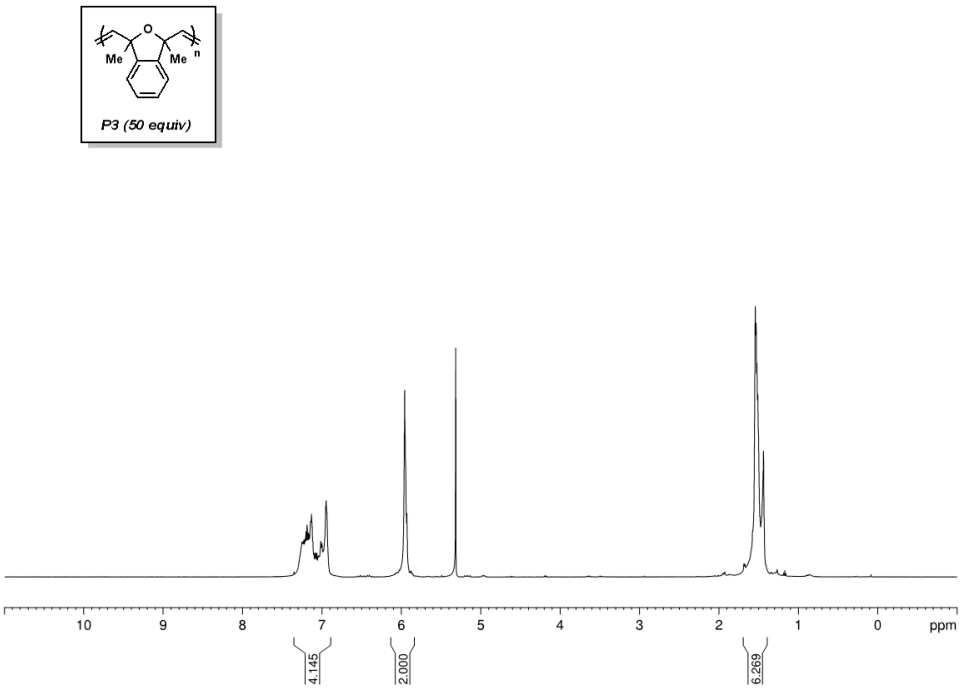

Figure 8-13. ^{1}H NMR spectrum of **P3** (50 equiv) (CD_2Cl_2).

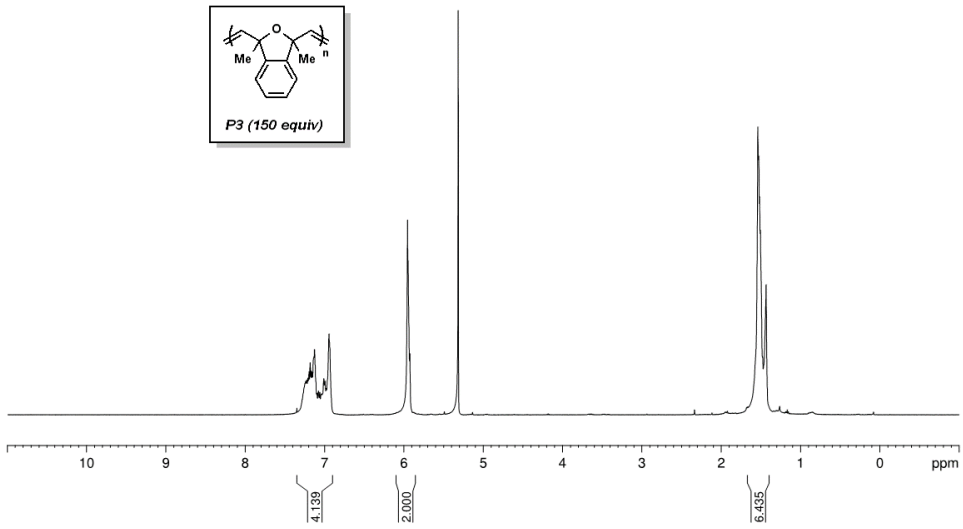

Figure 8-14. ^{1}H NMR spectrum of **P3** (150 equiv) (CD_2Cl_2).

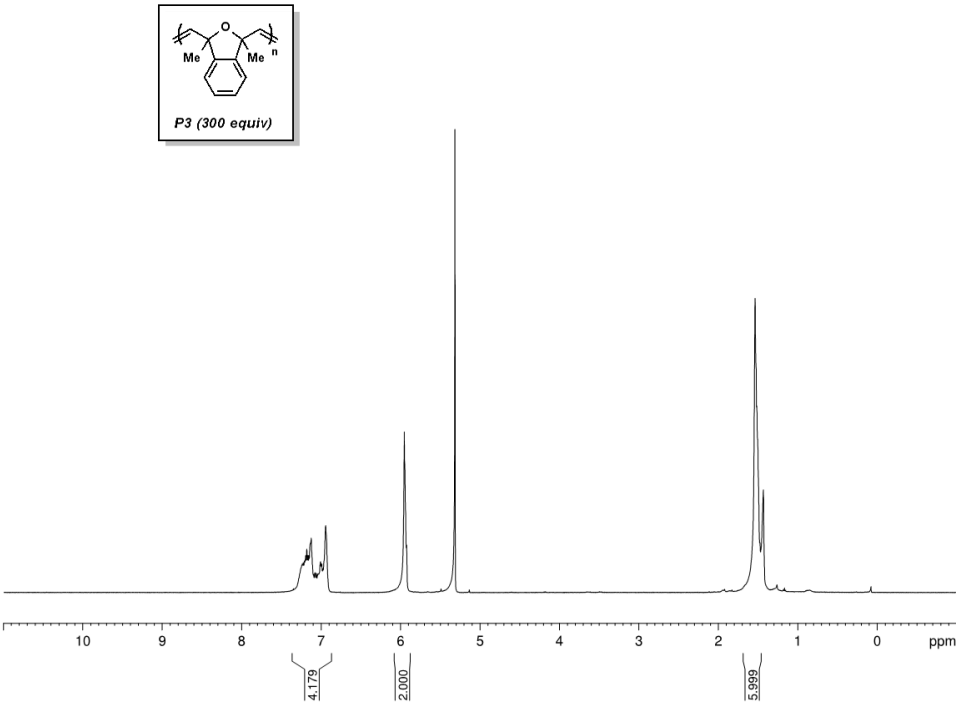

Figure 8-15. ^{1}H NMR spectrum of **P3** (300 equiv) (CD_2Cl_2).

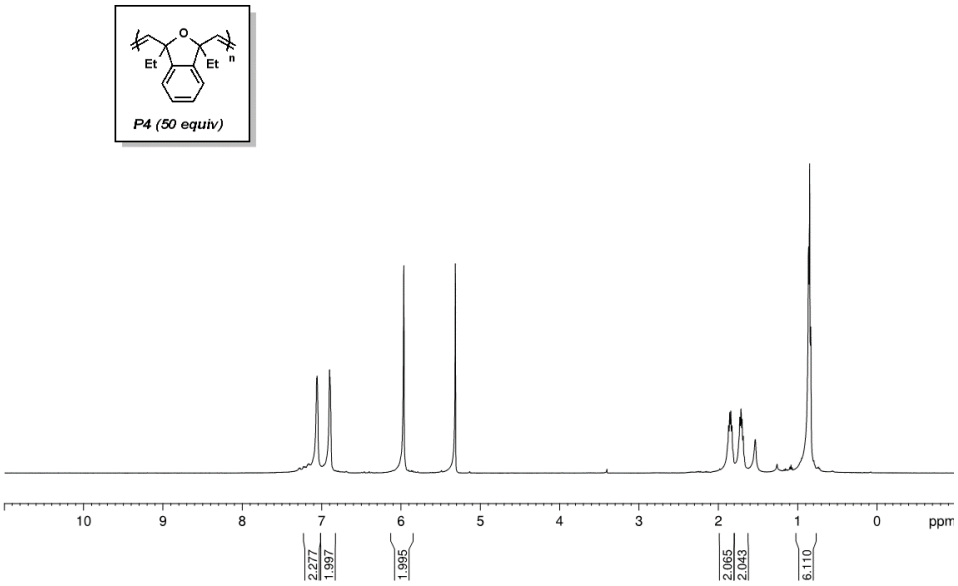

Figure 8-16. ^{1}H NMR spectrum of **P4** (50 equiv) (CD_2Cl_2).

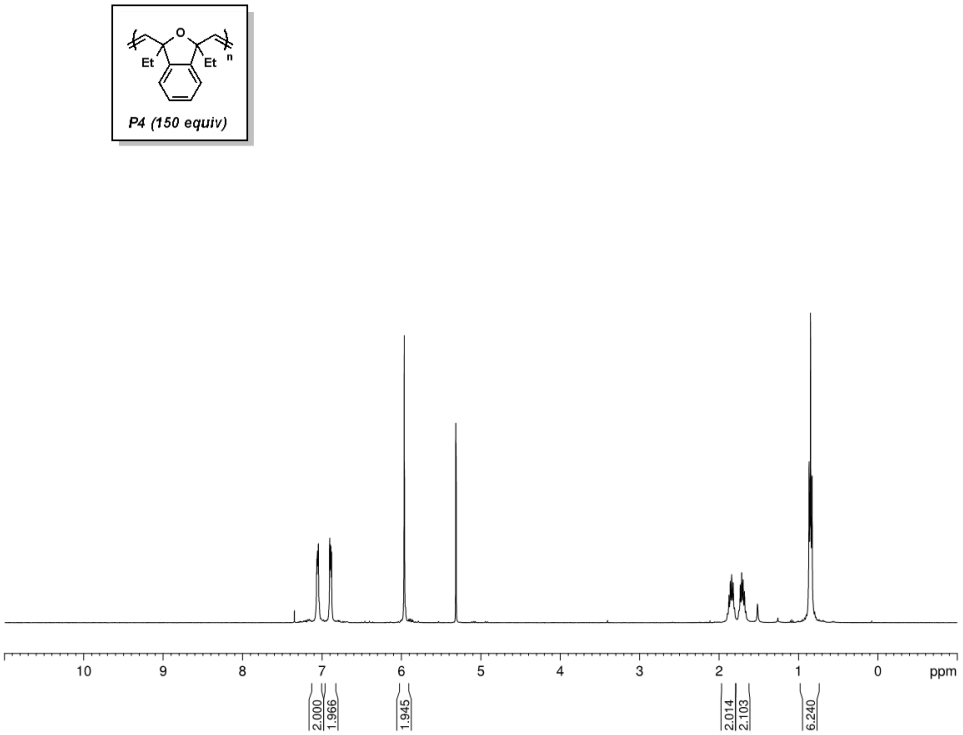

Figure 8-17. ^{1}H NMR spectrum of **P4** (150 equiv) (CD_2Cl_2).

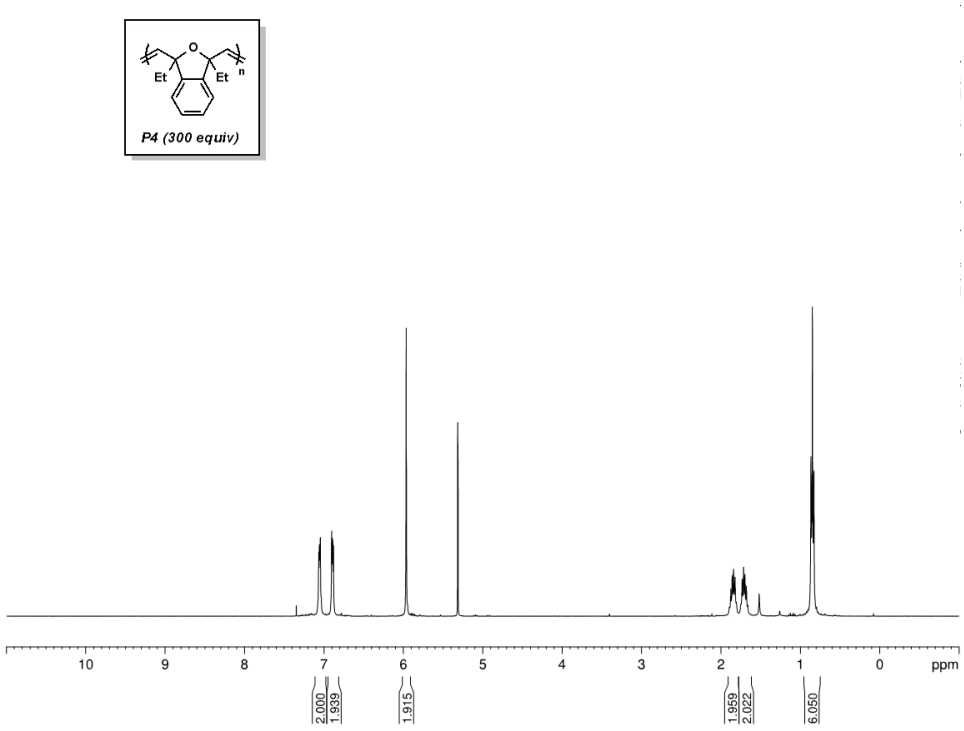

Figure 8-18. ^{1}H NMR spectrum of **P4** (300 equiv) (CD_2Cl_2).

8.5 References

(1) Callmann, C. E.; Barback, C. V.; Thompson, M. P.; Hall, D. J.; Mattrey, R. F.; Gianneschi, N. C. Therapeutic Enzyme-Responsive Nanoparticles for Targeted Delivery and Accumulation in Tumors. *Adv. Mater.* **2015,** *27*, 4611.

(2) Liao, L.; Liu, J.; Dreaden, E. C.; Morton, S. W.; Shopsowitz, K. E.; Hammond, P. T.; Johnson, J. A. A convergent synthetic platform for single-nanoparticle combination cancer therapy: ratiometric loading and controlled release of cisplatin, doxorubicin, and camptothecin. *J. Am. Chem. Soc.* **2014,** *136*, 5896.

(3) Rutenberg, I. M.; Scherman, O. A.; Grubbs, R. H.; Jiang, W.; Garfunkel, E.; Bao, Z. Synthesis of polymer dielectric layers for organic thin film transistors via surface-initiated ring-opening metathesis polymerization. *J. Am. Chem. Soc.* **2004,** *126*, 4062.

(4) Long, T. M.; Swager, T. M. Molecular design of free volume as a route to low-κ dielectric materials. *J. Am. Chem. Soc.* **2003,** *125*, 14113.

(5) Yoon, K.-Y.; Lee, I.-H.; Kim, K. O.; Jang, J.; Lee, E.; Choi, T.-L. One-Pot in Situ Fabrication of Stable Nanocaterpillars Directly from Polyacetylene Diblock Copolymers Synthesized by Mild Ring-Opening Metathesis Polymerization. *J. Am. Chem. Soc.* **2012,** *134*, 14291.

(6) Miyake, G. M.; Piunova, V. A.; Weitekamp, R. A.; Grubbs, R. H. Precisely Tunable Photonic Crystals From Rapidly Self-Assembling Brush Block Copolymer Blends. *Angew. Chem. Int. Ed.* **2012,** *51*, 11246.

(7) Schleyer, P. v. R.; Williams Jr, J. E.; Blanchard, K. Evaluation of strain in hydrocarbons. The strain in adamantane and its origin. *J. Am. Chem. Soc.* **1970,** *92*, 2377.

(8) Leitgeb, A.; Wappel, J.; Slugovc, C. The ROMP toolbox upgraded. *Polymer* **2010,** *51*, 2927.

(9) El-Saafin, I. F.; Feast, W. J. Metathesis polymerization of arylpolycyclic olefins. *J. Mol. Catal.* **1982,** *15*, 61.

(10) El-Saafin, I. F. Ring-opening polymerization of some aryl substituted polycyclic alkenes. Ph.D. Dissertation, Durham University, 1981.

(11) Cannizzo, L. F.; Grubbs, R. H. Block copolymers containing monodisperse segments produced by ring-opening metathesis of cyclic olefins. *Macromolecules* **1988,** *21*, 1961.

(12) Bazan, G.; Khosravi, E.; Schrock, R. R.; Feast, W.; Gibson, V.; O'Regan, M.; Thomas, J.; Davis, W. Living ring-opening metathesis polymerization of 2, 3-difunctionalized norbornadienes by Mo (: CHBu-tert)(: NC6H3Pr-iso2-2, 6)(OBu-tert) 2. *J. Am. Chem. Soc.* **1990,** *112*, 8378.

(13) Bazan, G. C.; Oskam, J. H.; Cho, H. N.; Park, L. Y.; Schrock, R. R. Living ring-opening metathesis polymerization of 2, 3-difunctionalized 7-oxanorbornenes and 7-oxanorbornadienes by Mo (CHCMe2R)(NC6H3-iso-Pr2-2, 6)(O-tert-Bu) 2 and Mo (CHCMe2R)(NC6H3-iso-Pr2-2, 6)(OCMe2CF3) 2. *J. Am. Chem. Soc.* **1991,** *113*, 6899.

(14) Kang, H. A.; Bronstein, H. E.; Swager, T. M. Conductive block copolymers integrated into polynorbornene-derived scaffolds. *Macromolecules* **2008,** *41*, 5540.

(15) Wolfberger, A.; Rupp, B.; Kern, W.; Griesser, T.; Slugovc, C. Ring Opening Metathesis Polymerization Derived Polymers as Photoresists: Making Use of Thiol-ene Chemistry. *Macromol. Rapid Commun.* **2011,** *32*, 518.

(16) Durmaz, H.; Butun, M.; Hizal, G.; Tunca, U. Postfunctionalization of polyoxanorbornene via sequential Michael addition and radical thiol-ene click reactions. *J. Polym. Sci., Part A: Polym. Chem.* **2012,** *50*, 3116.

(17) van Hensbergen, J. A.; Burford, R. P.; Lowe, A. B. Post-functionalization of a ROMP polymer backbone via radical thiol-ene coupling chemistry. *J. Polym. Sci., Part A: Polym. Chem.* **2013,** *51*, 487.

(18) Lowe, A. B. Thiol–ene "click" reactions and recent applications in polymer and materials synthesis: a first update. *Polym. Chem.* **2014,** *5*, 4820.

(19) Kauffmann, T. The Hetarynes. *Angew. Chem., Int. Ed. Engl.* **1965,** *4*, 543.

(20) Reinecke, M. G. Hetarynes. *Tetrahedron* **1982,** *38*, 427.

(21) Pellissier, H.; Santelli, M. The use of arynes in organic synthesis. *Tetrahedron* **2003,** *59*, 701.

(22) Wenk, H. H.; Winkler, M.; Sander, W. One century of aryne chemistry. *Angew. Chem. Int. Ed.* **2003,** *42*, 502.

(23) Sanz, R. Recent applications of aryne chemistry to organic synthesis. A review. *Org. Prep. Proced. Int.* **2008,** *40*, 215.

(24) Bronner, S. M.; Goetz, A. E.; Garg, N. K. Understanding and modulating indolyne regioselectivities. *Synlett* **2011,** *2011*, 2599.

(25) Tadross, P. M.; Stoltz, B. M. A comprehensive history of arynes in natural product total synthesis. *Chem. Rev.* **2012,** *112*, 3550.

(26) Gampe, C. M.; Carreira, E. M. Arynes and cyclohexyne in natural product synthesis. *Angew. Chem. Int. Ed.* **2012,** *51*, 3766.

(27) Bhunia, A.; Yetra, S. R.; Biju, A. T. Recent advances in transition-metal-free carbon–carbon and carbon–heteroatom bond-forming reactions using arynes. *Chem. Soc. Rev.* **2012,** *41*, 3140.

(28) Yoshida, H.; Takaki, K. Aryne insertion reactions into carbon–carbon σ-bonds. *Synlett* **2012,** *23*, 1725.

(29) Dubrovskiy, A. V.; Markina, N. A.; Larock, R. C. Use of benzynes for the synthesis of heterocycles. *Org. Biomol. Chem.* **2013,** *11*, 191.

(30) Wu, C.; Shi, F. A closer look at aryne chemistry: details that remain mysterious. *Asian J. Org. Chem.* **2013,** *2*, 116.

(31) Goetz, A. E.; Garg, N. K. Enabling the use of heterocyclic arynes in chemical synthesis. *J. Org. Chem.* **2014,** *79*, 846.

(32) Goetz, A. E.; Shah, T. K.; Garg, N. K. Pyridynes and indolynes as building blocks for functionalized heterocycles and natural products. *Chem. Commun.* **2015,** *51*, 34.

(33) Shah, T. K.; Medina, J. M.; Garg, N. K. Expanding the Strained Alkyne Toolbox: Generation and Utility of Oxygen-Containing Strained Alkynes. *J. Am. Chem. Soc.* **2016,** *138*, 4948.

(34) Medina, J. M.; Mackey, J. L.; Garg, N. K.; Houk, K. N. The role of aryne distortions, steric effects, and charges in regioselectivities of aryne reactions. *J. Am. Chem. Soc.* **2014,** *136*, 15798.

(35) Bronner, S. M.; Mackey, J. L.; Houk, K. N.; Garg, N. K. Steric effects compete with aryne distortion to control regioselectivities of nucleophilic additions to 3-silylarynes. *J. Am. Chem. Soc.* **2012,** *134*, 13966.

(36) Bronner, S. M.; Goetz, A. E.; Garg, N. K. Overturning indolyne regioselectivities and synthesis of indolactam V. *J. Am. Chem. Soc.* **2011,** *133*, 3832.

(37) Picazo, E.; Houk, K. N.; Garg, N. K. Computational predictions of substituted benzyne and indolyne regioselectivities. *Tetrahedron Lett.* **2015,** *56*, 3511.

(38) Im, G.-Y. J.; Bronner, S. M.; Goetz, A. E.; Paton, R. S.; Cheong, P. H.-Y.; Houk, K. N.; Garg, N. K. Indolyne experimental and computational studies: Synthetic applications and origins of selectivities of nucleophilic additions. *J. Am. Chem. Soc.* **2010,** *132*, 17933.

(39) Goetz, A. E.; Garg, N. K. Regioselective reactions of 3, 4-pyridynes enabled by the aryne distortion model. *Nat. Chem.* **2013,** *5*, 54.

(40) Bronner, S. M.; Bahnck, K. B.; Garg, N. K. Indolynes as electrophilic indole surrogates: fundamental reactivity and synthetic applications. *Org. Lett.* **2009,** *11*, 1007.

(41) Cheong, P. H.-Y.; Paton, R. S.; Bronner, S. M.; Im, G.-Y. J.; Garg, N. K.; Houk, K. N. Indolyne and aryne distortions and nucleophilic regioselectivites. *J. Am. Chem. Soc.* **2010,** *132,* 1267.

(42) Medina, J. M.; McMahon, T. C.; Jiménez-Osés, G.; Houk, K. N.; Garg, N. K. Cycloadditions of cyclohexynes and cyclopentyne. *J. Am. Chem. Soc.* **2014,** *136*, 14706.

(43) Mizukoshi, Y.; Mikami, K.; Uchiyama, M. Aryne polymerization enabling straightforward synthesis of elusive poly (ortho-arylene) s. *J. Am. Chem. Soc.* **2015,** *137*, 74.

(44) Ihara, E.; Kurokawa, A.; Koda, T.; Muraki, T.; Itoh, T.; Inoue, K. Benzyne as a monomer for polymerization: Alternating copolymerization of benzyne and pyridine to give novel polymers with o-phenylene and 2, 3-dihydropyridine units in the main chain. *Macromolecules* **2005,** *38*, 2167.

(45) Ito, S.; Takahashi, K.; Nozaki, K. Formal aryne polymerization: use of [2.2. 1] oxabicyclic alkenes as aryne equivalents. *J. Am. Chem. Soc.* **2014,** *136*, 7547.

(46) Sibi, M. P.; Sermadurai, S.; Zimmermann, N.; Serum, E.; Ma, G.; Moorthy, R.; Kalliokoski, K. Novel monomers from biomass. U. S. Patent 2016022943, Jun. 16, 2016.

(47) Himeshima, Y.; Sonoda, T.; Kobayashi, H. Fluoride-induced 1, 2-elimination of o-trimethylsilylphenyl triflate to benzyne under mild conditions. *Chem. Lett.* **1983,** *12*, 1211.

(48) MacRury, T.; McConnell, M. Measurement of the absolute molecular weight and molecular weight distribution of polyolefins using low-angle laser light scattering. *J. Appl. Polym. Sci.* **1979,** *24*, 651.

(49) Podzimek, S. The use of GPC coupled with a multiangle laser light scattering photometer for the characterization of polymers. On the determination of molecular weight, size and branching. *J. Appl. Polym. Sci.* **1994,** *54*, 91.

(50) Ganachaud, F.; Monteiro, M. J.; Gilbert, R. G.; Dourges, M.-A.; Thang, S. H.; Rizzardo, E. Molecular weight characterization of poly (N-isopropylacrylamide) prepared by living free-radical polymerization. *Macromolecules* **2000,** *33*, 6738.

(51) Roth, H. G.; Romero, N. A.; Nicewicz, D. A. Experimental and Calculated Electrochemical Potentials of Common Organic Molecules for Applications to Single-Electron Redox Chemistry. *Synlett* **2016,** *27*, 714.

(52) Amir-Ebrahimi, V.; Rooney, J. J. The remarkable activity of 7-oxa-benzonorbornadiene in metathesis copolymerization using Ru-based initiators. *J. Mol. Catal. A: Chem.* **2004,** *212*, 107.

(53) Simril, V. Internal plasticization: The effect of chemical structure. *J. Polym. Sci.* **1947,** *2*, 142.

(54) Khosravi, E.; Feast, W.; Al-Hajaji, A.; Leejarkpai, T. ROMP of n-alkyl norbornene dicarboxyimides: from classical to well-defined initiators, an overview. *J. Mol. Catal. A: Chem.* **2000,** *160*, 1.

(55) Jenekhe, S. A.; Roberts, M. F. Effects of intermolecular forces on the glass transition of polymers. *Macromolecules* **1993,** *26*, 4981.

(56) Love, J. A.; Morgan, J. P.; Trnka, T. M.; Grubbs, R. H. A practical and highly active ruthenium-based catalyst that effects the cross metathesis of acrylonitrile. *Angew. Chem. Int. Ed.* **2002,** *41*, 4035.

(57) Wang, B. Y.; Turner, D. A.; Zujović, T.; Hadad, C. M.; Badjić, J. D. The Role of Chirality in Directing the Formation of Cup-Shaped Porphyrins and the Coordination Characteristics of such Hosts. *Chem. Eur. J.* **2011,** *17*, 8870.

(58) Kitamura, T.; Yamane, M.; Inoue, K.; Todaka, M.; Fukatsu, N.; Meng, Z.; Fujiwara, Y. A new and efficient hypervalent iodine− benzyne precursor,(phenyl)[o-(trimethylsilyl) phenyl] iodonium triflate: Generation, trapping reaction, and nature of benzyne. *J. Am. Chem. Soc.* **1999,** *121*, 11674.

(59) Sumida, Y.; Kato, T.; Hosoya, T. Generation of arynes via ate complexes of arylboronic esters with an ortho-leaving group. *Org. Lett.* **2013,** *15*, 2806.